

**Design and Synthesis of Natural Product-Inspired, Cysteine Reactive
Probes toward Inhibition of Transcription Factors and Target
Identification Studies**

A Thesis

SUBMITTED TO THE FACULTY OF THE
UNIVERSITY OF MINNESOTA

BY

John C. Widen

IN PARTIAL FULFILLMENT OF THE REQUIREMENTS
FOR THE DEGREE OF
DOCTOR OF PHILOSOPHY

Advisor: Daniel A. Harki

January 2017

©John C. Widen 2017

Acknowledgments

I would first like to thank my advisor, Professor Daniel Harki, for providing me the opportunity to work and be trained in his laboratory. His advice and support throughout my graduate career was instrumental in my progress and growth as a medicinal chemist. He gave me freedom to pursue my research ideas and encouraged me to work hard in the laboratory, apply for fellowships, and present and publish my research. He also allowed me to travel to many research conferences, which contributed greatly to my professional development. His mentorship is greatly appreciated.

I would also like to thank our collaborators at the University of Minnesota, Professor Scott Dehm, Professor David Largaespada, and Professor Will Pomerantz for their advice and guidance throughout my graduate career. Their collaborations gave me the opportunity to expand my research skills into different fields and to approach scientific problems from different perspectives. I would like to thank Professor Kay Brummond and her two students, Paul Arthur Jackson and Sarah Wells, at the University of Pittsburgh for our fruitful collaboration, which has resulted in several publications and taught me a great deal about chemistry. Lastly, I would like to thank my dissertation committee Professor Carrie Haskell-Luevano, Professor Courtney Aldrich, and Professor Will Pomerantz for their guidance and support throughout my graduate career.

During my graduate studies I had the pleasure to work with and learn from many graduate students and researchers at the University of Minnesota. Special thanks to Maggie Olson for being a great lab mate and friend. Her discussions and advice were invaluable. Also, I would like to thank Dr. Aaron Kempema who worked with me on my main research project, taught me a wealth of chemistry, and remains a great friend. Without him my main research project would not have progressed as smoothly. I would like to acknowledge other members of the Harki Laboratory including Professor Angela Perkins, Nick Struntz, Tim Andrews, Dan Wang, Kellan Passow, Christopher Richards, Stephanie Bruenig, Torie Grover, Daniel Abate-Pella, Dibyendu Dana, Ruben Eckermann, and Ramkumar Moorthy for their guidance, helpful discussions, and

providing a fun work environment. Thanks to my undergraduate and professional school trainees, Jacob Edwards, Jordan Baur, David Cullen, Tenley Brown, and Hannah Skopec for their hard work and patience.

I would like to extend my gratitude to the Gunda Georg, Courtney Aldrich, David Largaspaeda, Natalia Tretyakova, Reuben Harris, and Rick Wagner group members for helpful discussions and lending chemicals and supplies; special thanks to Arnold Groehler IV and Aniekan Okon for great discussions and always being around late at night. I would like to acknowledge the Masonic Cancer Research Center, especially Dr. Peter Villalta, for providing training and guidance on mass spectrometry techniques. Lastly, I would like to thank the Bighley Family for their generous award during the second year of my graduate career.

Dedication

I'd like to dedicate this thesis to colleagues, friends, and family that supported me during my graduate career.

Abstract

Extra- and intracellular stimuli results in gene expression changes by controlling transcription factor activity. Transcription factors are at the hub of cellular signaling and are responsible for controlling virtually all cellular processes by binding DNA to directly modulate gene expression. Because transcription factors control many cell decisions based on cellular pathway signaling, aberrant transcription factor activity is involved in many human diseases, making them interesting targets for drug discovery. With the exception of nuclear receptors, which are the only class of transcription factors known to contain ligand-binding domains, there are no FDA approved drugs directly targeting transcription factors. Historically, transcription factors have been referred to as ‘undruggable’ protein targets. This is likely due to the difficulty in developing small molecules toward transcription factors because they typically contain no enzymatic activity, lack ligand binding pockets, and have non-discrete tertiary structure. Thus, directly targeting transcription factors with small molecules must occur at protein-protein or DNA-binding interfaces, which contain shallow binding pockets over large surface areas.

One strategy to overcome the difficulty in directly targeting transcription factors at protein-protein and DNA-binding interfaces with small molecules is through targeting nucleophilic amino acids within protein or DNA binding surfaces. This thesis describes efforts in developing cysteine reactive small molecules for direct targeting of transcription factors. Small molecule probes containing a cysteine reactive group(s) were developed, which were inspired by natural products. Chapter 2 discusses the design and synthesis of bis-electrophile probes based on the pseudoguaianolide natural product helenalin to target the transcription factor p65 of the NF- κ B (p50/p65) heterodimer. Chapter 3 describes the synthesis and testing of additional helenalin-based inhibitors containing a single Michael acceptor for targeted inhibition of the NF- κ B pathway. Chapter 6 explores small molecule probes that contain a chlorohydrin for covalent inhibition of the androgen receptor N-terminal domain for castration resistant prostate cancer inhibition.

Other projects discussed in this thesis relate to the development of cysteine reactive probes for target identification studies. Chapter 4 communicates the synthesis of cysteine reactive probes based on the sesquiterpene lactone natural product parthenolide and their ability to target leukemic stem cells versus healthy bone marrow cells. Chapter 5 presents the synthesis of parthenolide-based alkyne probes for target identification studies in primary human AML cells via pulldown and LC-MS/MS proteomic analysis. Chapter 7 examines the Nicholas reaction and its application toward the attachment of terminal alkynes to complex small molecules.

TABLE OF CONTENTS

LIST OF TABLES		ix
LIST OF FIGURES		x
LIST OF SCHEMES		xii
Chapter 1	INTRODUCTION	1
1.1	Overview of Transcription Factors	2
1.2	Structural Features of Transcription Factors	8
1.3	Overview of the NF- κ B Pathway	11
1.3.1	The Canonical NF- κ B Pathway	12
1.3.2	The Non-canonical NF- κ B Pathway	17
1.3.3	Involvement of the NF- κ B Pathway in Human Disease	19
1.4	Overview of Androgen Receptor Signaling	21
1.4.1	The Androgen Receptor Signaling Pathway	22
1.4.2	Targeting Androgen Receptor Signaling in Prostate Cancer	25
1.5	Why Develop Inhibitors Toward Transcription Factors?	27
1.5.1	Indirect Inhibition of Transcription Factor Activity	29
1.6	Direct Small Molecule Inhibitors of Transcription Factors	33
1.6.1	Small Molecules Targeting Protein-DNA Interfaces of Transcription Factors	34
1.7	Preface to this Thesis	40
Chapter 2	TARGETING NF- κ B p65 WITH A HELENALIN INSPIRED BIS-ELECTROPHILE	41
2.1	Introduction	42
2.2	Design and Synthesis of Simplified Helenalin Analogues	45
2.3	Stereochemical Determination of Simplified Helenalin Probes	49
2.4	Simplified Helenalin Probes Inhibit NF- κ B Signaling in Cell Culture	50
2.5	Simplified Helenalin Probes Covalently Bind Proteins in Cell Culture	52
2.6	Helenalin and Simplified Helenalin Probes Covalently Label Cys38 of Recombinant p65	54
2.7	Simplified Helenalin Probes Covalently Target p65 in Cell Culture	59
2.8	Conclusion	61
2.9	Materials and Methods	62
2.10	Spectral Data	79

2.11	HPLC Chromatograms of Tested Compounds	93
2.12	Enantiopurity Analysis of Synthesized Compounds	96
2.13	X-ray Crystallography Data for 2.11	100
2.14	Acknowledgements	105
Chapter 3	SYNTEHSIS AND BIOCHEMICAL EVALUATION OF BIS-MICHAEL ACCEPTOR INHIBITORS OF THE NF- κ B PATHWAY BASED ON THE NATURAL PRODUCT HELENALIN	106
3.1	Introduction	107
3.2	Monitoring Cysteamine Reactivity of 3.1a and 3.1b with ^1H NMR	109
3.3	Reduction of Simplified Helenalin Intermediates	114
3.4	Synthesis of Reduced Simplified Helenalin Analogues	116
3.5	Stereochemical Determination of Reduced Simplified Helenalin Analogues	118
3.6	Evaluation of Reduced Simplified Helenalin Analogues for NF- κ B inhibition	120
3.7	Conclusion	122
3.8	Experimental	123
3.9	Improved Synthesis of 3.2 and 3.3	134
3.10	Spectral Data	136
3.11	HPLC Purity Analysis of Synthesized Compounds	155
Chapter 4	SYNTHESIS AND ANTILEUKEMIC ACTIVITIES OF C1-C10-MODIFIED PARTHENOLIDE ANALOGUES	157
4.1	Introduction	158
4.2	Design and Synthesis of Parthenolide Analogues	160
4.3	Lipophilicity Analyses	163
4.4	Cellular Cytotoxicity Screening	164
4.5	Bone Marrow Toxicity Studies	165
4.6	Inhibition of Drug-resistant AML and Toxicity to LSCs	167
4.7	Induction of Reactive Oxygen Species	171
4.8	Conclusion	172
4.9	Experimental	173
4.10	Spectral Data	181
4.11	HPLC Chromatograms of Synthesized Compounds	185
4.12	Data and Analysis of X-ray Structures	189
4.13	Acknowledgements	202

Chapter 5	IDENTIFICATION OF PUTATIVE PARTHENOLIDE TARGETS IN ACTUE MYELOID LEUKEMIA CELLS	203
5.1	Introduction	204
5.2	Semi-synthesis of Parthenolide-based Probes	206
5.3	Cytotoxicity of Functional and Non-functional Alkyne Probes in HL-60	207
5.4	Flow Cytometry Analysis of Primary AML Samples	208
5.5	Pulldown in Primary AML Cells	210
5.6	Progress toward Validation of F12A/OSSA as a Key Regulator of LSC Survival	215
5.7	Additional Identified Protein Targets from Pulldown Studies	217
5.8	Conclusion	223
5.9	Experimental	224
5.10	Spectral Data	230
5.11	HPLC Chromatograms of Synthesized Compounds	234
5.12	Acknowledgements	235
Chapter 6	BIOCHEMICAL EVALUATION AND TARGET IDENTIFICAITON STUDIES OF EPI-002 AND EPI-054	236
6.1	Introduction	237
6.2	Synthesis of EPI002 and EPI054	240
6.3	Biological Evaluation of EPI-002 and EPI-054 in LnCaP Cells	241
6.4	In-gel Fluorescent Labeling of EPI-054 in LnCaP Cells	242
6.5	Conclusion	245
6.6	Experimental	246
6.7	HPLC Chromatograms of Synthesized Compounds	251
Chapter 7	ALKYNE LIGATION HANDLES: PROPARGYLATION OF HYDROXYL, SULFHYDRYL, AMINO, AND CARBOXYL GROUPS VIA THE NICHOLAS REACTION	253
7.1	Introduction	254
7.2	Optimization of Nicholas Reaction Conditions	256
7.3	Application of the Optimized Nicholas Reaction Condition to Amino Acids	258
7.4	Application of the Nicholas Reaction to Complex, Base-sensitive Small Molecules	263
7.5	Conclusions	264
7.6	Experimental	264

7.7	Spectral Data	292
7.8	Acknowledgements	321
	Bibliography	322

List of Tables

Table 2.13.1.	Crystal data and structure refinement for 2.11	104
Table 3.6.1.	Inhibition of synthesized compounds in a NF- κ B luciferase assay in A549 cells	121
Table 3.11.1.	Compound Purity by HPLC	156
Table 4.3.1.	Calculated LogD values of parthenolide analogues	163
Table 4.4.1.	Growth inhibitory activities of parthenolide analogues	165
Table 4.6.1.	Growth inhibitory activities of parthenolide and analogues against Murine AML cell lines B117P, B117H, B140P, and B140H	168
Table 4.6.2.	Growth inhibitory activities of parthenolide and analogues in TEX cells	169
Table 4.6.3.	Clonal growth assays with TEX cells	171
Table 4.12.1.	Crystal data and structure refinement for 4.3	192
Table 4.12.2.	Crystal data and structure refinement for 4.6	196
Table 4.12.3.	Crystal data and structure refinement for 4.7	200
Table 5.5.1.	Pulldown data for primary human AML and TEX samples	211
Table 5.5.2.	Prioritization of identified protein targets	212
Table 5.5.3.	List of identified protein targets that were found in 3-4 Functional samples and not any non-functional control samples	213
Table 6.3.1.	Cytotoxicity of EPI-002 and EPI-054 in LnCaP cells	241
Table 7.2.1.	Optimization of Nicholas Reaction with Alcohol 7.5	257
Table 7.3.1.	Synthesis of alkyne modified amino acids	260

List of Figures

Figure 1.1.1. General activation of the transcriptional machinery	4
Figure 1.1.2. Mechanisms of transcriptional activation	7
Figure 1.2.1. Three examples of common transcription factors bound to DNA	9
Figure 1.3.1. The canonical NF- κ B signal transduction pathway	14
Figure 1.3.2. Characterized phosphorylation and acetylation sites on p65	16
Figure 1.3.3. Non-canonical NF- κ B Signaling	18
Figure 1.4.1. Endogenous Agonists of androgen receptor	21
Figure 1.4.2. Structural Features of the androgen receptor	22
Figure 1.4.3. Androgen receptor signaling pathway	24
Figure 1.4.4. FDA approved drugs for the treatment of castration resistant prostate cancer	26
Figure 1.4.5. Structures of EPI-001 and EPI-054	27
Figure 1.5.1. Indirect methods to modulate transcription factor activity	30
Figure 1.5.2. Imatinib	31
Figure 1.5.3. FDA approved pan-HDAC inhibitors	32
Figure 1.6.1. Helenalin and crystal structure of p65 bound to DNA (PDB: 1VKX)	35
Figure 1.6.2. STAT DNA-binding domain inhibitors	36
Figure 1.6.3. Small molecule inhibitor of NM32-H2	37
Figure 1.6.4. Small molecule inhibitors of KLF10	38
Figure 1.6.5. Inhibitors of the androgen receptor DNA-binding domain	39
Figure 2.1.1. Structure of helenalin and design of helenalin mimics	44
Figure 2.2.1. The measured distances between the two electrophilic carbons of Helenalin and probes 2.1a-b and 2.6a-b	46
Figure 2.4.1. NF- κ B-luciferase inhibition assay in A549 cells	51
Figure 2.4.2. Alamar Blue cytotoxicity analysis of A549 NF- κ B-luciferase cells	52
Figure 2.5.1. Proteome labeling of 2.1a and 2.1b in HeLa cells	53
Figure 2.5.2. In-gel labeling assay: Helenalin competition with 2.1a	54
Figure 2.6.1. Annotation of compound binding sites on p65	55
Figure 2.6.2. MS ² fragmentation data for 2.1a	56

Figure 2.6.3.	MS ² fragmentation data for 2.1b	57
Figure 2.6.4.	MS ² fragmentation data for helenalin	58
Figure 2.6.5.	MS ² fragmentation data for 2.6a and 2.6b with Cys105 of p65	59
Figure 2.7.1.	Immunodetection of NF-κB signaling pathway proteins for covalent binding by 2.1a and 2.1b	61
Figure 3.1.1.	Helenalin and helenalin-based probes 3.1a and 3.1b	108
Figure 3.2.1	Reaction between cysteamine and 3.1a monitored by 1H NMR	111
Figure 3.2.2	Reaction between cysteamine and 3.1b monitored by 1H NMR	113
Figure 3.5.1.	Stereochemical determination of reduced simplified helenalin-based analogues	119
Figure 4.1.1.	Structures of parthenolide analogues	161
Figure 4.2.1.	Comparison of x-ray crystal structures of parthenolide and 4.7	163
Figure 4.5.1.	Toxicity of parthenolide and parthenolide analogues to human bone marrow cells	167
Figure 4.6.1.	Cellular viability to TEX cells treated with doxorubicin, Parthenolide, and parthenolide analogues	170
Figure 4.7.1.	Intracellular ROS induction in TEX cells	172
Figure 4.9.1.	Example of processing flow cytometry data	176
Figure 4.9.2.	Example of processing ROS assay flow cytometry data	178
Figure 4.12.1.	Alignment of the x-ray structures of parthenolide and 4.7	201
Figure 5.3.1.	48 h cytotoxicity dose response curves for probes 5.3 and 5.4 in HL-60 cells	208
Figure 5.4.1.	Human Primary AML and TEX cells CD34 and CD38 population flow cytometry data	209
Figure 5.6.1.	CRISPR/Cas9 knockout studies in HEK293 cells: Western blot analysis and surveyor nuclease assay (Cel-I)	217
Figure 6.1.1.	Structures of abiraterone, enzalutamide, and EPI analogues	239
Figure 6.3.1.	Relative mRNA levels of AR in the presence of EPI-001 and EPI-054	242
Figure 6.4.1.	In-gel fluorescence labeling of EPI-054 in LnCaP cells (time course)	244
Figure 6.4.2.	In-gel fluorescence labeling of EPI-054 in LnCaP cells (concentration gradient)	245
Figure 7.1.1.	Synthetic methods for alkyne incorporation	255

List of Schemes

Scheme 2.2.1. Racemic synthesis of bifunctional helenalin mimics and their alkyne analogues	47
Scheme 2.2.2. Enantioselective synthesis of 2.6a and 2.6b	49
Scheme 2.3.1. Synthesis and x-ray crystal structure of 2.11	50
Scheme 3.3.1. Reduction of the exocyclic methylene of silyl enol ether derivatives 3.2 and 3.3	116
Scheme 3.4.1. Deprotection and Saegusa oxidation of silyl enol ethers for synthesis Of helenalin-based analogues	117
Scheme 3.4.2. Esterification of 3.17	118
Scheme 3.9.1. Synthesis of Intermediates 3.23 and 3.24	135
Scheme 4.2.1. Synthesis of C1-C10 reduced parthenolide analogues	162
Scheme 5.2.1. Synthesis of functional and non-functional parthenolide-based Alkyne probes 5.3 and 5.4	207
Scheme 6.2.1. Synthesis of EPI-002 and EPI-054	241
Scheme 7.2.1. Decomplexation of $\text{Co}_2(\text{CO})_6$ -alkyne 7.7	258
Scheme 7.3.1. Reaction of 7.9h with BF_4^- 7.12	262
Scheme 7.4.1. Synthesis of alkyne probes 7.15 and 7.17	263

Chapter 1

INTRODUCTION

1.1 Overview of Transcription Factors

All intracellular signaling pathways converge to transcription factor modulation, which controls gene expression depending on stimuli. Eukaryotic and prokaryotic cells rely on transcription factors (TFs) to communicate external and internal signals to undergo all processes such as cell growth, division, differentiation, apoptosis, adhesion, energy regulation, metabolism, and immunity. Studying TFs is paramount to understanding how information encoded in DNA becomes a living organism and how it relates to development and disease.

Sequence specific TFs directly bind unique DNA response elements associated with a subset of genes and induce or repress gene transcription through recruitment of co-activators/repressors and chromatin remodeling proteins. During induction, general TFs and RNA polymerase II (pol II) (**Figure 1.1**) are recruited to the promoter region. Response elements are upstream sites from the start of genes (within promoter or enhancer regions) and contain a specific DNA sequence. Binding of TFs to enhancer or promoter regions significantly upregulates transcription by interacting with the initiation complex at the promoter region of genes.

In humans, six general TFs form the initiation complex with RNA pol II before the start of transcription (TFIIA, -B, -D, -E, -F, and -H).¹ General TFs bind to promoter sites of all genes and are required for starting transcription by RNA pol II.² Additionally, a large complex of 20-30 proteins referred to as the Mediator complex is required to start gene transcription.³ The Mediator complex consists of many structural proteins that bridge the interactions between TF complexes located at enhancer regions and initiation complex at the promoter region.⁴ Enhancer regions are typically thousands of base pairs away from promoter regions and physically interact by bending DNA to bring the regions into proximity (referred to as 'looping').⁵ As an extreme example, in mice the sonic hedgehog (ssh) gene promoter is over 1 Mb away from the enhancer region.⁶ The components and functional properties of Mediator change depending on TF interactions

and activation.⁷ The initiator complex only has a basal level of transcription until sequence specific TFs bind to DNA and increase expression.⁸

A single TF can be responsible for the expression of hundreds of genes; however, these genes are not expressed simultaneously upon activation. For instance, the Nuclear Factor κ B (NF- κ B) modulates over 600 genes but binds to only a subset of gene promoters and enhancers based on stimuli and post-translational modifications.⁹ Activation of the androgen receptor (AR) with synthetic testosterone in prostate cancer cells causes different levels of transcriptional activation or repression of hundreds of genes, including upregulation of the Inhibitor of κ B α (I κ B α) gene and down regulation of the myc and IL-6 receptor genes.¹⁰ Furthermore, during the course of the induction genes were activated or repressed over different time periods.

Genes can have multiple promoter and enhancer binding sites for the same or different TFs.¹¹ Different TFs often interact in a cooperative manner to increase or decrease gene transcription. One example of this occurs at the enhancer region of the Interferon- β (IFN- β) gene where the NF- κ B heterodimer and activating transcription factor 2 (ATF-2)/c-Jun heterodimer, along with multiple co-activators, are required for transcription upon viral infection.¹² In a separate example, the TNF- α gene is controlled by multiple TFs including NF- κ B and c-Jun. However, in this case NF- κ B and c-Jun activate transcription separately and no synergistic interactions were observed.¹³ Promoter and enhancer sites for the same TF can have different DNA sequences that can distort protein binding surfaces in unique ways, which are recognized by separate co-activators or repressors.¹⁴

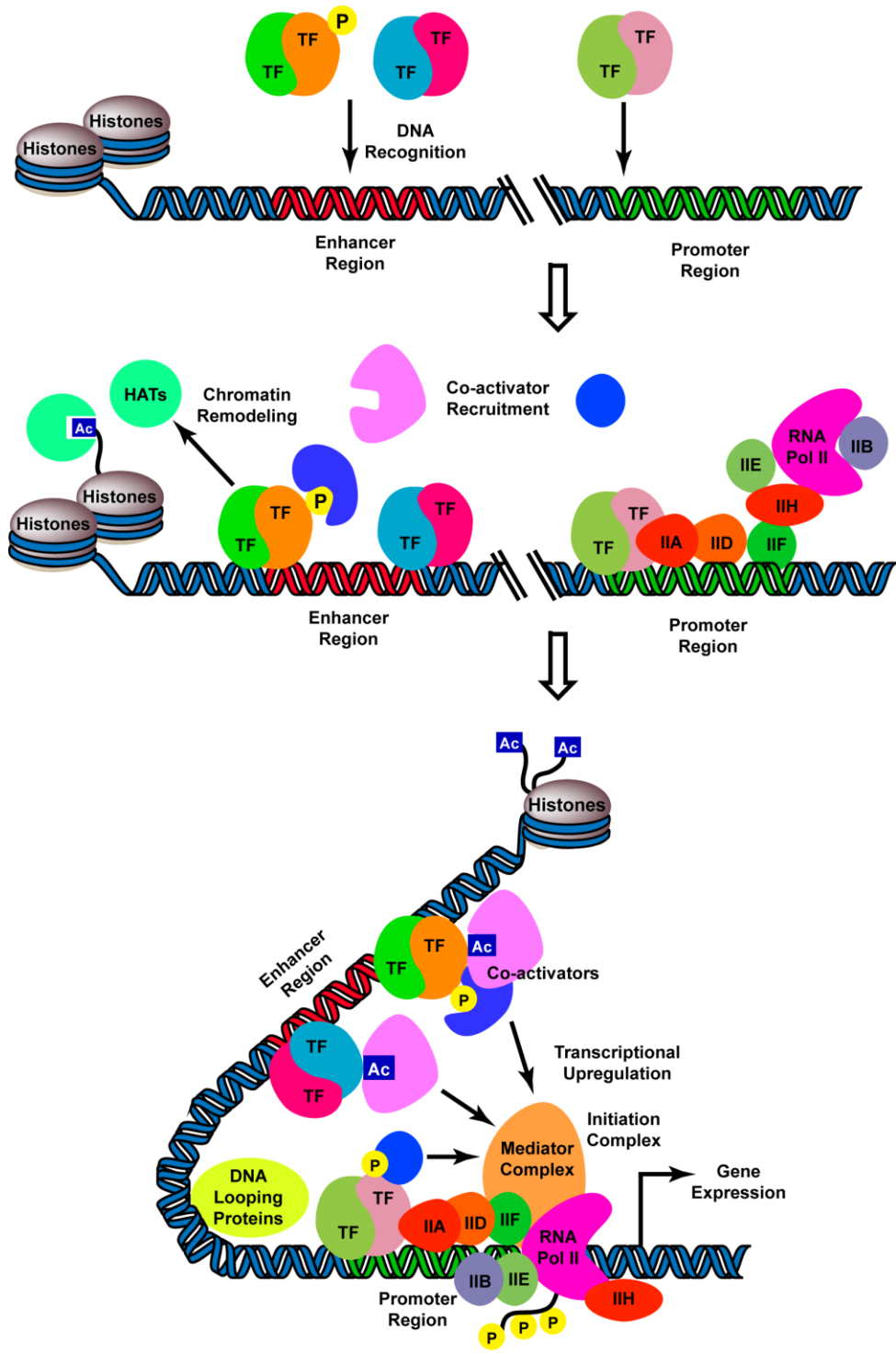


Figure 1.1.1. General activation of the transcriptional machinery. TFs bind to DNA response elements within promoter and enhancer regions and then recruit co-activators, which stimulate chromatin remodeling and post-translationally modify TFs. Co-activators also interact with the Mediator complex and Initiation complex to begin transcription with RNA Pol II.

Various cellular signals and interactions fine tune TF activity in a variety of ways to achieve unique gene expression profiles (**Figure 1.1.2**). Regulation of gene transcription is differentiated by binding affinity to specific DNA sequences within promoter and enhancer regions, post-translational modifications, and recruitment of co-activators/repressors. Differences in binding affinity between TFs and promoter/enhancer regions are taken advantage of to express specific genes by regulation of TF concentrations in the nucleus. For instance, the TF family signal transducers and activators of transcription (STATs) generally reside in the cytoplasm until activation through tyrosine phosphorylation. Phosphorylation of STATs causes a change in conformation, leading to dimerization and translocation to the nucleus.¹⁵ Another example includes the masking of the nuclear location sequence (NLS) of the NF- κ B heterodimer by I κ B α , therefore blocking nuclear translocation. When I κ B α is phosphorylated and subsequently targeted for degradation, the NF- κ B heterodimer translocates to the nucleus.¹⁶ Controlling the concentration of TFs in the nucleus determines the activation of high or low affinity promoter and enhancer sites.

Many examples of post-translational modifications made to TFs have been characterized and are often necessary for full activation of gene transcription.¹⁷ Post-translational modifications predominantly involve acetylation of lysine residues or phosphorylation of tyrosine, serine, and threonine residues. Post-translational modifications directly affect TF binding affinity for DNA through conformational changes, or through recruitment of other regulatory proteins. Other modifications such as methylation and oxidation also regulate many TFs. For instance, hypoxia-induced factor 1 α (HIF-1 α) regulation involves oxidation of two proline residues (Pro402 and Pro564), which target it for degradation under normoxic cellular conditions.¹⁸ Regulation of TFs via direct methylation has not been well studied compared to other well-known post-translational modifications, but within the past decade many examples of lysine and arginine methylations have been characterized for many signaling proteins including TFs.¹⁹ For example, methylation of Lys218 and Lys221 on p65 increases gene

transcription.²⁰ Arginine methylation has been shown to positively regulate several other TFs as well.²¹

Acetylation and phosphorylation sites can be recognized by co-activators, which are necessary for full transcriptional activity. Three common co-activators that ultimately form two heterodimers, the p300/CREB binding protein (CBP) dimer and p300/CREB binding protein association factor (PCAF) dimer, directly bind to many TFs, and also contain acetyl transferase activity resulting in direct chromatin remodeling and TF acetylation.²² Two other co-activators that form a heterodimer, p160 and steroid receptor co-activators (SRCs), interact directly with a host of TFs including activating protein-1 (AP-1), Smad3, NF- κ B, E2F1, retinoblastoma tumor suppressor (Rb), and p53.²³

Post-translational modifications can also act as negative regulators and recruit repressors to inhibit transcription. Co-repressors can recruit histone deacetylases (HDACs) and DNA methyl transferases (DMTs) resulting in chromatin repackaging and transcriptional repression. For example, two co-repressors silencing mediator for retinoid and thyroid hormone receptor (SMRT) and nuclear co-repressor (N-CoR) both bind to nuclear receptors to inhibit gene transcription.²⁴ SMRT has also been shown to undergo many post-translational modifications after activation of the NF- κ B and mitogen activated protein kinase (MAPK) pathways.²⁵ Variations in co-activator and repressor recruitment to post-translational modification sites fine tune the gene expression profile of a TF based on cellular stimuli.

In summary, general TFs bind to all transcribed genes at promoter regions and are required for the start of transcription by RNA pol II. Activated sequence specific TFs bind to promoter and enhancer sites by recognizing specific DNA sequences and cause bending of the DNA (e.g. looping) to directly interact with Mediator and the Initiation complex to upregulate gene transcription. Extracellular and intracellular signals activate TFs in a variety of different ways leading to gene expression. After activation of a TF, many interactions regulate their activity including the enhancer/promoter DNA sequence,

other TFs, co-activators/repressors, and post-translational modifications. TFs can also act as transcriptional repressors depending on cellular stimuli.

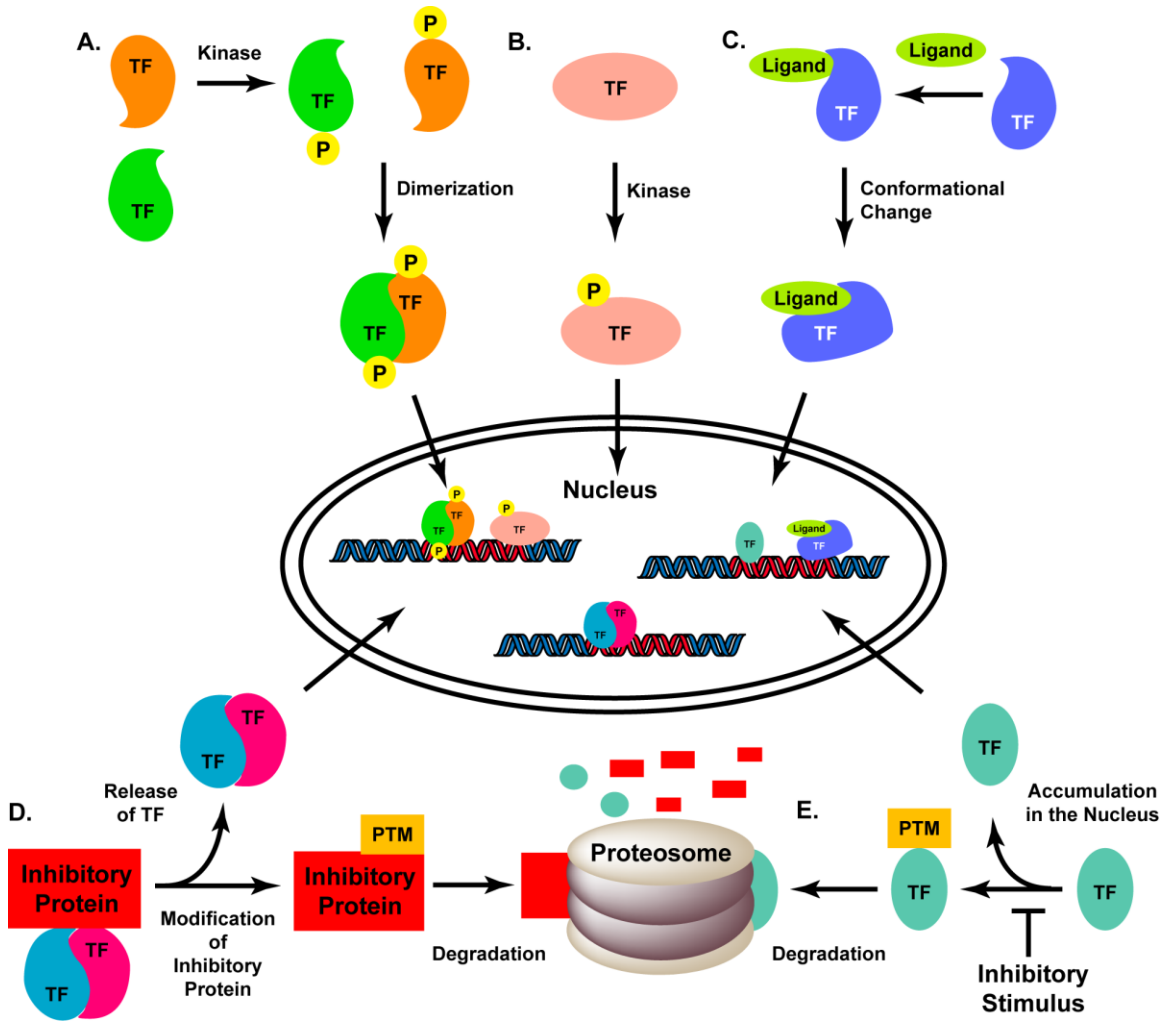


Figure 1.1.2. Mechanisms of transcriptional activation.

A. Phosphorylation can induce dimerization, causing translocation of TFs to the nucleus. **B.** Post-translational modifications (PTMs) such as phosphorylation can induce nuclear translocation of TFs. **C.** Ligands can induce conformational changes to TFs and cause nuclear translocation. This occurs predominantly with nuclear receptors. **D.** Inhibitory proteins can withhold TFs in the cytosol until a signal transduction pathway leads to PTMs and subsequent degradation, thereby releasing the TF to translocate to the nucleus. **E.** PTMs can target TFs to be degraded until a stimulus inhibits this process and allows TFs to accumulate and translocate to the nucleus.

1.2 Structural Features of Transcription Factors

Using data from several available databases, it has been estimated that there are 3,268 TFs coded in the human genome based on similarity to known DNA-binding motifs.²⁶ These TF DNA-binding domains (DBDs) are classified into ten superclasses and further divided into families and subfamilies. The ten superclasses are (1) basic, (2) zinc-coordinating, (3) helix-turn-helix, (4) other α -helical DNA-binding, (5) α -Helices exposed by β -structures, (6) immunoglobulin fold, (7) β -hairpin exposed by an α/β -scaffold, (8) β -sheet binding to DNA, (9) β -barrel DNA-binding, and (10) yet undefined DBDs. From these ten superclasses there are 112 family classifications and over 300 subfamilies to further categorize TFs. For example, there are seven classes within the immunoglobulin fold superclass, which are the rel homology, STAT, p53, runt, T-box, NDT80, and grainyhead domains. The rel homology domain is further broken down into five families including NF- κ B related TFs. An organized list and classification of all human TFs and their mouse orthologs can be found using TFClass, which is a free database of TFs published online. Characterized DNA-binding consensus sequences for each TF can also be found at this website.²⁷

Most sequence specific TFs bind to DNA through recognition of nucleotide bases in the major groove of the double helix. Many crystal structures of TFs, or truncated DBDs of TFs, have been reported showing how the tertiary structure of the DBD can recognize and differentiate between specific DNA sequences. Three examples including the c-Fos/c-Jun heterodimer²⁸ as a basic domain example, estrogen receptor homodimer²⁹ as an example of a zinc-coordinating domain, and p50/p65 heterodimer³⁰ as an immunoglobulin domain example are shown in **Figure 1.2.1**. The basic (**Figure 1.2.1A**) and zinc-coordinating (**Figure 1.2.1B**) domains use α -helical structures for DNA recognition compared to the p50/p65 heterodimer, which uses an unstructured loop region. Interestingly, the p50/p65 heterodimer binding affinity to its consensus sequence is higher than many eukaryotic TFs. The range of dissociation constants (K_d) measured for the p50/p65 heterodimer to its consensus sequence is 10^{-13} to 10^{-10} M, while most other TFs have K_d 's typically between 10^{-9} to 10^{-3} .³¹ This has been attributed to the large

surface area of the heterodimer protein-protein interaction and its contribution to binding cooperativity between the two TFs to the major grooves of the DNA helix.

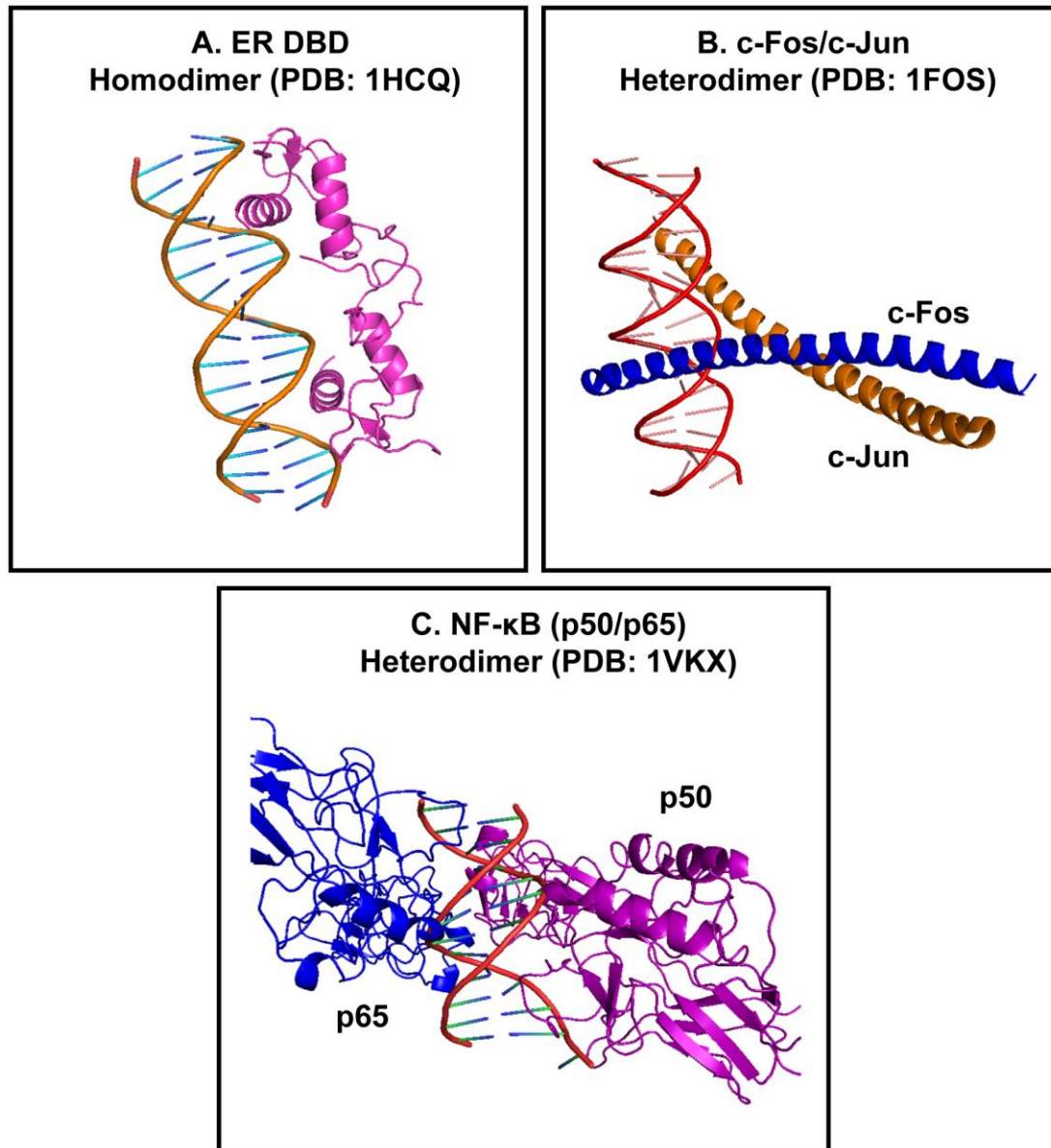


Figure 1.2.1. Three examples of common TFs bound to DNA. **A.** Estrogen Receptor (ER) DBD as an example of a zinc-coordinating domain. **B.** c-Fos/c-Jun heterodimer as an example of a basic domain. **C.** The NF- κ B (p50/p65) heterodimer as an immunoglobulin domain example.

A second structural feature present in most TFs is the transcription activation domain or transactivation domain (TAD), which is necessary to upregulate gene expression via direct or indirect interactions with the initiation complex. The TADs of TFs have been demonstrated to directly interact with many co-activators, general TFs, and Mediator proteins of the initiation complex.³² TADs are capable of interacting with multiple proteins at once and are subject to post-translational modification, which contribute to tightly regulated gene transcription.³³ Eukaryotic TADs are classified into three general groups based on amino acid composition. There are TADS rich in acidic amino acids, glutamine residues, or proline residues.^{32a} However, this classification doesn't allude to general protein interaction types among the transcriptional machinery.

Other protein-protein interactions are also essential to TF regulation and function. Many TFs exist as homo and heterodimers within cells and often can dimerize with multiple TFs or related proteins. For example, the Rel/NF- κ B family of transcription factors (p65/RelA, p50, RelB, p100/p52, and c-Rel) can dimerize to different extents with each other in a hetero- or homodimeric fashion.³⁴ Because all TFs contain unique DBDs that recognize specific consensus sequences, variation in dimerization leads to differential gene transcription. Interestingly, only p65, RelB, and c-Rel contain TADs, which directly lead to transcriptional activation whereas p50 and p52 do not. However, p50 homodimers utilize other protein-protein interactions to activate transcription.³⁵ In unstimulated cells p50 and p52 homodimers can also serve as transcriptional repressors through association with histone deacetylase 1 (HDAC1).³⁶

In summary, TFs contain a DBD and multiple binding surfaces for protein-protein interactions such as the NLS and TADs. Many TFs form dimers in a homodimeric or heterodimeric fashion with each other. DBDs recognize consensus sequences through interactions of amino acids and nucleobases primarily in the major groove of the DNA double helix. Upon binding to DNA, TFs can undergo conformational changes to be recognized by specific regulatory proteins. Many amino acid residues within these protein-protein interfaces and DBDs are subject to post-translational modifications by

regulatory proteins. TFs can be controlled spatially and temporally to give precise gene products depending on all of the stimuli exerted on the cell.

Thus far TF structure and function have been broadly discussed. The focus for the rest of the introduction will be on two signaling pathways and their TFs, the NF- κ B and androgen receptor pathways. How each of these subfamilies of TFs relates to human disease and ways to target them for inhibition utilizing small molecules will be discussed. Additionally, approaches for development of small molecule inhibitors towards TFs will be presented.

1.3 Overview of the NF- κ B Pathway

The NF- κ B/Rel transcription factor family is responsible for propagating immune, inflammatory, and stress-related responses within cells. Furthermore, the NF- κ B pathway is also deeply involved with differentiation, cell growth, and apoptosis. There is a canonical³⁷ and non-canonical³⁸ NF- κ B pathway, which activate separate transcription factors depending on stimuli. Activation of the canonical pathway predominantly involves the p50/p65 heterodimer, and activation of the non-canonical pathway predominantly involves the p100/p52 (aka NF- κ B2) and RelB heterodimer. A fifth transcription factor c-Rel dimerizes with p50; however, it is only expressed in hematopoietic tissue.³⁹ All NF- κ B transcription factors are related by a conserved Rel homology domain, which is necessary for DNA-binding, dimerization with other Rel transcription factors, and I κ B binding.

Activation of the canonical NF- κ B pathway can occur through a variety of signals including bacterial⁴⁰ and viral⁴¹ components, lipopolysaccharides (LPS),⁴² interleukins (IL-1 α / β ,⁴³ IL-2,⁴⁴ IL-12,⁴⁵ IL-15,⁴⁶ IL-17,⁴⁷ and IL-18⁴⁸), tumor necrosis factor α (TNF- α),^{43c} ultraviolet irradiation,⁴⁹ increase in reactive oxygen species (ROS), and many other small molecules and signals that cause cellular stress.⁵⁰ All known NF- κ B stimuli result

in activation of the canonical pathway, however, only some activate the non-canonical pathway concurrently.⁵¹

1.3.1 The Canonical NF- κ B Pathway

The canonical NF- κ B pathway (**Figure 1.3.1**) begins with the activation of the Inhibitor of κ B kinase (IKK) complex via phosphorylation by upstream kinases. The IKK complex consists of two kinases, IKK α and IKK β , and a regulatory unit NF- κ B essential modulator (NEMO, aka IKK γ).⁵² However, only IKK β and NEMO are required for activation of the canonical pathway.⁵³ Activation of the IKK complex can occur with phosphorylation of IKK β . The ubiquitin-dependent kinase TGF β -activating kinase 1 (TAK1) is an essential part of a larger complex that is necessary for phosphorylation of Ser177 and Ser181 in the activation loop of IKK β after certain stimuli.⁵⁴ Although NF- κ B inducing kinase (NIK) is required for non-canonical NF- κ B activation (involving IKK α) it is also capable of phosphorylating IKK β for canonical activation.^{53a} A third kinase shown to phosphorylate IKK β during TNF- α induction of the NF- κ B pathway is Mitogen-activated extracellular-signal induced kinase kinase 3 (MEKK3).⁵⁵ Phosphorylation of Tyr188 and Tyr199 within the IKK β activation loop by c-Src upon stimulation also leads to activation of the NF- κ B pathway in A549 lung cancer cells.⁵⁶ Activation of the IKK complex can also occur via trans-autophosphorylation.⁵⁷ Oligomerization of the IKK complex is suggested to be necessary for trans-autophosphorylation by bringing kinase domains in proximity to each other inducing full activation.⁵⁸ Activation of the NF- κ B pathway was induced in experiments where oligomerization of the IKK complex was forced by chemical modification.⁵⁹

After phosphorylation of the IKK β activation loop, K63-linked, non-degradative ubiquitination of NEMO is also required for full activation of the IKK complex involving.⁶⁰ There are still many mechanistic questions pertaining to how ubiquitination regulates the IKK complex; however, multiple lysine sites near the N-terminus zinc-finger motif of NEMO have been suggested to be ubiquitinated leading to activation.⁶¹

Phosphorylation and sumoylation of NEMO have also been shown to affect the regulation of the IKK complex under certain situations.⁶² All of the post-translational modifications that NEMO undergoes underscore its importance in regulation of the NF- κ B pathway, despite not containing a catalytic function.

Once fully activated, the IKK complex targets I κ B α for degradation by phosphorylating two proximal residues, Ser32 and Ser36.^{52a} Prior to targeted degradation, I κ B α is responsible for inhibiting the NF- κ B heterodimer in the cytosol from translocating into the nucleus by masking the nuclear location sequence (NLS) on p65.^{16,}⁶³ Upon phosphorylation, I κ B α is poly-ubiquitinated at Lys21 and Lys22 and degraded by the 26S proteasome, thus releasing the NF- κ B heterodimer into the nucleus to bind to κ B response elements.⁶⁴

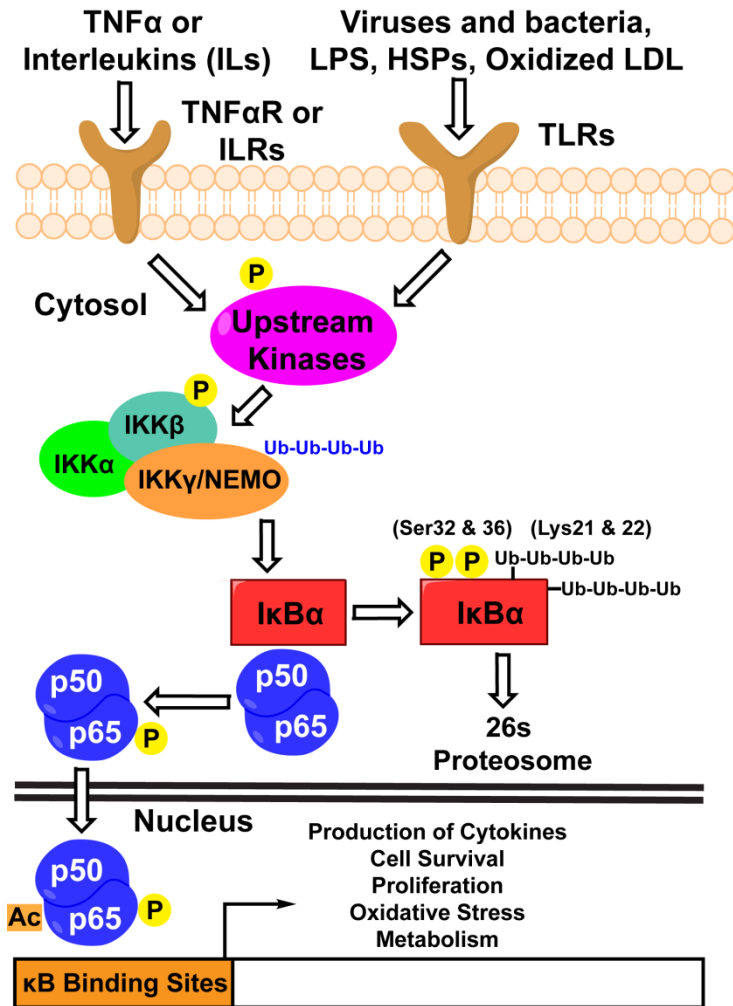


Figure 1.3.1. The canonical NF- κ B signal transduction pathway. Many extracellular and intracellular signals lead to activation of the canonical NF- κ B pathway, which begins by phosphorylation of IKK β and non-degradative ubiquitination of NEMO. Both are part of the IKK complex, which phosphorylate I κ B α upon activation and targets it for 26S proteasome degradation via phosphorylation of Ser32 and Ser36. I κ B α inhibits the NF- κ B (p50/p65) heterodimer from translocating to the nucleus until activation of the pathway. Upon release from I κ B α , the p50/p65 heterodimer translocates to the nucleus to bind to κ B sites causing increased gene transcription. P = phosphorylation, Ub (blue) is non-degradative ubiquitination, Ub (black) is degradative ubiquitination, Ac = acetylation.

Post-translational modifications including phosphorylation and acetylation of p65 further modulate its transcriptional activity after the NF- κ B heterodimer is released from I κ B α . **Figure 1.3.2** shows all of the phosphorylation and acetylation sites that have been characterized on p65. Protein Kinase A (PKA) and mitogen- and stress-activated protein

kinase 1/2 (MSK 1/2) stimulates transcriptional activity by phosphorylating Ser276 on p65. Phosphorylation of Ser276 is necessary for interactions with co-activators CBP and p300.⁶⁵

Other phosphorylation sites on p65 that have been identified are Ser529 by casein kinase II (CK-II) after IL-1 or TNF α treatment⁶⁶ and Ser536 by IKK β .⁶⁷ Stimulation with TNF- α has been proposed to cause NF- κ B-activating kinase (NAK) in complex with NAK associated protein 1 (NAP1) to phosphorylate the IKK complex and Ser536 on p65.⁶⁸ Phosphorylation of p65 at the C-terminus by glycogen synthase kinase 3 β (GSK3 β) has also been demonstrated to be important in NF- κ B transcriptional activation.⁶⁹ On the other hand, phosphorylation of p65 at Ser468 by GSK3 β was shown to negatively regulate transcription.⁷⁰ This discrepancy in regulation by GSK3 β may be due to the different cell types used in each study. Mouse embryonic fibroblasts were used in the previously mentioned study where activation of p65 was observed and HeLa cells were used where inactivation was observed.

The NF- κ B pathway can be differentially activated and expressed across multiple cell types. Protein Kinase C ζ (PKC ζ) was determined to phosphorylate Ser311 on p65 when stimulated with TNF- α and IL-6, which is largely required for transcriptional activation in mouse lung cells but not B-cells or embryonic fibroblasts.⁷¹ Compared to the above mentioned kinases, which phosphorylate p65 after I κ B degradation, Ribosomal S6 Kinase 1 (RSK 1) is activated directly by the transcription factor p53. Phosphorylation of p65 by RSK1 at Ser536 is independent of IKK complex activation or degradation of I κ B.⁷² Therefore, direct phosphorylation of p65 reduces the affinity of I κ B α for the NF- κ B heterodimer, thus releasing it from the cytosol.

Phosphorylation plays an important role in activation before and after p65 translocates into the nucleus. Some phosphorylations by kinases are not necessary for gene transcription but are implicated in modulating which genes are chosen to be transcribed. Phosphorylation of p65 can have different effects on gene transcription depending on cell type presumably through differentiated co-activator expression and

recruitment. Many phosphorylation sites serve as signals for the recruitment of other regulatory proteins to further modulate p65 transcriptional activity.

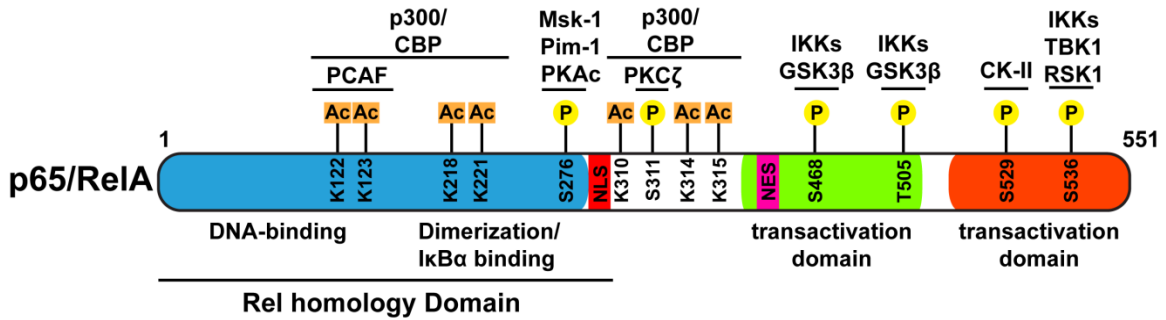


Figure 1.3.2. Characterized phosphorylation and acetylation sites on p65. P = phosphorylation, Ac = acetylation, NLS = nuclear translocation sequence, NES = nuclear exportation sequence.

Phosphorylation of p65 enhances transcriptional activity by recruiting histone acetyltransferases (HATs), which typically target DNA-bound histones and lysine residues on TFs. Acetylation of p65 at Lys218, Lys221, and Lys310 by p300/CBP affects its transcriptional activity and cellular localization.⁷³ When Lys218 and Lys221 are acetylated DNA binding is enhanced and nuclear export via IκBα is inhibited.⁷⁴ Transcription of the IκB gene by NF-κB driven activation acts as a negative feedback loop by removing the p50/p65 heterodimer from the nucleus after *de novo* synthesis.⁷⁵ Acetylation of Lys310 on p65 recruits transcriptional activators including bromodomain-containing protein 4 (Brd4) and is required for full transcriptional activity.⁷⁶ Negative regulation of p65 transcription can also occur after acetylation of Lys122 and Lys123 mediated by the p300/PCAF heterodimer (both residues are near the DNA-binding domain of p65).⁷⁷ When these two lysine residues are acetylated, p65 DNA-binding affinity is reduced allowing for IκBα to remove it from the nucleus. Additional acetylation sites at Lys314 and Lys315 on DNA-bound p65 regulate transcriptional activity at specific κB promoter sites.⁷⁸

Acetylation of p65 is a reversible process via histone deacetylase (HDAC) interactions. After the NF- κ B heterodimer is directly deacetylated by HDAC3, it is shuttled from the nucleus to the cytosol, inactivating the transcription factor. However, HDACs 1, 2, 4, 5, or 6 do not directly deacetylate the NF- κ B heterodimer.⁷³ It has been shown that HDAC 1 directly interacts with p65 to regulate histone acetylation at κ B sites to repress gene expression, but doesn't have deacetylase activity towards p65.⁷⁹ The Class III HDAC Sirt1 regulates many TFs including the p65 subunit by deacetylating Lys310 causing transcriptional repression.⁸⁰

1.3.2 The Non-canonical NF- κ B Pathway

The non-canonical NF- κ B pathway (**Figure 1.3.3**) begins with the essential activity of the NF- κ B inducing kinase (NIK).⁸¹ Once NIK becomes catalytically active, it then phosphorylates Ser176 within the activation loop of IKK α .⁸² IKK β and NEMO are not necessary for non-canonical NF- κ B activation.⁸³ The requirement of NIK for p100 processing is not only because of IKK α phosphorylation but also formation of a complex that directs IKK α to p100.⁸⁴ After induction, IKK α phosphorylates p100 at Ser866 and Ser870 near the C-terminus, which recruits an E3 ubiquitin ligase complex to ubiquitinate K856, targeting p100 for 26S proteasome processing.⁸⁵ The C-terminus ankrin repeats of p100 inhibit translocation of its heterodimeric partner RelB into the nucleus.⁸⁶ These ankrin repeats are selectively degraded to give the active transcription factor p52 allowing translocation of the p52/RelB heterodimer into the nucleus to bind κ B target genes.⁸⁷

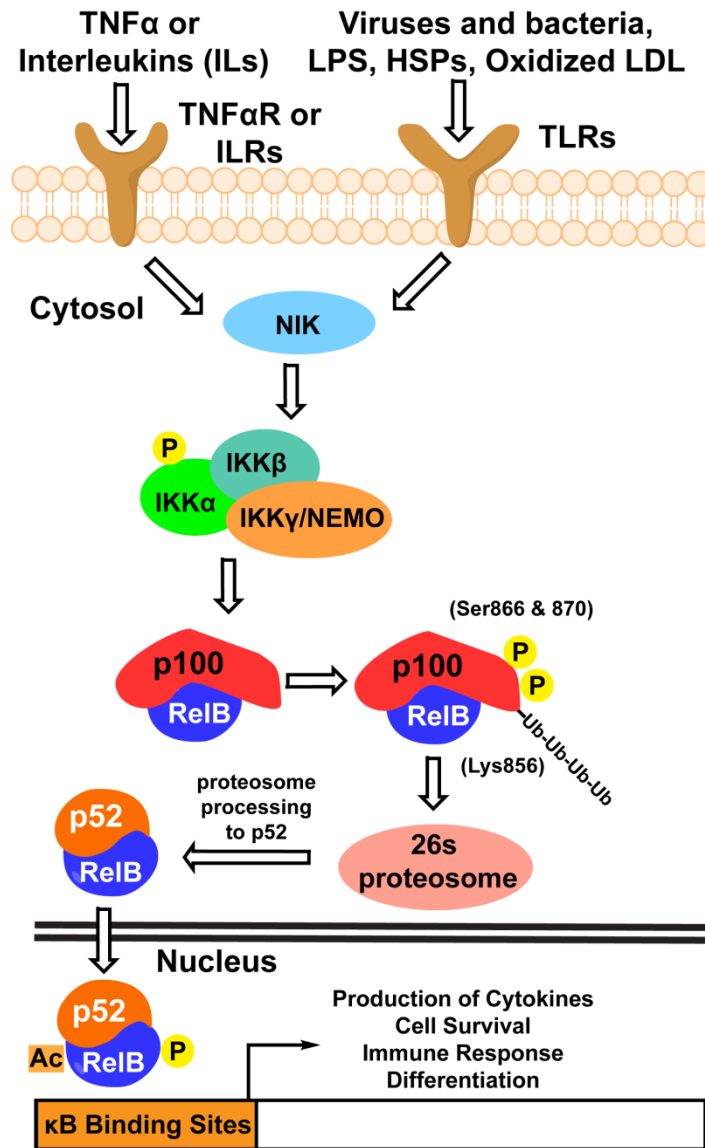


Figure 1.3.3. Non-canonical NF- κ B Signaling. Upon activation, NIK phosphorylates IKK α of the IKK complex, which phosphorylates p100 at Ser866 and Ser870. Phosphorylation of p100 causes ubiquitination and subsequent 26S proteasome processing to p52. p100 inhibits RelB translocation to the nucleus via C-terminal ankrin repeats until cleavage occurs after processing. The p52/RelB heterodimer translocates to the nucleus to bind to κ B sites increasing gene transcription. P = phosphorylation, Ac = acetylation, Ub = degradative ubiquitination.

Interestingly, *de novo* protein synthesis is also required for non-canonical activation.⁸⁸ The activation of the canonical pathway expresses proteins directly involved in stabilization of NIK activity and protein synthesis of the precursor p100. Under normal

conditions NIK is present in the cytosol at low levels due to constant degradation via ubiquitination.⁸⁹ Key players in the regulation of NIK levels are tumor necrosis factor receptor associated factor 2/3 (TRAF2/3) and cellular inhibitor of apoptosis 1/2 (cIAP1/2). TRAF2/3 binds to NIK and directs its ubiquitination by cIAP1/2 targeting it for degradation.⁹⁰ Upon a receptor stimulus, TRAF2/3 gets recruited to the activated receptors and then degraded leaving NIK to accumulate in the cytosol.⁹¹ Additionally, activation of the canonical NF- κ B pathway causes direct expression of p100, which is necessary for non-canonical activation as well.⁸⁷⁻⁸⁸

Activation kinetics of the NF- κ B non-canonical pathway is generally much slower compared to the canonical pathway.^{85b, 92} Degradation of p100 to the transcription factor p52 occurs over the time scale of hours compared to I κ B degradation in the canonical NF- κ B pathway, which occurs in minutes.⁹³ Additionally, stimulation of the non-canonical NF- κ B pathway results in a prolonged activation of p52/RelB compared to the activation of the canonical pathway, which is transient.⁵¹

There is significant overlap between canonical and non-canonical activation.⁹³ All stimuli that activate the non-canonical pathway also activate the canonical pathway.⁵¹ Furthermore, activation of the non-canonical pathway is dependent on protein expression of canonical NF- κ B driven genes.⁸⁷⁻⁸⁸ Overlap of the canonical and non-canonical NF- κ B pathways also occurs at the transcription factor level. For instance, the non-canonical proteins p100 and RelB can serve as negative regulators of the canonical pathway.⁹⁴ Alternatively, p65 can suppress RelB activity via dimerization in the nucleus when stimulated with TNF- α .⁹⁵

1.3.3 Involvement of the NF- κ B Pathway in Human Disease

As the key intracellular regulator of the immune and stress-related responses, the NF- κ B pathway is involved in immunity and inflammatory diseases. Knockouts or conditional knockouts of various genes involved in the NF- κ B pathway have demonstrated its importance in development and disease states.⁹⁶ Knockouts of p65 and

IKK β results in prenatal lethality⁹⁷ whereas other gene deletions and mutations result in immunodeficiencies.⁹⁶ Deletion of p65 in mice can be partially rescued with a liver transplant or an additional deletion of the TNF receptor gene.⁹⁸ Rare genetic disorders in humans involving the NF- κ B pathway also result in immune disorders.⁹⁹ On the other hand, hyperactivation of the NF- κ B pathway results in auto-immune and cardiovascular diseases, as well as the development and progression of cancers.

Increased NF- κ B activation has been implicated in a variety of autoimmune diseases including rheumatoid arthritis,¹⁰⁰ type 1 diabetes mellitus,¹⁰¹ inflammatory bowel disease,¹⁰² and multiple sclerosis.¹⁰³ Surprisingly, there are no selective NF- κ B inhibitors approved for treatment of these diseases.¹⁰⁴ Oxidative stress, chronic inflammation, and activation of the immune system are major contributors to atherogenesis as well.¹⁰⁵ It has been established that activation of the NF- κ B pathway within endothelial and immune response cells plays a crucial role in the development of plaques leading to atherosclerosis.¹⁰⁶ Plaque formation within blood vessels leads to a higher risk of myocardial infarctions, brain aneurisms, and other complications resulting from blood clots.¹⁰⁷ Within vascular tissue where plaque deposits have occurred, NF- κ B related gene expression is significantly up-regulated compared to normal tissues, and animal models suggest that inhibition of the NF- κ B pathway can reduce inflammation and atherosclerosis.¹⁰⁸

Inflammation and immunity also play important roles in cancer development and progression. The NF- κ B pathway is aberrantly regulated in many types of cancers including lymphoma, leukemia, glioblastoma, pancreatic, epithelial, lung, prostate, and liver tumors.¹⁰⁹ Chronic inflammation increases the likelihood of cancer development as evidenced by inflammation associated colon cancer in transgenic mouse models,¹¹⁰ v-rel induction of lymphoma and leukemia in chickens¹¹¹, and increased cancer risk associated with viral, bacterial, and chronic inflammatory diseases.¹¹² Furthermore, inflammation in the tumor microenvironment contributes to proliferation, angiogenesis, and metastasis.^{109,113} The NF- κ B pathway is a major factor in maintaining the cancer stem cell population in a variety of cancers.¹¹⁴ Cancer stem cells are a quiescent and drug-

resistant sub-population of tumor cells, which are responsible for relapse.¹¹⁵ It is clear that the NF- κ B pathway plays an important role in tumorigenesis and progression of cancer, inflammatory diseases, and immune related disorders making it an important target for inhibitor discovery.

1.4 Overview of Androgen Receptor Signaling

Nuclear receptors (NRs) are the only family of TFs that contain a ligand binding domain (LBD) allowing for direct binding to endogenous small molecule ligands. There are six subfamilies of NRs: (1) Thyroid hormone receptor-like, (2) Retinoid X receptor-like, (3) Estrogen receptor-like, (4) Nerve growth factor IB-like, (5) Steroidogenic factor-like, and (6) Germ cell nuclear factor-like receptors.¹¹⁶ Many of the NRs are orphan receptors or bind general types of molecules such as xenobiotics or fatty acids. The androgen receptor (AR) is part of the Estrogen receptor-like family, and has two endogenous ligands (**Figure 1.4.1**), testosterone (**1.1**) and 5- α -dihydrotestosterone (DHT, **1.2**)).

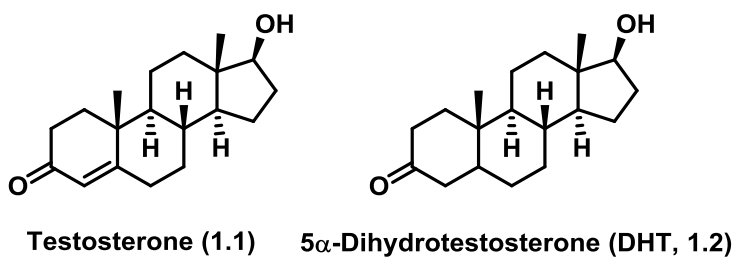


Figure 1.4.1. Testosterone (**1.1**) and 5 α -dihydrotestosterone (DHT, **1.2**) are endogenous agonists of AR.

AR has four domains (**Figure 1.4.2**): The N-terminal transactivation domain (NTD), DNA-binding domain (DBD), a hinge region, and ligand-binding domain (LBD).¹¹⁷ The NTD is intrinsically disordered. There are two activation function regions (AF-1 and AF-2) in AR.¹¹⁸ AF-1 is located in the NTD, and AF-2 is located in the LBD.

There are two transactivation units (Tau) within AF-1, referred to as Tau-1 and Tau-5, which are responsible for interactions with co-activators for transcriptional activity.¹¹⁹ Deletion of AF-1 eliminates AR activation, and deletion of AR-2 significantly attenuates transcriptional activation.¹²⁰ Expression of the truncated N-terminal AF-1 region results in constitutive transcriptional activity.^{120a} The hinge region is a flexible segment that connects the LBD and DBD.¹²¹ The NLS sequence is at the end of the DBD and spans into the hinge region.¹²²

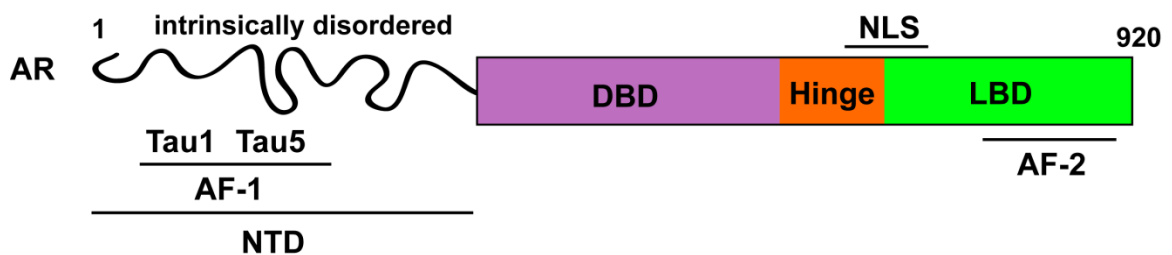


Figure 1.4.2. Structural Features of the Androgen Receptor (AR). There are four domains in AR: N-terminal domain (NTD), DNA-binding domain (DBD), the hinge region, and ligand-binding domain (LBD). The NTD contains activation function-1 (AF-1), which has two transactivation units (Tau1 and Tau5) responsible for co-activator/repressor interactions. The nuclear location sequence is within the hinge region and spans into the LBD. The LBD contains activation function-2 (AF-2), which is also responsible for interactions with co-activators/repressors.

1.4.1 The Androgen Receptor Signaling Pathway

Multiple heat shock proteins (Hsp) and other regulatory proteins bind to AR in the cytoplasm before activation including Hsp90, 70, 56, and p23 (**Figure 1.4.2**).¹²³ Hsp90 binds to the LBD of AR sequestering it in the cytosol.¹²⁴ The heat shock family of proteins is usually thought of as chaperones that target a host of unfolded proteins; however, in NR signaling they play an important role in signaling mechanisms. Hsp90 contributes to the stability of the tertiary structure of the unbound LBD of AR and is required for binding of testosterone or DHT.¹²⁵ Along with several adapter proteins, Hsp70 and Hsp56 are required to initially interact with AR, which then facilitates the

binding of Hsp90.¹²⁶ After Hsp90 is bound to AR, Hsp70 and Hsp56 dissociate from the complex and AR adopts a ligand-binding conformation with Hsp90 and p23.¹²⁷ The Hsp90/p23 complex with AR is then competent to bind androgens.¹²⁸

Binding of an androgen to the AR complex induces a conformational change in AR, which dissociates the Hsp90/p23 complex. Upon agonist binding, the NTD of AR, which is largely responsible for interacting with co-activators, also binds to the AF-2 region of the LBD in an intramolecular fashion.^{120b, 129} The two sequences largely responsible for this intramolecular interaction are ²³FQNL²⁷ and ⁴³³WHTLF⁴³⁷ within the NTD.¹³⁰ Interestingly, co-activators found to interact with AR also contain a similar motif suggesting that competition might occur for binding to the AF-2 region.¹³¹ This intramolecular interaction stabilizes the ligand bound state, causes homodimerization of AR, and exposes the NLS and TADs for transcriptional regulation by co-activators and repressors.¹³² Dimerized AR translocate to the nucleus to bind AR response elements and begin gene transcription.¹³³

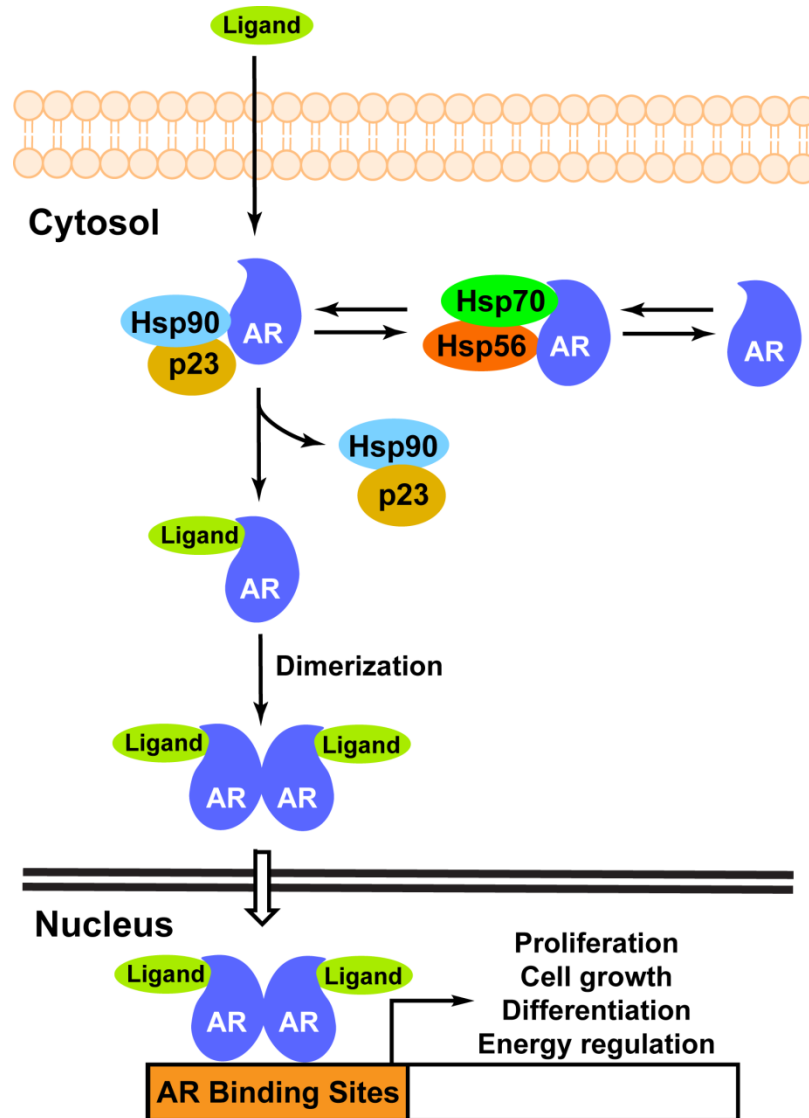


Figure 1.4.3. Androgen Receptor (AR) Signaling Pathway. A complex involving Hsp70 and Hsp56 facilitate binding of Hsp90 and p23 to AR, which maintains a ligand-binding competent state. Upon binding of ligand AR changes conformation and releases the Hsp90/p23 complex, dimerizes and translocates to the nucleus to bind to AR response elements.

AR interacts with many co-activators after DNA-binding. Over 200 co-activators have been described to interact with all NRs.¹³⁴ Only representative examples that interact with AR will be discussed here. Three proteins that are part of the p160 co-activator family, steroid receptor co-activators 1-3 (SRC1-3), bind to AR. These three co-activators were among the first to be discovered and are necessary for further recruitment

of chromatin remodeling proteins to TFs.¹³⁵ All SRCs interact primarily with the NTD, but they have also been demonstrated to interact with AF-2 within the LBD as well.¹³⁶ Although SRC1 and 2 have weak acetyltransferase activity (SRC3 does not), these proteins serve as ligand-dependent scaffolding proteins for other HATs to bind AR and have not been demonstrated to acetylate AR.^{136a} The ubiquitous co-activators that interact with many TFs, p300/CBP and PCAF, acetylate Lys630, Lys632, and Lys633 within the NLS of AR.¹³⁷ Another co-activator found to acetylate AR within the hinge region is Tat interacting protein 60 (Tip60).¹³⁸ The co-activator acetyltransferase-arrest defect 1 (ARD1) has been shown to acetylate AR at Lys618, which contributes directly to Hsp90 dissociation upon ligand binding.¹³⁹

Eighteen phosphorylation sites have been reported for AR and have recently been reviewed.¹⁴⁰ Constitutive phosphorylation of AR has been found to occur prior to activation with ligand at Ser94 and Ser650; however, the role of these phosphorylations is unclear and doesn't affect AR activity significantly.¹⁴¹ The phosphorylation sites occur at serine, threonine, and tyrosine residues spanning from the NTD to the LBD. Most of the phosphorylation sites occur within AF-1 or AF-2. Although phosphorylation doesn't globally affect the transcriptional activity of AR, certain phosphorylation sites play a role in differentiating between gene expression profiles.¹⁴² For example, phosphorylation of Ser81 by cyclin-dependent kinase 9 (CDK 9) causes differences in transcriptional activation of target genes compared to a S81A mutant of AR.¹⁴³ Other phosphorylation sites contribute to differences in transcriptional activation programs as well.¹⁴⁰

1.4.2 Targeting Androgen Receptor Signaling in Prostate Cancer

The AR signaling pathway is an important mechanism for prostate cancer proliferation and survival. Prostate cancer is initially treated with androgen deprivation therapy as a means to limit AR signaling activation. After a mean time of 2-3 years, castration resistant prostate cancer inevitably develops.¹⁴⁴ Castration resistant prostate cancer occurs through several mechanisms resulting in continued activation of the AR

signaling pathway despite androgen deprivation. These mechanisms include increasing agonist sensitivity, reduction of metabolic enzymes that degrade androgens, production of androgens within the tumor environment, mutations resulting in activation via other small molecule binders such as other endogenous steroids or antagonists, ligand independent activation, and upregulation of other signaling pathways.¹⁴⁵

Several FDA approved drugs for castration resistant prostate cancer target the synthesis of androgens or the LBD of AR. Abiraterone acetate (**1.3**) inhibits the synthesis of androgens and acts as an antagonist to the AR receptor; however this therapy is very limited due to the resistance mechanisms mentioned above, which inevitably lead to tumor progression and death after beginning treatment.¹⁴⁶ Enzalutamide (**1.4**) binds to the LBD of AR antagonizing nuclear translocation into the nucleus,¹⁴⁷ but, resistance still prevails over this drug as well.¹⁴⁸ Interestingly, a single point mutation (F876L) has recently been found in a prostate cancer mouse model after treatment with enzalutamide switching the drug from an antagonist to an agonist of AR.¹⁴⁹

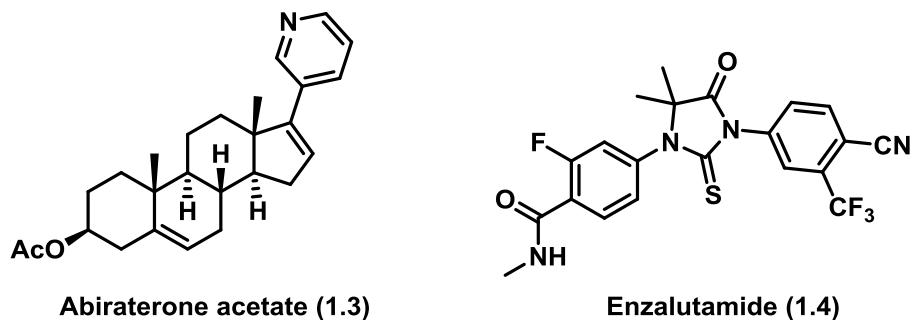


Figure 1.4.4. FDA approved drugs for the treatment of castration resistant prostate cancer. Abiraterone acetate (**1.3**) inhibits the synthesis of androgens and acts as an antagonist of AR. Enzalutamide (**1.4**) is an antagonist and inhibits nuclear translocation of AR.

A major contributor to castration resistant AR signaling is the formation of splice variants of AR without the LBD, resulting in ligand-independent constitutive activity.¹⁵⁰ These findings have turned attention to identifying inhibitors of the NTD of AR, which is

necessary for transcriptional activation. The natural product EPI-001 (**Figure 1.4.5, 1.5**) was isolated from the marine sponge *Geodia lindgreni*, which produced this natural product after exposure to bisphenol A waste, and was found to inhibit the NTD of AR presumably through a covalent modification.¹⁵¹ Later, studies identified a diastereomer of EPI-001, EPI-002 (**1.6**), to be slightly more active compared to the three other possible diastereomers.¹⁵² The reactive chloro hydrin group is necessary for EPI-001/002 activity and was found to covalently modify the NTD of AR, thereby inhibiting gene transcription. In a separate study, it was shown that EPI-001 is generally reactive towards biological thiols in buffer at physiological pH, suggesting other proteins may be targets for covalent modification by EPI compounds.¹⁵³

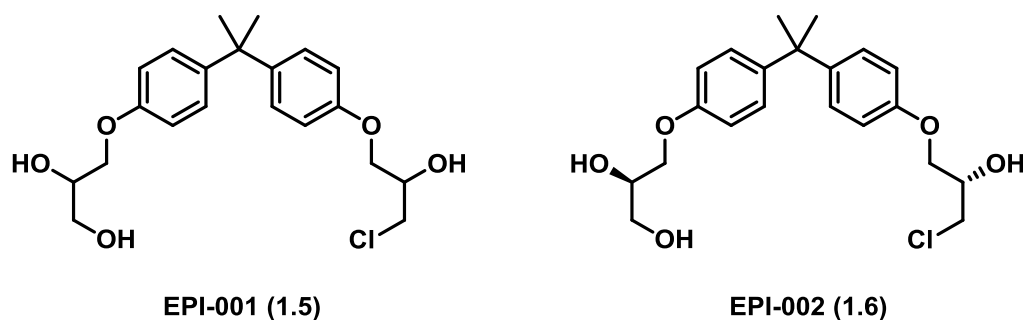


Figure 1.4.5. Structures of EPI-001 (**1.5**) and EPI-002 (**1.6**). EPI-001/002 inhibits AR by interacting with the NTD. EPI-002 is an isomer of EPI-001 found to be more potent than the three other possible isomers.

1.5 Why Develop Inhibitors Toward Transcription Factors?

TFs are commonly shown in simplistic form at the end of cellular pathways binding to DNA resulting in gene transcription; however, this process alone is subject to significant regulation. TFs have been under explored compared to other types of regulatory proteins. Despite finding thousands of TF genes after sequencing the human genome, under 100 TFs have been experimentally verified for DNA-binding and regulatory function.¹⁵⁴ From these characterized TFs, very few have been extensively studied in humans. Therefore, continuing research on TFs is important for a greater understanding of cellular signaling pathways and how it relates to human diseases.

To study TFs in depth requires specific inhibitors that target the regulatory processes involved in transcription including post-translational modifications, protein-protein interactions, and DNA-binding events. Specific small molecule probes targeting these regulatory events will provide insight into how dysregulation of TFs contribute to cancer and other human diseases. Furthermore, development of tool compounds towards inhibition of TFs could lead to discovery of new therapeutics.

Historically, TFs were labeled as ‘undruggable’ molecules for several reasons.¹⁵⁵ With the exception of nuclear receptors, TFs lack binding sites for endogenous small molecule ligands, which limits starting points for inhibitor discovery. Additionally, TFs have non-discrete tertiary structure making crystallization difficult for structural studies and for screening of small molecule binders. Despite limited structural data, *in silico* screening campaigns based on crystal structures and homology models have been an important method as a starting point for the discovery of small molecule inhibitors.

Because TFs lack both enzymatic activity and endogenous small molecule binding sites, the development of small molecule inhibitors towards TFs must target protein-protein interfaces or DBDs that are required for activity. Protein-protein interactions usually involve large surface areas (750-10,000 Å² for protein-protein interactions compared to 100-600 Å² for small molecule binding sites)¹⁵⁶ containing shallow, flexible clefts instead of discrete binding pockets, which make them difficult to inhibit with potent and selective small molecules.¹⁵⁷ Similarly, DBDs have large surface areas lacking binding sites with undefined, flexible structure until bound to DNA.¹⁵⁸

Multiple advantages could be realized by specifically targeting TFs with small molecule inhibitors. TFs are the last step of activation in most signal transduction pathways and often serve as a central hub for input from multiple stimuli, limiting the cells ability to upregulate other proteins to circumvent inhibition.¹⁵⁹ This is evident by the fact that multiple types of stimuli lead to activation of a common TF.

Development of small molecules towards TFs will increase the overall diversity of the druggable landscape. TFs make up approximately 14% of all coded proteins yet no drugs directly targeting TFs outside of inhibitors of NRs, which bind to the LBDs, have been FDA approved.¹⁵⁴ Continuing to identify new targetable TFs will lead to treatments that will target multiple hallmarks of cancer growth potentially reducing resistance and relapse in cancer patients. Additionally, TFs are also dysregulated in many other non-cancer related diseases including cardiovascular diseases, autoimmunity, chronic inflammation, acute lung injury, myocardial ischemia reperfusion injury, neurodegenerative diseases, and many others.^{104-105, 160} Developing inhibitors towards TFs can provide an opportunity to treat these diseases as well.

1.5.1 Indirect Inhibition of Transcription Factor Activity

The difficulty of developing selective and potent inhibitors towards TFs has placed focus on the development of small molecule inhibitors towards kinases and other regulatory proteins involved in human disease (**Figure 1.5.1**).^{159a, 161} These approaches have led to many success stories and are viable strategies for treatments of a multitude of diseases. However, it has become evident that in many cases targeting these proteins leads to resistance, reducing the efficacy of these drugs. Additionally, targeting upstream proteins in a signal transduction pathway complicates the study of direct effects resulting from inactivation of the pathway.

There have been hundreds of inhibitors demonstrated to decrease NF- κ B pathway activation, but many of these small molecules target upstream kinases or regulatory proteins that indirectly modulate NF- κ B activity.¹⁶² Other inhibitors target upstream canonical NF- κ B proteins. Many of these upstream proteins overlap with other signal transduction pathways limiting studies focused on specific NF- κ B control of transcription. Targeting redundant signaling proteins allow for resistance to therapeutics to occur.¹⁶³ Furthermore, overlap with other important cellular processes can lead to

unwanted effects and toxicity to normal, healthy cells from a therapeutic stand point. Since DNA-binding by TFs is the last crucial step in every signal transduction pathway targeting TFs may offer a means to avoid unwanted inhibition of other cellular processes and limit off-target affects. Therefore, targeting the p50/p65 heterodimer may lead to specific inhibition of this pathway with limited effects on other cellular processes.

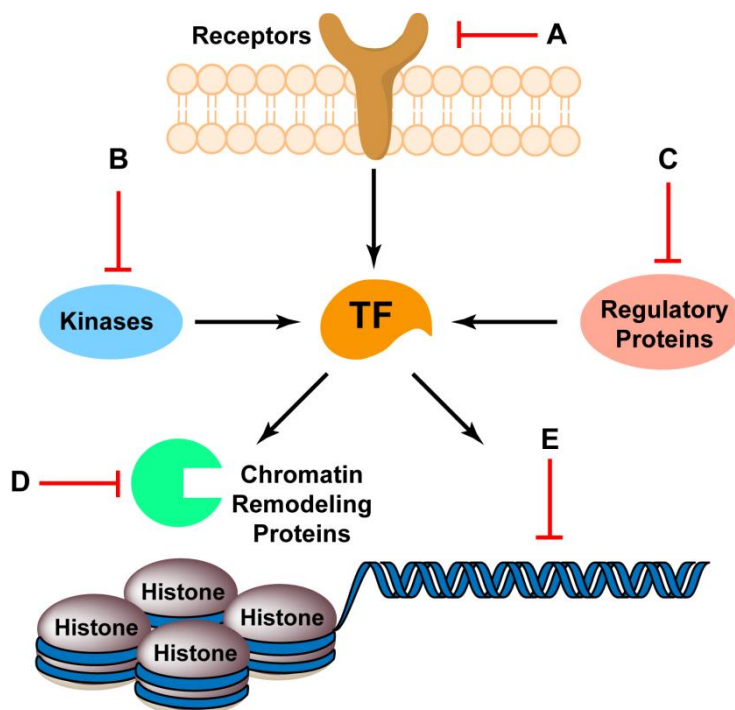
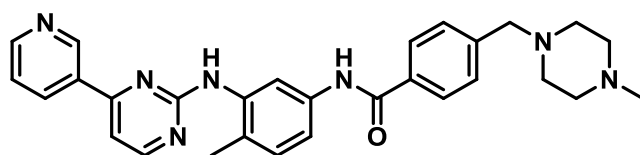


Figure 1.5.1. Indirect methods to modulate TF activity. **A.** Antagonists of receptor activation. **B.** Inhibition of kinase activity. **C.** Disruption of protein-protein interactions between regulatory proteins and TFs. **D.** Targeting of chromatin remodeling proteins. **E.** Small molecule DNA binders that inhibit TF DNA-binding.

Kinase inhibitors approved for cancer treatment inevitably fail due to resistance through a variety of mechanisms such as single point mutations within ligand binding pockets or deletion of LBDs resulting in constitutive activity.^{163a} For instance, the fusion protein Breakpoint Cluster Region-Abelson (BCR-ABL) kinase is responsible for progression of chronic myeloid leukemia (CML) in the majority of patients with this

disease. The FDA approved drug Imatinib (**Figure 1.5.2, 1.7**) targets BCR-ABL in patients expressing this fusion protein.¹⁶⁴ Treatment with Imatinib initially results in progression-free survival; notwithstanding, progression occurs in almost all patients due to mutations.¹⁶⁵ Additionally, redundant signal transduction pathways can circumvent inhibition of kinases or receptors through increased or modified activity of other proteins.^{163b} Inhibition of epidermal growth factor receptor (EGFR) can be overcome through a variety of mechanisms including upregulation of other tyrosine kinase receptors such as c-Met, which activate signal transduction pathways independent of ligand activation.¹⁶⁶



Imatinib (1.7)

Figure 1.5.2. Imatinib (**1.7**) is an FDA approved drug for the treatment for patients with CML containing a fusion protein BCR-ABL.

Other indirect approaches have been undertaken to inhibit or modify TF activity. These approaches include inhibition of regulatory proteins that directly modify or bind to TFs.^{159b, 167} As an example of indirectly targeting a protein-protein interaction involving a TF, many inhibitors have been designed to target mouse double-minute 2 (MDM2), a regulatory protein that interacts with the tumor suppressor TF p53.¹⁶⁸ MDM2 has E3 ligase activity and ubiquitinates p53 targeting it for degradation. In cancer cells with WT p53, MDM2 has increased activity towards p53 degradation causing aberrant cell proliferation.¹⁶⁹ Small molecule inhibitors block the protein-protein interaction between MDM2 and p53 allowing p53 to bind DNA and induce apoptosis in cancer cells. However, clinical trials and in vivo studies have shown that these inhibitors lack the ability to reduce tumor size over time, cause toxicity to normal cells, and select for p53 mutants that are resistant to MDM2 inhibition.

Another indirect way to control TF activity is inhibition of chromatin modifying proteins (i.e. HDACs, HATs, methyl transferases, and ATP-dependent remodeling proteins).¹⁷⁰ HDACs are predominantly responsible for removal of acetyl groups on histone lysine residues to repackage DNA in nucleosomes, typically associated with gene silencing. In contrast, HATs transfer acetyl groups to histone lysine residues and TFs, and are generally associated with unpacking DNA for transcriptional activation. Methyl transferases methylate lysine residues and DNA cytosine bases, which typically results in gene repression. ATP-dependent chromatin remodeling proteins rearrange histone organization in response to different stimuli. Dysregulation of these enzymes frequently occurs in cancerous cells, usually involving increased expression of oncogenes and decreased expression of tumor suppressor genes. Therefore, targeting these enzymes for inhibition has many consequences on transcriptional regulation.

Two pan HDAC inhibitors are FDA approved for treatment of refractory cutaneous T cell lymphoma and peripheral T cell lymphoma, suberanilohydroxamic acid (SAHA, a.k.a. vorinostat, **Figure 1.5.3, 1.8**) and romidespsin (**1.9**).¹⁷¹ Both inhibit HDACs by chelating to bound zinc in the enzyme active site, which is necessary for deacetylase activity. The limitation of both of these drugs is due to their lack of specificity against cancer cells over healthy cells.¹⁷² Both compounds are non-specific because they generally chelate zinc found in many enzyme active sites causing toxicity. Efforts are ongoing to selectively target HDACs to increase selectivity towards cancer cells over normal healthy cells.

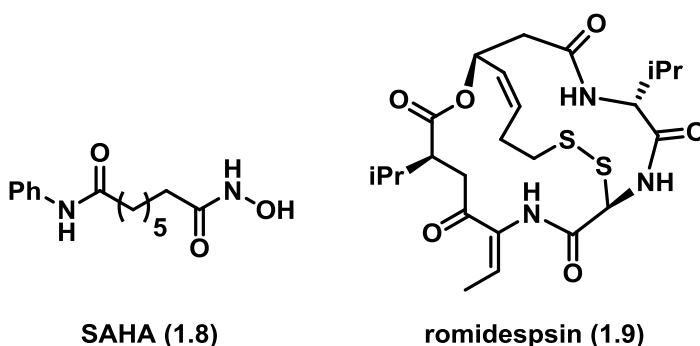


Figure 1.5.3. FDA approved pan-HDAC inhibitors.

In addition to toxicity effects due to lack of specificity, resistant mechanisms also occur to overcome HDAC inhibition in cancer cells.¹⁷³ A variety of TFs rely on HDAC activity to decrease transcription and therefore inhibition of HDACs paradoxically increase activation of pathways involved in cell survival and growth including the NF- κ B and STAT pathways.¹⁷⁴ Consequently, activation of these pathways can overcome general inhibition of HDACs and drive cancer proliferation.

DNA-binding small molecules are another indirect way to inhibit gene transcription of TFs.¹⁷⁵ By binding to DNA these small molecules can either sterically block TF binding or distort the helical structure of DNA making consensus sequences unrecognizable to TFs.¹⁷⁶ DNA-binding pyrole-imidzole (Py-Im) polyamides are able to read and bind to specific sequences of DNA based on minor groove interactions with nucleobases.¹⁷⁷ Many DNA-binding Py-Im polyamides have been developed including the targeted inhibition of HIF-1 α binding to the VEGF promoter and occupation of κ B sites recognized by the NF- κ B (p50/p65) heterodimer.¹⁷⁸ Inhibition of DNA-binding interactions of TFs using DNA-targeting Py-Im polyamides have become useful biochemical probes and is a promising approach for future clinical applications.

1.6 Direct Small Molecule Inhibitors of Transcription Factors

The indirect approaches to modify TF activity mentioned above have provided valuable information pertaining to TF function, but, also mentioned above, each approach has their own limitations and advantages. Targeting TFs directly with small molecules may address these issues.

Over the past two decades there have been multiple examples of targeting protein-protein or protein-DNA binding surfaces on TFs using small molecules despite the challenges associated with direct inhibition. Several excellent reviews covering small molecule inhibitors as recently as 2013 have summarized these efforts.^{155b, 158a, 179} Many

inhibitors of protein-protein interfaces on TFs have also been reviewed.^{159a, 167b} Therefore, this section will focus on recent advances towards the development of small molecule inhibitors that have been shown to directly bind to protein-DNA interfaces of TFs. Select historical examples will also be discussed because of their relevance to the research contributing to this thesis.

1.6.1 Small Molecules Targeting Protein-DNA Interfaces of Transcription Factors

Historically, small molecule inhibitors targeting the DBD of TFs have been limited. DBDs of TFs are large, flexible protein surfaces, which lack deep hydrophobic pockets.¹⁵⁸ Today this remains to be a challenge, but several recent examples have demonstrated the feasibility of such an endeavor. Targeting DBDs has several advantages. First, DBDs of activating TFs are rarely mutated and unlikely to gain resistance due to their requirement for recognition of specific DNA sequences and transcriptional regulation.¹⁸⁰ Many TFs are downstream regulators and central hubs of multiple signal transduction pathways. Several classes of TFs have been found to be necessary drivers of cancer development and progression making them ideal targets for treatment. The dependence for survival of cancer cells on idiosyncratic TF activation could offer selectivity over healthy cells and make it unlikely for redundant mechanisms to impart resistance.

Helenalin (**1.10**) is a pseudoguaianolide natural product isolated from the *Arnica* plant family and was one of the first natural products to be characterized as a direct DBD inhibitor.¹⁸¹ Helenalin features two potential Michael acceptors, an α -methylene- γ -lactone and cyclopentenone, which are responsible for its anti-inflammatory and anti-proliferative properties.¹⁸² Several studies have shown that both Michael acceptors react with biological thiols at different rates depending on the nucleophile.¹⁸³ Merfort and co-workers discovered in 1998 that helenalin targets the DBD of p65, part of the NF- κ B heterodimer, thereby sterically blocking DNA-binding.¹⁸⁴ Furthermore, it was demonstrated that helenalin alkylates Cys38 that is within the DBD of p65 and necessary

for DNA sequence recognition.¹⁸⁵ Using additional analogues, it was suggested that the cysteine reactivity was predominantly from hetero-Michael addition to the exocyclic methylene butyrolactone.^{183c} An additional Cys120 is found to be 7.7 Å away from Cys38, and in a later study it was hypothesized using computational methods that a second Michael addition could occur between Cys120 and the endocyclic enone because of the ideal distance between the two Michael acceptors of helenalin.¹⁸⁶ However, the double Michael addition event has never been demonstrated experimentally.

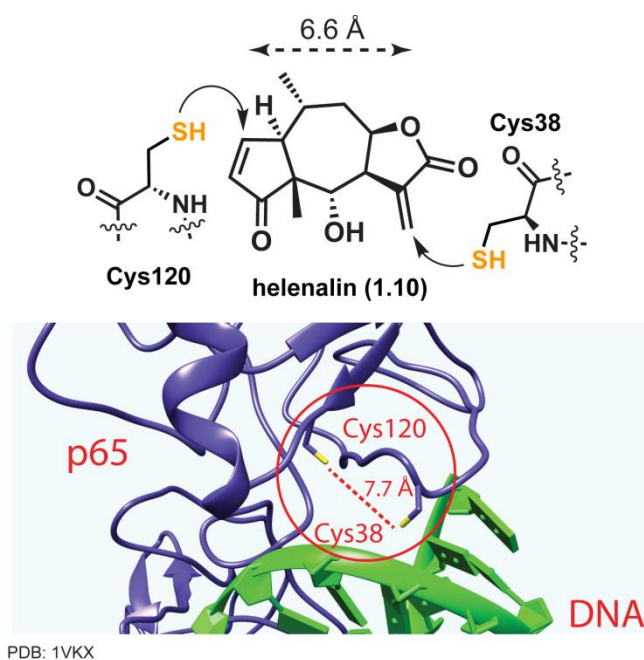


Figure 1.6.1. Helenalin (**1.10**) is a pseudoguaianolide that contains two Michael acceptors, an α -methylene- γ -lactone and cyclopentenone. Helenalin has been demonstrated to covalently modify Cys38 within the DBD of p65, blocking DNA-binding. Computational studies have suggested that a second Michael addition could occur with Cys120 and the cyclopentenone.

Many inhibitors of STAT3 target protein-protein interfaces responsible for binding to kinases or dimerization.¹⁸⁷ However, recent reports demonstrate that targeting the DBD of STATs is also possible with small molecules. An *in silico* screening approach was used to identify small molecule inhibitors of the STAT3 DBD.¹⁸⁸ The lead compound **1.11** had an IC_{50} of ~ 14 μ M in a 48 h luciferase reporter assay and time-dependent inhibition ($t_{1/2} \sim 30$ h). This study showed direct binding to the DBD of STAT3;

however, inhibition of STAT1 and additional off-target effects led to a follow-up SAR study. Testing of additional analogues uncovered **1.12** and **1.13** having reduced IC_{50} values between 8.8 and 12.6 μ M and $t_{1/2}$ values of 12.7 and 49.9 h respectively.¹⁸⁹ These analogues were found to directly target the STAT3 DBD over STAT1 and eliminated off-target alkylating effects. In a mouse xenograft model with A549 cells **1.11** reduced tumor size and metastases with no toxicity effects. Additionally, in tumor tissue STAT3 target gene transcription was reduced versus vehicle control.

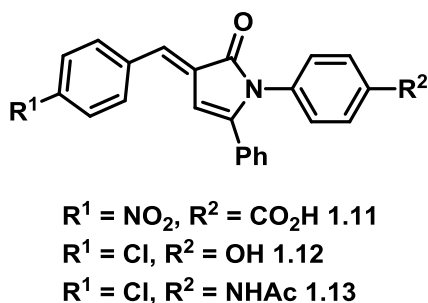


Figure 1.6.2. STAT DBD inhibitors. **1.11** was initially identified from an *in silico* screen. **1.12** and **1.13** were found to be more potent than the initial hit compound identified from a previous compound screen against the DBD of STAT.

Many examples of direct inhibition of c-myc with small molecules have been reported over the past decade.¹⁹⁰ An alternative approach to inhibiting c-myc is through transcriptional regulation by targeting an unconventional TF non-metastatic 23-H2 (NM23-H2) that controls c-myc gene transcription. The c-myc promoter contains G-rich regions, which form G-quadruplexes, and plays an important role in gene expression.¹⁹¹ NM23-H2 has DNA binding activity that specifically recognizes G-quadruplexes and resolves their formation; therefore, playing an important role in the expression of c-myc.¹⁹² In cancer cells it has been determined that NM23-H2 is overexpressed causing increased expression of c-myc, driving proliferation and cell survival. Inhibition of NM23-H2 might serve as a way to down regulate c-myc causing apoptosis in cancer cells.¹⁹³

In a recent study, screening of a small molecule library revealed a low micromolar inhibitor of the DNA-NM23-H2 interaction.¹⁹⁴ Further experiments showed that inhibition of DNA-binding of NM23-H2 was due to direct interaction with its DBD and not binding to G-quadruplexes using a variety of functional binding assays. The most potent inhibitor **1.14** maintained activity in HeLa cells and demonstrated knockdown of mRNA transcription and protein expression of c-myc at low micromolar concentrations, agreeing with previous binding assays. It was also discovered that inhibiting NM23-H2 resulted in increased or decreased regulation of a variety of other genes involved in cancer survival.

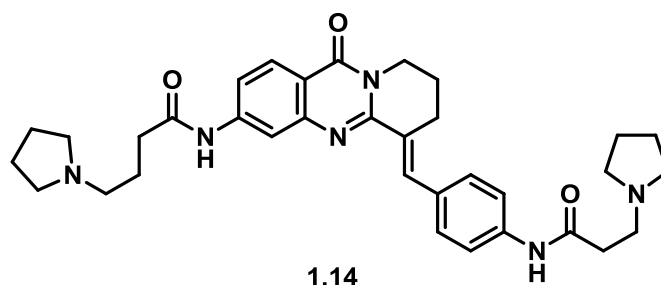


Figure 1.6.3. Small molecule inhibitor of NM32-H2. **1.14** was shown to bind to the DBD of NM32-H2, an unconventional transcription factor that binds to G-quadruplexes and controls the transcription of c-myc.

Small molecule inhibitors of the Kruppel-like Factor 10 (KLF10) DBD were discovered using an *in silico* screening approach based on homology modeling.¹⁹⁵ KLF10 is a TF important in T regulatory cell differentiation that is driven by TGF- β 1 signaling, and is therefore an interesting therapeutic target for diseases involving immunosuppression.¹⁹⁶ After identifying over 700 potential small molecule inhibitors with an *in silico* screen, 40 compounds were tested for inhibition of KLF10 transcription via a luciferase reporter assay. Of these 40 compounds, two had greater than 50% reduction in transcriptional activity (**1.15** and **1.16**). Derivatives based on scaffolds of **1.15** and **1.16** identified two additional inhibitors **1.17** and **1.18**. Direct binding to the DBD of KLF10 was confirmed with electric mobility shift assays (EMSAs). Compound **1.17** reduced DNA-binding by 45% and **1.18** reduced DNA-binding by 83% compared to a compound-free control. These inhibitors serve as first in-class inhibitors for KLF-10

opening the door for future SAR optimization and drugging other members of the KLF family of TFs.

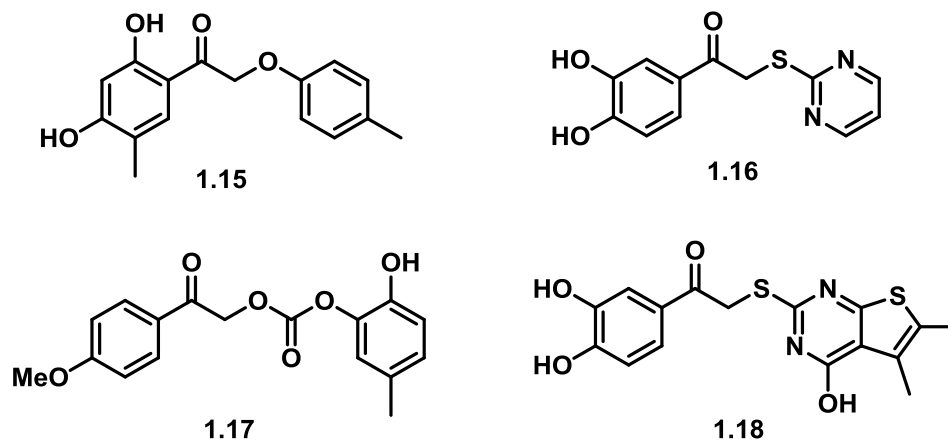


Figure 1.6.4. Small molecule inhibitors of KLF10.

Several inhibitors targeting AR have been discussed in section 1.4.2 of this introduction that bind to the LBD or NTD of AR. Abiraterone acetate (**1.3**) and enzalutamide (**1.4**) are FDA approved drugs for castration resistant prostate cancer but treatment eventually leads to resistance. EPI-001 (**1.5**) and related derivatives target the NTD. In an alternative approach, small molecules were discovered to target the DBD of AR.

Using crystal structure data of the DBD of AR, an *in silico* screen was used to identify lead compounds for testing of AR DNA-binding activity.¹⁹⁷ Three compounds were identified and chosen for further testing. Compounds **1.19**, **1.20** and **1.21** were shown to reduce AR transcriptional activity in a luciferase assay with IC₅₀ values of 2.36 μM, 0.340 μM, and 0.194 μM respectively; compared to enzalutamide, which had an IC₅₀ of 0.314 μM. Interestingly, **1.20** did not inhibit similar NRs including estrogen receptor, glucocorticoid receptor, and progesterone receptor, whereas enzalutamide and **1.19** inhibited ER at similar concentrations. Interestingly, in a luciferase reporter assay **1.19** and **1.20** still inhibited DNA-binding of the splice variant AR-V7 lacking the LBD compared to enzalutamide, which displayed no activity. Xenograft mouse models using

LnCaP cells demonstrated a significant reduction in tumor growth with similar activity to enzalutamide in the same mouse model.

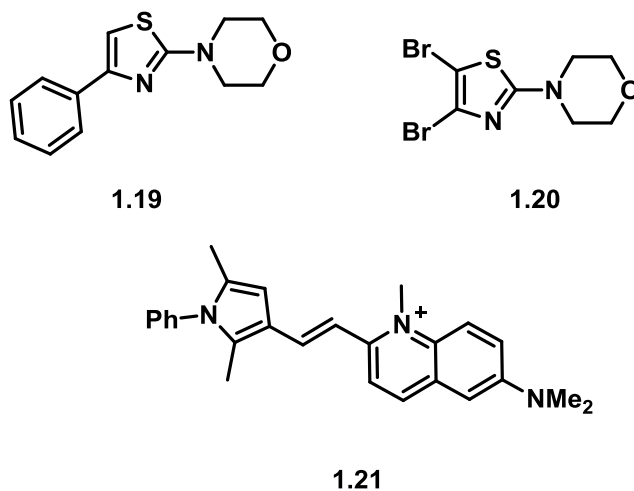


Figure 1.6.5. Inhibitors of the AR DBD.

From these examples it has become evident that targeting DBDs with small molecules is a viable strategy for TF inhibition. On rare occasions, discovery of small molecules that target DBDs come from natural products, but more commonly lead compounds have been found via *in silico* screening approaches using homology modeling or crystal structure data of TFs. This is most likely because of limited starting points for small molecule inhibitors of DBDs, which have large surface areas, lack deep binding pockets, and have non-discrete tertiary structure.

Many of the small molecule inhibitors discussed here have low micromolar inhibition of DNA-binding. This may not be ideal for drug candidates due to a lack of potency, but, these molecules serve as probes for biological experiments and starting points for the discovery of more potent inhibitors. In some instances, inhibitors of DBDs have been shown to act via a covalent mechanism of action and could be a valuable strategy to gain potency and specificity. Furthermore, covalent mechanism of actions could be useful for biochemical studies of TFs such as pulldowns, labeling experiments, and competitive binding assays. Continuing to discover small molecule inhibitors of TF

DBDs will expand the druggable landscape and may lead to better targeted therapy for a variety of diseases, including cancer.

1.7 Preface to this Thesis

The following chapters describe the development of cysteine reactive small molecule probes for protein target identification studies and targeting transcription factors. Chapter 2 reports the synthesis and biological evaluation of cysteine reactive probes inspired by the natural product helenalin, building upon the previous work described in **1.6.1**. The thiol reactivity of the α -methylene- γ -butyrolactone present on the synthetic helenalin-based analogues was used to demonstrate that our probes have the same mechanism of action as helenalin. Chapter 3 discusses the synthesis of additional helenalin-based small molecule probes. The synthesized derivatives were designed to explore how each Michael acceptor on our synthetic probes affect inhibition of the NF- κ B pathway. Chapter 4 describes the synthesis and biological testing of semi-synthetic derivatives from the natural product parthenolide. Several analogues of parthenolide are shown to target the cancer stem cell population ($CD34^+CD38^-$) of a model AML cancer cell line while not having toxic properties to normal, healthy primary bone marrow cells. The topic of Chapter 5 entails efforts to identify putative protein targets of the natural product parthenolide in human primary AML cells using a LC-MS/MS approach. Chapter 6 communicates the biological evaluation of an alkyne probe, EPI-054, based on EPI-001 as discussed in **1.4.2** of the introduction and progress towards the identification of its protein targets within the cell proteome. Chapter 7 describes the application of the Nicholas reaction for the attachment of propargyl groups to hydroxyl, thiol, phenol, amine, and carboxylic acid groups on both amino acids and complex small molecules.

Chapter 2

TARGETING NF- κ B p65 WITH A HELENALIN INSPIRED BIS-ELECTROPHILE

Adapted with Permission from:

Widen, J.C.; Kempema, A.M.; Villalta, P.W.; Harki, D.A. Targeting NF- κ B p65 with a Helenalin Inspired Bis-electrophile. *ACS Chem. Biol.* ASAP, DOI: 10.1021/acscchembio.6b00751. © American Chemical Society

This work was in collaboration with Dr. Aaron M. Kempema, Dr. Peter W. Villalta, and Professor Daniel A. Harki. Dr. Aaron M. Kempema assisted with aspects of the synthesis of the helenalin-based probes discussed below. Dr. Peter W. Villalta trained and assisted with operation of the LC-MS/MS. John Widen designed and synthesized the small molecules presented in this work and conducted all experiments including the NF- κ B luciferase assay, in-gel fluorescence labeling, pulldown experiments, and p65 labeling experiments.

2.1 Introduction

Aberrant activation of canonical p50/p65 NF- κ B transcription factors and concomitant expression of their target genes has been implicated in a spectrum of human diseases, including chronic inflammatory disease, atherosclerosis, arthritis, and cancer.¹⁹⁸ Consequently, interventional strategies to regulate canonical NF- κ B signaling may be broadly useful for multiple therapeutic indications.¹⁹⁹ Accordingly, significant research efforts have been devoted towards the discovery of inhibitors of canonical p50/p65 NF- κ B signaling with the targeting of upstream kinases that facilitate p50/p65 activation (via release from its repressor protein, I κ B α) being the prominent strategy.^{162, 200} However, most of these enzymes have degenerate activities with other cellular processes, and therefore, their inhibition as a strategy to regulate canonical NF- κ B signaling results in off-target effects.¹⁶² Targeting the most downstream proteins in the canonical NF- κ B signaling pathway, the p50/p65 transcription factor heterodimer itself, would ablate such specificity issues.

Chemical modulation of transcription factor-DNA interfaces has shown promise as a strategy to regulate aberrant transcription factor signaling. Pyrrole-imidazole polyamides that target the DNA minor groove with sequence specificity and disrupt transcription factor-DNA binding have demonstrated promising utilities in both cell culture and animal models, including modulation of canonical NF- κ B signaling.^{178b, 201} Conversely, targeting transcription factors with protein-binding small molecules has proven more problematic, which has been attributed to the typical shallow ligand binding pockets and non-discrete protein tertiary structure, which result in weak binding by putative inhibitors.^{155b, 158a} Irreversible covalent binding by inhibitors to nucleophilic amino acids on transcription factors may provide another strategy for transcriptional regulation via direct protein binding provided the amino acids that are covalently modified are intolerant of chemical modification (e.g., chemical modification prevents DNA binding and/or transcriptional activation).^{199b}

Many sesquiterpene lactone (SL) natural products are known modulators of NF- κ B signaling.^{182c, 202} In particular, helenalin (**Figure 2.1.1A**), a SL isolable from some *Arnica* and *Helenium* species,^{181, 203} has provided inspiration for the rational design of transcription factor-targeting NF- κ B inhibitors that disrupt DNA binding. The medicinal properties of helenalin have been known for over a century,²⁰⁴ which are structurally endowed, in part, by its α -methylene- γ -butyrolactone; a moiety found in scores of bioactive natural products.²⁰⁵ Exocyclic methylene butyrolactones undergo hetero-Michael addition with biological thiols to form covalent adducts. Helenalin also contains an endocyclic α,β -unsaturated ketone (cyclopentenone) that can also undergo hetero-Michael addition with thiols. Removal of one of the two Michael acceptors of helenalin, such as reduction of the cyclopentenone (yielding 2,3-dihydrohelenalin) or α -methylene- γ -butyrolactone (yielding 11,13-dihydrohelenalin; plenolin), significantly diminishes cytotoxicity in comparison to the parent natural product.^{182b, 206} Reduction of both Michael acceptors on helenalin ablates all activity.^{206b, 206c} The cyclopentenone and α -methylene- γ -butyrolactone of helenalin can engage biological thiols, such as glutathione and cysteine, yielding covalent adducts.^{182a, 183a} Previous studies by Merfort and colleagues have shown that helenalin covalently targets Cys38 of NF- κ B p65,^{183c, 184} which is positioned at the DNA-binding interface upon heterodimerization with p50 and DNA engagement (**Figure 2.1.1B**).^{31a} Alkylation of p65 by helenalin sterically prevents DNA binding of the p50/p65 heterodimer and inhibits its transcriptional activation.¹⁸⁶ Interestingly, molecular modeling of helenalin enabled the hypothesis that it may engage in tandem hetero-Michael additions with Cys38 and Cys120, which are 7.7 Å apart when bound to DNA,^{207,185} however, the lack of sensitivity of helenalin to a Cys120 \rightarrow Ser mutation has drawn this crosslinking model into question.^{182c, 186} Nonetheless, the non-disulfide, nucleophilic cysteines, Cys38 and Cys120, located at the p65 DNA-binding interface constitute unique structural features of p65 that lends itself towards the development of covalent chemical modulators. Furthermore, previous studies from other groups have demonstrated covalent engagement of p65 Cys38 with diverse small molecules,^{199b, 208} as well as covalent targeting of p65 Cys120.²⁰⁹

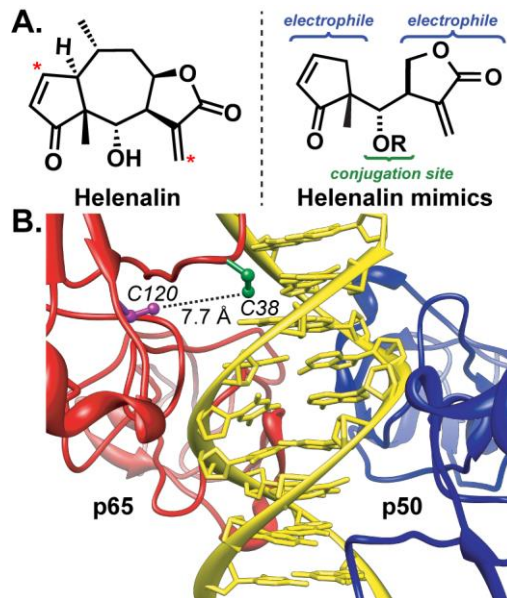


Figure 2.1.1. **A.** Structure of the sesquiterpene lactone helenalin and the design of helenalin mimics that contain both electrophiles found in the parent natural product. The secondary alcohol is amenable to chemical modifications to install reporter tags, such as alkynes. Based on two reported crystal structures of helenalin, the distance between the two electrophilic carbons (red asterisks) is 6.2-6.4 Å.²¹⁰ **B.** X-ray crystal structure of the NF-κB p50-p65 heterodimer bound to DNA (pdb 1VKX).³³ Notably, p65 cysteine residues 38 and 120 are adjacent in the DNA-binding interface (7.7 Å S-S distance, depicted with dashed line).

We hypothesized that chemical probes containing two structurally similar, electrophilic heterocycles configured in comparable chemical space as that of helenalin may recapitulate the interesting biological activity of the parent natural product. A similar strategy has been recently implemented for regulation of the Keap1/Nrf2/ARE pathway.²¹¹ Consequently, we devised a strategy to develop structurally simplified helenalin analogues that could be amenable to structure-activity relationship studies, serve as suitable chemical mimics of the parent natural product, and yield powerful chemical biology tools for specificity studies and target annotation by protein pulldown-mass spectrometry analysis. Our design would also enable rapid syntheses of analogues in comparison to the parent natural product, which required lengthy total syntheses.²¹² Herein, we report the design, synthesis, and characterization of simplified helenalin

analogues and their utilization in cell culture to target p65 of the canonical NF- κ B signaling pathway.

2.2 Design and Synthesis of Simplified Helenalin Analogues

The probe design was based on retaining both the cyclopentenone and α -methylene- γ -butyrolactone of helenalin, which are required for covalent reactivity at Cys38 and Cys120 of p65, but structurally simplifying the central 7-membered ring whereas the two above-mentioned ring systems would be tethered in only one position (**Figure 2.1.1A**). In support of this design, computational modeling of **2.6a** and **2.6b** predicted distances between the electrophilic carbons (analogous to the electrophilic carbons of helenalin denoted in **Figure 2.1.1A**) on both simplified analogues to be 6.2 Å, which is comparable to those distances measured from published x-ray crystal structures of helenalin (6.2-6.4 Å; **Figure 2.2.1** for modeling data).²¹⁰ Additionally, the calculated distances between the analogous electrophilic carbons on alkynylated probes **2.1a** and **2.1b** was similar (**2.1a**: 6.1 Å; **2.1b**: 5.4 Å). An additional consideration in our design was the utility of the diastereoselective, Barbier-type, aldehyde allylation chemistry developed by Hodgson and coworkers for synthesizing β -substituted α -methylene- γ -butyrolactones.²¹³

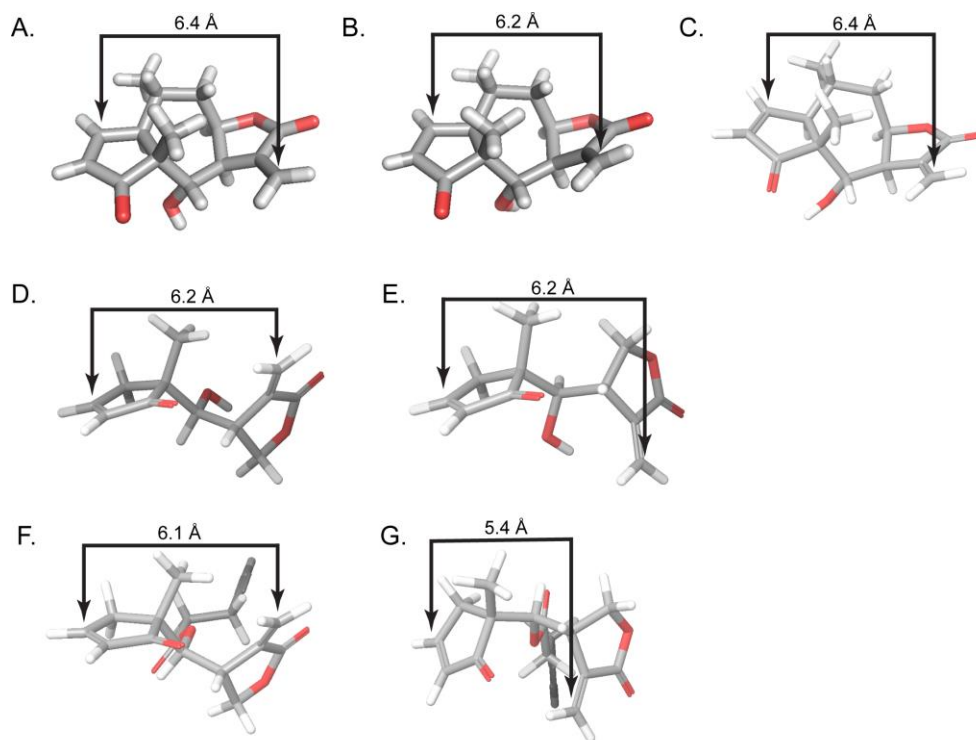
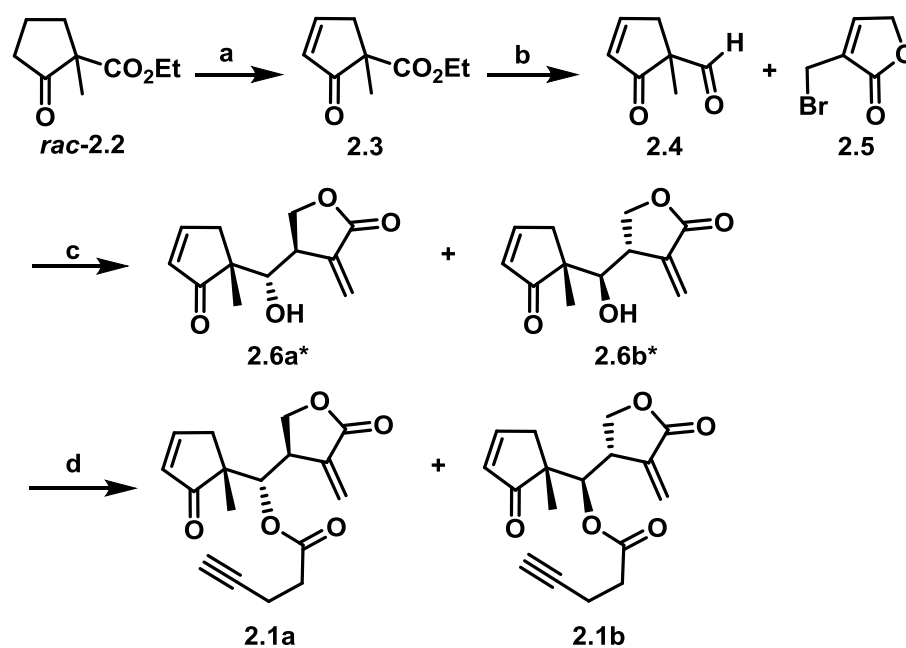


Figure 2.2.1. The measured distances between the two electrophilic carbons of helenalin and probes **2.1a**, **2.2b**, **2.6a**, and **2.6b**. Molecular modeling and structure minimization was performed with Maestro (Schrödinger, Inc., version 10.2.010). All *ab initio* equilibrium conformer minimizations were calculated with Jaguar (version 8.0) using the Density Functional Theory (DFT) B3LYP method and 6-31G** basis set in the gas phase (maximum iterations set to 48; calculation speed was set to ‘accurate’). The distances between the two electrophilic carbons were measured after minimization of each structure. **A.** Measured distance between both electrophilic carbons from a published crystal structure of helenalin.^{210a} **B.** Measured distance between both electrophilic carbons from a second published crystal structure of helenalin.^{210b} **C.** The predicted distance between the two electrophilic carbons of a minimized helenalin structure, which is in close agreement with **A** and **B**. Minimized structures and measured distances between electrophilic carbons for probes **2.6a** (**D**), **2.6b** (**E**), **2.1a** (**F**), and **2.1b** (**G**).

Accordingly, we devised the 5-step racemic synthesis of structurally simplified helenalin probe **2.1a/b** shown in **Scheme 2.2.1**. The known, racemic cyclopentanone *rac*-**2.2**²¹⁴ was oxidized to the α,β -unsaturated ketone **3** using IBX in moderate yield.²¹⁵ β -keto ester **2.3** was reduced to the diol with LiAlH₄, and then subsequently oxidized to the desired aldehyde **2.4** with PCC in a 40% yield over the two steps. Notably, aldehyde **2.4** is volatile and unstable and must be used immediately following careful purification and isolation. The α -(bromo)methyl unsaturated furanone **2.5** was synthesized in one step from α -methylene- γ -butyrolactone by a known procedure.^{213, 216} With building blocks **2.4**

and **2.5** in-hand, the diastereoselective Barbier coupling (*vide supra*) was performed, which resulted in inseparable diastereomers **2.6a*** and **2.6b***. Only one diastereomer was observed in the Barbier coupling with respect to β -substitution of α -methylene- γ -butyrolactone ring in accord with literature precedence of a 6-membered transition state. However, metal-catalyzed allylation of aldehyde **2.4**, bearing a stereogenic center, occurs without facial selectivity, yielding diastereomeric products **2.6a*** and **2.6b*** that are racemic. Coupling the inseparable mixture of **2.6a*** and **2.6b*** with 4-pentynoic acid and DCC yielded racemic **2.1a** and **2.1b** that were separable on silica gel. The overall yield for the synthesis of **2.1a** and **2.1b** was 13% (5 steps).

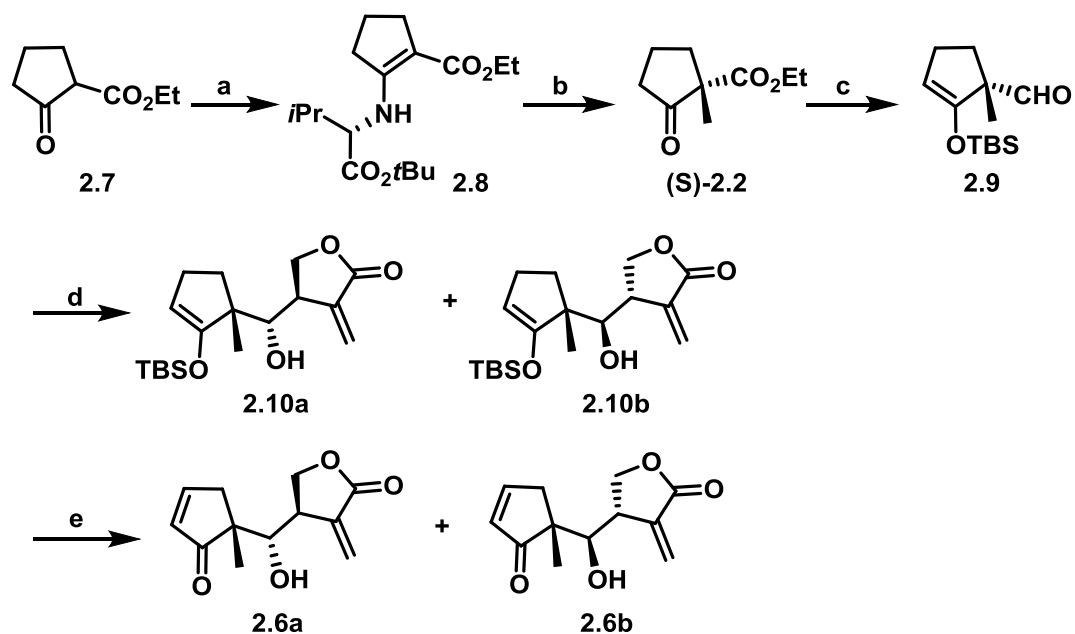


Scheme 2.2.1. Racemic synthesis of bifunctional helenalin mimics and their alkyne analogues.^a

^a**Reagents and Conditions:** (a) IBX, DMSO, 75 °C, 66%; (b) (i) LiAlH₄, Et₂O 0 °C; (ii) PCC, CH₂Cl₂, RT, 40% (2 steps); (c) Zn⁰, NH₄Cl (aq.), DMF, RT, 60%; (d) 4-pentynoic acid, DCC, DMAP, CH₂Cl₂, 40 °C, 80% (separable diastereomers). *Denotes **2.6a** and **2.6b** prepared from racemic starting materials.

A stereoselective synthesis of **2.6a** was also developed to deliver a simplified helenalin probe with the appropriate overall stereochemistry as that found in helenalin and to overcome our inability to separate diastereomers **2.6a*** and **2.6b*** from the Barbier

coupling in the racemic synthesis. Since our stereoselective synthesis would employ a different aldehyde coupling partner, an opportunity to separate the diastereomers resulting from the Barbier coupling would exist. Our synthesis began with the stereoselective introduction of the quaternary methyl group, yielding (*S*)-**2.2**, using an established protocol for the stereoselective methylation of 1,3-ketoesters (**Scheme 2.2.2**).²¹⁷ Accordingly, 1,3-ketoester **2.7** was condensed with *L*-*tert*-butylvaline to obtain enamine **2.8** in 75% yield. Enamine **2.8** was deprotonated with LDA in toluene at $-78\text{ }^{\circ}\text{C}$, and then two equivalents of THF were added, followed by the addition of excess CH_3I at the same temperature. After formation of the quaternary center, the crude product was isolated and the resulting Schiff base was hydrolyzed with aqueous HCl to obtain (*S*)-**2.2** in 53% yield and 93:7 er (85% ee) by chiral-GC analysis. Cyclopentanone (*S*)-**2.2** was then converted to the TBS-protected enol ether, followed by 2-electron reduction of the ester to aldehyde **2.9** using DIBAL-H in 27% yield (two steps). Notably, addition of the TBS protecting group resulted in a non-volatile and stable aldehyde **2.9** in comparison to **2.4**. Aldehyde **2.9** was then subjected to the aforementioned Barbier conditions with **2.5** to obtain diastereomers **2.10a** and **2.10b** in 1:1 dr (64% yield) that *were* separable by silica gel chromatography. Diastereomers **2.10a** and **2.10b** were oxidized separately to their corresponding cyclopentenones under catalytic Saegusa-Ito oxidation conditions²¹⁸ in DMSO under 1 atm of O_2 in 46% yield (for **2.6a**, 93:7 er) and 56% yield (for **2.6b**, 91:9 er). It is noteworthy that **2.10a**, **2.10b**, **2.6a**, and **2.6b** should not be dried under high vacuum because of their propensity to decompose (drying under low vacuum for a short period of time is recommended). Enantiomerically pure **2.6a** and **2.6b** were synthesized in six steps in 3% and 4% overall yields, respectively.

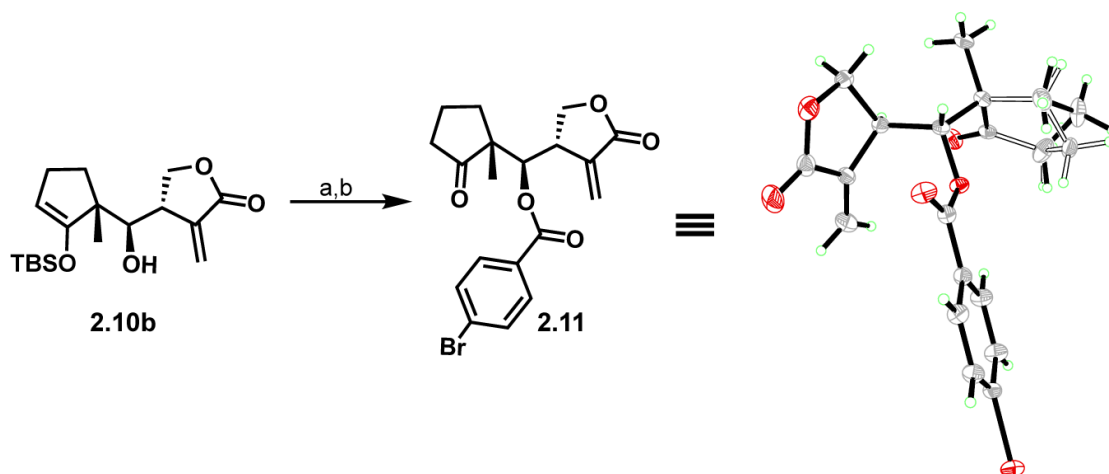


Scheme 2.2.2. Enantioselective synthesis of **2.6a** and **2.6b**.^a

^a**Reagents and Conditions:** (a) L-Valine *tert*-butyl ester, $\text{BF}_3 \cdot \text{OEt}$, PhH, reflux (Dean-Stark), 75%; (b) (i) LDA, toluene, THF (2 eq.), -78°C ; MeI; (ii) 3M HCl (aq.), THF, RT, 53% (2 steps), 93:7 er; (c) (i) LiHMDS, THF; TBSCl, -78°C to RT; (ii) DIBAL-H, CH_2Cl_2 , -78°C , 27% (2 steps); (d) **2.5**, Zn^0 , NH_4Cl (aq.), DMF, RT, 64% (separable diastereomers); (e) $\text{Pd}(\text{OAc})_2$, O_2 (1 atm), DMSO, 46% (**2.6a**, 93:7 er), 56% (**2.6b**, 91:9 er).

2.3 Stereochemical Determination of Simplified Helenalin Probes

The Barbier coupling utilized for the synthesis of our molecular probes resulted in a highly stereocontrolled β -substitution of the butyrolactone ring. However, the lack of facial selectivity for aldehyde allylation resulted in diastereomers with respect to the quaternary center on the cyclopentanone ring and secondary alcohol. To unambiguously assign the stereochemistry of our probes by x-ray crystallography, we esterified diastereomer **2.10b** from the enantioselective synthesis with 4-bromobenzoic acid, a moiety that bears a heavy atom for determination of absolute configuration (**Scheme 2.3.1**). Deprotection of the silyl enol ether to the ketone using TFA in DCM afforded **2.11**, which was crystallized and the x-ray structure solved (**Scheme 2.3.1**). Based on this information, diagnostic ^1H NMR coupling constants, and the known, absolute configuration of **2.9**, we unambiguously assigned the structures of our chemical probes.



Scheme 2.3.1. Synthesis and x-ray crystal structure of **2.11**^a

^a**Reagents and Conditions:** (a) 4-bromobenzoic acid, 4-DMAP, DCC, DCM, 40 °C (99%) (b) TFA, DCM, RT (53%). Right: ORTEPII plot of the x-ray diffraction data of **2.11**.

2.4 Simplified Helenalin Probes Inhibit NF- κ B Signaling in Cell Culture

Simplified helenalin analogues **2.6a** and **2.6b** and alkynylated probes **2.1a** and **2.1b** were screened for inhibitory activity towards canonical p50/p65 NF- κ B signaling with a cellular luciferase assay (**Figure 2.4.1**).²¹⁹ Helenalin was utilized as a benchmark and exhibited low micromolar inhibition of induced NF- κ B signaling ($53.7 \pm 14.1\%$ NF- κ B activity at $2.5 \mu\text{M}$). In comparison, alkyne-functionalized probes **2.1a** and **2.1b** were comparably active at $5 \mu\text{M}$ ($54.4 \pm 16.7\%$ and $52.9 \pm 7.1\%$ NF- κ B activity, respectively). Notably, **2.1a** elicits more cellular cytotoxicity ($64.5 \pm 3.0\%$ cell viability) during this 8-hour assay compared to **2.1b** ($97.8 \pm 15.1\%$ cell viability) at $10 \mu\text{M}$ treatment. Cellular cytotoxicity for **2.1a** at $20 \mu\text{M}$ treatment was comparable to that observed at $10 \mu\text{M}$, whereas cellular viability was $>80\%$ for all other doses of all compounds shown in **Figure 2.4.1** (refer to **Figure 2.4.2** for cellular viability data). Intriguingly, enantiomerically pure **2.6b**, the diastereomer with the ‘incorrect’ stereochemistry with respect to helenalin, has approximately 6-fold more NF- κ B inhibitory activity at $25 \mu\text{M}$ compared to **2.6a**, the enantiomerically pure ‘correct’ diastereomer from the Barbier coupling (**2.6b**: $14.5 \pm 7.4\%$ NF- κ B activity; **2.6a**: $88.8 \pm 4.9\%$ NF- κ B activity). Furthermore, **2.6b** achieves the same NF- κ B inhibitory activity as helenalin at only a 4-

fold higher dose (**2.6b**: $51.6 \pm 16.6\%$ NF- κ B activity at $10 \mu\text{M}$; helenalin: $53.7 \pm 14.1\%$ NF- κ B activity at $2.5 \mu\text{M}$). These data suggests the stereochemistries of our helenalin analogues are important with respect to cellular potency. The observation that **2.1a** and **2.1b** are equivalently potent in this assay hints at the possibility that **2.6a** may have poor uptake properties or may be poorly retained in cells; however, no data currently exists to support this proposal.

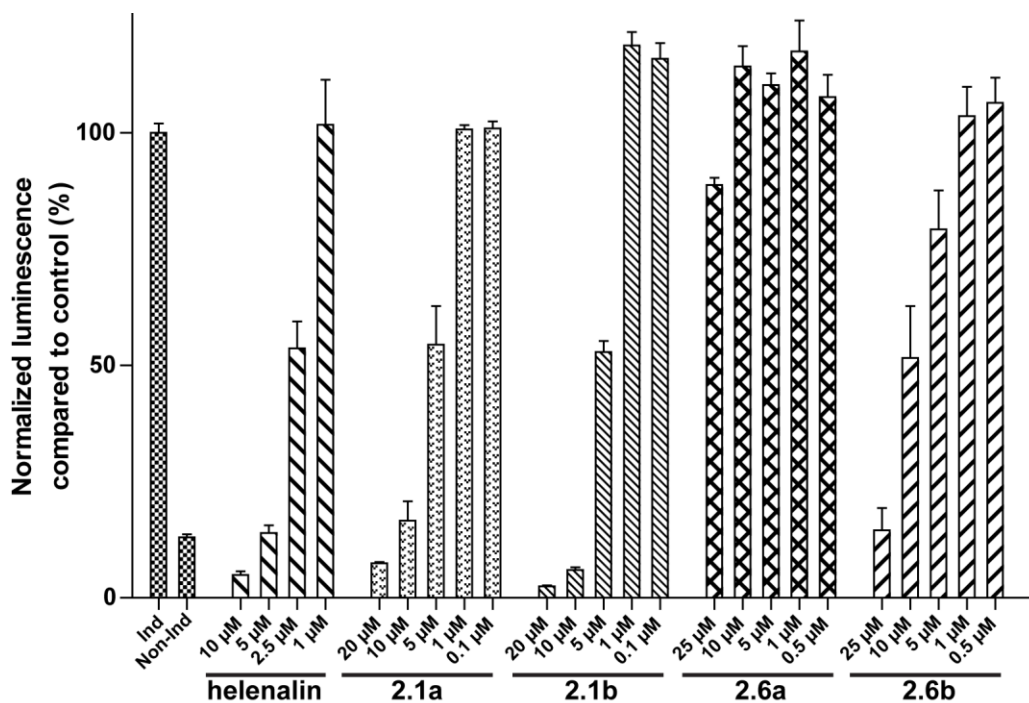


Figure 2.4.1. NF- κ B-luciferase inhibition assay in A549 cells. Compounds were dosed to A549 cells containing a stably transfected NF- κ B luciferase reporter construct and stimulated with TNF- α for eight hours (except for non-induced control, Non-Ind). Luminescence was normalized to the no compound induced (Ind) control and plotted as % NF- κ B luciferase activity. Mean \pm standard deviation values are shown ($n \geq 3$ biological replicates). Compound-mediated toxicity to A549 cells was measured concurrently (**Figure 2.4.2**) and no significant toxicity was observed under these assay conditions.

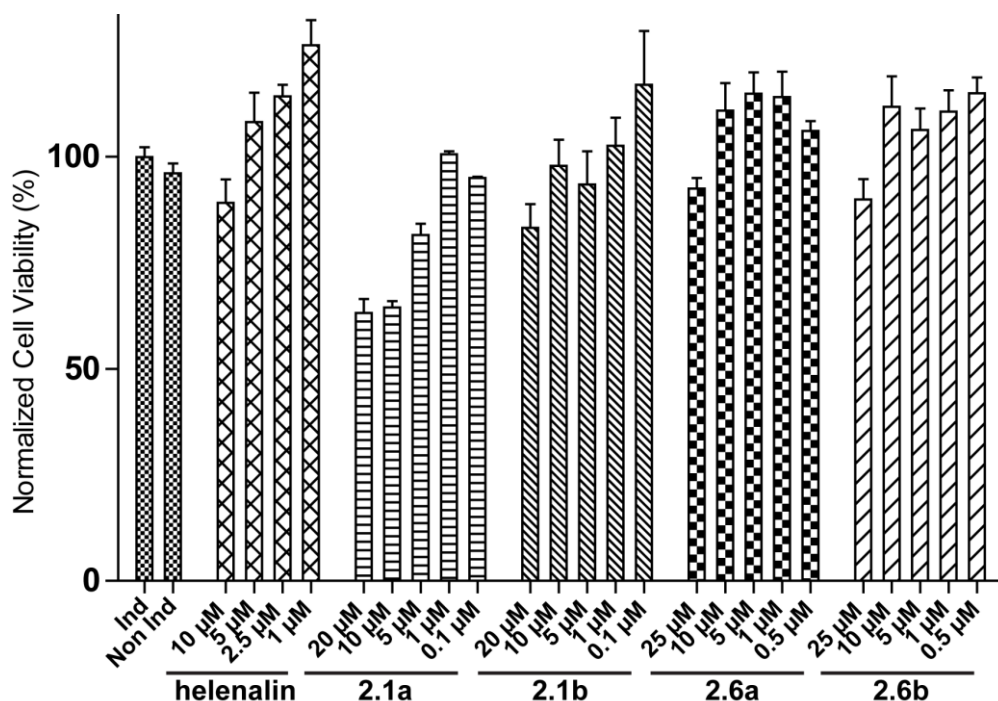


Figure 2.4.2. Alamar Blue cytotoxicity analysis of A549 NF- κ B-luciferase cells treated with compounds at varying concentrations. All compounds maintained greater than 80% cell viability throughout the assay with the exception of **2.1a** at 20 and 10 μ M where a cell viability greater than 60% was achieved. All wells were normalized to non-treated (1% v/v DMSO) control wells.

2.5 Simplified Helenalin Probes Covalently Bind Proteins in Cell Culture

To qualitatively assess the protein-binding properties of our probes in cell culture, we performed protein labeling studies in HeLa cells. Alkyne-functionalized **2.1a** and **2.1b** were dosed separately to HeLa cells for one hour, cells were then lysed and the lysate cleared, and then protein-probe adducts were labeled with tetramethylrhodamine-azide (TAMRA- N_3) via a copper mediated [3+2] Huisgen reaction (click chemistry).²²⁰ Protein-**2.1a/2.1b**-TAMRA adducts were separated by denaturing PAGE and fluorescence visualization of TAMRA (**Figure 2.5.1**). To demonstrate uniform protein labeling, total proteins were also imaged. Both **2.1a** and **2.1b** labeled multiple proteins in a concentration dependent manner (**Figure 2.5.1**). Gratifyingly, protein bands at approximately 65 kDa were observed for both **2.1a** and **2.1b**, which would be expected for targeting NF- κ B p65. Off-target binding by **2.1a** and **2.1b**, which is evident by the

multiple protein bands observed in our qualitative analysis, was observed and was certainly anticipated given the designed probes are bis-electrophiles. However, the distinct labeling patterns of **2.1a** and **2.1b** further reinforce the relevance of the stereochemistry of our probes with respect to protein targeting. Probe **2.1a** (which contains the correct stereochemistry with respect to helenalin) qualitatively labels more proteins compared to **2.1b** by visualization of the intense bands seen at 50 and 10 μM . Additionally, pre-treatment of cells with helenalin prior to labeling studies with **2.1a** competes away protein binding properties by **2.1a**, suggesting that our designed probe mimics the proteome reactivity properties of the parent natural product (**Figure 2.5.2**).

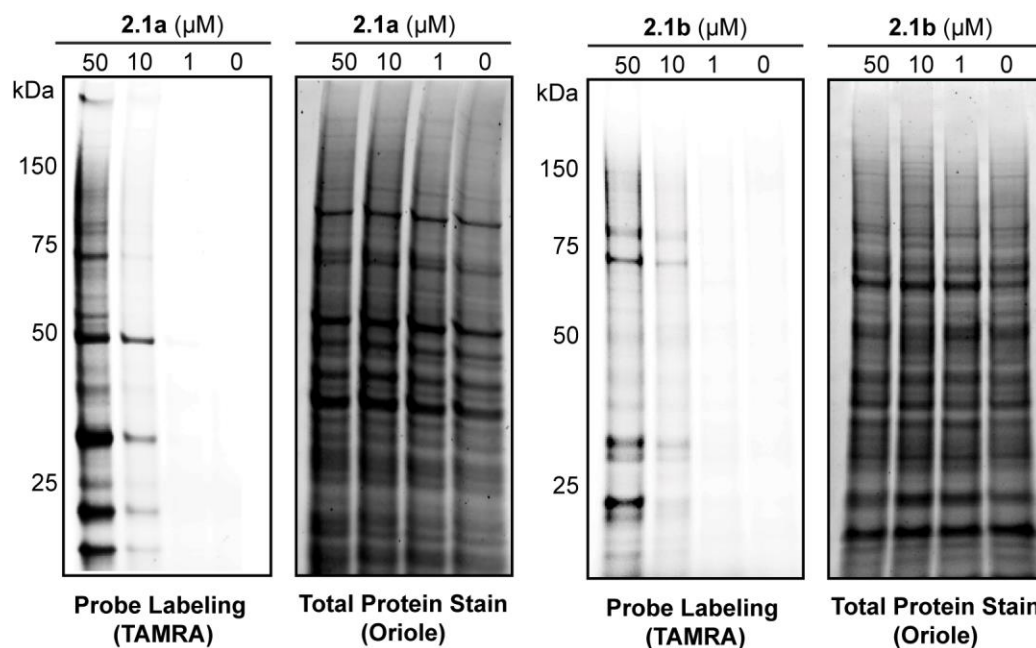


Figure 2.5.1. Proteome labeling of **2.1a** and **2.1b** in HeLa cells. Compounds were dosed to HeLa cells at the concentrations shown, the cells were lysed, and then TAMRA- N_3 was conjugated to **2.1a** and **2.1b** via azide-alkyne click chemistry. Proteins were separated by denaturing PAGE and gels were imaged for TAMRA fluorescence. Total proteins were then visualized by staining with Oriole[®] fluorescent protein stain followed by gel imaging.

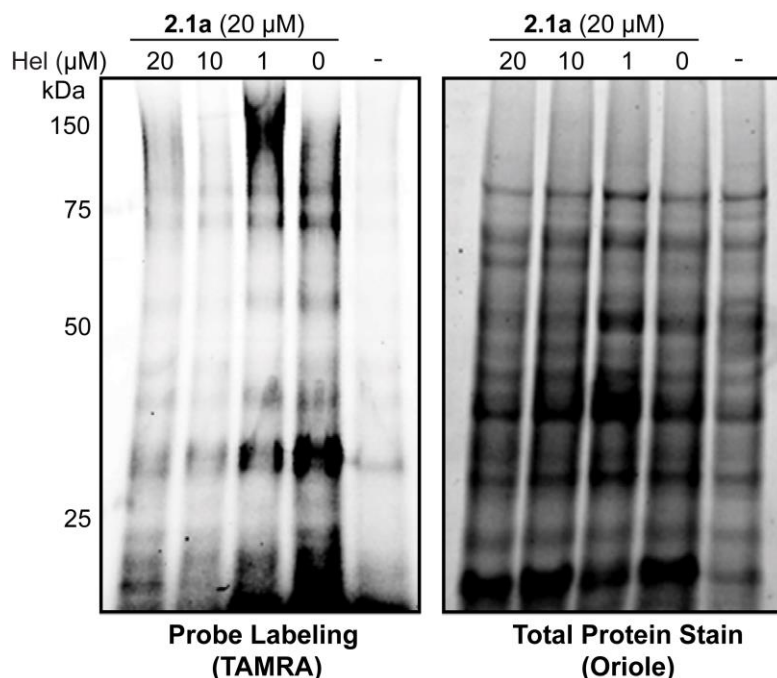


Figure 2.5.2. The natural product helenalin is able to compete away labeling of **2.1a** in a concentration dependent manner. Helenalin was dosed to live HeLa cells at the respective concentrations 30 min prior to dosing **2.1a** at 20 μM , which was incubated for an additional 30 min. The cells were lysed and TAMRA- N_3 was conjugated to **2.1a** via azide-alkyne click chemistry. Proteins were separated by denaturing PAGE and gels were imaged for TAMRA fluorescence. Total proteins were then visualized by staining with Oriole® fluorescent protein stain followed by gel imaging to show equal protein loading in all lanes.

2.6 Helenalin and Simplified Helenalin Probes Covalently Label Cys38 of Recombinant p65

Previous studies with wild-type p65 and Cys \rightarrow Ser mutant p65 proteins have demonstrated that helenalin covalently targets Cys38.¹⁸⁶ To evaluate if helenalin mimics **2.1a** and **2.1b** also target Cys38, recombinant human p65 was incubated with **2.1a** and **2.1b**, proteins were digested, and LC-MS/MS was performed to identify adducted thiols (**Figure 2.6.1-2.6.5**). The predicted trypsin digestion of p65 proximal to Cys38 yields $\text{C}^{38}\text{EGR}^{41}$ or $\text{Y}^{36}\text{KCEGR}^{41}$ if the cleavage site closest to Cys38 is missed. Searching for the exact masses of the probes as a cysteine modification found the expected probe-peptide adducts for helenalin ($\text{Y}^{36}\text{KCEGR}^{41}$ adduct), **2.1a** ($\text{C}^{38}\text{EGR}^{41}$ adduct) and **2.1b** ($\text{C}^{38}\text{EGR}^{41}$ adduct). Analysis of the MS² data for studies with **2.1a** and **2.1b** and recombinant p65 consistently revealed a fragment that was cleaved at the secondary

hydroxyl group, which demonstrates the α -methylene- γ -butyrolactone was reacting with Cys38 (**Figure 2.6.1** and **Figures 2.6.2-2.6.3**). On the other hand, no fragments were found to support reactivity at the endocyclic enones of **2.1a** and **2.1b**, although such adducts might be reversible and unstable to digestion and MS analysis. Our reactivity data is consistent with previous reports demonstrating that α -methylene- γ -butyrolactones form irreversible hetero-Michael addition adducts with cysteines.^{183a, 184} Interestingly, attempts to identify Cys38 adducts for **2.6a** and **2.6b** were unsuccessful, although adducts to a surface cysteine on p65, Cys105, was observed (**Figure 2.6.5**). Cys105 adducts were not found in experiments with **2.1a**, **2.1b**, or helenalin. The biological significance of labeling Cys105 on p65 remains unclear.

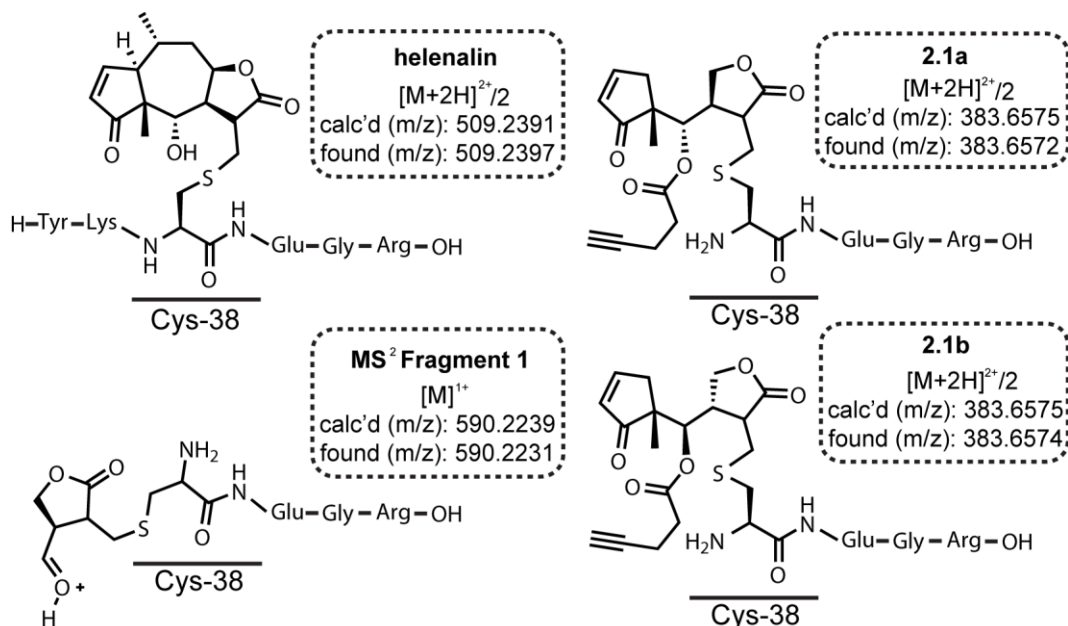


Figure 2.6.1. Annotation of compound binding sites on p65. Helenalin, **2.1a** and **2.1b** were incubated separately with recombinant human p65 in 1X PBS buffer for 1 hr. Proteins were digested with trypsin and peptides analyzed by LC-MS/MS. Peptide-probe adducts were identified by extracting the theoretical mass from the total ion chromatogram and then analysis of the MS² fragmentation pattern. Helenalin, **2.1a** and **2.1b** all bound Cys38 as expected. The MS² Fragment 1 (shown on the bottom left) was detected after dosing **2.1a** and **2.1b** indicating that covalent adducts are forming at the exocyclic methylene butyrolactone.

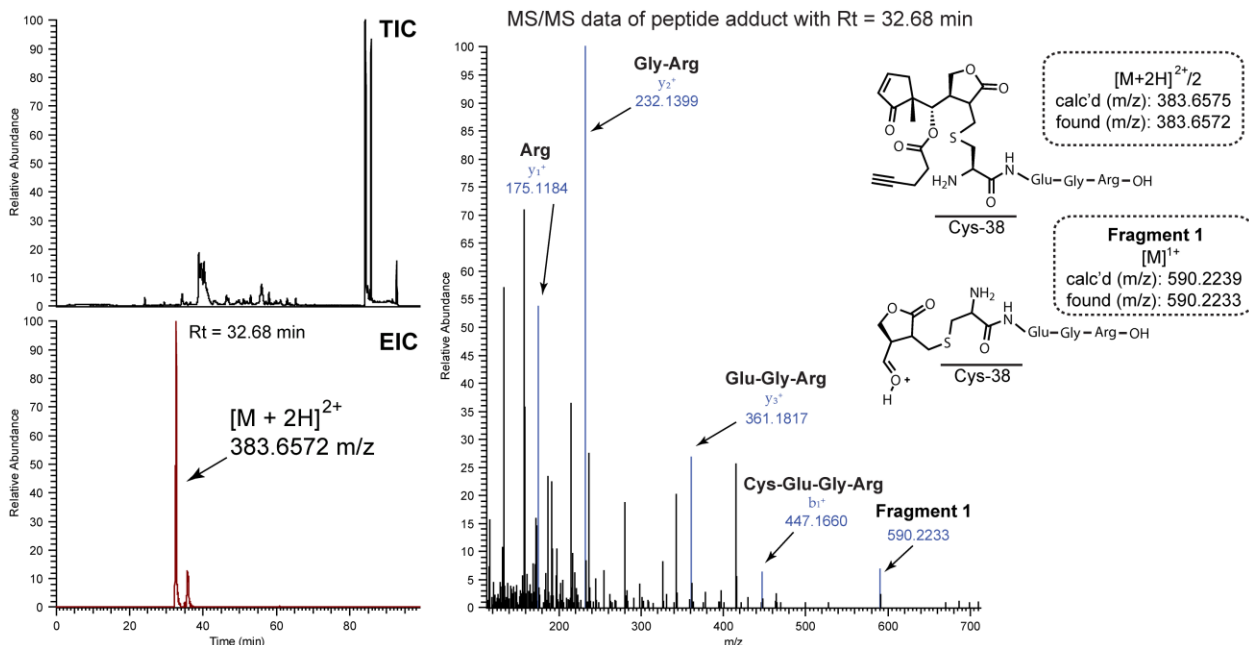


Figure 2.6.2. The extracted ion chromatogram (EIC) from the total ion chromatogram (TIC) is shown above with the MS² fragmentation data of **2.1a** covalently attached to the C³⁸EGR⁴¹ adduct of Cys38 within the p53 DNA binding pocket. This is the predicted peptide-probe adduct as shown above after trypsin digestion. **Fragment 1** identified in the MS² data suggests that Cys38 is reacting with the exocyclic methylene butyrolactone of **2.1a**.

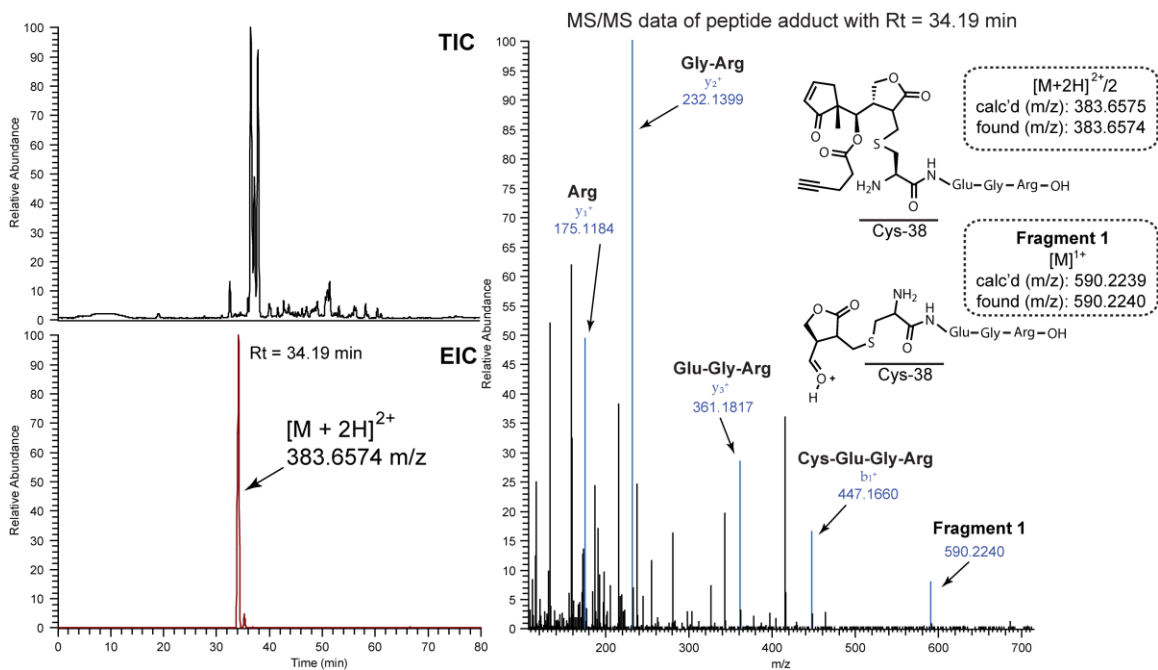


Figure 2.6.3. The extracted ion chromatogram (EIC) from the total ion chromatogram (TIC) is shown above with the MS² fragmentation data of **2.1b** covalently attached to the C³⁸EGR⁴¹ adduct of Cys38 within the p53 DNA binding pocket. This is the predicted peptide-probe adduct as shown above after trypsin digestion. **Fragment 1** identified in the MS² data suggests that Cys38 is reacting with the exocyclic methylene butyrolactone of **2.1b**.

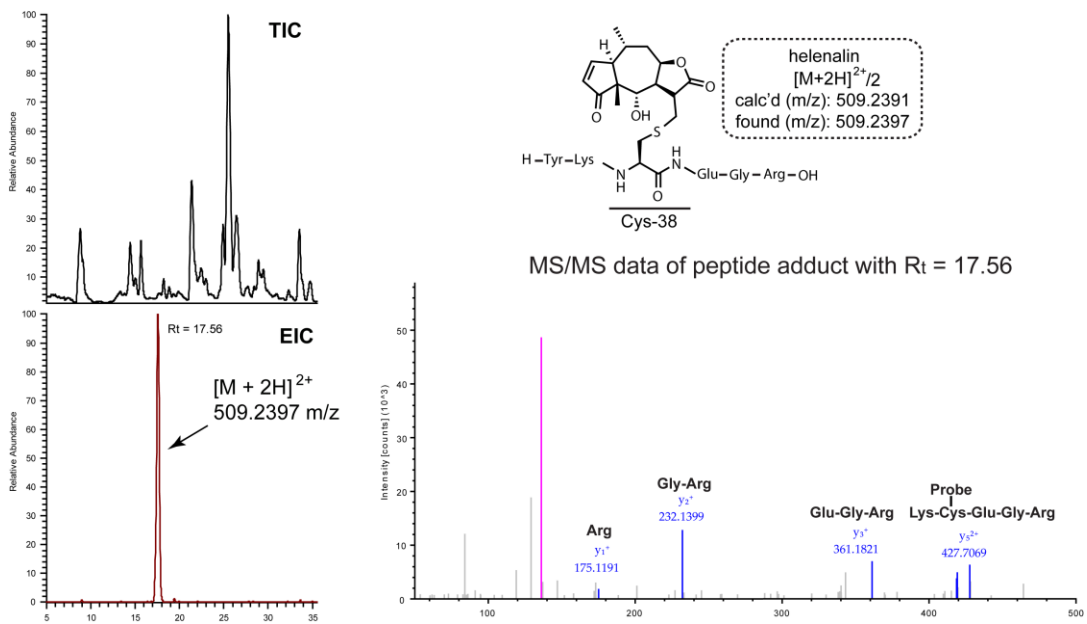


Figure 2.6.4. The extracted ion current (EIC) from the total ion chromatogram (TIC) is shown above with the MS² fragmentation data of helenalin covalently attached to the Y³⁶KCEGR⁴¹ adduct of Cys38 within the p53 DNA binding pocket. This is the predicted peptide-probe adduct as shown above after trypsin digestion, missing one cut site after the lysine residue.

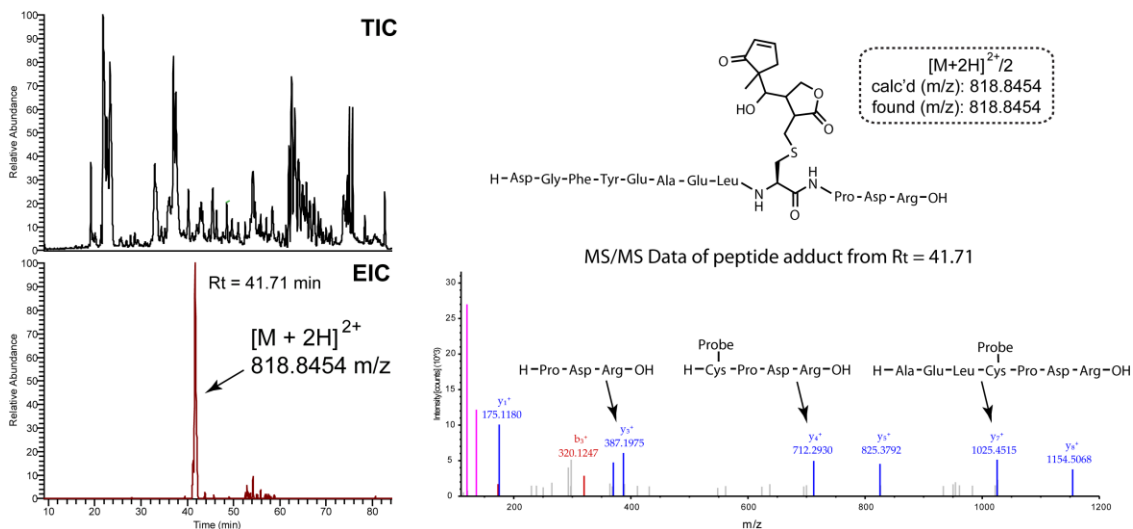


Figure 2.6.5. The extracted ion current (EIC) from the total ion chromatogram (TIC) is shown above with the MS² fragmentation data of **2.6a**. The same retention time and fragmentation data was observed with derivative **2.6b** as well. Both compounds covalently attached to surface exposed Cys105. After trypsin digestion the predicted peptide is D⁹⁷GFYEALCPDR¹⁰⁸.

2.7 Simplified Helenalin Probes Covalently Target p65 in Cell Culture

After determining that simplified helenalin probes **2.1a** and **2.1b** can inhibit canonical NF- κ B signaling in cell culture, covalently label cellular proteins, and target Cys38 of recombinant p65, we turned our attention to evaluating if **2.1a** and **2.1b** can directly bind p65 in cell culture and avoid other well-established canonical NF- κ B signaling enzymes. Accordingly, **2.1a** and **2.1b** were dosed to HeLa cells at 50 μ M and incubated for 30 minutes. Cells were then harvested, washed extensively to remove unincorporated probe, and then lysed by sonication. Protein-**2.1a/2.1b** adducts were then labeled with biotin-azide (biotin-N₃) via a copper mediated [3+2] Huisgen reaction (click chemistry).²²⁰ Protein-**2.1a/2.1b**-biotin adducts were enriched with a monomeric avidin column and separated by denaturing PAGE. Protein-**2.1a/2.1b**-biotin adducts were transferred to a membrane and then incubated with primary antibodies for p65 (primary target), I κ B α (p50/p65 repressor protein; for specificity assessment), p50 (forms transcription factor heterodimer with p65; for specificity assessment), and IKK α/β

(upstream kinases that contribute to activation of the NF- κ B signaling pathway; for specificity assessment; antibody recognizes both proteins). To our delight, simplified helenalin probes **2.1a** and **2.1b** successfully pulled down p65 from live HeLa cells, but does not target I κ B, p50, or IKK α/β (**Figure 2.7.1**). The negative control demonstrates no proteins are pulled down in the absence of probes and the input lysates show that all proteins being evaluated are present in the input lysate (prior to monomeric avidin isolation of protein-**2.1a/2.1b**-biotin adducts). Furthermore, a head-to-head comparison of the ability of **2.1a** and **2.1b** to target p65 reveals comparable efficiencies (**Figure 2.7.1C**).

We also wanted to determine if **2.6a** and **2.6b** could compete away binding of alkyne probes **2.1a** and **2.1b** in live cells; especially since p65 adducts were not observed with **2.6a** and **2.6b** by MS analysis. To this end, **2.6a** and **2.6b** were dosed to HeLa cells at 50 μ M for 20 minutes prior to dosing **2.1a** or **2.1b**. Interestingly, **2.6b** was able to completely block labeling and pulldown by both **2.1a** and **2.1b**, whereas **2.6a** exhibited only partial activity at the same concentration (**Figure 2.7.1**). These data suggest that **2.6a** and **2.6b** target Cys38 on p65. Additionally, the difference in efficiencies between the two compounds is consistent with the cellular reporter data (**Figure 2.4.1**), in which **2.6a** was dramatically less potent than **2.6b** for inhibition of canonical NF- κ B signaling.

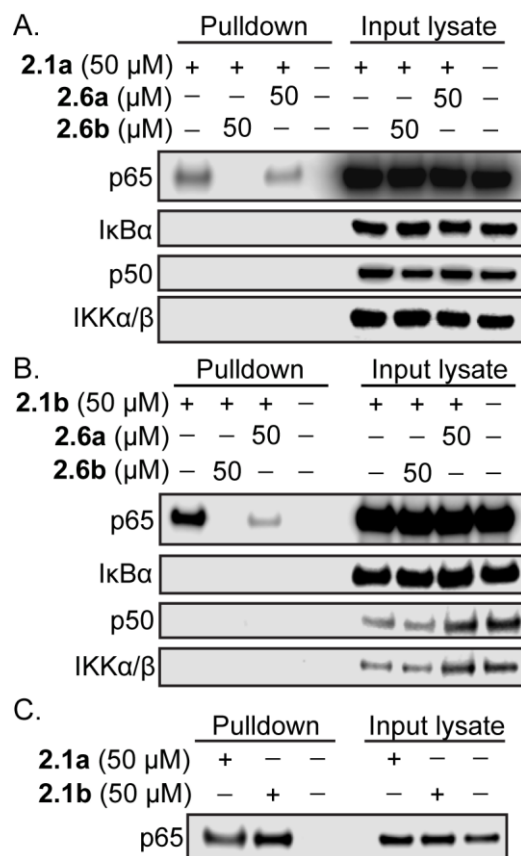


Figure 2.7.1. Immunodetection of NF- κ B signaling pathway proteins for covalent binding by **2.1a** and **2.1b**. Compounds were dosed to HeLa cells at the concentrations shown, the cells were lysed, and then Biotin- N_3 was conjugated to **2.1a** and **2.1b** via azide-alkyne click chemistry. Protein-**2.1a/2.1b** adducts were isolated on monomeric avidin resin and identified by Western blotting with the antibodies shown. Notably, IKK α/β is recognized with the same antibody. (A & B) **2.1a** (for A) and **2.1b** (for B) label p65, but not other NF- κ B pathway proteins, as shown in pulldown experiments. Competition experiments were performed by pre-treating cells with **2.6a** and **2.6b** 20 min before addition of **2.1a** (for A) or **2.1b** (for B). (C) Head-to-head comparison of labeling efficiency of **2.1a** and **2.1b**. Input lysate is the crude protein products before monomeric avidin enrichment.

2.8 Conclusion

We have developed simplified helenalin probes that target Cys38 of NF- κ B p65 by a covalent mechanism of action. Our chemical probes are easily accessed in 6 synthetic steps (to probes **2.1a** and **2.1b**) and contain an alkyne handle for imaging and protein pulldown applications. Simplified helenalin probes **2.1a** and **2.1b** inhibit induced, canonical NF- κ B signaling in a cellular reporter assay with low micromolar efficiencies and selectively engage p65 over other well-established proteins whose targeting by small

molecules affects canonical NF- κ B signaling; namely, I κ B α , p50, and IKK α/β . The strategy of covalent targeting of solvent accessible, nucleophilic amino acids at key transcription factor interfaces, such as the DNA-binding cleft for p65 in this work, represents a viable strategy to rationally design small molecule transcription factor binders with biochemical utilities for transcriptional control of aberrant gene expression in human diseases. Current efforts are focused on improving the specificities and potencies of the first-generation helenalin-based probes reported in this work, with a particular focus on the size and rigidity of the moieties that mimic the central 7-membered ring of helenalin.

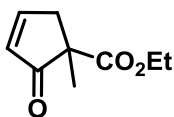
2.9 Materials and Methods

Unless otherwise noted, reactions were performed in flame-dried glassware under a nitrogen or argon atmosphere and stirred with a Teflon-coated magnetic stir bar. Liquid reagents and solvents were transferred via syringe and cannula using standard techniques. Reaction solvents dichloromethane (DCM), N,N-dimethylformamide (DMF), tetrahydrofuran (THF) and diethyl ether (Et₂O) were dried by passage over a column of activated alumina using a solvent purification system (MBraun). All other chemicals were used as received unless otherwise noted. Helenalin was purchased from Enzo Life Sciences and purified by SiO₂ flash column chromatography before use in biological assays. The molarities of n-butyllithium solutions were determined by titration against diphenylacetic acid as an indicator (average of three determinations). Reaction temperatures above 23 °C refer to oil bath temperature, which was controlled by a temperature modulator. Reaction progress was monitored by thin layer chromatography using EMD Chemicals Silica Gel 60 F₂₅₄ glass plates (250 μ m thickness) and visualized by UV irradiation (at 254 nm) and/or KMnO₄ stain. Silica gel chromatography was performed on a Teledyne-Isco Combiflash Rf-200 instrument utilizing Redisep Rf High Performance silica gel columns (Teledyne-Isco) or flash column chromatography was performed using SiliCycle silica gel (32-63 μ m particle size, 60 Å pore size). ¹H NMR (500 MHz), ¹³C NMR (125 MHz), and ¹⁹F NMR (470 MHz) spectra were recorded on a

Bruker Avance NMR spectrometer. ^1H and ^{13}C chemical shifts (δ) are reported relative to the solvent signal, CHCl_3 ($\delta = 7.26$ for ^1H NMR and $\delta = 77.00$ for ^{13}C NMR). Some spectra contain TMS (0.05% v/v). All NMR spectra were obtained at room temperature unless otherwise specified. High resolution mass spectral data were obtained at the Analytical Biochemistry Core Facility of the University of Minnesota Masonic Cancer Center on an LTQ OrbiTrap Velos Mass Spectrometer (Thermo Fisher).

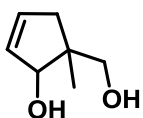
The purity of all compounds tested in biological assays were checked via analytical HPLC analysis on an Agilent 1200 series instrument equipped with a diode array detector (wavelength monitored = 215 nm) and a Zorbax SBC18 column (4.6 x 150 mm, 5 μm , Agilent Technologies). All compounds tested in biological assays were >95% pure by HPLC. Information regarding the HPLC method and purity traces can be found in **Section 2.11** of this chapter.

Enantiopurity of (**S**)- **2.2** was determined by chiral-GC/MS using an Agilent 7200B GC/Q-TOF with an Agilent J&W CycloSil-B GC column (30 m x 0.25 mm, 0.25 μm film). The injector port was set at 250 $^\circ\text{C}$ and the column flow (helium gas) at 1.0 mL/min. The temperature method began at 35 $^\circ\text{C}$ and increased to 180 $^\circ\text{C}$ (8 $^\circ\text{C}/\text{min}$) over 18.1 min. The mass spectrometer electron ionization source temperature was set to 250 $^\circ\text{C}$ for detection. Area under the peak for each enantiomer was used to determine the enantiopurity; reported as enantiomeric ratio (er). The enantiopurity of other compounds was determined using normal phase chiral-HPLC or ^{19}F analysis after derivatization with (**S**)-(-)- α -methoxy- α -(trifluoromethyl)phenylacetic acid ((**S**)-MTPA). Information regarding these two methods can be found in **Section 2.12**.

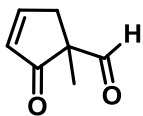


Ethyl 1-methyl-2-oxocyclopent-3-enecarboxylate (**2.3**).²¹⁴ To a stirred solution of *rac*-**2.2** (1.00 g, 5.88 mmol) in DMSO (20 mL) was added 4.11 g (14.7 mmol) of IBX²²¹ and

the solution was heated to 85 °C for 18 h. The reaction was cooled to 0 °C and aqueous NaHCO₃ (sat'd, 40 mL) was added slowly. The reaction was filtered to remove IBX decomposition products. The solution was extracted with Et₂O (30 mL, 3X), and the organic layer was dried over Na₂SO₄, and concentrated *in vacuo*. The crude mixture was SiO₂ purified with EtOAc (10-30%) in hexanes to afford **2.3** (0.52 g, 53% yield) as a slightly tinted yellow oil. ¹H NMR (CDCl₃): 7.76-7.71 (m, 1H), 6.19-6.15 (m, 1 H), 4.14 (q, *J* = 7.2 Hz, 2 H), 3.25 (d, *J* = 19.1 Hz, 1 H), 2.53 (d, *J* = 19.2 Hz, 1 H), 1.39 (s, 3H), 1.21 (t, *J* = 7.2 Hz, 3H) ppm. ¹³C NMR (CDCl₃): 206.9, 171.7, 163.2, 131.8, 61.7, 53.5, 42.9, 20.8, 14.2 ppm HRMS-ESI⁺ (*m/z*): calc'd [M+H]⁺ for C₉H₁₂O₃: 169.0859, found 169.0855.

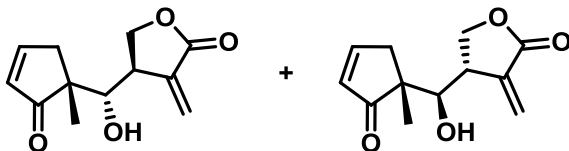


5-(Hydroxymethyl)-5-methylcyclopent-2-en-1-ol. To a stirred suspension of LiAlH₄ (0.66 g, 17 mmol) in EtO₂ (25 mL) at 0 °C was added **2.3** (0.75 g, 4.4 mmol) in EtO₂ (6 mL) dropwise. The reaction was stirred at 0 °C for 2 h. The reaction was carefully quenched with H₂O (1 mL), then aqueous NaOH (10%, 0.5 mL), and finally H₂O (2 mL) and stirred overnight. The reaction was then filtered through celite, and the filtrate was concentrated *in vacuo*. The crude mixture was SiO₂ purified with EtOAc (30-100%) in hexanes to afford a clear oil (0.46 g, 80% yield). ¹H NMR analysis was consistent with that reported previously.²²²



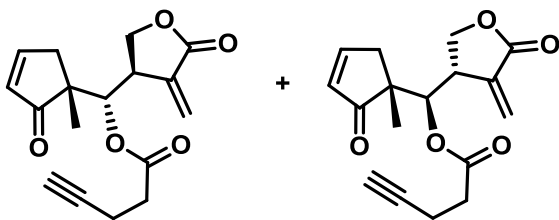
1-Methyl-2-oxocyclopent-3-enecarbaldehyde (**2.4**). The diol product (0.31 g, 2.3 mmol) from above was dissolved in DCM (20 mL) at room temperature and stirred. PCC (1.51 g, 7.03 mmol) was added in 3 equivalent portions over 4 h while stirring. This reaction

was not kept under an inert atmosphere. The reaction was vacuum filtered through celite. The resulting solution was carefully concentrated on a rotary evaporator (no water bath at 150 torr) until only a small amount of solution remained. This solution was introduced onto a silica column (1 in. diameter, 4 in. length) and quickly purified (10% Et₂O in pentanes). The fractions containing the desired compound were collected and concentrated carefully (as described above) to afford a volatile, clear oil **2.4** (0.16 g, 55% yield). *Note: Concentration until no residual solvent is left will result in loss of product and decreased yields; do not use high vacuum to dry product. After isolation, the product was used immediately in the next reaction. If stored at -20° C in DCM the compound degrades in the span of 24 h.* ¹H NMR (CDCl₃): 9.43 (s, 1H), 7.82-7.77 (m, 1H), 6.16-6.12 (m, 1H), 3.37 (dt, *J* = 19.4, 2.5 Hz, 1H), 2.41 (dt, *J* = 19.4, 2.3 Hz, 1H), 1.45 (s, 3H) ppm. ¹³C NMR (CDCl₃): 206.0, 198.1, 164.4, 132.0, 60.6, 37.4, 18.2 ppm. HRMS-ESI⁺ (*m/z*): calc'd [M+H]⁺ for C₇H₈O₂: 125.0597, found 125.0594.



Rac-(*R*)-4-((*S*)-Hydroxy((*R*)-1-methyl-2-oxocyclopent-3-en-1-yl)methyl)-3-methylenedihydrofuran-2(3H)-one (**2.6a***) and *rac*-(*S*)-4-((*R*)-hydroxy((*R*)-1-methyl-2-oxocyclopent-3-en-1-yl)methyl)-3-methylenedihydrofuran-2(3H)-one (**2.6b***). Compounds **2.4** (69 mg, 0.56 mmol) and **2.5**^{213, 216} (55 mg, 0.84 mmol) were combined in a round bottom containing DMF (3 mL) and a stir bar. Activated Zn⁰ (109 mg, 1.68 mmol) was added to the stirring solution. Zn⁰ was freshly activated before each reaction by stirring in aqueous HCl (4M) for 15 min, and then filtered, washed with H₂O (200 mL, 3X), MeOH (200 mL), EtOAc (200 mL), Et₂O (100 mL), and dried under high vacuum for at least 1 h. Aqueous NH₄Cl (sat'd, 1 drop) was added to the solution. The reaction was degassed and backfilled with Ar (g) 3X and then allowed to stir at RT for 16 h. The reaction was quenched with H₂O (15 mL) and extracted with Et₂O (20 mL, 3X) then

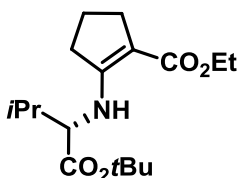
dried over Na₂SO₄, and concentrated *in vacuo* to a crude oil. The crude oil was SiO₂ purified with EtOAc (0 to 70%) in hexanes to give 74 mg (60% yield) of a clear oil containing **2.6a*** and **2.6b*** that was an inseparable mixture of diastereomers. The NMR characterization data for the separated, enantiomerically enriched compounds are below. See the **Section 2.11** for methodology used for enantiopurity analysis of synthesized compounds. For **2.6a***, a modest chiral induction was observed in the Barbier coupling reaction in a 32:68 dr for the resulting esterified, (S)-MTPA analogues by ¹⁹F NMR. For **2.6b***, no chiral induction was observed, as evidenced by the 1:1 er by chiral-HPLC analysis.



Rac-(S)-((R)-1-Methyl-2-oxocyclopent-3-en-1-yl)((R)-4-methylene-5-oxotetrahydrofuran-3-yl)methyl pent-4-ynoate (**2.1a**) and *rac*-(R)-((R)-1-methyl-2-oxocyclopent-3-en-1-yl)((S)-4-methylene-5-oxotetrahydrofuran-3-yl)methyl pent-4-ynoate (**2.1b**) – The previously isolated mixture of **2.6a*** and **2.6b*** (14 mg, 0.06 mmol) were dissolved in DCM (5 mL), then 4-pentynoic acid (12 mg, 0.13 mmol) was added to this solution. 4-DMAP (31 mg, 0.25 mmol) was then added followed by DCC (39 mg, 0.19 mmol). The reaction was heated to 40 °C for 4 h. The reaction was quenched with H₂O (5 mL) and extracted with DCM (10 mL, 3X). The organic layer was dried over Na₂SO₄, filtered, and concentrated *in vacuo* to afford a crude oil. The crude product was SiO₂ purified with EtOAc (0-70%) in hexanes to afford two white solids with an overall yield of 15 mg (80% yield, 1:1 ratio of **2.1a**:**2.1b**). **2.1a**: ¹H NMR (CDCl₃): 7.73-7.68 (m, 1H), 6.38 (s, 1H), 6.19-6.14 (m, 1H), 5.72 (s, 1H), 5.17 (d, *J* = 4.9 Hz, 1H), 4.36 (dd, *J* = 9.5, 7.6 Hz, 1H), 4.27 (dd, *J* = 9.6, 2.8 Hz, 1H), 3.60-3.52 (m, 1H), 2.97 (dt, *J* = 19.0, 2.4 Hz, 1H), 2.49-2.33 (m, 5H), 1.95 (t, *J* = 2.3 Hz, 1H), 1.20 (s, 3H) ppm. ¹³C NMR (CDCl₃):

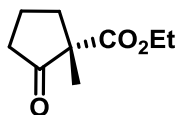
210.1, 170.4, 169.8, 163.2, 134.5, 132.0, 125.4, 82.0, 77.0, 69.9, 69.3, 49.8, 40.8, 40.2, 33.2, 20.3, 14.1 ppm. HRMS-ESI⁺ (m/z): calc'd [M+H]⁺ for C₁₈H₂₀O₃: 303.1227, found 303.1222.

2.1b: ¹H NMR (CDCl₃): 7.76-7.72 (m, 1H), 6.28 (s, 1H), 6.26-6.20 (m, 1H), 5.56 (s, 1H), 5.10 (d, *J* = 6.3 Hz, 1H), 4.30-4.27 (m, 2H), 3.56-3.50 (m, 1H), 2.92 (dt, *J* = 19.8, 2.4 Hz, 1H), 2.54-2.42 (m, 5H), 1.98 (t, *J* = 2.4 Hz, 1H), 1.19 (s, 3H) ppm. ¹³C NMR (CDCl₃): 209.8, 169.9, 168.8, 162.4, 133.5, 132.4, 124.3, 81.0, 76.8, 69.0, 68.5, 48.4, 40.2, 38.5, 32.4, 21.6, 13.2 ppm. HRMS-ESI⁺ (m/z): calc'd [M+H]⁺ for C₁₈H₂₀O₃: 303.1227, found 303.1222.

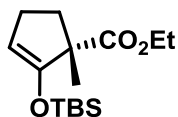


(S)-2-((1-(*tert*-Butoxy)-3-methyl-1-oxobutan-2-yl)amino)cyclopent-1-ene-1-carboxylate (**2.8**) – The synthetic procedure was adapted from that previously reported.²¹⁷ To remove the salt of L-valine *tert*-butyl ester hydrochloride, the material was dissolved in EtOAc (100 mL), and aqueous NaOH (0.5 M, 100 mL) was added and stirred for 10 minutes. The material was extracted with EtOAc (100 mL, 3X), washed with brine (15 mL, 1X), dried over Na₂SO₄, concentrated *in vacuo* to a clear oil, and then immediately used. To a stirred solution of **2.7** (2.99 g, 19.1 mmol) and L-valine *tert*-butyl ester (4.31 g, 24.9 mmol) in benzene (50 mL) was added BF₃·OEt₂ (1.18 mL, 9.55 mmol). The reaction mixture was refluxed with a Dean-Stark trap for 24 h. The reaction was allowed to cool to RT and quenched with aqueous NaHCO₃ (sat'd, 50 mL) and then extracted with Et₂O (50 mL, 3X), washed with brine (10 mL, 1X), and dried over Na₂SO₄. The organic layer was concentrated *in vacuo*. The crude product was SiO₂ purified with EtOAc (0-5%) in hexanes to afford **2.8** (4.46 g, 75%) as a white solid. ¹H NMR (500 MHz): 7.63 (bs, 1H), 4.22-2.11 (m, 2H), 3.64 (dd, *J* = 10.0, 5.5 Hz, 1H), 2.52 (t, *J* = 7.1 Hz, 2H), 2.47 (t, *J* = 7.6 Hz, 2H), 2.17-2.06 (m, 1H), 1.81 (p, *J* = 7.4 Hz, 2H), 1.46 (s, 9H), 1.27 (t, *J* = 7.1 Hz,

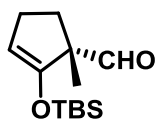
3H), 0.98 (app t, 6H) ppm. ^{13}C NMR (125 MHz): 171.3, 168.2, 163.1, 94.7, 81.6, 63.9, 58.6, 32.3, 31.8, 29.3, 28.0, 20.9, 19.2, 17.8, 14.8. HRMS-ESI⁺ (m/z): calc'd $[\text{M}+\text{H}]^+$ for $\text{C}_{17}\text{H}_{29}\text{NO}_4$: 312.2169, found 312.2163.



Ethyl (S)-1-methyl-2-oxocyclopentane-1-carboxylate ((S)-2.2). Stereoselective methylation was adapted from that previously reported.²¹⁷ n-BuLi in hexanes (2.0 M solution, 3.56 mL, 7.13 mmol) was added to a solution of DIPA (1.00 mL, 7.13 mmol) at $-78\text{ }^\circ\text{C}$ in anhydrous toluene (30 mL) and the reaction was warmed to $0\text{ }^\circ\text{C}$ and stirred for 30 min. The reaction mixture was cooled to $-78\text{ }^\circ\text{C}$ and **2.8** (1.85 g, 5.94 mmol) in anhydrous toluene (10 mL) was added dropwise and stirred for 1 h. THF (0.96 mL, 11 mmol) was added to the reaction and stirred for 2 h. MeI (1.85 mL, 29.7 mmol) was added and the reaction was stirred at $-78\text{ }^\circ\text{C}$ for 16 hours. The reaction was then quenched with aqueous NH_4Cl (sat'd, 50 mL) and extracted with Et_2O (30 mL, 3X), washed with brine (15 mL, 1X), dried over Na_2SO_4 , and concentrated *in vacuo*. The crude products were then dissolved in THF (50 mL) and aqueous HCl (3M, 50 mL) was added and stirred at RT for 6 hours. The reaction was extracted with Et_2O (50 mL, 3X), washed with water (10 mL, 1X), then brine (15 mL, 1X), and dried over Na_2SO_4 . The solvent was concentrated *in vacuo*. The crude mixture was SiO_2 purified with EtOAc (0%-20%) in hexanes to afford (S)-2.2 as a colorless oil (0.54 g, 53%, 93:7 er by chiral-GCMS). NMR characterization was consistent with previously reported data for this compound.^{214a}

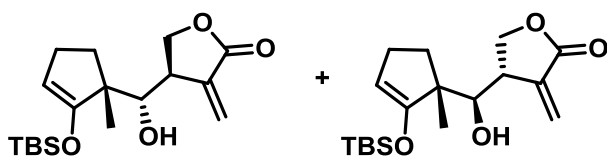


Ethyl (S)-2-((*tert*-butyldimethylsilyl)oxy)-1-methylcyclopent-2-ene-1-carboxylate. LiHMDS solution in THF (1 M solution, 4.20 mL, 4.19 mmol) was added to anhydrous THF (30 mL) at -78 °C. Next, a solution of **2.9** (0.59 g, 3.5 mmol) in THF (5 mL) was added dropwise and stirred for 1 hr at -78 °C. A solution of TBSCl (1.05 g, 6.98 mmol) in THF (10 mL) was then added dropwise at -78 °C and then the reaction was allowed to slowly come to RT and stirred for 16 h. The reaction mixture was quenched with aqueous NH_4Cl (sat'd, 30 mL) and extracted with Et_2O (30 mL, 3X). The organic layer was washed with brine (15 mL, 1X), and dried over Na_2SO_4 , and concentrated *in vacuo*. The crude material was SiO_2 purified with EtOAc (0 to 10%) in hexanes, resulting in a clear oil (0.78 g, 79% yield). ^1H NMR (500 MHz): 4.61 (t, $J = 2.2$ Hz, 1H), 4.12 (q, $J = 7.2$ Hz, 2H), 2.40-2.29 (m, 2H) 2.29-2.19 (m, 1H), 1.77-1.67 (m, 1H), 1.72 (m, 1H), 1.30 (s, 3H), 1.24 (t, $J = 7.1$ Hz, 3H), 0.90 (s, 9H), 0.16 (s, 3H), 0.15 (s, 3H). ^{13}C NMR (125 MHz): 176.1, 156.2, 101.2, 60.5, 54.3, 35.3, 26.2, 25.5, 21.3, 18.0, 14.2, -5.0, -5.2 ppm. HRMS-ESI⁺ (m/z): calc'd $[\text{M}+\text{H}]^+$ for $\text{C}_{15}\text{H}_{28}\text{O}_3\text{Si}$: 285.1881, found 285.1883.



(S)-2-((*tert*-Butyldimethylsilyl)oxy)-1-methylcyclopent-2-enecarbaldehyde (**2.9**). To a solution of anhydrous DCM (20 mL) was added the silyl enol ether from the above reaction (0.91 g, 3.19 mmol) and the resulting solution was cooled to -78 °C. A solution of DIBAL-H in DCM (1M, 3.19 mL, 3.19 mmol) was added dropwise to the reaction mixture and stirred for 4 h at -78 °C. The reaction was then carefully quenched with H_2O (1 mL), aqueous NaOH (0.5M, ~0.1 mL) was added, and then an additional aliquot of H_2O (1 mL). The reaction was gravity filtered through qualitative filter paper, washed with brine (10 mL, 1X), dried over Na_2SO_4 , and concentrated *in vacuo*. The crude

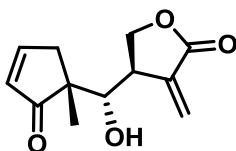
product was SiO₂ purified with EtOAc (0-5%) in hexanes to afford a clear oil (0.29 g, 38% yield). ¹H NMR (500 MHz): 9.53 (s, 1H), 4.75 (t, *J* = 2.3 Hz, 1H), 2.34-2.25 (m, 3H), 1.72 – 1.60 (m, 1H), 1.20 (s, 3H), 0.90 (s, 9H), 0.17 (s, 3H), 0.15 (s, 3H) ppm. ¹³C NMR (125 MHz): 202.5, 154.2, 103.2, 59.3, 30.7, 26.0, , 25.5, 18.0, 17.6, -4.9, -5.0; impurities at 25.7, -3.6 ppm. HRMS-ESI⁺ (*m/z*): calc'd [M+H]⁺ for C₁₃H₂₄O₂Si: 241.1618, found 241.1616.



(*R*)-4-((*S*)-((*R*)-2-((*tert*-Butyldimethylsilyl)oxy)-1-methylcyclopent-2-en-1-yl)(hydroxy)methyl)-3-methylenedihydrofuran-2(3H)-one (**2.10a**) and (*S*)-4-((*R*)-((*R*)-2-((*tert*-Butyldimethylsilyl)oxy)-1-methylcyclopent-2-en-1-yl)(hydroxy)methyl)-3-methylenedihydrofuran-2(3H)-one (**2.10b**). To a solution of DMF (3 mL), **2.9** (0.29 g, 1.2 mmol) and **2.5**^{213, 216} (0.32 g, 1.8 mmol) was added powdered Zn⁰ (0.32 g, 4.8 mmol, activated as described for **2.6a***/**2.6b***). Aqueous NH₄Cl (sat'd, one drop) was added and the reaction was degassed and backfilled with Ar (g) (3X). The reaction was then stirred at RT for 16 h. The reaction mixture was quenched with H₂O (15 mL) and extracted with Et₂O (15 mL, 3X). The organic layer was washed with H₂O (10 mL, 1X) and then brine (10mL, 1X). The subsequent organic layer was dried over Na₂SO₄ and concentrated *in vacuo*. The crude mixture was SiO₂ purified with an isocratic eluent system EtOAc (20%) in hexanes to afford the separated diastereomers **2.10a** and **2.10b** as white solids (0.41 g, 64% yield, 1:1 dr) *Note: 2.10a/2.10b will polymerize when concentrated and/or the silyl enol ether will be deprotected if allowed to sit at RT as a solid for an extended period of time. To avoid this, do not dry under high vacuum, and after concentration with a low vacuum pump immediately take 2.10a and 2.10b on to the next reaction.* **2.10a**: ¹H NMR (500 MHz): 6.42 (d, *J* = 1.6 Hz, 1H), 5.91 (d, *J* = 1.0 Hz, 1H), 4.66 (t, *J* = 2.4 Hz, 1H),

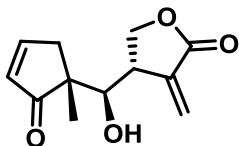
4.22 (dd, $J = 9.2, 4.1$ Hz, 1H), 4.22 (dd, $J = 9.2, 4.1$ Hz, 1H), 3.62 (dd, $J = 6.6, 4.1$ Hz, 1H), 3.29-3.22 (m, 1H), 2.27-2.19 (m, 2H), 2.17-2.08 (m, 1H), 2.0 (d, $J = 4.2$ Hz, 1H), 1.62-1.51 (m, 1H), 1.10 (s, 3H), 0.93 (s, 9H), 0.20 (s, 3H), 0.17 (s, 3H) ppm. ^{13}C NMR (125 MHz): 170.8, 156.9, 135.0, 126.2, 102.0, 76.1, 70.3, 51.9, 41.3, 31.1, 25.7, 25.4, 21.8, 18.0, -4.6, -5.3 ppm. HRMS-ESI⁺ (m/z): calc'd $[\text{M}+\text{H}]^+$ for $\text{C}_{18}\text{H}_{30}\text{O}_4\text{Si}$: 339.1986, found 339.1982.

2.10b: ^1H NMR (500 MHz): 6.40 (d, $J = 1.1$ Hz, 1H), 6.01 (s, 1H), 4.62 (t, $J = 2.3$ Hz, 1H), 4.24 (dd, $J = 9.4, 3.1$ Hz, 1H), 4.24 (dd, $J = 9.4, 5.3$ Hz, 1H), 3.64 (dd, $J = 8.6, 3.7$ Hz, 1H), 3.23 – 3.16 (m, 1H), 2.51 (d, $J = 3.7$ Hz, 1H), 2.30–2.12 (m, 2H), 2.07–1.99 (m, 1H), 1.63–1.55 (m, 1H), 1.20 (s, 3H), 0.94 (s, 9H), 0.22 (s, 3H), 0.18 (s, 3H) ppm. ^{13}C NMR 170.9, 157.4, 135.7, 126.0, 101.9, 77.4, 68.9, 51.3, 42.4, 30.7, 25.8, 25.6, 22.7, 18.0, -4.4, -5.5 (125 MHz). HRMS-ESI⁺ (m/z): calc'd $[\text{M}+\text{H}]^+$ for $\text{C}_{18}\text{H}_{30}\text{O}_4\text{Si}$: 339.1986, found 339.1978.

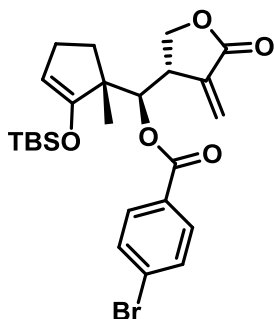


(R)-4-((S)-Hydroxy((R)-1-methyl-2-oxocyclopent-3-en-1-yl)methyl)-3-methylenedihydrofuran-2(3H)-one (**2.6a**). **2.10a** (22 mg, 0.074 mmol) was dissolved in DMSO (2 mL) and $\text{Pd}(\text{OAc})_2$ (7.0 mg, 0.013 mmol) was added. The reaction was placed under 1 atm of O_2 (g) and stirred at RT for 24 h. The reaction mixture was quenched with H_2O (10 mL) and extracted with Et_2O (15 mL, 3X). The organic layer was washed with H_2O (10 mL, 1X), then brine (10mL, 1X), dried over Na_2SO_4 , and concentrated *in vacuo*. The crude mixture was SiO_2 purified with EtOAc (0-80%) in hexanes to afford **2.6a** (10 mg, 46% yield, 93:7 er), as a clear oil. ^1H NMR (500 MHz): 7.78–7.72 (m, 1H), 6.46 (d, $J = 2.1$ Hz, 1H), 6.20–6.16 (m, 1H), 5.81 (d, $J = 1.9$ Hz, 1H), 4.43 (dd, $J = 9.4, 7.7$ Hz, 1H), 4.24 (dd, $J = 9.4, 3.1$ Hz, 1H), 3.97 (d, $J = 5.7$ Hz, 1H), 3.35–3.29 (m, 1H), 3.10 (app dt, $J = 18.9, 2.5$ Hz, 1H), 2.35 (app dt, $J = 18.9, 2.8$ Hz, 1H), 1.14 (s, 3H) ppm. ^{13}C

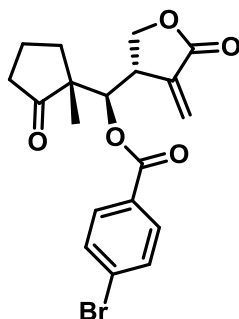
NMR (125 MHz): 213.0, 170.3, 164.3, 134.6, 132.0, 126.3, 75.9, 69.9, 51.4, 41.4, 39.5, 21.1 ppm. HRMS-ESI⁺ (m/z): calc'd [M+H]⁺ for C₁₂H₁₄O₄: 223.0965, found 223.0963.



(S)-4-((R)-Hydroxy((R)-1-methyl-2-oxocyclopent-3-en-1-yl)methyl)-3-methylenedihydrofuran-2(3H)-one (**2.6b**). **2.10b** (12 mg, 0.04 mmol) was dissolved in DMSO (2 mL) and Pd(OAc)₂ (1.00 mg, 0.004 mmol) was added. The reaction was placed under 1 atm of O₂ (g) and stirred at RT for 24 h. The reaction mixture was quenched with H₂O (10 mL) and extracted with Et₂O (15 mL, 3X). The organic layer was washed with H₂O (10 mL, 1X) and then brine (10 mL, 1X). The subsequent organic layer was dried over Na₂SO₄ and concentrated *in vacuo*. The crude mixture was SiO₂ purified with EtOAc (0-80%) in hexanes to afford **2.6b** (4.0 mg, 56% yield, 91:9 er) as a clear oil. ¹H NMR (500 MHz): 7.77–7.73 (m, 1H), 6.39 (d, *J* = 2.7 Hz, 1H), 6.24–6.16 (m, 1H), 5.98 (d, *J* = 2.3 Hz, 1H), 4.32–4.23 (m, 1H), 4.15 (dd, *J* = 9.4, 5.2 Hz, 1H), 3.77 (dd, *J* = 7.9, 2.6 Hz, 1H), 3.45 (d, *J* = 2.8 Hz, 1H), 3.41–3.32 (m, 1H), 2.87 (dt, *J* = 19.5, 2.5 Hz, 1H), 2.44 (dt, *J* = 19.4, 2.4 Hz, 1H), 1.26 (s, 3H). ¹³C NMR (125 MHz): 213.8, 170.4, 163.8, 134.9, 132.7, 126.4, 75.4, 68.5, 49.9, 42.0, 41.1, 20.8 ppm. HRMS-ESI⁺ (m/z): calc'd [M+H]⁺ for C₁₂H₁₄O₄: 223.0965, found 223.0963.



Rac-(*R*)-((*R*)-2-((*tert*-Butyldimethylsilyl)oxy)-1-methylcyclopent-2-en-1-yl)((*S*)-4-methylene-5-oxotetrahydrofuran-3-yl)methyl 4-bromobenzoate. **2.10b** (0.150 g, 0.443 mmol) was dissolved in DCM (4 mL). Next 4-DMAP (0.325 g, 2.66 mmol) and 4-bromobenzoic acid (0.445 g, 2.22 mmol) was added, followed by DCC (0.457 g, 2.22 mmol). The reaction was heated to 40 °C for 16 h. The reaction was allowed to cool to RT and quenched with H₂O (5 mL). The mixture was extracted with DCM (20 mL, 3X). The organic layer was dried over Na₂SO₄ and concentrated *in vacuo*. The crude reaction product was SiO₂ purified with EtOAc (0-20%) in hexanes. The reaction afforded 0.180 g (99% yield) of a white solid. ¹H NMR (500 MHz): 7.89-7.82 (m, 2H), 7.63-7.56 (m, 2H), 6.12 (d, *J* = 2.5 Hz, 1H), 5.51 (d, *J* = 2.1 Hz, 1H), 5.11 (d, *J* = 7.5 Hz, 1H), 4.71 (t, *J* = 2.3 Hz, 1H), 4.46 (dd, *J* = 9.5, 3.8 Hz, 1H), 4.34 (dd, *J* = 9.5, 7.9 Hz, 1H), 3.50–3.41 (m, 1H), 2.38-2.21 (m, 3H), 1.84-1.74 (m, 1H), 1.14 (s, 3H), 0.96 (s, 9H), 0.23 (s, 3H), 0.19 (s, 3H) ppm. ¹³C NMR (125 MHz): 170.1, 165.1, 155.8, 134.9, 132.0, 131.0, 128.7, 128.5, 125.2, 102.8, 79.5, 69.7, 51.5, 40.3, 30.5, 26.1, 25.7, 24.3, 18.1, 4.4, 5.4, impurity at 53.4 ppm. HRMS-ESI⁺ (*m/z*): calc'd [M+H]⁺ for C₂₅H₃₃BrO₅Si: 521.1353, found 521.1331.



Rac-(*R*)-((*R*)-1-Methyl-2-oxocyclopentyl)((*S*)-4-methylene-5-oxotetrahydrofuran-3-yl)methyl 4-bromobenzoate (**2.11**) –The 4-bromo benzoate silyl enol ether (0.180 g, 0.035 mmol) from the previous reaction was dissolved in DCM (2 mL) and TFA (200 μ L) was added to the reaction at RT. The reaction was stirred for 1 h, then quenched with aqueous NaHCO₃ (sat'd, 10 mL) and extracted with DCM (10 mL, 3X). The organic layer was dried over Na₂SO₄ and concentrated *in vacuo*. The crude product was SiO₂ purified with EtOAc (0-40%) in hexanes to afford a white solid (0.100 g, 53% yield). ¹H NMR (500 MHz): 7.83-7.4 (m, 2H), 7.62-7.54 (m, 2H), 6.14 (d, *J* = 2.4 Hz, 1H), 5.53 (d, *J* = 1.7 Hz, 1H), 5.19 (d, *J* = 6.7 Hz, 1H), 4.47-4.35 (m, 2H), 3.87-3.81 (m, 1H), 2.52-2.42 (m, 1H), 2.33-2.21 (m, 1H), 2.15-2.07 (m, 1H), 2.05-1.88 (m, 3H), 1.17 (s, 3H) ppm. ¹³C NMR (125 MHz): 220.0, 169.7, 164.8, 134.2, 132.1, 131.0, 128.9, 128.1, 126.0, 78.5, 69.8, 51.4, 39.9, 38.8, 34.2, 20.2, 18.6 ppm. HRMS-ESI⁺ (*m/z*): calc'd [M+H]⁺ for C₁₉H₁₉BrO₅: 407.0489, found 407.0471.

Cell Culture

All cell lines were maintained in a humidified 5% CO₂ environment at 37 °C in tissue culture flasks (Corning) under normoxic conditions. Adherent cells were dissociated using Trypsin-EDTA solution (0.25%, Gibco). A549-NF- κ B luciferase cells were cultured in DMEM media supplemented with 10% v/v FBS, penicillin (100 I.U./mL), streptomycin (100 μ g/mL), and hygromycin (plasmid selection reagent, 100 μ g/mL).²¹⁹ HeLa were cultured in MEM media (Cellgro) supplemented with 10% FBS (Gibco), penicillin (100 I.U./mL, ATCC), and streptomycin (100 μ g/mL, ATCC).

A549-Luciferase NF- κ B reporter assay

The NF- κ B-luciferase assay in stably transfected A549 cells was conducted according to a previously described protocol.²¹⁹ The protocol for this assay is as follows: A549-NF- κ B luciferase cells (Panomics, RC0002) were seeded (5,000 cells/mL) with cell culture media (50 μ L/well) in 96-well white plates with clear bottoms for measurement of luminescence signal. In parallel, 96-well clear plate with flat-bottoms were seeded at the same density and volume to determine cell viability. Cells were seeded 16-24 h prior to running the assay. Media used in this assay did not contain hygromycin (luciferase gene selection reagent). Compounds were serially diluted in cell culture media and cells were treated with compound or blank media containing 1 v/v % DMSO (50 μ L, total volume in wells equals 100 μ L). Media used for serial dilutions contained 1 v/v % DMSO with the exception of the first 1:100 dilutions from DMSO stock solutions. This was done to maintain the same DMSO concentration across all treated and control wells (0.5 v/v %).

After treating cells with compound for 30 min, TNF- α diluted in 1X PBS was added to wells treated with compound and the induced control wells without compound (10 μ L, 15 ng/mL final concentration). The non-induced control wells and wells without cells received 1X PBS (10 μ L). Cells were incubated for 7 h at 37 °C under normoxic conditions in a cell incubator. AlamarBlue™ (Invitrogen) was added to plates used for measuring cell viability 2-3 h prior to measuring luciferase activity. After 7 h, Bright-Glo luciferin reagent (Promega) was added to each well (100 μ L) and luminescence was immediately measured using a BioTek Synergy H1 microplate reader. Cell viability was obtained by measuring absorbance (560 nm) using the same plate reader. Measuring AlamarBlue™ at 560 nm yields a quantitative measure of cell viability by evaluating the ability of metabolically active cells (which are proportional to the number of living cells) to convert resorufin (non-fluorescent dye) to red-fluorescent resorufin. Background luminescence from reagents (no cell controls) were subtracted from all other wells. All luminescence signal was normalized to the induced, no compound control wells after background subtraction. The same calculations were completed for cell viability measurements. Each experiment was performed in at least biological triplicate with three

technical replicates per experiment. Mean activity values were obtained by averaging biological replicates and standard errors were calculated by propagating standard deviations from each biological replicate. Statistical analysis was performed using Microsoft Excel and GraphPad Prism (v. 5.0).

Labeling in HeLa Cell Culture

HeLa cells were grown to 90% confluency in a 75 cm² culture flask. The culture flasks were dosed with the respective probe concentrations or a DMSO control and incubated for 1 h at 37 °C under normoxic conditions. The cells were detached with non-enzymatic cell dissociation solution (Life Technologies) and washed with cold 1X PBS buffer (10 mL, 3X). The cells were pelleted after each suspension for five minutes at 1000 rpm. After the last wash the cells were suspended in cold 1X PBS buffer (1 mL) containing Complete EDTA-Free Protease Cocktail (Promega). The cells were lysed via sonication with a Vibra Cell VCX 750 (750 W, 20 kHz, 120 V) at 40% power for 30 seconds, while on ice. The lysates were stored at –80 °C until further use.

Lysate was allowed to thaw and kept on ice. The protein concentration was measured via BCA analysis (Pierce BCA Protein Assay Kit, Thermo Scientific) and all lysates were normalized to the sample with the lowest concentration. Click reagents were added to each sample (1 μL CuSO₄, 100 mM stock in ddH₂O; 1 μL TBTA, 20 mM stock in DMSO; 0.5 μL TAMRA-N₃²²³, 40 mM stock in DMSO; 2 μL TCEP, 100 mM in ddH₂O) and allowed to react for 3 h at room temperature. LDS 4X Sample Buffer (8 μL, NuPAGE) and of 10X Sample Reducing Agent (2 μL, NuPAGE) was then added to each sample and heated to 90 °C for five minutes before being pipetted into a 15-well NuPAGE Novex 4-12% polyacrylamide bis-tris gel and separated with electrophoresis (180V, 54 min) in NuPAGE MES SDS running buffer (1X). Gels were imaged using a TyphoonFLA7000 gel imager (General Electric). Images were analyzed using ImageQuant TL v7.0 software.

Pulldown Experiments

HeLa cells were allowed to grow to 90% confluency in a 150 cm² flask under normoxic conditions at 37 °C in a humidified CO₂ incubator. The media was replaced with 20 mL of fresh media and the competition compounds **2.6a**, **2.6b**, or a DMSO control was dosed to achieve the final concentration (50 μM, DMSO concentration <0.05%) in each flask and incubated for 20 min. Alkyne probes **2.1a** or **2.1b** were dosed at 50 μM and incubated for an additional 30 min. After incubation, the media was removed and the cells were washed with cold 1X PBS (10 mL). The cells were then dissociated from the flask using non-enzymatic dissociation media (4 mL, Life Technologies). The cells were collected in 1X PBS (8 mL) and centrifuged (1000 rpm, 5 min, RT) in a conical tube. The cells were washed with cold 1X PBS (10 mL) and centrifuged again. The cells were then taken up in 1X PBS (2.5 mL) containing protease inhibitor (Complete EDTA-free protease inhibitor cocktail, Life Technologies). The cells were lysed via sonication with a Vibra Cell VCX 750 (750 W, 20 kHz, 120 V) at 40% power for 30 seconds, while on ice. The lysates were stored at -80 °C until further use.

After thawing, the samples were centrifuged at 4000 RPM for 20 min at 0 °C to clear the lysate. The samples were transferred to clean conical tubes and 200 μL of 10 w/v% SDS in ddH₂O were added and heated to 65 °C for 10 minutes. The protein concentration of each sample was measured via BCA analysis (Pierce BCA Protein Assay Kit, Thermo Scientific) and all lysates were normalized to the sample with the lowest concentration (between 1.0 to 1.6 mg/mL). Click reagents were added (10 μL CuSO₄, 100 mM stock in ddH₂O; 20 μL TBTA, 20 mM stock in DMSO; 20 μL Biotin-N₃, 20 mM stock in DMSO [Sigma-Aldrich 762024; CAS: 875770-34-6]; 10 μL TCEP, 100 mM in ddH₂O) and allowed to react for 3 h at room temperature. After incubation 15 μL of each sample was collected and saved for the input lysate control.

The samples were then separated on a monomeric avidin column according to the manufacturer's instructions (Pierce) at 4 °C. The biotinylated samples were eluted using the regeneration buffer (0.1 M HCl glycine buffer, pH 2.8) *Note: biotinylated samples did not elute using the elution biotin buffer.* After the samples are collected they were

concentrated using a 10 kDa molecular weight cut-off filter (Amicon) and diluted with ddH₂O (20 mL, 2X) and then finally concentrated to ~500 μL. The samples were collected and concentrated to dryness in a SpeedVac for 10 h at RT. These samples were then dissolved in ddH₂O (20 μL), 10X reducing agent (2 μL, NuPAGE), and 4X sample buffer (10 μL, NuPAGE) and vortexed. Sample buffer and reducing agent was added to the input lysates in the same fashion and all samples were heated to 90 °C for five minutes before pipetting 15 μL of each sample into a 15-well NuPAGE Novex 4-12% polyacrylamide bis-tris gel and separated with electrophoresis (180V, 54 min) in NuPAGE MES SDS running buffer (1X). The samples were separated and transferred (30 V, 1 h, RT) in 1X TBE buffer to a PVDF membrane (Immobilon-FL) for Western blot analysis. Membranes were incubated with the respective primary antibodies (p65, Santa Cruz, sc-372; p50, Santa Cruz sc-8414; IκB, Santa Cruz sc-371; IKKα/β, Santa Cruz sc-7607) with a 1:1,000 dilution in 0.5% non-fat milk (BioRad) in 1X PBS (10 mL) overnight at 4 °C. Secondary HRP-conjugated antibodies (anti-rabbit poly-HRP, Pierce cat # 32260; secondary anti-mouse, Novex HRP cat # A16072) were added to 0.5% non-fat milk (BioRad) in 1X PBS (10 mL) at a 1:5,000 dilution for 1 h at RT. Membranes were washed in ddH₂O between each incubation (30 mL for 1 min, 5X). Super Signal West Dura Extended Duration Luminol/Enhancer Solution (1 mL) and Stable Peroxide Buffer (1 mL) were added to the top of the membrane and imaged with a Li-COR Odyssey Fc imaging system. After each antibody was detected the membrane was stripped with Restore PLUS Western Blot Stripping Buffer (Thermo), washed with ddH₂O for 30 min, and blocked over night at 4 °C in 0.5% w/v non-fat dry milk (BioRad) in 1X PBS before incubating with the next antibody.

Labeling Recombinant Human p65

Recombinant human p65 in buffer (this clone has five point mutations compared to the p65 sequence listed under accession no. AAA36408: L159V, P180S, F309S, A439V and V462M, Active Motif) was placed in an Eppendorf tube (3 μL, 100 ng/ μL) with ddH₂O (6 μL) and incubated with 100 μM of helenalin, **2.6a**, **2.6b**, **2.1a**, or **2.1b** for

1 h at RT. LDS 4X Sample Buffer (4 μ L, NuPAGE) and 10X Sample Reducing Agent (1 μ L, NuPAGE) was then added to each sample and heated to 90 °C for five minutes before being pipetted into a 15-well NuPAGE Novex 4-12% polyacrylamide bis-tris gel and run into the top of the gel with electrophoresis (180V, 5 min) in NuPAGE MES SDS running buffer (1X). The top of each well where the protein was located was excised and placed into an Eppendorf tube.

The gel pieces were then processed by in-gel trypsin digestion according to a previously reported protocol.²²⁴ The peptides were desalted using a P10 C₁₈ Zip-Tip (Millipore). Samples were dried with a SpeedVac for 3 h at RT and the dried peptides were dissolved in 95:5 H₂O:MeCN 0.1% formic acid solution (12 μ L) for HPLC-ESI⁺-MS/MS analysis.

HPLC-ESI⁺-MS/MS analyses of tryptic peptides were conducted using an OrbiTrap Fusion mass spectrometer (Thermo Scientific) equipped with a Dionex Ultimate UHPLC pump (Thermo Scientific), a nanospray source, and Xcalibur 3.0.63 software for instrument control. Peptide mixtures were directly injected onto a nanoHPLC column (75 μ m i.d., 10 cm packed bed, 15 μ m orifice) created by hand packing a commercially purchased fused-silica emitter (New Objective) with Zorbax SB-C18 5 μ m separation media (Agilent). The gradient program started from 0-17 min at 2% MeCN:H₂O (1% formic acid) with a flow rate of 0.3 μ L/min, followed by a linear increase to 30% MeCN:H₂O (1% formic acid) from 17-80 min, followed by a linear increase to 80% MeCN:H₂O (1% formic acid) from 80-91 min. Finally, the column was equilibrated with 2% MeCN:H₂O (1% formic acid) from 91-99 min with a flow rate of 0.9 μ L/min. Liquid chromatography was carried out at an ambient temperature. The mass spectrometer was calibrated prior to each analysis, and the spray voltage was adjusted to ensure a stable spray. The MS tune parameters were as follows: spray voltage of 2.460 kV, capillary temperature of 300 °C, and an S-lens RF level of 60%. MS/MS spectra were collected using simultaneous data-dependent scanning and target mass analysis, in which one full scan mass spectrum is acquired in the OrbiTrap detector (R = 120,000, scan range 320-2000 m/z), followed by a target list analyzing masses corresponding to

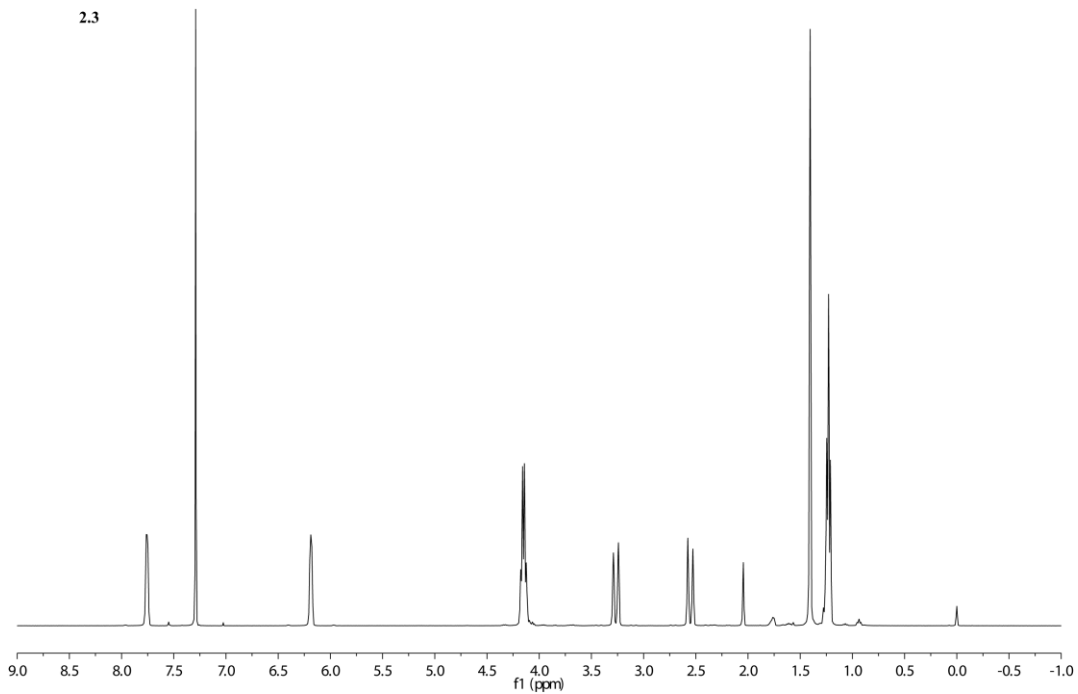
expected theoretical probe-peptide adducts (343.6443, 489.2235, 640.8083, 770.8567, 229.4320, 326.4848, 427.5413, 514.2402, 923.7783, 693.0855, 569.7730, 383.6574, 529.2365, 353.1601, 680.8214, 454.2167 m/z), followed by 12 data-dependent MS/MS spectra acquired with the OrbiTrap detector (R = 15,000) with charge states 2-7, dynamic exclusion after one detection for 20 s, an intensity threshold of 5.0×10^4 , and a mass tolerance of 10.00 ppm. The method uses an isolation width of 1.6 m/z, maximum injection time of 150 ms, 40% HCD collision energy, and 1 AGC microscan. Spectral data were analyzed using Proteomic Discoverer software package (v1.4.0.288, Thermo Fisher). Data was processed using the SEQUEST v.27 algorithm.²²⁵ Peptide spectra were searched against the UniProt Human Protein Database. Helenalin (+262.1205 Da), **2.6a** and **2.6b** (+222.0892), **2.1a** and **2.1b** (+302.3260 Da), and/or cysteine carboxamidomethylation (+57.0215 Da) was set as a dynamic modification. Precursor mass tolerance was set to 10 ppm within the calculated mass, and fragment ion mass tolerance was set to 10 mmu of their monoisotopic mass. Probe-peptide adducts found using the Proteome Discoverer software were further scrutinized by manually extracting the mass using the Xcalibur software from the total ion chromatogram. The MS² fragmentation data were analyzed manually to confirm the identity of probe-peptide adducts.

2.10 Spectral Data

¹H NMR (CDCl₃)



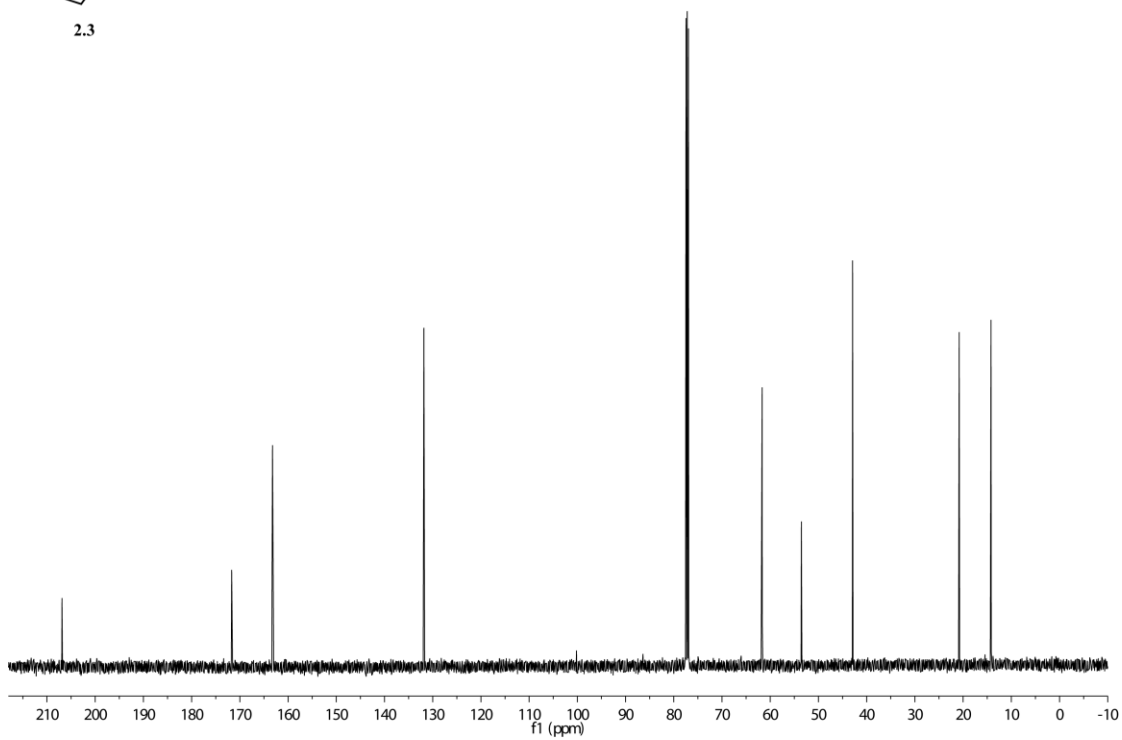
2.3



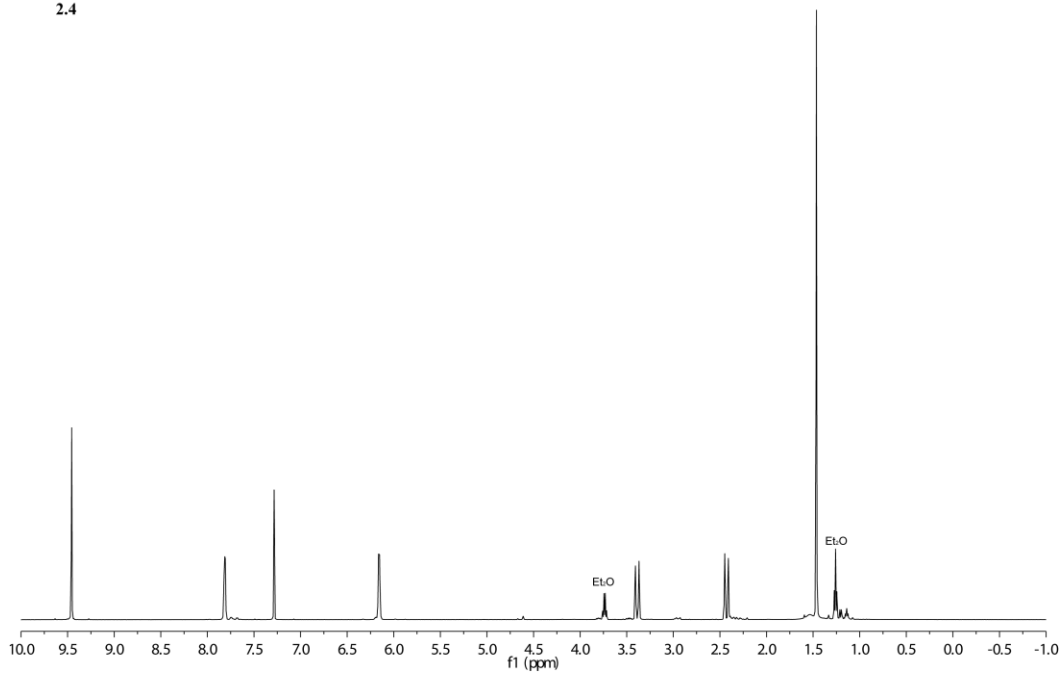
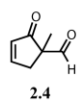
¹³C NMR (CDCl₃)



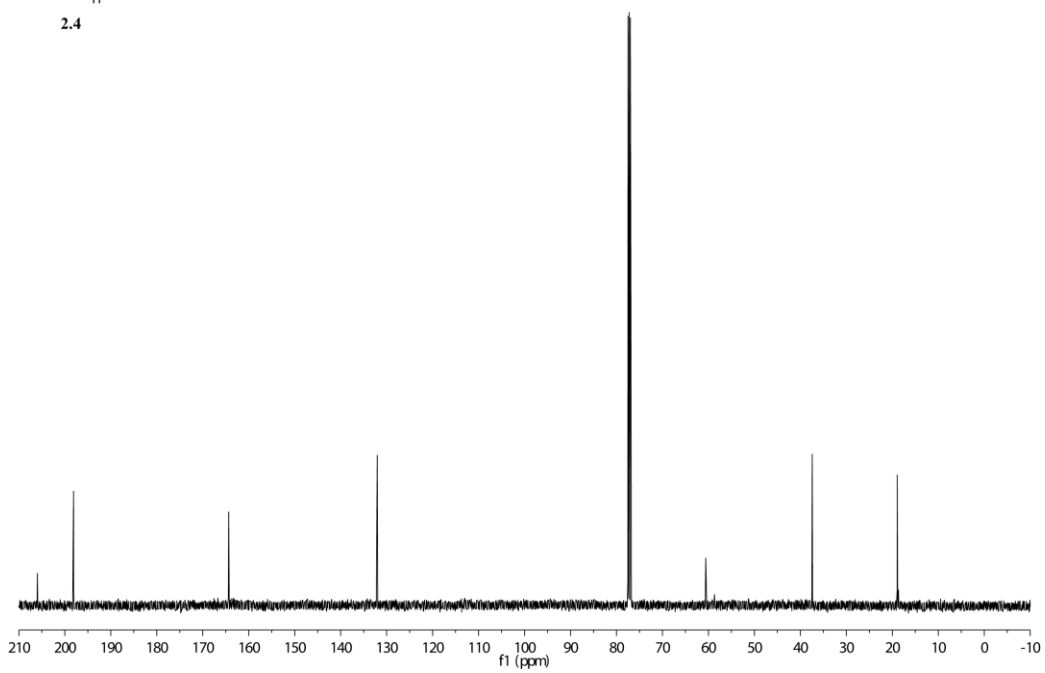
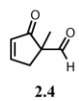
2.3

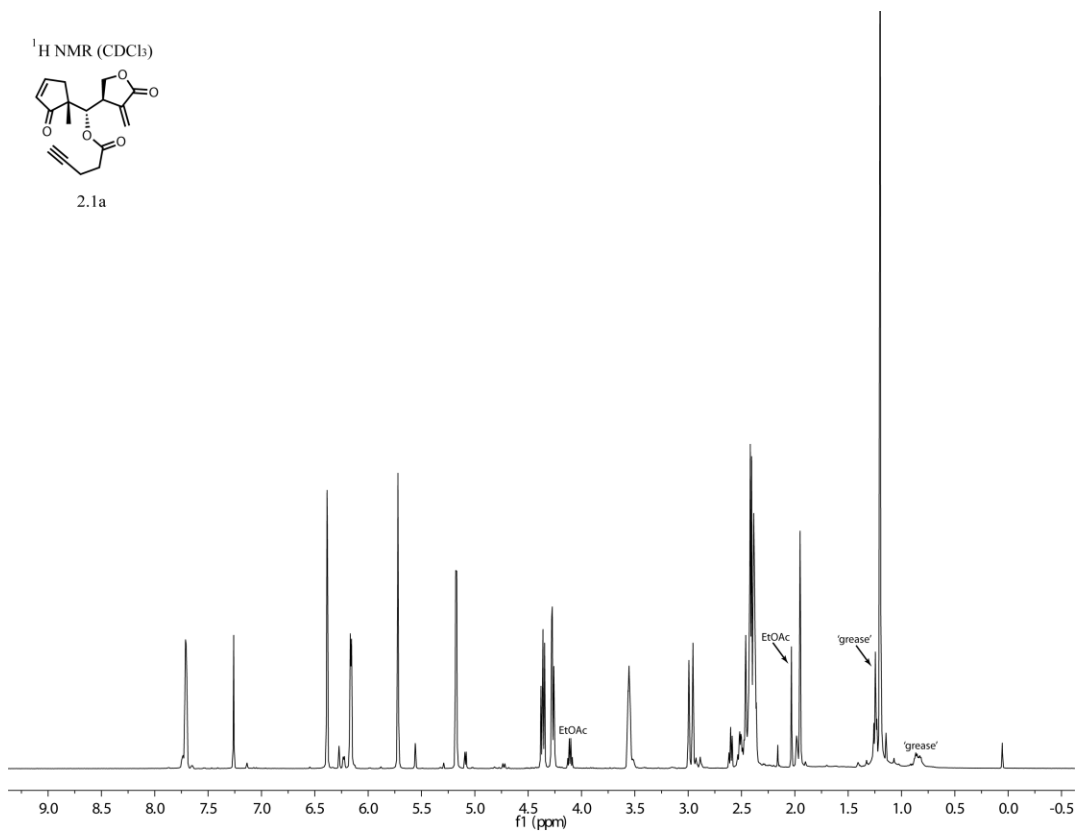
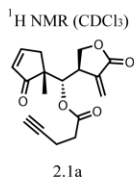


¹H NMR (CDCl₃)

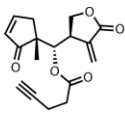


¹³C NMR (CDCl₃)

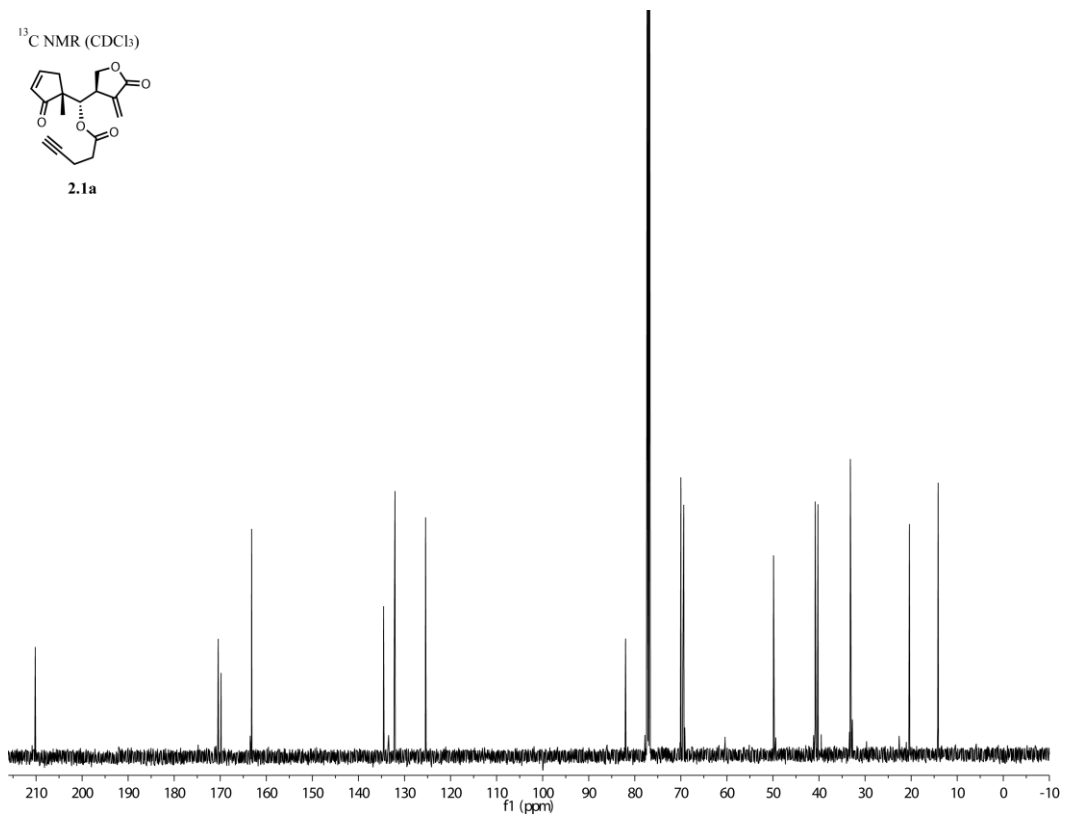




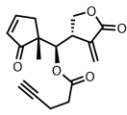
¹³C NMR (CDCl₃)



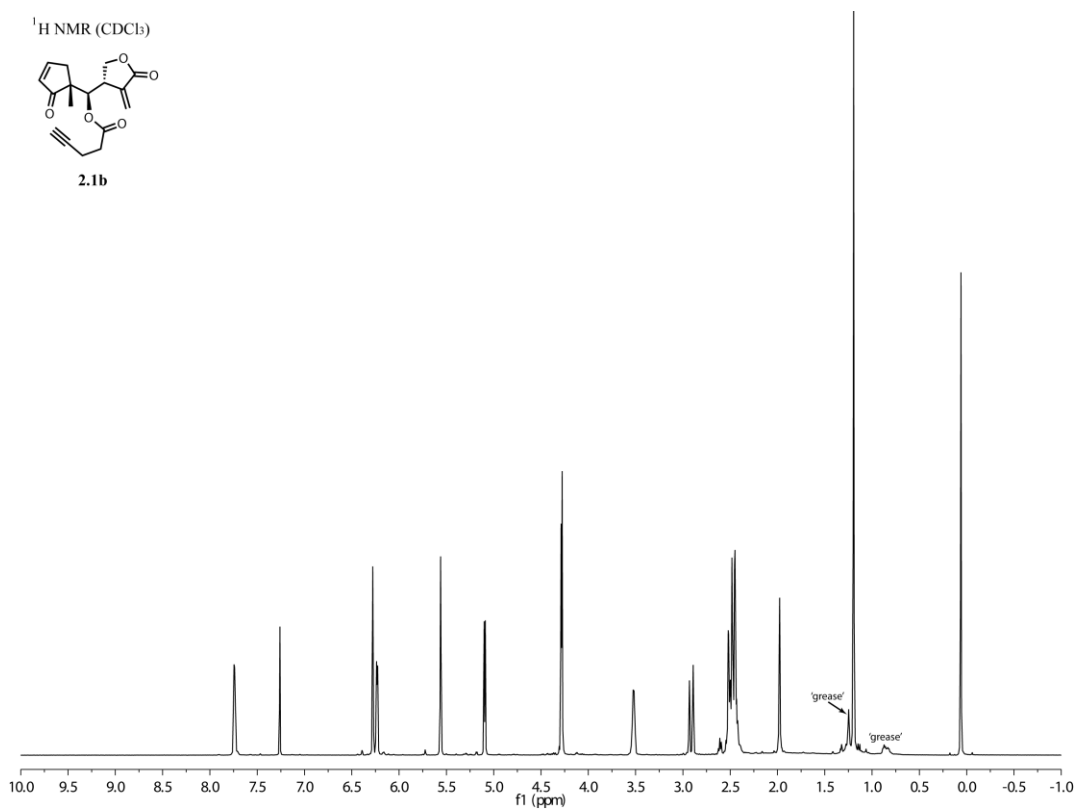
2.1a

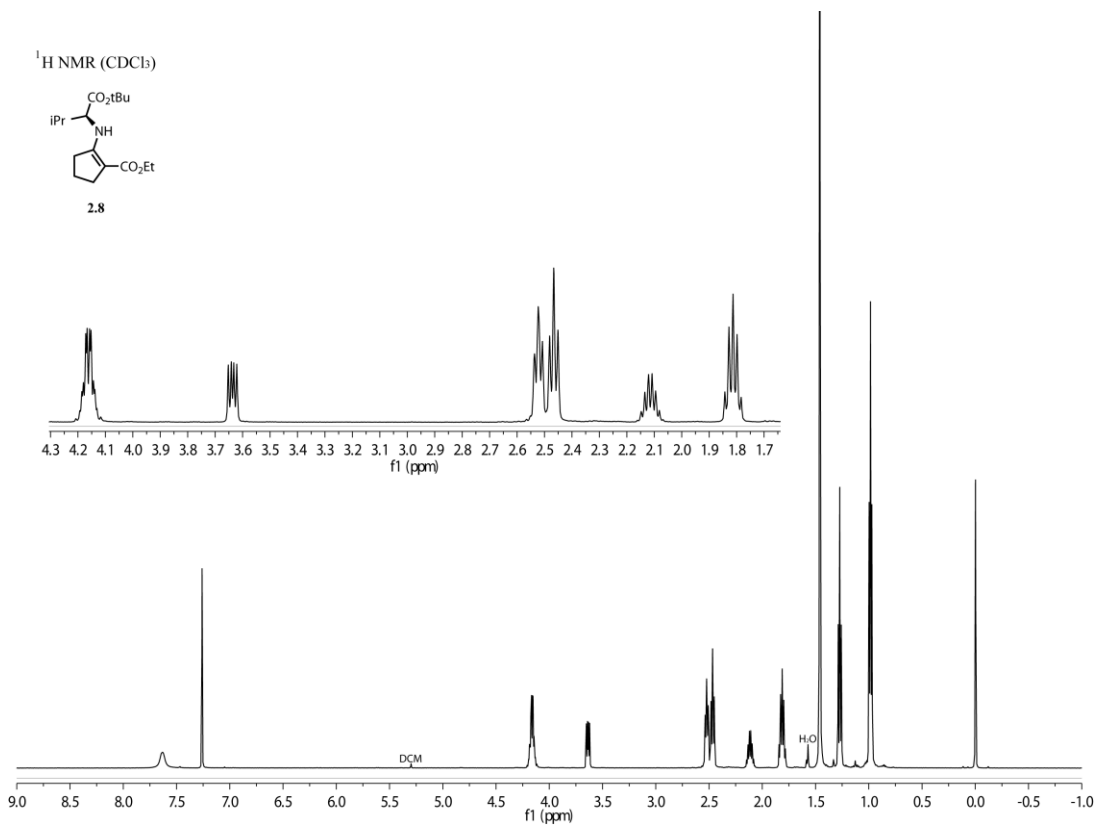
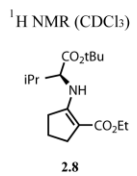
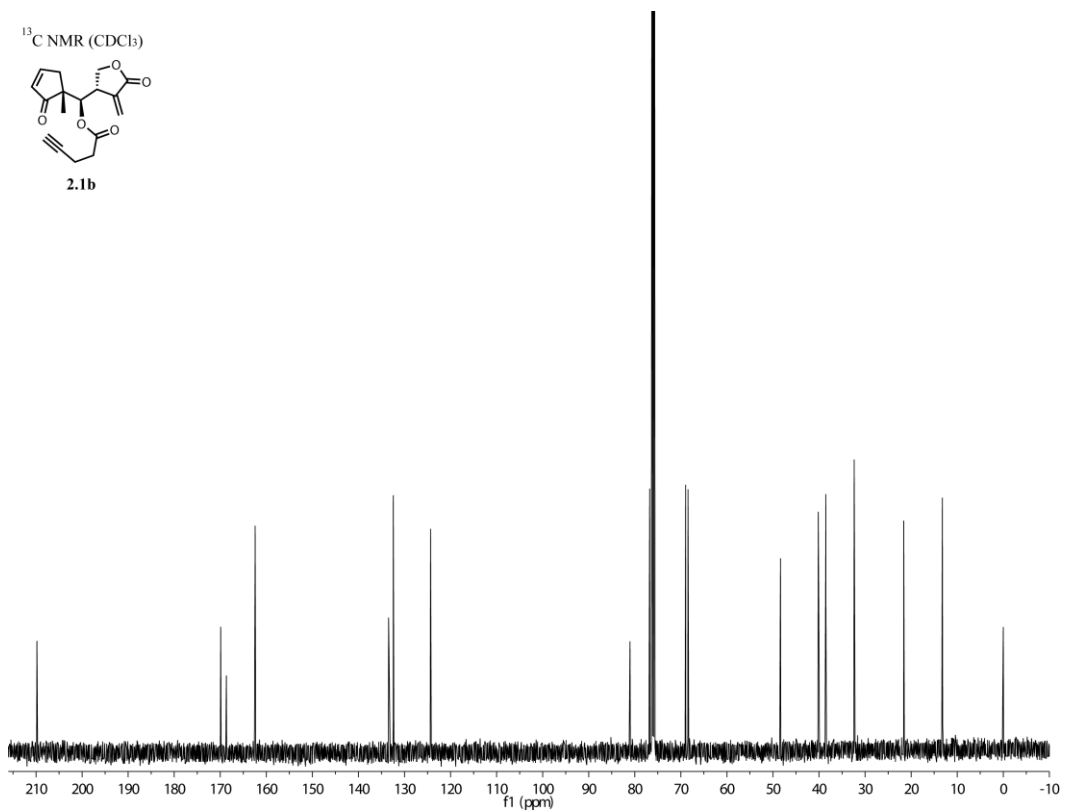
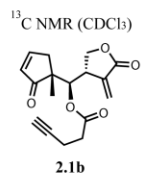


¹H NMR (CDCl₃)

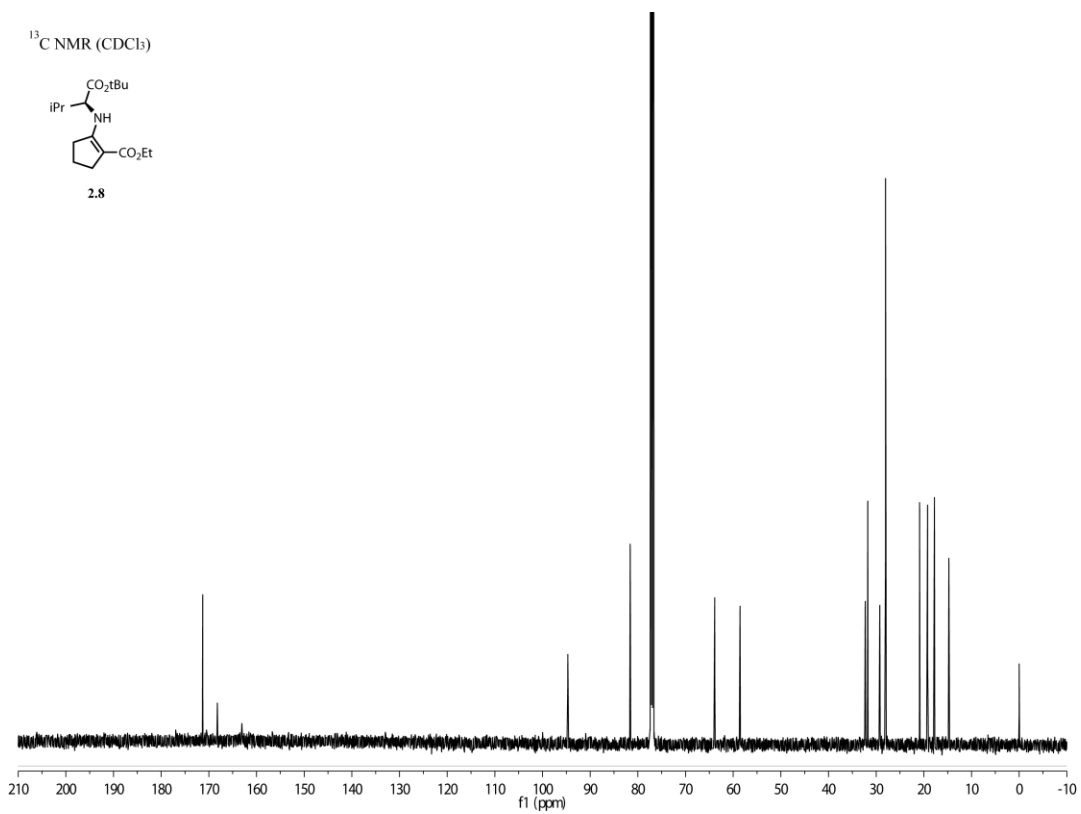
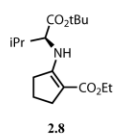


2.1b

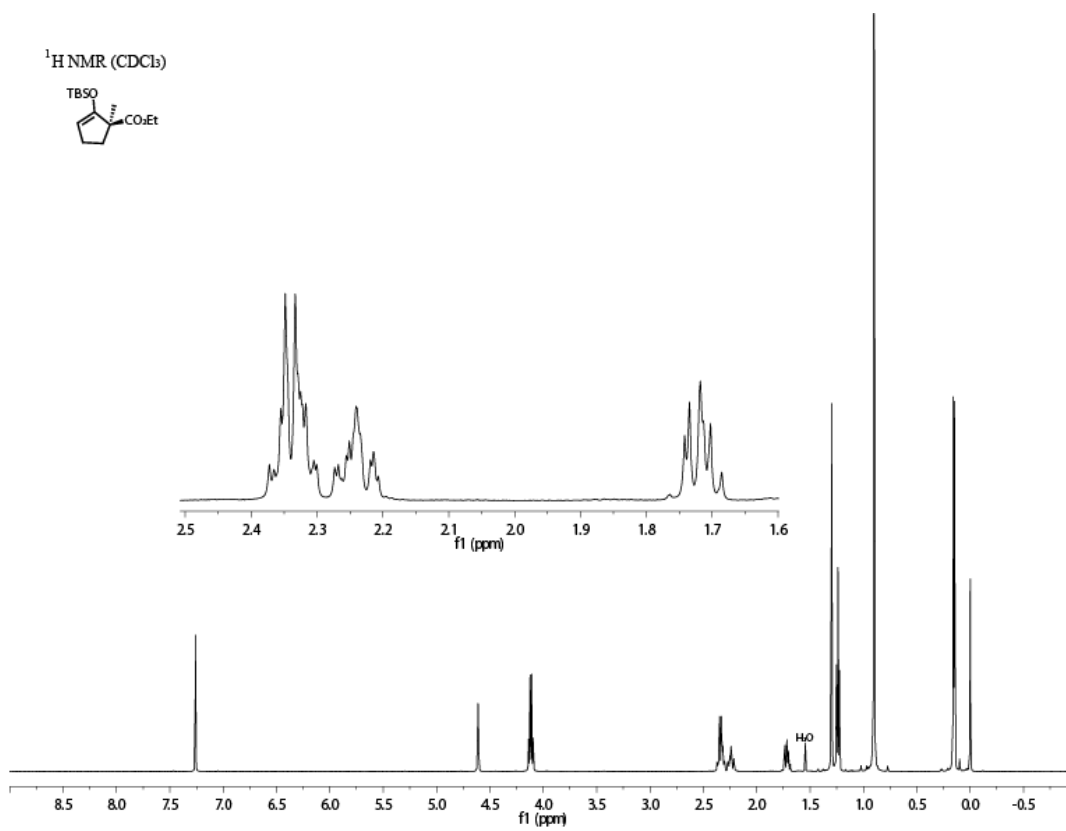
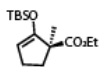




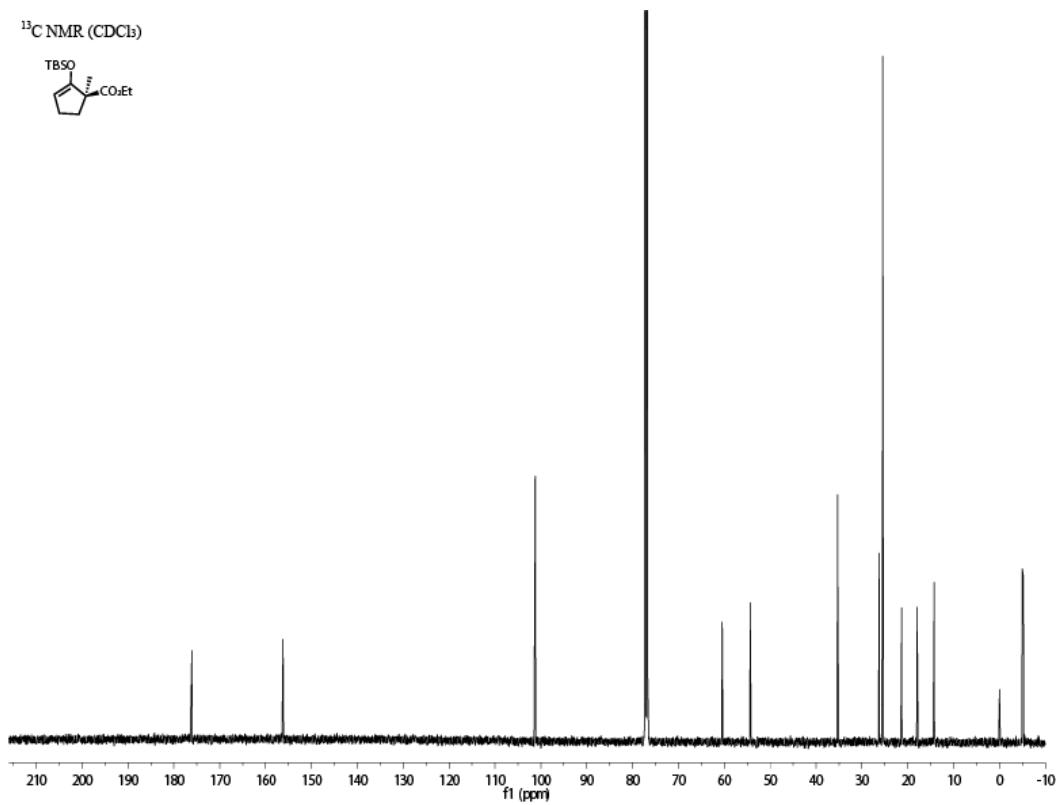
¹³C NMR (CDCl₃)



¹H NMR (CDCl₃)



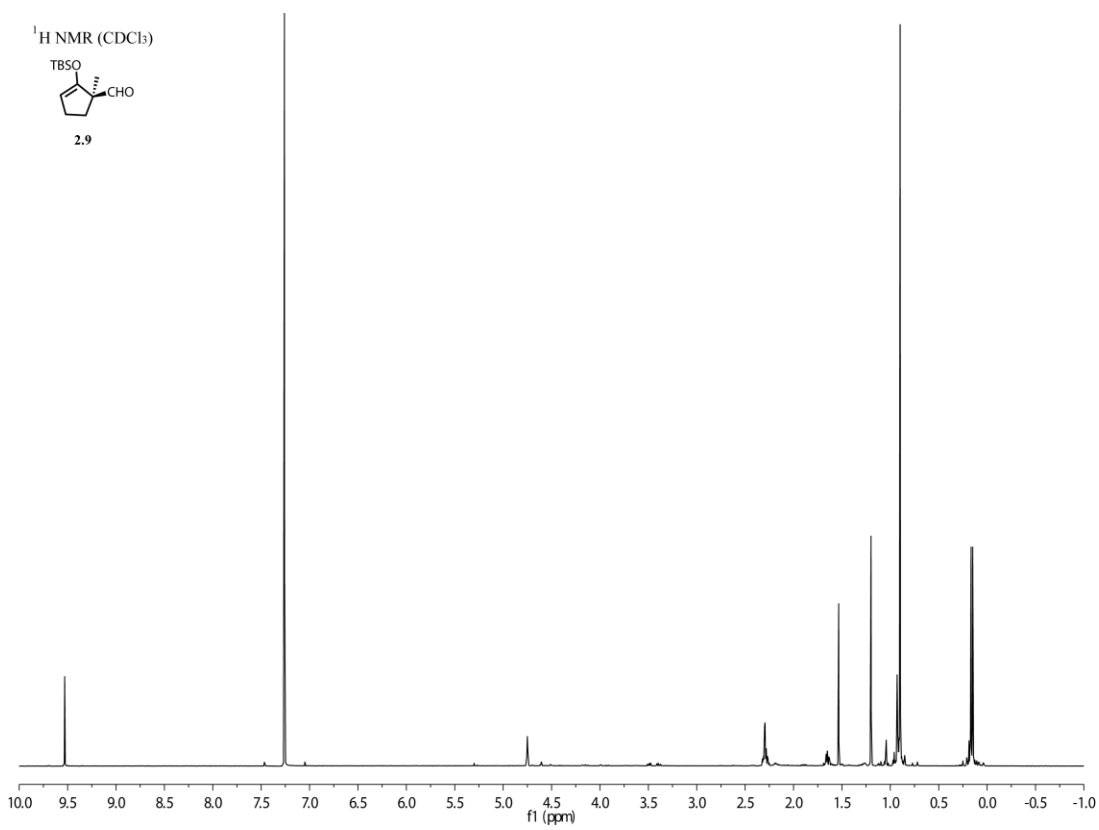
¹³C NMR (CDCl₃)

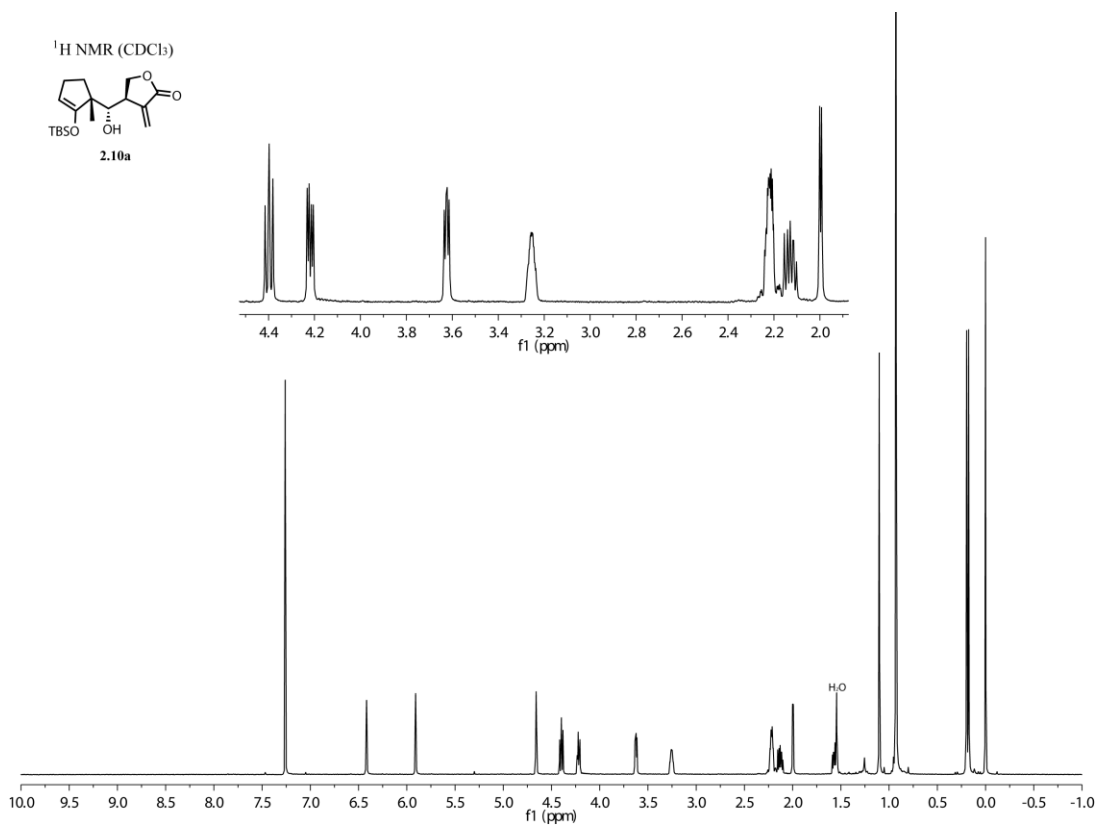
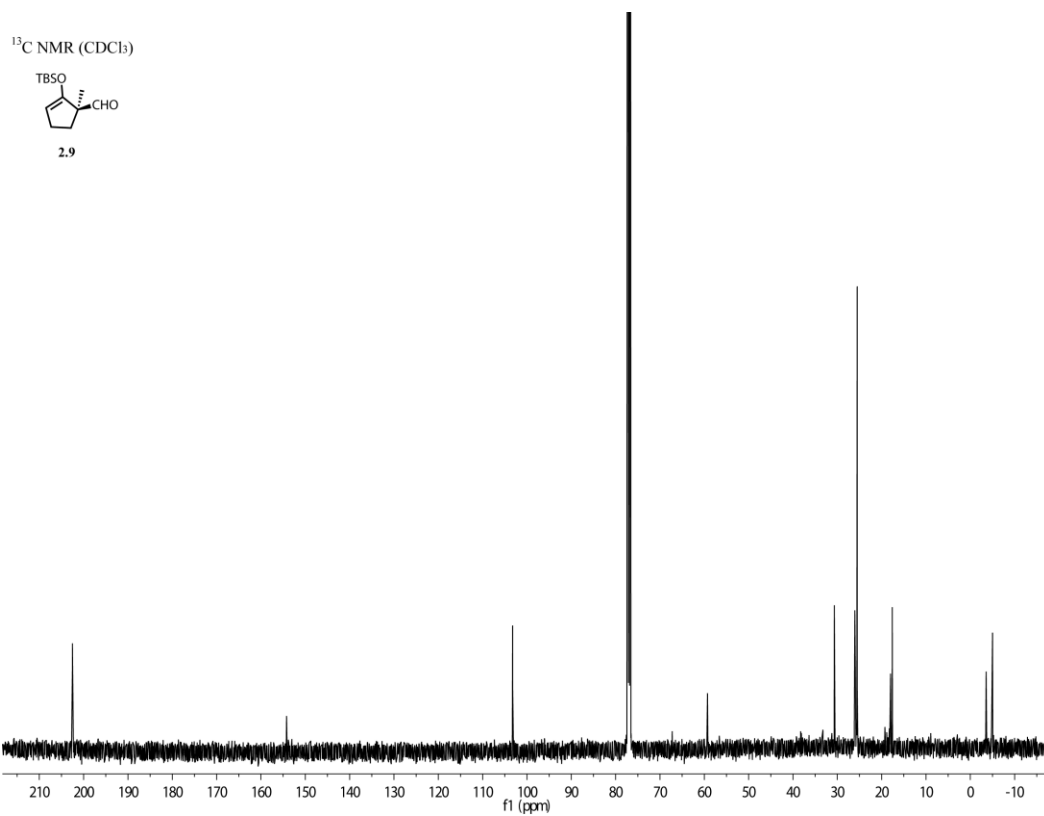


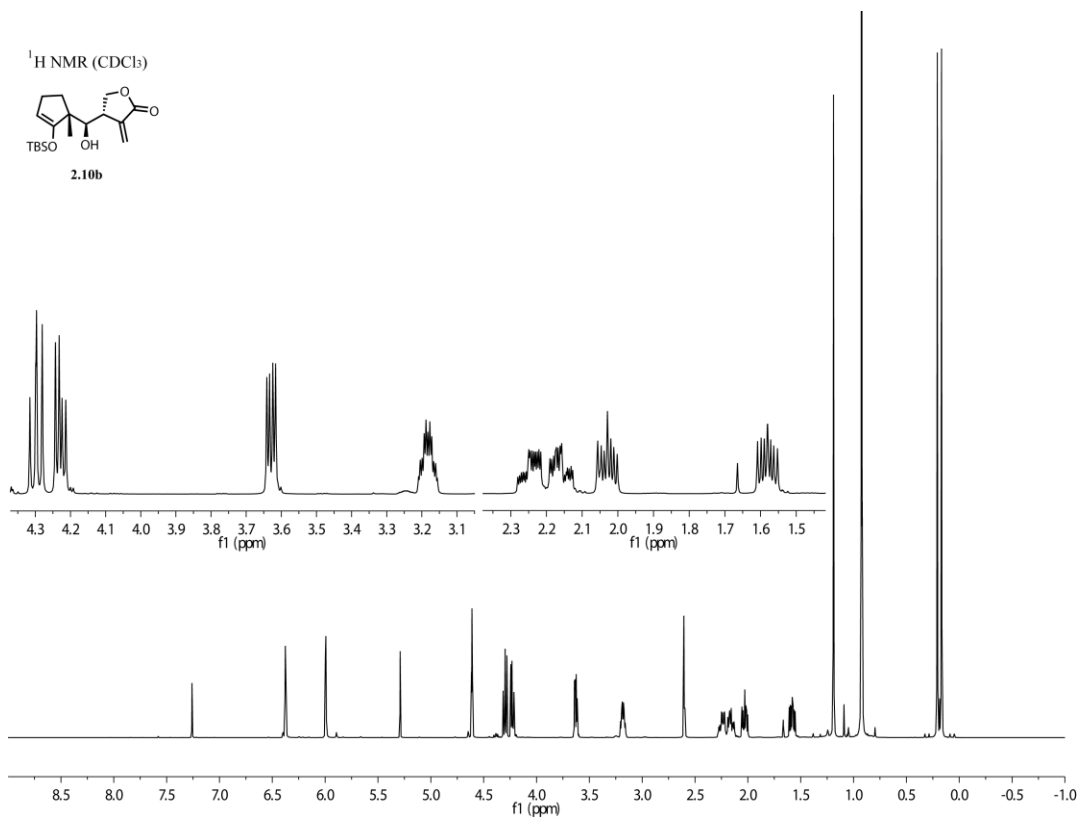
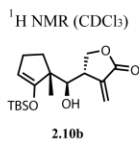
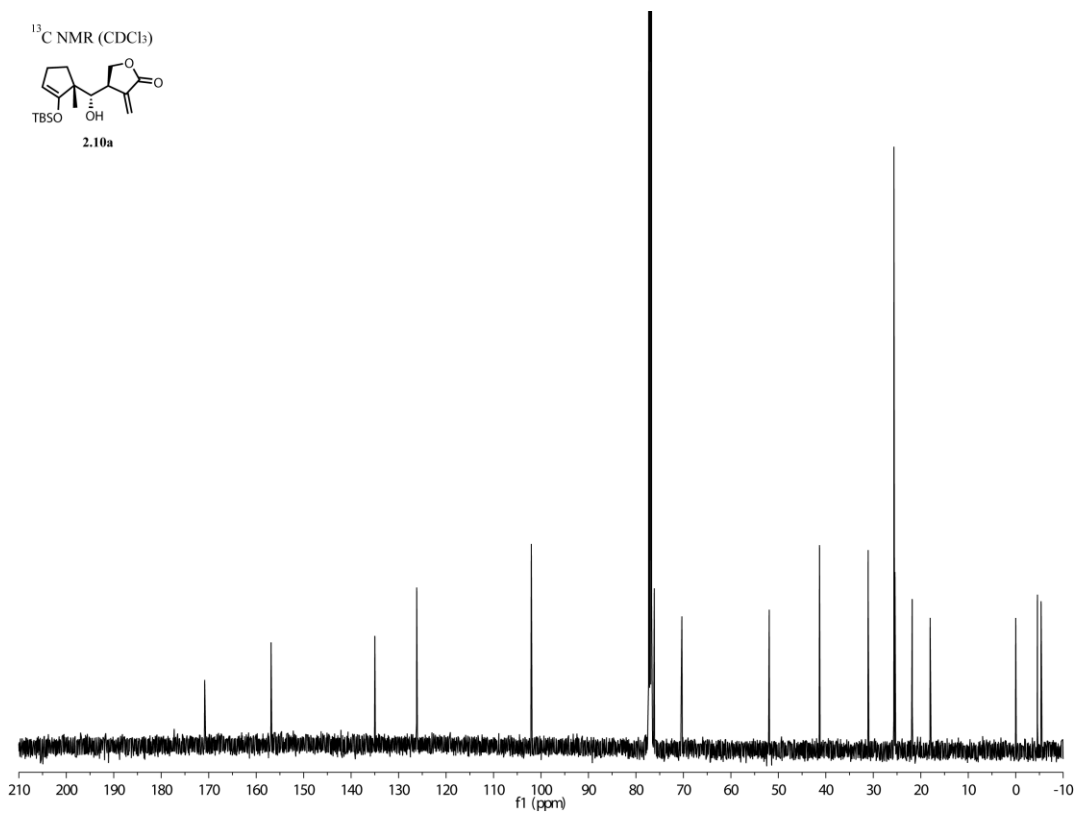
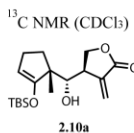
¹H NMR (CDCl₃)

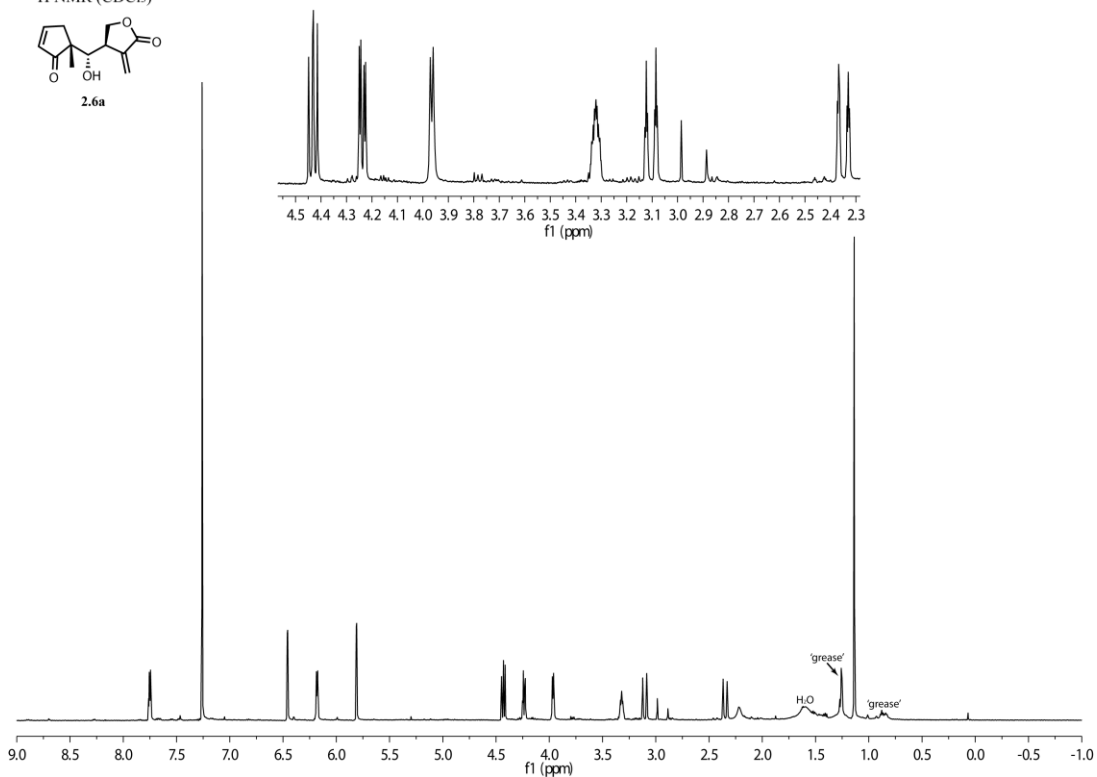
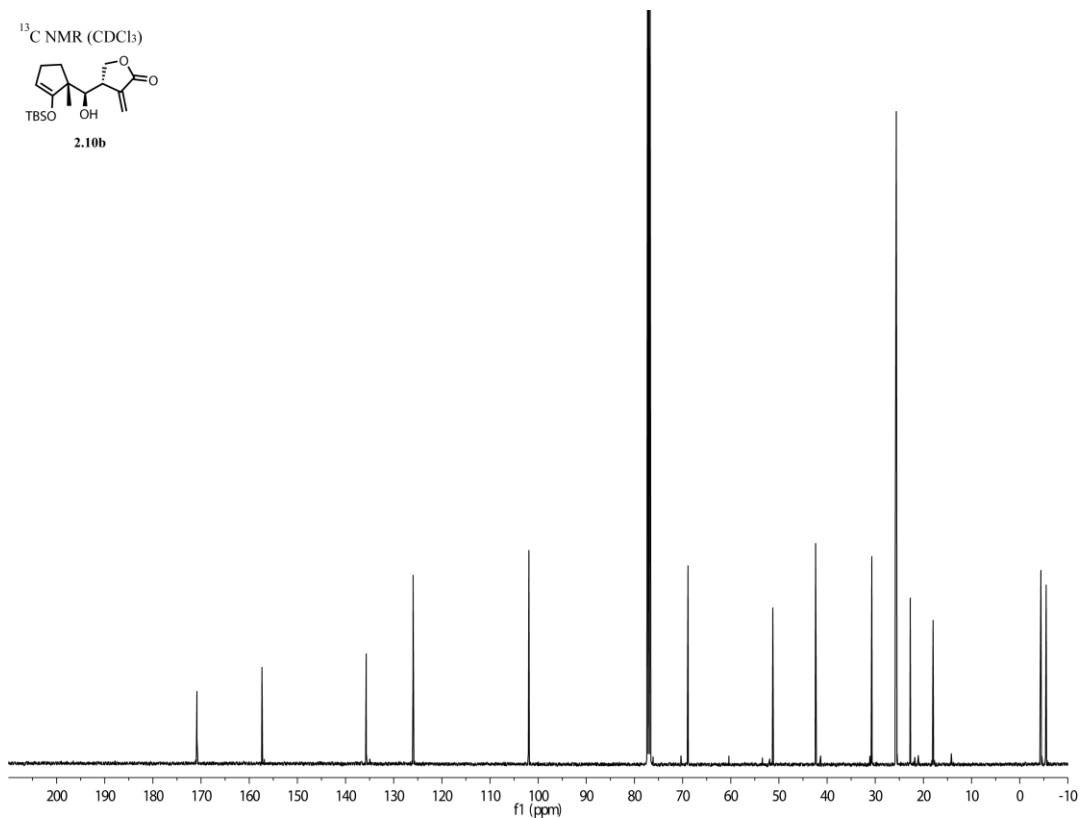
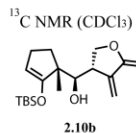


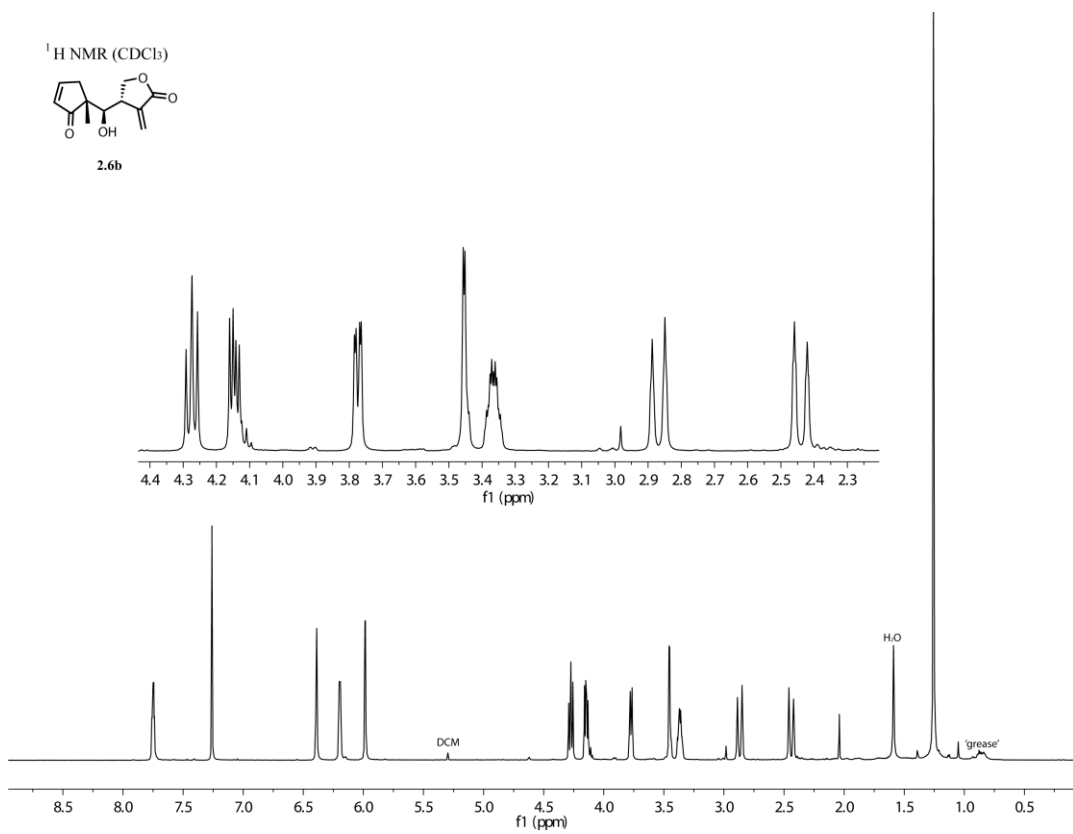
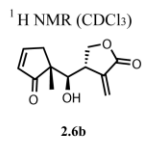
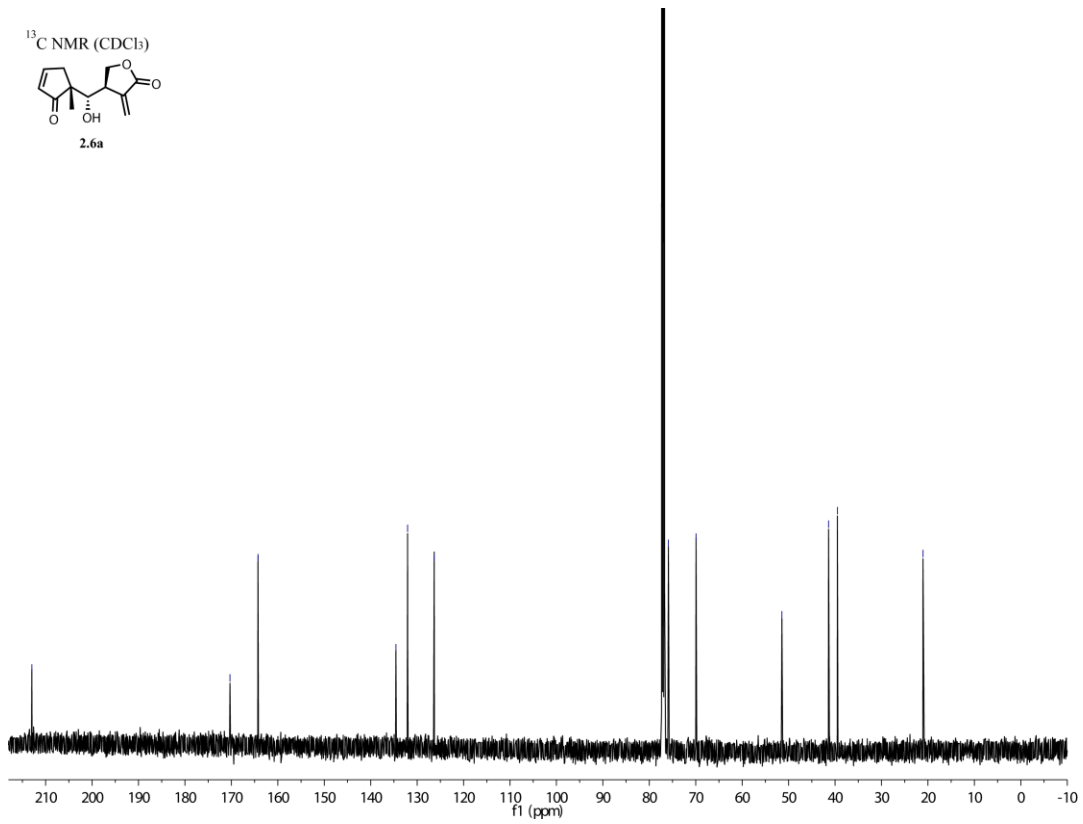
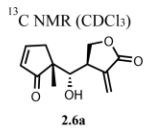
2.9

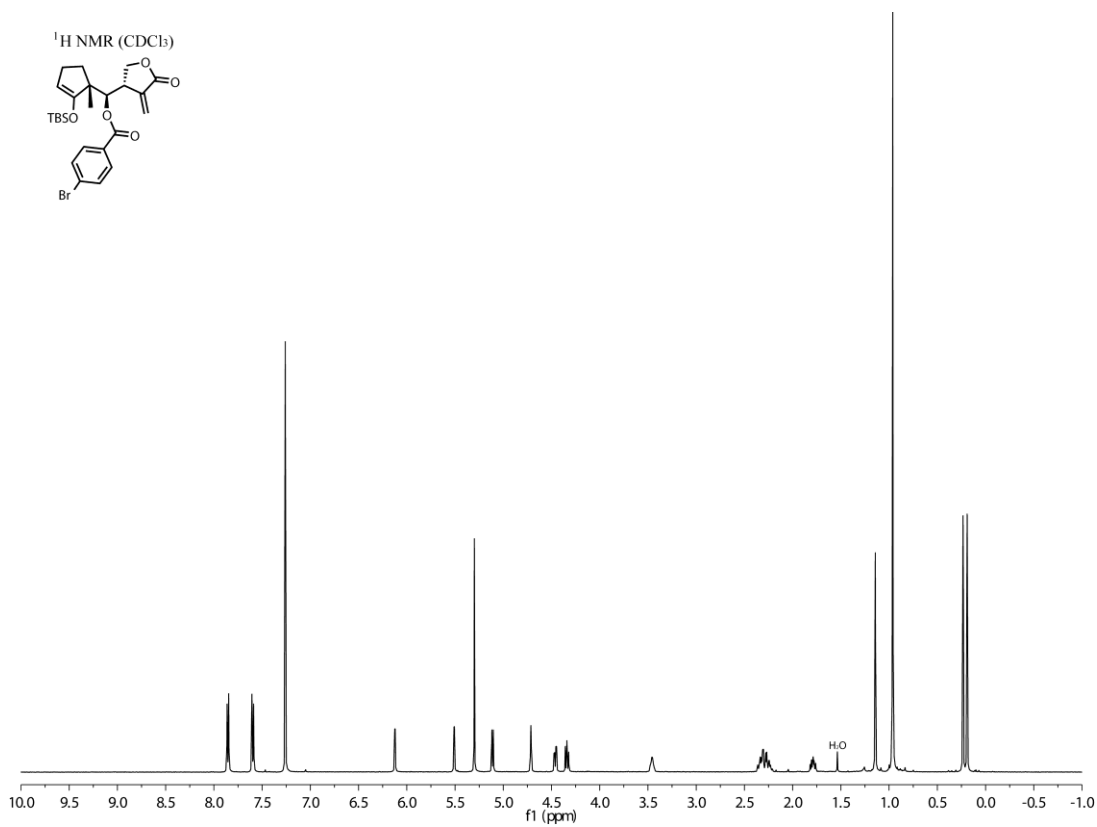
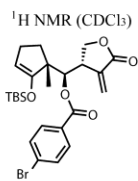
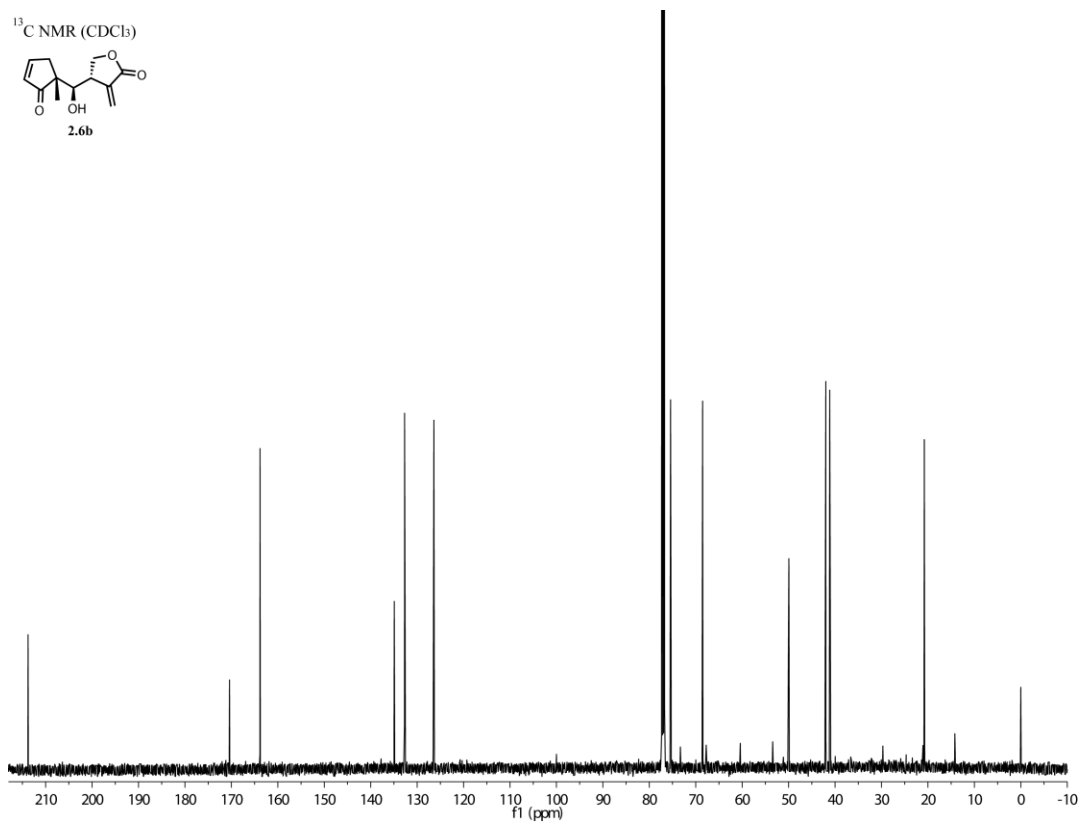
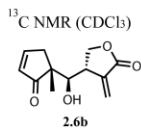


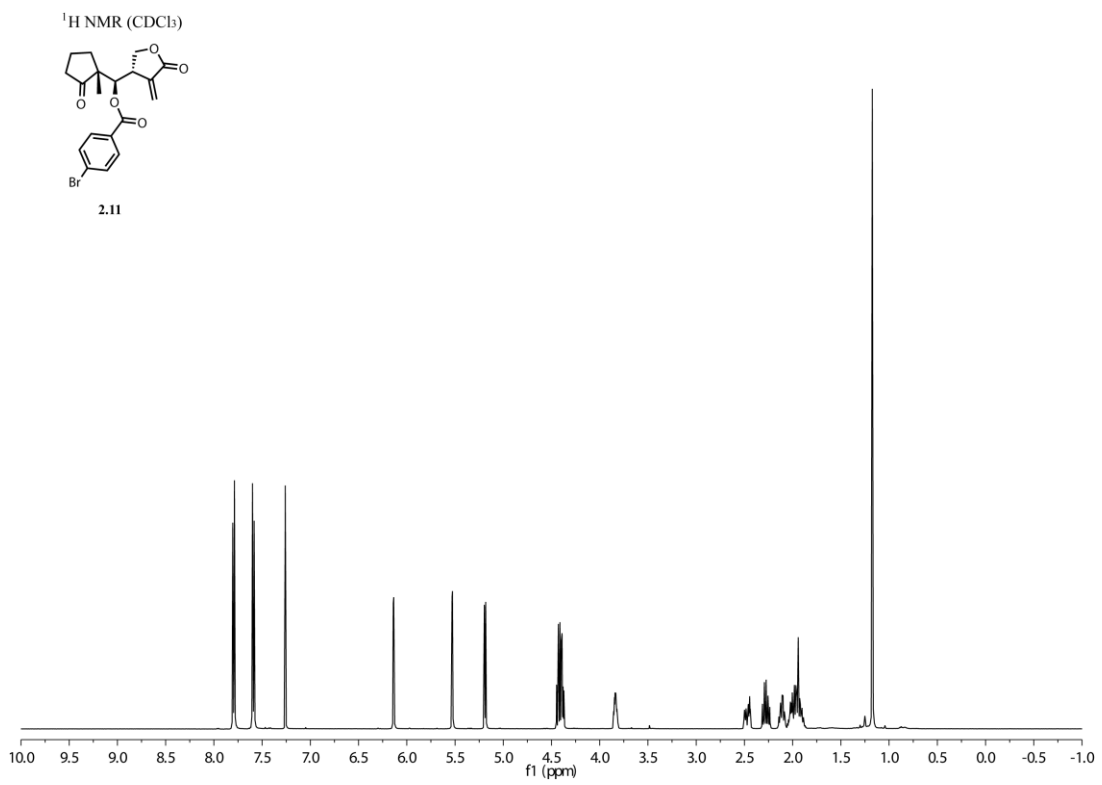
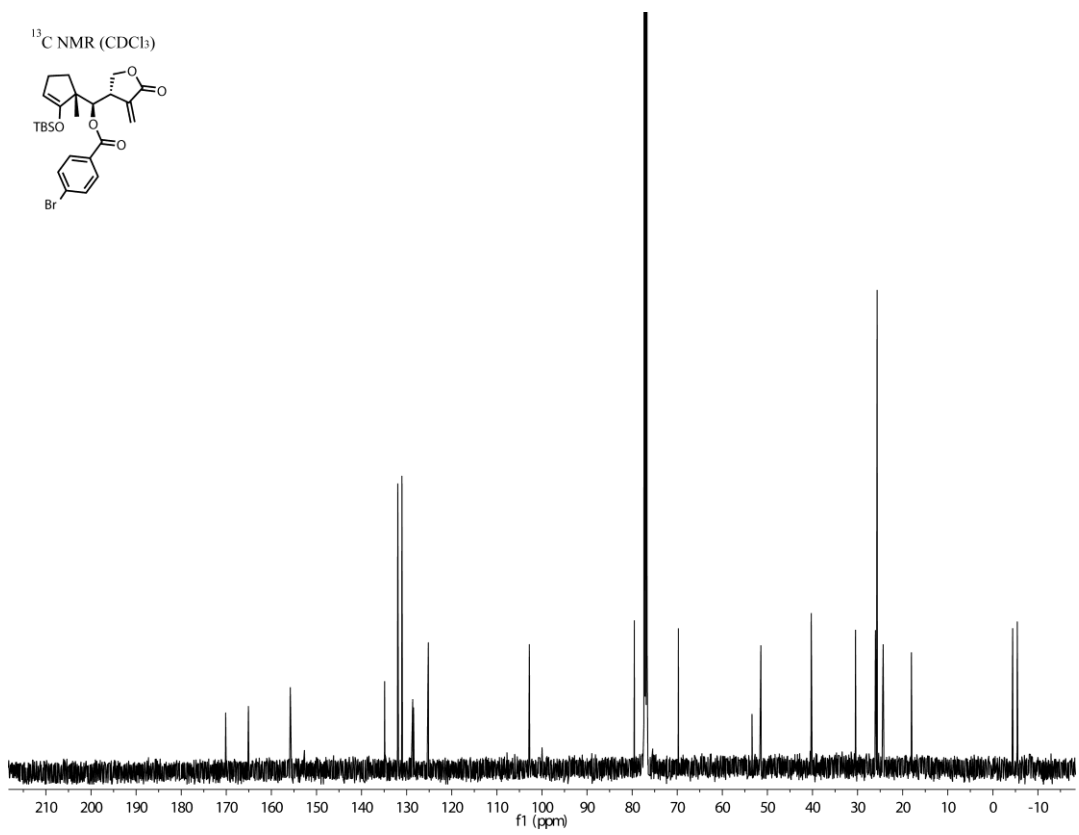


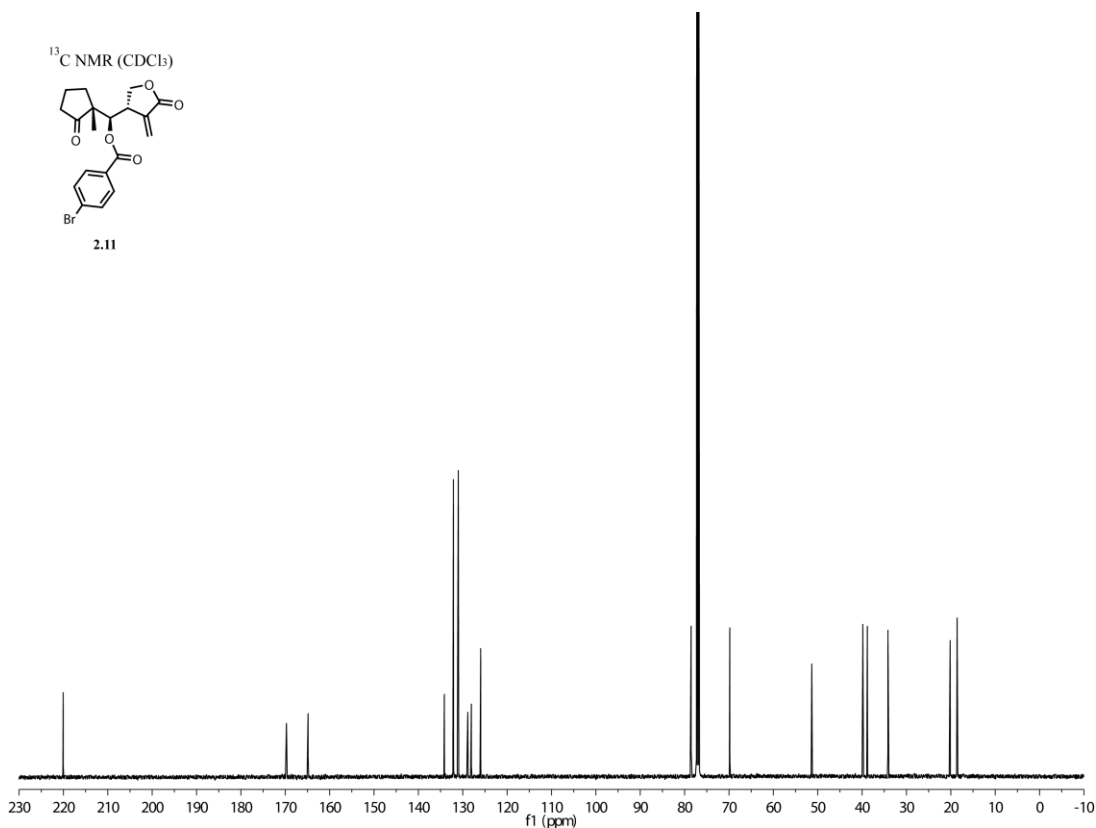












2.11 HPLC Chromatograms (Purity Analysis) of Tested Compounds

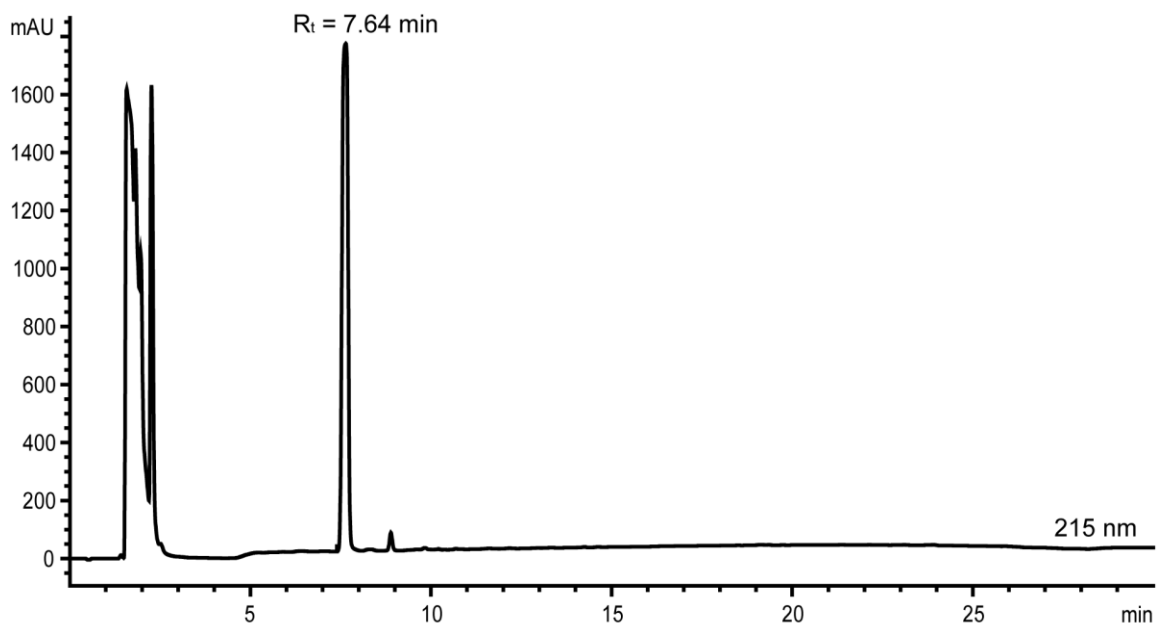
General Protocol for HPLC Analysis of Synthesized Compounds

DMSO stock solutions of newly synthesized molecules were dissolved in methanol and distilled and deionized water (ddH₂O) containing trifluoroacetic acid (TFA, 0.1% v/v) and analyzed on an Agilent 1200 series instrument equipped with a diode array detector and Zorbax SB-C18 column (4.6 x 150 mm, 3.5 μm, Agilent Technologies). The analysis method (1 mL/min flow rate) starts with an isocratic eluent system of 10% MeCN in ddH₂O from 0-2 minutes (both containing 0.1% TFA) followed by a linear gradient of 10% to 85% MeCN in ddH₂O from 2-24 minutes, followed by 85% to 95% MeCN in ddH₂O from 24-26 minutes, and finally an isocratic eluent system of 95% MeCN in ddH₂O from 26-30 minutes. Wavelengths monitored = 215 nm.

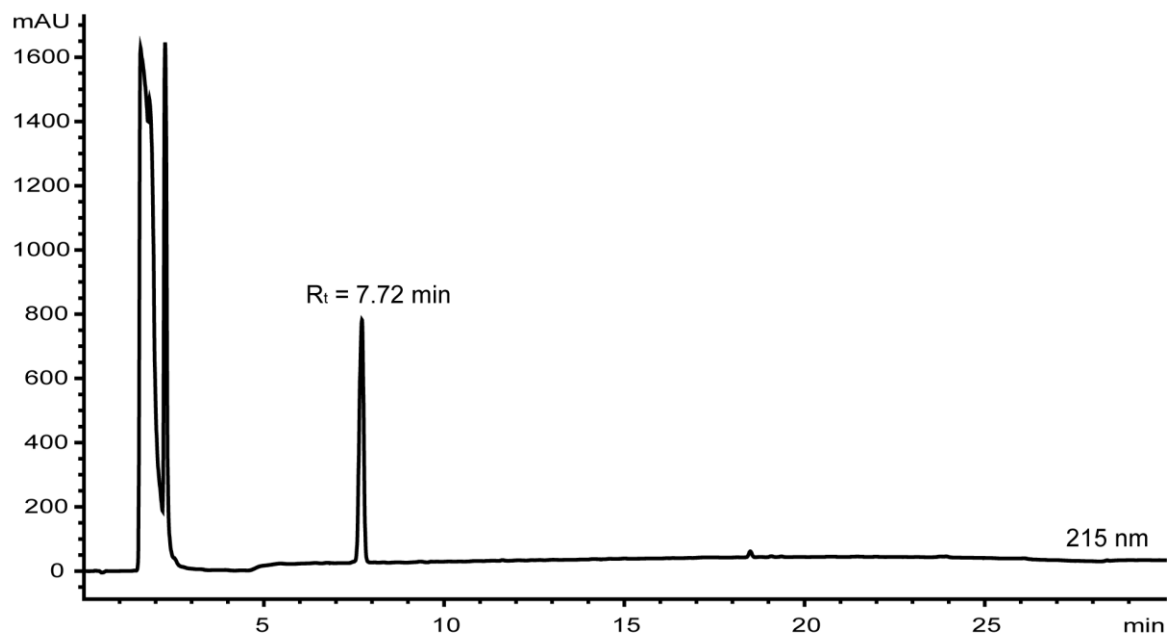
Preparation of Stock Solutions

Compound stock solutions were prepared in DMSO (40 mM to 100 mM concentrations) and stored at -20 °C when not in use. Compound purities were assessed frequently by analytical reverse-phase HPLC analysis and fresh solutions were prepared as needed.

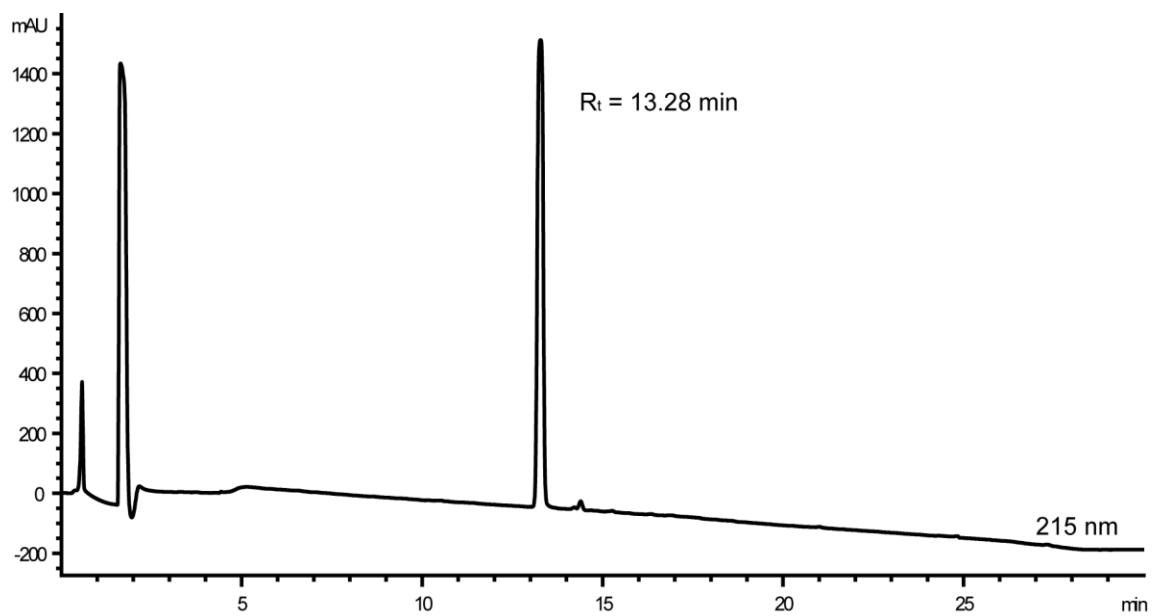
2.6a HPLC (98.4% pure):



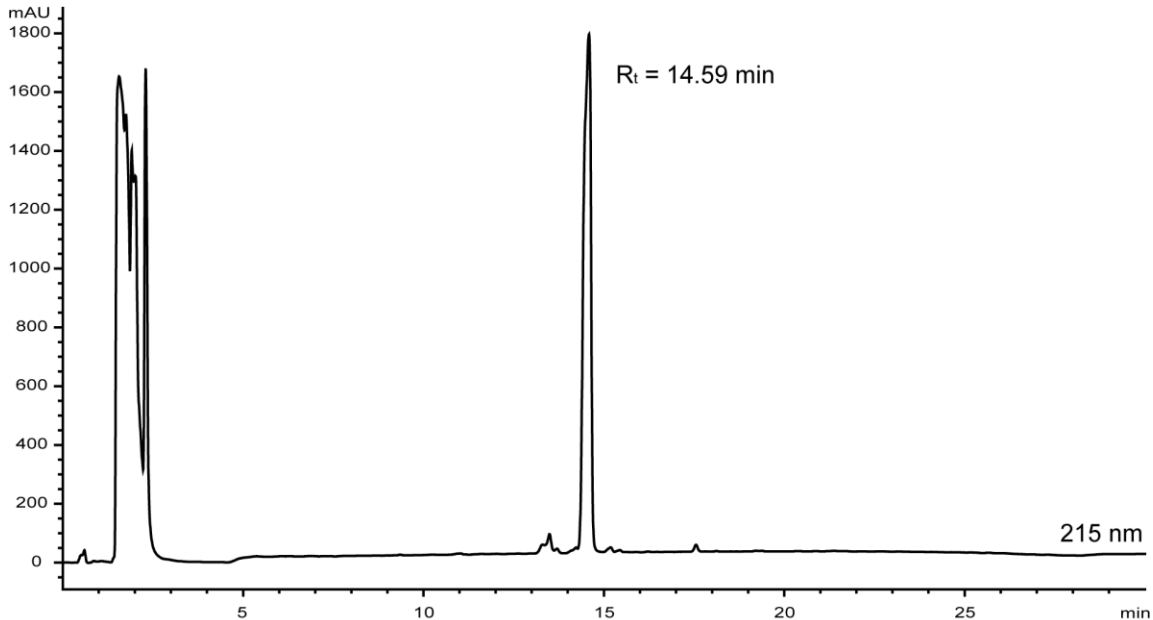
2.6b HPLC (>99% pure):



2.1a HPLC (>99% pure):

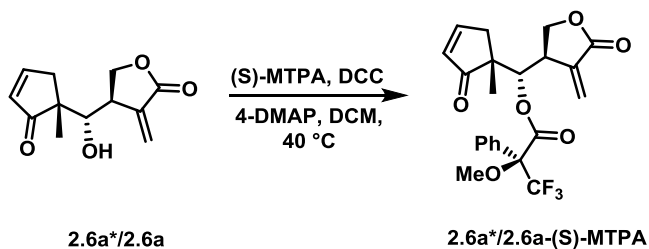


2.1b HPLC (96.4% pure):



2.12 Enantiopurity Analysis of Synthesized Compounds

During enantiopurity analysis via chiral-HPLC **2.6a**/**2.6a**^{*} was not separable; therefore, **2.6a**^{*} and **2.6a** were esterified with (S)-MTPA to determine enantiopurity with ¹⁹F NMR.

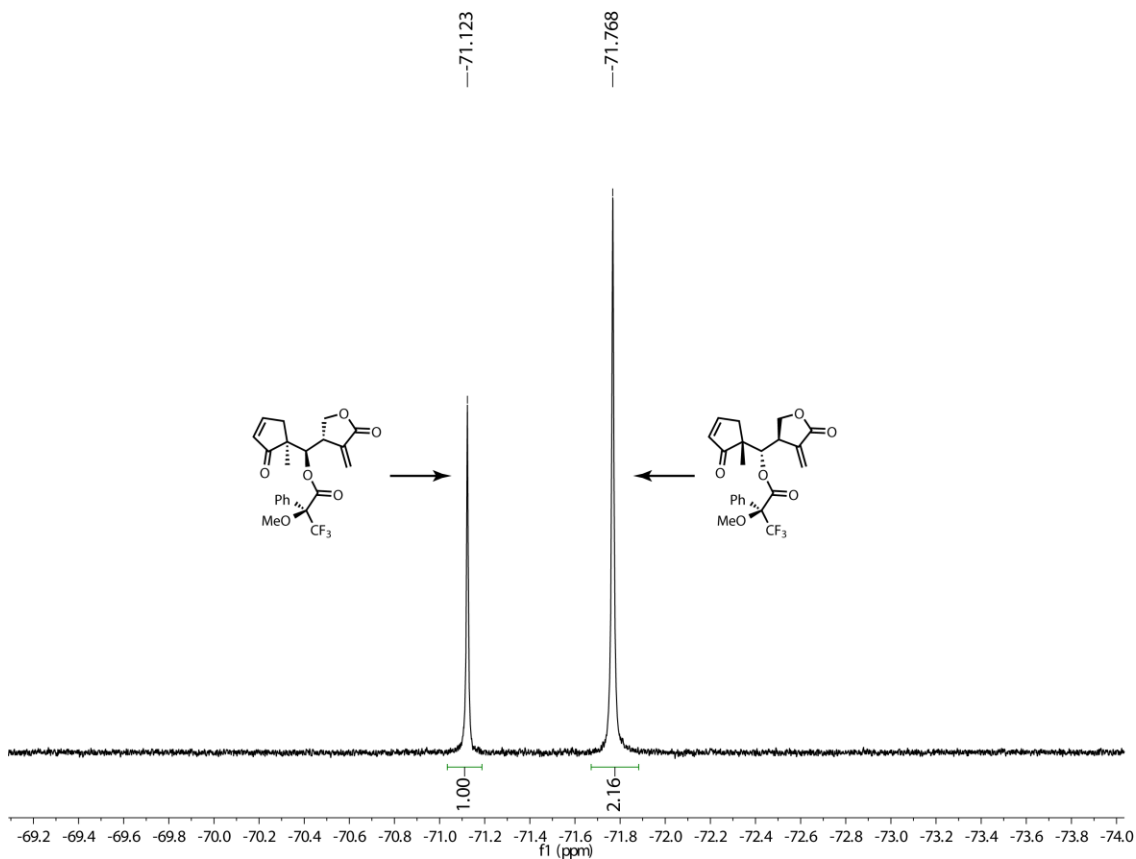


General Procedure for Esterification: **2.6a**^{*} or **2.6a**

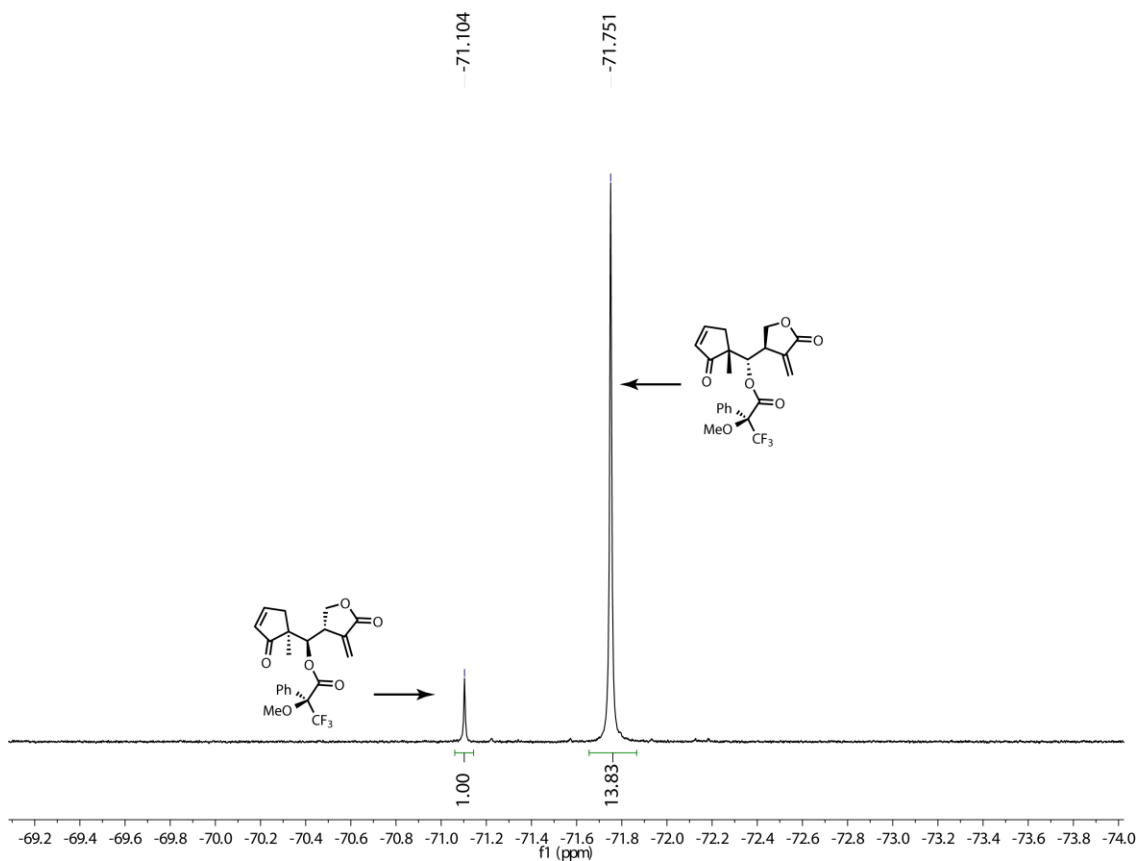
(1-5 mg scale) was dissolved in DCM (2 mL), then 4-DMAP (5 equiv) and (S)-MTPA (4 equiv) were added. DCC (5 equiv) was added last and the reaction was heated to 40 °C. Reaction progress was monitored by TLC and allowed to react until starting material was

no longer visible, typically after 16 h. The reaction mixture was allowed to cool to RT and pipetted onto a SiliCycle glass backed extra hard layer prep TLC plate (particle size: 60 Å, plate size: 20x20 cm, thickness: 1000 µm, indicator F-254) and purified with a 70% ethyl acetate in hexanes eluent system. After the eluent reached the top of the plate, the plate was allowed to dry and the silica where the product was contained was scraped off ($R_f = 0.6$) and washed through filter paper with ethyl acetate (30 mL, 5X). The organic layer was concentrated *in vacuo* and then the purified compound was dissolved in CDCl_3 (0.6 mL).

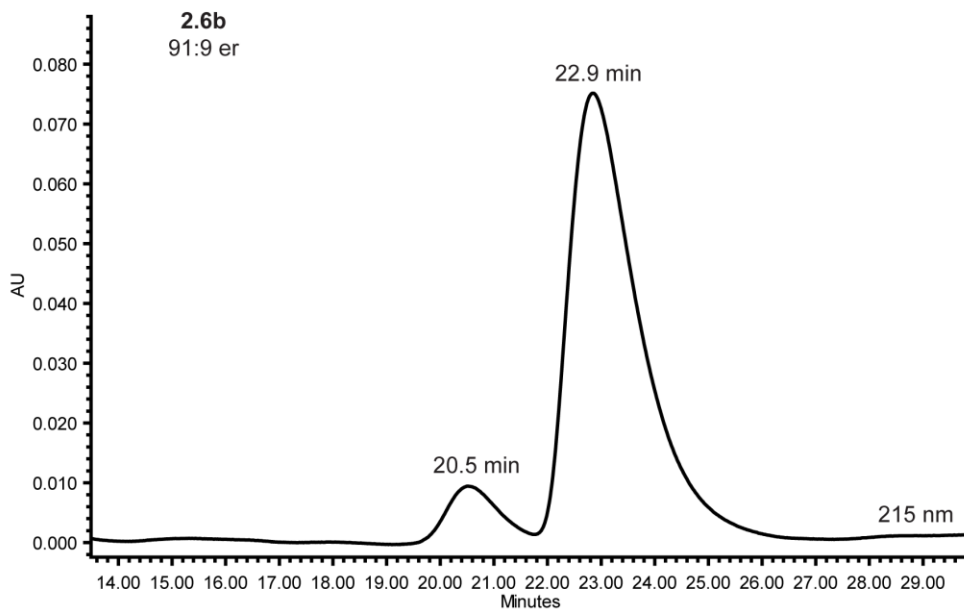
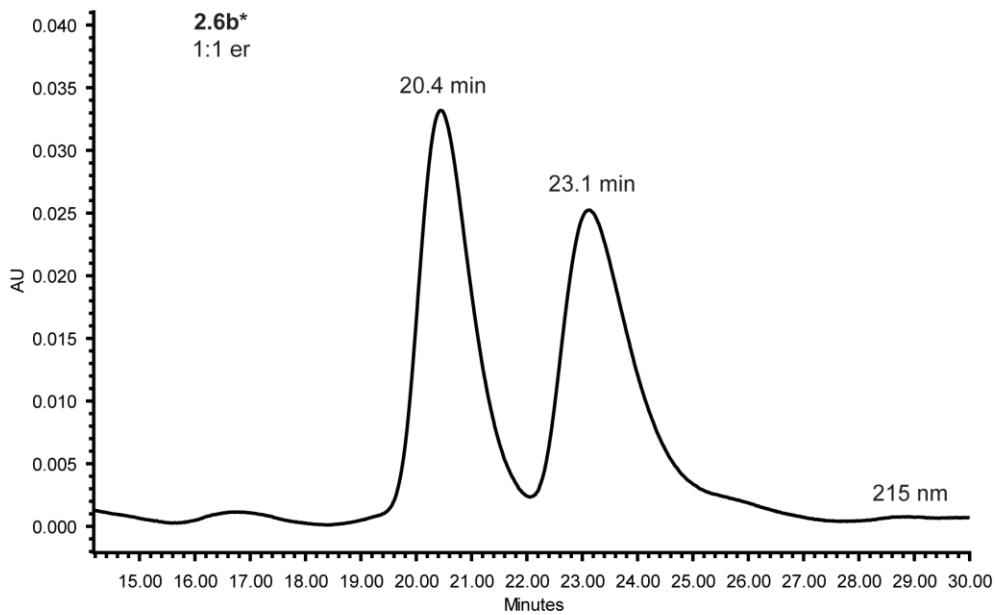
^{19}F NMR (CDCl_3) of **2.6a***-(S)-MTPA derivative (32:68 dr):



^{19}F NMR (CDCl_3) of **2.6a-(S)**-MTPA derivative (7:93 dr):

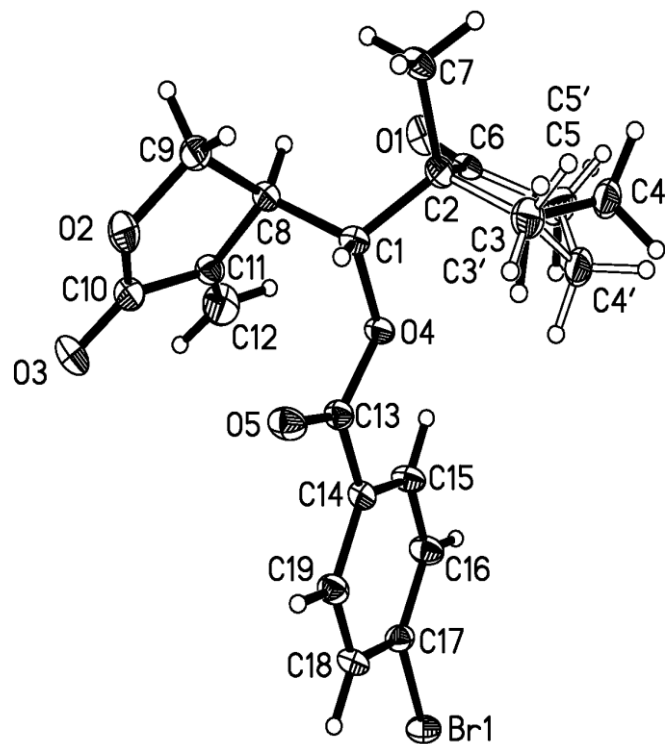


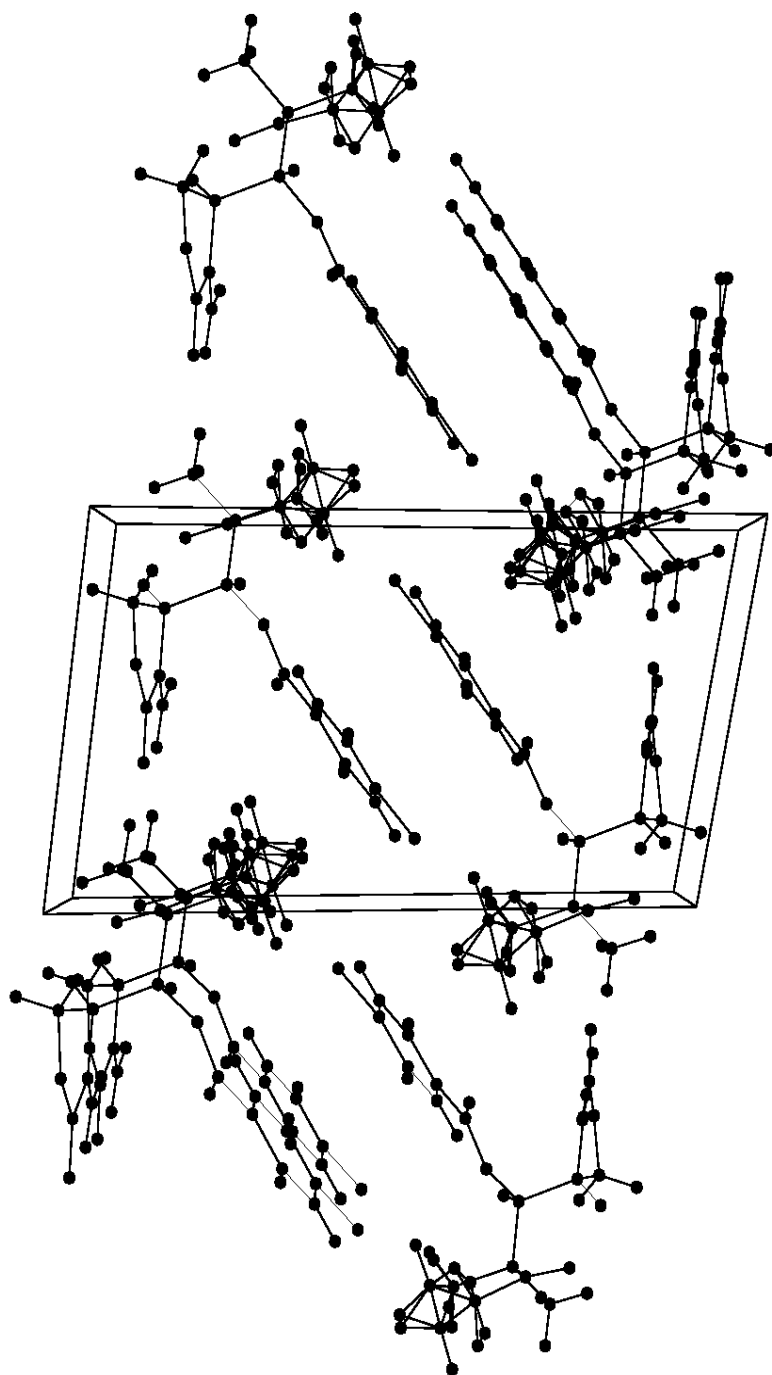
General Protocol for Chiral HPLC Analysis. DMSO stock solutions of newly synthesized molecules were dissolved in 1:1 *i*-PrOH:hexanes. A normal phase Chiralcel[®] OJ column (250 x 4.6 mm, 3 μm) was used for the separation. The analysis method used a 1 mL/min flow rate and isocratic 15% *i*-PrOH in hexanes eluent system for 45 minutes. Wavelength monitored = 215 nm. Enantioenriched derivatives were compared to their respective racemic derivatives and enantiopurity was determined by integrating peak area under the curve.



Comparison of chiral HPLC traces for **2.6b*** and **2.6b**. The top trace shows the separation of **2.6b*** (1:1 er) and the bottom trace is the enantiomerically enriched **2.6b** (91:9 er).

2.13. X-ray Crystallography Data for 2.11





Crystal growth conditions

Compound **2.11** was dissolved in a 1:1 mixture of ethyl acetate and methanol and allowed to slowly evaporate (cap loosely on) in a 1.5 dram vial over a 48 h period.

Data collection

A crystal (approximate dimensions 0.280 x 0.180 x 0.120 mm³) was placed onto the tip of a 0.1 mm diameter glass capillary and mounted on a Bruker-AXS Venture PHOTON-II diffractometer for a data collection at 123(2) K.²²⁶ A preliminary set of cell constants was calculated from reflections harvested from three sets of frames. These initial sets of frames were oriented such that orthogonal wedges of reciprocal space were surveyed. This produced an initial orientation matrix determined from 210 reflections. The data collection was carried out using CuK α radiation (parabolic mirrors) with a frame time of 2, 4, or 8 seconds and a detector distance of 4.0 cm. A strategy program was used to assure complete coverage of all unique data to a resolution of 0.80 Å. All major sections of frames were collected with 0.80° steps in ω or ϕ at different detector positions in 2θ . The intensity data were corrected for absorption and decay (SADABS).²²⁷ Final cell constants were calculated from 2980 strong reflections from the actual data collection after integration (SAINT).²²⁸ Please refer to Table 1 for additional crystal and refinement information.

Structure solution and refinement

The structure was solved using SHELXT-2014/5 (Sheldrick 2014) and refined using SHELXL-2014/6 (Sheldrick, 2014).²²⁷ The space group P-1 was determined based on systematic absences and intensity statistics. A direct-methods solution was calculated which provided most non-hydrogen atoms from the E-map. Full-matrix least squares/difference Fourier cycles were performed, which located the remaining non-

hydrogen atoms. All non-hydrogen atoms were refined with anisotropic displacement parameters. All hydrogen atoms were placed in ideal positions and refined as riding atoms with relative isotropic displacement parameters. The final full matrix least squares refinement converged to $R1 = 0.0277$ and $wR2 = 0.0730$ (F^2 , obs. Data).

Data collection and structure solution were conducted at the X-Ray Crystallographic Laboratory, 192 Kolthoff Hall, Department of Chemistry, University of Minnesota. All calculations were performed using Pentium computers using the current SHELXTL suite of programs. Victor G. Young, Jr. is gratefully acknowledged for solving the structure. The Bruker-AXS D8 Venture diffractometer was purchased through a grant from NSF/MRI (#1229400) and the University of Minnesota. Additional information pertaining to the crystal structure data and crystallographic information file (CIF) can be found in the supporting information of the original publication.²²⁹ The structure will be uploaded to the Cambridge Structural Database (CSD).

Table 2.13.1. Crystal data and structure refinement for **2.11**.

Identification code	16045A	
Empirical formula	C ₁₉ H ₁₉ BrO ₅	
Formula weight	407.25	
Temperature	123(2) K	
Wavelength	1.54178 Å	
Crystal system	triclinic	
Space group	P -1	
Unit cell dimensions	$a = 6.8412(4)$ Å	$\alpha = 94.527(2)^\circ$
	$b = 9.1081(6)$ Å	$\beta = 101.197(2)^\circ$
	$c = 15.4906(9)$ Å	$\gamma = 110.280(2)^\circ$
Volume	876.87(9) Å ³	
Z	2	
Density (calculated)	1.542 Mg/m ³	
Absorption coefficient	3.431 mm ⁻¹	
$F(000)$	416	
Crystal color, morphology	colorless, Block	
Crystal size	0.280 x 0.180 x 0.120 mm ³	
Theta range for data collection	2.945 to 74.595°	
Index ranges	$-8 \leq h \leq 8, -11 \leq k \leq 11, -19 \leq l \leq 19$	
Reflections collected	18642	
Independent reflections	3575 [$R(\text{int}) = 0.0336$]	
Observed reflections	3460	
Completeness to theta = 67.679°	99.7%	
Absorption correction	multi-scan	
Max. and min. transmission	0.7538 and 0.5639	
Refinement method	Full-matrix least-squares on F^2	
Data / restraints / parameters	3575 / 2 / 237	
Goodness-of-fit on F^2	1.113	
Final R indices [$I > 2\sigma(I)$]	$R1 = 0.0277, wR2 = 0.0730$	
R indices (all data)	$R1 = 0.0284, wR2 = 0.0736$	
Extinction coefficient	n/a	
Largest diff. peak and hole	0.598 and -0.697 e.Å ⁻³	

6.14 Acknowledgements

The work was generously supported by the University of Minnesota (Academic Health Center Seed Grant #2010.01), The V Foundation for Cancer Research (V Scholar Award to DAH), Hyundai Hope on Wheels (Hope Grant), and the NIH (R21-CA194661). J.C.W. acknowledges the University of Minnesota, College of Pharmacy for a Bighley Graduate Fellowship. Mass spectrometry was performed at the Analytical Biochemistry Core Facility of the Masonic Cancer Center, which is supported by the NIH (P30-CA77598 and S10 RR-024618). We gratefully acknowledge Victor G. Young, Jr. (University of Minnesota, Department of Chemistry, X-Ray Crystallographic Laboratory) for solving the structure of **2.11** and funding from the NSF/MRI (#1229400) and the University of Minnesota for the purchase of the Bruker-AXS D8 Venture diffractometer. The Minnesota Supercomputing Institute (MSI) at the University of Minnesota is acknowledged for molecular modeling resources.

Chapter 3

SYNTHESIS AND BIOCHEMICAL EVALUATION OF BIS-MICHAEL ACCEPTOR INHIBITORS OF THE NF- κ B PATHWAY BASED ON THE NATURAL PRODUCT HELENALIN

This work was performed in collaboration with Dr. Aaron M Kempema, Jordan W. Baur, Tenley J. Brown, Jacob T. Edwards, Hannah M. Skopec, and Professor Daniel A. Harki.

John Widen designed and synthesized the helenalin-based derivatives, completed the NMR studies, and conducted the NF- κ B-luciferase assay on all compounds presented in this work. All authors assisted with aspects of the synthesis of the analogues contributing to this work.

3.1 Introduction

The NF- κ B pathway regulates the immune and inflammatory response within cells.^{96, 230} When the NF- κ B pathway is hyper-activated, it can lead to tumorigenesis and progression of cancer, coronary disease, and autoimmunity.^{104, 106, 231} Hundreds of small molecules have been reported that inhibit the NF- κ B pathway, but many target up-stream regulatory proteins that overlap with other cellular pathways.^{162, 232} This leads to off-target effects and limits the ability to study specific NF- κ B processes using small molecule probes. Targeting the furthest downstream protein in the pathway, the p65 transcription factor of the NF- κ B (p50/p65) heterodimer, could potentially avoid these off-target effects and lead to specific NF- κ B pathway inhibitors.

Targeting transcription factors with small molecule inhibitors remains a challenging endeavor.^{155a} This is because transcription factors typically have shallow ligand binding surfaces and non-discrete tertiary structures.^{155b, 158a} Nevertheless, over the past two decades, researchers have discovered some small molecule inhibitors that directly bind to transcription factor protein binding surfaces or DNA-binding domains.^{155b, 158a} One strategy that has shown promise for probe and inhibitor discovery is utilizing thiol reactive small molecules that covalently attach to solvent exposed cysteines within the DNA-binding domain, sterically blocking DNA recognition and transcriptional activity.^{185, 189}

Helenalin is a pseudoguaianolide isolated from plants in the *Arnica* and *Helenium* genera with a 5-7-5 fused ring system.^{181, 203} Helenalin contains two Michael acceptors (**Figure 3.1.1**), an α -methylene- γ -butyrolactone and cyclopentenone, which are 6.2-6.4 Å apart based on two reported crystal structures.²¹⁰ The exocyclic methylene has been demonstrated to alkylate Cys38 within the DNA binding pocket of p65.¹⁸⁴ Based on a crystal structure of the p50/p65 heterodimer bound to DNA, Cys38 is 7.8 Å away from Cys120.³⁰ Computational studies have suggested that a second Michael addition is possible between the endocyclic enone with Cys120, but this has not been empirically validated.¹⁸⁶ Additionally, a mutant of p65 containing a Cys120→Ser mutation is still

sensitive to inhibition by helenalin, suggesting that Cys120 is not the primary cysteine targeted by helenalin.^{182c, 186}

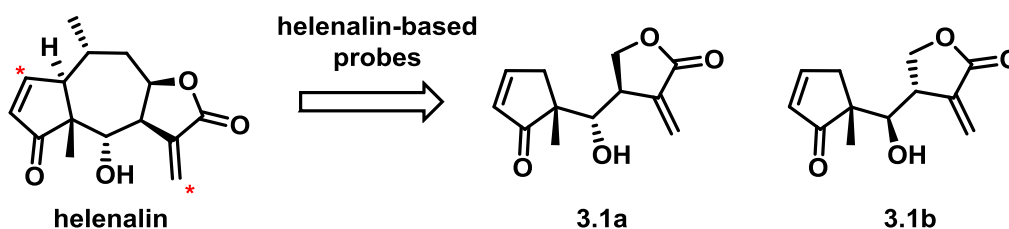


Figure 3.1.1. Helenalin is a pseudoguaianolide natural product with two Michael acceptors, which are 6.2-6.4 Å apart (distance between carbons with red asterisks), based on two reported crystal structures.²¹⁰ Helenalin-based analogues **3.1a** and **3.1b** were synthesized and shown to mimic the biological activity of helenalin.²²⁹ Simplified helenalin derivatives **3.1a** and **3.1b** were previously described in Chapter 2 of this thesis as compounds **2.6a** and **2.6b** respectively.

Recently, our group synthesized structurally simplified helenalin-based small molecules (**3.1a** and **3.1b**) containing bis-Michael acceptors.²²⁹ The simplified helenalin derivatives **3.1a** and **3.1b** were previously shown in Chapter 2 of this thesis as compounds **2.6a** and **2.6b** respectively. The helenalin-based probes were shown to inhibit the NF- κ B pathway and alkylate Cys38 within the DNA binding pocket of p65. However, it is still unclear how the endocyclic enone and exocyclic methylene butyrolactone contribute separately to the mechanism of action of the simplified helenalin probes. Previous studies suggest that helenalin derivatives without the exocyclic methylene butyrolactone lose much of their activity compared to helenalin.^{206a} Direct comparison of reduced helenalin-based derivatives only differing in their number of Michael acceptors, as well as the different diastereomers resulting from reduction of the exocyclic methylene has not been evaluated for inhibition of the NF- κ B pathway. This is especially important because differences in stereochemistry of previously synthesized helenalin-based analogues have a direct effect on inhibition of p65.²²⁹

To determine the general thiol reactivity of the α -methylene- γ -butyrolactone and endocyclic enone, compounds **3.1a** and **3.1b** were reacted with cysteamine in DMSO- d_6

and monitored by ^1H NMR.²³³ The results of these studies led us to pursue how each Michael acceptor present on **3.1a** and **3.1b** affects inhibition of the NF- κ B pathway in correlation to its thiol reactivity. Thus, a small molecule library of helenalin-based analogues was synthesized containing only one Michael acceptor and evaluated for inhibition of the NF- κ B pathway in a cellular reporter assay.

3.2 Monitoring Cysteamine Reactivity of **3.1a** and **3.1b** with ^1H NMR

Endocyclic enones that undergo a hetero-Michael addition reaction with cysteines are typically reversible at physiological pH.^{183a} Alternatively, hetero-Michael additions to exocyclic methylene butyrolactones are irreversible at physiological pH in most cases.^{183b, 183c} Evaluation of the reversibility of both Michael acceptors present on **3.1a** and **3.1b** was conducted using a previously reported procedure for small molecules containing bis-Michael acceptors.²³³ Both compounds were reacted with cysteamine in DMSO- d_6 and monitored using ^1H NMR to follow the reactivity and reversibility of both Michael acceptors. The chemical assignments of protons H₃ and H₄ are based on previous shift assignments of exocyclic methylene butyrolactones.^{183a, 234}

Addition of one equivalent of cysteamine to a solution with **3.1a** resulted in disappearance of signal corresponding to the two exocyclic methylene protons (peaks 3 and 4, **Figure 3.2.1**). Both signals from the exocyclic methylene protons were below 50% of the original signal within 10 min of cysteamine addition. Within 20 min, the exocyclic methylene completely reacted with cysteamine. Comparing integrations with the TMS internal standard revealed that the signal from both of the endocyclic enone protons initially decreased within the first ten minutes of the reaction but then increased in signal as the signal from the exocyclic methylene protons continued to decrease. This suggests that cysteamine could be reacting at both Michael acceptors simultaneously, but the hetero-Michael addition with the endocyclic enone is quickly reversible (faster than the NMR measurement time scale) compared to the largely irreversible hetero-Michael

addition to the exocyclic methylene, resulting in a permanent decrease in signal from the exocyclic methylene protons.

After addition to the exocyclic methylene of **3.1a**, additional equivalents of cysteamine was added until signal from the endocyclic enone decreased to near undetectable levels, which required a total of four equivalents. Addition of cysteamine past four equivalents did not cause further reduction in signal of the endocyclic enone protons. To determine the reversibility of the hetero-Michael addition of cysteamine to the endocyclic enone, the reaction was then diluted 1:10 in CDCl₃, which induces retro hetero-Michael addition because of the decrease in solvent polarity and increased solubility of cysteamine.^{233b} Upon dilution of the reaction mixture in CDCl₃, the endocyclic enone signals (normalized across NMR acquisitions using a TMS internal standard) increased approximately 6-fold, but not the exocyclic methylene signals, indicating that the hetero-Michael addition to the endocyclic enone is reversible and addition to the exocyclic methylene is not.

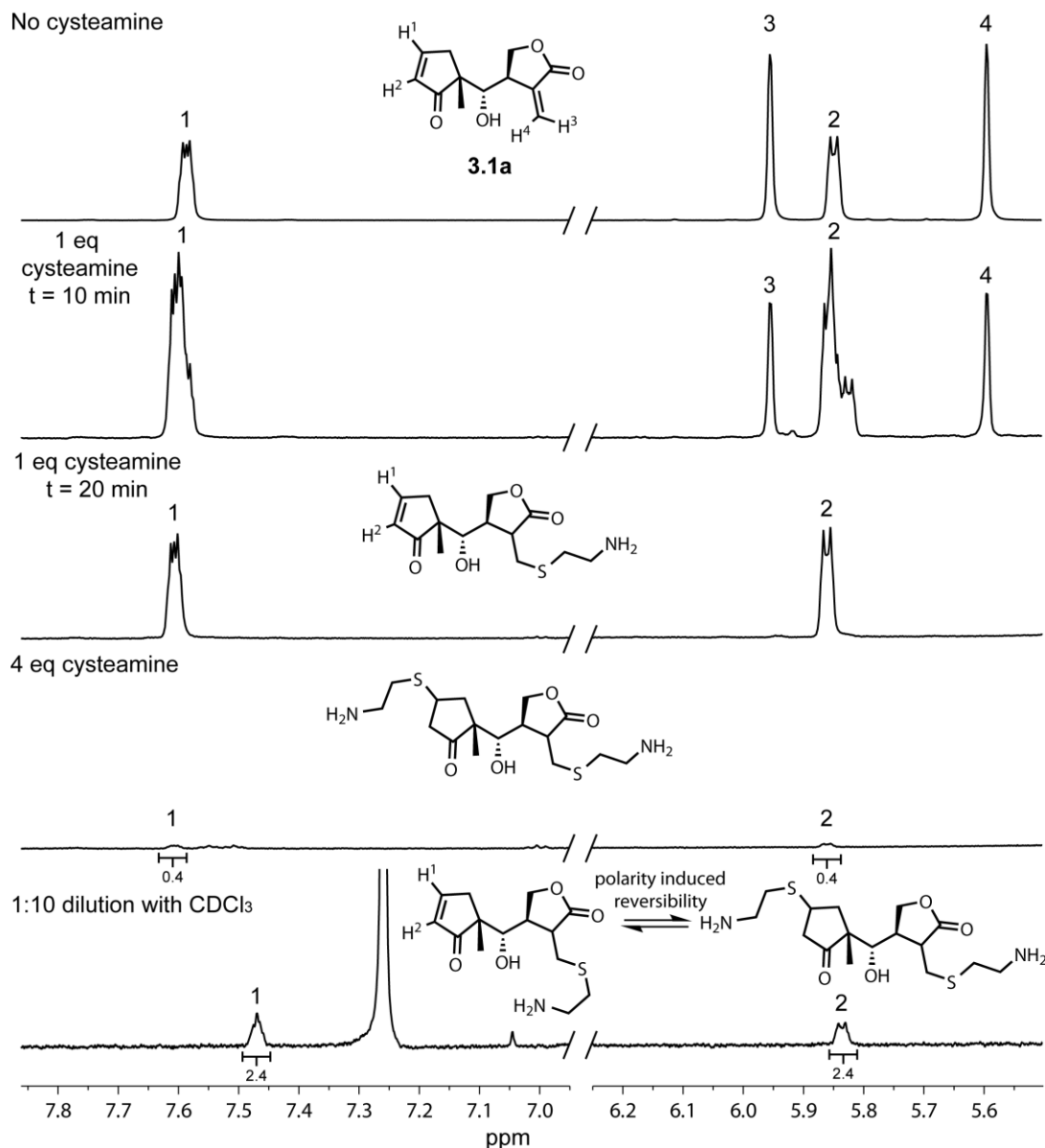


Figure 3.2.1. Reaction between cysteamine and **3.1a** monitored by ^1H NMR ($\text{DMSO-}d_6$). The signals corresponding to the exocyclic methylene protons 3 and 4 were undetectable after 20 min. After addition of cysteamine in 1 eq aliquots, the endocyclic enone peaks 1 and 2 were consumed after a total of 4 eq were added. Upon dilution in CDCl_3 (1:10), peaks 1 and 2 increase in signal relative to the tetramethylsilane (TMS) internal standard by approximately 6-fold, indicating addition of cysteamine to the endocyclic enone is reversible, whereas addition to the exocyclic methylene is not, as evidenced by the absence of peaks 3 and 4 after dilution. Peaks 1 and 2 correspond to endocyclic enone protons H_1 and H_2 . Peaks 3 and 4 correspond to the exocyclic methylene protons H_3 and H_4 .

The same thiol reactivity and reversibility experiment was carried out for helenalin mimic **3.1b**, which yielded similar results (**Figure 3.2.2**). After addition of one equivalent of cysteamine, the exocyclic methylene proton signals decreased to below detection limits within 20 min. Near complete disappearance of the endocyclic enone proton signals occurred after a total of four equivalents of cysteamine were added to the reaction. Upon a 1:10 dilution in CDCl₃, the endocyclic proton signals (normalized across NMR acquisitions using a TMS internal standard) increased by approximately 7-fold compared to the spectra obtained prior to dilution, but the exocyclic methylene proton signals did not, again reinforcing that hetero-Michael addition of cysteamine to the endocyclic enone is reversible, whereas addition of cysteamine to the exocyclic methylene is irreversible.

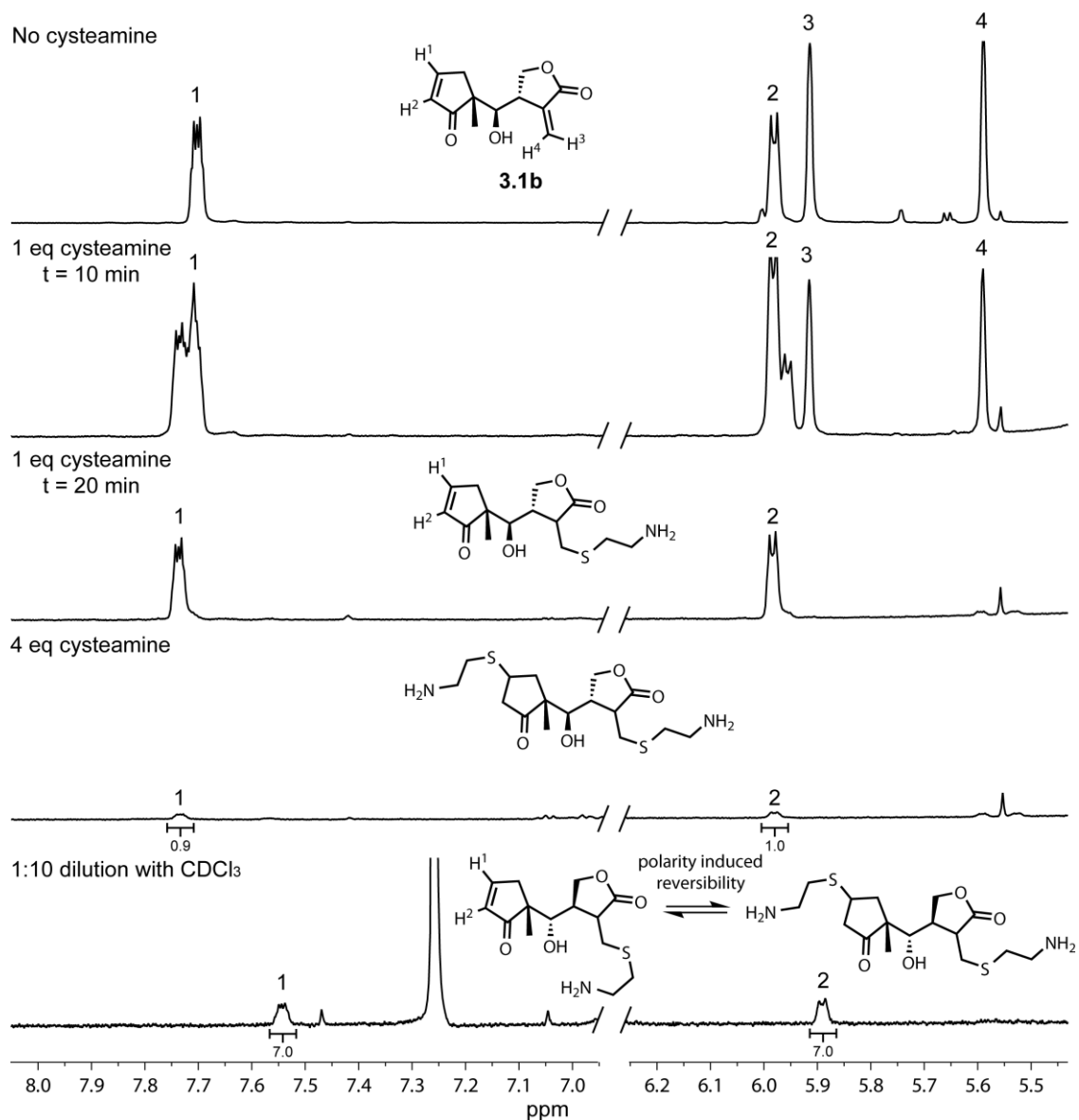


Figure 3.2.1. Reaction between cysteamine and **3.1b** monitored by ^1H NMR ($\text{DMSO}-d_6$). The signals corresponding to the exocyclic methylene protons 3 and 4 were undetectable after 20 min. After addition of cysteamine in 1 eq aliquots, the endocyclic enone peaks 1 and 2 were consumed after a total of 4 eq were added to the reaction. Upon dilution in CDCl_3 (1:10), peaks 1 and 2 increase in signal relative to the tetramethylsilane (TMS) internal standard by approximately 7-fold, indicating addition of cysteamine to the endocyclic enone is reversible, whereas addition to the exocyclic methylene is not, as evidenced by the absence of peaks 3 and 4 after dilution. Peaks 1 and 2 correspond to olefin protons H^1 and H^2 . Peaks 3 and 4 correspond to the exocyclic methylene protons H^3 and H^4 .

The irreversible addition of cysteamine to the exocyclic methylene of helenalin-based probes **3.1a** and **3.1b** agrees with previous reports of thiol addition to α -methylene- γ -butyrolactones.^{183a} Comparatively, addition to the endocyclic enone is reversible, which is also in agreement with previous reports.^{181b,181c,233} This thiol reactivity data suggests that the endocyclic enone may play a role in the NF- κ B inhibitory properties of **3.1a** and **3.1b** because of its propensity to undergo a hetero-Michael addition in the presence of cysteamine after reaction of the exocyclic methylene. There is a possibility that cysteamine is reacting with the endocyclic enone and exocyclic methylene concurrently, but the reversibility of the hetero-Michael addition with the endocyclic enone and irreversible hetero-Michael addition to the α -methylene- γ -butyrolactone leads to formation of a single cysteamine adduct at the α -methylene- γ -butyrolactone by Le Châtelier's principle.

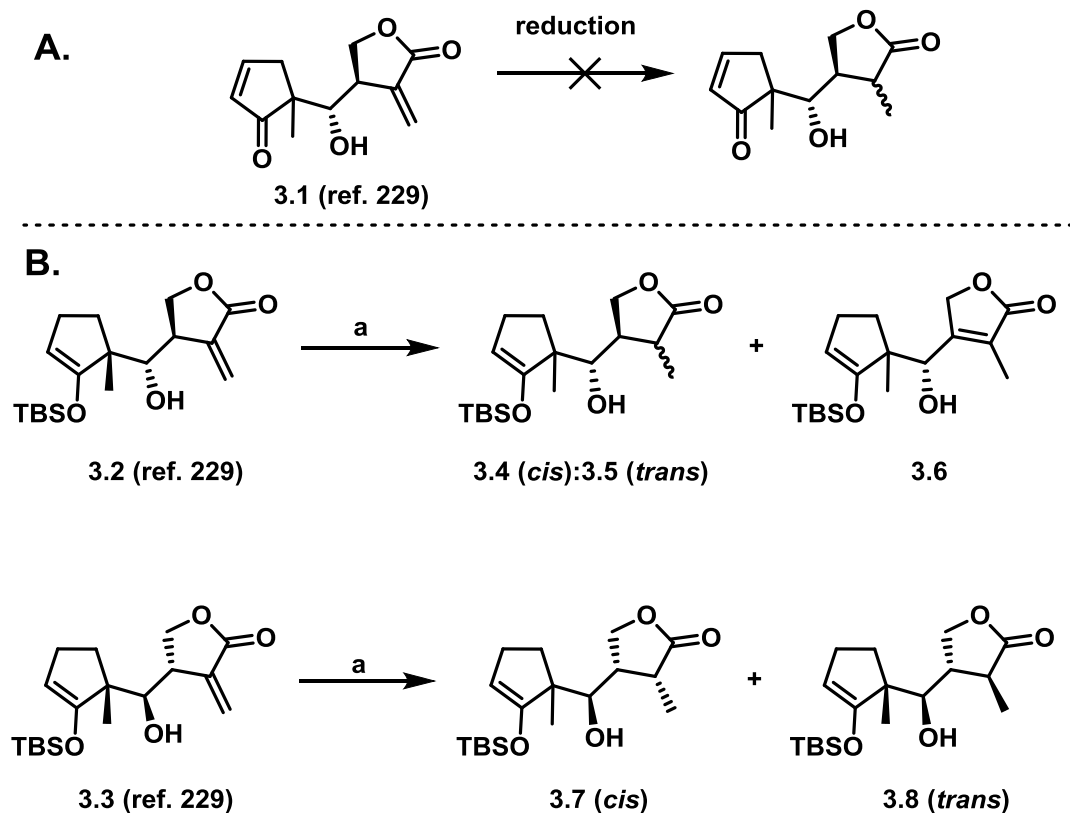
Helenalin-based probes **3.1a** and **3.1b** have been demonstrated to directly interact at the DNA-binding surface of p65 containing Cys38 and Cys120, two solvent exposed cysteines important for DNA-binding interactions.^{31a, 229} Small molecules containing an α -methylene- γ -butyrolactone typically react with many proteins containing solvent exposed cysteines, which can lead to off-target toxicity. Because the endocyclic enone undergoes a reversible hetero-Michael addition with cysteamine, removal of the α -methylene- γ -butyrolactone but leaving the cyclopentenone intact could lead to an inhibitor of the NF- κ B pathway that forms a *reversible* covalent bond to p65. Thus, helenalin-based probes were designed containing only the endocyclic enone as the sole Michael acceptor.

3.3 Reduction of Simplified Helenalin Intermediates

To determine how both Michael acceptors contribute to the inhibition of the NF- κ B pathway, a synthesis was designed to differentiate the Michael acceptors from a common intermediate. Initial attempts to selectively reduce the exocyclic methylene over the cyclopentenone starting from the previously synthesized simplified helenalin probes

3.1a/b²²⁹ resulted in non-selective reduction of both Michael acceptors or decomposition (**Scheme 3.3.1A**). Utilizing boron or aluminum derived hydride sources for selective reduction of the exocyclic methylene over the cyclopentenone were unsuccessful because of the compounds' inherent base-sensitive nature. Short reaction times (1-10 min) under 1 atm of H₂ or utilizing ammonium formate as the source of hydrogen in the presence of Pd/C were unsuccessful.²³⁵ Because selectively reducing the exocyclic methylene over the cyclopentenone was unfruitful, a synthetic strategy was developed to install the endocyclic enone after reduction of the exocyclic methylene.

Intermediates **3.2** and **3.3** were previously synthesized containing a *tert*-butyl dimethyl silyl enol ether to protect the ketone.²²⁹ This approach would allow for installation of the endocyclic enone via a Saegusa-Ito oxidation after reduction of the exocyclic methylene (see **Section 3.9** for improved synthesis of **3.2** and **3.3**).²¹⁸ Hydrogenation of **3.2** and **3.3** with PtO₂ under 1 atm of H₂ for 30 minutes was successful at reducing the exocyclic methylene of diastereomers **3.2** and **3.3** in the presence of the silyl enol ether (**Scheme 3.3.1B**). Hydrogenation of **3.2** resulted in an inseparable mixture of **3.4** and **3.5** in 78% overall yield in a 3:2 dr favoring the *cis*-methyl product. Interestingly, an isomerized product **3.6** was also isolated in 20% yield. This compound likely arises due to the Pt center forming a complex with the resulting enolate of the lactone ring (after delivering one hydride to the exocyclic methylene), which enables a β -hydride elimination, and gives the less reactive quaternary olefin.²³⁶ The other silyl enol ether diastereomer **3.3** was subjected to the same reducing conditions and resulted in two separable diastereomers **3.7** and **3.8** with a 9:1 dr favoring the *cis*-methyl group (89% overall yield). The isomerized product was surprisingly not observed in this reaction, although β -hydride elimination is theoretically possible. This is especially interesting considering the preferred diastereomer **3.7** requires hydride addition and complexation to the top face of the exocyclic methylene, resulting in the required position for β -hydride elimination.



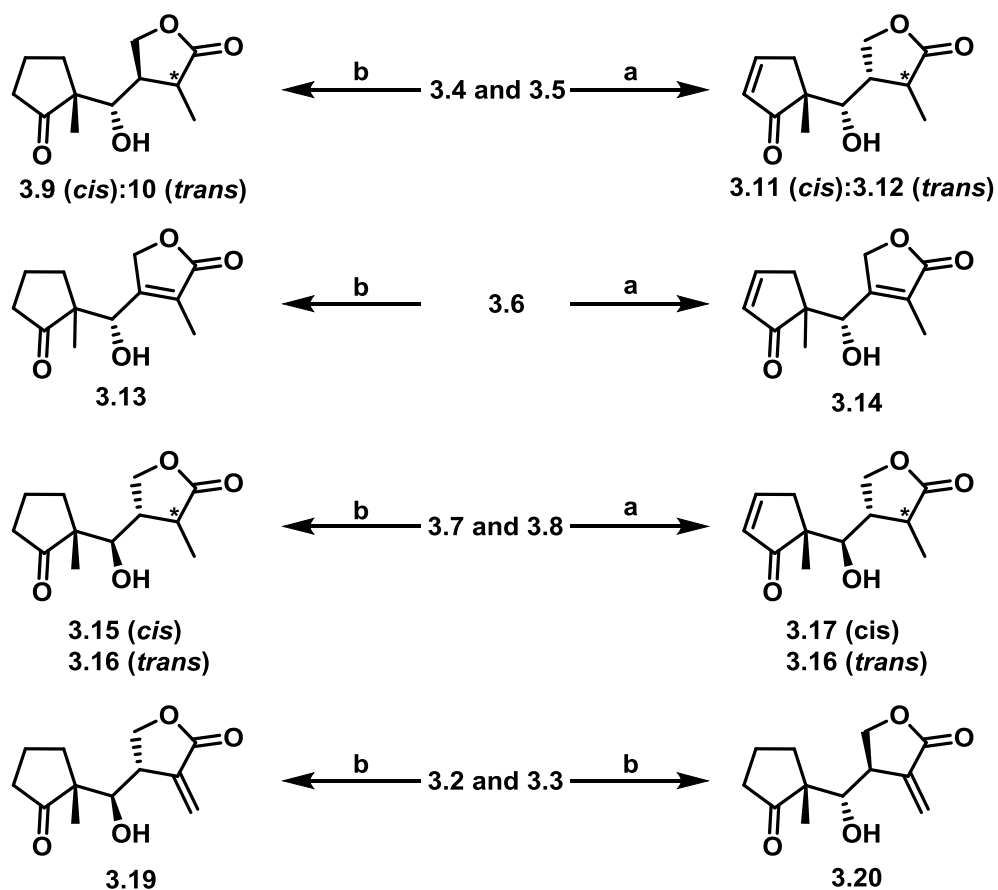
Scheme 3.3.1. **A.** Attempts to selectively reduce helenalin-based analogues **3.1a/b** resulted in complete reduction of both α,β -unsaturated carbonyls or degradation products. **B.** Reduction of the exocyclic methylene of silyl enol ether derivatives **3.2** and **3.3**.^a

^a**Reagents and Conditions:** (a) PtO_2 , 1 atm H_2 , 78% for **3.4(cis)**:**3.5(trans)**, 3:2 dr (inseparable); 20% for **3.6**; 89% for separable compounds **3.7(cis)**:**3.8(trans)**, 9:1 dr (separable).

3.4 Synthesis of Reduced Simplified Helenalin Analogues

The mixture of diastereomers **3.4** and **3.5**, the isomerized product **3.6**, and the separated diastereomers **3.7** and **3.8** were all further derivatized, either by deprotection in the presence of TFA, resulting in compounds without Michael acceptors, or subjected to Saegusa-Ito oxidation conditions to install the endocyclic enone as the single Michael acceptor (**Scheme 3.4.1**). Deprotecting the mixture of diastereomers **3.4** and **3.5** with TFA over 15 minutes resulted in two separable diastereomers **3.9** and **3.10** in a 3:2 dr and 76% overall yield. Intermediates **3.4** and **3.5** were reacted as a mixture with $\text{Pd}(\text{OAc})_2$ in DMSO under 1 atm of O_2 for 48 hours and again resulted in two separable diastereomers **3.11** and **3.12** in a 3:2 dr and 85% overall yield. The isomerized product **3.6** was also

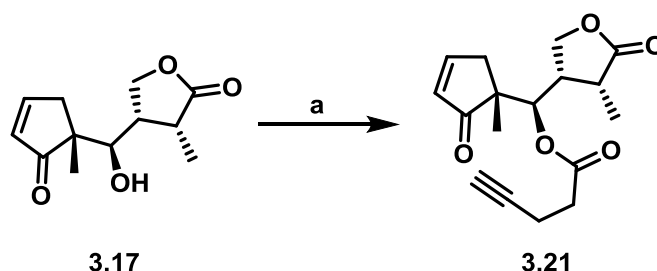
subjected to deprotection and Saegusa-Ito oxidation to give **3.13** and **3.14** in 71% and 35% yield respectively. Intermediates **3.7** and **3.8** were deprotected to give **3.15** and **3.16** in 84% and 86% yield respectively. Exposing **3.7** and **3.8** to the Saegusa-Ito oxidation conditions gave enones **3.17** and **3.18** in modest yields (22% and 55% yield respectively). Intermediates **3.2** and **3.3** were deprotected to obtain **3.19** and **3.20** in 79% and 36% yield respectively, which lack the endocyclic enone but maintains the exocyclic methylene butyrolactone Michael acceptor.



Scheme 3.4.1. Deprotection and Saegusa oxidation of silyl enol ethers for synthesis of helenalin-based analogues.^a

^a**Reagents and Conditions:** (a) Pd(OAc)₂, DMSO, 1 atm O₂, 85% yield for **3.11(cis):3.12(trans)**, 3:2 dr (separable), 31% for **3.14**, 22% for **3.17**, 55% for **3.18**; (b) TFA, DCM, 76% for **3.9(cis):3.10(trans)**, 3:2 dr (separable), 71% for **3.13**, 84% for **3.15**, 86% for **3.16**, 79% for **3.19**, 36% for **3.20**. *Represents carbon center with *cis* or *trans* stereochemistry.

Previously, esterifying the simplified helenalin analogues **3.1a/b** with 4-pentynoic acid caused an increased in the inhibition of the NF- κ B pathway in a cellular reporter assay.²²⁹ To determine if esterifying a reduced analogue containing only an endocyclic enone would lead to more potent inhibition of the NF- κ B pathway, **3.17** was esterified with 4-pentynoic acid (**Scheme 3.4.2**). The esterified derivative **3.21** was synthesized using DCC as the coupling reagent, resulting in a 32% yield.



Scheme 3.4.2. Esterification of **3.17**.^a

^a**Reagents and Conditions:** (a) DCC, 4-DMAP, 4-pentynoic acid, 40 °C, 16 h, 32%.

3.5 Stereochemical Determination of Reduced Simplified Helenalin Analogues

The stereochemistry of **3.2** and **3.3** were previously defined;²²⁹ however, the stereochemistry of the methyl group resulting from reduction with PtO₂ needed to be determined for each derivative. Attempts to define the stereochemistry of the reduced methyl group using the TBS protected derivatives (**3.4**, **3.5**, **3.7**, and **3.8**) were unsuccessful because of instability over the course of the NOESY experiments and interference of signals from the silyl *tert*-butyl and methyl groups. Therefore, analogues **3.9–3.11**, **3.15**, and **3.16** were used to define the stereochemistry of the reduced methyl group of each analogue. Diagnostic NOE correlations are shown in **Figure 3.5.1**.

Derivative **3.9** displayed an NOE correlation between the reduced methyl substituent and the proton geminal to the secondary hydroxyl group, compared to compound **3.10** that showed an NOE correlation between the β -lactone proton and the methyl group, suggesting both substituents are on the same face of the lactone ring.

Based on these correlations, the methyl substituent of **3.9** was assigned *cis* to the lactone ring stereocenter and the methyl substituent of **3.10** was determined to be in the *trans* configuration. The stereochemistry of **3.11** was also determined by a distinct NOE correlation between the reduced methyl group and the proton geminal to the hydroxyl group.

The stereochemistry of the reduced derivatives synthesized from silyl enol ether **3.3** was determined using fully reduced compounds **3.15** and **3.16**. The stereochemistry of **3.15** was assigned *cis* to the lactone ring based on an NOE between the reduced methyl group and the proton geminal to the hydroxyl group. For compound **3.16**, NOE correlations between the methyl group and β -lactone proton, as well as an NOE correlation between the α -lactone proton and proton geminal to the hydroxyl group led to assigning the methyl group *trans* to the lactone ring stereocenter.

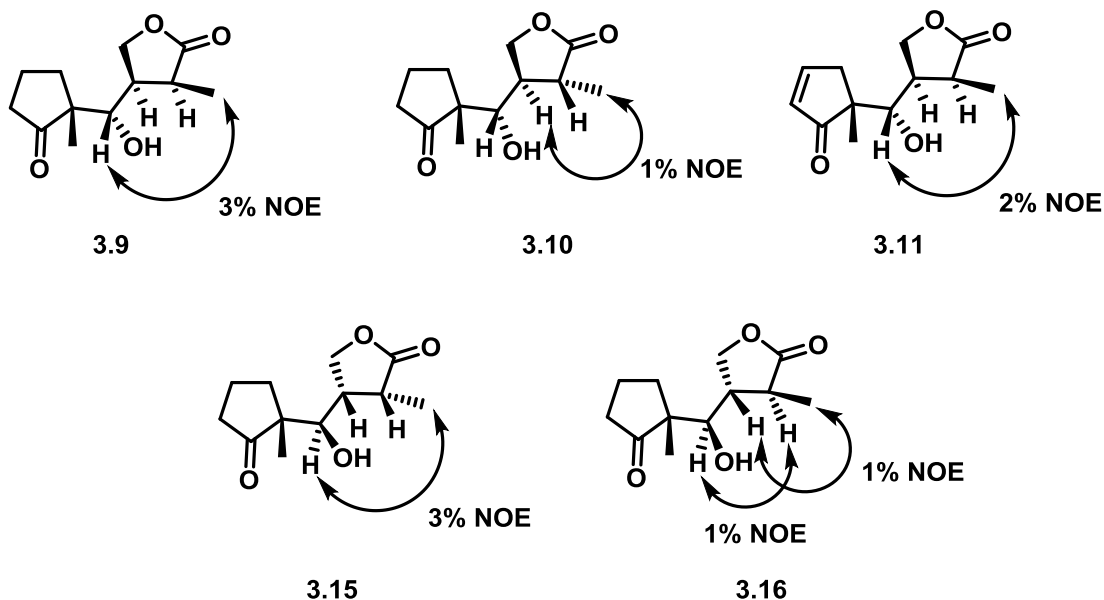


Figure 3.5.1. Stereochemical determination of reduced simplified helenalin-based analogues using NOESY. Diagnostic NOE correlations are shown above with the calculated percent NOE normalized from the total irradiation signal. The stereochemistry of compounds not shown above was deduced based on common intermediates.

3.6 Evaluation of reduced simplified helenalin analogues for NF- κ B inhibition

All of the synthesized reduced helenalin-based analogues were screened for NF- κ B inhibitory activity to determine the contribution of each Michael acceptor to inhibition of the NF- κ B pathway. A549 cells with a stably transfected NF- κ B luciferase gene was used to determine inhibitory activity (**Table 3.6.1**).²¹⁹ As expected, all fully reduced compounds containing no Michael acceptors did not significantly inhibit activation of the NF- κ B pathway at 250 μ M, the highest concentration tested. Cells dosed with 250 μ M of **3.9** and **3.10** had $86 \pm 1\%$ and $96 \pm 5\%$ signal from NF- κ B activation remaining respectively compared to the no compound, induced control. Cells dosed with **3.15** and **3.16** at 250 μ M had $99 \pm 8\%$ and $79 \pm 6\%$ NF- κ B activation remaining respectively. The isomerized product **3.13** without the endocyclic enone displayed little inhibitory activity as well when dosed at 250 μ M and 100 μ M ($78 \pm 5\%$ and $84 \pm 1\%$ respectively).

Compounds containing the endocyclic enone but not the exocyclic methylene had only slightly improved activity compared to the fully reduced analogues. Cells dosed at 100 μ M with **3.11** and **3.12** reduced NF- κ B activation to $85 \pm 3\%$ and $69 \pm 4\%$ respectively, and **3.11** displayed inhibition at 250 μ M ($50 \pm 5\%$ NF- κ B activity). Similarly, dosing cells with 250 μ M of **3.12** resulted in $34 \pm 4\%$ activity remaining. Derivatives **3.17** and **3.18** had little inhibitory activity against the NF- κ B pathway at 100 μ M ($86 \pm 12\%$ and $83 \pm 8\%$ NF- κ B activation respectively). At 250 μ M, **3.17** showed little inhibition ($78 \pm 9\%$) similar to **3.18** ($63 \pm 4\%$ activity remaining). Altogether, the stereochemistry of the reduced methyl group seemed to have little effect on the inhibitory activity of compounds **3.11-3.12** and **3.17-3.18** containing the endocyclic enone. Cells dosed with isomerize product **3.14** containing the endocyclic enone, had $43 \pm 4\%$ and $73 \pm 3\%$ luciferase activity at 250 μ M and 100 μ M respectively.

Analogues only containing an endocyclic enone displayed weak activity at high micromolar concentrations compared to the two derivatives with the exocyclic methylene intact but with no endocyclic enone. At 50 μ M, **3.19** and **3.20** showed complete inhibition of the NF- κ B pathway with only $12 \pm 1\%$ and $11 \pm 2\%$ luciferase activity remaining. Dosing **3.19** and **3.20** at 20 μ M reduced NF- κ B activity to $42 \pm 2\%$ and $43 \pm 1\%$

respectively. All cells maintained a cell viability $\geq 80\%$ throughout the 8 h assay (right side of **Table 3.6.1**).

Table 3.6.1. Inhibition of NF- κ B luciferase activity in A549 cells by synthesized compounds. Values are the mean \pm S.D. ($n \geq 3$) and were normalized to a 1% v/v DMSO, induced control. ^aInhibition data was obtained from ref. 229.

Compound	NF- κ B Activity \pm S.D. (%)			Cell Viability \pm S.D. (%)		
	250 μ M	100 μ M	50 μ M	250 μ M	100 μ M	50 μ M
3.9	86 \pm 1	91 \pm 3	-	94 \pm 1	113 \pm 25	-
3.10	86 \pm 5	97 \pm 8	-	96 \pm 5	99 \pm 8	-
3.11	50 \pm 5	85 \pm 3	92 \pm 6	88 \pm 3	96 \pm 3	102 \pm 2
3.12	34 \pm 4	69 \pm 4	93 \pm 11	109 \pm 5	111 \pm 14	105 \pm 6
3.13	78 \pm 5	84 \pm 1	-	103 \pm 5	102 \pm 5	-
3.14	43 \pm 4	73 \pm 3	-	89 \pm 6	98 \pm 8	-
3.15	99 \pm 8	99 \pm 7	-	99 \pm 1	95 \pm 11	-
3.16	79 \pm 6	82 \pm 2	-	103 \pm 4	102 \pm 3	-
3.17	78 \pm 9	86 \pm 12	95 \pm 5	104 \pm 7	96 \pm 11	95 \pm 3
3.18	63 \pm 4	83 \pm 8	88 \pm 6	97 \pm 5	93 \pm 17	96 \pm 8
3.21	23 \pm 4	62 \pm 2	76 \pm 1	80 \pm 3	84 \pm 2	97 \pm 3
Compound	50 μ M	20 μ M	10 μ M	50 μ M	20 μ M	10 μ M
3.19	12 \pm 1	42 \pm 2	69 \pm 2	70 \pm 6	87 \pm 14	93 \pm 6
3.20	11 \pm 2	43 \pm 1	71 \pm 2	67 \pm 6	86 \pm 4	90 \pm 5
3.1b^a	-	7 \pm 1	16 \pm 8	-	90 \pm 17	112 \pm 25

Screening these compounds for inhibitory activity towards the NF- κ B pathway showed that analogues without either Michael acceptor are inactive. Furthermore, analogues containing only the endocyclic enone (**3.11-3.12**, **3.14**, and **3.17-3.18**) had little activity, except at 250 μ M and 100 μ M. Despite limited inhibitory activity, these derivatives still demonstrate that the endocyclic enone contributes somewhat to inhibition against the NF- κ B pathway. Interestingly, **3.21**, which has the same stereochemistry as

3.15 but esterified with 5-pentynoic acid at the secondary hydroxyl group, has increased activity compared to the non-esterified derivatives, where only $23 \pm 4\%$ and $62 \pm 2\%$ NF- κ B activity is left at 250 μ M and 100 μ M respectively. This may be due to the decreased polarity of the compound compared to non-esterified derivatives resulting in better cell penetration.

3.7 Conclusion

In conclusion, thiol reactivity studies demonstrated that cysteamine forms an irreversible bond with the exocyclic methylene of compounds **3.1a/b**, compared to a reversible bond with the endocyclic enone. Analogues were synthesized that differentiated between the NF- κ B inhibitory contributions of the two Michael acceptors on **3.1a/b**. Because selective reduction of an exocyclic methylene lactone over a cyclopentenone was not possible, a new method was developed to reduce an exocyclic methylene in the presence of a silyl protected ketone, which served as a latent enone using a Saegusa-Ito oxidation. This method produced a variety of analogues for testing in a NF- κ B luciferase reporter assay. Complete reduction of the two Michael acceptors abolished all inhibitory activity in the NF- κ B luciferase assay. Reducing the exocyclic methylene to a methyl group decreased activity significantly, whereas removal of the endocyclic enone had little effect on inhibition of the NF- κ B pathway. The stereochemistry of the reduced methyl group did not significantly affect activity between analogues. This suggests that the endocyclic enone is not sufficient for significant inhibition of the NF- κ B pathway, despite the endocyclic enones of **3.1a/b** being reactive towards cysteamine. The reversibility of the hetero-Michael addition between thiols and the endocyclic enone could play a key role in the reduction of inhibitory activity.

3.8 Experimental

General Methods and Materials

Unless otherwise noted, reactions were performed in flame-dried glassware under a nitrogen or argon atmosphere and stirred with a Teflon-coated magnetic stir bar. Liquid reagents and solvents were transferred via syringe and cannula using standard techniques. Reaction solvents dichloromethane (DCM), N,N-dimethylformamide (DMF), tetrahydrofuran (THF) and diethyl ether (Et₂O) were dried by passage over a column of activated alumina using a solvent purification system (MBraun). All other chemicals were used as received unless otherwise noted. Reaction temperatures above 23 °C refer to oil bath temperature, which was controlled by a temperature modulator. Reaction progress was monitored by thin layer chromatography using EMD Chemicals Silica Gel 60 F254 glass plates (250 μm thickness) and visualized by UV irradiation (at 254 nm) and/or KMnO₄ stain. Silica gel chromatography was performed on a Teledyne-Isco Combiflash R_f-200 instrument utilizing Redisep R_f High Performance silica gel columns (Teledyne-Isco) or flash column chromatography was performed using SiliCycle silica gel (32-63 μm particle size, 60 Å pore size). ¹H NMR (400, 500, or 600 MHz) and ¹³C NMR (100, 125, 150 MHz) spectra were recorded at room temperature on a Bruker NMR spectrometer. ¹H and ¹³C chemical shifts (δ) are reported relative to the solvent signal, CHCl₃ (δ = 7.26 for ¹H NMR and δ = 77.00 for ¹³C NMR). Some spectra contain TMS (0.05% v/v). High resolution mass spectral data were obtained at the Analytical Biochemistry Core Facility of the Masonic Cancer Center on an LTQ OrbiTrap Velos Mass Spectrometer (Thermo Fisher).

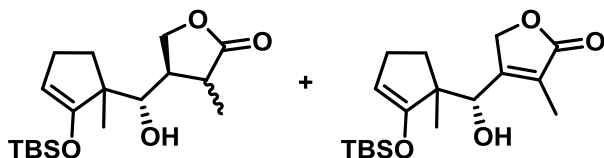
The purity of all UV active compounds tested in biological assays were analyzed via analytical HPLC analysis on an Agilent 1200 series instrument equipped with a diode array detector (wavelength monitored = 215 nm) and a Zorbax SBC18 column (4.6 x 150 mm, 5 μm, Agilent Technologies). All compounds tested in biological assays were >95% pure by HPLC. See **Section 3.11** for compound purities.

General Procedures

General Procedure A: Reduction of the exocyclic methylene butyrolactone. The substrate was dissolved in EtOAc, PtO₂ was added, and the reaction was stirred at RT. The reaction flask was degassed (3X) and backfilled with H₂ (1 atm) and then allowed to react for 30 minutes. The reaction flask was then degassed (3 min, 1X) and backfilled to the open air. The suspension was filtered through celite and rinsed with EtOAc (3X, 10 mL). The resulting solution was concentrated *in vacuo*.

General Procedure B: Deprotection of the silyl enol ether. The substrate was dissolved in DCM and stirred. The reaction was not anhydrous or kept under an inert atmosphere. TFA was added to the reaction and stirred for 15 minutes at RT. The reaction was quenched with aqueous NaHCO₃ (sat'd, 20 mL) and extracted with DCM (3X). The resulting organic layer was dried over Na₂SO₄ and concentrated *in vacuo*.

General Procedure C: Saegusa-Ito oxidation. The substrate was dissolved in DMSO and Pd(OAc)₂ was added. The reaction was degassed and backfilled with O₂ (1X, 1 atm). The reaction was stirred for 48 hrs at RT. Then, water (40 mL) was added to the reaction and extracted with EtOAc (3X, 20 mL). The resulting organic layer was washed with H₂O (1X, 15 mL) and brine (1X, 10 mL). The organic layer was dried over Na₂SO₄ and concentrated *in vacuo*.

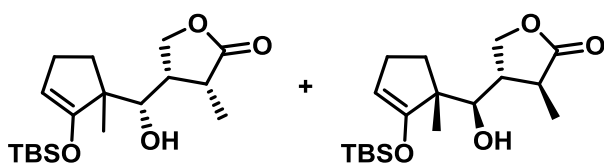


(3*S*,4*R*)-4-((*S*)-((*R*)-2-((tert-butyldimethylsilyl)oxy)-1-methylcyclopent-2-en-1-yl)(hydroxy)methyl)-3-methyldihydrofuran-2(3*H*)-one (**3.4**), (3*R*,4*R*)-4-((*S*)-((*R*)-2-((tert-butyldimethylsilyl)oxy)-1-methylcyclopent-2-en-1-yl)(hydroxy)methyl)-3-methyldihydrofuran-2(3*H*)-one (**3.5**), and 4-((*S*)-((*R*)-2-((tert-butyldimethylsilyl)oxy)-1-methylcyclopent-2-en-1-yl)(hydroxy)methyl)-3-methylfuran-2(5*H*)-one (**3.6**). Followed **General Procedure A**: Compound **3.2** (100 mg, 0.295 mmol); EtOAc (5 mL); PtO₂ (7 mg, 0.030 mmol). The crude product was SiO₂ (deactivated with 1% TEA) purified with EtOAc (0-25%) in hexanes to give an inseparable mixture of diastereomers **3.4** and **3.5** (78 mg, 78% yield) and the isomerized product **3.6** (20 mg, 20% yield).

Data for **3.4** (major diastereomer, 3:2 dr): ¹H NMR (500 MHz, CDCl₃): δ 4.64 (t, *J* = 2.4 Hz, 1H)*, 4.29 (dd, *J* = 8.8, 7.6 Hz, 1H), 4.07 (dd, *J* = 11.3, 8.8 Hz, 1H), 3.62 (dd, *J* = 9.9, 3.9 Hz, 1H), 2.82 – 2.74 (m, 1H), 2.73 – 2.66 (m, 1H)*, 2.30 – 2.21 (m, 1H), 2.21 – 2.13 (m, 1H)*, 1.97 (d, *J* = 4.0 Hz, 1H), 1.95 – 1.87 (m, 1H)*, 1.60 – 1.48 (m, 1H)*, 1.34 (d, *J* = 7.6 Hz, 3H)*, 1.01 (s, 3H), 0.93 (s, 9H)*, 0.21 (s, 3H)*, 0.18 (s, 3H)*. ¹³C NMR (125 MHz, CDCl₃): δ 180.2, 156.9, 101.6, 73.2, 68.6, 51.7, 42.8, 37.9, 29.4, 25.56*, 25.53*, 22.1, 17.9, 10.4, -4.65*, -5.32*. *Overlapping signals for diastereomers.

Data for **3.5** (minor diastereomer): ¹H NMR (500 MHz, CDCl₃): δ 4.66 (t, *J* = 2.4 Hz, 1H)*, 4.36 (app t, *J* = 8.7 Hz, 1H), 4.01 (app t, *J* = 8.8 Hz, 1H), 3.57 (dd, *J* = 6.1, 4.2 Hz, 1H), 2.73 – 2.66 (m, 1H)*, 2.41 – 2.32 (m, 1H), 2.30 – 2.21 (m, 1H)*, 2.21 – 2.13 (m, 1H)*, 2.03 (d, *J* = 4.3 Hz, 1H), 2.01 – 1.94 (m, 1H)*, 1.60 – 1.48 (m, 1H)*, 1.36 (d, *J* = 7.4 Hz, 3H)*, 1.06 (s, 3H), 0.93 (s, 9H)*, 0.21 (s, 3H)*, 0.18 (s, 3H)*. ¹³C NMR (125 MHz, CDCl₃): δ 180.3, 156.7, 101.9, 76.9, 70.3, 51.8, 45.0, 36.7, 30.0, 25.62*, 25.54*, 22.3, 18.0, 16.9, -4.69*, -5.33*. *Overlapping signals for diastereomers. HRMS-ESI⁺ (*m/z*): calc'd [M+H]⁺ for C₁₈H₃₂O₄Si 341.2143, found 341.2133.

Data for **3.6**: ^1H NMR (500 MHz, CDCl_3): δ 4.91 (dq, $J = 17.2, 1.9$ Hz, 1H), 4.82 – 4.75 (m, 1H), 4.72 (d, $J = 4.3$ Hz, 1H), 4.70 (t, $J = 2.4$ Hz, 1H), 2.39 (d, $J = 4.4$ Hz, 1H), 2.29 – 2.20 (m, 1H), 2.18 – 2.11 (m, 1H), 2.00 – 1.92 (m, 1H), 1.87 (t, $J = 2.0$ Hz, 3H), 1.56 – 1.48 (m, 1H), 1.08 (s, 3H), 0.96 (s, 9H), 0.23 (s, 3H), 0.20 (s, 3H). ^{13}C NMR (125 MHz, CDCl_3): δ 175.0, 159.4, 155.9, 125.3, 102.6, 77.3, 76.8, 71.8, 70.2, 52.4, 30.1, 25.6, 25.4, 21.8, 18.0, 9.7, -4.6, -5.4. HRMS-ESI $^+$ (m/z): calc'd $[\text{M}+\text{H}]^+$ for $\text{C}_{18}\text{H}_{30}\text{O}_4\text{Si}$ 339.1986, found 339.1980.

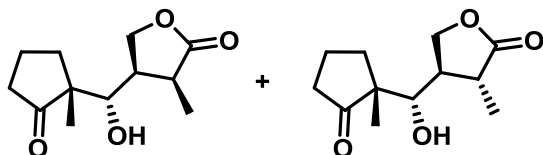


(3R,4S)-4-((R)-((R)-2-((tert-butyldimethylsilyl)oxy)-1-methylcyclopent-2-en-1-yl)(hydroxy)methyl)-3-methyldihydrofuran-2(3H)-one (**3.7**) and (3S,4S)-4-((R)-((R)-2-((tert-butyldimethylsilyl)oxy)-1-methylcyclopent-2-en-1-yl)(hydroxy)methyl)-3-methyldihydrofuran-2(3H)-one (**3.8**). Followed **General Procedure A**: Compound **3.3** (50 mg, 0.148 mmol); EtOAc (5 mL); PtO_2 (4 mg, 0.015 mmol). The crude product was SiO_2 purified with EtOAc (0-25%) in hexanes to give separable diastereomers **3.7** (40 mg) and **3.8** (4 mg) with an 89% overall yield (9:1 dr).

Data for **3.7** (major diastereomer, contains <5% of minor diastereomer): ^1H NMR (500 MHz, CDCl_3): δ 4.58 (t, $J = 2.4$ Hz, 1H), 4.30 – 4.23 (m, 1H), 4.03 (dd, $J = 11.2, 9.0$ Hz, 1H), 3.73 (dd, $J = 9.7, 2.6$ Hz, 1H), 3.09 (d, $J = 3.1$ Hz, 1H), 2.81 – 2.70 (m, 2H), 2.30 – 2.21 (m, 1H), 2.21 – 2.12 (m, 1H), 1.73 – 1.63 (m, 1H), 1.54 – 1.46 (m, 1H), 1.32 (d, $J = 6.9$ Hz, 3H), 1.14 (s, 3H), 0.93 (s, 9H), 0.22 (d, $J = 1.9$ Hz, 3H), 0.17 (s, 3H). ^{13}C NMR (125 MHz, CDCl_3): δ 180.4, 158.6, 101.2, 75.6, 68.1, 49.8, 43.1, 37.5, 31.6, 25.6, 25.5, 19.7, 18.0, 10.2, -4.4, -5.6. HRMS-ESI $^+$ (m/z): calc'd $[\text{M}+\text{H}]^+$ for $\text{C}_{18}\text{H}_{32}\text{O}_4\text{Si}$ 341.2143, found 341.2139.

Data for **3.8** (minor diastereomer): ^1H NMR (500 MHz, CDCl_3): δ 4.59 (t, $J = 2.4$ Hz, 1H), 4.32 (dd, $J = 9.2, 8.3$ Hz, 1H), 3.95 (app t, $J = 9.1$ Hz, 1H), 3.65 (dd, $J = 7.4, 3.5$ Hz,

1H), 2.74 (d, $J = 3.6$ Hz, 1H), 2.73 – 2.65 (m, 1H), 2.41 – 2.31 (m, 1H), 2.30 – 2.21 (m, 1H), 2.21 – 2.12 (m, 1H), 1.83 – 1.74 (m, 1H), 1.59 – 1.51 (m, 1H), 1.38 (d, $J = 7.2$ Hz, 3H), 1.13 (s, 3H), 0.93 (s, 9H), 0.21 (s, 3H), 0.18 (s, 3H). Impurities: 1.56 (H₂O). ¹³C NMR (125 MHz, CDCl₃): δ 180.2, 158.3, 101.1, 80.0, 69.9, 50.7, 45.9, 38.0, 31.7, 25.7, 25.5, 20.5, 18.0, 17.0, -4.4, -5.5. HRMS-ESI⁺ (m/z): calc'd [M+H]⁺ for C₁₈H₃₂O₄Si 341.2143, found 341.2137.

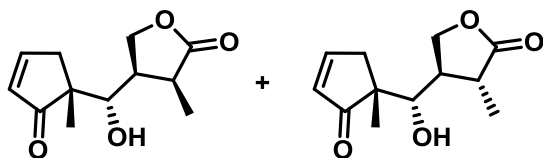


(3S,4R)-4-((S)-hydroxy((R)-1-methyl-2-oxocyclopentyl)methyl)-3-methyldihydrofuran-2(3H)-one (**3.9**) and (3R,4R)-4-((S)-hydroxy((R)-1-methyl-2-oxocyclopentyl)methyl)-3-methyldihydrofuran-2(3H)-one (**3.10**). Followed **General Procedure B**: Mixture of diastereomers **3.4** and **3.5** (78 mg, 0.288 mmol); DCM (5 mL); TFA (0.1 mL). The crude product was SiO₂ purified with EtOAc (0-50%) in hexanes to give separable diastereomers **3.9** (25 mg) and **3.10** (14 mg) with a 76% overall yield (3:2 dr).

Data for **3.9** (major diastereomer): ¹H NMR (500 MHz, CDCl₃): δ 4.30 (dd, $J = 8.9, 7.6$ Hz, 1H), 4.06 (dd, $J = 11.1, 8.8$ Hz, 1H), 3.97 (dd, $J = 9.7, 3.8$ Hz, 1H), 2.82 – 2.69 (m, 2H), 2.48 – 2.40 (m, 1H), 2.29 – 2.21 (m, 1H), 2.20 – 2.12 (m, 1H), 2.12 – 2.07 (m, 1H), 2.07 – 2.01 (m, 1H), 1.95 – 1.83 (m, 1H), 1.75 – 1.68 (m, 1H), 1.32 (d, $J = 7.2$ Hz, 3H), 0.91 (s, 3H). Impurities: 1.56 (H₂O). ¹³C NMR (125 MHz, CDCl₃): δ 222.7, 179.5, 72.2, 68.0, 54.0, 42.8, 37.6, 37.4, 30.2, 18.8, 18.3, 10.5. HRMS-ESI⁺ (m/z): calc'd [M+H]⁺ for C₁₂H₁₈O₄ 227.1278, found 227.1270.

Data for **3.10** (minor diastereomer): ¹H NMR (500 MHz, CDCl₃): δ 4.39 (app t, $J = 8.8$ Hz, 1H), 4.00 (dd, $J = 9.1, 8.1$ Hz, 1H), 3.90 (t, $J = 4.7$ Hz, 1H), 2.77 – 2.65 (m, 1H), 2.45 – 2.34 (m, 2H), 2.32 – 2.23 (m, 1H), 2.20 – 2.09 (m, 1H), 2.07 – 1.99 (m, 1H), 1.93 – 1.81 (m, 1H), 1.74 – 1.67 (m, 1H), 1.35 (d, $J = 7.3$ Hz, 3H), 0.95 (s, 3H). ¹³C NMR

(125 MHz, CDCl₃): δ 222.9, 179.8, 75.5, 69.8, 54.0, 44.9, 37.7, 36.5, 30.5, 19.3, 18.4, 16.8. HRMS-ESI⁺ (m/z): calc'd [M+H]⁺ for C₁₂H₁₈O₄ 227.1278, found 227.1271.

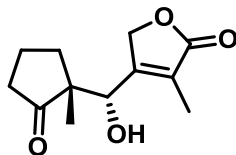


(3S,4R)-4-((S)-hydroxy((R)-1-methyl-2-oxocyclopent-3-en-1-yl)methyl)-3-methyldihydrofuran-2(3H)-one (**3.11**) and (3R,4R)-4-((S)-hydroxy((R)-1-methyl-2-oxocyclopent-3-en-1-yl)methyl)-3-methyldihydrofuran-2(3H)-one (**3.12**). Followed **General Procedure C**: Mixture of diastereomers **3.4** and **3.5** (8 mg, 0.022 mmol); Pd(OAc)₂ (3 mg, 0.011 mmol); DMSO (2 mL). The crude product was purified using a SiliCycle glass backed extra hard layer prep TLC plate (particle size: 60 Å, plate size: 20x20 cm, thickness: 1000 μ m, indicator F-254) with an EtOAc (70%) in hexanes eluent system to give the separated diastereomers **3.11** (3 mg) and **3.12** (2 mg) in a 3:2 dr and 85% overall yield.

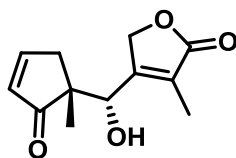
Data for **3.11** (major diastereomer): ¹H NMR (500 MHz, CDCl₃): δ 7.80 – 7.76 (m, 1H), 6.20 – 6.15 (m, 1H), 4.28 (dd, *J* = 8.8, 7.5 Hz, 1H), 4.10 (dd, *J* = 11.1, 8.8 Hz, 1H), 4.01 – 3.95 (m, 1H), 2.90 (dt, *J* = 18.9, 2.5 Hz, 1H), 2.81 – 2.70 (m, 2H), 2.45 – 2.37 (m, 1H), 2.14 (d, *J* = 6.1 Hz, 1H), 1.34 (d, *J* = 7.3 Hz, 3H), 1.07 (s, 3H). Impurities: 1.56 (H₂O). ¹³C NMR (125 MHz, CDCl₃): δ 213.7, 179.3, 164.3, 132.2, 72.7, 68.0, 51.5, 43.6, 38.8, 37.6, 21.2, 10.6. HRMS-ESI⁺ (m/z): calc'd [M+H]⁺ for C₁₂H₁₆O₄ 225.1121, found 225.1113.

Data for **3.12** (minor diastereomer): ¹H NMR (500 MHz, CDCl₃): δ 7.80 – 7.77 (m, 1H), 6.21 – 6.17 (m, 1H), 4.37 (app t, *J* = 8.8 Hz, 1H), 4.03 (app t, *J* = 8.9 Hz, 1H), 3.94 (t, *J* = 5.6 Hz, 1H), 2.99 (dt, *J* = 18.7, 2.5 Hz, 1H), 2.77 – 2.68 (m, 1H), 2.48 – 2.36 (m, 2H), 2.18 (d, *J* = 6.1 Hz, 1H), 1.35 (d, *J* = 7.2 Hz, 3H), 1.09 (s, 3H). Impurities: 1.56 (H₂O), 1.26 and 0.86 (grease). ¹³C NMR (125 MHz, CDCl₃): δ 213.8, 179.7, 164.6, 132.4, 74.7,

69.6, 51.6, 45.3, 39.1, 36.0, 21.5, 16.8. Impurities: 29.9 (grease). HRMS-ESI⁺ (m/z) calc'd [M+H]⁺ for C₁₂H₁₆O₄ 225.1121, found 225.1113.

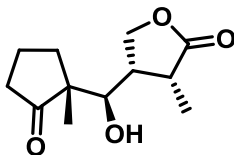


4-((S)-hydroxy((R)-1-methyl-2-oxocyclopentyl)methyl)-3-methylfuran-2(5H)-one (**3.13**). Followed **General Procedure B**: Compound **3.6** (11 mg, 0.033 mmol); DCM (3 mL); TFA (0.1 mL). The crude product was SiO₂ purified with EtOAc (0-80%) in hexanes to give **13** (5 mg, 71% yield) as a white solid. ¹H NMR (500 MHz, CDCl₃): δ 5.00 (bs, 1H), 4.90 (dq, *J* = 17.5, 2.0 Hz, 1H), 4.73 – 4.66 (m, 1H), 2.50 – 2.45 (m, 1H), 2.43 (dt, *J* = 8.3, 1.8 Hz, 1H), 2.32 – 2.23 (m, 1H), 2.23 – 2.13 (m, 1H), 2.10 – 2.01 (m, 1H), 1.94 – 1.81 (m, 1H), 1.89 (t, *J* = 2.0 Hz, 3H), 1.68 – 1.62 (m, 1H), 0.95 (s, 3H). ¹³C NMR (125 MHz, CDCl₃): δ 222.0, 174.6, 157.9, 125.5, 70.5, 70.1, 53.9, 38.0, 30.3, 19.4, 18.4, 9.7. HRMS-ESI⁺ (m/z): calc'd [M+H]⁺ for C₁₂H₁₆O₄ 225.1121, found 225.1115.

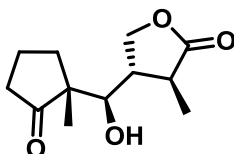


4-((S)-hydroxy((R)-1-methyl-2-oxocyclopent-3-en-1-yl)methyl)-3-methylfuran-2(5H)-one (**3.14**). Followed **General Procedure C**: Compound **3.6** (31 mg, 0.092 mmol); Pd(OAc)₂ (10 mg, 0.046 mmol); DMSO (2 mL). The crude product was SiO₂ purified with EtOAc (0-70%) in hexanes to give **14** (7 mg, 35% yield) as a white solid. ¹H NMR (500 MHz, CDCl₃): δ 7.80 – 7.75 (m, 1H), 6.26 – 6.21 (m, 1H), 5.04 (d, *J* = 5.6 Hz, 1H), 4.95 – 4.88 (m, 1H), 4.69 – 4.62 (m, 1H), 2.93 (dt, *J* = 18.5, 2.5 Hz, 1H), 2.60 (d, *J* = 5.7 Hz, 1H), 2.41 – 2.34 (m, 1H), 1.93 (t, *J* = 2.0 Hz, 3H), 1.08 (s, 3H). Impurities: 1.26 and 0.86 (grease) ¹³C NMR (125 MHz, CDCl₃): δ 212.6, 174.4, 164.3, 157.4, 132.3, 126.2,

70.4, 69.8, 51.1, 38.7, 21.6, 9.6. HRMS-ESI⁺ (m/z): calc'd [M+H]⁺ for C₁₂H₁₄O₄ 223.0965, found 223.0958.

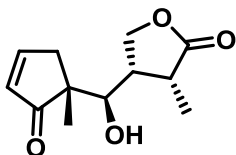


(3R,4S)-4-((R)-hydroxy((R)-1-methyl-2-oxocyclopentyl)methyl)-3-methyldihydrofuran-2(3H)-one (**3.15**). Followed **General Procedure B**: Compound **7** (21 mg, 0.062 mmol); DCM (3 mL); TFA (0.1 mL). The crude product was SiO₂ purified with EtOAc (0-50%) in hexanes to give **15** (12 mg, 84% yield) as a white solid. ¹H NMR (500 MHz, CDCl₃): δ 4.47 (s, 1H), 4.19 (t, *J* = 8.0 Hz, 1H), 3.95 (t, *J* = 9.9 Hz, 1H), 3.75 (d, *J* = 9.1 Hz, 1H), 2.87 – 2.75 (m, 2H), 2.49 (dd, *J* = 19.6, 8.7 Hz, 1H), 2.30 – 2.18 (m, 1H), 2.08 – 1.99 (m, 1H), 1.99 – 1.87 (m, 1H), 1.72 – 1.59 (m, 2H), 1.34 (d, *J* = 6.7 Hz, 3H), 1.14 (s, 3H). Impurities: 1.56 (H₂O), 1.26 and 0.86 (grease) ¹³C NMR (125 MHz, CDCl₃): δ 225.8, 179.8, 73.0, 67.4, 50.4, 41.9, 37.1, 37.0, 34.0, 18.7, 15.0, 10.2. HRMS-ESI⁺ (m/z): calc'd [M+H]⁺ for C₁₂H₁₈O₄ 227.1278, found 227.1270.

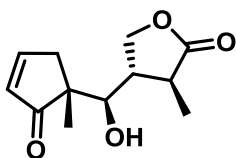


(3S,4S)-4-((R)-hydroxy((R)-1-methyl-2-oxocyclopentyl)methyl)-3-methyldihydrofuran-2(3H)-one (**3.16**). Followed **General Procedure B**: Compound **3.8** (6 mg, 0.002 mmol); DCM (3 mL); TFA (0.1 mL). The crude product was SiO₂ purified with EtOAc (0-40%) in hexanes to give **3.16** (4 mg, 86% yield) as a white solid. ¹H NMR (500 MHz, CDCl₃): δ 4.25 (bs, 1H), 4.20 (t, *J* = 8.7 Hz, 1H), 3.84 (t, *J* = 9.1 Hz, 1H), 3.61 (d, *J* = 7.2 Hz, 1H), 2.70 – 2.59 (m, 1H), 2.41 (dd, *J* = 19.5, 8.6 Hz, 1H), 2.33 – 2.22 (m, 1H), 2.22 – 2.09 (m, 1H), 2.02 – 1.77 (m, 2H), 1.69 – 1.55 (m, 2H), 1.34 (d, *J* = 7.1 Hz, 3H), 1.06 (s, 3H).

Impurities: 1.56 (H₂O), 1.26 and 0.86 (grease). ¹³C NMR (125 MHz, CDCl₃): δ 225.4, 179.8, 72.1, 68.7, 51.1, 45.3, 37.9, 37.0, 34.1, 18.6, 16.8, 15.2. Impurities: 29.8 (grease). HRMS-ESI⁺ (m/z): calc'd [M+H]⁺ for C₁₂H₁₈O₄ 227.1278, found 227.1270.

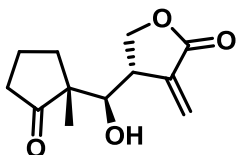


(3R,4S)-4-((R)-hydroxy((R)-1-methyl-2-oxocyclopent-3-en-1-yl)methyl)-3-methyldihydrofuran-2(3H)-one (**3.17**). Followed **General Procedure C**: Compound **3.7** (27 mg, 0.080 mmol); Pd(OAc)₂ (9 mg, 0.040 mmol); DMSO (4 mL). The crude product was SiO₂ purified with EtOAc (0-100%) in hexanes to give **17** (4 mg, 22% yield). ¹H NMR (500 MHz, CDCl₃): δ 7.78 – 7.70 (m, 1H), 6.23 – 6.17 (m, 1H), 4.14 – 4.06 (m, 1H), 4.02 – 3.95 (m, 2H), 3.78 (d, *J* = 9.3 Hz, 1H), 2.87 – 2.74 (m, 2H), 2.58 – 2.49 (m, 1H), 2.43 – 2.33 (m, 1H), 1.33 (d, *J* = 6.0 Hz, 3H), 1.24 (s, 3H). Impurities: 1.56 (H₂O). ¹³C NMR (125 MHz, CDCl₃): δ 214.8, 179.6, 163.6, 132.1, 72.0, 67.5, 48.7, 42.8, 40.4, 37.2, 19.1, 10.1. HRMS-ESI⁺ (m/z): calc'd [M+H]⁺ for C₁₂H₁₆O₄ 225.1121, found 225.1114.

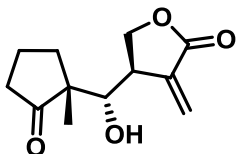


(3S,4S)-4-((R)-hydroxy((R)-1-methyl-2-oxocyclopent-3-en-1-yl)methyl)-3-methyldihydrofuran-2(3H)-one (**3.18**). Follows **General Procedure C**: Compound **3.8** (21 mg, 0.063 mmol); Pd(OAc)₂ (7 mg, 0.031 mmol); DMSO (4 mL). The crude product was SiO₂ purified with EtOAc (0-100%) in hexanes to give **3.18** (8 mg, 55% yield). ¹H NMR (500 MHz, CDCl₃): δ 7.77 – 7.72 (m, 1H), 6.22 – 6.16 (m, 1H), 4.20 (app t, *J* = 8.7 Hz, 1H), 3.91 (app t, *J* = 10.2 Hz, 1H), 3.74 – 3.68 (m, 2H), 2.76 – 2.68 (m, 1H), 2.66 –

2.59 (m, 1H), 2.46 – 2.38 (m, 1H), 2.36 – 2.28 (m, 1H), 1.40 (d, $J = 6.9$ Hz, 3H), 1.23 (s, 3H). Impurities: 1.56 (H₂O). ¹³C NMR (125 MHz, CDCl₃): δ 214.4, 179.5, 163.6, 132.3, 76.2, 69.1, 49.7, 45.9, 40.5, 37.8, 19.5, 16.8. HRMS-ESI⁺ (m/z): calc'd [M+H]⁺ for C₁₂H₁₆O₄ 225.1121, found 225.1115.

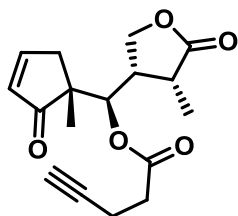


(S)-4-((R)-hydroxy((R)-1-methyl-2-oxocyclopentyl)methyl)-3-methylenedihydrofuran-2(3H)-one (**3.19**). Followed **General Procedure B: 3.3** (20 mg, 0.059 mmol); DCM (1 mL); TFA (0.1 mL). The crude product was SiO₂ purified with EtOAc (0-70%) in hexanes to give **3.19** (10 mg) in 79% yield. ¹H NMR (500 MHz, CDCl₃): δ 6.39 (dd, $J = 2.8, 1.1$ Hz, 1H), 6.15 (dd, $J = 2.5, 1.1$ Hz, 1H), 4.37 (d, $J = 1.5$ Hz, 1H), 4.33 (app t, $J = 8.5$ Hz, 1H), 4.09 (dd, $J = 9.1, 6.6$ Hz, 1H), 3.78 (dd, $J = 8.3, 1.5$ Hz, 1H), 3.40 – 3.34 (m, 1H), 2.52 – 2.42 (m, 1H), 2.30 – 2.19 (m, 1H), 2.08 – 2.00 (m, 1H), 1.98 – 1.88 (m, 1H), 1.88 – 1.80 (m, 1H), 1.78 – 1.71 (m, 1H), 1.15 (s, 3H). Impurities: 1.56 (H₂O), 1.26 and 0.86 (grease). ¹³C NMR (125 MHz, CDCl₃): δ 224.9, 170.5, 135.0, 126.4, 76.1, 67.6, 51.2, 41.8, 37.2, 34.8, 18.7, 15.8. HRMS-ESI⁺ (m/z): calc'd [M+H]⁺ for C₁₂H₁₆O₄ 225.1121, found 225.1115.



(R)-4-((S)-hydroxy((R)-1-methyl-2-oxocyclopentyl)methyl)-3-methylenedihydrofuran-2(3H)-one (**3.20**). Followed **General Procedure B: 2** (20 mg, 0.059 mmol); DCM (1 mL); TFA (0.1 mL). The crude product was SiO₂ purified with EtOAc (0-70%) in hexanes to give **3.20** (5 mg) in 36% yield. ¹H NMR (500 MHz, CDCl₃): δ 6.44 – 6.42 (m,

1H), 5.88 – 5.86 (m, 1H), 4.41 (dd, $J = 9.3, 7.8$ Hz, 1H), 4.19 (dd, $J = 9.3, 3.9$ Hz, 1H), 3.94 – 3.89 (m, 1H), 3.28 – 3.21 (m, 1H), 2.45 – 2.29 (m, 3H), 2.23 – 2.13 (m, 1H), 2.07 – 1.98 (m, 1H), 1.92 – 1.80 (m, 1H), 1.76 – 1.69 (m, 1H), 1.01 (s, 3H). Impurities: 1.56 (H₂O), 1.26 and 0.86 (grease). ¹³C NMR (125 MHz, CDCl₃): δ 222.3, 170.4, 134.6, 126.5, 75.5, 69.6, 53.8, 41.6, 38.0, 30.9, 19.5, 18.6. HRMS-ESI⁺ (m/z): calc'd [M+H]⁺ for C₁₂H₁₆O₄ 225.1121, found 225.1114.



(R)-((R)-1-methyl-2-oxocyclopent-3-en-1-yl)((3S,4R)-4-methyl-5-oxotetrahydrofuran-3-yl)methyl pent-4-ynoate (**3.21**). Compound **3.17** (15 mg, 0.065 mmol) was dissolved in DCM (3 mL). Then, 4-pentyonic acid (19 mg, 0.194 mmol) and 4-DMAP (24 mg, 0.194 mmol) were added, followed by addition of EDCI (37 mg, 0.194 mmol). The reaction was heated to 40 °C for 16 h. The reaction was quenched with H₂O (5 mL), extracted with DCM (3X, 10 mL), and the organic layer was concentrated in vacuo. The crude product was SiO₂ purified with EtOAc (0-60%) in hexanes to give **3.21** (6 mg) in 32% yield. ¹H NMR (500 MHz, CDCl₃): δ 7.78 – 7.71 (m, 1H), 6.26 – 6.12 (m, 1H), 5.38 (d, $J = 10.2$ Hz, 1H), 4.02 – 3.88 (m, 2H), 3.03 – 2.92 (m, 1H), 2.86 (m, 1H), 2.71 – 2.45 (m, 5H), 2.46 – 2.31 (m, 1H), 2.00 (t, $J = 2.5$ Hz, 1H), 1.18 (d, $J = 7.5$ Hz, 3H), 1.15 (s, 3H). Impurity: 1.56 (H₂O). ¹³C NMR (125 MHz, CDCl₃): δ 210.1, 178.8, 171.0, 163.1, 132.9, 82.2, 73.9, 69.7, 67.8, 50.3, 42.3, 39.9, 37.4, 33.7, 23.1, 14.7, 10.6. Impurity: 29.9 ('grease'). HRMS-ESI⁺ (m/z): calc'd [M+H]⁺ for C₁₇H₂₀O₅ 305.1384, found 305.1374.

Stereochemical determination by NOESY

The stereochemistry assignments for newly synthesized compounds were made using NOESY experiments with a Bruker Avance 500 MHz NMR. All samples were run at RT. All protons were assigned using COSY, HMBC, and HSQC prior to assigning stereochemistry based on NOE correlations. All NOE signals are normalized to the respective excitation signal to obtain percent NOE. The silyl enol ethers were not well suited for stereochemical determination because of their instability in solvent over the course of the 2D experiments and signal interference from the silyl methyl and *tert*-butyl protons.

All protons found to have diagnostic NOE correlations were predicted to be within a distance of 4 Å based on computationally minimized structures. All *ab initio* minimizations were completed using Jaguar (version 8.0) within Maestro (Schrödinger, Inc., version 10.2.010). All equilibrium conformer minimizations were calculated using the B3LYP method with the 6-31G** basis set in the gas phase (maximum iterations set to 48, calculation speed set to ‘accurate’).

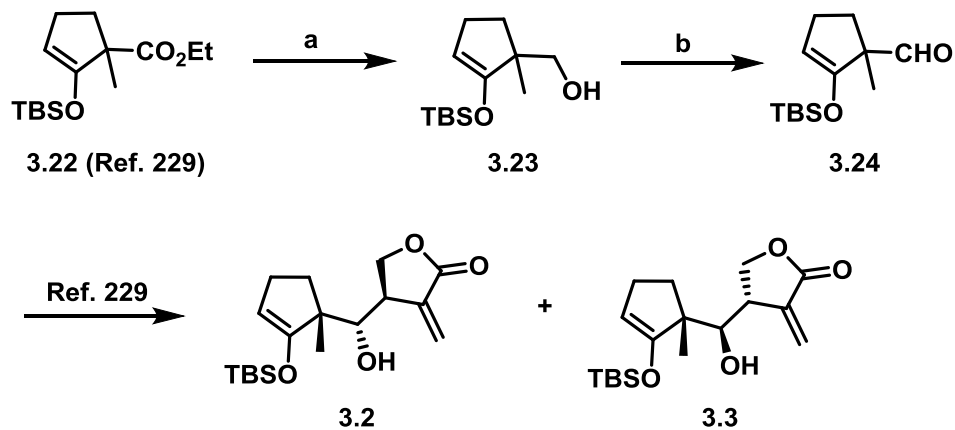
NF-κB Luciferase Reporter Assay

Compounds were tested for inhibition of the NF-κB pathway in stably transfected A549 cells containing an NF-κB driven luciferase gene as previously described.^{219,237} Additional details for this assay are also described in Chapter 2 of this thesis.

3.9 Improved synthesis of 3.2 and 3.3

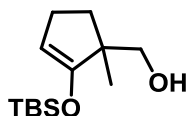
The synthesis of **3.2** and **3.3** has been previously reported but involves a reduction of the ester **3.22** to aldehyde **3.24** in the presence of 1 equivalent of DIBAL-H, which gave poor yields because of over-reduction to the alcohol **3.23**. To improve the overall yield of the synthesis of **3.2** and **3.3**, a two step procedure was used to first reduce **3.22** to

the alcohol **3.23** with 2 equivalents of DIBAL-H (96% yield), and then oxidize to the aldehyde **3.24** using a Pfitzner-Moffatt oxidation (91% yield, **Scheme 3.9.1**).



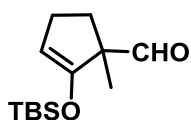
Scheme 3.9.1. Synthesis of Intermediates **3.23** and **3.24**. This is an improved synthesis of **3.2** and **3.3** from a previously reported synthesis from our lab.^{229, a}

^a**Reagents and Conditions:** (a) 2 equiv. DIBAL-H, THF, $-78\text{ }^{\circ}\text{C}$, 4 h. (b) 1:1 DMSO:DCM, DCC, H_3PO_4 , RT, 16 h.



(2-((tert-butyldimethylsilyl)oxy)-1-methylcyclopent-2-en-1-yl)methanol (**3.23**). Starting material **3.22** (0.75 g, 2.6 mmol) was dissolved in THF (20 mL) and cooled to $-78\text{ }^{\circ}\text{C}$. Then, DIBAL-H (5.2 mL, 5.2 mmol) was added dropwise at the same temperature and allowed to stir for 4 h. The reaction was quenched at $-78\text{ }^{\circ}\text{C}$ with H_2O (0.5 mL) and stirred for 5 min. Then, aqueous NaOH (0.5M, 0.5 mL) was added followed by addition H_2O (2 mL). The reaction mixture was allowed to warm to RT and then the precipitate was filtered. The resulting solution was concentrated *in vacuo* and SiO_2 purified with EtOAc (0-50%) in hexanes to give **3.23** (0.61 g, 96% yield). ^1H NMR (500 MHz, CDCl_3): δ 4.60 (t, $J = 2.4$ Hz, 1H), 3.49 (dd, $J = 10.5, 5.6$ Hz, 1H), 3.39 (dd, $J = 10.5, 6.6$ Hz, 1H), 2.22 – 2.16 (m, 2H), 1.93 – 1.86 (m, 1H), 1.68 – 1.64 (m, 1H), 1.63 – 1.56 (m,

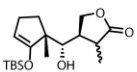
1H), 1.04 (s, 3H), 0.93 (s, 9H), 0.19 (s, 3H), 0.17 (s, 3H). Impurities: 5.33 (DCM), 1.56 (H₂O). ¹³C NMR (125 MHz, CDCl₃): δ 157.4, 100.9, 69.3, 48.6, 32.2, 25.6, 25.4, 21.0, 18.0, -4.7, -5.2. HRMS-ESI⁺ (m/z): calc'd [M+H]⁺ for C₁₃H₂₆O₂Si 243.1775, found 243.1170.



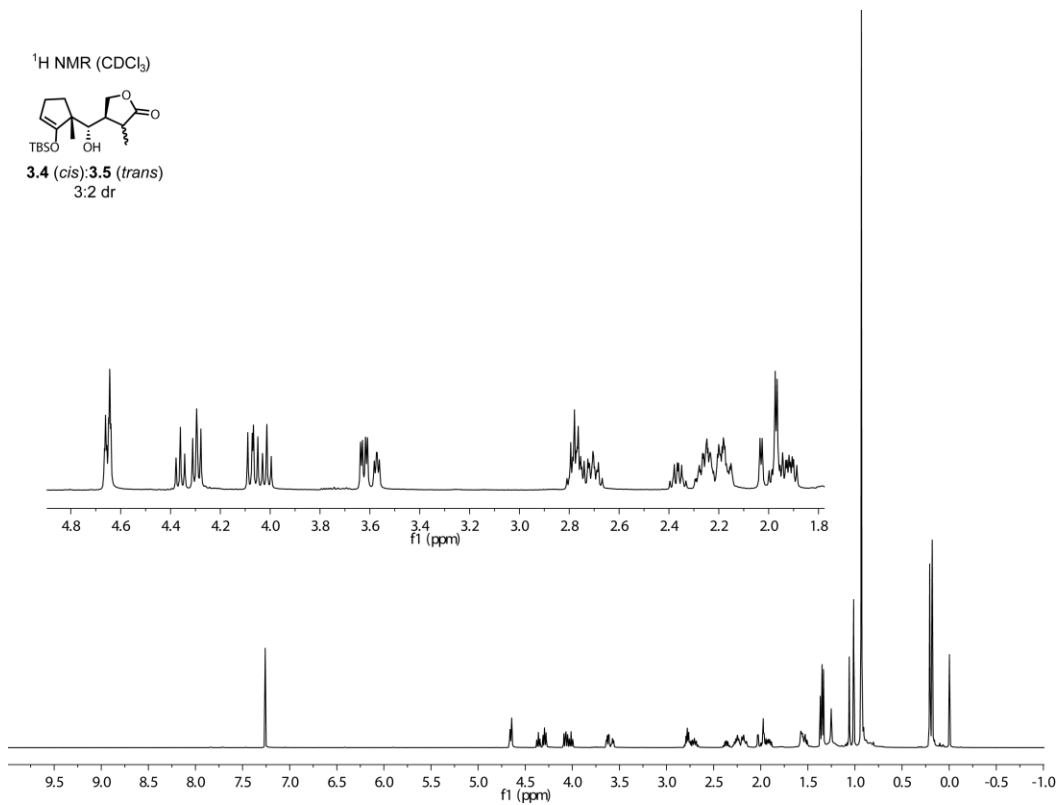
2-((tert-butyldimethylsilyl)oxy)-1-methylcyclopent-2-ene-1-carbaldehyde (3.24). Intermediate **3.23** (0.43 g, 1.8 mmol) was dissolved in a solution of DCM (3 mL) and DMSO (3 mL). Then, DCC (1.1 g, 5.3 mmol) was added followed by addition of H₃PO₄ (0.1 mL, 0.9 mmol). The reaction mixture was stirred for 16 h at RT. The reaction was quenched with H₂O (20 mL) and extracted with Et₂O (3X, 20 mL). The combined organic layer was washed with H₂O (10 mL), then brine (10 mL), and then concentrated *in vacuo*. The crude product was SiO₂ purified with EtOAc (0-10%) in hexanes to give **3.24** (0.40 g, 91% yield). This compound has been characterized previously.

3.10 Spectral Data

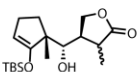
¹H NMR (CDCl₃)



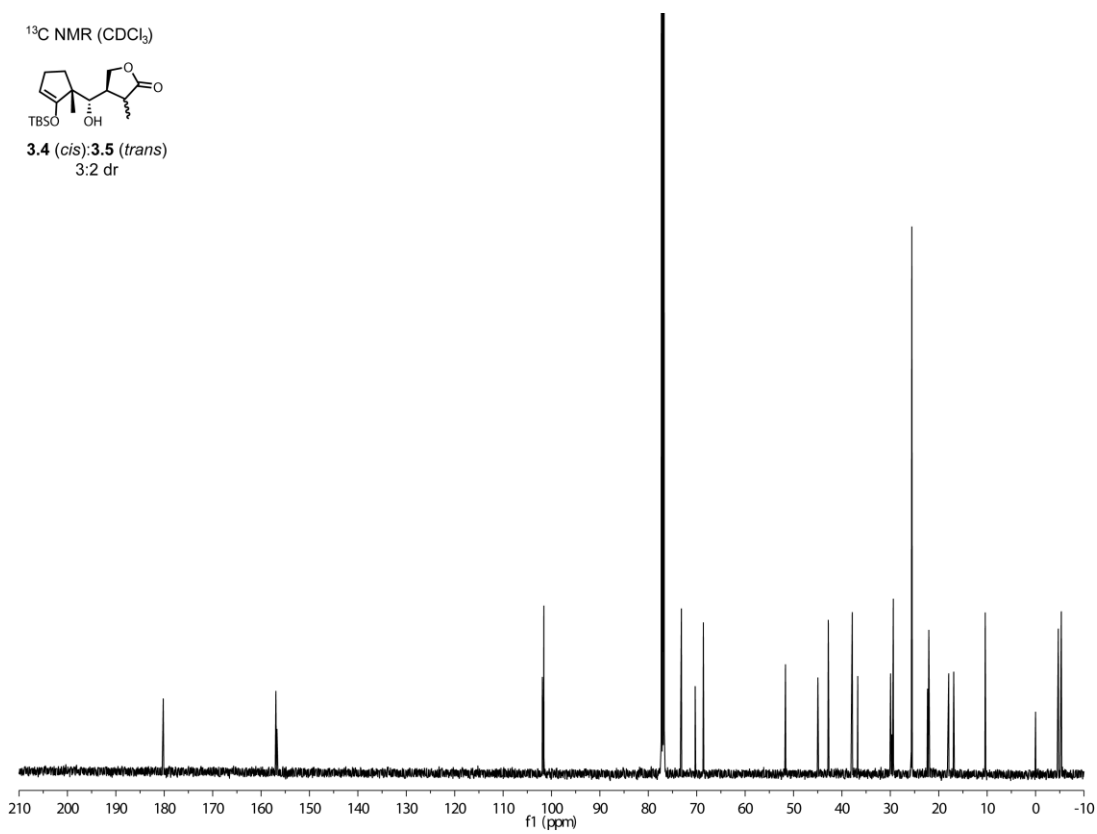
3.4 (*cis*):**3.5** (*trans*)
3:2 dr



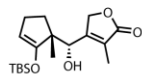
¹³C NMR (CDCl₃)



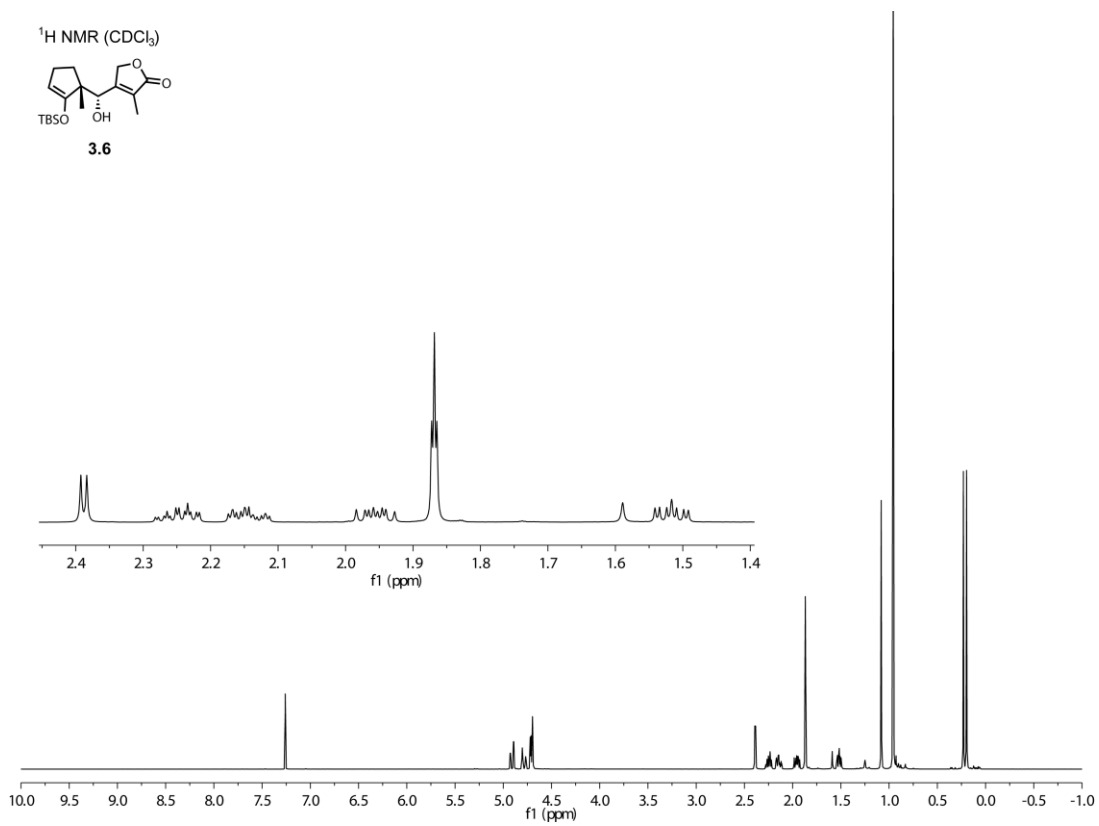
3.4 (*cis*):**3.5** (*trans*)
3:2 dr



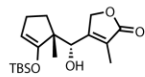
¹H NMR (CDCl₃)



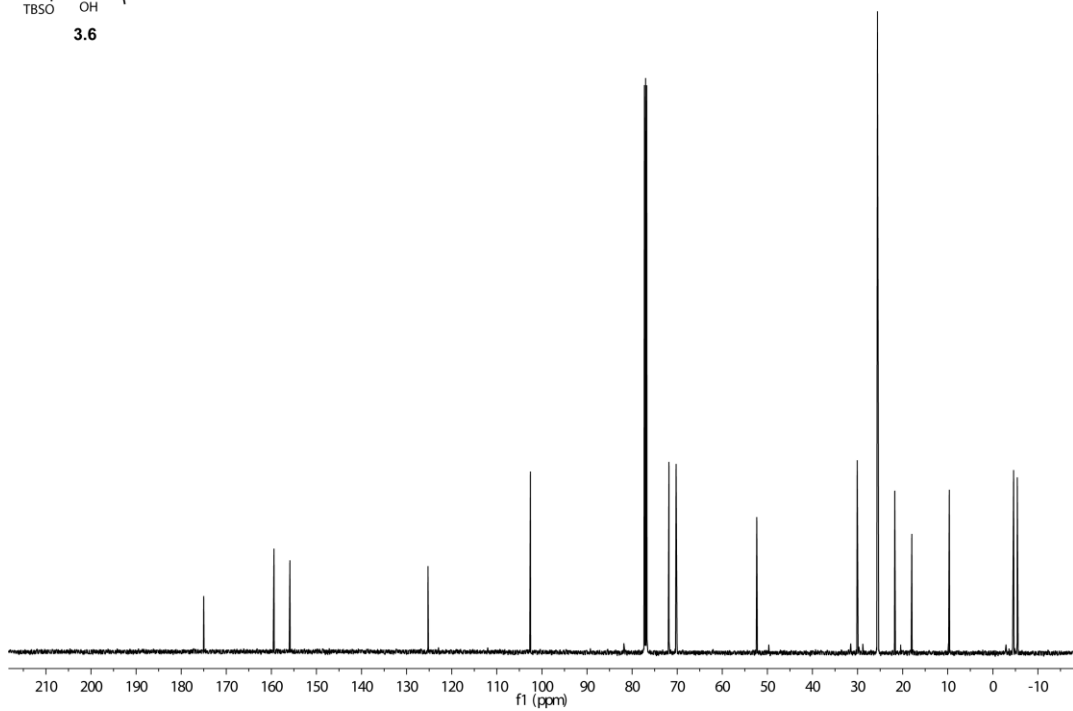
3.6

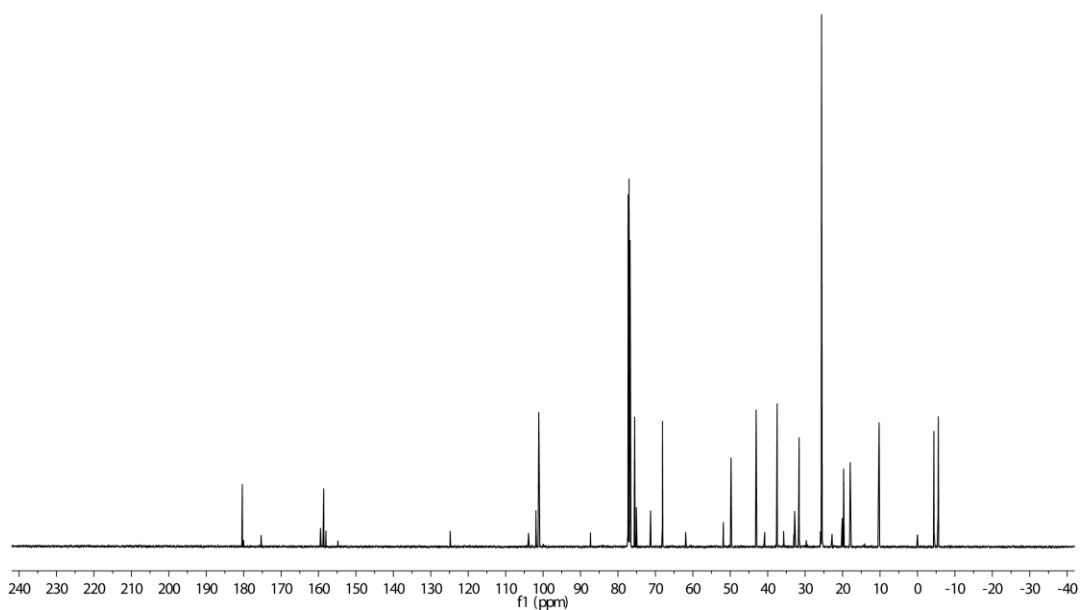
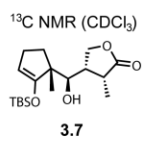
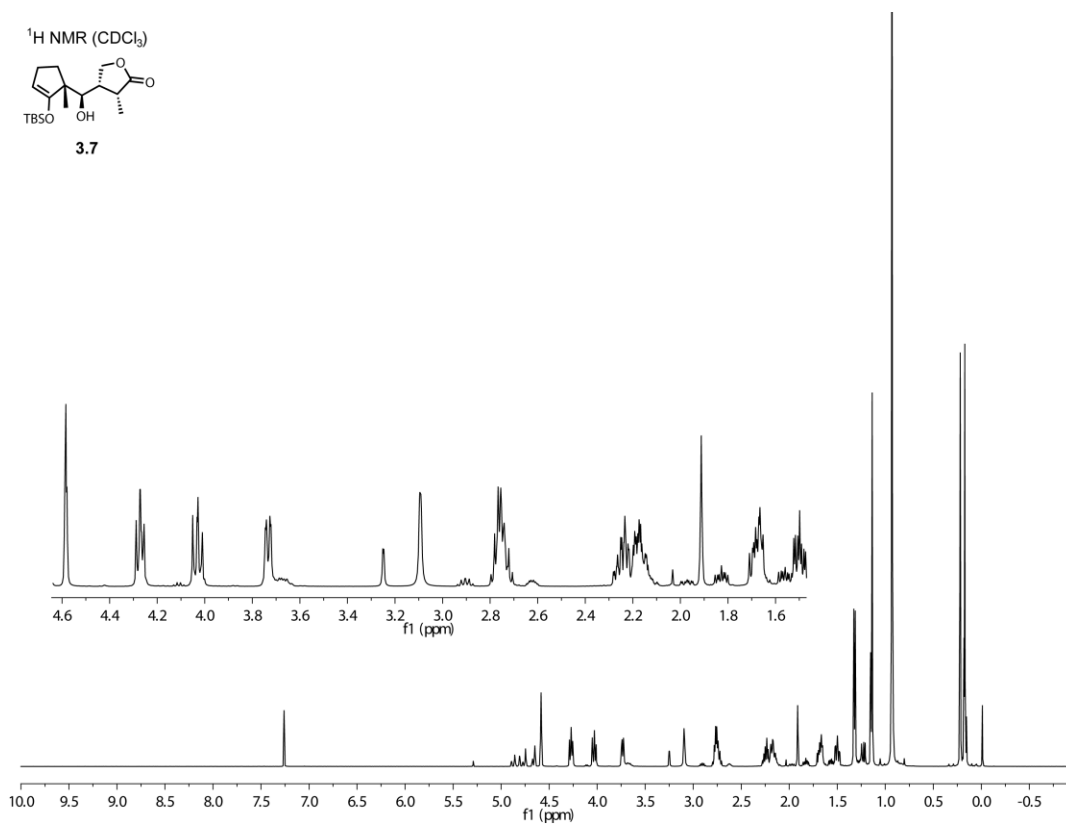
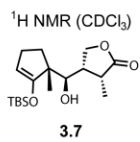


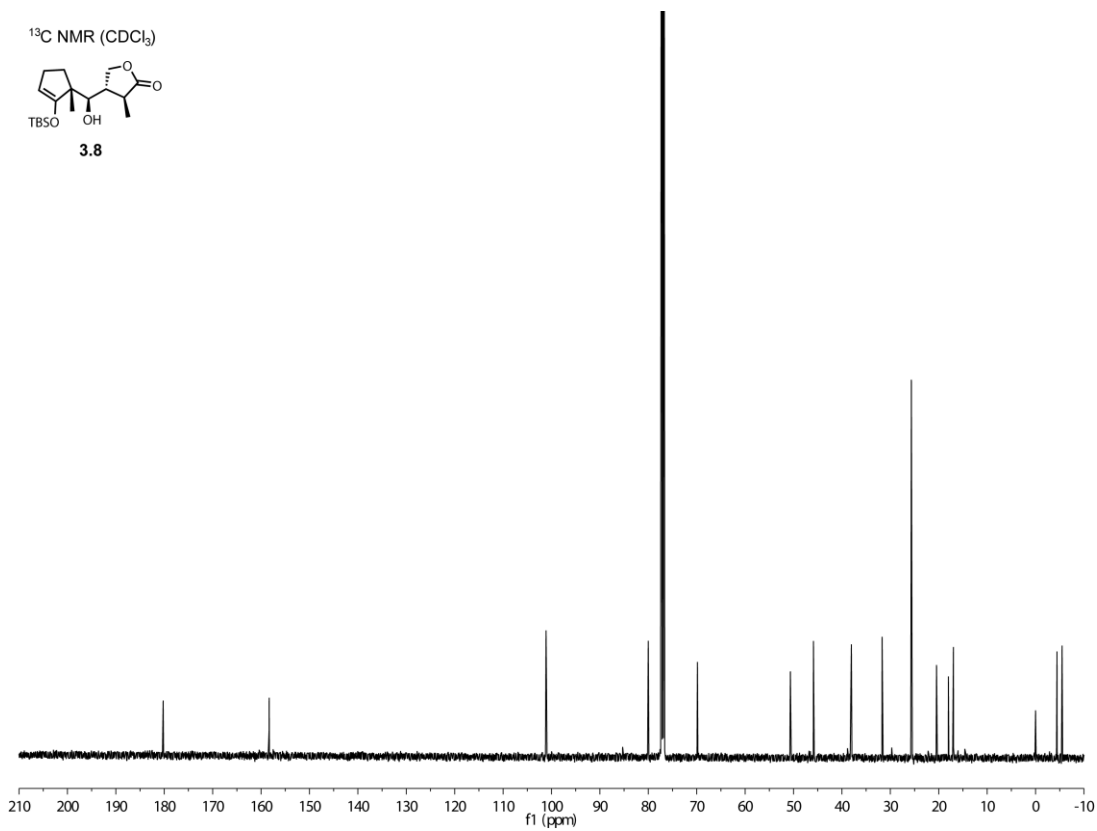
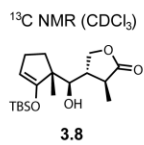
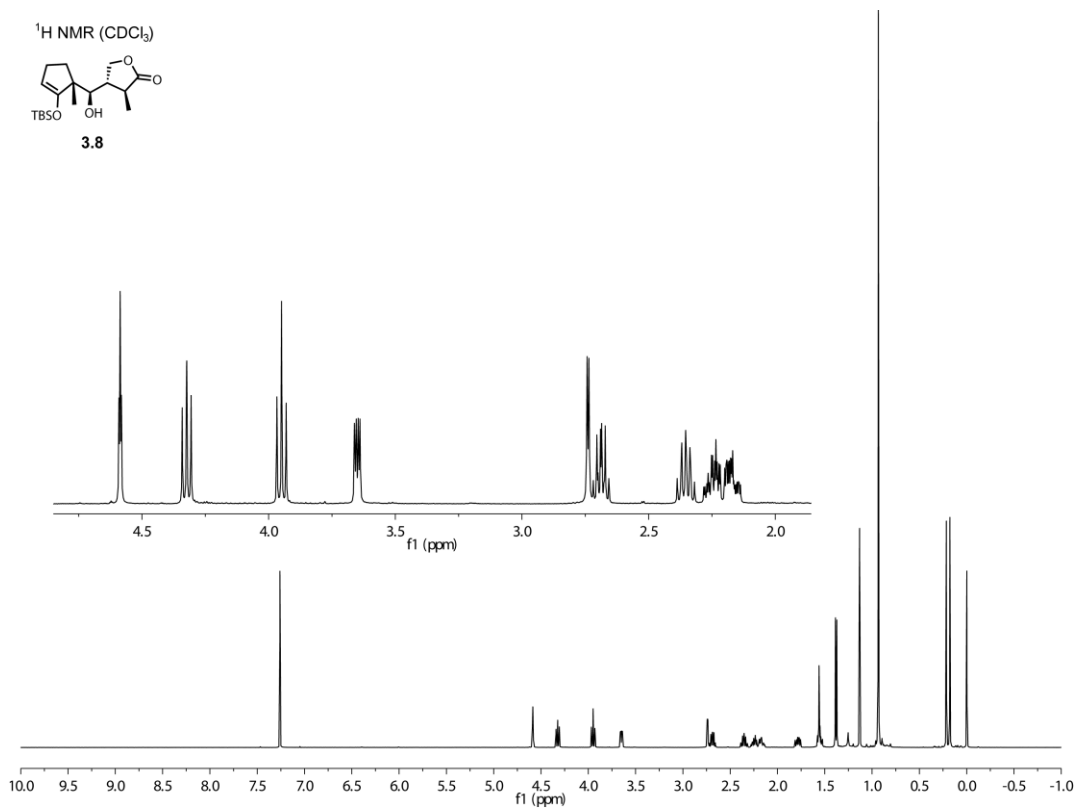
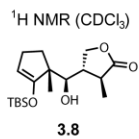
¹³C NMR (CDCl₃)

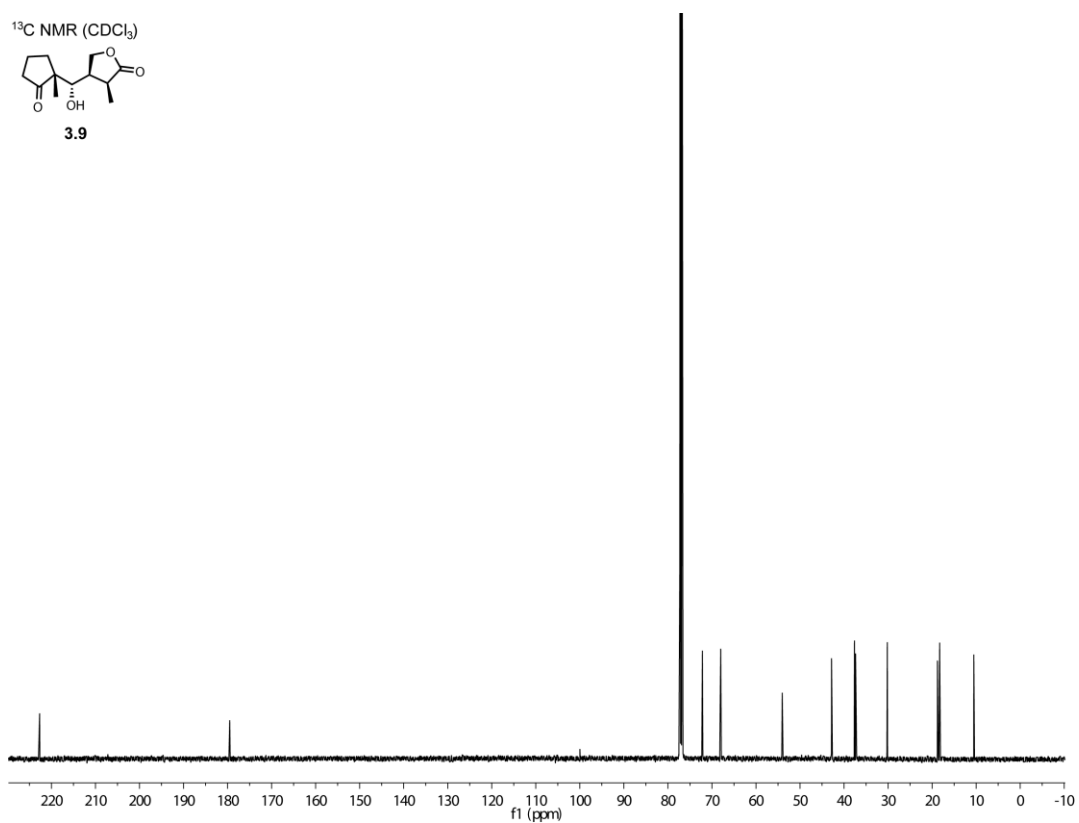
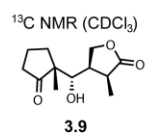
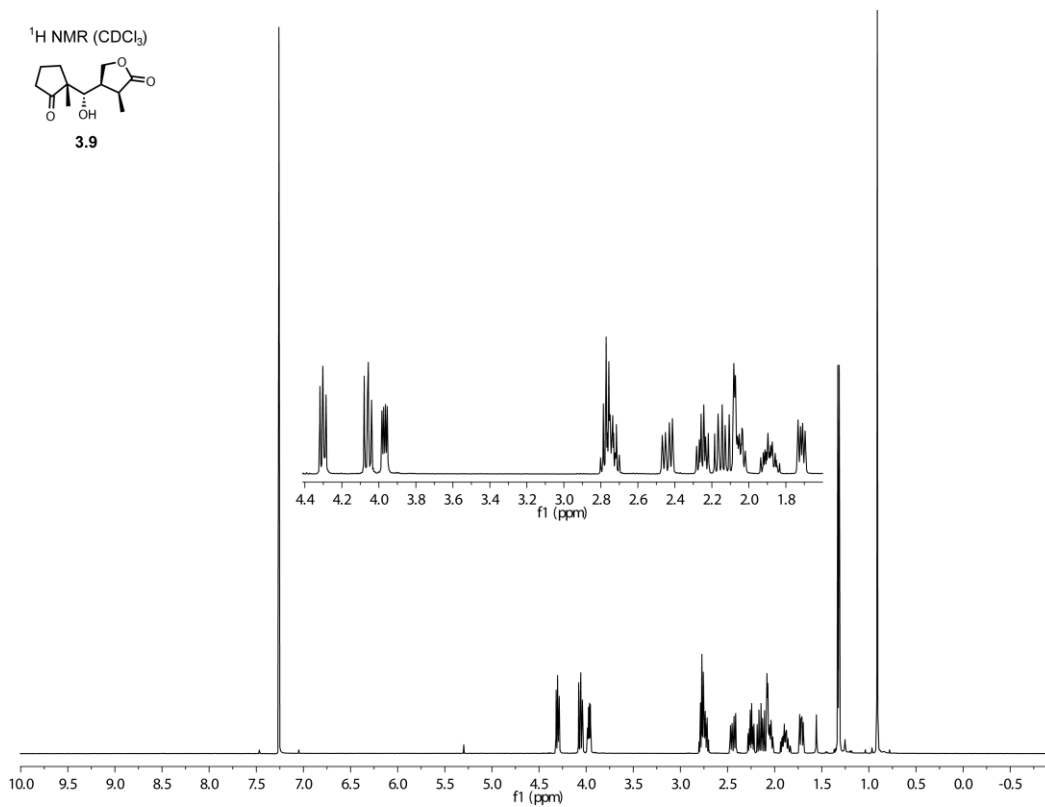
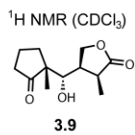


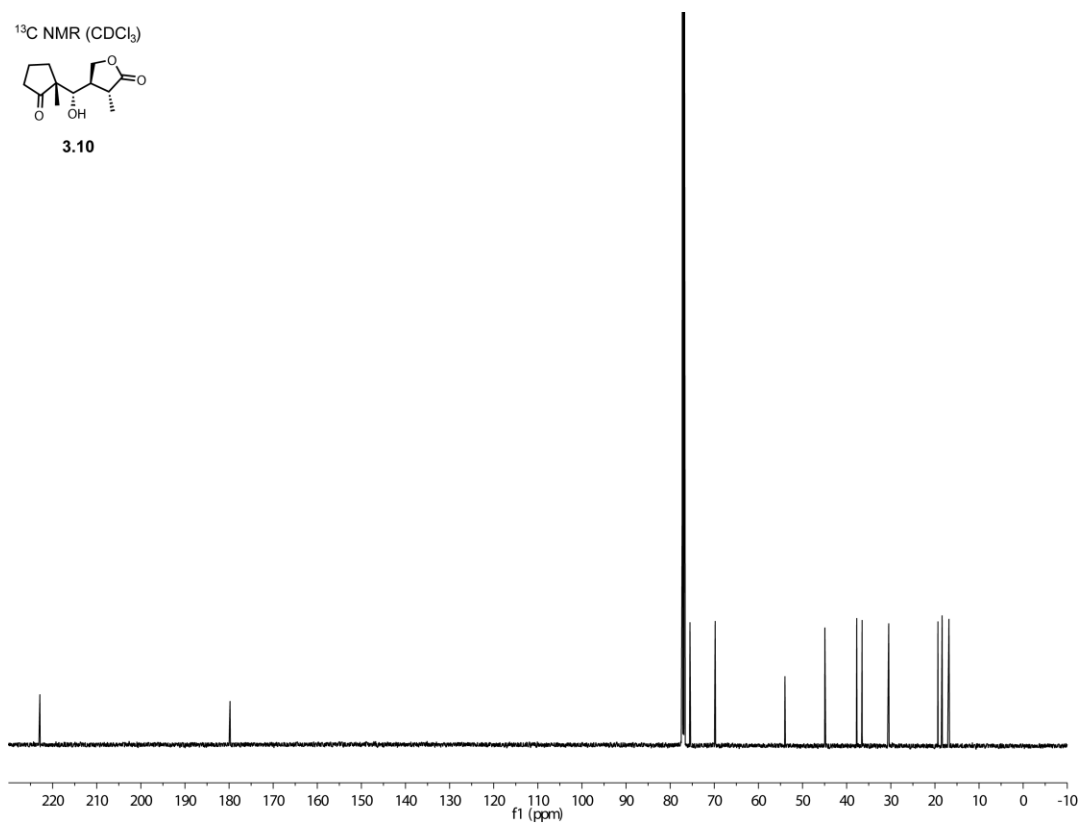
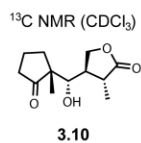
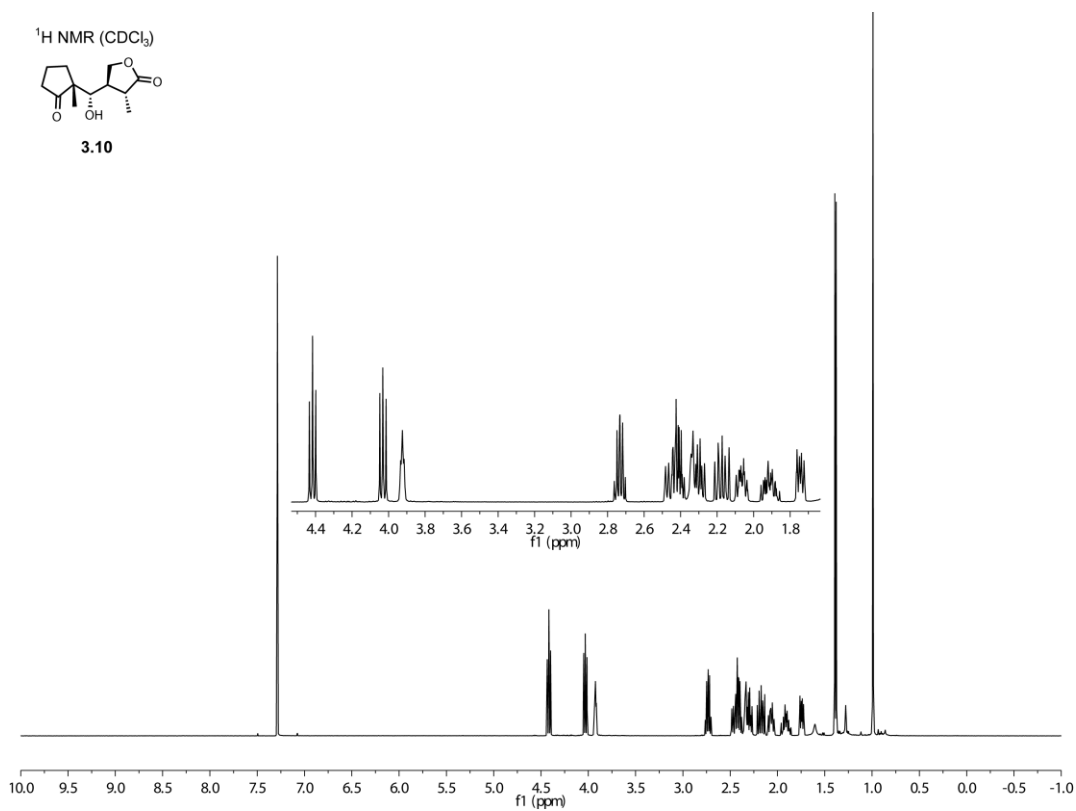
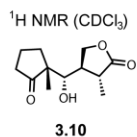
3.6

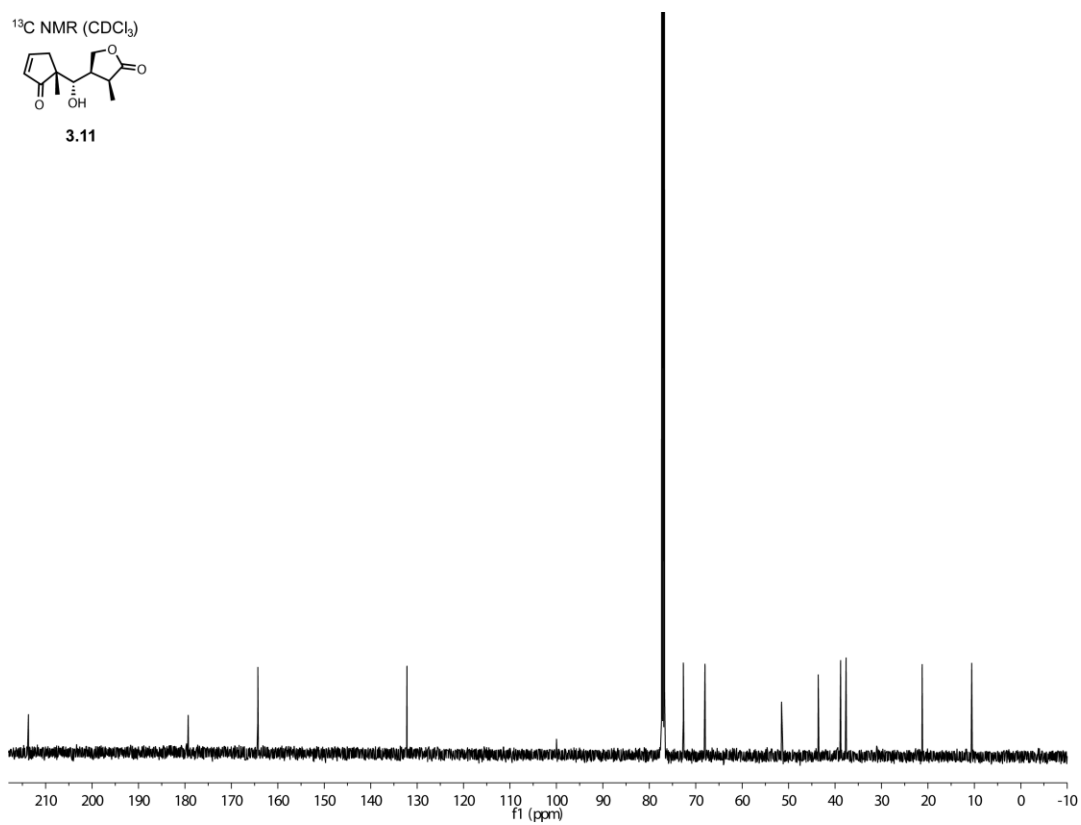
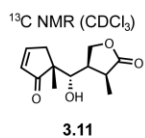
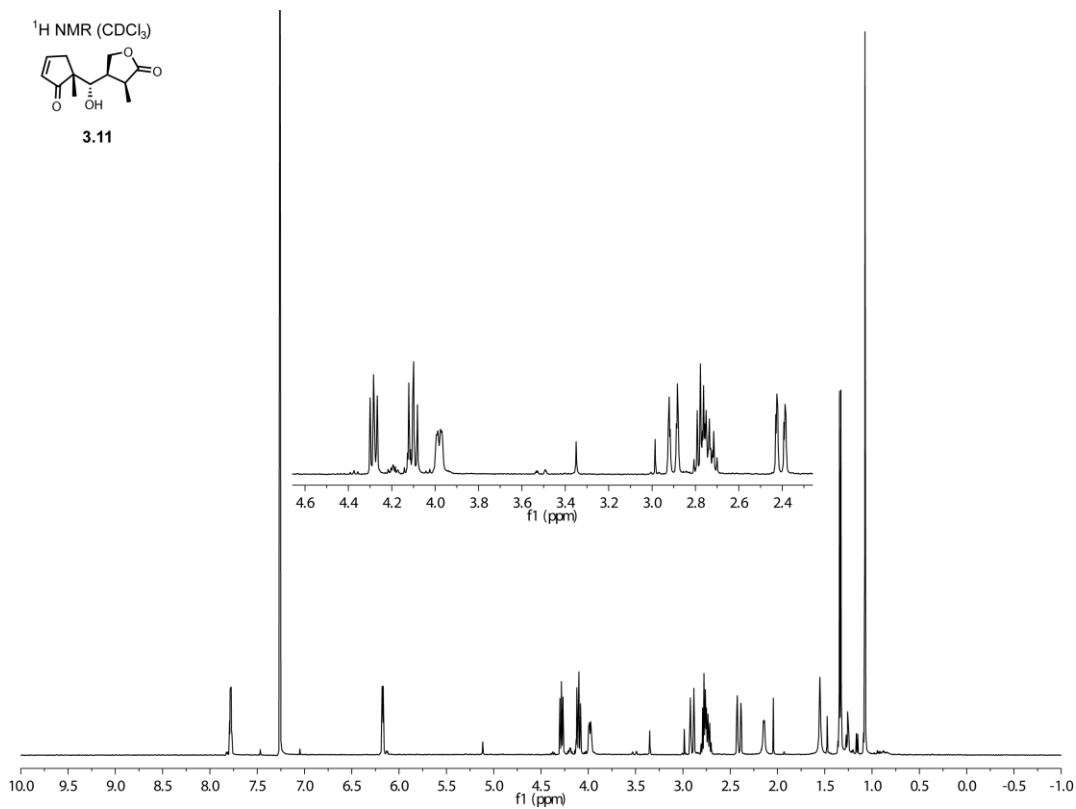
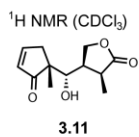




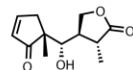




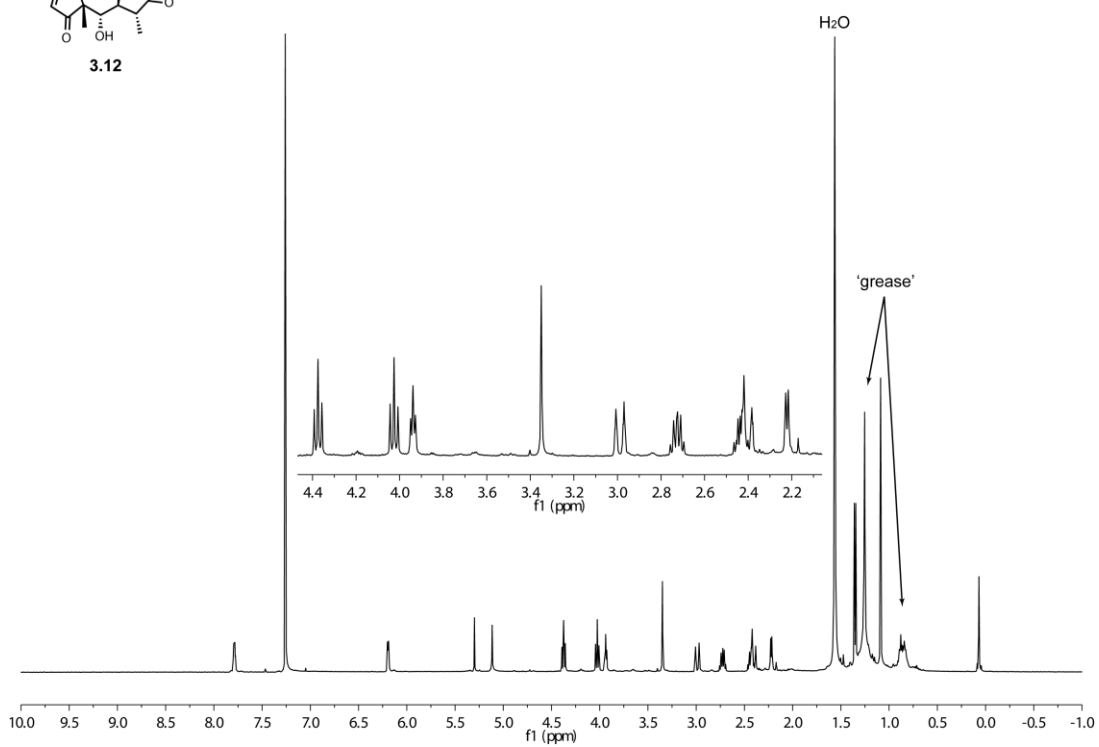




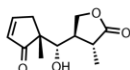
¹H NMR (CDCl₃)



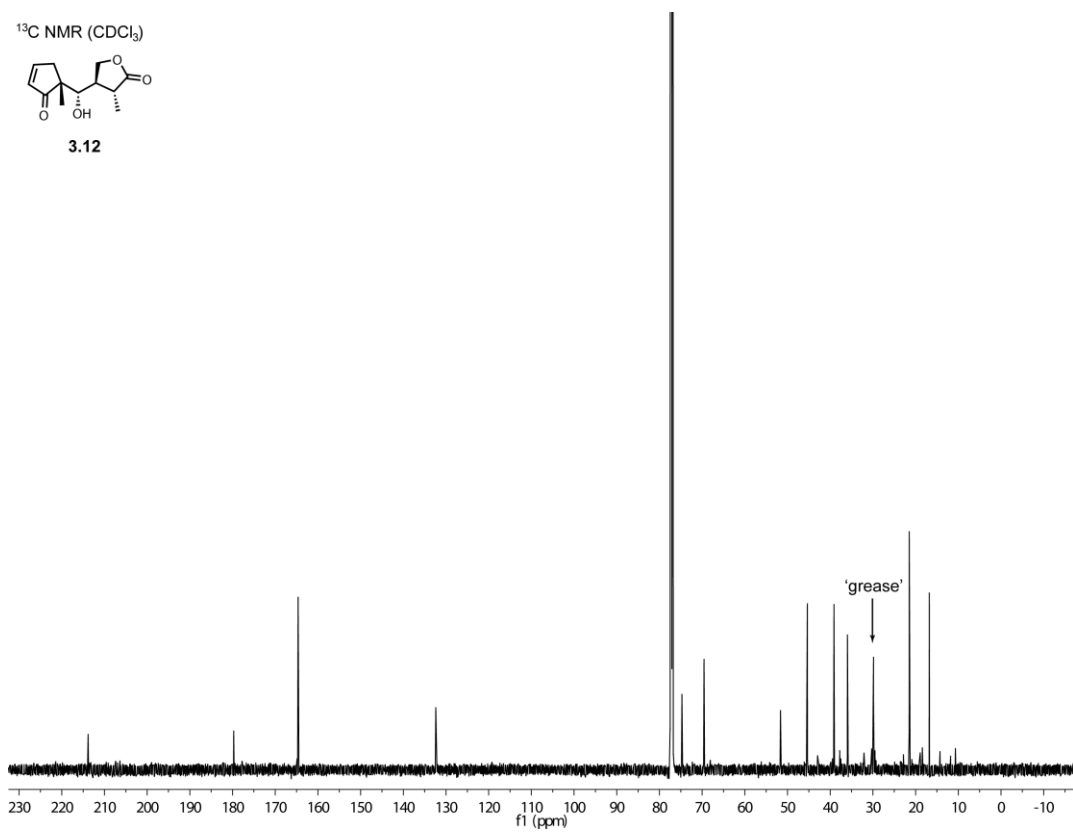
3.12



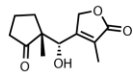
¹³C NMR (CDCl₃)



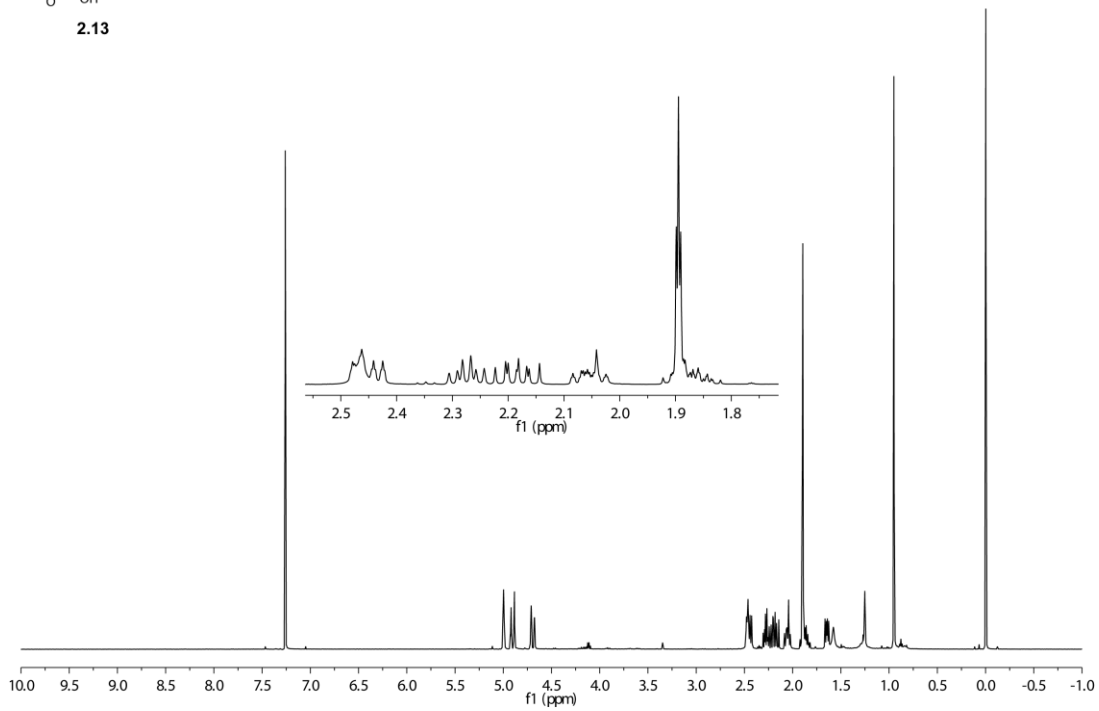
3.12



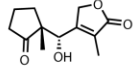
¹H NMR (CDCl₃)



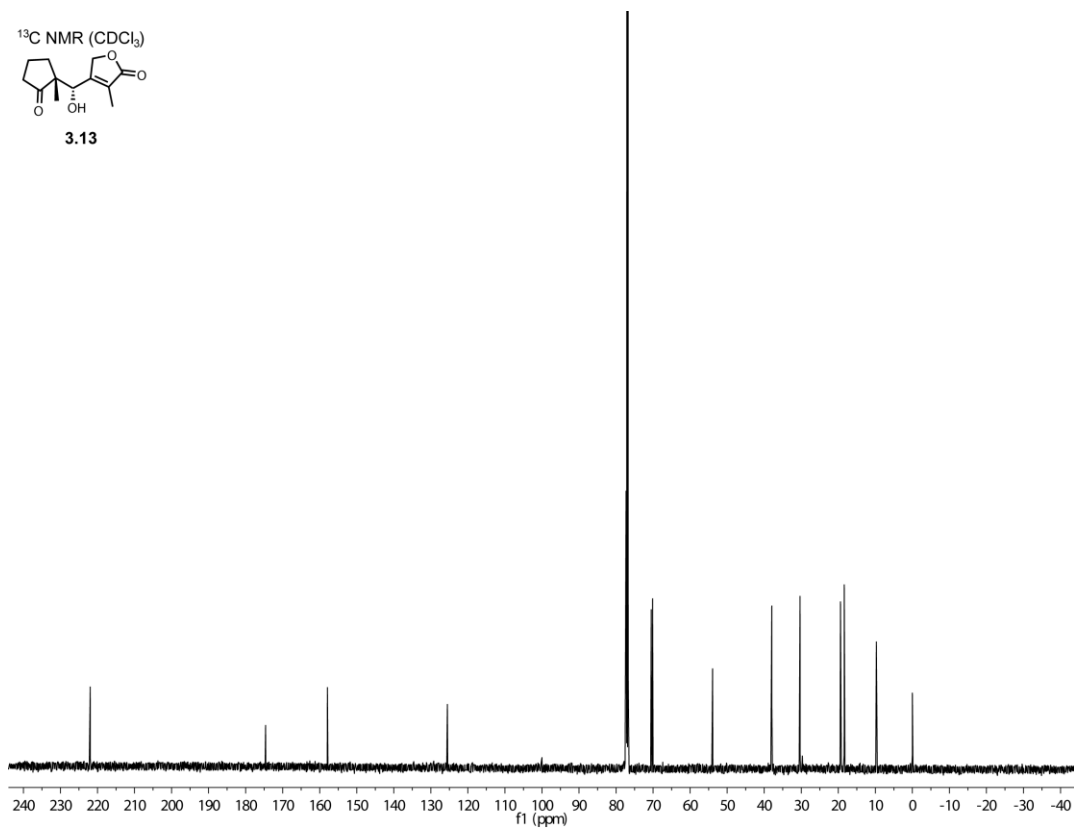
2.13



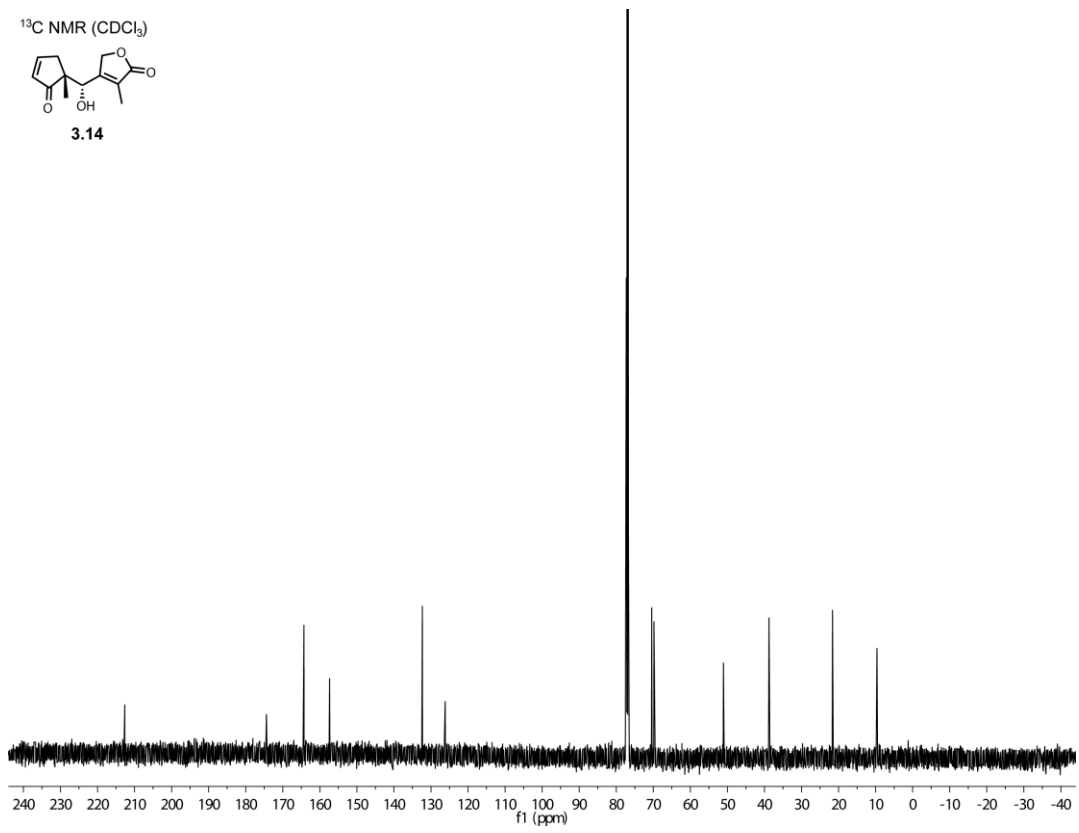
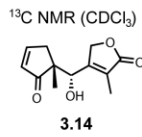
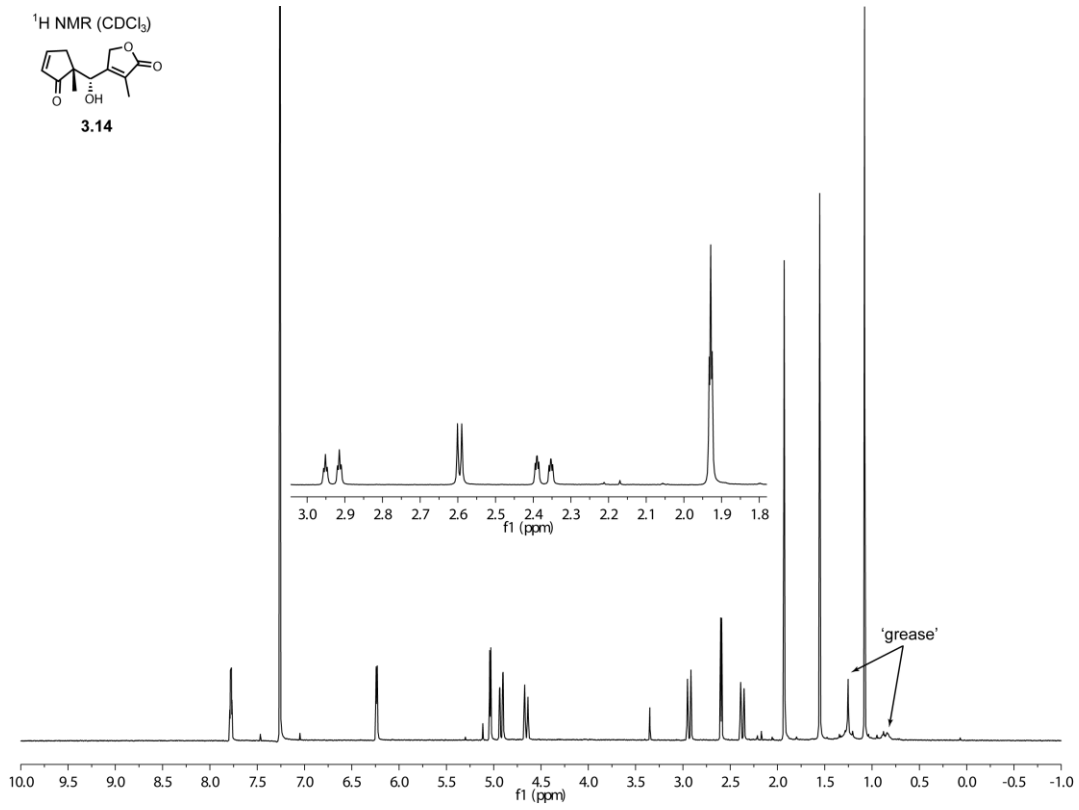
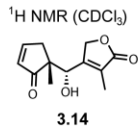
¹³C NMR (CDCl₃)

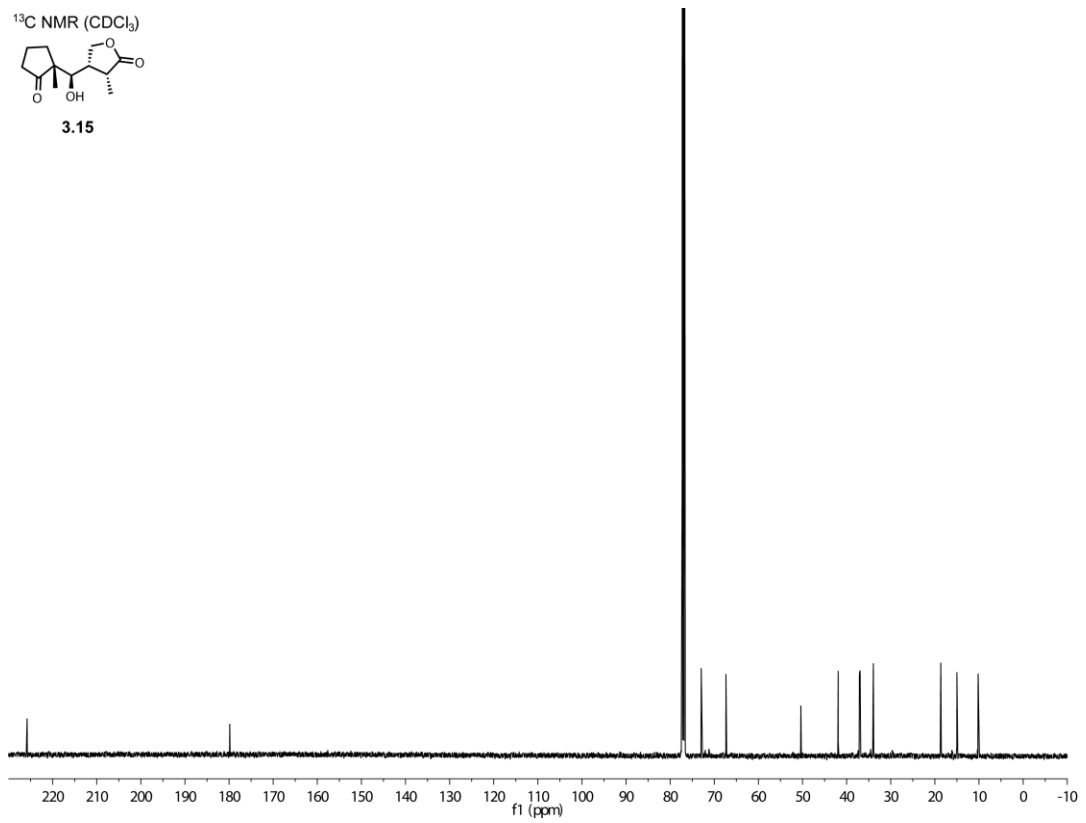
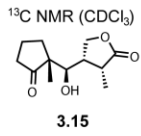
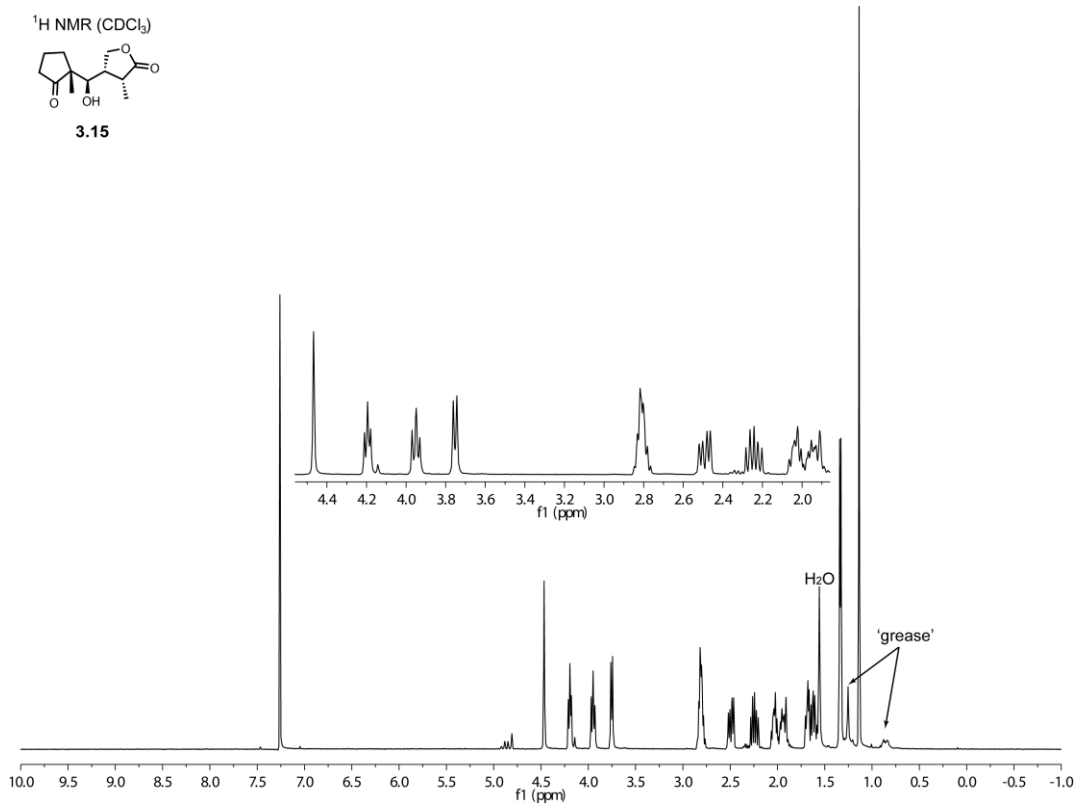
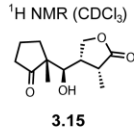


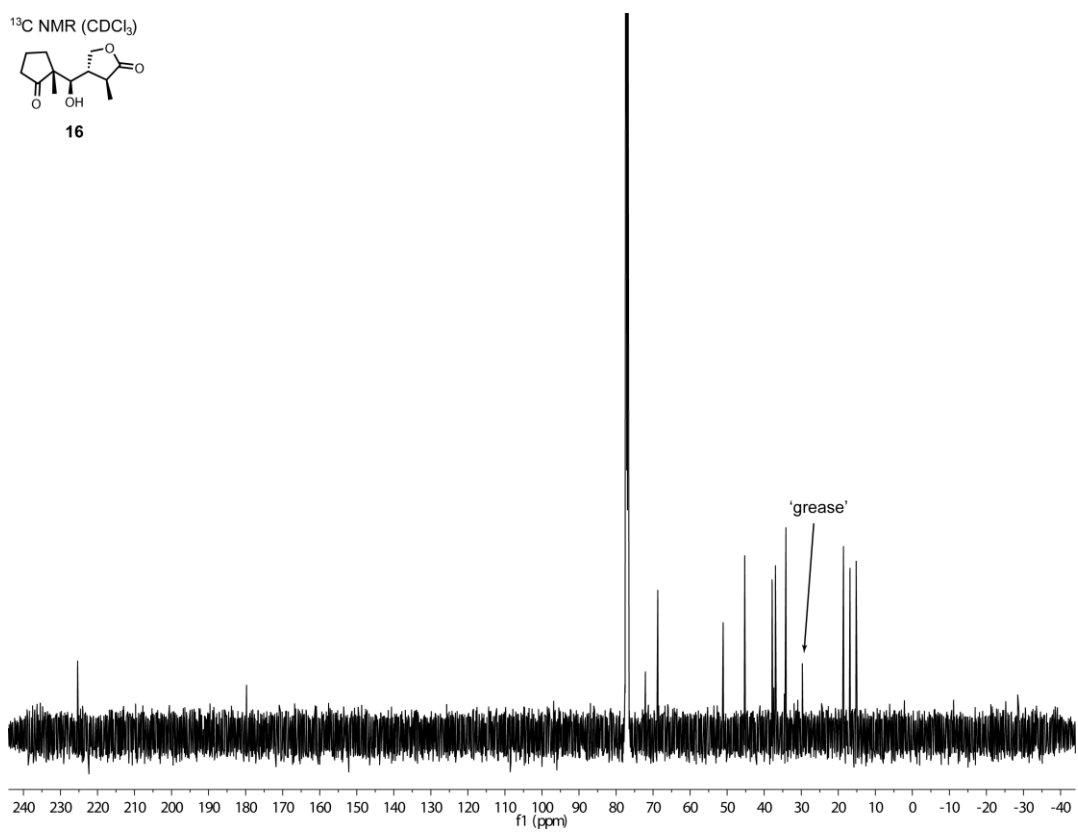
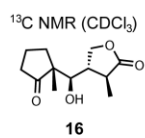
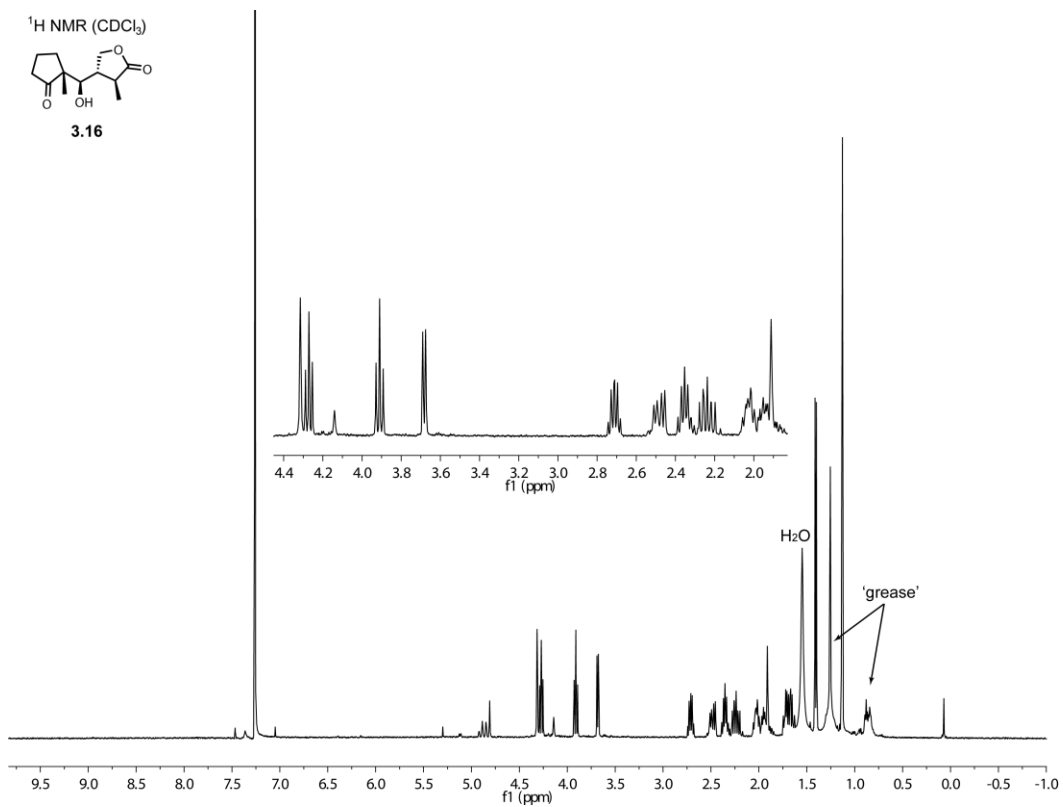
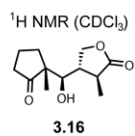
3.13

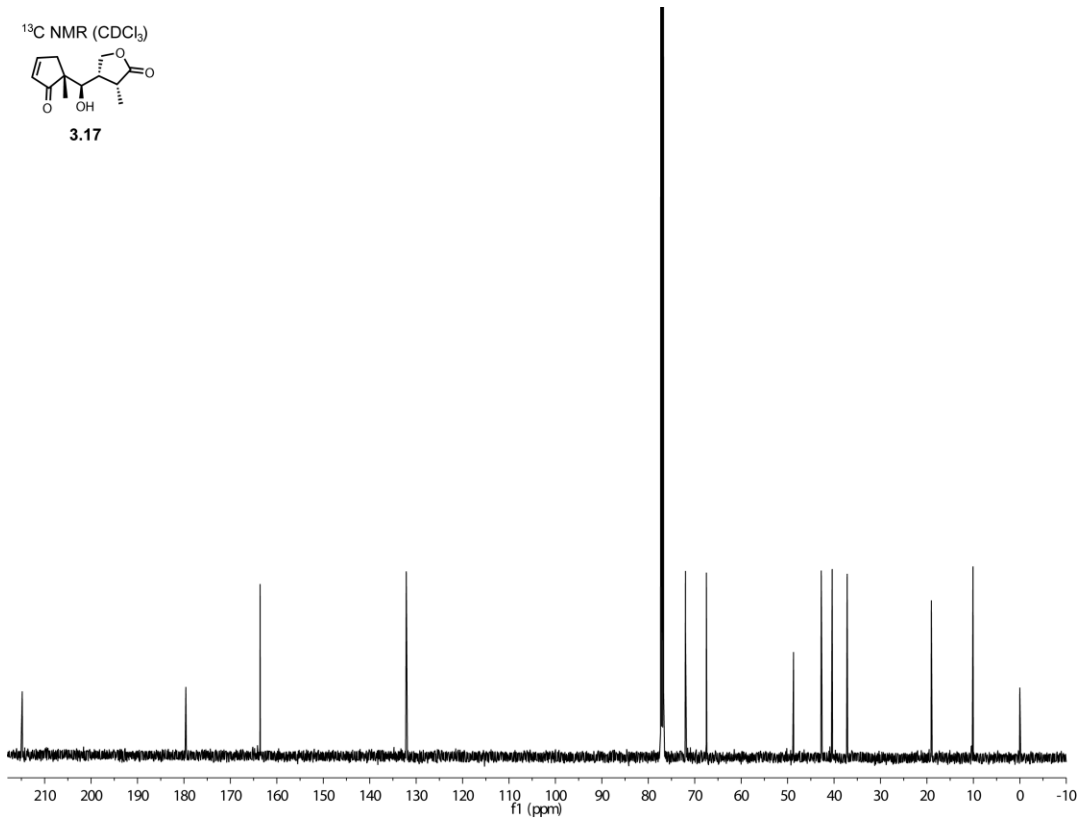
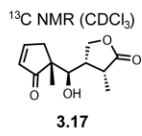
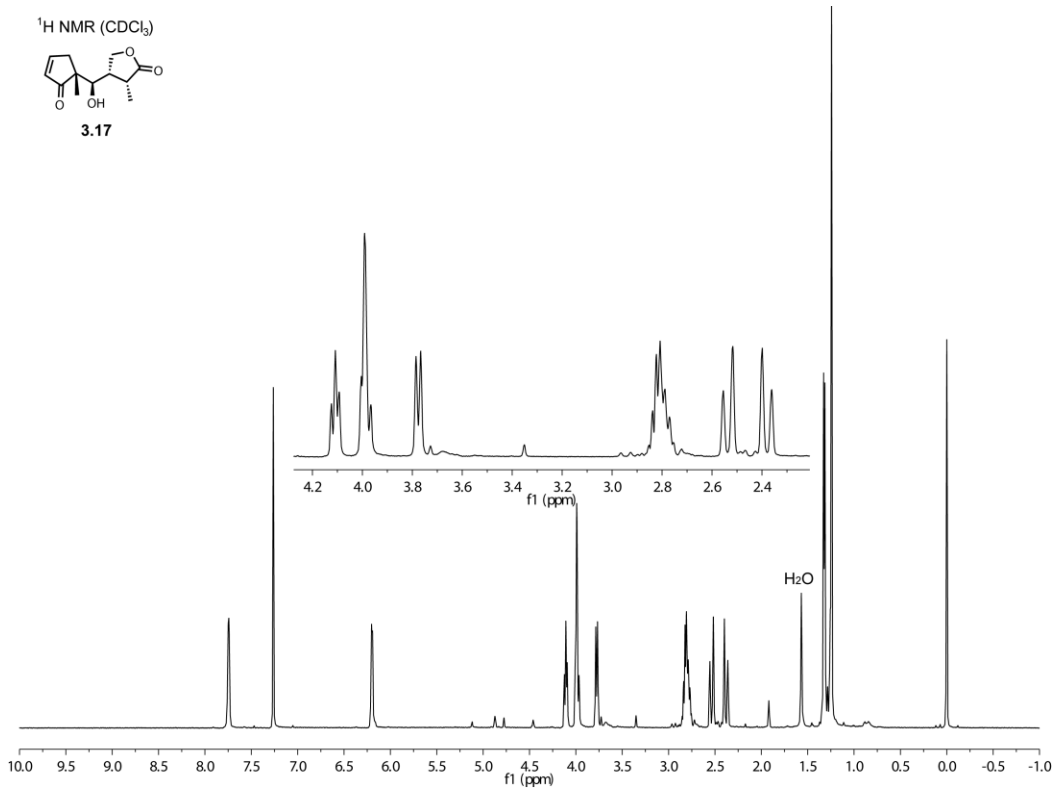
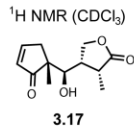


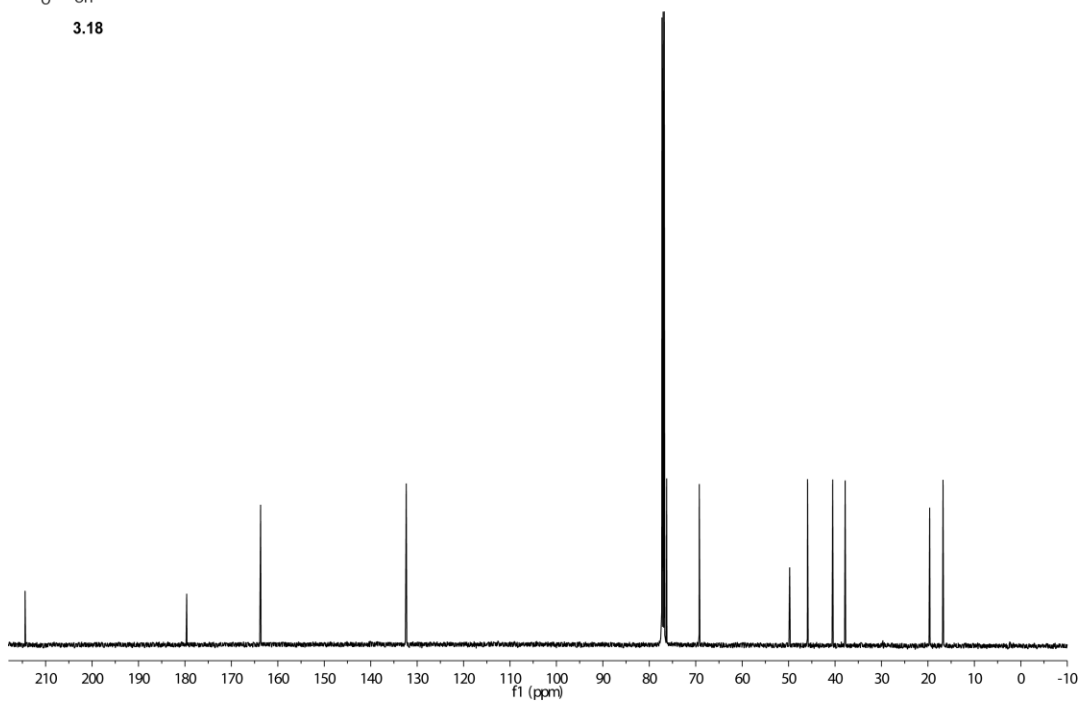
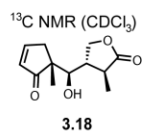
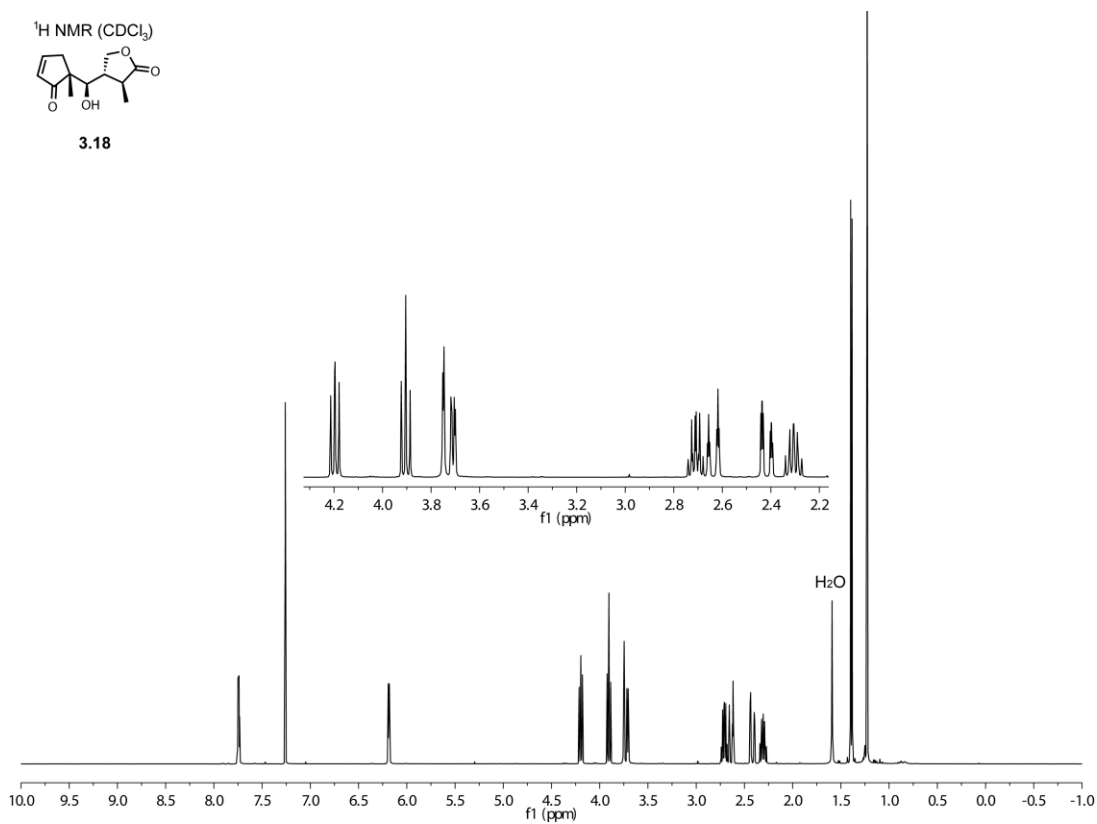
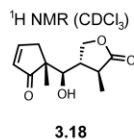
146



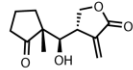




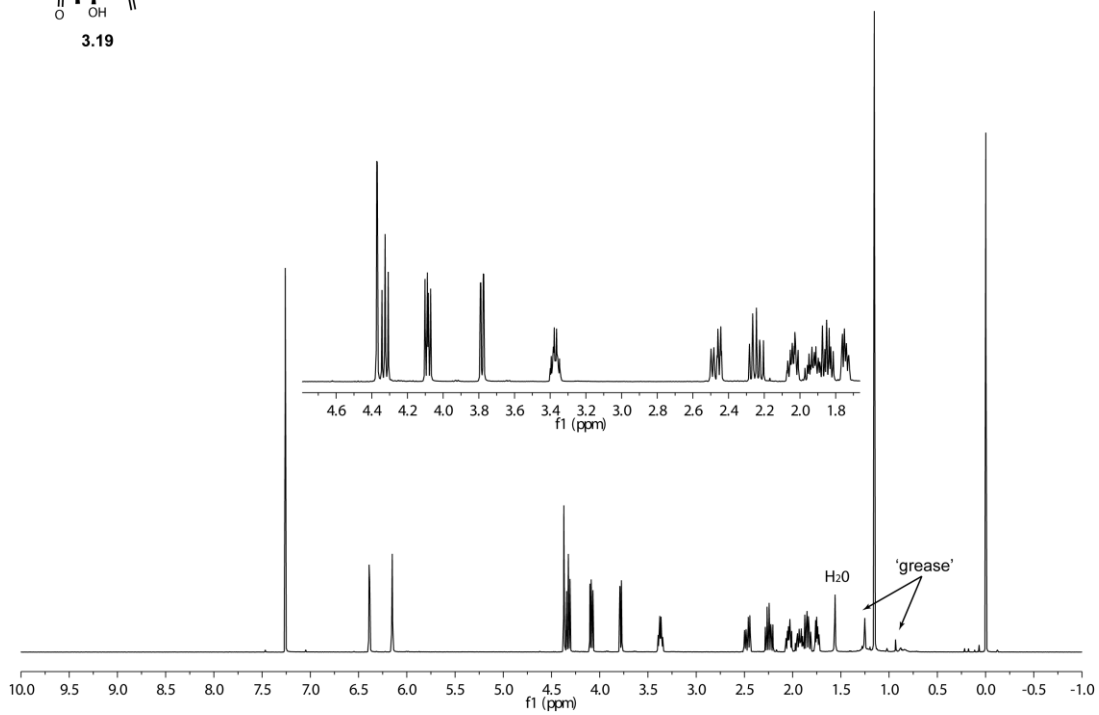




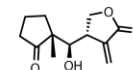
¹H NMR (CDCl₃)



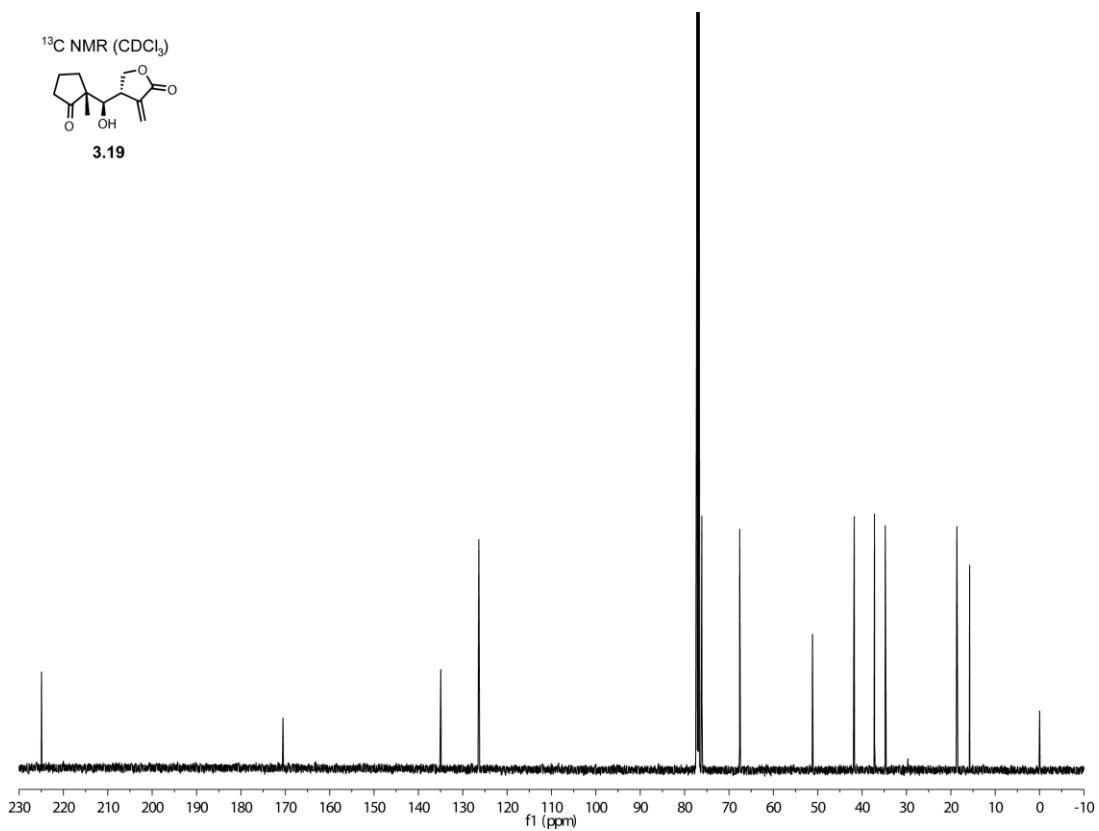
3.19

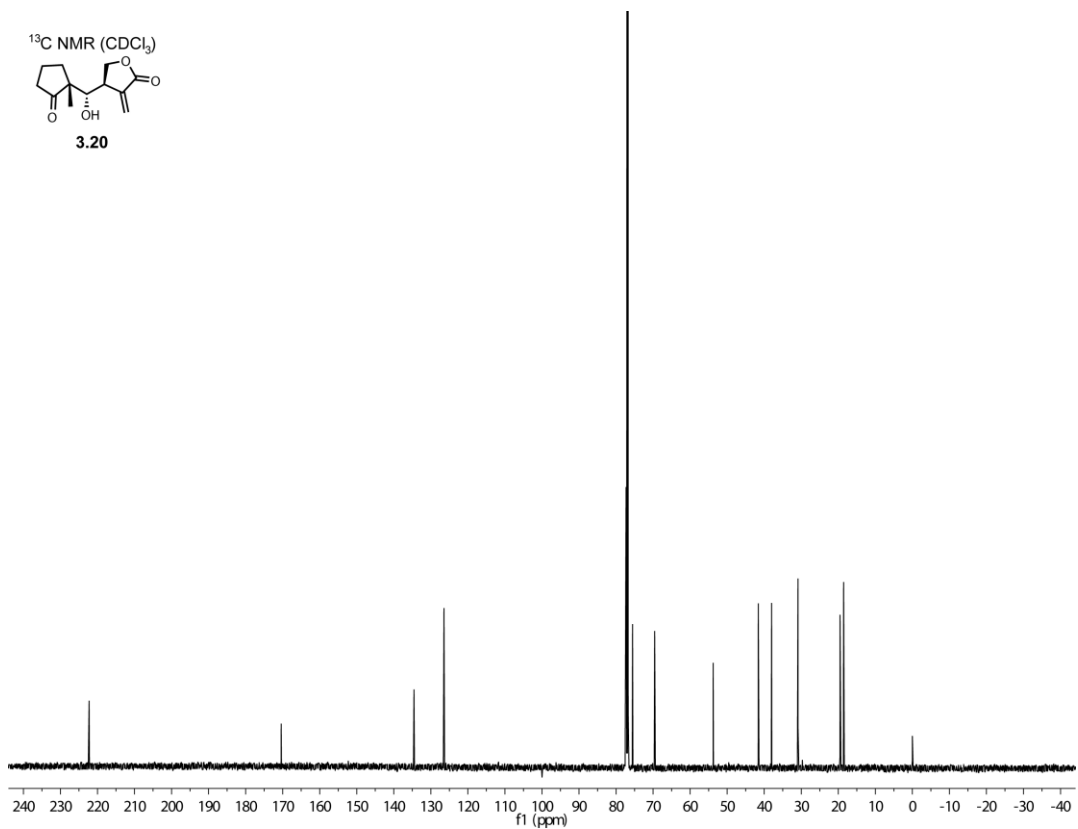
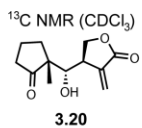
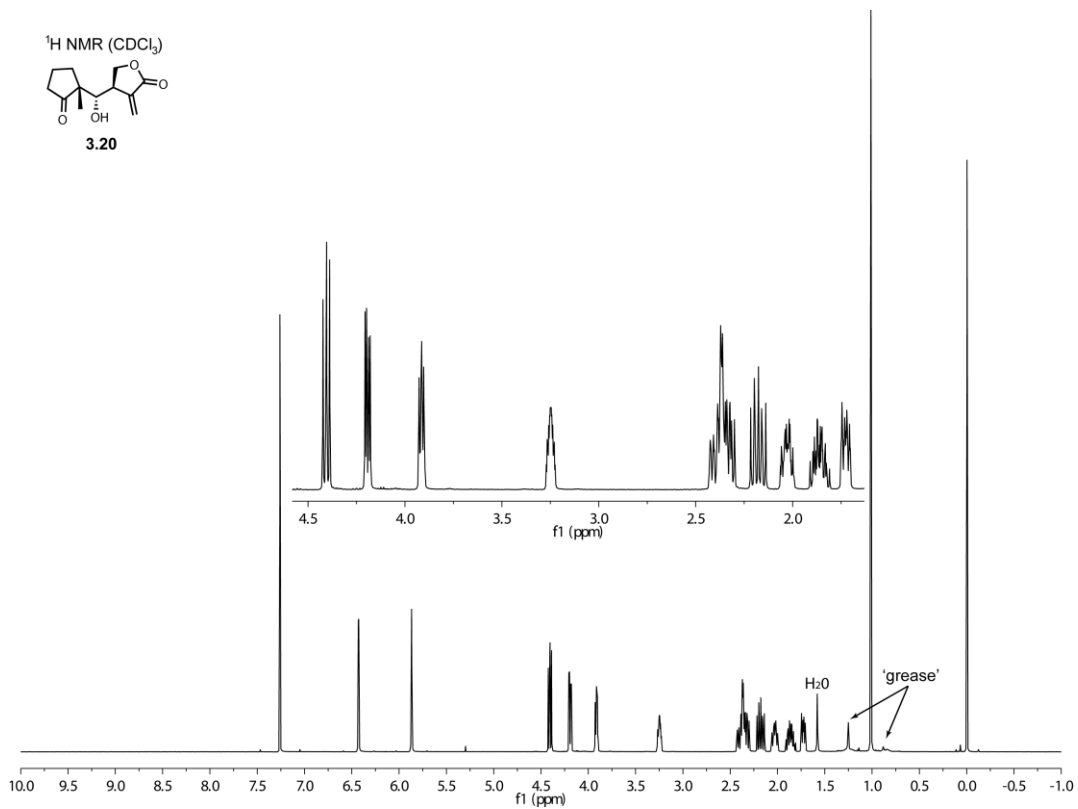
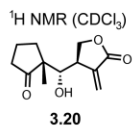


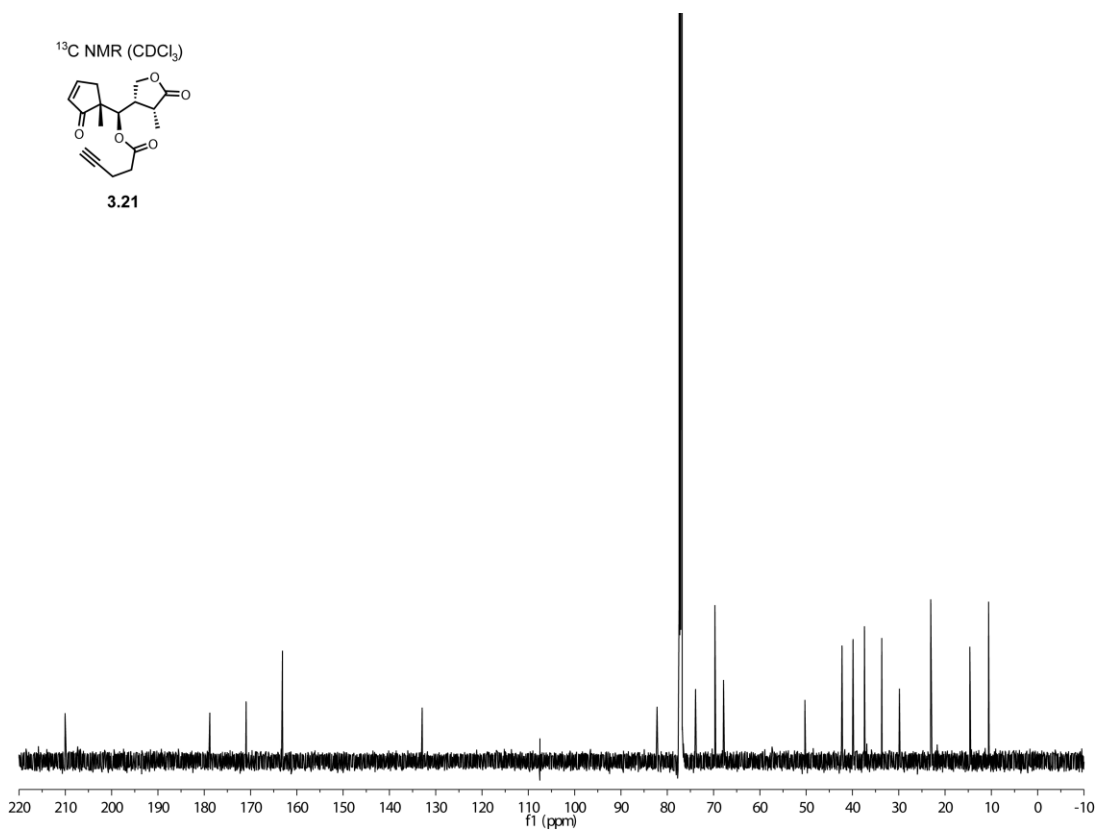
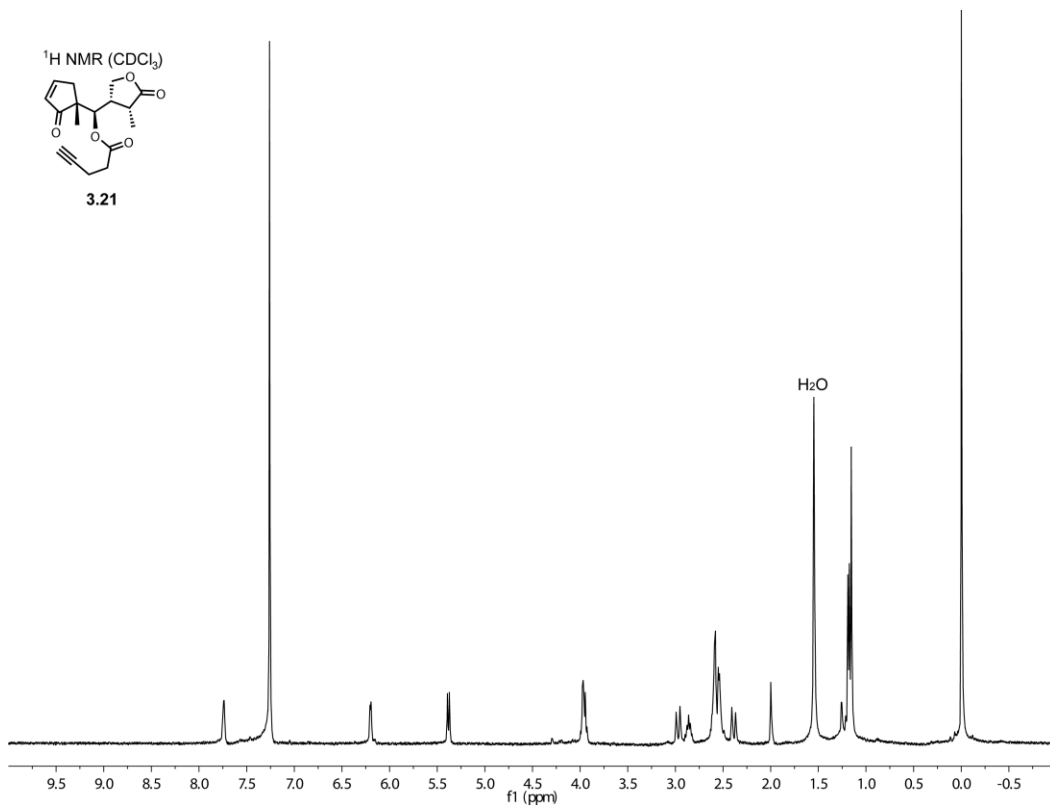
¹³C NMR (CDCl₃)



3.19



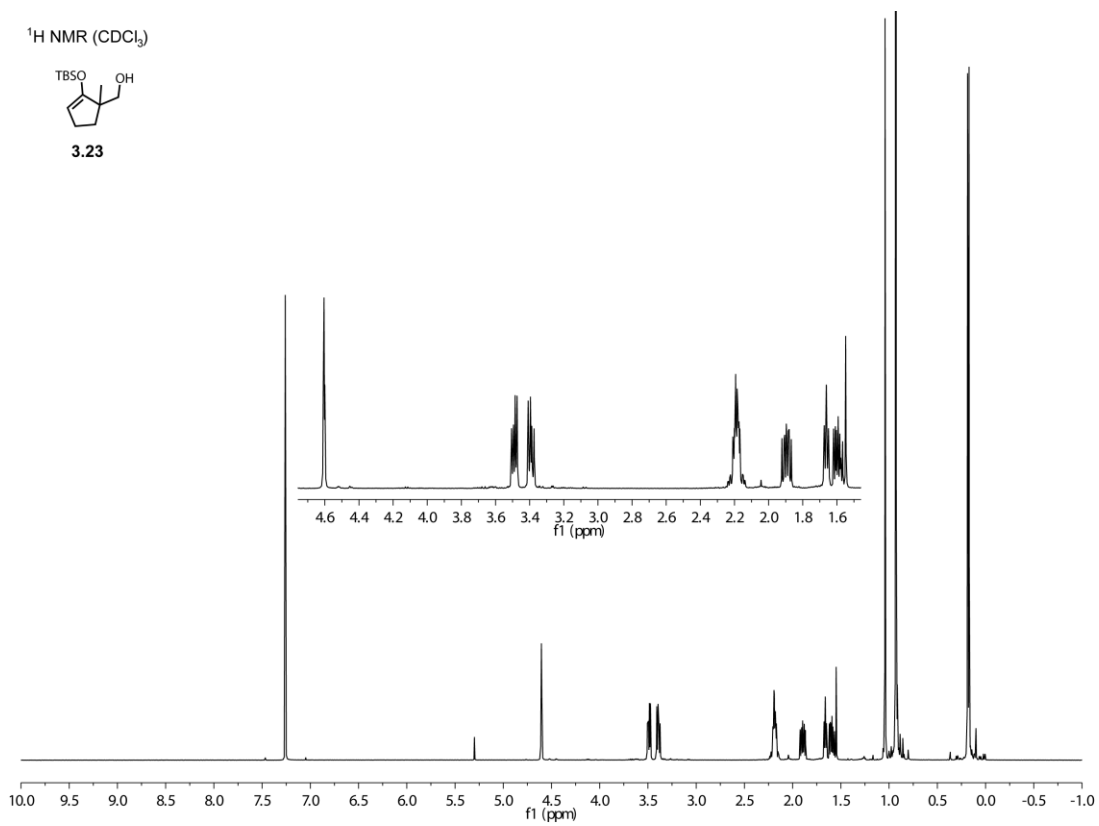




¹H NMR (CDCl₃)



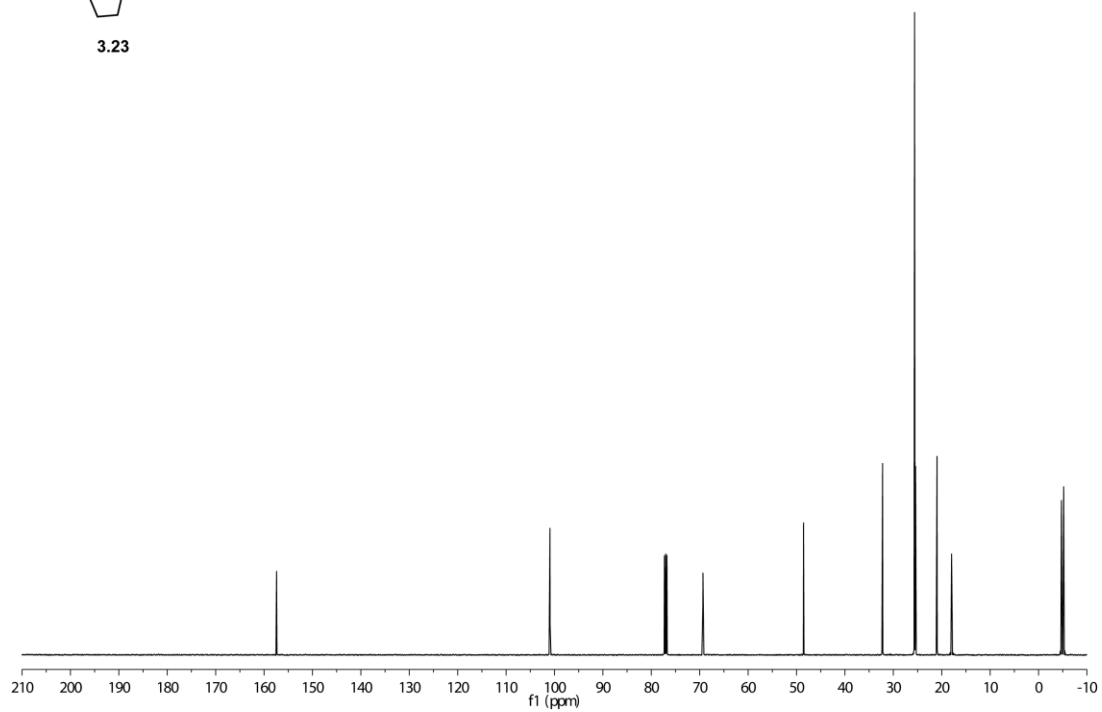
3.23



¹³C NMR (CDCl₃)



3.23



3.11. HPLC Purity Analysis of Synthesized Compounds

General Protocol for HPLC Analysis of Synthesized Compounds

DMSO stock solutions of newly synthesized molecules were dissolved in methanol and distilled and deionized water (ddH₂O) and analyzed on an Agilent 1200 series instrument equipped with a diode array detector and Zorbax SB-C18 column (4.6 x 150 mm, 5 μm, Agilent Technologies). The analysis method (1 mL/min flow rate) starts with an isocratic eluent system of 10% MeCN in ddH₂O from 0-2 minutes followed by a linear gradient of 10% to 85% MeCN in ddH₂O from 2-24 minutes, followed by 85% to 95% MeCN in ddH₂O from 24-26 minutes, and finally an isocratic eluent system of 95% MeCN in ddH₂O from 26-30 minutes. No TFA was added to the eluent solvents. Wavelengths monitored = 215 nm.

Preparation of Stock Solutions

Compound stock solutions were prepared in DMSO (40 mM to 100 mM concentrations) and stored at -20 °C when not in use. Compound purities were assessed frequently by analytical reverse-phase HPLC analysis and fresh solutions were prepared as needed.

Table 3.11.1. Compound Purity by HPLC. All compounds were tested for purity by HPLC with the exception of **3.9**, **3.10**, **3.15**, and **3.16** due to their lack of UV absorbance. These compounds were determined to be $\geq 95\%$ pure by ^1NMR analysis.

Compound	R _T (min)	HPLC Purity (%)
3.11	9.0	96
3.12	9.1	>99
3.13	11.4	>99
3.14	9.9	>99
3.17	7.7	>99
3.18	8.0	>99
3.19	9.7	>99
3.20	9.6	>99
3.21	15.7	>99

Chapter 4

SYNTHESIS AND ANTILEUKEMIC ACTIVITIES OF C1-C10-MODIFIED PARTHENOLIDE ANALOGUES

Adapted with Permission from:

Kempema, A.M.; Widen, J.C.; Hexum, J.K.; Andrews, T.E.; Wang, D.; Rathe, S.K.; Meece, F.A.; Noble, K.E.; Sachs, Z.; Largaespada, D.A.; Harki, D.A. *Bioorg. Med. Chem.* **2015**, *23*, 4737-4745.

This work was performed in collaboration with Dr. Aaron M. Kempema, Joseph K. Hexum, Timothy E. Andrews, Dr. Dan Wang, Dr. Susan K. Rathe, Dr. Frederick A. Meece, Klara E. Noble, Professor Zohar Sachs, Professor David A. Largaespada, and Professor Daniel A. Harki. Compounds were synthesized or purified after purchase by Aaron Kempema, John Widen, Timothy Andrews, Dan Wang, or Fred Meece. Klara Noble and Zohar Sachs trained me on the clonal growth assay. Sue Rathe conducted growth inhibitory assays on leukemic mouse cell lines. Aaron Kempema, Joseph Hexum, Timothy Andrews, Dan Wang assisted with growth inhibitory assays on human cancer cells lines. Joseph Hexum assisted with the intracellular ROS production assay. John Widen conducted the flow cytometry assays, assisted with growth inhibition assays on human cells lines, conducted the clonal growth assays, and assisted with the intracellular ROS production assay.

4.1 Introduction

Sesquiterpene lactones (SL) are a diverse family of plant-derived natural products with utilities in treating inflammatory diseases and cancer.^{182c, 238} Parthenolide (**PTL**, **4.1**) is a well-studied SL derived from the feverfew plant *Tanacetum parthenium*,²³⁹ bearing broad-spectrum anti-proliferative activities to a variety of cancer types through multiple mechanisms of inhibition.²⁴⁰ The seminal discovery that **PTL** induces apoptosis in acute myeloid leukemia (AML) stem and progenitor cells without exhibiting comparable toxicity to healthy hematopoietic stem cells (HSCs) has anointed **PTL** as the prototypical member of next-generation therapies for eradicating leukemic stem cells (LSCs).²⁴¹ AML growth is hierarchical and originates from LSCs.²⁴² Therefore, small molecules that eliminate LSCs are expected to confer more durable and potentially curative therapies.²⁴³ In addition to its anti-leukemic activity, **PTL** has been explored as a potential therapeutic for a spectrum of indications.²⁴⁴

Chemical optimizations of **PTL** have been required to optimize the natural product for *in vivo* applications. A Phase I dose escalation trial of feverfew extract failed to achieve measurable levels of **PTL** in serum and oral dosing (40 mg/kg) of **PTL** in mice yielded approximately 200 nM concentrations in serum, which is not sufficient to confer anti-proliferative activity.²⁴⁵ Conversion of **PTL** to prodrug dimethylamino-parthenolide fumarate, **DMAPT** (or **LC-1**, **4.2**), increased water solubility by ~1000-fold and yielded an analogue with substantially improved pharmacokinetic parameters (mice: $C_{\max} = 25 \mu\text{M}$, $t_{1/2} = 0.6 \text{ hr}$; canine: $C_{\max} = 61 \mu\text{M}$, $t_{1/2} = 1.9 \text{ hr}$) with oral dosing (100 mg/kg).²⁴⁶ Hetero-Michael addition of aliphatic amines to natural products and synthetic analogues bearing α -methylene- γ -butyrolactones has constituted a modular strategy to enhance water solubility through prodrug formation.²⁴⁷ Semisynthetic modifications to **PTL** outside of the α -methylene- γ -butyrolactone warhead, however, are significantly less developed. Acid-catalyzed conversion of **PTL** to 5-7-5 guaianolide, Micheliolide (**4.3**), has been achieved, yielding a derivative with anti-proliferative activity comparable to its predecessor.^{247c, 248} Photochemical isomerization of the C1-C10 olefin of **PTL** has also been reported, yielding *cis*-olefin **4.4**.²⁴⁹ Allylic oxidation of the C1-C10 vinyl methyl

group of **PTL** results in formation of another natural product, Melampomagnolide B (**MeIB**, **4.5**), which exhibits comparable anti-proliferative activity as **PTL**, but contains an allylic alcohol, which is useful for further transformations (e.g., synthesis of affinity pull-down reagents and O-functionalized analogues).²⁵⁰ Recently, the Fasan laboratory has utilized P450 enzymes to oxygenate proximal to the C1-C10 olefin of **PTL**, yielding alcohols at C9 and C14, which were subsequently esterified with substituted benzoic acids to yield **PTL** analogues with anti-leukemic activities.²⁵¹

In this study, we examined the necessity of the **PTL** C1-C10 olefin and its tolerance to structural modification with respect to sustained anti-proliferative activities to cancer cells through the synthesis and biochemical screening of C1-C10 modified **PTL** analogues. Included among our small library of compounds are established **PTL** analogues, such as Micheliolide (**4.3**), *cis*-**PTL** (**4.4**), and **MeIB** (**4.5**), as well as additional mechanistic probes, such as **4.6** (reduced C1-C10 olefin) and **4.7** (cyclopropanated C1-C10 olefin). Interestingly, cyclopropanated analogue **4.7** was found to exhibit similar anti-proliferative activity to cancer cells as **PTL**, but conferred less toxicity to healthy bone marrow and more potently induced cellular reactive oxygen species (ROS), which is known to promote cell death to AML stem cells and other cancer cells.²⁵²

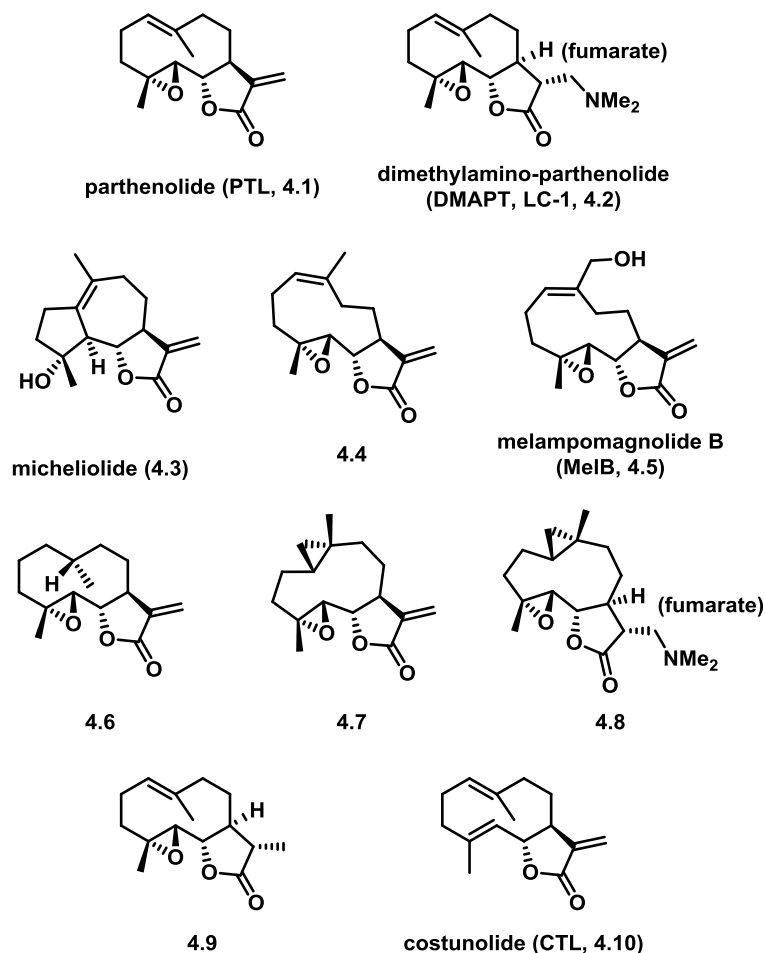
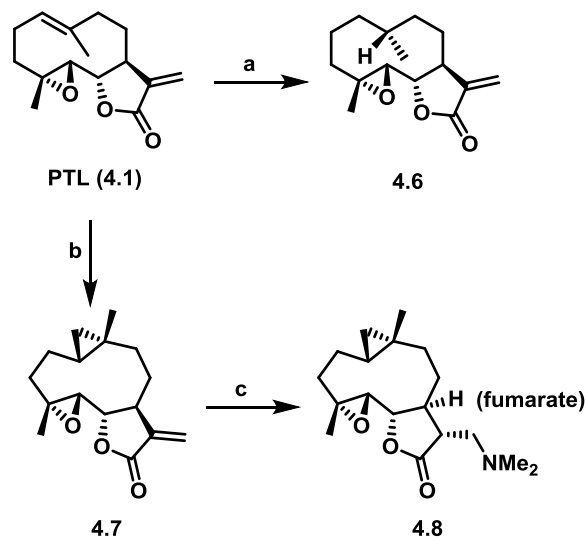


Figure 4.1.1. Structures of **PTL** and **DMAPT**, C1-C10 modified **PTL** analogues **4.3-4.4**, **MelB**, **4.5** and **4.6-4.8**), and control compounds for biochemical assays (**4.9** and **CTL**, **4.10**).

4.2 Design and synthesis of **PTL** analogues

A small library of C1-C10 olefin modified **PTL** analogues and control compounds were synthesized or purchased commercially (**Figure 4.1.1**). Previous studies have found that the C1-C10 olefin of **PTL** can participate in electrophilic transannular cyclizations with the C4-C5 epoxide under Brønsted or Lewis acid conditions to yield guaianolide analogues.^{249a} Therefore, we synthesized reduced analogue **4.6** to eliminate any potential for acid instability. The exocyclic methylene on the α -methylene- γ -butyrolactone of **PTL** was transiently protected by dimethylamine addition to yield dimethylamino-**PTL**, which was not converted to the fumarate salt for this application

(**Scheme 4.2.1**). Hydrogenation of dimethylamino-**PTL** free base with PtO₂ catalyst at 50 psi H₂ resulted in facial selective reduction (~15:1). The exocyclic methylene was deprotected under Hofmann elimination conditions (excess MeI, THF, H₂O)^{247b, 253} to yield **4.6** in 32% yield (over three steps). The stereochemistry of the methyl group was assigned by X-ray crystallography (see **Section 4.12** for crystal structure data).



Scheme 4.2.1. Synthesis of C1-C10 reduced **PTL** analogues.^a

^a**Reagents and Conditions:** a) NHMe₂, MeOH; Pt₂O, H₂ (50 psi), EtOAc; MeI, THF, H₂O, 45 °C, 32% (3 steps); b) Zn(CH₂I)₂, DME, CH₂Cl₂, 41%; c) NHMe₂, MeOH; fumaric acid, 85%.

Cyclopropanes are unique ring systems with significant sp²-character, thereby mimicking the electronics of double bonds.²⁵⁴ Such modifications can be valuable for increasing the stability of a drug candidate. In the case of **PTL**, replacement of the C4-C5 epoxide with a cyclopropane significantly enhanced plasma half-life ($t_{1/2}$ = 13.9 hr versus 1.6 hr for **PTL**; testing in mouse plasma).²⁵⁵ To further probe the role of the C1-C10 olefin in **PTL** with a structurally analogous mimetic, we synthesized C1-C10-cyclopropanated **4.7**. Utilizing the Furukawa modification (ZnEt₂) to the classical Simmons-Smith reaction,²⁵⁶ **PTL** was treated with pre-formed Zn(CH₂I)₂ in a solution of DME and CH₂Cl₂, which yielded (1*S*,10*R*) **4.7** in 41% yield following silica gel chromatography (**Scheme 4.2.1**). Interestingly, no attack to the exocyclic olefin was

observed, with the remaining mass balance consisting of mostly unreacted **PTL**. The structure of **4.7** was assigned by X-ray crystallography (**Figure 4.2.1**). As expected, the solid-state structure of cyclopropane **4.7** was highly similar to a recently reported **PTL** X-ray structure)²⁵⁵ with a root-mean-square deviation of 0.167 Å (**Figure 4.2.1**; alignment of structures provided below in **Section 4.12, Figure 4.12.1**). Recognizing that **4.7** may suffer from poor aqueous solubility akin to **PTL**, we synthesized dimethylamine congener **4.8**, which was converted to the fumarate salt for consistency with **DMAPT (4.2)**.^{246b} **PTL** and Costunolide (**CTL, 4.10**) were purchased from commercial vendors and the remaining analogues in our library (**4.3, MeIB (4.5)**, and **4.6**) were synthesized as previously reported.^{246b, 247c-g, 248a, 249a, 250a-d} The structure of synthesized Micheliolide (**4.3**) was verified by X-ray crystallography (**Section 4.12**) and compared to a previous report.²⁵⁷

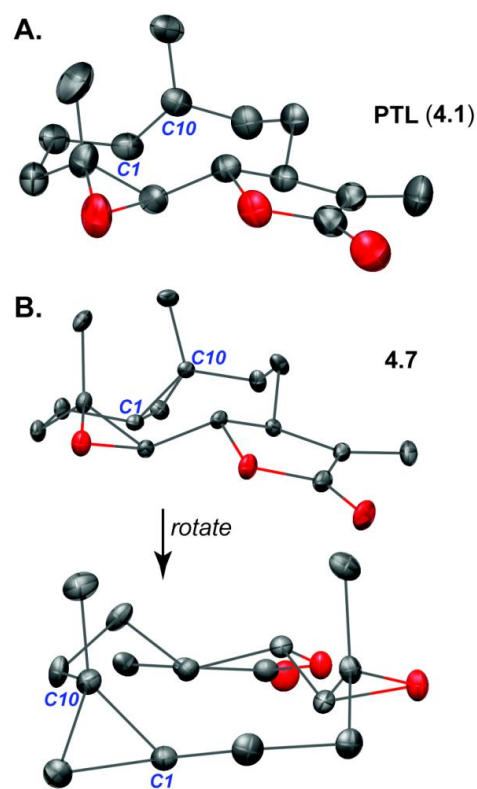


Figure 4.2.1. X-ray crystal structures. (A) **PTL**^{246b} and (B) cyclopropane **4.7** adopt similar conformations in the solid-state. Root-mean-square deviation between the two structures is 0.167 Å.

4.3 Lipophilicity Analyses

The distribution coefficients (LogD) of select C1-C10 **PTL** analogues were assessed through calculated and measured analyses (**Table 4.3.1**). Calculated LogD values were less predictive in comparison to experimentally derived measurements for **PTL** ($c\text{LogD}_{7.4} = 3.07$ versus $\text{LogD}_{7.4} = 1.79$) and *cis*-**PTL** isomer **4.4** ($c\text{LogD}_{7.4} = 3.07$ versus $\text{LogD}_{7.4} = 2.00$), whereas calculated and measured values were generally consistent for the remaining analogues (**Table 4.3.1**). Both reduction and cyclopropanation of the C1-C10 olefin increased the overall lipophilicity of the **PTL** skeleton ($\text{LogD}_{7.4} = 2.30$ for **4.6** and $\text{LogD}_{7.4} = 2.29$ for **4.7**). **CTL**, which contains a C4-C5 olefin in place of the epoxide in **PTL**, was substantially more lipophilic ($\text{LogD}_{7.4} = 2.90$ for **CTL** versus $\text{LogD}_{7.4} = 1.79$ for **PTL**). The distribution coefficients of dimethylamine fumarate salts of **PTL** and **4.7**, analogues **DMAPT** and **4.8**, respectively, were not measured because their calculated LogD values ($c\text{LogD}_{7.4} = 0.50$, **DMAPT**; $c\text{LogD}_{7.4} = 0.56$, **5**) were outside the measurable range of the assay (1-5 units).

Table 4.3.1. Calculated LogD values ($c\text{LogD}_{7.4}$; MarvinSketch) and measured LogD values ($\text{LogD}_{7.4}$; Sirius Analytical, average of two measurements) at pH 7.4 for select C1-C10 **PTL** analogues.

Compound	$c\text{LogD}_{7.4}$	$\text{LogD}_{7.4}$
PTL (4.1)	3.07	1.79
4.3	1.97	2.18
4.4	3.07	2.00
4.6	3.48	2.30
4.7	3.16	2.29
CTL (4.10)	4.22	2.90

4.4 Cellular Cytotoxicity Screening

All compounds were screened for anti-proliferative activity against 7 cell lines representing blood lineage cancers (HL-60 and CCRF-CEM) and solid tumors (U-87 MG, GBM6, MCF-7, DU-145, and NCI/ADR-RES). An established drug-resistant tumor cell line, NCI/ADR-RES, was included in our screen to determine if **PTL** and related analogues possess activity against cancer cell lines with high P-glycoprotein expression.²⁵⁸ Clinically used chemotherapeutic drugs gemcitabine and doxorubicin are inactive ($IC_{50} > 500 \mu\text{M}$) against NCI/ADR-RES cells,²³⁷ and cancer stem cells (CSCs) are known to have high expression levels of drug efflux machinery.²⁵⁹ Additionally, we included the GBM6 glioblastoma multiforme (GBM) cell line in our primary screen because it possesses a CD133⁺ population of cells,²⁶⁰ which is a frequently used marker of GBM stem cells.²⁶¹

Screening of **PTL** and related analogues revealed broad-spectrum, low-micromolar IC_{50} growth inhibitory activity to all cancer cell lines regardless of modification to the C1-C10 olefin (**Table 4.4.1**). In contrast, **4.9**, which bears a reduced exocyclic methylene on the α -methylene- γ -butyrolactone, was found to be completely inactive against all cell lines examined ($IC_{50} > 500 \mu\text{M}$). These data are consistent with previous reports,^{246b, 262} and reinforce the necessity of the α -methylene- γ -butyrolactone for anti-proliferative activity of molecules of this class.^{182c, 205, 247b, 247e} **CTL** was found to be equipotent to the C1-C10 modified analogues, suggesting the C4-C5 epoxide is non-essential for activity, which is also consistent with a previous report.²⁵⁵ All compounds except for exocyclic methylene-reduced **4.9** were active against drug-resistant NCI/ADR-RES cells (IC_{50} range: 9.4 – 22.0 μM).

Table 4.4.1. Growth inhibitory activities (IC₅₀) of **PTL**, C1-C10-modified **PTL** analogues, and related probes to cell lines: HL-60 (acute promyelocytic leukemia), CCRF-CEM (acute lymphoblastic leukemia), U-87 MG (glioblastoma multiforme), GBM6 (glioblastoma multiforme), MCF-7 (breast adenocarcinoma), DU-145 (prostate cancer), and NCI/ADR-RES (ovarian cancer; adriamycin-resistant), IC₅₀ values are mean ± S.D. in μM (n ≥ 3 analyses). ^aObtained previously.^{219, 237} ^bSlightly lower than previously reported (57.6 μM).²³⁷

Compound	HL-60	CCRF-CEM	U-87 MG	GBM6	MCF-7	DU-145	NCI/ADR-RES
PTL (4.1)	9.3 ± 3.8 ^a	4.7 ± 1.6	8.8 ± 2.1 ^a	3.4 ± 1.1 ^a	9.7 ± 2.8	8.9 ± 4.6 ^a	11.4 ± 2.4 ^b
LC-1 (4.2)	7.1 ± 0.4	1.9 ± 0.4	8.8 ± 1.9 ^a	3.5 ± 1.1 ^a	10.4 ± 1.2	8.4 ± 4.5	12.3 ± 2.7
4.3	9.2 ± 2.2	2.7 ± 1.1	17.8 ± 5.0	8.5 ± 0.7	9.6 ± 1.0	14.8 ± 4.0	22.0 ± 5.3
4.4	8.0 ± 1.1	2.2 ± 1.0	9.1 ± 4.4	3.3 ± 0.8	7.5 ± 0.8	6.0 ± 4.2	9.4 ± 2.1
MelB (4.5)	7.5 ± 3.0	5.5 ± 1.2	16.3 ± 6.8	4.5 ± 1.9	9.5 ± 1.9	14.3 ± 5.9	15.0 ± 4.9
4.6	9.0 ± 2.1	2.5 ± 2.1	7.5 ± 0.4	2.0 ± 0.3	20.1 ± 1.3	5.5 ± 1.5	15.6 ± 3.1
4.7	4.4 ± 1.3	2.0 ± 0.6	11.6 ± 1.4	2.3 ± 0.5	14.1 ± 1.0	14.8 ± 6.7	12.0 ± 2.5
4.8	6.5 ± 2.7	2.9 ± 0.6	10.5 ± 0.9	3.2 ± 0.7	16.9 ± 2.0	13.3 ± 2.2	11.7 ± 3.1
4.9	>500	>500	>500	>500	>500	>500	>500
CTL (4.10)	13.0 ± 0.2	2.3 ± 0.2	9.6 ± 0.8	7.0 ± 1.8	17.5 ± 3.7	7.7 ± 2.8	17.1 ± 0.9

4.5 Bone Marrow Toxicity Studies

The CD34⁺CD38⁻ bone marrow (BM) immunophenotype is enriched for self-renewing stem cells.²⁶³ Previous studies have demonstrated that **PTL** is non-toxic to total BM and CD34⁺CD38⁻ BM cells when dosed at 5 μM for 18 hrs.²⁴¹ To assess BM toxicity of the synthesized C1-C10 **PTL** analogues in comparison to **PTL**, we performed flow cytometry assays with human BM cells and measured cellular viability by flow cytometry using markers for apoptosis (Annexin V) and necrosis (7-AAD). Since **PTL** has been shown to elicit some overall BM toxicity at a dose of 7.5 μM for 18 hrs,²⁴¹ we elected to utilize a slightly higher dose to exacerbate the toxicity of **PTL** so that analogues with less toxicity to BM in comparison to **PTL** could be measured. Doxorubicin (**DOX**) was included as a positive control since it is known to elicit BM toxicity.²⁶⁴ The mean overall

viability of the BM specimen utilized in our study was 78% (**Figure 4.5.1A**) and 94% for the CD34⁺CD38⁻ population (**Figure 4.5.1B**). Treatment with 0.5 μ M **DOX** for 12 hr resulted in a 56% reduction in total BM viability and an 85% reduction in the primitive CD34⁺CD38⁻ BM population (**Figure 4.5.1**). **PTL** treatment at 25 μ M resulted in a 48% reduction in total BM viability, whereas C1-C10 modified **PTL** analogues **4.3**, **MeIB**, and **4.7**, as well as control analogue, **CTL**, were less toxic (range: 22-26% average reduction of total BM viable cells). **PTL** was found to elicit no significant toxicity to primitive CD34⁺CD38⁻ BM cells at 25 μ M dose and the C1-C10 **PTL** analogues were similarly non-toxic at the same concentration (**Figure 4.5.1B**). Therefore, modification to the C1-C10 olefin of **PTL** significantly lowers its overall toxicity to BM cells. However, the observed toxicity of **PTL** to total BM would be expected to be transient since little cell death was measured in the CD34⁺CD38⁻ BM population upon **PTL** treatment, which is responsible for BM clonal growth.²⁶³ Studies in our group using **PTL** prodrug, **DMAPT**, have revealed no measurable toxicity to mice upon continuous oral dosing (100 mg/kg, daily) for over four weeks.^{262b}

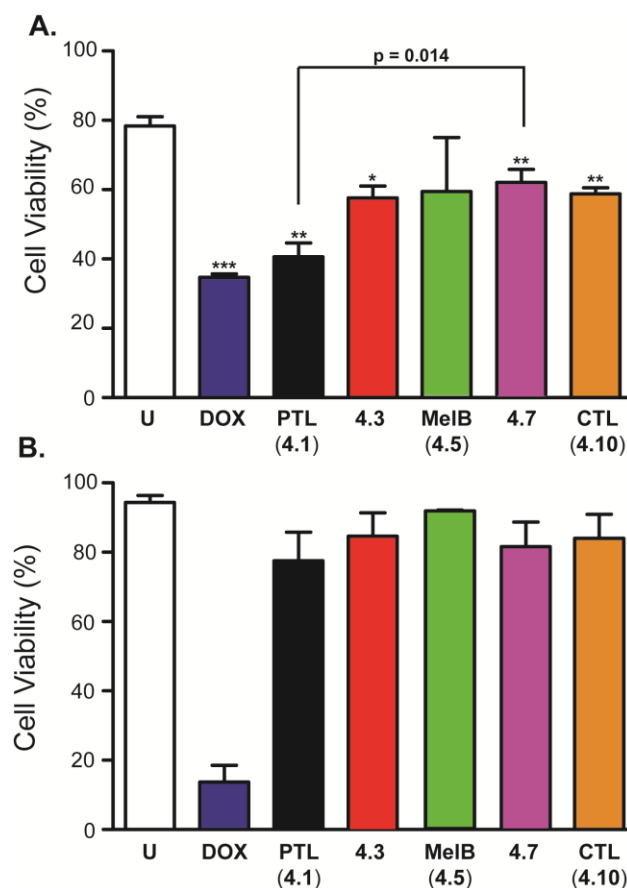


Figure 4.5.1. Toxicity of PTL and analogues to human bone marrow cells. BM was dosed with DOX (0.5 μ M), and PTL (4.1), 4.3, MeIB (4.5), 4.7, and CTL (4.10) (25 μ M) for 12 h. Cellular viability was then measured by flow cytometry and viable cells (%) were those not stained by Annexin V (apoptosis) and 7-AAD (necrosis) reagents. (A) Viability of the total bone marrow cell population and (B) viability of the CD34⁺CD38⁻ population. Data is the mean ($n \geq 3$ analyses) \pm S.D. * $p = 0.05$, ** $p \leq 0.01$, *** $p \leq 0.001$ in comparison to untreated control.

4.6 Inhibition of Drug-resistant AML and Toxicity to LSCs

Given the selectivity of our compounds for inhibiting growth of blood lineage cancer cells (e.g., HL-60 and CCRF-CEM, **Table 4.6.1**) and their lack of toxicity to healthy BM (**Figure 4.5.1**), we focused subsequent efforts on characterizing the anti-leukemic activities of our molecules. Four murine AML cell lines were utilized for our initial screen (**Table 4.6.1**). B117P and B140P are murine cell lines isolated from the BXH-2 mice strain that spontaneously develops AML due to the presence of a murine leukemia virus.²⁶⁵ These cells are sensitive to cytarabine (AraC), which is used in

standard-of-care AML therapy. Continual low dosing of B117P and B140P with cytarabine resulted in cytarabine-resistant cell lines B117H and B140H, respectively.²⁶⁶ Cytarabine resistance is conferred in B117H and B140H by loss-of-function mutations in the deoxycytidine kinase gene *Dck*, which inhibits intracellular metabolism of cytarabine to its 5'-monophosphate.²⁶⁷ **PTL** and C1-C10-modified analogues **4.3**, **MeIB**, and **4.7**, and control analogue **CTL** all inhibited the growth of this panel of cell lines with low micromolar activity (IC₅₀ range: 1.1 – 13.5 μM). No loss in potency was observed between cytarabine-sensitive (parental) cell lines B117P and B140P and cytarabine-resistant lines B117H and B140H for any of the molecules tested. These data suggest that **PTL** analogues have the potential to sustain anti-proliferative activities to AML cell lines that become sensitive to cytarabine.

Table 4.6.1. Growth inhibitory activities (IC₅₀) of **PTL**, C1-C10-modified **PTL** analogues, and related probes to murine AML cell lines B117P, B117H, B140P, and B140H. IC₅₀ values are mean ± S.D. in μM (n ≥ 3 analyses).

Compound	B117P	B117H	B140P	B140H
PTL (4.1)	1.1 ± 0.2	4.7 ± 1.6	5.8 ± 2.3	3.4 ± 1.1
4.3	6.4 ± 1.0	8.8 ± 1.7	10.0 ± 0.4	9.3 ± 1.5
MeIB (4.5)	2.1 ± 0.8	2.5 ± 1.0	2.9 ± 1.0	2.2 ± 0.7
4.7	2.9 ± 0.6	6.4 ± 2.1	13.5 ± 2.3	5.9 ± 2.4
CTL (4.10)	3.5 ± 0.4	4.8 ± 0.7	3.6 ± 1.2	2.8 ± 0.7

PTL is known to eradicate LSCs,²⁴¹ and therefore, we investigated if the C1-C10-modified **PTL** analogues could inhibit LSCs with similar potency as the parent natural product. We utilized an engineered leukemia cell line, TEX, for these assays. TEX cells are derived from lineage depleted (Lin⁻) human cord blood cells transduced with the fusion gene *TLS-ERG*. TEX cells effectively mimic human AML by maintaining the potential for multi-lineage differentiation through their heterogeneous population of cells with hierarchical growth properties. A large population of primitive CD34⁺ cells are

present in the TEX model system, which has also been utilized in high-throughput screening for small molecule inhibitors of LSCs.²⁶⁸ Screening of **PTL** and related analogues (**4.3**, **MelB**, **4.7**, and **CTL**) revealed broad-spectrum inhibitory activity (IC₅₀ range: 2.7 – 6.8 μM) by metabolic viability staining following 48 hr treatment (**Table 4.6.2**).

Table 4.6.2. Growth inhibitory activities (IC₅₀) of **PTL**, C1-C10-modified **PTL** analogues, and related probes to TEX cells. IC₅₀ values are mean ± S.D. in μM (n ≥ 3 analyses).

Compound	TEX
PTL (4.1)	2.8 ± 0.2
4.3	2.7 ± 0.4
MelB (4.5)	6.8 ± 2.3
4.7	3.8 ± 0.2
CTL (4.10)	4.9 ± 0.4

Analysis of the LSC-enriched CD34⁺CD38⁻ population of TEX cells treated with 25 μM **PTL**, **1**, **MelB**, and **CTL** for 12 hr revealed a nearly complete reduction in cellular viability by flow cytometry analysis (cell viability range: 1–10%, **Figure 4.6.1**), with the majority of cells staining positive for 7-AAD, indicating necrotic cell death. Treatment of cells with 15 μM **PTL** analogues yielded slightly higher amounts of viable cells (cell viability range: 10–25%) with no statistical significant differences in potencies between the analogues tested. A relatively low dose of **DOX** (0.5 μM) was sufficient to reduce the viability of CD34⁺CD38⁻ TEX cells to 6%. Consequently, all of the **PTL** analogues tested were able to induce cell death in the LSC-enriched CD34⁺CD38⁻ population of TEX cells.

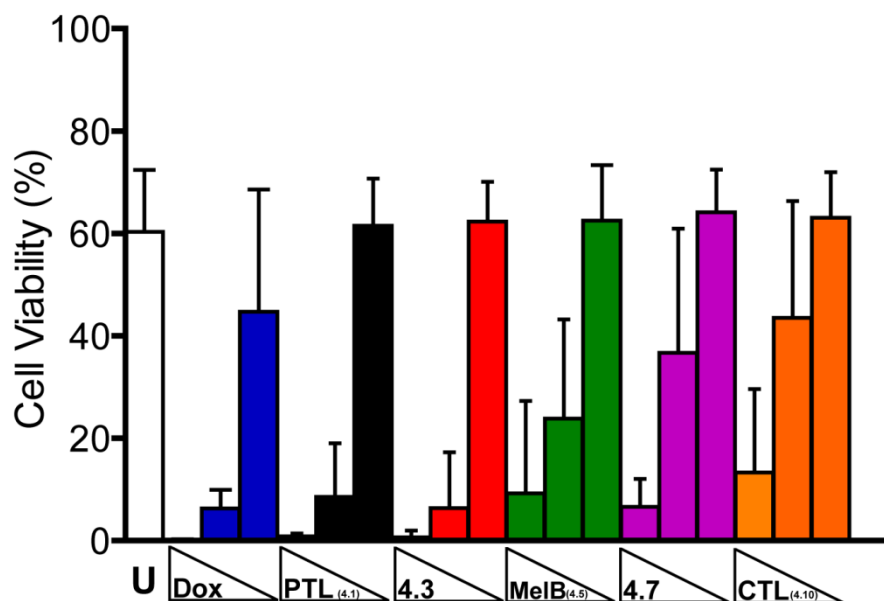


Figure 4.6.1. Cellular viability (%) of CD34⁺CD38⁻ TEX cells treated with **DOX** (2.5, 0.5, 0.05 μM) and **PTL**, **4.3**, **MeIB**, **4.7**, **CTL** (25, 15, 2.5 μM). Viable cells were those not stained by Annexin V (apoptosis) and 7-AAD (necrosis) markers. Values are mean ± S.D. (n ≥ 5 analyses). * p = 0.05, ** p ≤ 0.01, *** p ≤ 0.001 in comparison to untreated control.

To corroborate that the observed inhibition of primitive CD34⁺CD38⁻ TEX cells also affects the LSC population, we performed methylcellulose clonal growth assays of TEX cells in the presence of our compounds. As previously mentioned, AML is characterized by hierarchical growth properties that originate from LSCs,²⁴² and therefore, small molecule inhibition of LSCs will prevent clonal growth of cells in methylcellulose. Control (DMSO) treated TEX cells yield on average 20.8 clones per assay (**Table 4.6.3**). Treatment with **PTL** or analogues **4.3**, **MeIB**, **4.7**, or **CTL** all potently inhibit clonal outgrowth of TEX cells at 15 μM dose, with **PTL** and **4.3** yielding no measurable clones. Decreasing the dosage to 2.5 μM with the same compounds also elicits inhibition of TEX clonal growth (range: 2.6 – 7.0 clone average). **DOX** and **AraC** were both able to inhibit TEX clonal growth in our assay, with 0.5 μM treatment of both compounds completely inhibiting cell growth. Taken together, these data demonstrate **PTL** and related analogues are proficient at inhibiting LSCs, which is likely mediated through their common pharmacophore, the α-methylene-γ-butyrolactone.

Table 4.6.3. Clonal growth assay with TEX cells. TEX cells were plated 6,000 cells/well and dosed with DMSO (0.05%, control wells) or compounds at the concentrations noted. Values are the mean number of colonies \pm S.D. (3 biological replicates) observed after 11 d growth on methylcellulose. N.D., clonal growth not detected. $p \leq 0.001$ in comparison to DMSO control for all samples, except **4.7** at 2.5 μ M ($p \leq 0.01$).

Compound	Colonies \pm S.D.	
	2.5 μ M	15 μ M
PTL (4.1)	2.6 \pm 2.7	N.D.
4.3	4.2 \pm 2.5	N.D.
MelB (4.5)	5.3 \pm 1.6	0.1 \pm 0.3
4.7	7.0 \pm 5.1	0.6 \pm 0.9
CTL (4.10)	6.9 \pm 3.6	5.6 \pm 4.7
	0.1 μ M	0.5 μ M
DOX	0.7 \pm 1.3	N.D.
AraC	2.6 \pm 1.0	N.D.
DMSO	20.8 \pm 9.0	

4.7 Induction of Reactive Oxygen Species

The mechanism by which **PTL** eradicates cancer cell viability is an area of substantial debate. **PTL** has been shown to affect a variety of cellular processes, including (among many others) inhibition of NF- κ B signaling and microtubule deetyrosination, reduction in DNA methylation, and induction of cellular ROS (reviewed in^{182c, 239-240, 268b, 269}). Multiple studies have implicated ROS induction as a mechanism of **PTL**-mediated cancer cell death.^{252c, 252f, 252i, 252j} Consequently, we measured changes in intracellular ROS in TEX cells resulting from treatment with **PTL**, **CTL**, **4.3**, **MelB**, and **4.7** to rank order the pharmacological utility of our compounds. Treatment of TEX cells with hydrogen peroxide results in a 3.1-fold induction of intracellular ROS after 30 min, which is consistent with a previous study where a similar induction of ROS was measured by flow cytometry in HL-60 cells.²⁷⁰ Dosage of TEX cells with **4.3** (2.9-fold),

4.7 (2.6-fold), and **CTL** (2.2-fold) all substantially induced ROS levels at 100 μ M dose in comparison to untreated control (**Figure 4.7.1**). **PTL** induced ROS as well, but to a lower level (1.6-fold). No observable induction of ROS was detected with **MelB** at either concentration tested. Decreasing the concentration of compounds to 25 μ M also resulted in a significant induction of ROS levels for **4.3** (1.7-fold) and **4.7** (1.6-fold). Consequently, these data suggest that **4.3** and **4.7** more potently induce ROS than parent natural product, **PTL**.

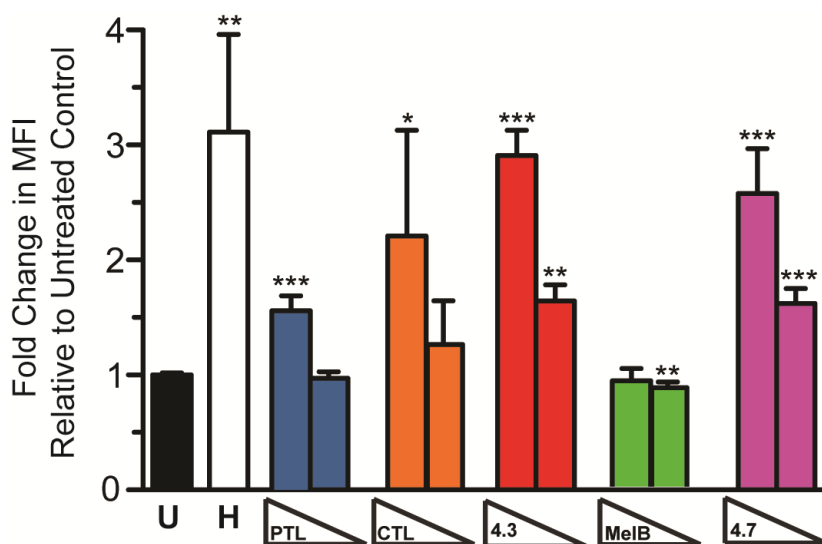


Figure 4.7.1. Intracellular ROS induction by **PTL** and analogues. TEX cells were treated with 100 μ M hydrogen peroxide (H) and **PTL**, **CTL**, **4.3**, **MelB**, and **4.7** (100, 25 μ M) and ROS activity was measured by flow cytometry using CellROX Green reagent. The median fluorescence intensity (MFI) of each sample was normalized to the untreated control (U) and averaged. Values are mean MFI \pm S.D. ($n \geq 3$ analyses). * $p = 0.05$, ** $p \leq .01$, *** $p \leq 0.001$ in comparison to untreated control.

4.8 Conclusions

A small library of C1-C10 **PTL** analogues was synthesized and evaluated for anti-proliferative activity to cancer cells, toxicity to healthy BM, ability to inhibit drug-resistant AML and target LSCs, and proficiency at inducing intracellular ROS. All compounds with the exception of **4.9** were capable of inducing cancer cell death with low micromolar potency. However, Micheliolide (**4.3**) and cyclopropane **4.7** were found to inhibit the growth of drug-resistant AML and eliminate LSCs similarly to **PTL** (**4.1**), but

offer the advantages of being less toxic to healthy BM and more potently activating ROS in AML cells than **PTL**. Additionally, elaboration of **4.7** to its dimethylamine congener **4.8** provided an analogous prodrug to **DMAPT (LC-1)**. Given the continued interest in **PTL**, highlighted by its first total synthesis,²⁴⁴ and the rekindled popularity of covalent drugs in general,²⁷¹ C1-C10 modifications such as cyclopropanation may be useful for optimizing **PTL** and related germacranolides for therapeutic applications.

4.9 Experimental

LogD measurements

Calculated LogD values were obtained using MarvinSketch (ChemAxon). cLogD_{7.4} was calculated using 0.1 mol/dm³ electrolyte concentrations (Cl⁻, Na⁺, K⁺) at pH 7.4. Experimental LogD_{7.4} measurements were performed by Sirius Analytical. The LogD_{7.4} of each sample was determined using the LDA (liquid-liquid distribution chromatography) method. The data is the average of two measurements.

Preparation of stock solutions

Compound stock solutions were prepared in DMSO (20-100 mM concentrations) and stored at -20 °C when not in use. Compound purities were assessed frequently by analytical reverse-phase HPLC analysis and fresh solutions were prepared as needed.

Cell culture

All cell lines were maintained in a humidified 5% CO₂ environment at 37 °C in tissue culture flasks (Corning) under normoxic conditions. Adherent cells were dissociated using either Trypsin-EDTA solution (0.25%, Gibco) or TrypLE Express solution (Invitrogen). HL-60, CCRF-CEM, U-87 MG, GBM6, DU-145, and NCI/ADR-RES cells were cultured as described previously.^{219, 237, 262b} MCF-7 cells (ATCC, HTB-22) were cultured in MEM media (Cellgro) supplemented with 10% FBS (Gibco), bovine

insulin (0.01 mg/mL, Sigma), penicillin (100 I.U./mL, ATCC), and streptomycin (100 µg/mL, ATCC). TEX cells^{268a, 272} were cultured in IMDM containing L-glutamine (Cellgro) supplemented with 15% FBS (Gibco), Stem Cell Factor (20 ng/mL, PeproTech), Interleukin-3 (2 ng/mL, PeproTech), penicillin (100 I.U./mL, ATCC), and streptomycin (100 µg/mL, ATCC).

Human cancer cell line cytotoxicity assays

Alamar blue cellular cytotoxicity assays and data analyses were performed as previously described.^{219, 237, 262b} Suspension cell lines (HL-60, CCRF-CEM and TEX^{268a, 272}) were seeded at a density of 10,000 cells/well in media (50 µL) and adherent cell lines (U-87 MG, GBM6, MCF-7, DU-145, and NCI/ADR-RES) were seeded at a density of 5,000 cells/well in media (50 µL) 24 h prior to treatment with compounds in 96-well plates (Costar 3595, Corning, Inc.). IC₅₀ values (n ≥ 3 biological replicates) are the mean ± S.D.

Murine cytotoxicity assay

Cell culture and cytotoxicity assays with murine cell lines B117P, B117H, B140P, and B140H were performed as previously described.^{266b, 267} Cells were seeded at a density of 25,000, 28,000, 36,000 and 44,000 cells/well for B117P, B117H, B140P, and B140H cell lines, respectively, in media (200 µL) in 96-well plates (Costar 3596, Corning, Inc.). Assays were conducted in biological triplicate and IC₅₀ values are the mean ± S.D.

Bone marrow cell culture

Frozen human mononuclear bone marrow cells were purchased from AllCells (Cat. #ABM011F). These bone marrow cells were from two donors (#5630 [Lot #BM4565] and #4887 [Lot #BM4118]). The cells were thawed according to vendor instructions and then cultured in StemSpan SFEM (STEMCELL Technologies, Inc.) media supplemented with StemSpan CC100 cytokine cocktail (STEMCELL

Technologies, Inc.) in a humidified 5% CO₂ environment at 37 °C in tissue culture flasks (Corning) under normoxic conditions.

Flow cytometry analysis of cytotoxicity in bone marrow and TEX cells

Human bone marrow or TEX cells were plated in their respective media at 1×10^6 cells/mL (1 mL/well) in a 24-well plate format (Corning). Cells were dosed with compounds or 1% DMSO/media and incubated for 12 h at 37 °C, 20% O₂, and 5% CO₂. The final DMSO concentration was 0.03% (v/v) per well. After 12 h of incubation, each sample was transferred into FACS tubes and centrifuged for 5 min at 800 rpm. The supernatant was decanted and each sample was washed with cold 1X PBS (1 mL) and centrifuged again. After centrifugation, the supernatant was decanted and the samples were stained with Brilliant Violet 421 mouse anti-human CD34 (BD Biosciences [Cat. #562577]; 5 µL/sample) and APC mouse anti-human CD38 (BD Biosciences [Cat. #555462]; 20 µL/sample) antibodies in FACS buffer (1X PBS, 2% FBS, 0.1% sodium azide; 100 µL total volume/sample) for 10 minutes at 4 °C. The cells were then diluted with FACS buffer (1 mL) and centrifuged. The supernatant was decanted and stained with Annexin V-FITC (BD Biosciences [Cat. #556420]; 5 µL/sample) and 7-AAD (eBioscience [Cat. #00-6993-50]; 5 µL/sample) in FACS buffer (100 µL total volume/sample) for 10 minutes at room temperature in the dark. The samples were diluted with FACS buffer (300 µL), and kept on ice during analysis by flow cytometry using a BD Biosciences LSR II flow cytometer. Greater than 5×10^4 events were measured for each sample during analysis. All antibodies and stains were stored at 4 °C in the dark. After data collection, each sample was processed using FlowJo (Tree Star; v 7.6.5). The cell viability is expressed as a mean of 3-5 biological replicates \pm S.D. Statistical significance was determined using unpaired t-tests (GraphPad Prism v. 5.0). An example of the data processing is shown below.

Figure 4.9.1 is a graphical representation of the work-up process completed for all presented samples starting from the initial forward scatter (FSC-A) vs. side scatter (SSC-A) dot plot. Following data collection each sample was processed with FlowJo (Tree Star; v 7.6.5). A primary gate was used before further data processing to eliminate

cell debris from the analysis of apoptotic and necrotic cells in a forward scatter (FSC-A) vs. side scatter (SSC-A) dot plot. After the primary gate was in place the stains were compensated using single stain samples compared to a non-stain control and isotype controls for the CD34 and CD38 stains. OneComp eBeads (CD34) and UltraComp eBeads (CD38) were used for positive compensation controls (eBioscience). Fluorescence minus one (FMO) controls were used to verify proper compensation of the samples. Gating of the CD34 and CD38 population was completed by comparing non-stain and isotype controls to positive control populations. The CD34⁺CD38⁻ population was then gated for Annexin V and 7-AAD to obtain cell viability. The percentage of cells within the Annexin V and 7-AAD negative quadrant was used for comparison of cell viability between samples (lower left quadrant). Cells that stained positive for Annexin V, 7-AAD, or both were considered to be apoptotic or necrotic. Below is an example of gating analysis of cell viability after dosing 15 μM PTL to TEX cells and gating for the CD34⁺CD38⁻ population.

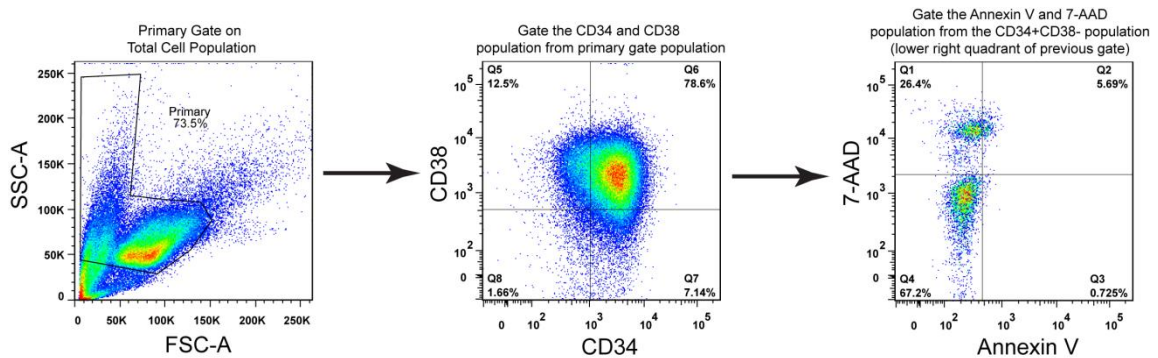


Figure 4.9.1. Example of processing to obtain cell death percentages for the CD34⁺CD38⁻ population of TEX cells after flow cytometry analysis.

Colony growth assay

TEX cells were added to Methocult H4230 (STEMCELL Technologies Inc.) supplemented with penicillin (100 I.U./mL, ATCC) and streptomycin (100 µg/mL, ATCC) at a final cell density of 1.2×10^4 cells/mL. Compounds were diluted in TEX cell media and dosed to each cell suspension to obtain the respective concentration. Each sample was vortexed vigorously to evenly distribute the cells before and after compound dosing. Each sample (1.5 mL) was plated into three wells (0.5 mL/well, three technical replicates) of a 24-well plate (Corning) and incubated under normoxic conditions at 37 °C, 5% CO₂ for 11 days before scoring colonies. Colonies were counted for each well at 10X magnification with a light microscope by two people independently and averaged for each sample. The data is the mean number of colonies for three biological replicate \pm S.D. Statistical significance was determined using unpaired t-tests (GraphPad Prism v. 5.0).

ROS Assay

TEX cells were seeded in 24-well plates at 5×10^5 cells/mL/well and incubated overnight at 37°C and 5% CO₂. The cells were then treated with compounds (25 and 100 µM), including H₂O₂ (100 µM; positive control). Immediately after treatment with compounds, CellROX Green (Invitrogen) reagent was added to the appropriate samples at a final concentration of 5 µM. The cells were then incubated for 30 minutes at 37°C and 5% CO₂. Following incubation, the samples were transferred to 5 mL FACS tubes and washed with FACS buffer (3 mL, 2X). The samples were run using a BD Biosciences LSR II flow cytometer and 5×10^4 events were recorded for each sample. Flow cytometry data was analyzed using FlowJo software (Tree Star; version 7.6.5). Samples were run in quadruplicate with the exception of H₂O₂ (triplicate data). Median fluorescence intensity (MFI) values were obtained for each sample and were normalized to the untreated control. Data are shown as mean MFI value \pm S.D. Statistical significance was determined using unpaired t-tests (GraphPad Prism v. 5.0).

The data for the TEX ROS assays were worked up using FlowJo (Tree Star;

version 7.6.5) following acquisition. A scatter gate was first set using the FSC-A vs. SSC-A dot plot. This subpopulation was then gated for singlets (doublet exclusion) using the FSC-A vs. FSC-W (width parameter) dot plot. Finally, a CellROX Green histogram was prepared from the singlet population. Shown below is a representative analysis using one of the 100 μ M PTL-treated samples:

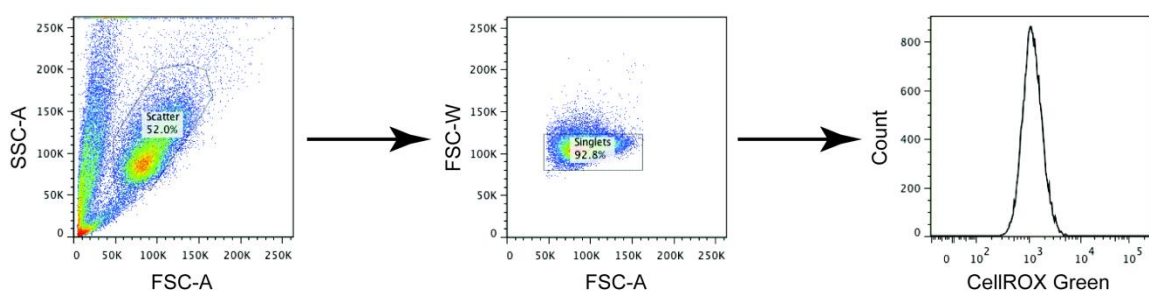
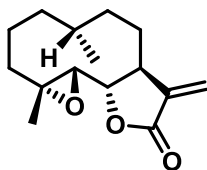


Figure 4.9.2. Graphical representation of processing to obtain total intracellular ROS within TEX cells after flow cytometry analysis.

General synthesis information

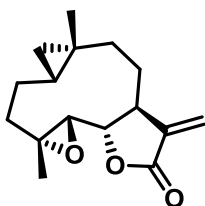
Chemical reagents were typically purchased from Sigma-Aldrich and used without additional purification unless noted. Bulk solvents were from Fisher Scientific. **PTL (4.1)** was purchased from Enzo Life Sciences and **CTL (4.10)** was purchased from Santa Cruz Biotechnology. Previously reported analogues **DMAPT (4.2)**, **MeIB (4.5)**, **4.3**, **4.4** and **4.10** were synthesized as described.^{246b, 247c-g, 248a, 249a, 250a-d} The structure of **4.3** was further confirmed by small molecule X-ray crystallography (SI; CCDC 1033012) and compared to the previous report.²⁵⁷ Tetrahydrofuran (THF) was rendered anhydrous by passing through the resin column of a solvent purification system (MBraun). Reactions were performed under an atmosphere of dry N₂ unless noted. Silica gel chromatography was performed on a Teledyne-Isco Combiflash Rf-200 instrument utilizing Redisep Rf Gold High Performance silica gel columns (Teledyne-Isco). Analytical HPLC analysis was performed on an Agilent 1200 series instrument equipped with a diode array detector and a Zorbax SB-C18 column (4.6 x 150 mm, 3.5 μ m, Agilent Technologies). The method started with 10% CH₃CN (with 0.1% trifluoroacetic acid

(TFA)) in H₂O (0.1% TFA). The 10% CH₃CN (with 0.1% TFA) was increased to 85% over 22 minutes, and then increased to 95% CH₃CN (with 0.1% TFA) over 2 more minutes. Nuclear magnetic resonance (NMR) spectroscopy was employed by using either a Bruker Avance (400 MHz for ¹H; 100 MHz for ¹³C) or Bruker Ascend (500 MHz for ¹H; 125 MHz for ¹³C) NMR operating at ambient temperature. Chemical shifts are reported in parts per million and normalized to internal solvent peaks or tetramethylsilane. High-resolution masses were obtained from the University of Minnesota Department of Chemistry Mass Spectrometry lab, employing a Bruker BioTOF II instrument.



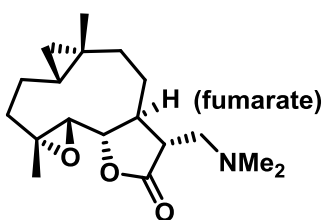
C1-C10 Reduced (**4.6**). To a stirred solution of **PTL** (**4.1**) (0.050 g, 0.201 mmol) in MeOH (2 mL) was added dimethylamine (2.0 M in MeOH, 1 mL). The reaction was allowed to stir at RT overnight and then concentrated *in vacuo*. The crude material was used without further purification. The residual material was dissolved in EtOAc (3 mL) and PtO₂ (0.005 g, 0.022 mmol) was added. The reaction mixture was degassed, then shaken for 8 hr in a Parr shaker under an atmosphere of H₂ (50 psi). The mixture was then degassed, filtered through celite, and concentrated *in vacuo*. The crude material was taken on to the next step without further purification. The reaction mixture was dissolved in THF (3 mL) and iodomethane was added in excess (0.10 mL, 1.60 mmol). The reaction was allowed to stir at RT for 2 h. The solvent and excess iodomethane were removed *in vacuo* resulting in a white solid. Water (10 mL) was added and the reaction was heated to 45 °C. Complete solvation of the yellowish material resulted within minutes of heating. The reaction was allowed to stir with heating for 3 h, and then solvent was removed *in vacuo*. Aqueous NaHCO₃ (sat'd, 5 mL) was added to the reaction mixture, and the product was extracted with DCM (3 x 20 mL). The combined organic

layers were washed with brine (20 mL), and dried with Na₂SO₄. The reaction was purified by flash chromatography over SiO₂ (10%-50% ethyl acetate in hexanes gradient) to yield **4.6** as a white solid (0.014 g, 32 %). ¹H NMR (CDCl₃, 500 MHz): δ 6.24 (d, *J* = 2.8 Hz, 1H), 5.53 (d, *J* = 2.4 Hz, 1H), 3.84 (t, *J* = 7.6 Hz, 1H), 3.10 (d, *J* = 7.6 Hz, 1H), 2.99-2.94 (m, 1H), 2.20-2.14 (m, 2H), 1.81-1.75 (m, 2H), 1.75-1.56 (m, 2H), 1.51 (s, 3H), 1.51-1.40 (m, 2H), 1.26 (m, 2H), 1.17-1.14 (m, 2H), 0.93 (d, *J* = 4.8 Hz, 3H). ¹³C NMR (CDCl₃, 125 MHz): 169.7, 139.5, 119.7, 81.0, 66.4, 61.3, 43.9, 36.7, 36.1, 30.1, 27.9, 24.7, 21.3, 20.6, 19.2. HRMS (ESI⁺) *m/z* calc'd for [C₁₈H₂₂O₃+Na]⁺ 273.1467; found 273.1470. The structure of **4.6** was further confirmed by small molecule X-ray crystallography (SI; CCDC 1033013).



Cyclopropane (**4.7**). A 0.20 M solution of Zn(CH₂I)₂·DME complex was made in the following manner: To a stirred solution of diethyl zinc (1.0 M solution in hexanes, 4.0 mL, 4.00 mmol) in CH₂Cl₂ (20 mL) and DME (0.50 mL) at 0 °C was added diiodomethane (0.80 mL, 9.92 mmol) under N₂. The mixture was stirred for 10 minutes. **PTL (4.1)** (0.090 g, 0.36 mmol) in CH₂Cl₂ (3 mL) was added dropwise over 10 min to the (CH₂I)₂·DME complex at 0 °C. The reaction was allowed to warm to RT over 12 h. The reaction was quenched with aqueous NH₄Cl (sat'd, 5 mL) and extracted with CH₂Cl₂ (3 x 20 mL). The combined organic layers were washed with aqueous NaHCO₃ (sat'd, 20 mL), brine (20 mL), dried over Na₂SO₄ and concentrated *in vacuo*. The crude mixture was purified using silica gel chromatography (gradient 10-30% EtOAc in hexanes over 15 min) to yield **4.7** (0.036 g, 40%) as a colorless oil and recovered **PTL (4.1)** (0.037 g, 41%). ¹H NMR (400 MHz, CDCl₃) δ: 6.28 (d, *J* = 3.7 Hz, 1H), 5.57 (d, *J* = 3.3 Hz, 1H), 3.96 (t, *J* = 9.1 Hz, 1H), 2.98 (d, *J* = 9.0 Hz, 1H), 2.67 (m, 1H), 2.39 (dd, *J* = 8.0 Hz, *J* =

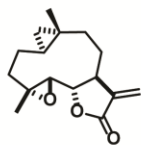
14.7 Hz, 1H), 2.19 (dd, $J = 2.3$ Hz, $J = 8.3$ Hz, 1H), 1.95 (m, 2H), 1.70 (m, 1H), 1.40 (s, 3H), 1.28 (m, 2H), 1.09 (s, 3H), 0.85 (dd, $J = 11.1$ Hz, $J = 14.7$, 1H), 0.64 (td, $J = 6.0$ Hz, $J = 9.5$ Hz, 1H), 0.39 (dd, $J = 4.3$ Hz, $J = 9.4$ Hz, 1H), -0.08 (dd, $J = 4.6$ Hz, $J = 5.6$ Hz, 1H). ^{13}C NMR (100 MHz, CDCl_3) δ : 169.4, 139.9, 120.5, 82.7, 65.5, 60.6, 48.0, 42.3, 38.4, 25.7, 24.5, 22.3, 20.4, 18.8, 18.5, 17.1. HRMS (ESI^+) m/z calc'd for $[\text{C}_{16}\text{H}_{22}\text{O}_3+\text{Na}]^+$ 285.1467; found 285.1470. The structure of **4.7** was further confirmed by small molecule X-ray crystallography (SI; CCDC 1033014).



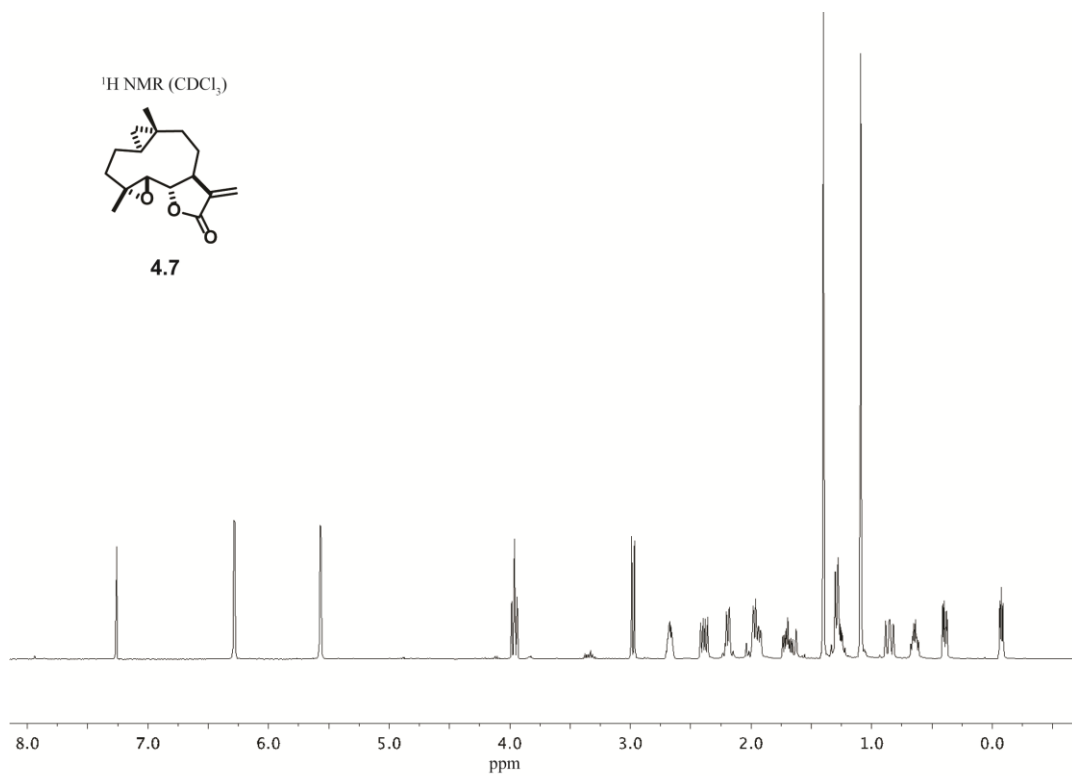
Cyclopropyl-PTL Dimethylamine Fumarate (**4.8**). To a stirred solution of **4.7** (0.009 g, 0.034 mmol) in MeOH (2 mL) was added dimethylamine (2.0 M in MeOH, 1.5 mL). The reaction was stirred for 12 h at RT. The reaction mixture was concentrated *in vacuo* purified by silica gel chromatography (gradient 0% - 50% EtOAc in hexanes over 10 min, then gradient 0%-25% MeOH in CH_2Cl_2 over 10 min) to yield the dimethylamino product as a white solid (0.009 g). To a stirred solution of this product in THF (5 mL) was added fumaric acid (0.0034 g, 0.029 mmol). A white precipitate was observed after stirring overnight at RT. The reaction mixture was concentrated *in vacuo* to give the fumarate salt **4.8** as white solid (0.0124 g, 85%). ^1H NMR ($\text{DMSO}-d_6$, 400 MHz): δ 6.61 (s, 2H), 4.09 (t, $J = 9.5$ Hz, 1H), 3.04 (d, $J = 9.2$ Hz, 1H), 2.64 (m, 3H), 2.24 (s, 6H), 2.14 (m, 2H), 2.05 (m, 1H), 1.78 (m, 2H), 1.59 (m, 1H), 1.31 (s, 3H), 1.19 (m, 2H), 1.02 (s, 3H), 0.74 (m, 2H), 0.28 (dd, $J = 3.8$ Hz, $J = 9.2$ Hz, 1H), -0.18 (t, $J = 4.8$ Hz, 1H). ^{13}C NMR ($\text{DMSO}-d_6$, 100 MHz): 176.6, 166.1, 134.1, 81.8, 64.3, 60.3, 57.2, 47.4, 45.6, 45.3, 41.7, 38.0, 24.2, 24.0, 21.6, 20.1, 18.4, 18.3, 16.7. HRMS (ESI^+) m/z calc'd for $[\text{C}_{18}\text{H}_{30}\text{NO}_3+\text{H}]^+$ 308.2226; found 308.2216.

4.10 Spectral Data

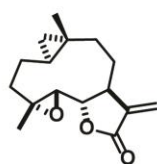
$^1\text{H NMR}$ (CDCl_3)



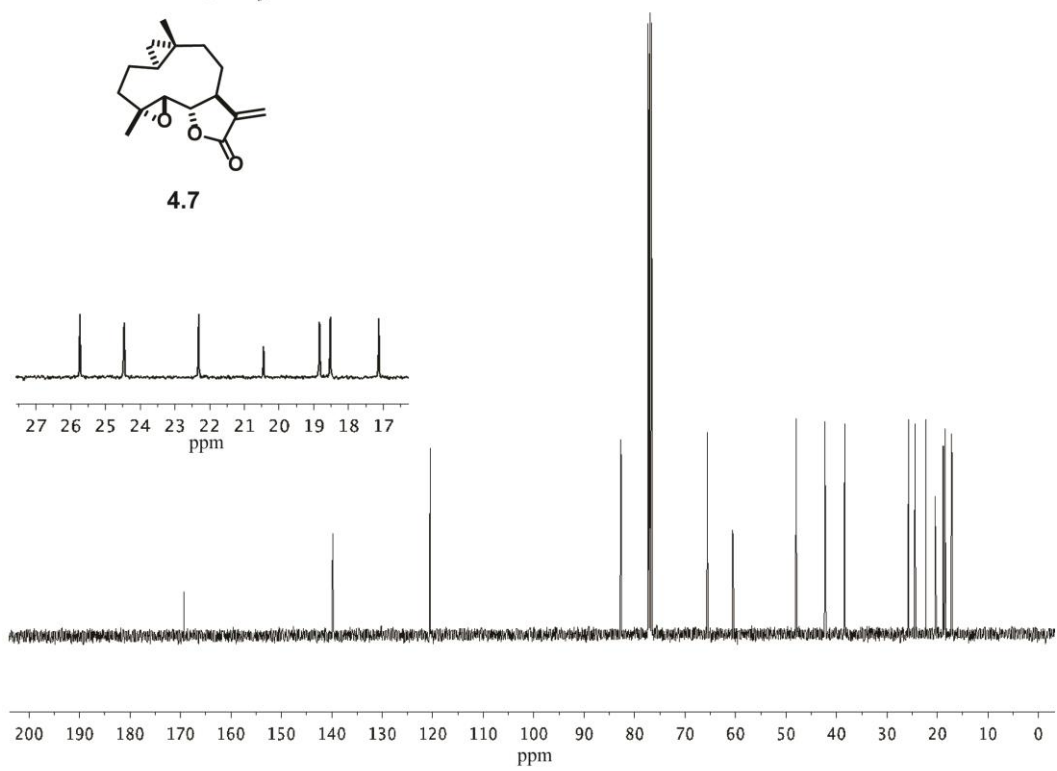
4.7

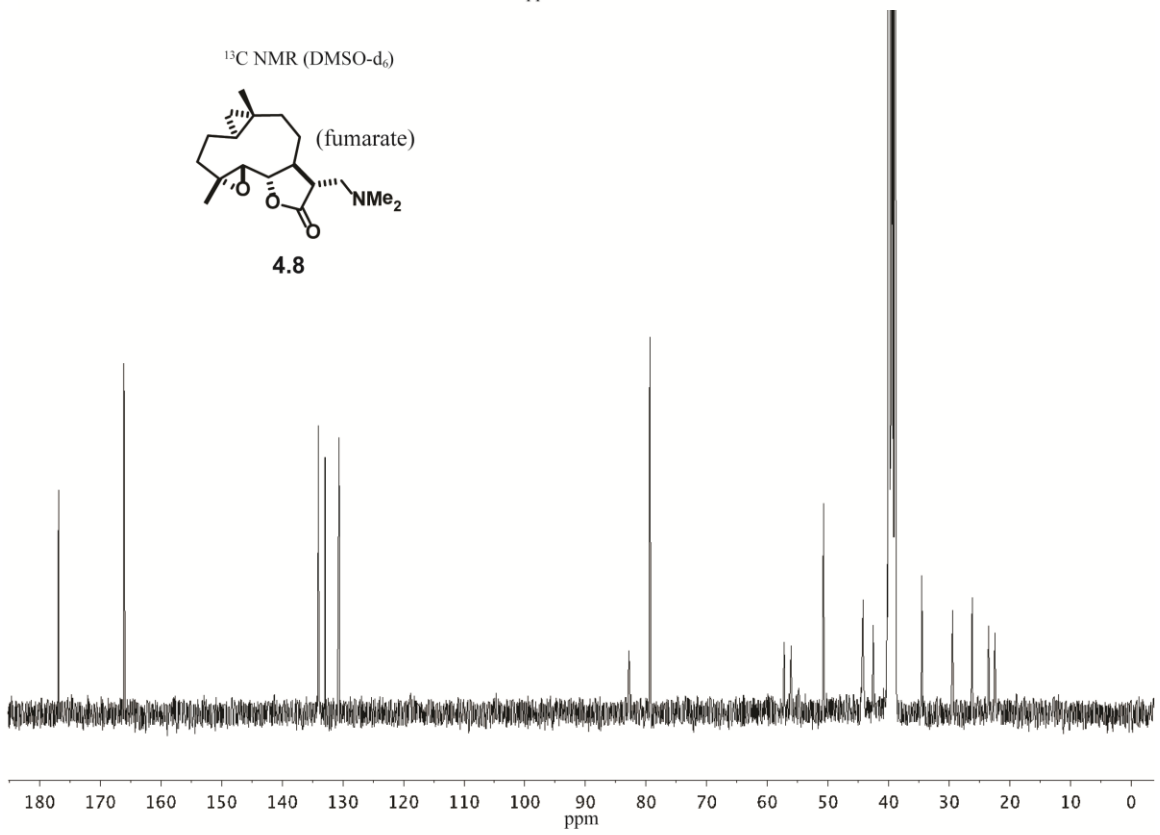
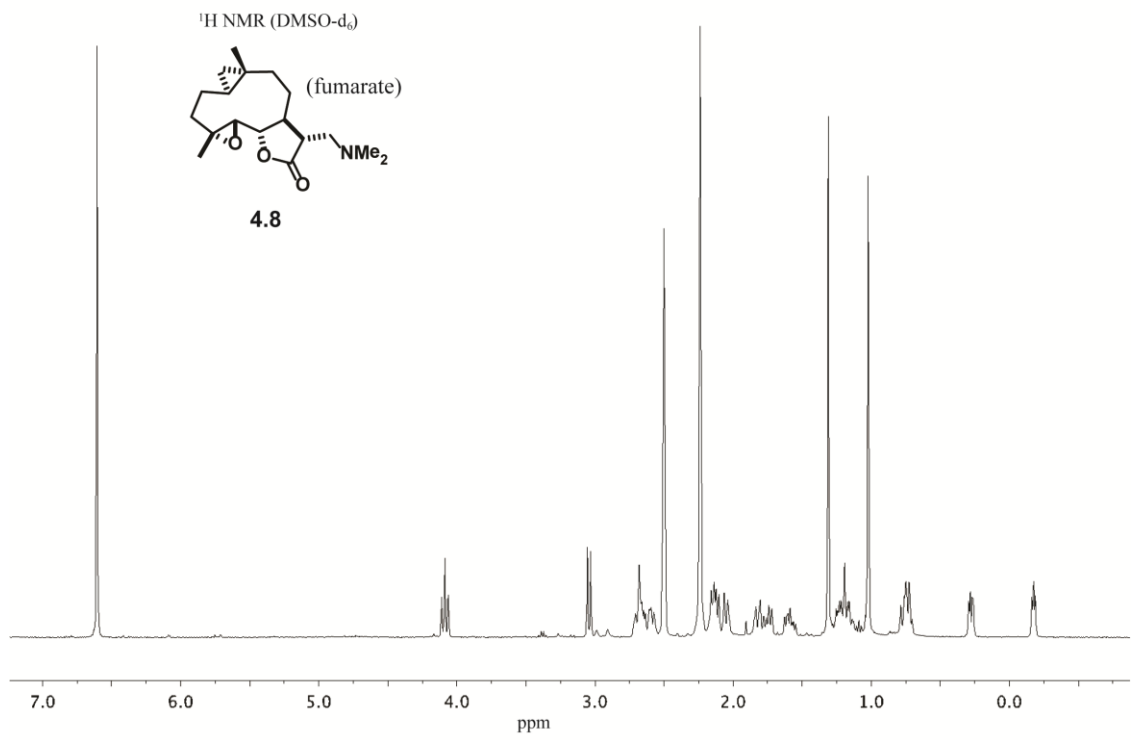


$^{13}\text{C NMR}$ (CDCl_3)

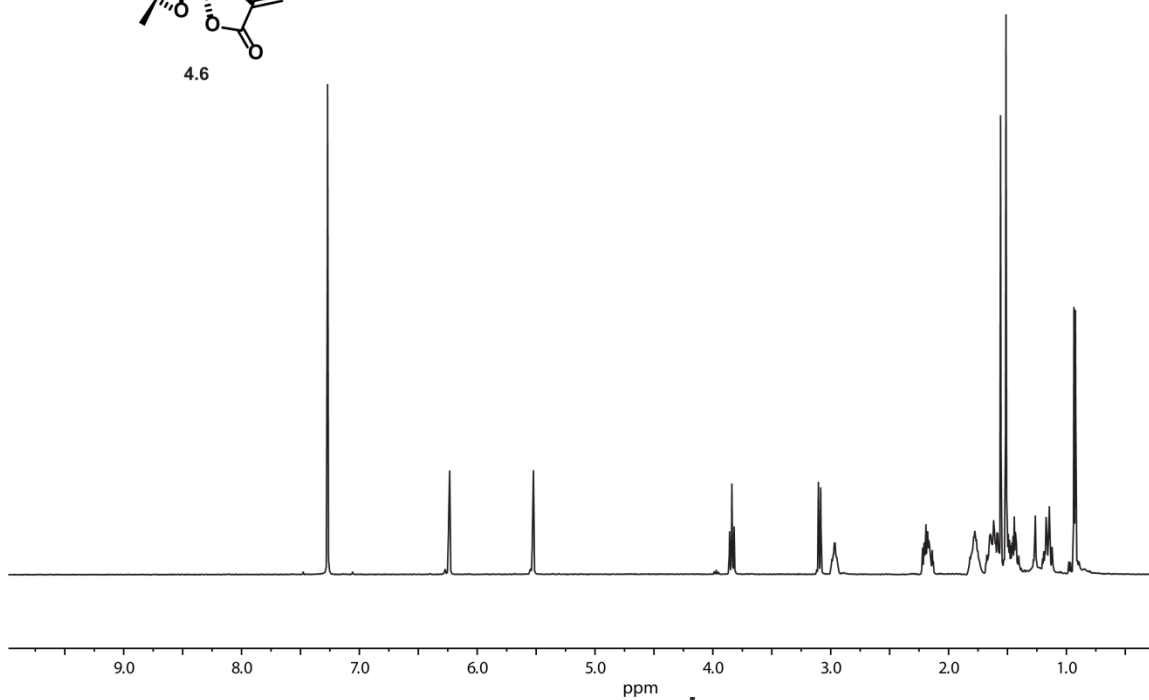
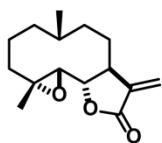


4.7

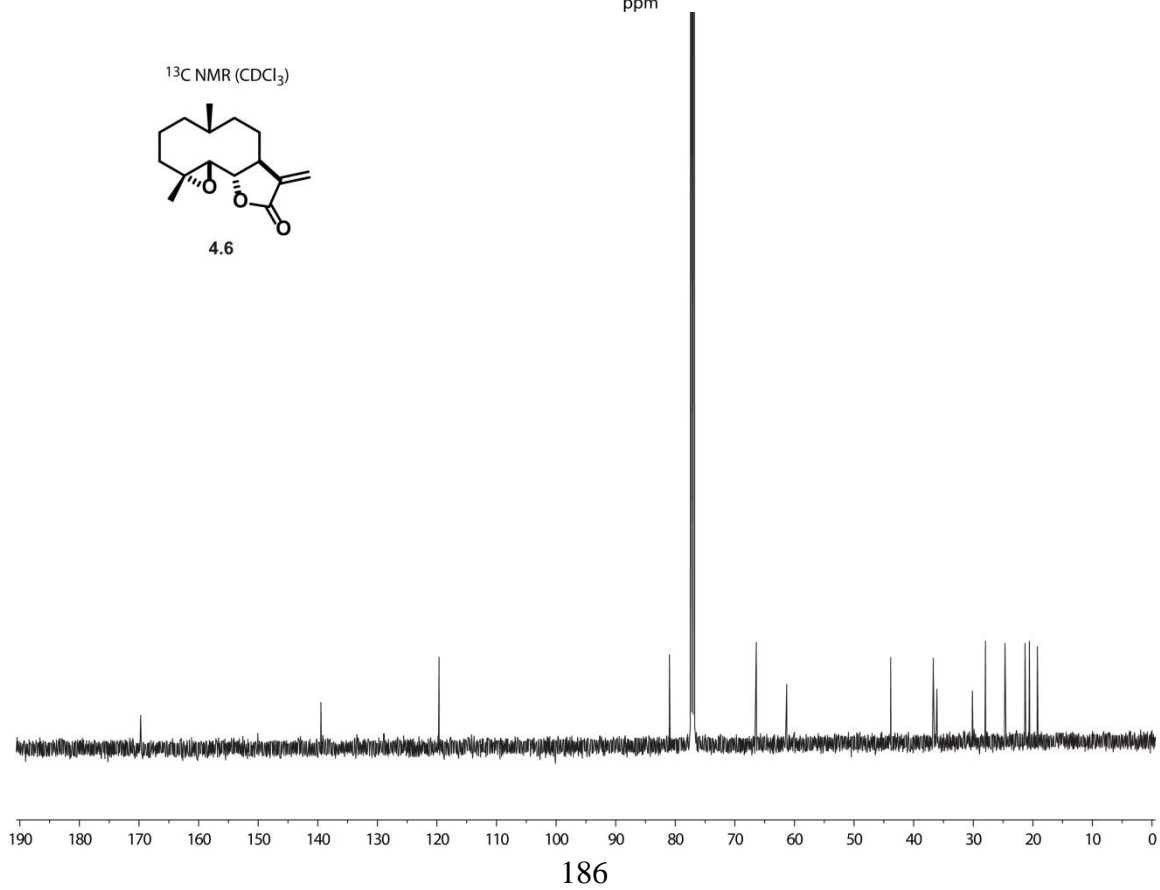
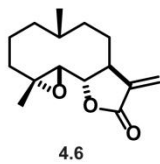




¹H NMR (CDCl₃)



¹³C NMR (CDCl₃)

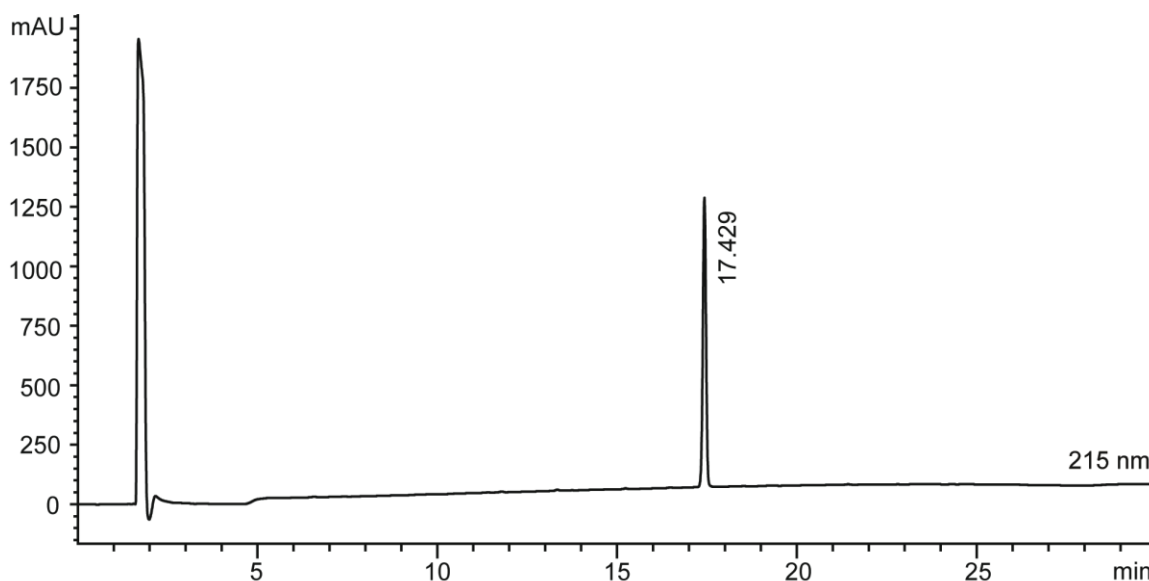


4.11 HPLC Chromatograms of Synthesized Compounds

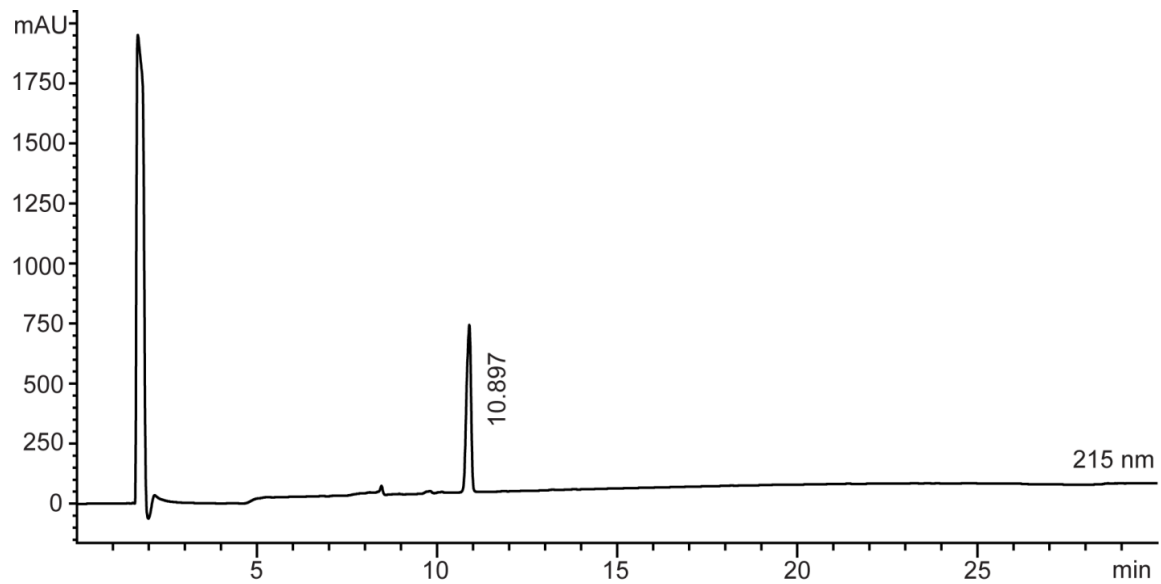
General Protocol for HPLC Analysis of Synthesized Compounds

DMSO stock solutions of newly synthesized molecules were dissolved in distilled and deionized water (ddH₂O) containing trifluoroacetic acid (TFA, 0.1% v/v) and analyzed on an Agilent 1200 series instrument equipped with a diode array detector and Zorbax SB-C18 column (4.6 x 150 mm, 3.5 μm, Agilent Technologies). The analysis method (1 mL/min flow rate) involved isocratic 10% MeCN in ddH₂O (both containing 0.1% TFA; 0 to 2 mins) followed by linear gradients of 10% to 85% MeCN in ddH₂O 2 to 24 mins followed by 85% to 95% MeCN in ddH₂O (both containing 0.1% TFA; 24 to 26 mins). Wavelengths monitored = 215 nm. HPLC chromatograms are not displayed for **DMAPT (LC-1, 4.2), 4.8 and 4.9** because of poor 215 nm absorbance.

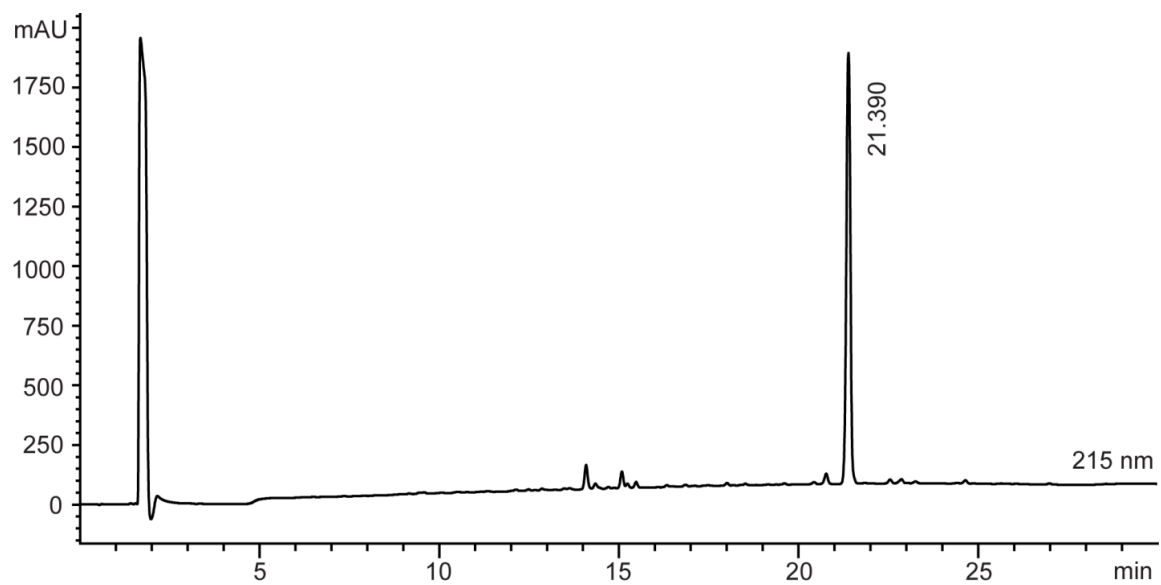
PTL (4.1) HPLC (>99% pure):



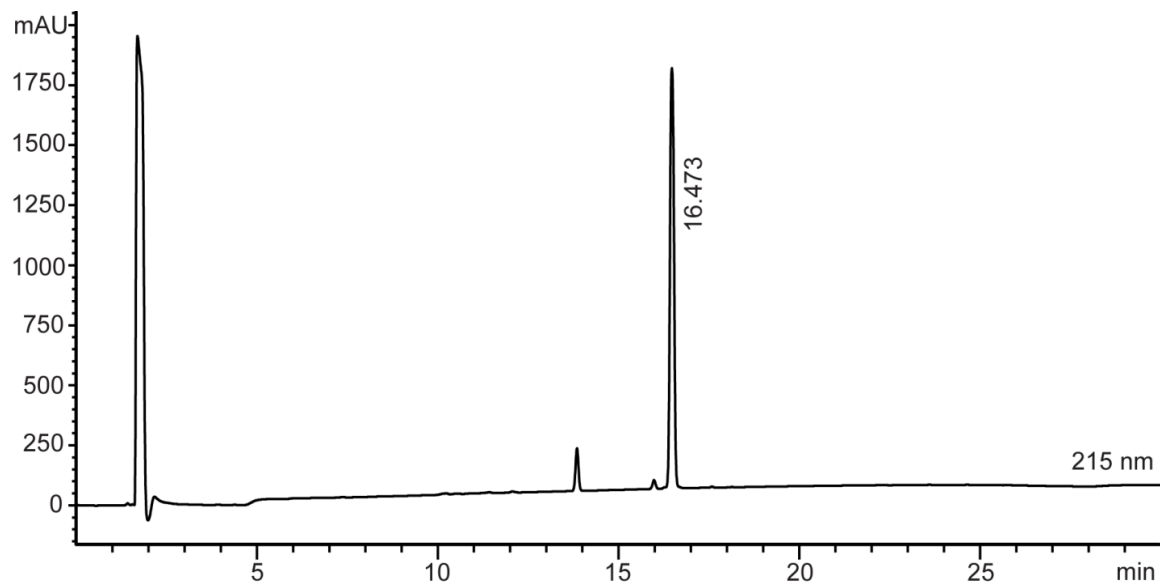
MelB (4.5) HPLC (97.7% pure):



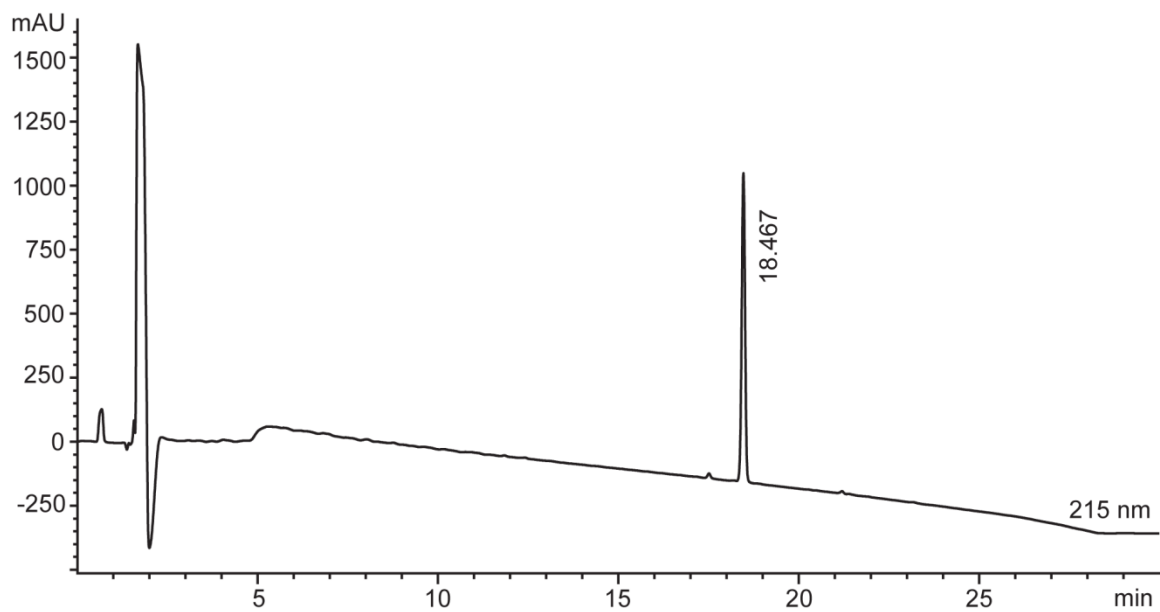
CTL (4.10) HPLC (96.7% pure):



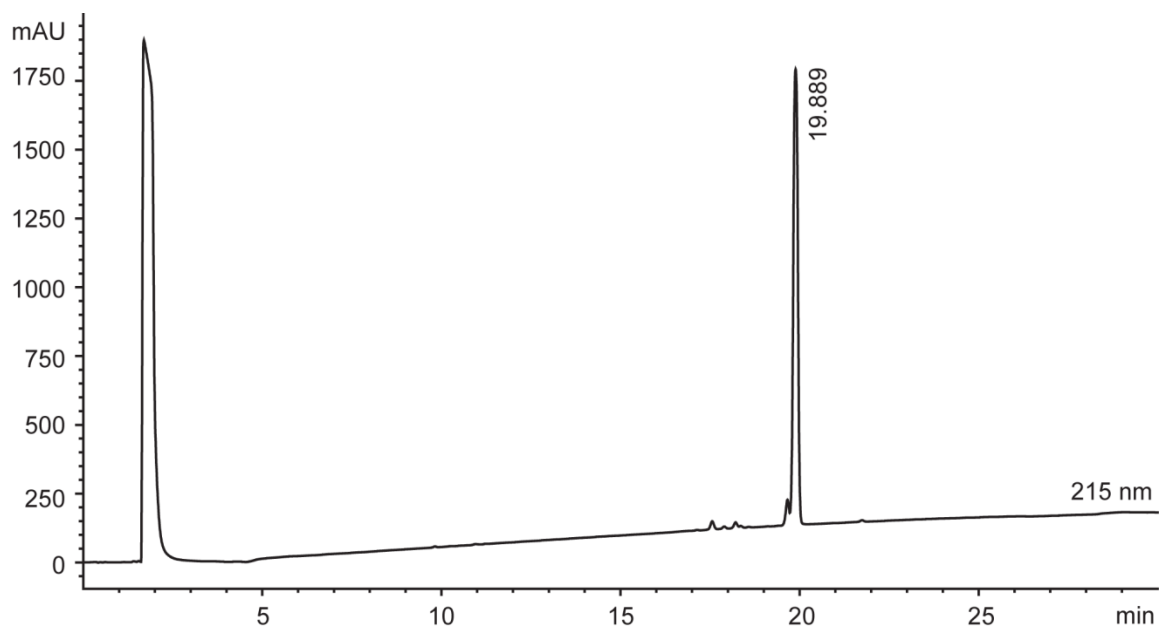
4.3 HPLC (94.5% pure):



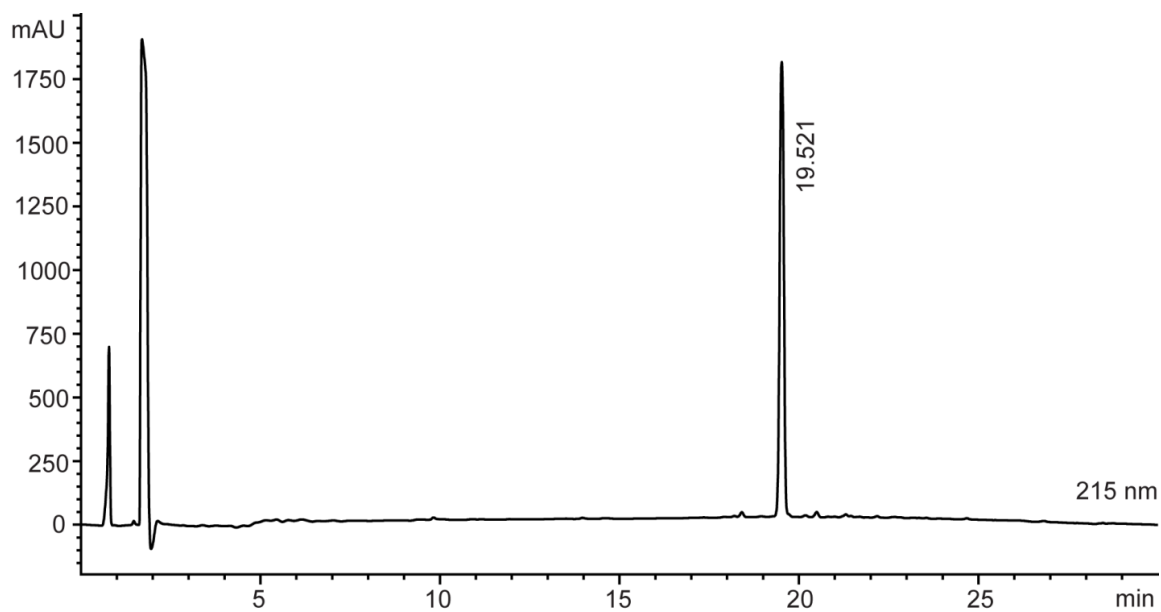
4.4 HPLC (97.9% pure):



4.6 HPLC (95.9% pure):

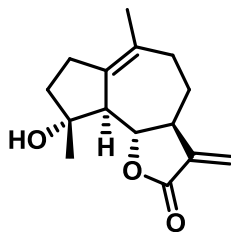


4.7 HPLC (97.5% pure):



4.12 Data and Analysis of X-ray Structures

X-ray Structure Information for Micheliolide (4.3)



Micheliolide (4.3)

Data collection

A crystal (approximate dimensions 0.50 x 0.08 x 0.04 mm³) was placed onto the tip of a 0.1 mm diameter glass capillary and mounted on a Bruker APEX-II CCD diffractometer for a data collection at 173(2) K.²²⁶ A preliminary set of cell constants was calculated from reflections harvested from four sets of 20 frames. These initial sets of frames were oriented such that orthogonal wedges of reciprocal space were surveyed. This produced initial orientation matrices determined from 755 reflections. The data collection was carried out using MoK α radiation (graphite monochromator) with a frame time of 120 seconds and a detector distance of 6.0 cm. A randomly oriented region of reciprocal space was surveyed to the extent of one sphere and to a resolution of 0.77 Å. Four major sections of frames were collected with 0.50° steps in ω at four different ϕ settings and a detector position of -28° in 2θ . The intensity data were corrected for absorption and decay (SADABS).²⁷³ Final cell constants were calculated from 2972 strong reflections from the actual data collection after integration (SAINT).²⁷⁴

Structure solution and refinement

The structure was solved using SHELXS-97 (Sheldrick, 2008/4) and refined using SHELXL-97 (Sheldrick, 2008/4).²²⁷ The space group C222₁ was determined based on systematic absences and intensity statistics. A direct-methods solution was calculated which provided most non-hydrogen atoms from the E-map. Full-matrix least squares / difference Fourier cycles were performed which located the remaining non-hydrogen

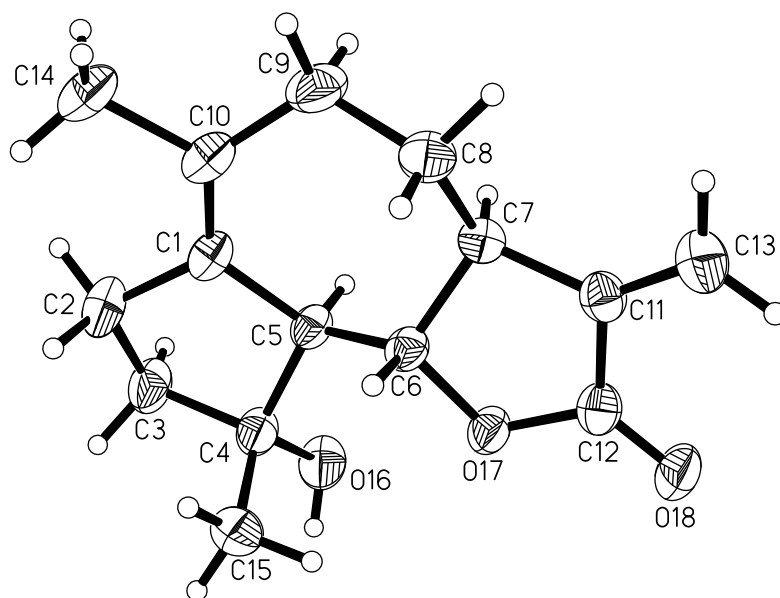
atoms. All non-hydrogen atoms were refined with anisotropic displacement parameters. All hydrogen atoms were placed in ideal positions and refined as riding atoms with relative isotropic displacement parameters. The final full matrix least squares refinement converged to $R1 = 0.0373$ and $wR2 = 0.1008$ (F^2 , all data).

Structure description

The structure is the one suggested. The data merged as though the structure was centrosymmetric since absolute configuration could not be determined experimentally for lack of a heavy atom. In the case the Flack parameter is meaningless and the enantiomer was chosen based on known chiral centers: these are C4-R, C5-S, C6-S, and C7-S.

Data collection and structure solution were conducted at the X-Ray Crystallographic Laboratory, 192 Kolthoff Hall, Department of Chemistry, University of Minnesota. All calculations were performed using Pentium computers using the current SHELXTL suite of programs. Additional crystallographic information, including the crystallographic information file (CIF), can be found in the supporting information of the original publication.²⁷⁵ This structure has also been deposited to the Cambridge Structural Database (CSD) under the Cambridge Crystallographic Database Center (CCDC) identifier: 1033012.

Thermal ellipsoid drawing of 4.3

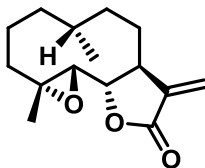


Crystallographic information for 4.3

Table 4.12.1. Crystal data and structure refinement for 4.3.

Identification code	11143a
Empirical formula	C ₁₅ H ₂₀ O ₃
Formula weight	248.31
Temperature	173(2) K
Wavelength	0.71073 Å
Crystal system	Orthorhombic
Space group	P222 ₁
Unit cell dimensions	$a = 7.4777(9)$ Å $\alpha = 90^\circ$ $b = 15.4839(18)$ Å $\beta = 90^\circ$ $c = 22.319(3)$ Å $\gamma = 90^\circ$
Volume	2584.2(5) Å ³
Z	8
Density (calculated)	1.276 Mg/m ³
Absorption coefficient	0.087 mm ⁻¹
$F(000)$	1072
Crystal color, morphology	Colorless, Needle
Crystal size	0.50 x 0.08 x 0.04 mm ³
Theta range for data collection	2.63 to 27.52°
Index ranges	$0 \leq h \leq 9, 0 \leq k \leq 19, 0 \leq l \leq 29$
Reflections collected	7790
Independent reflections	1458 [$R(\text{int}) = 0.0779$]
Observed reflections	1475
Completeness to theta = 27.52°	99.6%
Absorption correction	Multi-scan
Max. and min. transmission	0.9965 and 0.9576
Refinement method	Full-matrix least-squares on F^2
Data / restraints / parameters	1686 / 0 / 166
Goodness-of-fit on F^2	1.042
Final R indices [$I > 2\sigma(I)$]	$R1 = 0.0373, wR2 = 0.0958$

X-ray Structure Information for 4.6



4.6

Data collection

A crystal (approximate dimensions 0.45x 0.45 x 0.05mm³) was placed onto the tip of a 0.1 mm diameter glass capillary and mounted on a CCD area detector diffractometer for a data collection at 123(2) K.²⁷⁶ A preliminary set of cell constants was calculated from reflections harvested from four sets of 30 frames. These initial sets of frames were oriented such that orthogonal wedges of reciprocal space were surveyed. This produced initial orientation matrices determined from 109 reflections. The data collection was carried out using MoK α radiation (graphite monochromator) with a frame time of 90 seconds and a detector distance of 4.8 cm. A randomly oriented region of reciprocal space was surveyed to the extent of one sphere and to a resolution of 0.84 Å. Four major sections of frames were collected with 0.30° steps in ω at four different ϕ settings and a detector position of -28° in 2θ . The intensity data were corrected for absorption and decay (SADABS).²⁷³ Final cell constants were calculated from 2976 strong reflections from the actual data collection after integration (SAINT).²²⁸

Structure solution and refinement

The structure was solved using Bruker SHELXTL and refined using Bruker SHELXTL.²⁷⁷ The space group P2₁2₁2₁ was determined based on systematic absences and intensity statistics. A direct-methods solution was calculated which provided most non-hydrogen atoms from the E-map. Full-matrix least squares / difference Fourier cycles were performed which located the remaining non-hydrogen atoms. All non-hydrogen atoms were refined with anisotropic displacement parameters. All hydrogen atoms were placed in ideal positions and refined as riding atoms with relative isotropic displacement

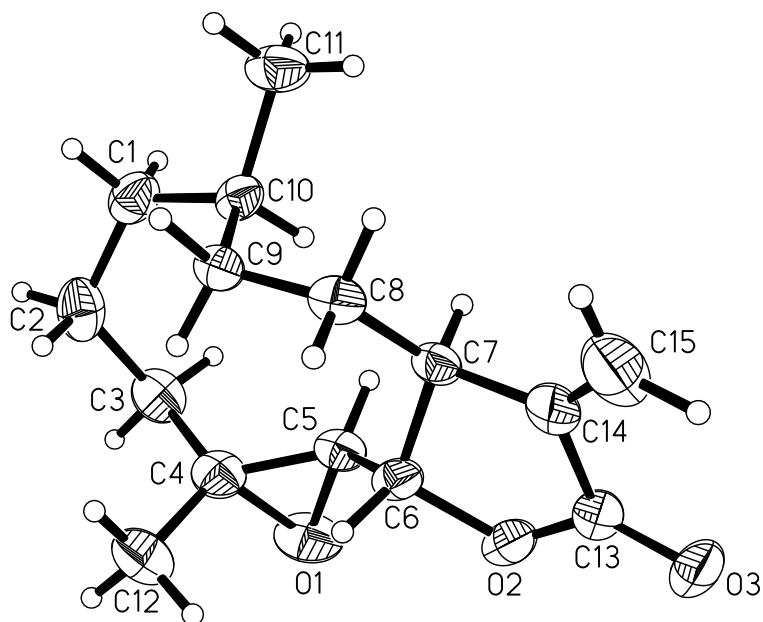
parameters. The final full matrix least squares refinement converged to $R1 = 0.0668$ and $wR2 = 0.1839$ (F^2 , all data).

Structure description

The structure is the one suggested. The chiralities of the following atoms are: C4-R, C5-R, C6-S, C7-S, and C10-R. While there is no question about the accuracy of the structure, the very thin specimen provided only data of moderate quality. The correct enantiomer was set by known chiral centers. The data were merged as though the data were centrosymmetric according to IUCr guidelines. The Flack X parameter is understood to be meaningless in this situation.

Data collection and structure solution were conducted at the X-Ray Crystallographic Laboratory, 192 Kolthoff Hall, Department of Chemistry, University of Minnesota. All calculations were performed using Pentium computers using the current SHELXTL suite of programs. Additional crystallographic information, including the CIF, can be found in the supporting information of the original publication.²⁷⁵ This structure has also been deposited to the CSD under the CCDC identifier: 1033013.

Thermal Ellipsoid Drawing of 4.6

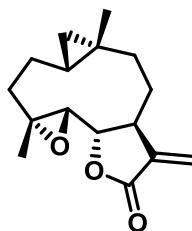


Crystallographic information for 4.6

Table 4.12.2. Crystal data and structure refinement for 4.6.

Identification code	10067a	
Empirical formula	C ₁₅ H ₂₂ O ₃	
Formula weight	250.33	
Temperature	123(2) K	
Wavelength	0.71073 Å	
Crystal system	Orthorhombic	
Space group	P2 ₁ 2 ₁ 2 ₁	
Unit cell dimensions	$a = 6.3639(19)$ Å	$\alpha = 90^\circ$
	$b = 7.595(2)$ Å	$\beta = 90^\circ$
	$c = 28.621(8)$ Å	$\gamma = 90^\circ$
Volume	1383.3(7) Å ³	
Z	4	
Density (calculated)	1.202 Mg/m ³	
Absorption coefficient	0.082 mm ⁻¹	
$F(000)$	544	
Crystal color, morphology	Colorless, Plate	
Crystal size	0.45 x 0.45 x 0.05 mm ³	
Theta range for data collection	1.42 to 25.07°	
Index ranges	$0 \leq h \leq 7, 0 \leq k \leq 9, 0 \leq l \leq 34$	
Reflections collected	7790	
Independent reflections	1458 [$R(\text{int}) = 0.0779$]	
Observed reflections	1195	
Completeness to theta = 25.07°	99.7%	
Absorption correction	Multi-scan	
Max. and min. transmission	0.9959 and 0.9640	
Refinement method	Full-matrix least-squares on F^2	
Data / restraints / parameters	1458 / 0 / 165	
Goodness-of-fit on F^2	1.195	
Final R indices [$I > 2\sigma(I)$]	$R1 = 0.0668, wR2 = 0.1777$	
R indices (all data)	$R1 = 0.0807, wR2 = 0.1839$	
Absolute structure parameter	-4(4)	
Largest diff. peak and hole	0.301 and -0.286 e.Å ⁻³	

X-ray Structure Information for 4.7



4.7

Data collection

A crystal (approximate dimensions 0.45x 0.40 x 0.05mm³) was placed onto the tip of a 0.1 mm diameter glass capillary and mounted on a CCD area detector diffractometer for a data collection at 123(2) K.²⁷⁶ A preliminary set of cell constants was calculated from reflections harvested from three sets of 20 frames. These initial sets of frames were oriented such that orthogonal wedges of reciprocal space were surveyed. This produced initial orientation matrices determined from 61 reflections. The data collection was carried out using MoK α radiation (graphite monochromator) with a frame time of 60 seconds and a detector distance of 4.8 cm. A randomly oriented region of reciprocal space was surveyed to the extent of one sphere and to a resolution of 0.77 Å. Four major sections of frames were collected with 0.30° steps in ω at four different ϕ settings and a detector position of -28° in 2θ . The intensity data were corrected for absorption and decay (SADABS).²⁷³ Final cell constants were calculated from 2944 strong reflections from the actual data collection after integration (SAINT).²⁷⁸

Structure solution and refinement

The structure was solved using Bruker SHELXTL and refined using Bruker SHELXTL.²⁷⁷ The space group P2₁ was determined based on systematic absences and intensity statistics. A direct-methods solution was calculated which provided most non-hydrogen atoms from the E-map. Full-matrix least squares / difference Fourier cycles were performed which located the remaining non-hydrogen atoms. All non-hydrogen atoms were refined with anisotropic displacement parameters. All hydrogen atoms were

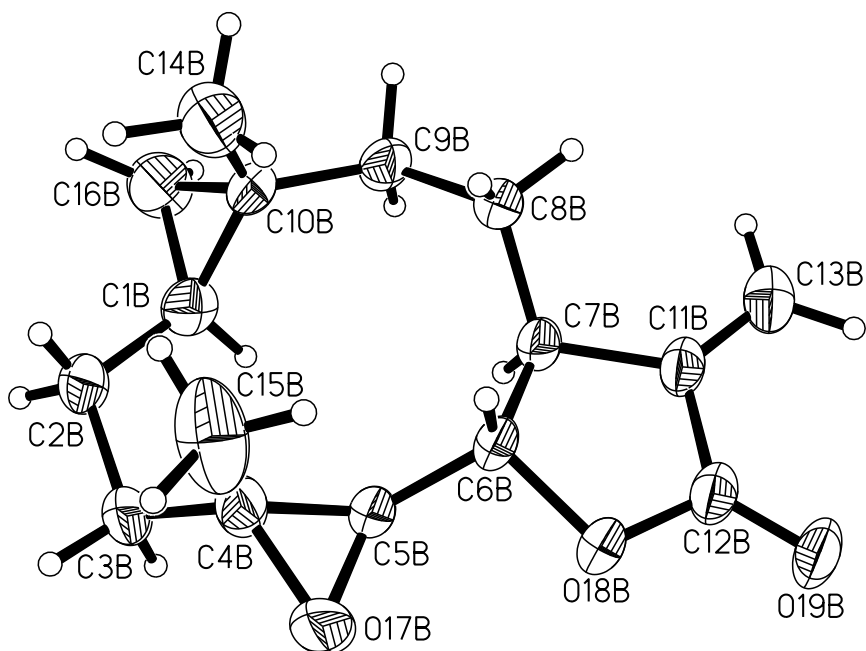
placed in ideal positions and refined as riding atoms with relative isotropic displacement parameters. The final full matrix least squares refinement converged to $R1 = 0.0496$ and $wR2 = 0.1335$ (F^2 , all data).

Structure description

The structure is the one suggested. There are two identical, unique molecules per asymmetric unit with $Z' = 2$. The chirality is as follows: C4-R, C5-R, C6-S, and C7-S. The CheckCIF program made no assignment at C1 due to its geometry. There is only slight pseudo-symmetry between the two unique molecules resulting in a pseudo 2_1 relationship along an irrational axis in the monoclinic setting.

Data collection and structure solution were conducted at the X-Ray Crystallographic Laboratory, 192 Kolthoff Hall, Department of Chemistry, University of Minnesota. All calculations were performed using Pentium computers using the current SHELXTL suite of programs. Additional crystallographic information, including the CIF, can be found in the supporting information of the original publication.²⁷⁵ This structure has also been deposited to the CSD under the CCDC identifier: 1033014.

Thermal Ellipsoid Drawing of 4.7



Crystallographic information for 4.7

Table 4.12.3. Crystal data and structure refinement for 4.7.

Identification code	10191a	
Empirical formula	C ₁₆ H ₂₂ O ₃	
Formula weight	262.34	
Temperature	123(2) K	
Wavelength	0.71073 Å	
Crystal system	Monoclinic	
Space group	P2 ₁	
Unit cell dimensions	$a = 11.106(2)$ Å	$\alpha = 90^\circ$
	$b = 7.9397(16)$ Å	$\beta = 104.024(2)^\circ$
	$c = 16.668(3)$ Å	$\gamma = 90^\circ$
Volume	1426.0(5) Å ³	
Z	4	
Density (calculated)	1.222 Mg/m ³	
Absorption coefficient	0.083 mm ⁻¹	
$F(000)$	568	
Crystal color, morphology	Colorless, Plate	
Crystal size	0.45 x 0.40 x 0.05 mm ³	
Theta range for data collection	1.26 to 27.47°	
Index ranges	$-14 \leq h \leq 13, 0 \leq k \leq 10, 0 \leq l \leq 21$	
Reflections collected	12785	
Independent reflections	3465 [$R(\text{int}) = 0.0291$]	
Observed reflections	3001	
Completeness to theta = 27.47°	98.9%	
Absorption correction	Multi-scan	
Max. and min. transmission	0.9959 and 0.9637	
Refinement method	Full-matrix least-squares on F^2	
Data / restraints / parameters	3465 / 1 / 347	
Goodness-of-fit on F^2	1.046	
Final R indices [$I > 2\sigma(I)$]	$R1 = 0.0496, wR2 = 0.1256$	
R indices (all data)	$R1 = 0.0599, wR2 = 0.1335$	
Absolute structure parameter	0.1(15)	
Largest diff. peak and hole	0.621 and -0.368 e.Å ⁻³	

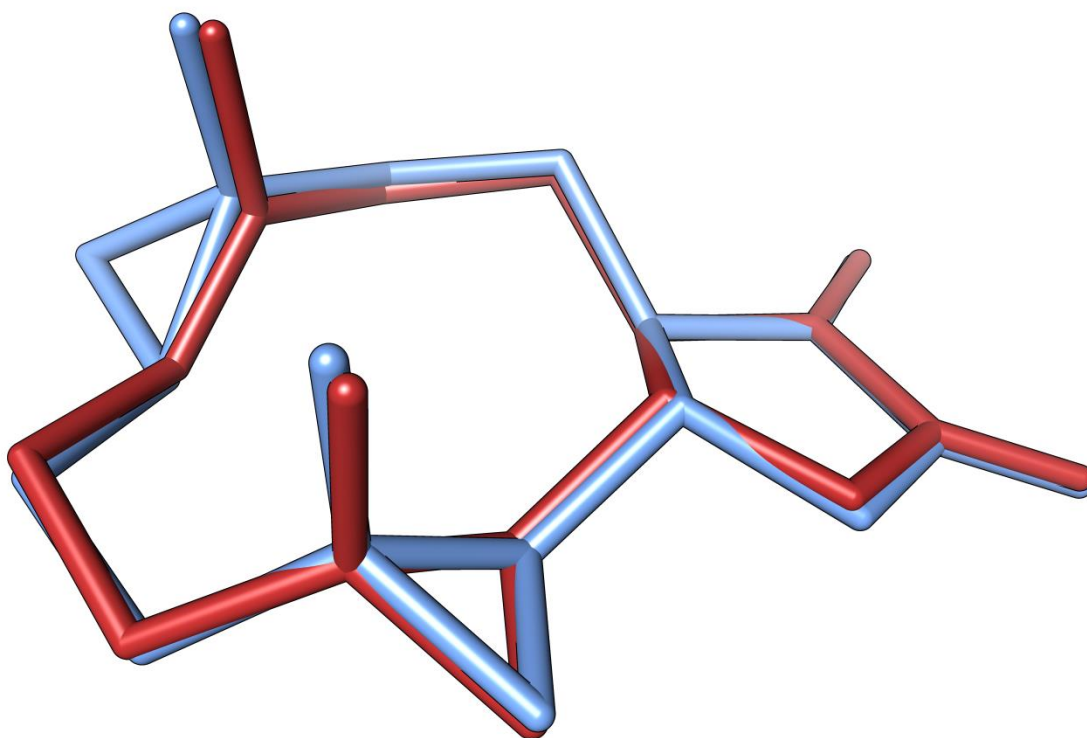


Figure 4.12.1. Alignment of the x-ray structures of **PTL (4.1)**, red²⁵⁵ and **4.7** (blue) using UCSF Chimera. Root-mean-square deviation was 0.167 Å (all non-hydrogen atoms). The X-ray structures of **4.7** and **PTL (4.1)** were analyzed for root-mean-square deviation (RMSD) and graphics were rendered using UCSF Chimera.²⁷⁹ Thermal ellipsoids were drawn at the 50% probability level. RMSD was calculated for all non-hydrogen atoms.

4.13 Acknowledgments

We thank Ezra Menon and Margaret Olson (University of Minnesota, UMN) for assistance with anti-proliferative activity experiments and Victor G. Young, Jr. of the Department of Chemistry, X-Ray Crystallographic Laboratory (UMN) for solving the X-ray structures of **4.3**, **4.6**, and **4.7**. We thank Professor Michael Verneris (UMN) for assistance with flow cytometry analysis and NIH P30 CA77598, which supports the Flow Cytometry shared resource of the Masonic Cancer Center (UMN). Professor John Dick (University of Toronto) is gratefully acknowledged for the gift of the TEX cell line. GBM6 cells were a gift from the late Professor John Ohlfest (UMN). This research was supported by grants from the UMN, Academic Health Center (Seed Grant 2010.01); UMN, Leukemia Research Fund – Danny Thompson Memorial Golf Tournament; Children’s Cancer Research Fund, Minneapolis, MN; American Cancer Society (IRG-58-001-52-IRG68); Hyundai Hope on Wheels, Hope Grant Award; The V Foundation for Cancer Research, V Scholar Award to D.A.H.; and startup funds to D.A.H. from the UMN. J.C.W. thanks the UMN, College of Pharmacy for a Bighley Graduate Fellowship. D.W. acknowledges the American Heart Association for a predoctoral fellowship (11PRE7240035).

Chapter 5

IDENTIFICATION OF PUTATIVE PARTHENOLIDE PROTEIN TARGETS IN ACUTE MYELOID LEUKEMIA CELLS

This work was performed in collaboration with Dr. Dan Wang, Dr. Morito Kurata, Professor David A. Largaespada, and Professor Daniel A. Harki. Dan Wang completed the synthesis of parthenolide-based probes **5.3** and **5.4**, growth inhibition assays in HL-60 cells, and assisted with method development for pulldown of the putative targets of the parthenolide-based probes. The pulldown method reported in this chapter was based on a previously developed method published in Dan Wang's M.S. thesis.²⁸⁰ Morito Kurata assisted with the CRISPR/Cas9 studies described in **Section 5.6**.

5.1 Introduction

Leukemia stem cells (LSCs) have been characterized as a sub-population of cells within the tumor hierarchy that have quiescent, self-renewing, and drug resistant properties.²⁸¹ Using fluorescence activated cell sorting (FACS) of cells labeled with fluorescent antibodies it was discovered that normal hematopoietic stem cells and LSCs have a combination of cell surface markers that allowed for identification and enrichment from healthy bone marrow and bulk cancer cells.^{242a, 282} Clonal in vivo repopulation assays were developed to show that CD34⁺CD38⁻ cells could give rise to growth and maintenance of a new tumor when serially transplanted into non-obese diabetic/severe combined immunodeficiency disease (NOD/SCID) mice.²⁸³ Similar studies showed that CD34⁺CD38⁺ cells also have the ability to maintain tumor growth and stem cell properties in over half of the leukemic samples injected into mice.²⁸⁴

The current standard of care for acute myeloid leukemia (AML) has not changed considerably in the past four decades and consists of taking two chemotherapeutic agents over the course of ten days: a DNA intercalator/topoisomerase inhibitor (daunorubicin or idarubicin) and a DNA synthesis inhibitor, cytarabine (Ara-c).²⁸⁵ In younger patients, bone marrow transplants can be successful in preventing relapse after chemotherapy due to the immunologic antileukemic graft-versus-leukemia effect,²⁸⁶ which is currently not a well understood process. However, the more common population that is diagnosed with AML (average age at diagnoses is 65) are typically not bone marrow transplant candidates due to their advanced age.²⁸⁷ The standard chemotherapeutics for AML therapy work well at eradicating the majority of the tumor and cause complete remission in most patients under the age of 60, but after remission is achieved, relapse typically occurs within 1-3 years.²⁸⁸ Relapse has been contributed to the LSC population that is able to avoid eradication by therapeutic treatments, which target rapidly dividing cells, by becoming dormant, gaining further mutations, and changing protein expression and pathway activation.^{281a} The ability of LSCs to avoid chemotherapy makes it difficult to design therapeutics that eliminate the LSC population, and currently no FDA approved drugs or clinical trial candidates have been shown to do so.²⁸⁵

Few small molecules exist that have been found to eradicate LSCs. This may be due to the lack of understanding of the cellular pathways and gene products that are required for cancer stem cell maintenance and survival. However, a sesquiterpene lactone natural product isolated from the plant *Tanacetum parthenium*, parthenolide (**PTL**, **5.1**) and other similar analogues have been shown to eradicate LSCs while being non-cytotoxic to normal bone marrow cells.^{153, 241, 262b, 275} **PTL** contains an α -methylene- γ -lactone, which undergoes hetero-Michael addition with solvent exposed cysteines within a cell and is responsible for much of its biological activity. When the α -methylene is reduced to a methyl group, anti-proliferative activity is lost.^{246b, 247b, 247e, 250a, 289} Because α -methylene- γ -butyrolactones are very reactive towards cysteines, many targets have been identified related to its biological activity including IKK β ^{250a} and p65²⁹⁰ of the NF- κ B pathway, as well as proteins related to oxidative stress.²⁵²ⁱ Yet, all of these protein targets identified have not been definitively linked to LSC survival and fitness. Furthermore, the **PTL**-based probe used in previous target identification studies includes a large linker attached to a biotin, which can change biological function and reactivity due to its size and hydrophobicity compared to the small parent compound.²⁹¹

The objective of this study is to synthesize a minimalistic **PTL**-based probe containing a terminal alkyne to avoid off-target effects from adding large molecules (e.g., dyes or biotin) to the parent compound that could affect its original biological activity. Conducting target identification studies in primary human AML cells containing a large population of CD34⁺ cells with the **PTL**-based probes will enable the identification of putative protein targets that are important to LSC survival. Identifying proteins responsible for LSC maintenance and survival would be beneficial toward the development of curative therapies for AML.

PTL is an ideal molecule to identify protein targets associated with LSC survival because it is known to target LSCs while sparing healthy bone marrow cells. Additionally, **PTL** has an irreversible covalent mechanism of action, allowing for covalent attachment to protein targets without the need for the incorporation of a light activated group, such as a benzophenone or diazirine for covalent protein engagement.²⁹² Attachment of a terminal alkyne via a small carbon linker enables the ligation of biotin

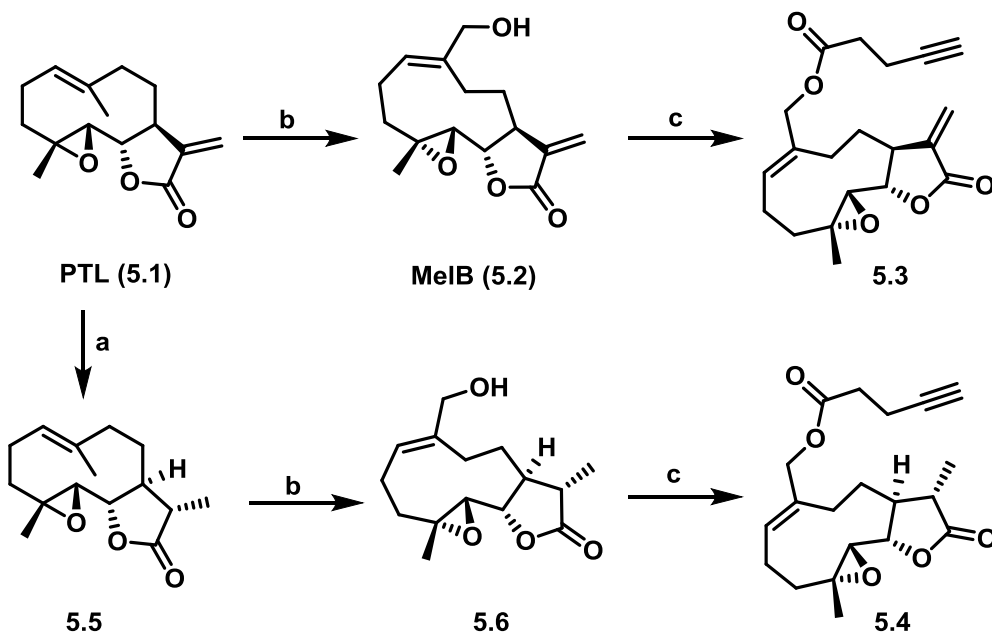
for enrichment after covalent bonds to target proteins are made using the copper-catalyzed [3+2] Huisgen reaction (click chemistry).²²⁰ The advent of click chemistry allows for the elimination of large, bulky linkers and the design of small molecules with little perturbation compared to the parent small molecule.

To design a minimalistic **PTL**-based probe for target identification studies, we took a semi-synthetic approach starting from the natural product itself. The alkyne was attached to the allylic hydroxyl group of Melampomagnolide B (**MelB**, **5.2**), which was synthesized by an allylic oxidation of **PTL**.²⁹³ We reduced the exocyclic methylene to a methyl group, which is responsible for **PTL**'s biological activity, to serve as a negative control for our target identification studies. This negative control can eliminate protein targets found that may have binding affinity to the non-functional probe but are not related to the parent compound's biological activity. By designing a functional and non-functional probe we sought to identify protein targets by dosing them to human primary AML cells and an LSC model cell line, TEX,²⁷² that contain a large population of CD34⁺ cells. After dosing our compounds we used monomeric avidin to enrich for proteins covalently modified by our probe, trypsin digested the enriched proteins, and used LC-MS/MS to identify putative protein targets. We prioritized the putative protein targets based on the frequency of identification in six replicates of the functional and negative control samples.

5.2 Semi-synthesis of **PTL**-based Functional and Non-functional Probes

The parthenolide-based functional alkyne probe **5.3** was synthesized in two steps and the non-functional probe **5.4** in three steps (**Scheme 5.2.1**) starting from **PTL**. A known allylic oxidation procedure was used to produce **MelB**.²⁹³ After installing the allylic hydroxyl group handle, 4-pentynoic acid was coupled with **MelB** using EDCI in the presence of 4-DMAP to produce **5.3** in 82% yield. The non-functional alkyne probe **5.4** was synthesized in a similar fashion. First, **PTL** was reduced with Pd/C and H₂.^{247e} The crude mixture from this reaction was taken on and subjected to the same allylic oxidation conditions as mentioned for the synthesis of **MelB** using selenium dioxide and *tert*-butylperoxide to produce **5.5** in 61% yield over two steps. Finally, 4-pentynoic acid

was coupled to **5.6** in the same fashion as **5.3** to obtain our desired non-functional alkyne probe **5.4** in 53% yield.



Scheme 5.2.1. Synthesis of functional and non-functional **PTL**-based alkyne probes.^a

^a**Reagents and Conditions:** (a) Ref. 246e, crude product taken on to next step; (b) Ref. 292, 74% for **MelB** (**5.2**), 61% (2 steps from **PTL**) for **5.6**; (c) (i) EDCI, 4-DMAP, DCM, 82% for **5.3**, 53% for **5.4**.

5.3 Cytotoxicity of Functional and Non-Functional Alkyne Probes in HL-60

As a model cancer cell line for AML we chose HL-60 to determine the cytotoxic effects of both synthesized alkyne probes (**Figure 5.3.1**). As expected, **5.3** maintains a low micromolar IC₅₀ value of $7.5 \pm 1.2 \mu\text{M}$ in a 48 h cytotoxicity assay compared to **5.4**, which has minimal cytotoxic effects below 500 μM . **PTL**, **MelB**, and other published **PTL** analogues maintain low micromolar IC₅₀ values similar to **5.3** in HL-60 cells demonstrating that the alkyne tag is not affecting the activity compared to the parent compound, **PTL**.²⁷⁵

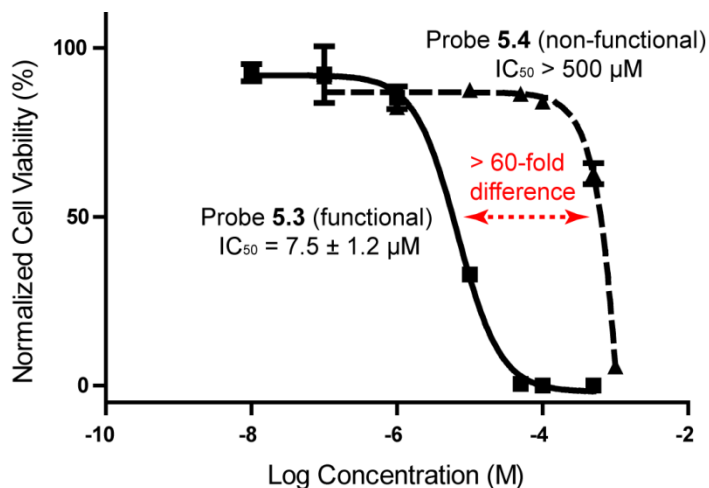


Figure 5.3.1. 48 h cytotoxicity dose response curves for probes **5.3** and **5.4** in HL-60 cells as a model AML cell line. **5.3** has similar activity to **PTL**, **MeIB**, and other **PTL**-based analogues.²⁷⁵ Probe **5.4**, which does not contain a Michael acceptor, is minimally cytotoxic below 500 μM . IC_{50} values are the average of $n \geq 3$ replicates \pm S.D. Solid line = curve fit for **5.3**, dashed line = curve fit for **5.4**.

5.4 Flow Cytometry Analysis of Primary AML Samples

Three separate primary human AML samples were chosen from the Leukemia MDS Tissue Bank at the University of Minnesota. Leukemic cells were isolated from each patient at the time of diagnosis (before treatment) and maintained in liquid nitrogen. FACS was used to determine the expression levels of the cell surface markers CD34 and CD38 for each patient sample (**Figure 5.4.1A**). Additionally, the CD34 and CD38 cell population in TEX cells was determined for comparison to the primary AML cells (**Figure 5.4.1B**). Cells with high expression levels of CD34 have previously been identified as an indication of LSCs;^{283a, 284} therefore, it is desirable to have a high CD34 population in the primary human leukemia samples for the identification of **PTL** probe protein targets that could be related to LSC survival. It has also been shown that cells with low CD38 expression levels also have LSC properties.^{283a} Prior to the pulldown experiments, the primary human leukemia samples were tested for their CD34 and CD38 expression levels to ensure that the samples contained an LSC population as a model system for identification of putative LSC-related protein targets.

The sample from **Patient 1** contained a 57% CD34⁺ cell population but only 6% of those were CD38⁻. **Patient 2** had a 52% CD34⁺ population and a 47% CD38⁻

population. **Patient 3** contained the largest CD34⁺ population at 88% but only 8% of those were CD38⁺. All three patients contained a majority of a CD34⁺ cell population while only **Patient 2** had a substantial CD34⁺CD38⁻ population. These results indicated that all three patient samples contain high levels of cells known to possibly confer LSCs for identification of **PTL** probe-protein targets that could be related to LSC survival. Three different patients were used for the target identification experiments to more broadly cover the proteome landscape as protein expression of leukemic cells in individual patients can be vastly different.²⁹⁴

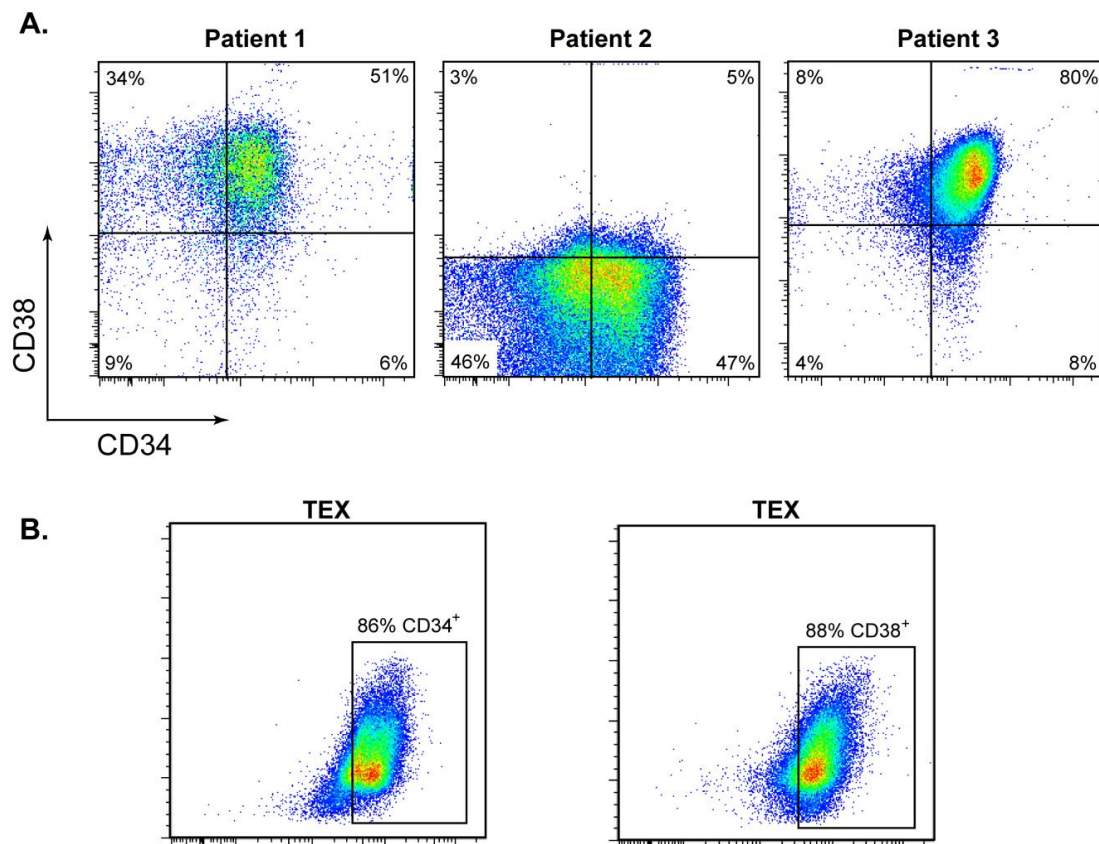


Figure 5.4.1. A. Human primary AML samples were characterized using Brilliant Violet 421 anti-CD34 and Allophycocyanin (APC) anti-CD38 cell surface markers and analyzed with FACS. All patients used in the pulldown studies had >50% CD34⁺ population while **Patient 2** had >46 % CD34⁺CD38⁻ population. Samples from **Patient 1** and **Patient 3** contained 6-8 % CD34⁺CD38⁻ population. **B.** TEX cells have been used as a model system for LSCs and were characterized in the same manner as primary human AML samples. 86% of TEX²⁷² cells have high expression of CD34 and 88% of cells have high expression of CD38, comparable to the three AML samples.

The TEX cell line is an engineered leukemia cell line derived from lineage depleted (lin⁻) human cord blood cells transduced with the fusion gene TLS-ERG that mimic the hierarchical growth properties of human primary AML cells.²⁷² TEX cells were determined to have a large CD34⁺ cell population (86%), similar to the three primary human AML samples tested (**Figure 5.4.1B**). A high CD38⁺ population was also found in the TEX cell line. Altogether, the TEX cells display similar CD34 and CD38 populations compared to the three primary human AML samples tested. Primary human AML cells typically are not able to be cultured for long periods of time, are limited in samples, and are highly variable between patients.²⁹⁴⁻²⁹⁵ As an alternative to primary human samples, it would be desirable to have a LSC cancer cell line model that would contain the same putative LSC target proteins as primary human cells for follow-up studies. Since the primary human AML cells and TEX cells have similar CD34 and CD38 expression levels and the TEX cell line has been demonstrated to have LSC properties, a pulldown experiment was also conducted in TEX cells for comparison to the primary human AML samples.

5.5 Pulldown in Primary AML Cells.

Four pulldown experiments were conducted in three different human primary AML samples (two pulldowns were done with two separate samples from **Patient 2**). Two additional pulldown experiments were done in TEX cells for comparison to the human primary AML samples. The functional probe **5.3** or the non-functional probe **5.4** was dosed to primary AML or TEX cells for two hours. The cells were lysed and then biotin-azide was attached to the probe-protein adducts using a copper-mediated Huisgen [3+2] cycloaddition (click chemistry).^{220, 296} The biotinylated probe-protein adducts were enriched using a monomeric avidin column. The enriched samples were then digested with trypsin and processed for proteomic analysis. All samples were analyzed with LC-MS/MS and putative protein targets were identified from peptide fragmentation data at the Taplin Mass Spectrometry Facility, Harvard School of Medicine (contracted work).

The overall number of proteins identified in each sample and patient information is in **Table 5.5.1**. In each case, the numbers of unique proteins identified were higher in

the functional samples versus the non-functional samples. The high number of protein hits from the non-functional sample can be attributed to non-specific binding of protein to the monomeric avidin column during probe-protein enrichment or binding to the non-functional probe **5.4**. The functional protein targets range was 776-1721 while the non-functional protein targets range was 94-1658. The number of identified protein targets is comparable between the primary human AML samples and TEX cells.

Table 5.5.1. Primary AML samples from three patients and TEX cells were used for pulldown and identification of target proteins using probes **5.3** (functional) and **5.4** (non-functional). All primary human samples were collected from patients at the time of diagnosis prior to therapy. Two separate samples were completed for **Patient 2** for a total of four independent pulldown experiments. The total number of proteins identified by at least two peptides is displayed for each replicate.

Patient	Functional (5.3) proteins identified	Non-functional (5.4) proteins identified	Cytogenetics	Blast (%)
1	1668	1658	Normal	87
2-1	1609	1577	Del(11)	88
2-2	807	569		
3	776	94	Normal	60
TEX	1721	485	-	-
TEX	1317	128	-	-

The goal of this pulldown study is to identify putative protein targets in AML cells that could be responsible for maintenance and survival of LSCs. Given the large number of putative targets identified in the functional probe samples, identified protein targets were categorized based on the frequency of the protein hit occurring in the functional samples versus the non-functional, negative control samples. Prioritization was given to samples that were not identified in any non-functional samples but identified in multiple functional samples. For instance, one high priority protein, bifunctional aminoacyl-tRNA synthetase (gene name: SYEP), was identified in all four functional samples and none of the non-functional negative controls. The number of proteins identified in each category can be seen in **Table 5.5.2**.

There were an additional ten protein targets identified in three of the four functional samples and not found in any of the non-functional samples. Other categories that include proteins that were also found in at least one non-functional sample have > 20

proteins for the primary human AML samples. Between the two pulldowns conducted in TEX cells, 176 protein targets were identified in both functional samples but not the non-functional samples. Notably, 21 proteins were identified in at least three functional primary human AML samples and one of the functional TEX samples, while two proteins were found in three functional primary human AML samples and both functional TEX samples.

Table 5.5.2. Identified protein targets were prioritized by comparing the proteins found in the functional pulldown with **5.3** to the pulldown with the negative control compound **5.4**. Protein targets identified in 3-4 functional pulldowns but not in any negative control pulldowns were considered to be high priority targets while proteins found in any negative control samples were low priority.

Primary AML	Number of proteins	TEX	Number of proteins
4 Functional/ 0 Non-Functional	1	2 Functional/0 Non-Functional	176
4 Functional/ 2 Non-Functional	25	2 Functional/ 1 Non-Functional	2
4 Functional/ 3 Non-Functional	62	1 Functional/ 0 Non-Functional	184
4 Functional/ 4 Non-Functional	25	Targets found in primary AML and TEX	Number of proteins
3 Functional/ 0 Non-Functional	10	3 Primary AML/1 TEX	21
3 Functional/ 1 Non-Functional	51	3 Primary AML/2 TEX	2
3 Functional/ 2 Non-Functional	222		
3 Functional/ 3 Non-Functional	122		
2 Functional/ 0 Non-Functional	60		

The eleven high priority protein targets identified in at least three functional AML samples but not in any of the non-functional samples are listed with the associated gene name and function in **Table 5.5.3**. The target genes were identified with a minimum of three unique peptides with a Z-score greater than 2.0, which considers the quality of the fragmentation data for each identified peptide. All of the high priority proteins contain at least one cysteine according to sequence data found in the Uniprot database. However, there is no information correlating covalent cysteine modification to inhibitory effects for

any of the 11 proteins. Many of the identified protein targets are not well characterized. None of the identified protein targets have been related to maintenance of LSCs to date, but several protein targets have been suggested to be important in cancer cell regulation.

Table 5.5.3. List of identified protein targets that were found in 3-4 functional samples and not any non-functional, negative control samples. Each gene name is associated with a function, Z-score, and unique peptides found. ^aIndicates protein identified in both functional TEX samples.

Gene Name	Function	Average Z-score	# of unique peptides
SYEP	glutamate and proline tRNA transferase	2.74	4
DDX46	ATP-dependent RNA helicase (probable)	2.77	3
DHB11	Hydroxysteroid (17- β) dehydrogenase 11	3.05	6
F120A ^a	Fam120A, Oxidative Stress-associated Src activator (OSSA)	3.01	4
FAS	Fatty acid synthase	3.21	3
HNRL1	Heterogeneous Nuclear Ribonucleoprotein U-like 1, basic transcriptional regulator, mRNA processing	3.12	3
MCM6 ^a	Minichromosome maintenance complex component 6, part of MCM complex for helicase activity	2.60	3
MTCH2	Mitochondria Carrier 2	2.58	3
MYADM	Myeloid-associated differentiation Marker	3.69	3
PSMD6	Regulatory proteasome subunit	2.85	4
SMHD1	Scaffolding protein for methylation of CpG islands of DNA	2.34	3

Several proteins that were identified are not likely to be good target proteins for inhibition of LSC survival, tumorigenesis, or cancer progression. The FAS gene encodes for fatty acid synthase, which is involved in catabolism of fatty acids.²⁹⁷ The HNRL1 gene encodes for heterogeneous nuclear ribonucleoprotein U-like protein 1, which is involved in general gene regulation and processing of mRNA.²⁹⁸ It was originally identified as a target of the early adenovirus E1B-55 kDa protein during infection.²⁹⁹ The MCM6 gene produces the protein minichromosome maintenance complex component 6, which is a part of the helicase complex during replicative DNA transcription.³⁰⁰ The MTCH2 gene encodes for mitochondrial carrier homolog 2, which is a mitochondria membrane-associated protein.³⁰¹ This protein has been found to positively affect

apoptosis by recruiting the pro-apoptotic regulator BH3-interacting domain (BID) death agonist.³⁰² MTCH2 has also been implicated in maintaining the normal hematopoietic stem cell population.³⁰³ The gene SMHD1 encodes for structural maintenance of chromosomes flexible hinge domain-containing protein 1. This protein is involved in silencing of the X chromosome in female development, and serves as a scaffolding protein for DNA methyl transferases (DMTs).³⁰⁴ The gene DDX46 encodes for ATP-dependent RNA helicase, which is involved in general processing of mRNA.³⁰⁵ Based on the known functions of these six proteins it is unlikely that they are involved in LSC survival or a driver of leukemia progression.

Shifting focus to the remaining five proteins, several have interesting functions. PSMD6 encodes for a regulatory subunit of the 26s proteasome, which is involved in processing and degradation of proteins within cells. Many inhibitors targeting the 26s proteasome have been discovered and some have been FDA approved for treatment of multiple myeloma (MM).³⁰⁶ Targeting the 26s proteasome has been found to be most efficacious for treatment of MM due to sensitivity to antigen processing.³⁰⁷ Patients with MM treated with a proteasome inhibitor eventually leads to drug resistance and relapse of the disease.³⁰⁸ This suggests that targeting the proteasome is not likely to be linked to cancer stem cell survival.

The SYEP gene encodes for a glutamate and proline tRNA transferase (glutamyl-prolyl-tRNA-synthetase, EPRS).³⁰⁹ This enzyme is part of the multisynthetase complex responsible for attaching amino acids to tRNA for protein synthesis. EPRS also has a separate function involving repressing the translation of mRNA involved in the pro-inflammatory response.³¹⁰ Interferon- γ (IFN- γ) has been shown to stimulate the dissociation of EPRS from the multisynthetase complex to form an IFN- γ -activated inhibitor of translation (GAIT) complex.³¹¹ The GAIT complex is responsible for inhibiting the translation of inflammatory response genes.³¹² The negative regulatory effect on the inflammation process makes this protein undesirable as an anti-cancer target.

The MYADM gene expresses myeloid-associated differentiation marker. As the name suggests, this protein is upregulated during myeloid-associated differentiation of

hematopoietic progenitor cells.³¹³ Although this protein may serve as a useful marker for differentiation in normal and leukemic cells, targeting this protein would not be beneficial in eradicating LSCs. The DHB11 gene encodes for estradiol 17- β -dehydrogenase 11, which is involved in androgen metabolism.³¹⁴ Its role in LSC survival is currently unclear.

The F120A gene encodes for constitutive coactivator or PPAR- γ -like protein 1, also known as oxidative stress-associate Src activation protein (OSSA). This protein was found in three of the four functional samples from primary human AML cells and both functional TEX samples, but not in any non-functional samples. The OSSA protein was first identified as an RNA binding protein and later was shown to play an important role in regulation of oxidative stress.³¹⁵ It has been demonstrated that OSSA binds directly to Src family kinases upon an increase in oxidative stress.³¹⁶ Activation of kinases including phosphatidylinositol-3 kinase (PI3K) activates cancer cell survival pathways. Regulation of oxidative stress has been shown to be a key regulator of LSC survival and maintenance.^{243b, 252d} Furthermore, it has been demonstrated that PTL and related analogues induce oxidative stress intracellularly.^{275, 317} The role of OSSA in the regulation of oxidative stress and cancer cell survival and the known effects of PTL and related compounds make OSSA an interesting protein target for further validation studies.

5.6 Progress toward Validation of F120A/OSSA as a Key Regulator of LSC Survival

Attempts to knockdown the F120A gene in TEX cells have been unsuccessful thus far. Transfection of plasmids containing the CRISPR/Cas9 system with several different guide-RNAs using electroporation or transfection reagents has not been able to modify the F120A gene.³¹⁸ Retroviral transduction of plasmids containing CRISPR/Cas9 was also unsuccessful.^{272, 319} The inability to transfect plasmids into TEX cells is most likely because of their small size and sensitivity to transfection reagents.

Due to the difficulty in transducing plasmids into TEX cells, attention was turned to HEK293 cells because of their propensity to accept foreign plasmids. Knockout of the F120A gene in HEK293 cells was demonstrated using the CRISPR/Cas9 system (**Figure**

5.6.1). Two guide-RNA constructs were chosen containing a PAM (Protospacer Adjacent Motif) sequence for directed gene modification (**Figure 5.6.1A**). Both plasmids were transduced into HEK293 cells and cells containing plasmid were selected with puromycin. After selection for cells containing the plasmid, doxycycline was used to induce the CRISPR/Cas9 system. The cells were tested for F120A protein via Western blot. The F120A gene was successfully knocked out in HEK293 cells by Western blotting for F120A compared to the parental control and a β -actin loading control (**Figure 5.6.1B**). Both guide-RNA sequences accomplished the knockout with and without doxycycline induction. Gene modification can occur without doxycyclin induction because of a baseline expression of the Cas9 protein with the guide-RNA sequence in some cell lines.

Next, a surveyor nuclease assay was conducted to validate that the CRISPR/Cas9 system made modifications to the F120A gene (**Figure 5.6.1C**).³²⁰ The surveyor nuclease assay uses an endonuclease derived from celery (Cel-I) that recognizes single base mismatches, small insertions, or deletions within DNA.³²¹ The CRISPR/Cas9 system makes modifications to the gene of interest that result in base pair mismatches or deletions that can be detected by the Cel-I endonuclease. After detection of the mismatched base pairs, the Cel-I enzyme cleaves the DNA. The DNA fragments resulting from the cleavage by Cel-I can be compared to the parent gene DNA to detect mutation sites. Mutations were detected in exon 2 of the F120A gene where the guide-RNAs were designed to modify the gene compared to the parental HEK293 cellular DNA (**Figure 5.6.1C**). The F120A gene was spliced in one site generating two DNA strands (indicated by arrows) compared to the single band corresponding to the unmodified F120A gene from parental HEK293 cells (identified by asterisks). This suggests both CRISPR/Cas9 systems modified the F120A gene, agreeing with the Western blot results.

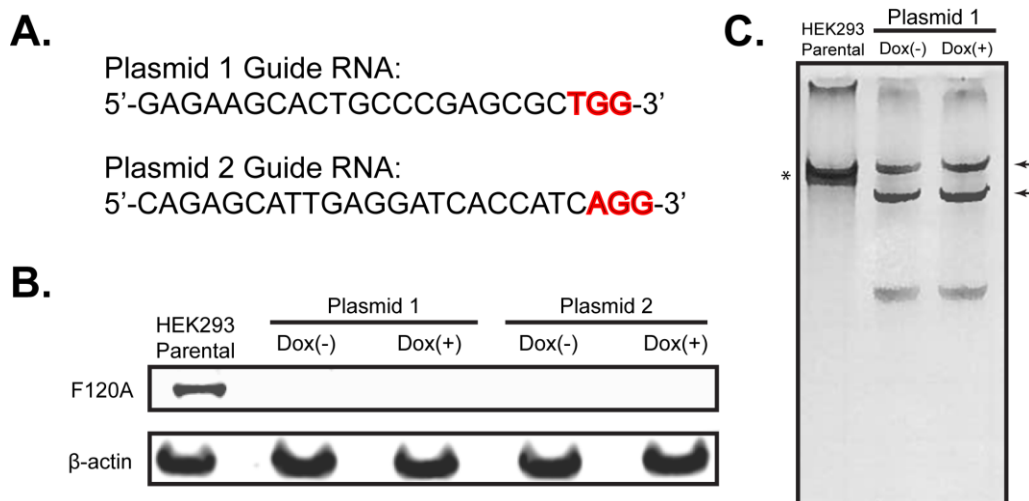


Figure 5.6.1. **A.** The sequences for both guide-RNAs are displayed with the PAM sequence highlighted in red. **B.** F120A was successfully knocked out in HEK293 using doxycycline inducible CRISPR/Cas9 plasmids containing two separate guide-RNA sequences. The knockout occurred successfully with and without doxycycline as seen in the Western blot compared to the parental HEK293 cell line. **C.** The surveyor nuclease assay shows that the CRISPR/Cas9 system was successfully expressed and made modifications to the cellular DNA within the F120A gene. The Cel-I endonuclease cleaved the F120A gene at the site of modification generating two strands of DNA compared to the single strand of DNA from the parental HEK293 cells. *Indicates the full length DNA of the unmodified F120A gene. Arrows indicate two DNA strands generated after cleavage by Cel-I.

5.7 Additional Identified Protein Targets from Pulldown Studies

Other proteins identified and categorized from the pulldown studies in primary human AML cells and TEX cells are listed below. Each identified putative target is categorized based on the frequency of identification in the functional and non-functional samples. These proteins may be relevant targets for LSC survival and maintenance but require further validation as potential PTL targets.

Proteins founds in 4 functional and 2 non-functional samples: APEX1_HUMAN, FKBP5_HUMAN, FUMH_HUMAN, H2B1B_HUMAN, HNRPF_HUMAN, HNRPL_HUMAN, HNRPQ_HUMAN, ILEU_HUMAN, IMMT_HUMAN, LMNA_HUMAN, MOES_HUMAN, NONO_HUMAN, NOP56_HUMAN, PERI_HUMAN, PGK1_HUMAN, PRDX6_HUMAN, PRKDC_HUMAN, PROF1_HUMAN, RL3_HUMAN, RS15A_HUMAN, RS3A_HUMAN, RS6_HUMAN, SF3B1_HUMAN, TERA_HUMAN, XRCC5_HUMAN

Proteins found in 4 functional and 3 non-functional samples: 1433Z_HUMAN,
LDHA_HUMAN, RS14_HUMAN, ANXA1_HUMAN, LDHB_HUMAN,
RS20_HUMAN, ATPA_HUMAN, LMNB1_HUMAN, RS3_HUMAN,
CAH2_HUMAN, LPPRC_HUMAN, RSMB_HUMAN, COF1_HUMAN,
LRRF1_HUMAN, SMD3_HUMAN, COR1A_HUMAN, MATR3_HUMAN,
SRSF3_HUMAN, EFTU_HUMAN, MDHM_HUMAN, TAGL2_HUMAN,
ETF A_HUMAN, MYH9_HUMAN, TKT_HUMAN, FLNA_HUMAN,
MYL6_HUMAN, TOP2B_HUMAN, GLU2B_HUMAN, NUCL_HUMA,
TPIS_HUMAN, GRP75_HUMAN, PCBP1_HUMAN, UGGG1_HUMAN,
GSTP1_HUMAN, PDIA1_HUMAN, VIME_HUMAN, H2B1C_HUMAN,
PDIA3_HUMAN, HBA_HUMAN, PERM_HUMAN, HBB_HUMAN, PPIA_HUMAN,
HNRCL_HUMAN, PPIB_HUMAN, HNRH1_HUMAN, PRDX1_HUMAN,
HNRPC_HUMAN, PRDX5_HUMAN, HNRPM_HUMAN, PTBP1_HUMAN,
HNRPU_HUMAN, RA1L2_HUMAN, HS90A_HUMAN, RAB10_HUMAN,
IDHP_HUMAN, RL9_HUMAN, IF5A1_HUMAN, ROA2_HUMAN, KP YM_HUMAN,
ROA3_HUMAN, LBR_HUMAN, RPN1_HUMAN

Proteins found in 4 functional and 4 non-functional samples: ACTA_HUMAN,
ACTB_HUMAN, AHNK_HUMAN, ATPB_HUMAN, EF1A1_HUMAN,
ENOA_HUMAN, FABP5_HUMAN, G3P_HUMAN, GDIR2_HUMAN,
GRP78_HUMAN, H2A1A_HUMAN, H31T_HUMAN, H4_HUMAN,
HNRPK_HUMAN, HS71L_HUMAN, HSP7C_HUMAN, ODO2_HUMAN,
PRDX2_HUMAN, PRDX3_HUMAN, RL40_HUMAN, RS7_HUMAN,
SFPQ_HUMAN, SRSF1_HUMAN, TBA1A_HUMAN, THIO_HUMAN

Proteins found in 3 functional and 1 non-functional samples: ACSL1_HUMAN,
ADT2_HUMAN, AL9A1_HUMAN, ANM1_HUMAN, AP1G1_HUMAN,
ARP3_HUMAN, AT2A3_HUMAN, CAB39_HUMAN, COPG1_HUMAN,
CRKL_HUMAN, CSK_HUMAN, DCPS_HUMAN, DDB1_HUMAN,
DDX21_HUMAN, DYHC1_HUMAN, EIF3L_HUMAN, HACD3_HUMAN,
HSP76_HUMAN, HXK1_HUMAN, KCAB2_HUMAN, LKHA4_HUMAN,
M2OM_HUMAN, MAOM_HUMAN, MAP4_HUMAN, MBOA7_HUMAN,

MET7A_HUMAN, MYH11_HUMAN, MYO1G_HUMAN, PP1A_HUMAN,
PSB6_HUMAN, PSMD3_HUMAN, QOR_HUMAN, RAB3D_HUMAN,
RB33B_HUMAN, RBM39_HUMAN, RECQ1_HUMAN, RHG01_HUMAN,
RL18A_HUMAN, RS21_HUMAN, SC11A_HUMAN, SERA_HUMAN,
SMCA2_HUMAN, STT3A_HUMAN, SYDC_HUMAN, SYG_HUMAN,
SYTC_HUMAN, THAS_HUMAN, UN13D_HUMAN, USO1_HUMAN,
XPO2_HUMAN, XPP1_HUMAN

Proteins found in 3 functional and 2 non-functional samples: 1433E_HUMAN,
LEG1_HUMAN, 1433F_HUMAN, LMAN2_HUMAN, 2AAA_HUMAN,
MCM5_HUMAN, 6PGD_HUMAN, ML12A_HUMAN, AATM_HUMAN,
MNDA_HUMAN, ACADM_HUMAN, MPCP_HUMAN, ACADV_HUMAN,
MYH10_HUMAN, ACLY_HUMAN, NB5R3_HUMAN, ACPH_HUMAN,
NOP58_HUMAN, ACTN1_HUMAN, NPM_HUMAN, ACTN4_HUMAN,
NUP50_HUMAN, ADDA_HUMAN, OST48_HUMAN, ADDG_HUMAN,
PA2G4_HUMAN, ADT1_HUMAN, PDC6I_HUMAN, AIFM1_HUMAN,
PLEC_HUMAN, ALDOC_HUMAN, PM14_HUMAN, AMPB_HUMAN,
PNPH_HUMAN, ANXA4_HUMAN, PO210_HUMAN, ANXA5_HUMAN,
PPAC_HUMAN, ANXA6_HUMAN, PRAF3_HUMAN, AP1B1_HUMAN,
PRP19_HUMAN, APMAP_HUMAN, PRP8_HUMAN, APT_HUMAN,
PRS10_HUMAN, ARC1B_HUMAN, PSA1_HUMAN, ARF6_HUMAN,
PSA3_HUMAN, ARK72_HUMAN, PSA4_HUMAN, ARL8B_HUMAN,
PSA5_HUMAN, ARP2_HUMAN, PSA7_HUMAN, ARPC2_HUMAN,
PSA7L_HUMAN, ARPC3_HUMAN, PSB3_HUMAN, ARPC4_HUMAN,
PSB4_HUMAN, ASC_HUMAN, PSD11_HUMAN, ATG3_HUMAN, PSIP1_HUMAN,
ATIF1_HUMAN, PTN6_HUMAN, B3AT_HUMAN, PTPRC_HUMAN,
ATG3_HUMAN, PYGB_HUMAN, ATIF1_HUMAN, PYGL_HUMAN,
B3AT_HUMAN, QCR1_HUMAN, BUB3_HUMAN, QCR7_HUMAN,
C1TC_HUMAN, RAB14_HUMAN, CAN1_HUMAN, RAB2A_HUMAN,
CAND1_HUMAN, RALY_HUMAN, CAP1_HUMAN, RINI_HUMAN,
CAPG_HUMAN, RL15_HUMAN, CAPZB_HUMAN, RL22_HUMAN,
CATA_HUMAN, RL23_HUMAN, CAZA1_HUMAN, RL7_HUMAN,

CBX3_HUMAN, RLA0_HUMAN, CH60_HUMAN, RLA0L_HUMAN,
 CISK_HUMAN, ROA1_HUMAN, CLH1_HUMAN, RPN2_HUMAN,
 CLIC1_HUMAN, RS15A_HUMAN, COPA_HUMAN, RS2_HUMAN,
 COPB_HUMAN, RS28_HUMAN, COPB2_HUMAN, RS8_HUMAN, COPD_HUMAN,
 RS9_HUMAN, COR1C_HUMAN, RTCB_HUMAN, COTL1_HUMAN,
 RUVB2_HUMAN, COX2_HUMAN, S10A4_HUMAN, CPSF5_HUMAN,
 SAHH_HUMAN, CPT1A_HUMAN, SAMH1_HUMAN, CPZIP_HUMAN,
 SAR1A_HUMAN, CREG1_HUMAN, SC22B_HUMAN, CYTB_HUMAN,
 SC31A_HUMAN, DBNL_HUMAN, SEPT7_HUMAN, DBPA_HUMAN,
 SEPT9_HUMAN, DCXR_HUMAN, SF3B3_HUMAN, DDX17_HUMAN,
 SND1_HUMAN, DDX3X_HUMAN, SP16H_HUMAN, DECR_HUMAN,
 SYIC_HUMAN, DHX15_HUMAN, SYWC_HUMAN, DHX9_HUMAN,
 TBB3_HUMAN, DOCK2_HUMAN, TCPA_HUMAN, DPYL2_HUMAN,
 TCPB_HUMAN, DX39A_HUMAN, TCPD_HUMAN, DX39B_HUMAN,
 TCPE_HUMAN, ECH1_HUMAN, TCPG_HUMAN, ECP_HUMAN, TCPH_HUMAN,
 EIF3A_HUMAN, TCPQ_HUMAN, ENPL_HUMAN, TLN1_HUMAN,
 ERLN1_HUMAN, TMEDA_HUMAN, ESTD_HUMAN, TOP2A_HUMAN,
 ESYT1_HUMAN, TPP1_HUMAN, ESYT2_HUMAN, TRA2B_HUMAN,
 EZRI_HUMAN, TRAP1_HUMAN, FLNB_HUMAN, U2AF2_HUMAN,
 G6PI_HUMAN, U520_HUMAN, GBB1_HUMAN, U5S1_HUMAN, GBLP_HUMAN,
 UB2L3_HUMAN, GDIA_HUMAN, UBA1_HUMAN, GDIB_HUMAN,
 UGPA_HUMAN, GELS_HUMAN, URP2_HUMAN, GLYM_HUMAN,
 VAPA_HUMAN, GNAI1_HUMAN, VATA_HUMAN, GNAI2_HUMAN,
 VATB2_HUMAN, GSHR_HUMAN, VDAC1_HUMAN, GSTK1_HUMAN,
 VDAC2_HUMAN, H90B2_HUMAN, VDAC3_HUMAN, H90B3_HUMAN,
 VPS35_HUMAN, HCDH_HUMAN, WDR1_HUMAN, HCLS1_HUMAN,
 XPO1_HUMAN, HMGA1_HUMAN, XRCC6_HUMAN, HNRPR_HUMAN,
 HPRT_HUMAN, HS90B_HUMAN, HSP71_HUMAN, HSP72_HUMAN,
 HSP74_HUMAN, HYOU1_HUMAN, I2BP2_HUMAN, IDHC_HUMAN,
 IF4A1_HUMAN, IF4A3_HUMAN, IQGA1_HUMAN, IQGA2_HUMAN,
 K6PL_HUMAN, K6PP_HUMAN, KAD2_HUMAN, LA_HUMAN, LAP2B_HUMAN

Proteins found in 3 functional and 3 non-functional samples: 1433T_HUMAN,
ACINU_HUMAN, AINX_HUMAN, ALDOA_HUMAN, ARF1_HUMAN,
ASAH1_HUMAN, AT5F1_HUMAN, ATP5I_HUMAN, ATPA_HUMAN,
AT5F1_HUMAN, ATP5I_HUMAN, C1QBP_HUMAN, CAH1_HUMAN,
CALR_HUMAN, CALX_HUMAN, CATC_HUMAN, CHM4B_HUMAN,
COX5B_HUMAN, CPNS1_HUMAN, DHB4_HUMAN, DHE3_HUMAN,
DKC1_HUMAN, DLDH_HUMAN, ECHA_HUMAN, ECHB_HUMAN,
ECHM_HUMAN, EF1G_HUMAN, EF2_HUMAN, ELAV1_HUMAN,
ERP29_HUMAN, F13A_HUMAN, FUBP1_HUMAN, FUBP2_HUMAN,
GANAB_HUMAN, GGH_HUMAN, H11_HUMAN, H12_HUMAN, H1X_HUMAN,
H2A1B_HUMAN, H2AY_HUMAN, HBD_HUMAN, HCD2_HUMAN,
HCFC1_HUMAN, HDGF_HUMAN, HGB1A_HUMAN, HMGB1_HUMAN,
HMGB2_HUMAN, HNRDL_HUMAN, HNRH3_HUMAN, HNRL1_HUMAN,
HNRPD_HUMAN, HP1B3_HUMAN, ILF2_HUMAN, ILF3_HUMAN,
IMB1_HUMAN, K1967_HUMAN, LAP2A_HUMAN, LASP1_HUMAN,
LYSC_HUMAN, MTPN_HUMAN, NDUS3_HUMAN, NNTM_HUMAN,
NUMA1_HUMAN, ODPB_HUMAN, PAIRB_HUMAN, PARK7_HUMAN,
PARP1_HUMAN, PCBP2_HUMAN, PDIA4_HUMAN, PDIA6_HUMAN,
PEBP1_HUMAN, PGAM1_HUMAN, PHB_HUMAN, PHB2_HUMAN,
PLSL_HUMAN, PSA2_HUMAN, PSA6_HUMAN, QCR2_HUMAN,
RAB7A_HUMAN, RAC2_HUMAN, RAP1A_HUMAN, RB11A_HUMAN,
RBMX_HUMAN, RL11_HUMAN, RL13_HUMAN, RL23A_HUMAN,
RL27_HUMAN, RL31_HUMAN, RL35A_HUMAN, RL38_HUMAN, RL7A_HUMAN,
RL8_HUMAN, ROA0_HUMAN, RS13_HUMAN, RS19_HUMAN, RS25_HUMAN,
RS4X_HUMAN, RSSA_HUMAN, RTN4_HUMAN, RUVB1_HUMAN,
SARNP_HUMAN, SARNP_HUMAN, SARNP_HUMAN, SEPT2_HUMAN,
SF01_HUMAN, SF3A1_HUMAN, SMD2_HUMAN, SSBP_HUMAN,
SSRD_HUMAN, TADBP_HUMAN, TALDO_HUMAN, TBB1_HUMAN,
TBB4A_HUMAN, TBB5_HUMAN, TCP4_HUMAN, TCPZ_HUMAN,
THOC4_HUMAN, TIF1B_HUMAN, TR150_HUMAN, UCRIL_HUMAN

Proteins found in 2 functional TEX and 2-3 functional AML samples:

MCM6_HUMAN, FAS_HUMAN, F120A_HUMAN, TEBP_HUMAN,
TCTP_HUMAN, SHIP1_HUMAN, S10AB_HUMAN, RAD50_HUMAN,
PRS6B_HUMAN, OXSR1_HUMAN, MAVS_HUMAN, IF2P_HUMAN,
HS105_HUMAN, HN1L_HUMAN, FUBP3_HUMAN, DOK3_HUMAN,
D6RBZ0_HUMAN, CYC_HUMAN, CHCH3_HUMAN, ARI1A_HUMAN,
AP3D1_HUMAN

Proteins found in 2 functional and no non-functional TEX samples:

1433B_HUMAN, AT5EL_HUMAN, CSTFT_HUMAN, ETFB_HUMAN,
1433E_HUMAN, AT5F1_HUMAN, CTF8A_HUMAN, EVL_HUMAN,
1433G_HUMAN, ATF1_HUMAN, CWC15_HUMAN, EWS_HUMAN,
1433T_HUMAN, ATOX1_HUMAN, CX7A2_HUMAN, F10A1_HUMAN,
1433Z_HUMAN, ATP5H_HUMAN, CYBP_HUMAN, F136A_HUMAN,
2B13_HUMAN, B4DY08_HUMAN, CYC_HUMAN, F192A_HUMAN,
2B18_HUMAN, BACH_HUMAN, D6RBZ0_HUMAN, F195B_HUMAN,
2B1B_HUMAN, BAF_HUMAN, D6RI10_HUMAN, F207A_HUMAN,
3BP1_HUMAN, BAP18_HUMAN, DAZP1_HUMAN, FA32A_HUMAN,
4F2_HUMAN, BAS1_HUMAN, DBNL_HUMAN, FCL_HUMAN, 6PGL_HUMAN,
BCCIP_HUMAN, DC1L1_HUMAN, FEN1_HUMAN, AAAT_HUMAN,
BCLF1_HUMAN, DCTN1_HUMAN, FIS1_HUMAN, AAMDC_HUMAN,
BLVRB_HUMAN, DCTN2_HUMAN, FKB1A_HUMAN, AATM_HUMAN,
BOLA1_HUMAN, DD19A_HUMAN, FKBP4_HUMAN, ACO13_HUMAN,
BRD4_HUMAN,, DDX1_HUMAN, FSCN1_HUMAN, ACON_HUMAN,
C1TC_HUMAN, DDX21_HUMAN, FUBP3_HUMAN, ACPH_HUMAN,
CAF17_HUMAN, DDX42_HUMAN, FUMH_HUMAN, AHSA1_HUMAN,
CALX_HUMAN, DDX5_HUMAN, FYB_HUMAN, AIMP1_HUMAN,
CAP1_HUMAN, DDX6_HUMAN, G3BP1_HUMAN, AIP_HUMAN, CAPG_HUMAN,
DHE3_HUMAN, G3BP2_HUMAN, AK1A1_HUMAN, CAPR1_HUMAN,
DHRS4_HUMAN, G6PI_HUMAN, ALDOC_HUMAN, CAPZB_HUMAN,
DHX15_HUMAN, GBRL2_HUMAN, ALDR_HUMAN, CAZA1_HUMAN,
DNJB1_HUMAN, GDIA_HUMAN, AMPN_HUMAN, CBX3_HUMAN,

DNMT1_HUMAN, GDIB_HUMAN, AMPL_HUMAN, CBX5_HUMAN,
 DOPD_HUMAN, GDIR1_HUMAN, AN32A_HUMAN, CC124_HUMAN,
 DPYL2_HUMAN, GGCT_HUMAN, ANX11_HUMAN, CCAR1_HUMAN,
 DRA_HUMAN, GL1AD_HUMAN, ANXA1_HUMAN, CD109_HUMAN,
 E9PAU2_HUMAN, GLO2_HUMAN, APEX1_HUMAN, CD2A1_HUMAN,
 ECHA_HUMAN, GLOD4_HUMAN, ARF1_HUMAN, CD97_HUMAN,
 EF1D_HUMAN, GLRX5_HUMAN, ARFG2_HUMAN, CDC37_HUMAN,
 EF1G_HUMAN, GLU2B_HUMAN, ARI1A_HUMAN, CDK12_HUMAN,
 EF2_HUMAN, GLYG_HUMAN, ARL3_HUMAN, CELF2_HUMAN,
 EFHD2_HUMAN, GMFB_HUMAN, ARP5L_HUMAN, CGBP1_HUMAN,
 EGLN_HUMAN, GMFG_HUMAN, ARPC3_HUMAN, CHCH3_HUMAN,
 EIF1B_HUMAN, GNAI2_HUMAN, ARPC5_HUMAN, CHM4B_HUMAN,
 EIF3C_HUMAN, GPX1_HUMAN, ASC_HUMAN, CHSP1_HUMAN,
 EIF3H_HUMAN, GRB2_HUMAN, ASHWN_HUMAN, CI078_HUMAN,
 ELOB_HUMAN, GRHPR_HUMAN, CISY_HUMAN, ELYS_HUMAN,
 GRPE1_HUMAN, CKS1_HUMAN, EMSA1_HUMAN, GSTO1_HUMAN,
 CLIC1_HUMAN, ERLN2_HUMAN, GSTP1_HUMAN, CN166_HUMAN,
 ESYT1_HUMAN, CNDP2_HUMAN, CNN2_HUMAN, COA4_HUMAN,
 COR1A_HUMAN, COTL1_HUMAN, COX5A_HUMAN, CPIN1_HUMAN,
 CPNE1_HUMAN, CPSF5_HUMAN, CREB1_HUMAN, CRKL_HUMAN,
 CSRP1_HUMAN, CSTF2_HUMAN

5.8. Conclusion

Protein target identification studies were conducted in primary human AML cells and TEX cells containing high levels of CD34⁺ positive cells (indicative of LSCs) with a novel **PTL**-based alkyne probe. **PTL** has been shown to selectively eradicate LSCs while being non-toxic to healthy hematopoietic stem cells. The designed **PTL**-based alkyne probe, which maintains low micromolar growth inhibition against leukemia cells, could be used to identify putative targets responsible for the ability of **PTL** to target LSCs. These pulldown studies revealed that F120A/OSSA is a putative target of **PTL** and may

be responsible for LSC survival and maintenance because of its role in the regulation of oxidative stress. **PTL** and similar analogues have been shown to modulate ROS levels and cause oxidative stress intracellularly. LSCs have been shown to be sensitive to ROS levels and targeting proteins involved in regulation of oxidative stress could prove to be valuable targets for the inhibition of LSC survival and tumor relapse.

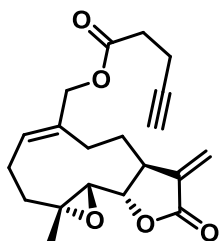
Further validation of F120A/OSSA as a target of **PTL** and a necessary protein for LSC survival and maintenance needs to be completed. Validation can be done by Western blot analysis of F120A after pulldown with the **PTL**-based alkyne probe **5.4** and demonstrating that **PTL** is also able to compete away this interaction in cells. Genetic modification experiments to the F120A gene in relevant LSC models will also be needed to show that F120A is necessary for LSC survival. This work is currently in progress.

5.9 Experimental

Unless otherwise noted, all reactions were performed in flame-dried glassware sealed with rubber septa under a nitrogen or argon atmosphere and the reaction mixture stirred with a Teflon-coated magnetic stir bar. Commercial grade reagents (Aldrich, Acros, Enzo Life Sciences, and Alfa Aesar) were used without further purification unless otherwise noted. Liquid reagents and solvents were transferred via syringe and cannula using standard techniques. The reaction solvent dichloromethane (DCM) was dried by passage over a column of activated alumina using a solvent purification system (MBraun). Reaction temperatures above 23 °C refer to oil bath temperature, which was controlled by a temperature modulator. Reaction progress was monitored by thin layer chromatography using EMD Chemicals Silica Gel 60 F254 glass plates (250 μm thickness) and visualized by UV irradiation (at 254 nm) and/or KMnO_4 stain. Silica gel chromatography was performed on a Teledyne-Isco Combiflash Rf-200 instrument utilizing Redisep Rf High Performance silica gel columns (Teledyne-Isco) or flash column chromatography was performed using SiliCycle silica gel (32-63 μm particle size, 60 Å pore size). ^1H NMR (400 or 500 MHz) and ^{13}C NMR (100 or 125 MHz) spectra were recorded on a Bruker NMR spectrometer. ^1H and ^{13}C chemical shifts (δ) are reported relative to the solvent signal, CHCl_3 ($\delta = 7.26$ for ^1H NMR and $\delta = 77.00$ for ^{13}C

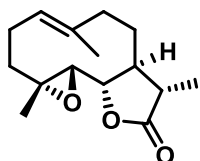
NMR). Some spectra contain 0.5% v/v TMS. All NMR spectra were obtained at room temperature. High resolution mass spectral data were obtained from the Masonic Cancer Center Mass Spectrometry Facility on an LTQ Orbitrap Velos Mass Spectrometer (Thermo Fisher) or at the University of Minnesota mass spectrometry lab with a BioTOF II Mass Spectrometer (Bruker). References located after compound names refer to literature protocols for the preparation and characterization of these or similar compounds by comparable methods.

Compounds with absorbance properties at or above 215 nm that were used in biological assays were tested for purity using analytical HPLC analysis on an Agilent 1200 series instrument equipped with a diode array detector (wavelength monitored = 215 nm) and a Zorbax SBC18 column (4.6 x 150 mm, 5 μ m, Agilent Technologies). All compounds tested in biological assays were > 95% pure by HPLC. Compounds that do not have sufficient absorbance at 215 nm or above are shown to be pure by ^1H NMR analysis.

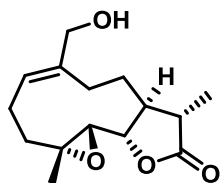


MelB-functional alkyne probe (5.3) – **MelB**²⁹³ (50.0 mg, 0.189 mmol) was dissolved in DCM (10 mL). Then, 4-pentynoic acid (21.0 mg, 0.208 mmol) and 4-DMAP (16.0 mg, 0.095 mmol) were added at RT. Finally, EDCI (39.9 mg, 0.208 mmol) was added to the solution and the reaction was allowed to stir for 24 hr at RT. The reaction was quenched with H₂O (20 mL) and extracted with DCM (20 mL, 3X). The organic layer was dried over Na₂SO₄, filtered and concentrated *in vacuo*. The resulting crude oil was SiO₂ purified with a gradient of 0 to 20% ethyl acetate in hexanes to afford 53.4 mg as a white solid in 82% yield. ^1H NMR (CDCl₃, 400 MHz): 6.26 (d, J = 3.5 Hz, 1H), 5.71 (t, J = 8.1 Hz, 1H), 5.55 (d, J = 3.2 Hz, 1H), 4.72 (d, J = 12.4 Hz, 1H), 4.49 (d, J = 12.4 Hz, 1H), 3.85 (t, J = 9.3 Hz, 1H), 2.86 (m, 2H), 2.54 (m, 4H), 2.30 (m, 6H), 1.98 (t, J = 2.4 Hz,

1H), 1.76 (m, 1H), 1.55 (s, 3H), 1.11 (t, $J = 12.4$ Hz, 1H) ppm. ^{13}C NMR (CDCl_3 , 100 MHz): 171.5, 169.3, 138.7, 134.8, 130.9, 120.3, 82.3, 81.0, 69.2, 67.0, 63.3, 59.9, 42.7, 36.6, 33.3, 25.7, 24.4, 23.8, 18.0, 14.4 ppm. HRMS (ESI^+) m/z calc'd for $[\text{C}_{20}\text{H}_{24}\text{O}_5+\text{Na}]^+$ 367.1521; found 367.1537 ppm.

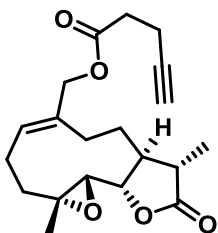


11,13-dihydroparthenolide (5.5) – Parthenolide (132 mg, 0.534 mmol) was dissolved in EtOH (15 mL) and the reaction was degassed and backfilled with H_2 (1 atm) 3X and allowed to stir at RT for 6 h. The reaction mixture was filtered through celite and concentrated *in vacuo*. The crude mixture was taken on to the next step without further purification. This compound has been previously synthesized and characterized.^{247e}



11,13-dihydroMelB (5.6) – Crude 11,13-dihydroparthenolide (**5.5**) (134 mg, 0.534 mmol) was dissolved in DCM (15 mL). Next, SeO_2 (65.1 mg, 0.587 mmol) and *t*BuOOH (0.5 mL, 3 mmol, 5M solution in decanes) was added at RT.²⁹³ The reaction was refluxed for 4 h. The reaction mixture was allowed to cool, quenched with H_2O (30 mL), and extracted with DCM (30 mL, 3X). The organic layer was dried over Na_2SO_4 and concentrated *in vacuo*. The crude material was SiO_2 purified with a gradient of 0 to 60% ethyl acetate in hexanes to yield the desired product (86 mg, 61%, over 2 steps) as a white solid. ^1H NMR (CDCl_3 , 500 MHz): 5.62 (t, $J = 8.2$ Hz, 1H), 4.13 – 4.01 (m, 2H), 3.83 (t, $J = 9.5$ Hz, 1H), 2.75 (d, $J = 9.4$ Hz, 1H), 2.47 – 2.37 (m, 1H), 2.37 – 2.09 (m, 7H), 1.95 – 1.84 (m, 1H), 1.62 – 1.56 (m, 1H), 1.54 (s, 3H), 1.25 (d, $J = 6.9$ Hz, 3H), 1.11 – 1.01 (m, 1H) ppm. ^{13}C NMR (CDCl_3 , 100 MHz): 178.0, 139.8, 127.0, 81.2, 65.6, 63.6,

60.0, 46.4, 41.5, 37.0, 26.7, 24.2, 23.6, 17.9, 13.0 ppm. HRMS (ESI⁺) m/z calc'd for [C₁₅H₂₂O₄+H]⁺ 267.1591; found 267.1588.



11,13-dihydroMelB-nonfunctional alkyne probe (5.6): Compound **5.5** (6.2 mg, 0.02 mmol), pentynoic acid (2.6 mg, 0.03 mmol), and 4-DMAP (2.8 mg, 0.02 mmol) were added to a stirred solution of DCM (5 mL) at RT. Then, EDCI (4.9 mg, 0.3 mmol) was added to the reaction and stirred for 24 h at RT. The reaction was quenched with H₂O (20 mL) and extracted with DCM (20 mL, 3X). The organic layer was dried over Na₂SO₄ and concentrated *in vacuo*. The crude material was SiO₂ purified with a gradient of 0 to 40% ethyl acetate in hexanes to yield the desired product (4.8 mg, 53%) as a white solid. ¹H NMR (CDCl₃, 400 MHz): δ 5.67 (t, J = 8.1 Hz, 1H), 4.71 (d, J = 12.5 Hz, 1H), 4.46 (d, J = 12.5 Hz, 1H), 3.83 (t, J = 9.5 Hz, 1H), 2.75 (d, J = 9.4 Hz, 1H), 2.55 (m, 5H), 2.30 (m, 6H), 1.98 (t, J = 2.5 Hz, 1H), 1.91 (m, 1H), 1.60 (m, 1H), 1.55 (s, 3H), 1.29 (d, J = 6.9 Hz, 3H), 1.08 (t, J = 12.8 Hz, 1H) ppm. ¹³C NMR (CDCl₃, 100 MHz): 177.7, 171.4, 135.0, 130.1, 82.3, 81.0, 69.2, 66.4, 63.5, 59.8, 46.3, 41.5, 36.8, 33.4, 26.7, 24.3, 23.7, 17.9, 14.4, 13.1 ppm. HRMS (ESI⁺) m/z calc'd for [C₂₀H₂₆O₅+K]⁺ 385.1417; found 385.1412.

Cell Culture

All cell lines were maintained in a humidified 5% CO₂ environment at 37 °C in tissue culture flasks (Corning) under normoxic conditions. Adherent cells were dissociated using Trypsin-EDTA solution (0.25%, Gibco). Primary human AML cells were cultured in Isocove's Modified Dubelco's Media (IMDM) media that contained 2% BSA, 10 μ g/mL insulin, 200 μ g/mL transferrin, 40 μ g/mL low density lipoproteins, 50

μM 2-mercaptoethanol, 100 I.U./mL penicillin, and 100 $\mu\text{g}/\text{mL}$ streptomycin. TEX cells were cultured in IMDM that contained 15% v/v FBS (Gibco), stem cell factor (SCF, 20 ng/mL, PeproTech), IL-3 (2 ng/mL, PeproTech), penicillin (100 I.U./mL, ATCC), and streptomycin (100 $\mu\text{g}/\text{mL}$, ATCC). HL-60 cells were cultured in IMDM supplemented with 20% v/v FBS (Gibco), penicillin (100 I.U./mL, ATCC), and streptomycin (100 $\mu\text{g}/\text{mL}$, ATCC). HEK293 cells were cultured in Eagle's Minimum Essential Medium (EMEM) that contained 10% v/v FBS, penicillin (100 I.U./mL, ATCC), and streptomycin (100 $\mu\text{g}/\text{mL}$, ATCC).

Human cancer cell line cytotoxicity assays

Alamar blue cellular cytotoxicity assays and data analyses were performed as previously described.^{219, 237} HL-60 cells were seeded at a density of 10,000 cells/well in media (50 μL) in 96-well plates (Costar 3595, Corning, Inc.). IC₅₀ values (n \geq 3 biological replicates) are the mean \pm SD.

Flow Cytometry Analysis

Primary human AML cells from each patient were plated in media at 10^6 cells/mL (1 mL/well) in a 24-well plate (Corning) in conjunction with each pulldown experiment. After allowing the cells to incubate overnight, each sample was transferred into FACS tubes and centrifuged for 5 min at 800 rpm. The supernatant was decanted and each sample was washed with cold 1X PBS (1 mL) and centrifuged again. After centrifugation, the supernatant was decanted and the samples were stained with Brilliant Violet 421 mouse anti-human CD34 (BD Biosciences, 5 $\mu\text{L}/\text{sample}$) and APC mouse anti-human CD38 (BD Biosciences, 20 $\mu\text{L}/\text{sample}$) antibodies in FACS buffer (1X PBS, 2% FBS, 0.1% sodium azide; 100 μL total volume/sample) for 10 minutes at 4 °C. The cells were then diluted with FACS buffer (1 mL) and centrifuged. The supernatant was decanted and stained with Annexin V-FITC (BD Biosciences, 5 $\mu\text{L}/\text{sample}$) and 7-AAD (eBioscience, 5 $\mu\text{L}/\text{sample}$) in FACS buffer (100 μL total volume/sample) for 10 minutes at room temperature in the dark in order to gate the live cell population. The samples

were diluted with FACS buffer (300 μ L), and kept on ice during analysis by flow cytometry using a BD Biosciences LSR II flow cytometer. Greater than 50,000 events were measured for each sample during analysis. All antibodies and stains were stored at 4 $^{\circ}$ C in the dark when not in use. After data collection, each sample was processed using FlowJo (Tree Star; v 7.6.5). Data was processed according to a previously published protocol.²⁷⁵

Protein Identification in Primary Human AML cells

Each primary cell aliquot was kept in N_2 (l) in 5% DMSO/IMDM media after collection from each patient until it was thawed over 2-4 min in a 37 $^{\circ}$ C water incubator and then diluted with IMDM media (10 mL) in a canonical tube before centrifuging at 300 RPM for 5 min. The supernatant was decanted off and the cell pellet was suspended to have a concentration of 10^6 cells/mL in IMDM media and placed (20 mL) in a 150 cm^2 flask under normoxic conditions at 37 $^{\circ}$ C in a humidified CO_2 incubator overnight. Alkyne probes **5.3** or **5.4** were dosed to separate flasks at 50 μ M and incubated for 2 h. After incubation, the cells were centrifuged at 300 RPM for 5 min and the media was decanted. The cells were washed once with 1X PBS buffer at 4 $^{\circ}$ C and centrifuged 300 RPM for 5 min. The supernatant was decanted and RIPA buffer ((Thermo Fisher, 1 mL) containing Complete EDTA-free protease inhibitor cocktail (Life Technologies)) was added to the cells and mixed via pipetting continuously (20X) and then lightly vortexed. The cells were incubated at 4 $^{\circ}$ C for 1 hour and then mixed via pipetting again. The cells were incubated for an additional 15 minutes at 4 $^{\circ}$ C then centrifuged at 4 $^{\circ}$ C at 4000 rpm for 20 minutes. The supernatant was isolated and protein concentration was determined (Pierce BCA Protein Assay Kit, Thermo Scientific). The protein concentrations were in the range between 1.5-2.0 mg/mL of lysate. The lysates were either stored overnight at -80 $^{\circ}$ C before further use or used immediately.

After thawing, click reagents were added to the lysates (20 μ L $CuSO_4$, 50 mM stock in H_2O ; 20 μ L TBTA, 10 mM stock in DMSO; 40 μ L Biotin- N_3 , 20 mM stock in DMSO [Sigma-Aldrich 762024; CAS: 875770-34-6]; 40 μ L sodium ascorbate, 100 mM in H_2O) and allowed to react for 2 h at room temperature.

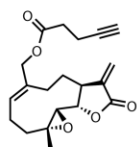
The samples were then separated on a monomeric avidin column according to the manufacturer's instructions (Pierce) at RT. After the enriched protein samples were collected they were concentrated using a 3 kDa molecular weight cut-off filter (Amicon) and diluted with ddH₂O (20 mL, 2X) and then finally concentrated to ~500 μL. Protein was precipitated from these proteins by adding 13 M trichloroacetic acid (TCA) in ddH₂O to a final concentration in the lysate of 1.3 M. The samples were incubated at -20 °C for 6 h. The samples were then centrifuged at 15,000 RPM for 10 min at 4 °C. The pellets were washed with -20 °C acetone (500 μL) and centrifuged at the same speed, time, and temperature (2X). The samples were then dried in a SpeedVac for 3 h and kept at -20 °C until further analysis. The samples were shipped overnight for LC-MS/MS and proteomic analysis at the Taplin Mass Spectrometry Facility at the Harvard Medical School (contracted work; Boston, MA).

CRISPR/Cas9 Knockout of F120A in HEK293 Cells

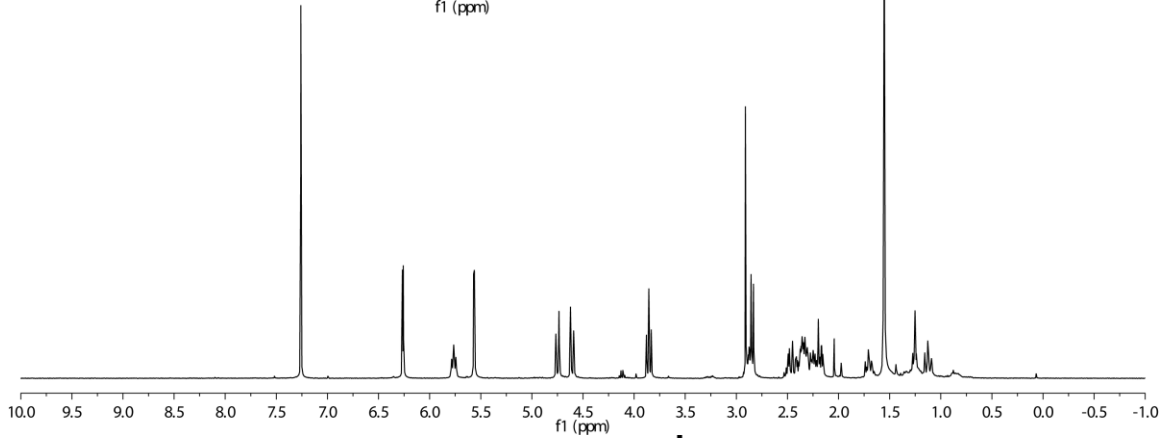
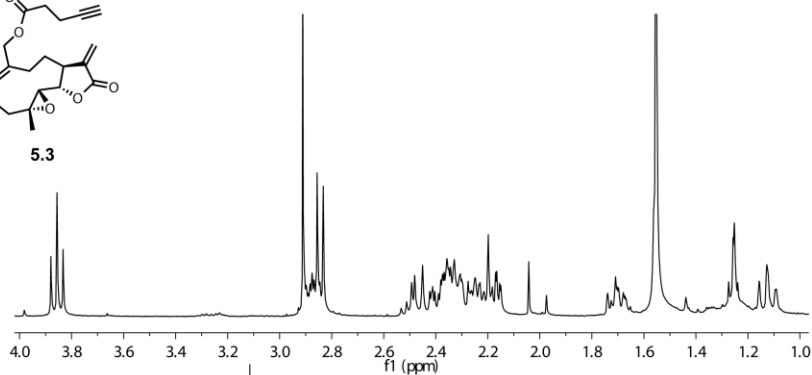
Two CRISPR/Cas9 plasmids containing separate guide RNA sequences (plasmid 1: 5'-GAGAAGCACTGCCCGAGCGCTGG-3'; plasmid 2: 5'-CAGAGCATTGAGGAT CACCATTCAGG-3') were generated and transduced into HEK293 cells as previously described.³²² Cells containing the transfected plasmid were then selected using puromycin (1 μg/mL in cell media) by dosing to the cell media for three passages. After selection, the CRISPR/Cas9 system was induced with doxycycline (5 μg/mL in cell media) for two weeks. The expression of FAM120A (Pierce, Cat# PA5-31766) was followed via Western blot analysis and β-actin (Sigma Aldrich, Cat# A1978) was used as the gel-loading control. Western blot analysis was carried out as previously described.²²⁹ The surveyor nuclease (Cel-1) assay was carried out as previously described.³²⁰

5.9 Spectral Data

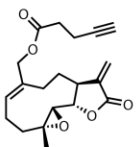
¹H NMR (CDCl₃)



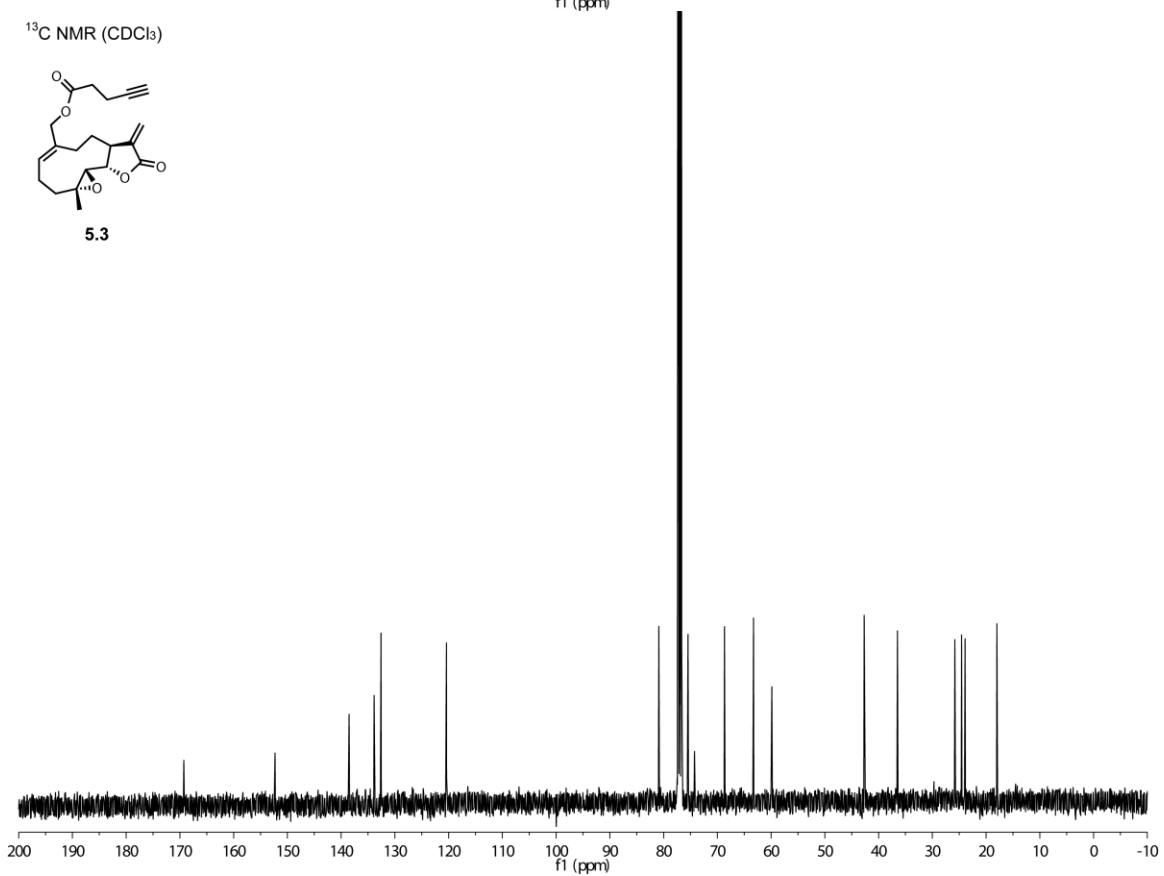
5.3



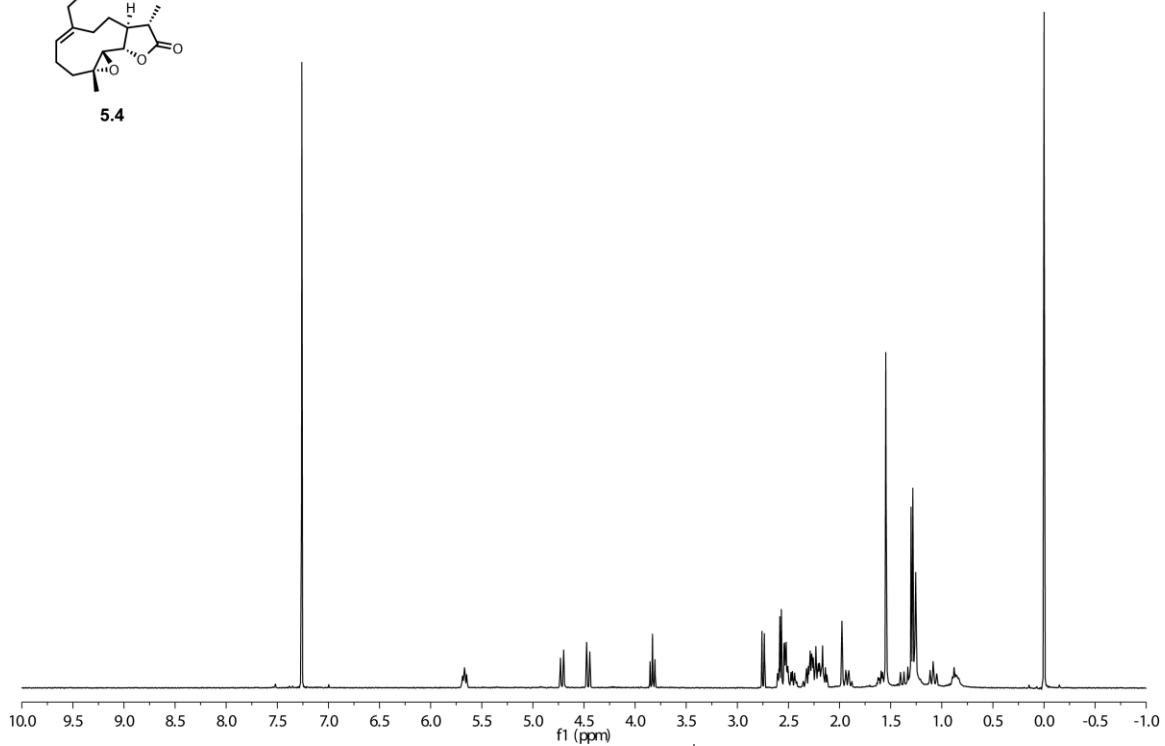
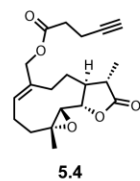
¹³C NMR (CDCl₃)



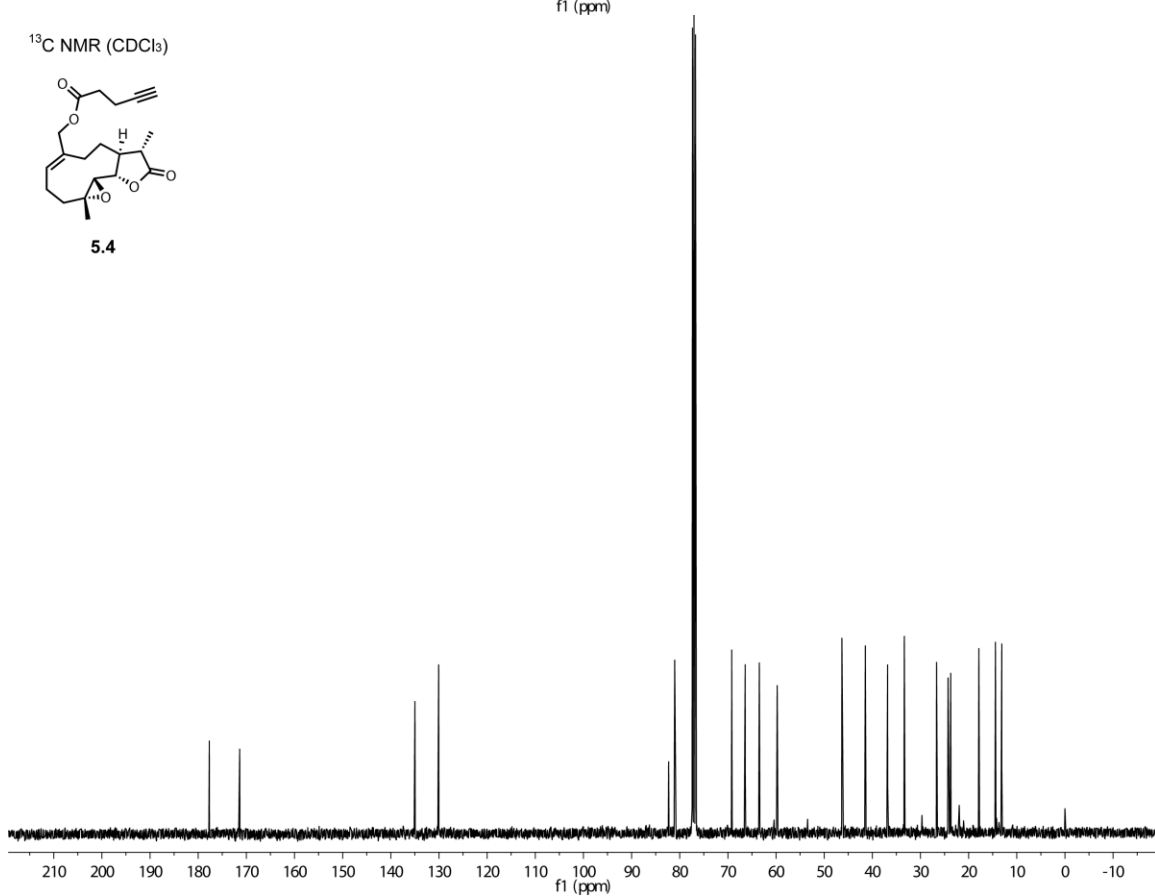
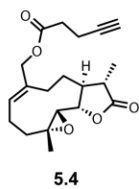
5.3



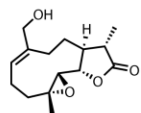
¹H NMR (CDCl₃)



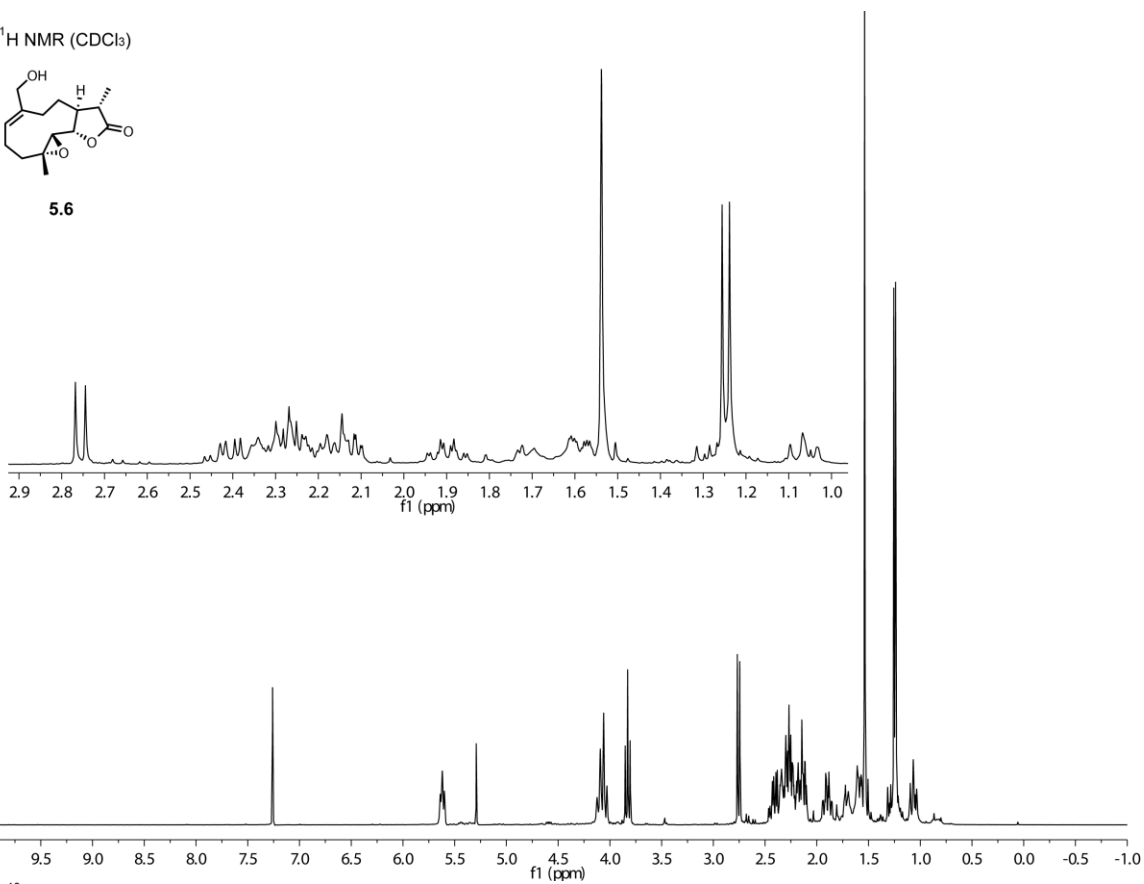
¹³C NMR (CDCl₃)



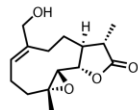
¹H NMR (CDCl₃)



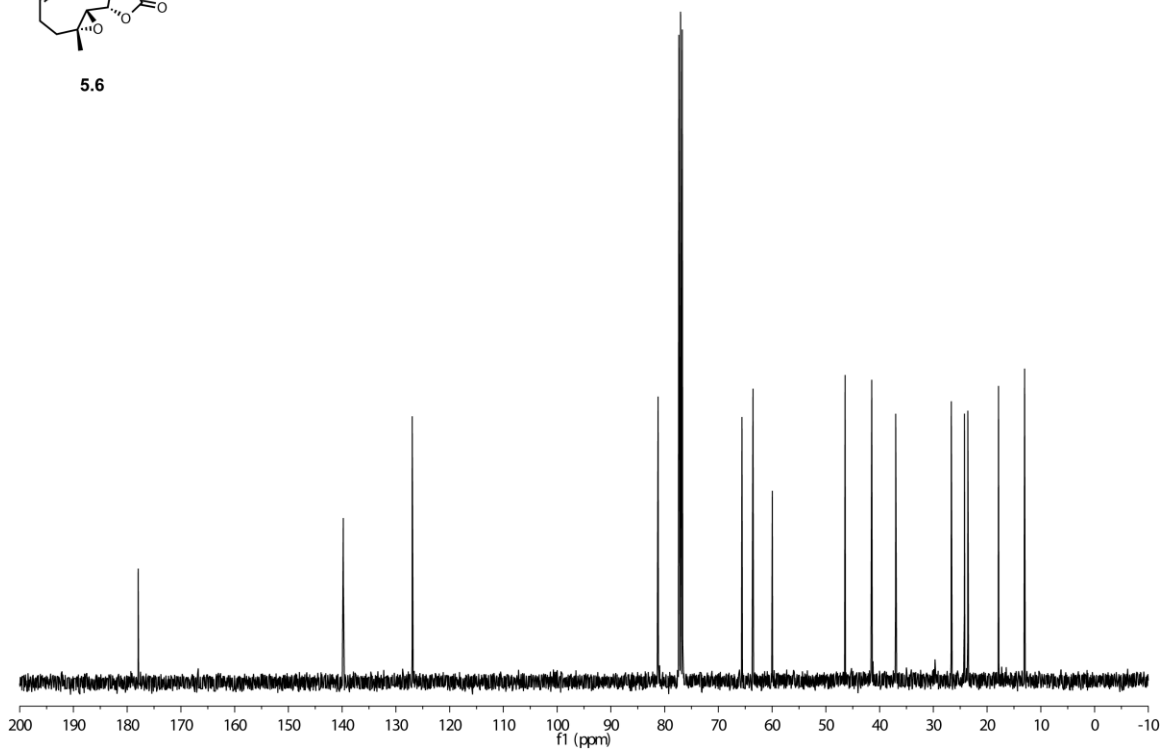
5.6



¹³C NMR (CDCl₃)



5.6

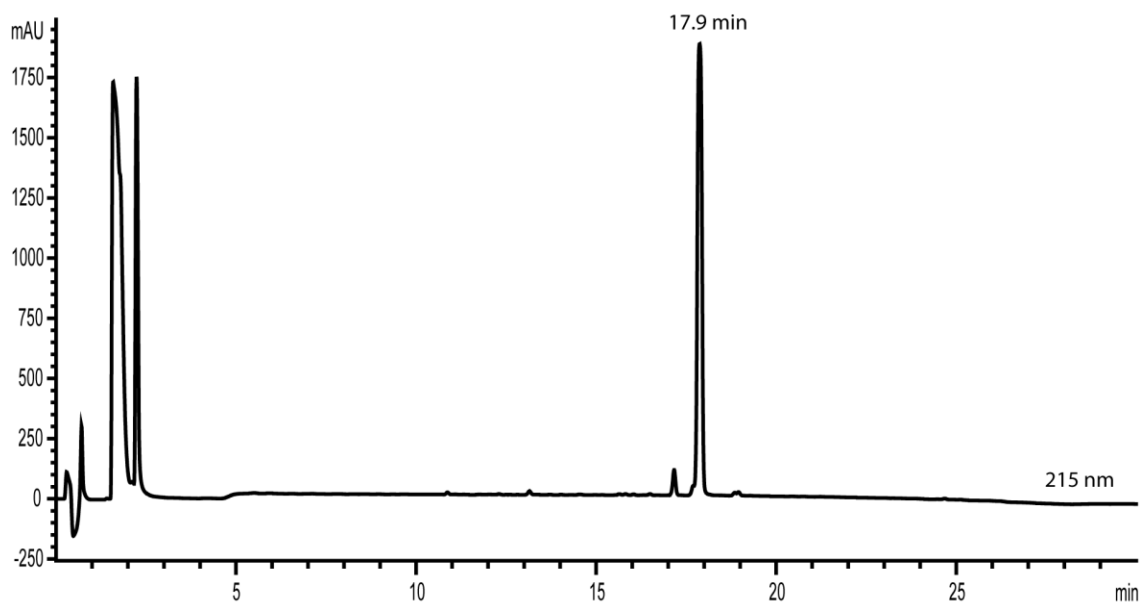


5.11 HPLC Chromatograms of Synthesized Compounds

General Protocol for HPLC Analysis of Synthesized Compounds. DMSO stock solutions of newly synthesized molecules were dissolved in 1:1 solution of methanol and distilled and deionized water (ddH₂O) containing trifluoroacetic acid (TFA, 0.1% v/v) and analyzed on an Agilent 1200 series instrument equipped with a diode array detector and Zorbax SB-C18 column (4.6 x 150 mm, 5 μ m, Agilent Technologies). The analysis method (1 mL/min flow rate) starts with an eluent system of 10% MeCN in ddH₂O from 0-2 minutes (both containing 0.1% TFA) followed by a linear gradient of 10% to 85% MeCN in ddH₂O from 2-24 minutes, followed by 85% to 95% MeCN in ddH₂O from 24-26 minutes, and finally an isocratic eluent system of 95% MeCN in ddH₂O from 26-30 minutes. Wavelengths monitored = 215 nm.

Preparation of Stock Solutions. Compound stock solutions were prepared in DMSO (40 mM to 100 mM concentrations) and stored at -20 °C when not in use. Compound purities were assessed frequently by analytical reverse-phase HPLC analysis and fresh solutions were prepared as needed. Compound **5.4** was not UV active and therefore purity was determined to be $\geq 95\%$ by ¹NMR analysis.

Probe 5.3 HPLC (96.5% pure):



5.12 Acknowledgements

We thank Professor Michael Verneris (UMN) for assistance with flow cytometry analysis and NIH P30 CA77598, which supports the Flow Cytometry shared resource of the Masonic Cancer Center (UMN). The TEX cell line was a gift from Professor John Dick (University of Toronto). The Leukemia MDS Tissue Bank (UMN) is acknowledged for supplying the human, primary AML samples.

Chapter 6

BIOCHEMICAL EVALUATION AND TARGET IDENTIFICATION STUDIES OF EPI-002 AND EPI-054

This work was performed in collaboration with Jordan Baur, Dr. Meixia Che, Mark Daniel, Professor Scott M. Dehm, and Professor Daniel A. Harki. Jordan Baur assisted with synthesis of the EPI analogues. Meixia Che and Mark Daniel assisted with aspects of biochemical evaluation of the synthetic EPI analogues. John Widen synthesized the presented compounds, conducted the cytotoxicity assays, and conducted the in-gel labeling assays.

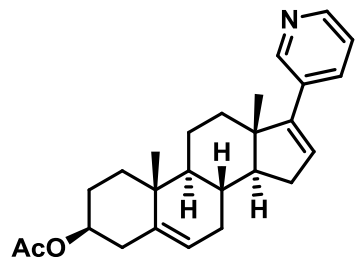
6.1 Introduction

In the United States, prostate cancer is the most diagnosed form of malignancy among men and is estimated to account for more than 26,000 deaths in the United States in 2016; second most among all cancers.³²³ Based on the Cancer of the Prostate Strategic Urologic Research Endeavor (CaPSURE) database, 46% of men at the time of diagnoses with prostate cancer are younger than 65 years of age with the overall mean age at the time of diagnosis being 66 years of age.³²⁴ Among these patients, many are initially treated with surgical or chemical androgen deprivation therapy.³²⁵ Prostate cancer initially relies on endogenous androgens to activate the androgen receptor (AR) for growth and progression.³²⁶ Androgen deprivation therapy includes removal of the testicular tissue or treatment with luteinizing hormone-releasing agonists, which inhibits the testicles from releasing testosterone.³²⁷ This treatment is effective until the malignancy transforms to castration resistant prostate cancer (CRPC).³²⁸

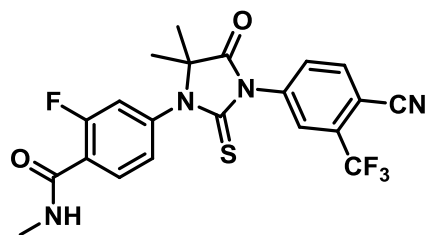
CRPC becomes independent of hormone signaling and continues to progress in the absence of androgen in blood serum. Despite this independence of androgen production by the testes, CRPC still relies on AR signaling for progression. This is evident considering the efficacy of second generation AR antagonists abiraterone (**6.1**) and enzalutamide (**6.2**) against CRPC.³²⁹ Both compounds bind to the AR ligand-binding domain (LDB), but abiraterone also inhibits production of androgens via inhibition of the CYP17A enzyme. Eventually, both AR signaling antagonists lead to selection of resistant cancer through multiple mechanisms. Resistance to AR inhibition occurs by overexpression of AR, mutation to the AR ligand-binding domain (LBD) that converts antagonists to agonists, splice variants of AR conferring constitutive AR signaling, intratumor production of androgens, non-canonical activation of AR in the absence of ligand, and increased cytokine signaling.^{145, 150} Currently, a variety of AR antagonists are in clinical trials for the treatment of CRPC, but many of these therapeutics still target the LBD of AR or synthesis of androgens despite a wealth of data demonstrating that drug resistance to these inhibitors inevitably occurs in patients, ultimately leading to death.³³⁰

Studies have shown that truncations to AR yielding only the N-terminal domain (NTD) resulting in AR variants with constitutive signaling.^{118, 331} Similar splice variants containing only the NTD of AR have also been found in patients with CRPC.³³² The NTD of AR is required for transcriptional activation, which contains an activation function 1 (AF 1) region and the DNA-binding domain (DBD).³³³ Currently, there are no FDA-approved treatment options for patients containing splice variants without the LBD of AR. One potential therapeutic, EPI-506 (structure has not been disclosed), which is a pro-drug of EPI-001 (**6.3**), is currently in clinical trials for CRPC.³³⁴ The natural product EPI-001 was isolated from the marine sponge *Geodia lindgreni*, most likely from contaminated water containing bisphenol A, a common industrial chemical used in plastics.¹⁵¹ Sadar and co-workers demonstrated that EPI-001 interacts with the NTD of AR inhibiting transcriptional activity independent of the LBD or non-canonical activation pathways. In vivo xenograft mouse models demonstrated tumor regression with no toxic effects to mice at a maximum dosage of 50 mg/kg.

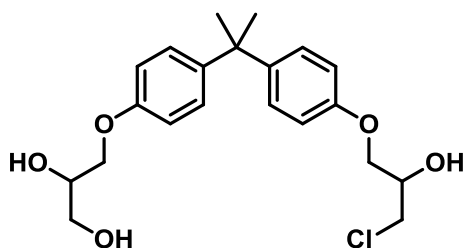
EPI-001 has two racemic stereocenters and thus four possible stereoisomers exist for this racemic compound. Identification of EPI-001 as an AR NTD antagonist led to further work identifying EPI-002 (**6.4**) as the most active and least toxic stereoisomer in cell culture assays and in vivo.¹⁵² Testing of additional analogues suggested that the chlorohydrin of the EPI compounds were necessary for inhibition of AR transcription. Pulldown experiments using analogues of EPI-001 bearing a terminal alkyne demonstrated these compounds are able to undergo irreversible covalent interaction with the NTD of AR. The alkyne containing analogue EPI-054 (**6.5**) has the same stereochemistry as EPI-002 and was able to pulldown AR from live LnCaP cells. However, analysis of the enriched protein-EPI-biotin adducts via Western blot suggests that EPI-054 (and, generally, other EPI compounds) have additional protein targets other than AR.¹⁵²



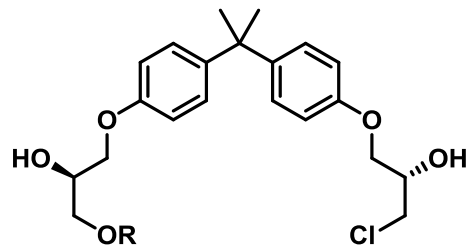
Abiraterone acetate (6.1)



Enzalutamide (6.2)



EPI-001 (6.3)



R = H, EPI-002 (6.4)

R = CH₂CCH, EPI-054 (6.5)

Figure 6.1.1. Abiraterone acetate (6.1) and Enzalutamide (6.2) are FDA approved drugs for CRPC. EPI-001 (6.3) is a natural product that consists of four stereoisomers, which target the NTD of AR. EPI-002 (6.4) is the most active and least toxic stereoisomer of EPI-001. EPI-054 (6.5) contains a propargyl group that enables ligation chemistry for biochemical studies.

In a separate study, EPI-001 was shown to have other potential mechanisms of inhibition within cells that is independent of AR activity.¹⁵³ These studies demonstrate that EPI-001 inhibits expression of full length and truncated AR, and activates PPAR- γ signaling independent of AR. Furthermore, EPI-001 undergoes thiol addition with cysteamine at physiological pH and to a greater extent at pH of 9.4, raising the possibility that covalent modification of solvent exposed cysteines within the cell proteome could occur.

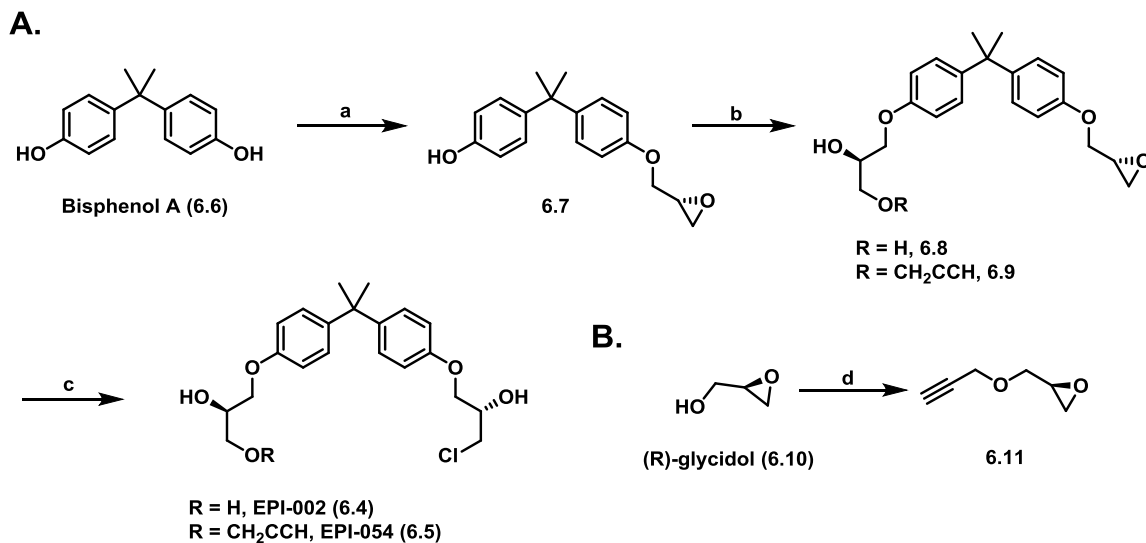
Currently, no other protein targets of EPI derivatives have been reported. The goal of this study is to further evaluate the biological activity and identify other protein targets of EPI-002 within the cell proteome. The derivative EPI-054 serves as a biological probe containing a terminal alkyne with the same stereochemistry as EPI-002. This study shows that EPI-054 maintains similar activity against LnCaP cells and decreases AR expression

compared to EPI-001 and EPI-002. Additionally, in-gel labeling studies demonstrate that EPI-054 labels other proteins besides AR within LnCaP cells. Ongoing experiments are being conducted to identify the protein targets of EPI-001 that could relate to its non-specific activity against prostate cancer cells. This work could be important to enable further optimization of the compound to yield more specific and potent AR NTD inhibitors.

6.2 Synthesis of EPI-002 and EPI-054

The stereoselective synthesis of derivatives EPI-002 and EPI-0054 have been previously described.³³⁵ In this chapter, EPI-002 and EPI-054 are synthesized using different procedures in three linear steps starting from commercial materials.

The synthesis of EPI-002 begins by coupling Bisphenol A (**6.6**) with (S)-glycidol employing the Mitsunobu reaction to give mono-alkylated **6.7** in 49% yield (**Scheme 6.2.1A**). The phenol of intermediate **6.7** opens the epoxide of (R)-glycidol (**6.10**) in the presence of K_2CO_3 at 50 °C to give the diol **6.8** in 49% yield. The epoxide of **6.8** is opened with $CeCl_3$ in refluxing MeCN to give EPI-002 (74% yield, overall yield over three steps is 18%). EPI-054 is synthesized using the same strategy, but (R)-glycidol is first coupled to propargyl bromide using a Williamson ether synthesis to give **6.11** (60% yield, **Scheme 6.2.1B**), which is then reacted with intermediate **6.7** to form the propargyl ether-epoxide **6.9** in 28% yield. Opening of the epoxide ring with $CeCl_3$ produces EPI-054 in 79% yield (11% overall yield over three steps).



Scheme 6.2.1. A. Synthesis of EPI-002 (**6.4**) and EPI-054 (**6.5**).^a

^a**Reagents and Conditions:** (a) (S)-glycidol, Ph₃P, DIAD, THF, 49%; (b) NaH, DMF, (R)-glycidol (**6.10**) or **6.11**, 80 °C, 49% for **6.8**, 28% for **6.9**; (c) CeCl₃, MeCN, reflux, 74% for EPI-002 (**6.4**), 79% for EPI-054 (**6.5**). **B.** Synthesis of propargyl (R)-glycidol precursor **6.11**. (d) NaH, propargyl bromide, TBAI, THF, 60% yield.

6.3 Biological evaluation of EPI-002 and EPI-054

To determine the effect of the propargyl group on EPI-054 compared to EPI-002, both compounds were tested for their cytotoxic properties against LnCaP cells. In a 48 h cytotoxicity assay with LnCaP cells (**Table 6.3.1**), EPI-002 has a high micromolar IC₅₀ value of 108 ± 5 μM. EPI-054 also has a high micromolar IC₅₀ value of 61 ± 6 μM, approximately a 2-fold difference compared to EPI-002.

Table 6.3.1. Cytotoxicity of EPI-002 and EPI-054 in LnCaP cells. Cells were dosed for 48 h and cell viability was indirectly determined by metabolic activity using Alamar Blue. IC₅₀ values are Mean ± S.D. (n ≥ 3).

Compound	IC ₅₀ ± S.D. (μM)
EPI-002	108 ± 5 μM
EPI-054	61 ± 6 μM

The alkyne derivative EPI-054 was further tested for its effects on AR mRNA expression levels compared to that of EPI-001 (**Figure 6.3.1**). Both compounds were dosed to LnCaP cells at 50 μM for 16 h with or without 1 nM of dihydrotestosterone (DHT). The AR mRNA expression levels were determined using qRT-PCR. Dosing DHT

to LnCaP cells has a modest effect on AR mRNA expression levels compared to the non-treated control. Co-dosing DHT with EPI-001 and EPI-054 should cause a further decrease in AR mRNA expression.³³⁶ EPI-001 and EPI-054 have similar inhibition of AR mRNA expression levels in the presence or absence of DHT, and suggests that EPI-001 and EPI-054 inhibit AR mRNA expression indirectly of AR. Approximately a 50% reduction in AR mRNA levels occurs when EPI-001 and EPI-054 are dosed at 50 μ M compared to the non-treated control. These data suggest that EPI-001 and EPI-054 have the same effect on AR expression levels and behave similarly in LnCaP cells. Thus, EPI-054 serves as a probe mimic for EPI-002 for protein identification studies.

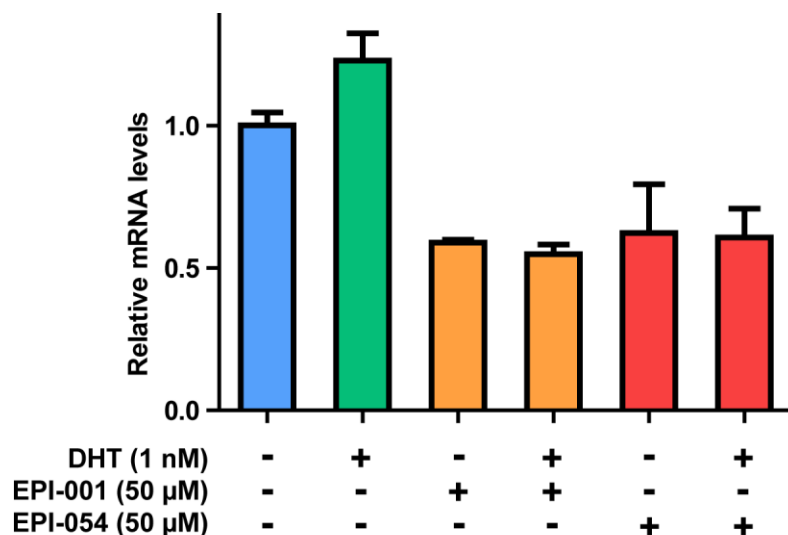


Figure 6.3.1. Relative mRNA levels of AR were determined in LnCaP cells. EPI-001 and EPI-054 were dosed to LnCaP cells at 50 μ M for 16 hours with or without dihydrotestosterone (1 nM). Expression levels were normalized to AR mRNA level of non-treated LnCaP cells and GAPDH mRNA control. Data shown is the mean relative mRNA level \pm S.D. (n = 3).

6.4 In-gel Fluorescent Labeling of EPI-054 in LnCaP Cells

EPI-054 has previously been reported to pull down AR in LnCaP cells. From this study, Western blot analysis of biotin labeled proteins used to identify AR also suggested that other proteins form covalent adducts with EPI-054.¹⁵² To confirm this result an in-gel

fluorescent labeling assay was used to demonstrate that EPI-054 labels multiple proteins within the LnCaP cell proteome.

EPI-054 was dosed to LnCaP cells at 50 μM for 36, 24, and 16 hours (**Figure 6.4.1**). Previous reports suggest that 24 h exposure of EPI-054 is optimal. After dosing the cells for the time indicated the cells were lysed via three freeze thaw cycles and the lysate was cleared by centrifugation. Lysate protein concentrations were normalized to the lowest value and TAMRA- N_3 was attached to the EPI-054-protein adducts with the copper catalyzed [3+2] Huisgen reaction (click chemistry).²²⁰ The proteins were separated with a denaturing PAGE gel and labeled proteins were visualized. The most significant labeling intensity was seen at the 24 h time point. After visualization of the labeled proteins, Oriole® total protein stain was used to show equal total protein concentration loading. Notably, at the 36 h time point the total protein is slightly reduced compared to other time points potentially because of premature cell death due to the long incubation time with EPI-054. The IC_{50} value of EPI-054 is $61 \pm 6 \mu\text{M}$, so presumably significant cell death would occur at 50 μM for 36 h. Therefore, 24 h incubation was determined to be optimal for labeling experiments.

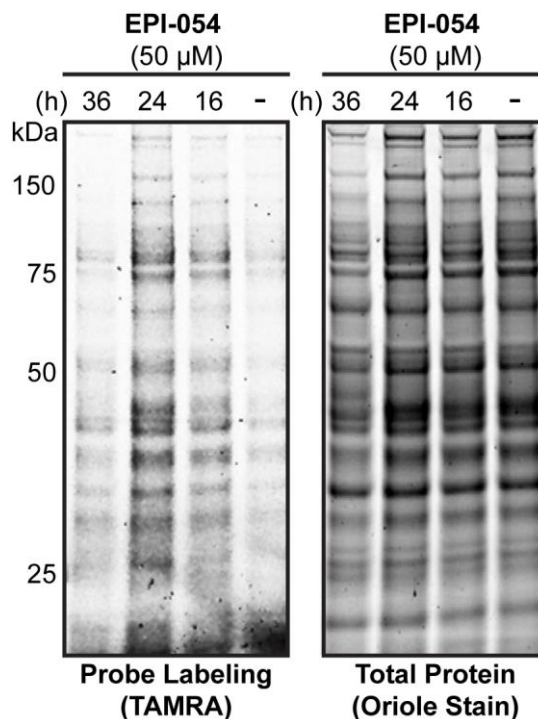


Figure 6.4.1. In-gel fluorescence labeling of EPI-054 in LnCaP cells. Cells were dosed with 50 μM of EPI-054 or a DMSO control for 36, 24, and 16 h. The cells were lysed and TAMRA- N_3 was attached to the EPI-054-protein adducts for visualization. After visualization of labeled protein, the gel was stained with Oriole® total protein stain to demonstrate equal protein loading.

After determining the optimal time for dosing, LnCaP cells were dosed with a DMSO control or EPI-054 at 100, 50, and 25 μM for 24 h (**Figure 6.4.2**). Cells were lysed and protein adducts were conjugated to TAMRA- N_3 in the same manner as the previous labeling experiment (*vide supra*). The fluorescent signal for labeled proteins was strongest at 100 μM , but significant cell death occurred (50% cell viability detected with trypan blue) over the 24 h period. At 50 and 25 μM the same bands can still be visualized compared to the 100 μM dose, but less cytotoxicity was observed (80% cell viability detected with trypan blue). Because of the differences in cell viability, a 50 μM dose was chosen for target identification studies.

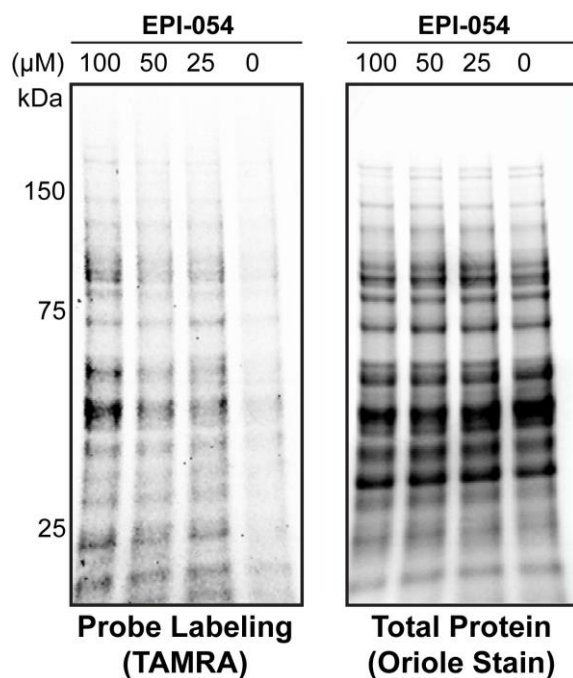


Figure 6.4.2. EPI054 was dosed to LnCaP cells at 100, 50, and 25 μM or a DMSO control for 24 hours. The cells were lysed and TAMRA- N_3 was attached to the probe-protein adducts via click chemistry. After labeling visualization the gel was stained with Oriole total protein stain to demonstrate equal lane loading.

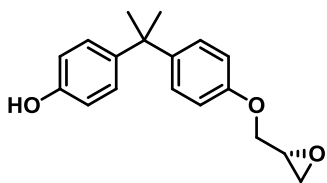
6.5 Conclusion

EPI-002 and EPI-054 were synthesized and shown to be cytotoxic to LnCaP cells at high micromolar concentrations in a 48 h assay. Both compounds inhibit AR mRNA expression levels in LnCaP cells in the presence and absence of DHT suggesting that the decrease of AR mRNA expression is occurring indirectly of AR signaling inhibition. The in-gel fluorescence labeling experiments shows that EPI-054 interacts with many proteins within the LnCaP cell proteome and not just AR. Identifying protein targets using an LC-MS/MS chemoproteomics platform could be useful for future development of EPI based compounds. Work is currently ongoing to identify the putative protein targets of EPI-002 in LnCaP cells.

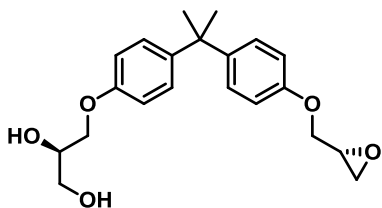
6.6 Experimental

Unless otherwise noted, all reactions were performed in flame-dried glassware sealed with rubber septa under a nitrogen or argon atmosphere and the reaction mixture stirred with a Teflon-coated magnetic stir bar. Commercial grade reagents (Aldrich, Acros, Enzo Life Sciences, and Alfa Aesar) were used without further purification unless otherwise noted. Liquid reagents and solvents were transferred via syringe and cannula using standard techniques. The reaction solvents tetrahydrofuran (THF) and dimethylformamide (DMF) were dried by passage over a column of activated alumina using a solvent purification system (MBraun). Reaction temperatures above 23 °C refer to oil bath temperature, which was controlled by a temperature modulator. Reaction progress was monitored by thin layer chromatography using EMD Chemicals Silica Gel 60 F254 glass plates (250 μm thickness) and visualized by UV irradiation (at 254 nm) and/or KMnO_4 stain. Silica gel chromatography was performed on a Teledyne-Isco Combiflash Rf-200 instrument utilizing Redisep Rf High Performance silica gel columns (Teledyne-Isco) or flash column chromatography was performed using SiliCycle silica gel (32-63 μm particle size, 60 \AA pore size). All NMR spectra to identify compounds were obtained at room temperature and matched to previously reported data unless otherwise specified. References located after compound names refer to literature protocols for the preparation and characterization of these or similar compounds by comparable methods.

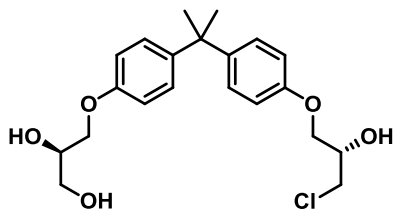
Compounds with absorbance properties at or above 215 nm that were tested in biological assays were tested for purity using analytical HPLC analysis on an Agilent 1200 series instrument equipped with a diode array detector (wavelength monitored = 215 nm) and a Zorbax SBC18 column (4.6x150 mm, 5 μm , Agilent Technologies). All compounds tested in biological assays were > 95% pure by HPLC.



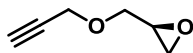
(R)-4-(2-(4-(oxiran-2-ylmethoxy)phenyl)propan-2-yl)phenol (**6.7**). Bisphenol A (**6.6**) (0.50 g, 2.20 mmol), Ph_3P (0.86 g, 3.29 mmol), and (S)-glycidol (0.18 mL, 2.63 mmol) were dissolved in THF (40 mL). DIAD (0.65 mL, 3.29 mmol) was added drop wise at RT and the reaction was stirred for 16 h. The reaction was quenched with aqueous $\text{Na}_2\text{S}_2\text{O}_5$ (sat'd, 20 mL). The reaction was extracted with EtOAc (30 mL, 3X). The combined organic layer was washed with H_2O (20 mL, 1X), brine (20 mL, 1X), and then dried over Na_2SO_4 and concentrated *in vacuo*. The crude product was SiO_2 purified in DCM and EtOAc (0-10%) to afford 0.31 g in 49% yield. The spectral data for this compound matches previously reported data.^{335b}



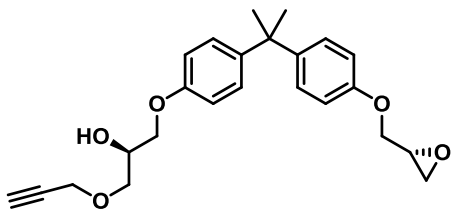
(R)-3-(4-(2-(4-(((R)-oxiran-2-yl)methoxy)phenyl)propan-2-yl)phenoxy)propane-1,2-diol (**6.8**). Compound **6.7** (0.23 g, 0.81 mmol) was dissolved in DMF (20 mL). Then, K_2CO_3 (0.22 g, 1.62 mmol) and (R)-glycidol (**6.10**) (0.16 mL, 2.43 mmol) was added. The reaction was heated to 65 °C for 16 h. The reaction was allowed to cool to RT, quenched with H_2O (25 mL), and extracted with EtOAc (25 mL, 3X). The organic layer was washed with H_2O (20 mL) and brine (20 mL, 1X), then dried over Na_2SO_4 and concentrated *in vacuo*. The crude product was SiO_2 purified in DCM and EtOAc (0-50%) to afford 0.14 g in 49% yield. The spectral data for this compound matches previously reported data.^{335b}



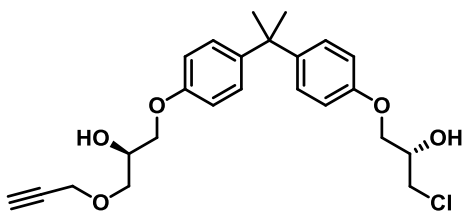
EPI-002 (6.4). The starting material **6.8** (0.14 g, 0.40 mmol) was dissolved in MeCN (5 mL) and $\text{CeCl}_3 \cdot 7\text{H}_2\text{O}$ (0.37 g, 0.98 mmol) was added. The reaction was heated to reflux for 16 h and then allowed to cool to RT before adding H_2O (25 mL). The reaction was extracted with EtOAc (20 mL, 3X). The organic layer was washed with H_2O (20 mL) and brine (20 mL, 1X), dried over Na_2SO_4 , and concentrated *in vacuo*. The crude product was SiO_2 purified in DCM and MeOH (0-10%) to afford 0.11 g in 74% yield. The spectral data for this compound matches previously reported data.^{335b}



(S)-2-((prop-2-yn-1-yloxy)methyl)oxirane (6.11). (R)-glycidol (0.45 mL, 6.75 mmol) was dissolved in THF (10 mL). The reaction was cooled to 0 °C and NaH (0.18 g, 7.43 mmol) was added and allowed to stir for 20 min at the same temperature. *tert*-Butyl ammonium iodide (TBAI) (0.25 g, 0.67 mmol) was added, and then propargyl bromide (2.0 mL, 13.49 mmol, 80% by mass in toluene) was added dropwise. The reaction was allowed to come to RT and stirred for 4 h. The reaction was quenched with aqueous NH_4Cl (sat'd, 10 mL), extracted with Et_2O (20 mL, 3X), dried over Na_2SO_4 , and concentrated *in vacuo*. The crude product was SiO_2 purified in hexanes and EtOAc (0-20%) to afford 0.46 g in 60% yield. The spectral data for this compound matches previously reported data.³³⁷



(R)-1-(4-(2-(4-(((R)-oxiran-2-yl)methoxy)phenyl)propan-2-yl)phenoxy)-3-(prop-2-yn-1-yloxy)propan-2-ol (6.9). Compound **6.7** (1.03 g, 3.52 mmol) and **6.11** (1.01 g, 8.79 mmol) were dissolved in DMF. K_2CO_3 (0.99 g, 7.03 mmol) was added and the reaction was heated to 65 °C for 16 h. The reaction was allowed to cool to RT and quenched with H_2O (40 mL). The reaction was extracted with EtOAc (40 mL, 3X). The organic layer was washed with H_2O (20 mL) and brine (20 mL, 1X), then dried over Na_2SO_4 and concentrated *in vacuo*. The crude product was SiO_2 purified in hexanes and EtOAc (0-40%) to afford 0.38 g in 28% yield. The spectral data for this compound matches previously reported data.^{335a}



EPI-054 (6.5). The starting material **6.9** (0.38 g, 1.06 mmol) was dissolved in MeCN (15 mL) and $CeCl_3 \cdot 7H_2O$ (0.99 g, 2.65 mmol) was added. The reaction was heated to reflux for 16 h and then allowed to cool to RT before adding H_2O (40 mL). The reaction was extracted with EtOAc (30 mL, 3X). The organic layer was washed with H_2O (20 mL) and brine (20 mL, 1X), then dried over Na_2SO_4 and concentrated *in vacuo*. The crude product was SiO_2 purified in hexanes and EtOAc (0-50%) to afford 0.33 g in 79% yield. The spectral data for this compound matches previously reported data.^{335a}

Cell Culture

LnCaP cells were maintained in a humidified 5% CO₂ environment at 37 °C in tissue culture flasks (Corning) under normoxic conditions and cultured in Roswell Park Memorial Institute (RPMI) 1640 media that contains 10% FBS, 100 I.U./mL penicillin, and 100 µg/mL streptomycin. Adherent cells were dissociated using Trypsin-EDTA solution (0.25%, Gibco).

Human cancer cell line cytotoxicity assays

Alamar blue cellular cytotoxicity assays and data analyses were performed as previously described.^{219, 237} LnCaP cells were seeded at a density of 5,000 cells/well in media (50 µL) in 96-well plates (Costar 3595, Corning, Inc.).

Relative AR mRNA expression assay

LnCaP cells were grown to 80% confluency in 10 cm cell plates and were dosed with DMSO, EPI-001, or EPI-054 at 50 µM with or without DHT (1 nM) for 16 h. After the incubation period total RNA isolated according and qRT-PCR was conducted for relative quantitation of AR mRNA expression levels according to a previously published procedure.³³⁸ The primers used for qRT-PCR are as follows, GAPDH-F: 5'-GAA GGT GAA GGT CGG AGT C-3'; GAPDH-R: 5'-GAA GAT GGT GAT GGG ATT TC-3', AR-F 5'-TGG ATG GAT AGC TAC TCC GG-3', AR-R: 5'-CCC AGA AGC TTC ATC TCC AC-3'. Expression levels were normalized to the non-treated control and GAPDH control gene.

In-gel labeling assay

LnCaP cells were grown in T-75 cm² flasks to 90% confluency and dosed with DMSO or EPI-054 at the respective concentration for the time indicated. Cells were dissociated from the flask using trypsin-free EDTA buffer (Gibco) then washed with 1X

PBS (10 mL, 2X). Cells were centrifuged at 1000 rpm for 5 minutes between washes. The cells were suspended in 1X PBS containing EDTA-free protease inhibitor cocktail (Pierce) and lysed using three freeze thaw cycles. The freeze thaw cycles were conducted by snap freezing the samples in an acetone/dry ice bath for 5 minutes and then immediately transferring them to a 37 °C water bath until completely thawed (typically 3-5 minutes). After the third freeze thaw cycle, the cells were kept at -80 °C until further use.

Cell lysates were allowed to thaw and lysates were cleared by centrifugation at 4000 RPM for 20 minutes at RT. Lysates were processed and visualized according to a previously reported procedure.²²⁹

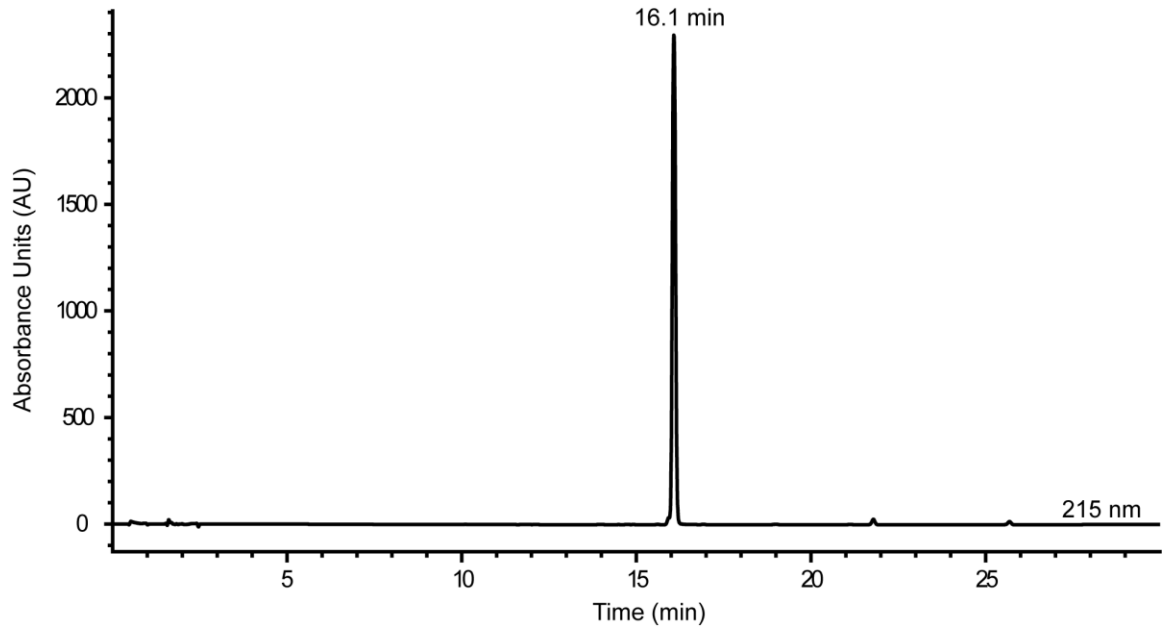
6.7 HPLC Chromatograms of Synthesized Compounds

General Protocol for HPLC Analysis of Synthesized Compounds

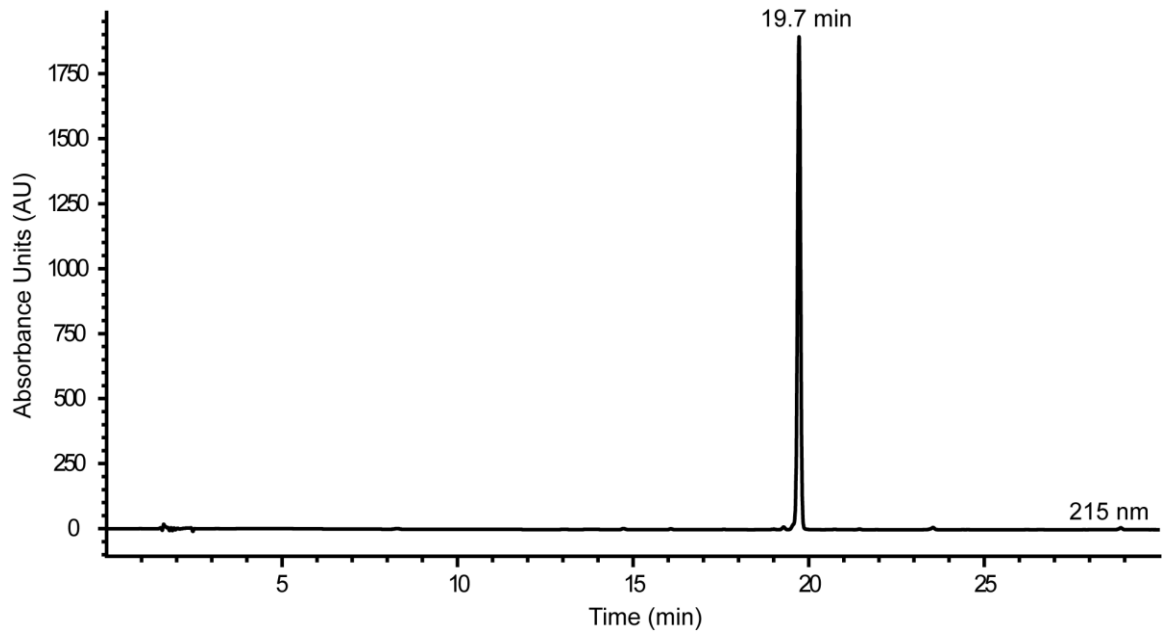
DMSO stock solutions of newly synthesized molecules were dissolved in 1:1 solution of methanol and distilled and deionized water (ddH₂O) containing trifluoroacetic acid (TFA, 0.1% v/v) and analyzed on an Agilent 1200 series instrument equipped with a diode array detector and Zorbax SB-C18 column (4.6 x 150 mm, 5 μm, Agilent Technologies). The analysis method (1 mL/min flow rate) starts with an eluent system of 10% MeCN in ddH₂O from 0-2 minutes (both containing 0.1% TFA) followed by a linear gradient of 10% to 85% MeCN in ddH₂O from 2-24 minutes, followed by 85% to 95% MeCN in ddH₂O from 24-26 minutes, and finally an isocratic eluent system of 95% MeCN in ddH₂O from 26-30 minutes. Wavelengths monitored = 215 nm.

Preparation of Stock Solutions. Compound stock solutions were prepared in DMSO (40 mM to 100 mM concentrations) and stored at -20 °C when not in use. Compound purities were assessed frequently by analytical reverse-phase HPLC analysis and fresh solutions were prepared as needed.

Probe EPI-002 (6.4) HPLC (>99% pure):



Probe EPI-054 (6.5) HPLC (>99% pure):



Chapter 7

ALKYNE LIGATION HANDLES: PROPARGYLATION OF HYDROXYL, SULFHYDRYL, AMINO, AND CARBOXYL GROUPS VIA THE NICHOLAS REACTION

Adapted with Permission from:

Wells, S.M.; Widen, J.C.; Harki, D.A.; Brummond, K.M. *Org. Lett.* **2016**, *18*, 4566-4569.

This work was performed in collaboration with Dr. Sarah M. Wells, Professor Daniel A. Harki, and Professor Kay M. Brummond. Sarah Wells completed the reaction optimization studies in **Table 7.2.1** and conducted the Nicholas reaction on substrates included in **Table 7.3.1**, **Scheme 7.3.1**, and **Scheme 7.4.1**. John Widen also synthesized analogues presented in **Table 7.3.1**, **Scheme 7.3.1**, and **Scheme 7.4.1**.

7.1 Introduction

Widespread use of the Huisgen 1,3-dipolar cycloaddition between azides and alkynes to form 1,2,3-triazoles, a click reaction,^{220, 296} has led to increased interest in transformations used to synthesize and/or install alkynyl groups.³³⁹ Typically, when readying substrates for a click reaction, late-stage propargylation or 5-hexynoation reactions of hydroxyl or amino groups are used to attach the desired alkynes.³³⁹ Propargylation of a hydroxyl group is usually achieved by a Williamson ether synthesis under basic conditions where the corresponding alkoxide is reacted with propargyl bromide (**Figure 7.1.1, eq 1**). Src-directed probe **7.1** was prepared using this approach but required protection of the 3'- and 5'-hydroxyl groups and 6-amino group to avoid over propargylation.³⁴⁰ Propargylation has also been accomplished by converting a hydroxyl group into a leaving group (i.e., a mesylate) and replacing it with propargylamine.³⁴¹

Another commonly used protocol for installing an alkynyl group is a carbodiimide-mediated coupling reaction between 5-hexynoic acid and a hydroxyl or amino group (**Figure 7.1.1, eq 2**).^{296a, 342} The Duocarmycin probe **7.2** exemplifies a product obtained from an EDCI-mediated coupling reaction between a cyclic, secondary amino group and 5-hexynoic acid.³⁴³ While carbodiimide couplings offer non-basic, neutral conditions, they require expensive reagents and/or the tedious removal of urea-related byproducts.

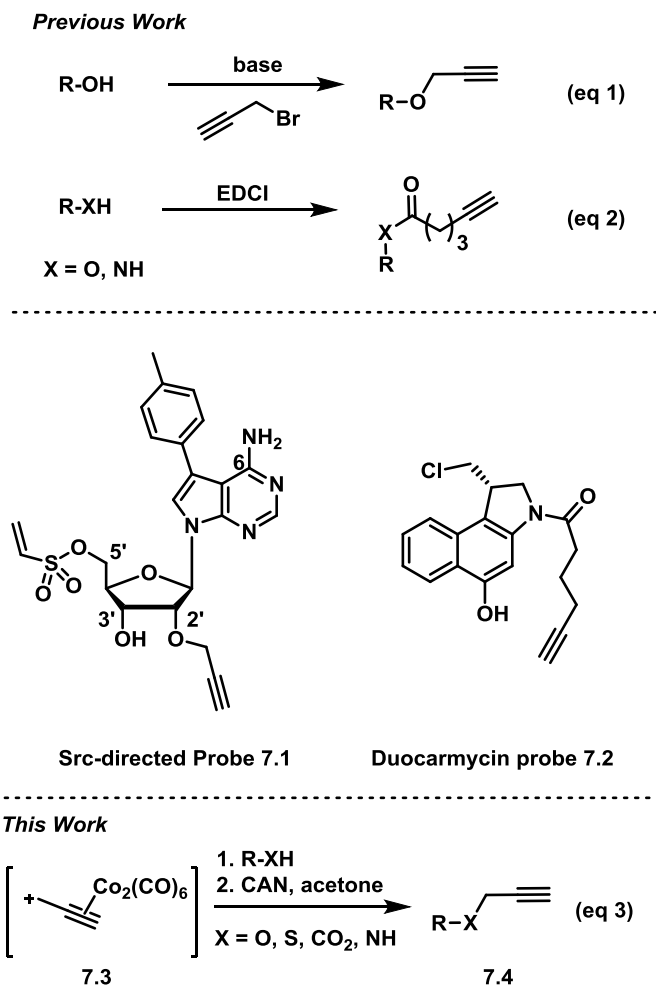


Figure 7.1.1. Synthetic methods for alkyne incorporation.

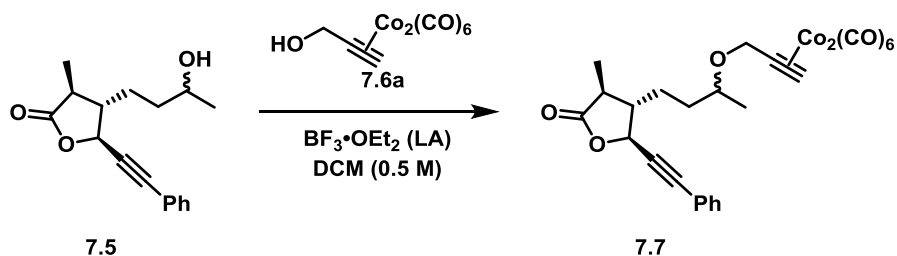
Many other methods are available for the functionalization of a compound with an alkynyl group,^{339, 344} however, despite these options, challenges still arise when alkynylating functionally dense natural products and chemical probes for applications such as activity-based protein profiling³⁴⁵ for target identification.³⁴⁶ For example, during investigations to label two different sesquiterpene analogues with alkynyl groups (*vide infra*), these analogues were unstable to the basic conditions required for propargylation. Although the hexynoylation reaction could serve as an alternative for appendage of an alkyne ligation handle via an allylic ester linkage, concerns about the metabolic stability of ester-containing probes in cell culture lowered enthusiasm for this approach.³⁴⁷

Consequently, a method for propargylation of these sesquiterpene analogues and other biomechanistic probes under non-basic conditions was needed.

We report our studies to establish the Nicholas reaction as an alternative protocol for the propargylation of high-value small molecules. The Nicholas reaction involves the addition of a nucleophile to the Co-stabilized propargylic carbocation **7.3**, generated by treating the corresponding dicobalt hexacarbonyl complexed ($\text{Co}_2(\text{CO})_6$)-propargyl alcohol with acid. Alkyne **7.4** is formed after oxidative decomplexation (**Figure 1, eq 3**).³⁴⁸ While it is well-known that the Nicholas reaction can be used to effect propargylation reactions of heteronucleophiles, classical conditions require excess nucleophile relative to the cobalt–carbonyl complex, even as the solvent in some cases, limiting its utility in the preparation of alkyne ligation handles.³⁴⁹ Conditions where the nucleophile is the limiting reagent would expand the utility of this approach.

7.2 Optimization of Nicholas Reaction Conditions

To increase the efficiency of the Nicholas reaction, we began our investigations using molecularly complex alcohol **7.5** as the limiting reagent. Initially, a reaction was carried out with a 1:1.1:1.4 ratio of nucleophile **7.5/7.6a**/ BF_3OEt_2 . However, these conditions led to a moderate yield of 40%, so we focused on using higher equivalents of **7.6a** and BF_3OEt_2 . We varied the molar equivalencies of **7.6a** and the Lewis acid (BF_3OEt_2) while keeping the order of addition constant. To reduce the likelihood of the alcohol and ester groups of **7.5** tying up the BF_3OEt_2 , $\text{Co}_2(\text{CO})_6$ -propargyl alcohol **7.6a** was added to BF_3OEt_2 to form the propargyl cation, followed by the addition of alcohol **7.5**. Using this addition order and a 1:2:2.5 molar ratio of alcohol **7.5/7.6a**/ BF_3OEt_2 , $\text{Co}_2(\text{CO})_6$ -propargyl ether **7.7** was obtained in 47% yield (**Table 7.1, entry 1**) after stirring 4.5 h at 0 °C. Increasing the equivalents of BF_3OEt_2 and **7.6a** afforded **7.7** in 36% yield (**entry 2**). Adding alcohol **7.5** more slowly lowered the yield of **7.7** to 28% (**entry 3**).

Table 7.2.1. Optimization of Nicholas Reaction with Alcohol **7.5**

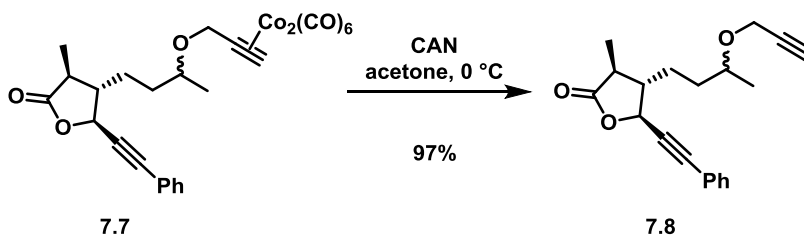
entry	equiv (7.5 : 7.6a :LA)	order of addition	temp (°C)	time (h)	yield (%)
1 ^a	1:2:2.5	LA, 7.6a , 7.5	0	4.5	47
2	1:3:5	LA, 7.6a , 7.5	0	4	36
3	1:2:2.5	LA, 7.6a , 7.5 ^c	0	4	28
4 ^a	1:2:2.5	LA, 7.5 , 7.6a	0	4.5	44
5 ^b	1:2:2.5	7.6a , 7.5 , LA	0	4	55
6	1:3:5	7.6a , 7.5 , LA	0	5	22
7 ^b	1:2:2.5	7.6a , 7.5 , LA ^d	0	3.5	60

^aDimerized product of **7.6a** was isolated in 33-34% yield. ^bDimerized product of **7.6a** was isolated in 25-28% yield. ^cAlcohol **7.5** was added dropwise over 5 min.

^dComplex **7.6a** was generated *in situ* from propargyl alcohol and Co₂(CO)₈.

Due to these results, the order of addition was examined. Adding **7.5** to BF₃OEt₂ prior to addition of **7.6a** did not affect the yield of **7.7**, obtained in 44% yield (**entry 4**). Next, **7.5** (1 equiv) and BF₃OEt₂ (2.5 equiv) were added sequentially to **7.6a** (2 equiv), which increased the yield of **7.7** to 55% (**entry 5**). With this same order of addition, increasing the amount of **7.6a** and BF₃OEt₂ lowered the yield of **7.7** to 22% (**entry 6**). For all of these examples, **7.6a** was prepared, isolated, and purified by column chromatography before the reaction. Although this complex is stable to air and moisture, it was reasoned that forming **7.6a** *in situ* may be advantageous.^{349c} To this end, **7.6a** was formed *in situ* from propargyl alcohol and dicobalt octacarbonyl, followed by the sequential addition of **7.5** and BF₃OEt₂ to afford the highest yield of **7.7** (60%, **entry 7**). A final attempt to improve the reaction conditions by lowering the reaction temperature only resulted in decreased yields of **7.7**. Reactions at -40 °C and -10 °C afforded **7.7** in

23 and 38% yield, respectively. Decomplexation of cobalt complex **7.7** was achieved using ceric ammonium nitrate (CAN) in acetone to readily afford alkyne **7.8** in 97% yield without the need for purification (**Scheme 7.2.1**). Use of N-methylmorpholine-N-oxide as an oxidant in this transformation resulted in decomposition of **7.7**.³⁵⁰



Scheme 7.2.1. Decomplexation of $\text{Co}_2(\text{CO})_6$ -alkyne **7.7**.

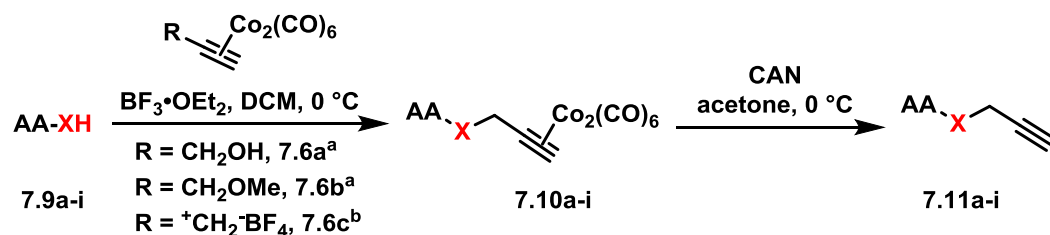
7.3 Application of the Optimized Nicholas Reaction Conditions to Amino Acids

Next, the generality of these optimized reaction conditions was tested on hydroxyl-, sulfhydryl-, amino-, and carboxyl-containing amino acids: a class of compounds selected for their richness of functionality and the utility of propargylated peptides for biochemical applications.^{296c, 339a, 351} Unfortunately, when subjecting N-Boc-L-serine methyl ester (**7.9a**) to the optimized reaction conditions, **7.10a** was obtained in 20% yield while 76% of the starting material **7.9a** was recovered (**Table 2, entry 1**). Similarly, when N-Fmoc-L-serine methyl ester (**7.9b**) was subjected to the same conditions, **7.10b** was isolated in 29% yield with 63% recovered **7.9b** (**entry 3**). In both of these examples, **7.6a** was fully consumed and the dimerized product of **7.6a** was obtained, resulting from the propargylium cation reacting more readily with the hydroxyl group of **7.6a**. To overcome this competing homodimerization reaction, $\text{Co}_2(\text{CO})_6$ -methyl propargyl ether **7.6b** was examined.^{348c} Reaction of **7.9a** with **7.6b** afforded **7.10a** in 97% yield (**entry 2**). The yield of **7.10b** also increased significantly to 54% when using **7.6b** (**entry 4**). Use of propargyl acetate for the synthesis of **7.10a** and **7.10b** gave yields comparable to those of **7.6a**.

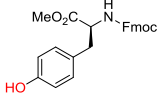
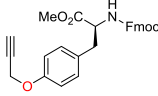
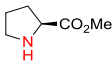
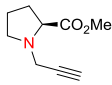
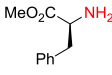
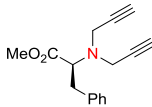
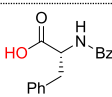
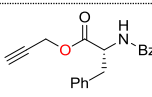
Next, we tested this method for the propargylation of cysteine thiols; a transformation typically accomplished using basic alkylation conditions.^{220, 352} Thiols react efficiently in the Nicholas reaction; however, application has been limited to the synthesis of sulfur-containing macrocycles.^{348c, 353} N-Acetyl- and N-Fmoc-L-cysteine ethyl ester (**7.9c** and **7.9d**) were reacted with **7.6a**, giving the corresponding Co₂(CO)₆-alkynes **7.10c** and **7.10d** in high yields of 86 and 71% (**entries 5** and **6**). N-Fmoc cysteine **7.9d** was also reacted with **7.6b**, which gave a comparable yield of 67% for **7.10d** (**entry 7**).

To evaluate the phenolic side chain of tyrosine in the Nicholas reaction, N-Boc-L-tyrosine methyl ester (**7.9e**) was reacted with **7.6a**.^{349a} Two major products were observed; the desired product, **7.10e**, was isolated in 45% yield (57% based on recovered **7.9e**) (**entry 8**), and an unstable byproduct was obtained in trace amounts. ¹H NMR analysis of this byproduct revealed aromatic signals integrating for three protons, resulting from electrophilic aromatic substitution (**7.19**).^{348c} Because **7.9e** was recovered along with complete consumption of **7.6a**, **7.6b** was tested. This reaction required a longer reaction time and did not improve the yield of **7.10e** (23% yield, **entry 9**) due to Boc instability.³⁵⁴ When the N-Fmoc tyrosine ester **7.9f** was reacted with complex **7.6a**, **7.10f** was formed in 6% yield (56% based on recovered starting material) (**entry 10**). Employing **7.6b** resulted in a significantly improved yield to 73% (**entry 11**). A byproduct, presumably formed by electrophilic aromatic substitution, was also observed by TLC for these reactions.

Table 7.3.1. Synthesis of alkyne modified amino acids (AA).



entry	AA-XH, 7.9	7.6	time (h)	7.10, yield (%)	7.11, yield (%)
1	 7.9a	7.6a	1	7.10a, 20	 7.11a, 90
2	7.9a	7.6b	1	7.10a, 97	
3	 7.9b	7.6a	1	7.10b, 29	 7.11b, 90
4	7.9b	7.6b	1	7.10b, 54	
5	 7.9c	7.6a	2	7.10c, 86	 7.11c, 83
6	 7.9d	7.6a	0.75	7.10d, 71	 7.11d, 92
7	7.9d	7.6b^c	2	7.10d, 67	
8	 7.9e	7.6a	1	7.10e, 45	 7.11e, 75
9	7.9e	7.6b	3	7.10e, 23	

10		7.6a	1	7.10f , 6	
	7.9f				7.11f , 81
11	7.9f	7.6b	1	7.10f , 73	
12		7.6a	0.25	7.10g , 0	
	7.9g				7.11g^d
13	7.9g	7.6c	1.5	7.10g , 46	
14		7.6c	1.5	7.10h , 59	
	7.9h				7.11h , 56
15		7.6a	2	7.10i , 60	
	7.9i				7.11i , 90
16	7.9i	7.6c	2	7.10i , 18	

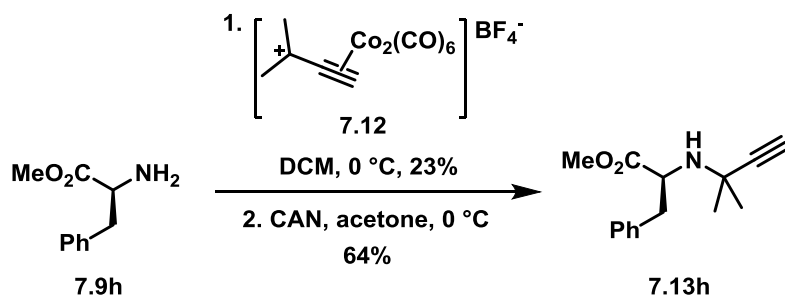
Nucleophilic group (-XH) of amino acid (AA) highlighted in red. ^aComplexes **7.6a** and **7.6b** were formed *in situ*. ^bBF₃OEt₂ is not used when using **7.6c**. ^cUse of isolated **7.6b** gave highest yield. ^d**7.11g** is unstable.

Amino groups were tested by subjecting L-proline methyl ester (**7.9g**) to the Nicholas reaction with **7.6a**. Consumption of **7.9g** was observed by TLC within 15 min with no evidence of **7.10g** (**entry 12**). We presume the BF₃OEt₂ coordinates with the nitrogen of proline. To circumvent this issue, the cationic propargylium ion was prepared as tetrafluoroborate salt **7.6c** by reacting complex **7.6a** with tetrafluoroboric acid in diethyl ether at 0 °C.^{348b, 355} Reaction of **7.6c** with **7.9g** in DCM at 0 °C afforded Co₂(CO)₆-alkyne **7.10g** in 46% yield (**entry 13**). The primary amine of L-phenylalanine methyl ester (**7.9h**) also proved to be an effective nucleophile; when reacted with **7.6c**, dialkylation afforded amine **7.10h** in 59% yield (**entry 14**).

Carboxyl groups were also subjected to the Nicholas reaction conditions. Only a few examples of carboxyl groups serving as a nucleophile in the Nicholas reaction have been reported.³⁵⁶ Reaction of N-Bz-D-phenylalanine (**7.9i**) with **7.6a** and BF_3OEt_2 afforded $\text{Co}_2(\text{CO})_6$ -propargyl ester **7.10i** in 60% yield (**entry 15**). Reaction of **7.9i** with **7.6c** afforded a lower yield for **7.10i** (18%, **entry 16**); thus, the utility of preformed propargylium salt is not necessarily general.

$\text{Co}_2(\text{CO})_6$ -alkyne-modified amino acids **7.10a–i** underwent oxidative decomplexation with CAN. Propargyl derivatives of serine, cysteine, tyrosine, and phenylalanine **7.11a–f,i** were afforded in high yields (75–94%). A moderate yield of 56% was observed for the formation of dipropargylamine **7.11h** (**entry 14**). Proline alkyne derivative **7.11g** appeared to be unstable, permitting isolation and NMR characterization only once prior to decomposition (**entry 12**).

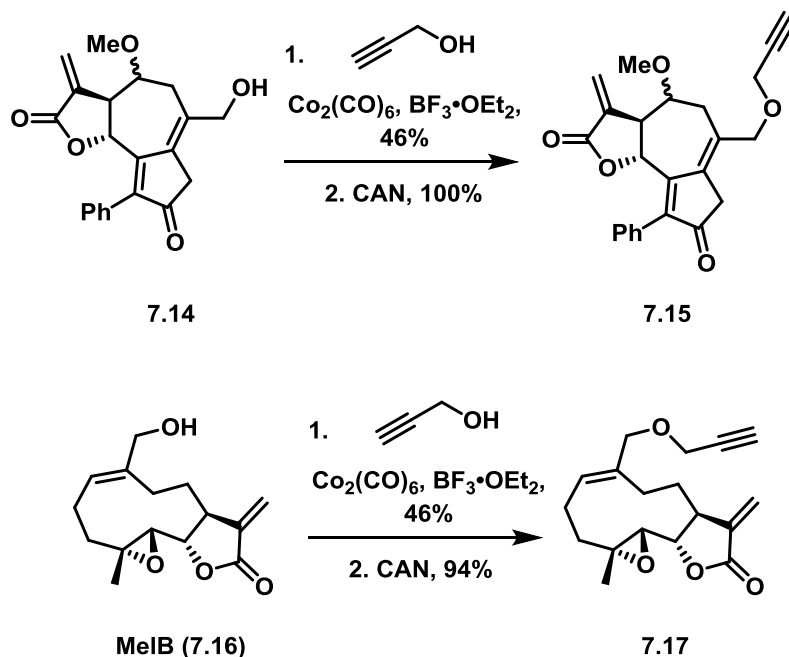
To effect monoalkynylation of primary amines, an alternative tetrafluoroborate salt **7.12** was prepared from $\text{Co}_2(\text{CO})_6$ -2-methyl-3-butyn-2-ol (**Scheme 7.3.1**). Reaction of **7.12** with **7.9h** afforded the monoalkynylated propargylamine **7.13** after oxidative decomplexation.



Scheme 7.3.1. Reaction of **7.9h** with BF_4^- **7.12**.

7.4 Application of the Nicholas Reaction to Complex, Base-sensitive Small Molecules

Finally, to show the synthetic utility of these conditions for base-sensitive, functionally dense molecules, we applied the Nicholas reaction conditions to two sesquiterpene analogues (**Scheme 7.4.1**). Base-sensitive guaianolide analogue **7.14**, previously synthesized in the Brummond group,²³⁷ was reacted with **7.6a**, formed in situ, and BF_3OEt_2 to give the $\text{Co}_2(\text{CO})_6$ -alkyne derivative in 46% yield. Reaction with CAN generated alkyne probe **7.15** in quantitative yield.



Scheme 7.4.1. Synthesis of alkyne probes **7.15** and **7.17**.

Melampomagnolide B (**MeIB**, **7.16**) was used as a parthenolide mimic for conjugation to biotin via an ester linkage.^{262a, 357} However, these biotinylated compounds may have metabolic stability issues for in vivo biochemical experiments. Formation of the alternative ether linkage using the allylic alcohol handle has proven to be difficult; **MeIB** is base-sensitive, and the allylic hydroxyl group was unreactive in our hands toward oxidation or bromination. Attempts to manipulate the allylic alcohol of **MeIB** included use of PCC, PDC, Dess-Martin periodinane, and PBr_3 . Reaction of **MeIB** with

7.6a and BF_3OEt_2 afforded the corresponding $\text{Co}_2(\text{CO})_6$ -alkyne product after 1 h in 19% yield. A shortened reaction time of 10 min gave a 41% yield (45% yield based on recovered **7.16**), suggesting the $\text{Co}_2(\text{CO})_6$ -alkyne product was unstable to the reaction conditions. Reacting **7.16** with **7.6b** gave a 39% yield of the coupled product. Cobalt decomplexation afforded the MeIB alkyne probe **7.17** in 94% yield.

7.5 Conclusion

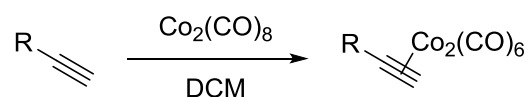
The Nicholas reaction conditions described provide an acid-mediated alternative for propargylation of molecularly complex compounds. Reaction conditions were optimized for use of high-value nucleophiles as limiting reagents, a practice atypical for the Nicholas reaction. A number of functional groups acted as the nucleophilic species, including hydroxyl, sulfhydryl, carboxyl, and amino groups. For substrates that react slower than the competing dimerization of **7.6a**, use of **7.6b** improved yields. Propargylation of amino groups required the preparation of propargylium tetrafluoroborate salts. Mono- and dialkynylation of a primary amino group was achieved selectively depending on the steric nature of the propargylium ion. Bz, Cbz, Ac, and Fmoc amine protecting groups were all tolerated. Finally, these conditions provided an alternative propargylation strategy for base-sensitive sesquiterpene analogues.

7.6 Experimental

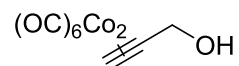
All commercially available compounds were used as received unless otherwise noted. Dichloromethane, diethyl ether, and tetrahydrofuran were purified by passing through alumina using a solvent purification system. Deuterated chloroform (CDCl_3) was stored over 4 Å molecular sieves. $\text{BF}_3\cdot\text{OEt}_2$ was used as received or redistilled under a nitrogen atmosphere. Dicobalt octacarbonyl ($\text{Co}_2(\text{CO})_8$) was used as purchased and was stored at $-20\text{ }^\circ\text{C}$ and opened only in a nitrogen filled glove box. Purification of compounds via manual flash column chromatography or with a CombiFlash Rf200 instrument (Teledyne Isco) was performed using silica gel (40-63 μm particle size, 60 Å pore size) purchased from Sorbent Technologies or SiliCycle. TLC analyses were

performed on SiliCycle SiliaPlate G silica gel glass plates (250 μm thickness) or EMD Chemicals Silica Gel 60 F254 glass plates (250 μm thickness) and visualized by UV irradiation (at 254 nm) and KMnO_4 stain. ^1H NMR and ^{13}C NMR spectra were recorded on Bruker Avance 300 MHz, 400 MHz, 500 MHz, or 600 MHz. Spectra were referenced to residual chloroform with or without 0.05% v/v TMS (7.26 ppm, ^1H ; 77.16 ppm, ^{13}C). Chemical shifts are reported in ppm, multiplicities are indicated by s (singlet), bs (broad singlet), d (doublet), t (triplet), q (quartet), p (pentet), and m (multiplet). Coupling constants, J , are reported in hertz (Hz). All NMR spectra were obtained at room temperature. IR spectra were obtained using a Nicolet Avatar E.S.P. 360 or a Perkin Elmer Spectrum 100 (NaCl plate) FT-IR. ESI mass spectrometry was performed on a Waters Q-TOF Ultima API, Micromass UK Limited or a Thermo Fisher OrbiTrap Velos high resolution mass spectrometer.

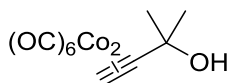
General Procedures



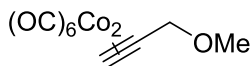
General Procedure A: Coordination of alkyne to cobalt carbonyl complex. A single-necked, round-bottomed flask, equipped with a stir bar and a septum, was charged with dicobalt octacarbonyl (1 equiv) in a N_2 filled glove box. The flask was transferred out of the glove box and the septum was pierced with a nitrogen inlet needle. The flask was charged with dichloromethane, followed by the alkyne (1 equiv), dissolved in dichloromethane. The reaction stirred for 2 h, until evolution of CO gas, visible by small bubbles, was no longer observed. The contents were loaded directly onto a silica gel column for purification by flash column chromatography to afford the dicobalt hexacarbonyl complexed alkyne ($\text{Co}_2(\text{CO})_6$ -alkyne).



Dicobalt hexacarbonyl complexed propargyl alcohol (**7.6a**). Followed general procedure A: Dicobalt octacarbonyl (793 mg, 2.3 mmol, 1.3 equiv), dichloromethane (1.5 mL), propargyl alcohol (0.10 mL, 1.8 mmol, 1 equiv), dissolved in dichloromethane (2.5 mL). The reaction was stirred for 2 h. The silica gel flash column chromatography was run with a gradient of 10-20% ethyl acetate in hexanes to afford 615 mg of $\text{Co}_2(\text{CO})_6$ -propargyl alcohol **7.6** in quantitative yield, as a dark red solid. ^1H NMR (300 MHz, CDCl_3) 6.08 (s, 1H), 4.81 (d, $J = 6.0$ Hz, 2H), 1.79 (t, $J = 6.0$ Hz, 1H) ppm. Melting Point: 48-52 °C. $R_f = 0.28$ (10% ethyl acetate in hexanes) Silica gel, visible (red).

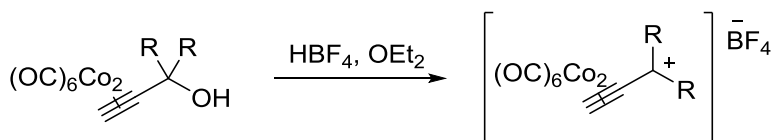


Dicobalt hexacarbonyl complexed 2-methyl-3-butyn-2-ol (**7.18**). Followed general procedure A: Dicobalt octacarbonyl (1.37 g, 4.0 mmol, 1.0 equiv), dichloromethane (15 mL), 2-methyl-3-butyn-2-ol (344 mg, 4.0 mmol, 1 equiv), dissolved in dichloromethane (5 mL). The reaction was stirred for 2 h. The silica gel flash column chromatography was run with a gradient of 10-30% ethyl acetate in hexanes to afford 1.36 g of $\text{Co}_2(\text{CO})_6$ -2-methyl-3-butyn-2-ol **7.18** in 92% yield, as a dark red solid. ^1H NMR (300 MHz, CDCl_3) 6.03 (s, 1H), 1.71 (s, 1H), 1.59 (s, 6H) ppm. Impurities observed at 1.54, 1.27, 0.88 ppm. Melting Point: 37.9-40.1 °C. $R_f = 0.26$ (20% diethyl ether in hexanes) Silica gel, visible (red).

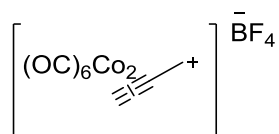


Dicobalt hexacarbonyl complexed methyl propargyl ether (**7.6b**). Followed general procedure A: Dicobalt octacarbonyl (195 mg, 0.57 mmol, 1 equiv), dichloromethane (1.5 mL), methyl propargyl ether (40 mg, 0.57 mmol, 1 equiv), dissolved in dichloromethane (3.0 mL). The reaction was stirred for 1.5 h. The silica gel flash column chromatography was run with a gradient of 0-2.5% diethyl ether in hexanes to afford 94 mg of $\text{Co}_2(\text{CO})_6$ -methyl propargyl ether **7.6b** in 45% yield, as a dark red oil. Drying under high vacuum

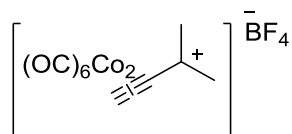
was not performed due to the volatility of the parent compound. ^1H NMR (300 MHz, CDCl_3) 6.06 (s, 1H), 4.60 (s, 2H), 3.49 (s, 3H) ppm. $R_f = 0.59$ (10% diethyl ether in hexanes) Silica gel, visible (red).



General Procedure B: Formation of propargylium tetrafluoroborate salts. A flame-dried 100 mL Schlenk flask equipped with a stir bar and septum was charged with either $\text{Co}_2(\text{CO})_6$ -propargyl alcohol **7.6a** or $\text{Co}_2(\text{CO})_6$ -2-methyl-3-butyn-2-ol (**7.18**), dissolved in diethyl ether. The flask was cooled to $-10\text{ }^\circ\text{C}$ on an ice/acetone bath. Tetrafluoroboric acid (54% by weight solution in diethyl ether, 1.5 equiv) was added dropwise and the solution stirred for 2 h. Formation of a dark red precipitate was observed. The reaction was diluted with diethyl ether. The septum was replaced with a Schlenk filtration apparatus. The apparatus was inverted and partial vacuum was applied to separate the solid from the ether solution within the apparatus. The ether filtrate was removed via syringe and the crystals were dried under vacuum. The apparatus was transferred to the nitrogen filled glove box, where the crystals were isolated and stored.

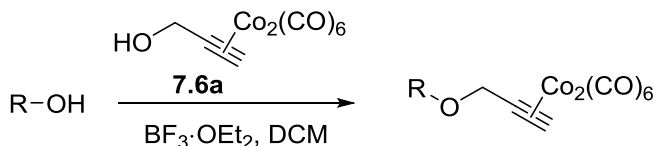


α -(Ethynyl)dicobalt hexacarbonyl carbonium tetrafluoroborate salt (**7.6c**).³⁵⁸ Follows General procedure B: $\text{Co}_2(\text{CO})_6$ -propargyl alcohol **7.6a** (500 mg, 1.46 mmol, 1 equiv), diethyl ether (5 mL), tetrafluoroboric acid (356 mg of a 54% by weight solution in diethyl ether, 2.19 mmol, 1.5 equiv). The reaction was diluted with diethyl ether (20 mL) prior to filtration and drying which afforded 601 mg of salt **7.6c** in 60% yield as a red solid. Due to sensitivity to water and air, the salt was stored in the glove box and used within 24 h of isolation for best results.



α -(Dimethylethynyl)dicobalt hexacarbonyl carbonium tetrafluoroborate salt (**7.12**). Follows General procedure B: $\text{Co}_2(\text{CO})_6$ -2-methyl-3-butyn-2-ol **7.18** (774 mg, 2.09 mmol, 1 equiv), diethyl ether (10 mL), tetrafluoroboric acid (509 mg of a 54% by weight in diethyl ether, 3.14 mmol, 1.5 equiv). The reaction was diluted with diethyl ether (10 mL) prior to filtration and drying which afforded 558 mg of salt **7.12** in 61% yield as a red solid. Due to sensitivity to water and air, the salt was stored in the glove box and used within 24 h of isolation for best results.

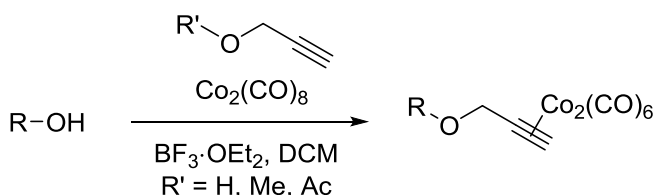
General Procedure C: Nicholas Reaction Procedures



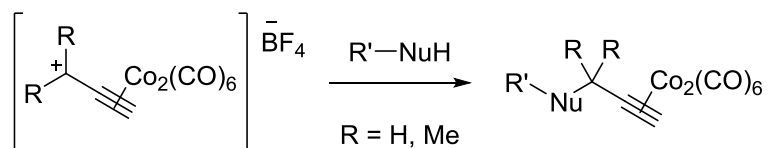
General Procedure C1: Use of pre-made dicobalt hexacarbonyl complexed alkyne.

A single-necked, round-bottomed flask equipped with a stir bar and a septum pierced with a needle was charged with dichloromethane (0.05 M), $\text{Co}_2(\text{CO})_6$ -propargyl alcohol **7.6a** or $\text{Co}_2(\text{CO})_6$ -methyl propargyl ether **7.6b** (2 equiv), and the nucleophilic species (1 equiv). The solution was cooled in an ice bath to 0 °C. Boron trifluoride diethyl etherate (2.5 equiv) was added dropwise and the reaction stirred until the nucleophile was fully consumed, or the reaction was no longer progressing, as determined by TLC. The reaction was quenched by the addition of saturated sodium bicarbonate. The mixture was transferred to a separatory funnel, the layers were separated and the aqueous layer was extracted with dichloromethane (3x). The combined organics were dried over magnesium sulfate, filtered, and concentrated under reduced pressure. The crude residue was purified

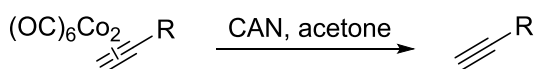
by silica gel flash column chromatography to afford the dicobalt hexacarbonyl complexed alkyne.



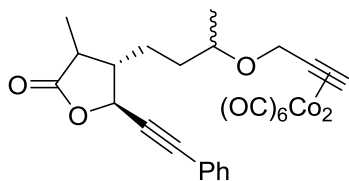
General Procedure C2: *In situ* formation of dicobalt hexacarbonyl complexed alkyne. A single necked, round-bottomed flask, equipped with a stir bar and a septum was charged with dicobalt octacarbonyl (2 equiv) in a N₂ filled glove box. The flask was transferred out of the glovebox and the septum was pierced with a nitrogen inlet needle. Either propargyl alcohol, methyl propargyl ether, or propargyl acetate (2 equiv), dissolved in dichloromethane (0.1 M), was added and the reaction stirred for 1.5 h until evolution of CO gas was no longer observed. The solution was cooled to 0 °C in an ice bath. The nucleophilic species (1 equiv) was dissolved in dichloromethane and added to the flask via syringe, followed by the dropwise addition of boron trifluoride diethyl etherate (2.5 equiv). The reaction stirred until the nucleophilic species was fully consumed, or the reaction was no longer progressing, as determined by TLC. The reaction was quenched by addition of saturated sodium bicarbonate. The mixture was transferred to a separatory funnel, the layers were separated, and the aqueous layer was extracted with dichloromethane (3X). The combined organic layers were dried over magnesium sulfate, filtered, and concentrated under reduced pressure rotary evaporation. The crude residue was purified by silica gel flash column chromatography to afford the dicobalt hexacarbonyl complexed alkyne.



General Procedure C3: Reaction of Tetrafluoroborate salts with nucleophiles. A single-necked, round-bottomed flask, equipped with a stir bar and a septum was charged with propargylium tetrafluoroborate salt **7.6c** or **7.12** (1.3 equiv) in a nitrogen filled glove box. The flask was transferred out of the glove box and the septum was pierced with a nitrogen inlet needle. The flask was cooled to 0 °C in an ice and water bath. Dichloromethane was added followed by the amine nucleophile (1 equiv) dissolved in dichloromethane (0.05 M overall). The reaction stirred for 2 h or until complete as determined by TLC. The reaction was quenched by the addition of saturated sodium bicarbonate. The mixture was transferred to a separatory funnel; the layers were separated and the aqueous layer was extracted with dichloromethane (3x). The combined organics were dried over magnesium sulfate, filtered, and concentrated under reduced pressure rotary evaporation. The crude residue was purified by silica gel flash column chromatography to afford the dicobalt hexacarbonyl complexed alkyne.

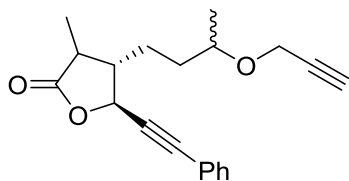


General Procedure D: Oxidative decomplexation of $\text{Co}_2(\text{CO})_6$ -alkynes. A single-necked, round-bottomed flask, equipped with a stir bar and a septum pierced with a nitrogen inlet needle was charged with the dicobalt hexacarbonyl complexed alkyne (1 equiv), dissolved in acetone (0.01 M). The solution was cooled in an ice bath to 0° C. Ceric ammonium nitrate (5 equiv) was added to the flask in a single portion. The reaction stirred until complete as evidenced by TLC. The reaction was diluted with distilled water and diethyl ether. The mixture was transferred to a separatory funnel. The layers were separated and the aqueous layer was extracted with diethyl ether (3x). The combined organics were dried over magnesium sulfate, filtered, and concentrated under reduced pressure rotary evaporation. If necessary, the residue was purified by silica gel flash column chromatography to afford the alkyne.

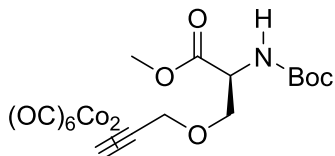


Dicobalt hexacarbonyl complexed 3-methyl-5-(phenylethynyl)-4-(3-(prop-2-yn-1-yloxy)butyl)dihydrofuran-2(3H)-one (**7.7**). **Method A:** Follows general procedure C1: $\text{Co}_2(\text{CO})_6$ -propargyl alcohol **7.6a** (25 mg, 0.073 mmol, 2 equiv), alcohol **7.5** (10 mg, 0.037 mmol, 1 equiv), dichloromethane (0.75 mL), and boron trifluoride diethyl etherate (12 μL , 0.93 mmol, 2.5 equiv) The reaction stirred for 4 h. The crude residue was purified by silica gel flash column chromatography (gradient of 5-10% ethyl acetate/hexanes) to afford 12 mg of **7** in 55% yield as a dark red/brown oil.

Method B: Follows general procedure C2: propargyl alcohol (4 μL , 0.064 mmol, 2.2 equiv), dichloromethane (0.36 mL), dicobalt octacarbonyl (20 mg, 0.058 mmol, 2 equiv), alcohol **5** (8 mg, 0.029 mmol, 1 equiv), dissolved in dichloromethane (0.25 mL), and boron trifluoride diethyl etherate (9 μL , 0.073 mmol, 2.5 equiv). The reaction stirred for 3.5 h. The crude residue was purified by silica gel flash column chromatography (gradient of 5-10% ethyl acetate in hexanes) to afford 10 mg of **7** in 60% yield as a dark red/brown oil. The product was a 1:1 mixture of diastereomers that were inseparable by column chromatography. ^1H NMR (500 MHz, CDCl_3) 7.46-7.44 (m, 2H), 7.37-7.33 (m, 3H), 6.01 (d, $J = 4.5$ Hz, 1 H), 4.79 (d, $J = 9.0$ Hz, 1H), 4.69 (dd, $J = 13.0, 4.5$ Hz, 1 H), 4.51 (d, $J = 13.0$, 1H), 3.71-3.64 (m, 1H), 2.34-2.19 (m, 2H), 1.95-1.87 (m, 0.5H)*, 1.80-1.61 (m, 3.5H), 1.33 (d, $J = 6.8$ Hz, 1.5H), 1.32 (d, $J = 6.8$ Hz, 1.5H)*, 1.24 (d, $J = 3.6$ Hz, 1.5H), 1.23 (d, $J = 6.3$ Hz, 1.5H)* ppm.* Discernable signal for one of two diastereomers. ^{13}C NMR (125 MHz, CDCl_3) 199.8 (6C), 177.9, 131.9 (2C), 129.2, 128.5 (2C), 121.9, 92.7, 87.9, 85.1, 75.2, 75.0*, 73.1, 71.3, 68.6, 51.2, 51.0*, 41.3, 34.5, 34.3*, 27.8, 27.5*, 19.3, 14.6, 14.4* ppm. IR (thin film) 2971, 2934, 2094, 2052, 2022, 1784, 1491, 1456, 1377, 1327, 1164, 1086, 992, 758, 691 cm^{-1} . HRMS (FTMS + p ESI Full ms) $[\text{M}+\text{Na}]^+$ calc'd for $\text{C}_{26}\text{H}_{22}\text{O}_9\text{Co}_2\text{Na}$, 618.9820; found, 618.9807. $R_f = 0.47$ (20% ethyl acetate in hexanes) Silica gel, visible UV.



3-Methyl-5-(phenylethynyl)-4-(3-(prop-2-yn-1-yloxy)butyl)dihydrofuran-2(3H)-one (**7.8**). Follows general procedure D: cobalt complex **7** (15 mg, 0.025 mmol, 1 equiv), acetone (3.0 mL), and ceric ammonium nitrate (69 mg, 0.13 mmol, 5 equiv) The reaction stirred for 30 min. The crude residue was purified by silica gel flash column chromatography (15% ethyl acetate in hexanes) to afford 8 mg of alkyne **7.8** in 97% yield as a clear oil. The product was a 1:1 mixture of diastereomers that were inseparable by column chromatography. ^1H NMR (400 MHz, CDCl_3) 7.46-7.43 (m, 2H), 7.36-7.33 (m, 3H), 4.83 (d, $J = 8.8$ Hz, 1 H), 4.22 (dd, $J = 15.6, 2.4$ Hz, 0.5 H), 4.21 (dd, $J = 15.6, 2.4$ Hz, 0.5 H)*, 4.122 (dd, $J = 15.6, 2.4$ Hz, 0.5H), 4.115 (dd, $J = 15.6, 2.4$ Hz, 0.5H)*, 3.74-3.66 (m, 1H), 2.394 (t, $J = 2.4$ Hz, 0.5H), 2.387 (t, $J = 2.4$ Hz, 0.5H)*, 2.33-2.31 (m, 2H), 1.92-1.83 (m, 0.5H)*, 1.77-1.67 (m 3.5H), 1.35 (d, $J = 6.8$ Hz, 1.5H), 1.34 (d, $J = 6.8$ Hz, 1.5H)*, 1.19 (d, $J = 6.0$ Hz, 1.5H), 1.17 (d, $J = 6.0$ Hz, 1.5H)* ppm. ^{13}C NMR (100 MHz, CDCl_3) 177.9, 131.93 (2C), 131.91 (2C)*, 129.2, 128.6 (2C), 121.8, 87.9, 85.0, 80.4, 74.1, 73.7, 73.1, 55.8, 55.7*, 51.0, 50.6*, 41.3, 34.2, 19.2, 14.7, 14.5* ppm.* Discernable signal for one of two diastereomers. IR (thin film) 3291, 2924, 2853, 2232, 1780, 1491, 1457, 1166, 1076, 992, 759, 692 cm^{-1} . HRMS (FTMS + p ESI Full ms) $[\text{M}+\text{H}]^+$ calc'd for $\text{C}_{20}\text{H}_{23}\text{O}_3$, 311.1642; found, 311.1631. $R_f = 0.50$ (30% ethyl acetate in hexanes) Silica gel, UV active.

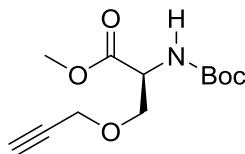


$\text{Co}_2(\text{CO})_6$ -*N*-[(1,1-dimethylethoxy)carbonyl]-*O*-(prop-2-yn-1-yl)serine methyl ester (**7.10a**). **Method A**. Follows general procedure C1: $\text{Co}_2(\text{CO})_6$ -propargyl alcohol **7.6a**

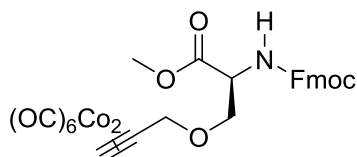
(505 mg, 1.48 mmol), *N*-Boc-L-serine methyl ester **7.9a** (150 mg, 0.74 mmol)³⁵⁹, dichloromethane (3 mL), and boron trifluoride diethyl etherate (230 μ L, 1.85 mmol). The reaction stirred for 1 h. The crude residue was purified by silica gel flash column chromatography (gradient of 0-25% ethyl acetate in hexanes) to afford 78 mg of **7.10a** in 20% yield as a dark red/brown oil.

Method B: Follows general procedure C2: Methyl propargyl ether (69.0 mg, 0.984 mmol), dichloromethane (5 mL), dicobalt octacarbonyl (337 mg, 0.984 mmol), *N*-Boc-L-serine methyl ester **7.9a** (69.0 mg, 0.984 mmol), dissolved in dichloromethane (5 mL), and boron trifluoride diethyl etherate (152 μ L, 1.230 mmol). The crude residue was purified by silica gel flash column chromatography (gradient of 10-25% ethyl acetate in hexanes) to afford 252.8 mg of **7.10a** in 97% yield.

Method C: Follows general procedure C2: Propargyl acetate (96.5 mg, 0.984 mmol), dichloromethane (5 mL), dicobalt octacarbonyl (337 mg, 0.984 mmol), *N*-Boc-L-serine methyl ester **7.9a** (100.0 mg, 0.492 mmol), dissolved in dichloromethane (5 mL), and boron trifluoride diethyl etherate (150 μ L, 1.230 mmol). The crude residue was purified by silica gel flash column chromatography (gradient of 10-25% ethyl acetate in hexanes) to afford 75.7 mg of **7.10a** in 29% yield. ¹H NMR (500 MHz, CDCl₃) 6.02 (s, 1H), 5.35 (d, *J* = 7.5 Hz, 1H), 4.64 (s, 2H), 4.49 (broad d, *J* = 8.5 Hz, 1H), 4.07 (d, *J* = 8.0 Hz, 1H), 3.85 (d, *J* = 7.0 Hz, 1H), 3.74 (s, 3H), 1.45 (s, 9H) ppm. ¹³C NMR (125 MHz, CDCl₃) 199.3 (6C), 170.8, 155.5, 80.0, 72.0, 71.3, 71.0, 54.0, 52.5, 28.3 (3C), 27.3 ppm. IR (thin film) 3451, 2978, 2874, 2096, 2054, 2022, 1750, 1718, 1500, 1454, 1438, 1391, 1367, 1347, 1298, 1248, 1207, 1165, 1110, 1062, 1021, 519, 494 cm⁻¹. HRMS (FTMS + p ESI Full ms) [M+Na]⁺ calc'd for C₁₈H₁₉Co₂NO₁₁Na 565.9514 m/z; found 565.9500 m/z. R_f = 0.50 (20% ethyl acetate in hexanes) Silica gel, visible UV.



N-[(1,1-dimethylethoxy)carbonyl]-*O*-(prop-2-yn-1-yl)serine methyl ester (**7.11a**). Follows general procedure D: cobalt complex **7.10a** (68 mg, 0.13 mmol, 1 equiv), acetone (5 mL), and ceric ammonium nitrate (700 mg, 1.28 mmol, 10 equiv). The reaction stirred for 30 min. The crude residue was purified by silica gel flash column chromatography (gradient of 0-30% ethyl acetate in hexanes) to afford 28.3 mg of alkyne **7.11a** in 90% yield as a clear oil. ^1H NMR (500 MHz, CDCl_3) 5.35 (d, $J = 8.0$ Hz, 1H), 4.45 (dd, $J = 5.0, 3.0$ Hz, 1H), 4.14 (d, $J = 2.5$ Hz, 2H), 4.08-3.85 (m, 1H), 3.77 (s, 3H), 3.76 (m, 1H), 2.44 (t, $J = 2.5$ Hz, 1 H), 1.46 (s, 9H) ppm. ^{13}C NMR (125 MHz, CDCl_3) 170.9, 155.5, 80.0, 78.8, 75.1, 69.7, 58.6, 53.8, 52.5, 28.3 (3C) ppm. IR (thin film) 3429, 3297, 2951, 2922, 2851, 2341, 1748, 1717, 1501, 1462, 1440, 1388, 1366, 1300, 1248, 1210, 1165, 1108, 1062, 1024 cm^{-1} . HRMS (FTMS + p ESI Full ms) $[\text{M}+\text{Na}]^+$ calc'd for $\text{C}_{12}\text{H}_{19}\text{NO}_5\text{Na}$ 280.1155 m/z; found 280.1148 m/z. $R_f = 0.31$ (20% ethyl acetate in hexanes) Silica gel, potassium permanganate stain.

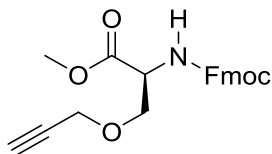


$\text{Co}_2(\text{CO})_6$ -*N*-[(((9H-fluoren-9-yl)methoxy)carbonyl)]-*O*-(prop-2-yn-1-yl)serine methyl ester (**7.10b**). **Method A.** Follows general procedure C2: propargyl alcohol (65.7 mg, 1.17 mmol), dichloromethane (10 mL), dicobalt octacarbonyl (400 mg, 1.17 mmol), *N*-Fmoc-L-serine methyl ester **7.9b** (200 mg, 0.59 mmol)³⁶⁰ and boron trifluoride diethyl etherate (200 μL , 1.46 mmol). The reaction stirred for 1 h. The crude residue was purified by silica gel flash column chromatography (gradient of 10-30% ethyl acetate in hexanes) to afford 114 mg of **7.10b** in 29% yield as a dark red/brown sticky solid.

Method B: Follows general procedure C2: Methyl propargyl ether (24.1 mg, 0.34 mmol), dichloromethane (5 mL), dicobalt octacarbonyl (117.4 mg, 0.34 mmol), *N*-Fmoc-L-serine

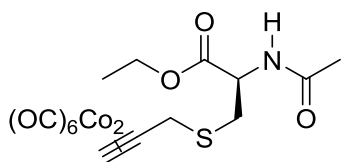
methyl ester **7.9b** (58.6 mg, 0.172 mmol), dissolved in dichloromethane (0.4 mL), and boron trifluoride diethyl etherate (50 μ L, 0.429 mmol). The crude residue was purified by silica gel flash column chromatography (gradient of 10-50% ethyl acetate in hexanes) to afford 61.9 mg of **7.10b** in 54% yield.

Method C: Follows general procedure C2: Propargyl acetate (57.4 mg, 0.586 mmol), dichloromethane (5 mL), dicobalt octacarbonyl (200.3 mg, 0.586 mmol), *N*-Fmoc-L-serine methyl ester **7.9b** (100.0 mg, 0.293 mmol), dissolved in dichloromethane (5 mL), and boron trifluoride diethyl etherate (90 μ L, 0.73 mmol). The crude residue was purified by silica gel flash column chromatography (gradient of 10-25% ethyl acetate in hexanes) to afford 45.6 mg of **7.10b** in 23% yield. ^1H NMR (500 MHz, CDCl_3) 7.77 (d, $J = 7.5$ Hz, 2H), 7.60 (app t, $J = 6.5$ Hz, 2H), 7.41 (app t, $J = 7.5$ Hz, 2H), 7.32 (app t, $J = 7.5$ Hz, 2H), 6.03 (s, 1H), 5.66 (d, $J = 8.5$ Hz, 1H), 4.66 (s, 2H), 4.59 (d, $J = 8.0$ Hz, 1H), 4.45-4.41 (m, 1H), 4.34-4.30 (m, 1H), 4.25-4.23 (m, 1H), 4.13 (d, $J = 9.0$ Hz, 1H), 3.91 (br d, $J = 3.5$ Hz, 1H), 3.77 (s, 3H) ppm. ^{13}C NMR (125 MHz, CDCl_3) 199.4 (6C), 170.5, 156.0, 143.9, 143.8, 141.3 (2C), 127.7 (2C), 127.07, 127.05, 125.23, 125.15, 120.0 (2C), 90.2, 72.0, 71.2, 70.8, 67.3, 54.4, 52.7, 47.1 ppm. IR (thin film) 3450, 3069, 3038, 3016, 2954, 2879, 2830, 2095, 2054, 2022, 1728, 1510, 1450, 1338, 1297, 1243, 1208, 1108, 1085, 1059, 760, 741, 621, 519, 495 cm^{-1} . HRMS (FTMS + p ESI Full ms) $[\text{M}+\text{Na}]^+$ calc'd for $\text{C}_{28}\text{H}_{21}\text{Co}_2\text{NO}_{11}\text{Na}$ 687.9657 m/z; found 687.9671 m/z. $R_f = 0.41$ (20% ethyl acetate in hexanes) Silica gel, visible UV.

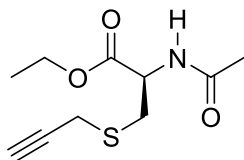


N-[[(9H-fluoren-9-yl)methoxy]carbonyl]-*O*-(prop-2-yn-1-yl)serine methyl ester (**7.11b**). Follows general procedure D: cobalt complex **7.10b** (41.1 mg, 0.06 mmol, 1 equiv), acetone (5 mL), and ceric ammonium nitrate (339 mg, 0.62 mmol). The reaction stirred for 30 min. The crude residue was purified by silica gel flash column chromatography (gradient of 0-40% ethyl acetate in hexanes) to afford 21 mg of alkyne **7.11b** in 90%

yield as a clear oil. ^1H NMR (500 MHz, CDCl_3) 7.77 (d, $J = 7.5$ Hz, 2H), 7.62 (app t, $J = 7.0$ Hz, 2H), 7.41 (app t, $J = 7.5$ Hz, 2H), 7.32 (app t, $J = 7.0$ Hz, 2H), 5.66 (d, $J = 8.0$ Hz, 1H), 4.47-4.35 (m, 1H), 4.41 (m, 2H), 4.25 (t, $J = 7.5$ Hz, 1H), 4.17 (s, 2H), 4.01 (dd, $J = 9.5, 3.0$ Hz, 1H), 3.81 (dd, $J = 9.5, 3.0$ Hz, 1H), 3.80 (s, 3H), 2.44 (t, $J = 2.0$ Hz, 1H) ppm. ^{13}C NMR (125 MHz, CDCl_3) 170.6, 156.0, 143.9, 143.8, 141.31, 141.30, 127.7 (2C), 127.1 (2C), 125.2, 125.1, 120.0 (2C), 78.8, 75.2, 69.5, 67.2, 58.6, 54.2, 52.7, 47.1 ppm. IR (thin film) 3287, 3060, 3038, 3016, 2952, 2890, 2115, 1745, 1717, 1515, 1476, 1465, 1450, 1341, 1298, 1240, 1210, 1106, 1084, 1059, 1032, 760, 741, 645, 621, 535 cm^{-1} . HRMS (FTMS + p ESI Full ms) $[\text{M}+\text{H}]^+$ calc'd for $\text{C}_{22}\text{H}_{21}\text{Co}_2\text{NO}_5$ 380.1493 m/z; found 380.1485 m/z. $R_f = 0.22$ (20% ethyl acetate in hexanes) Silica gel, visible UV.

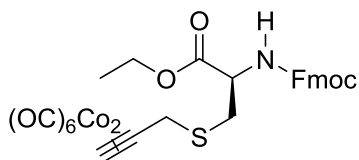


Dicobalt octacarbonyl complexed *N*-acetyl-*S*-(prop-2-yn-1-yl)cysteine ethyl ester (**7.10c**). Followed general procedure C2: Dicobalt octacarbonyl (107 mg, 0.31 mmol), propargyl alcohol (18 mg, 0.314 mmol) dissolved in dichloromethane (1.5 mL), *N*-acetyl-*L*-cysteine ethyl ester (**7.9c**) (30 mg, 0.16 mmol)³⁶¹ in dichloromethane (1.5 mL), and BF_3OEt_2 (49 μL , 0.39 mmol). The reaction was stirred for 2 h. The crude residue was purified by silica gel flash column chromatography (gradient of 10-30% ethyl acetate in hexanes) to yield 70 mg of **7.10c** in 86% yield, as a red oil. ^1H NMR (300 MHz, CDCl_3) 6.31 (d, $J = 4.5$ Hz, 1H), 6.14 (s, 1H), 4.87-4.85 (m, 1H), 4.25-4.23 (m, 2H), 4.02-3.91 (m, 2H), 3.19 (dd, $J = 13.5, 4.4$ Hz, 1H), 3.06 (dd, $J = 13.8, 4.7$ Hz, 1H), 2.03 (s, 3H), 1.30 (t, $J = 6.9$ Hz, 3H) ppm. ^{13}C NMR (100 MHz, CDCl_3) 199.5 (6 C), 170.8, 170.0, 92.0, 73.4, 62.2, 52.2, 36.8, 34.7, 23.3, 14.3 ppm. IR (thin film) 3295, 2984, 2093, 2052, 2020, 1742, 1655, 1543, 1374, 1208, 1032 cm^{-1} . HRMS (FTMS + p ESI Full ms) $[\text{M}+\text{Na}]^+$ calc'd for $\text{C}_{16}\text{H}_{15}\text{O}_9\text{NC}_2\text{NaS}$, 537.9024; found, 537.9035. $R_f = 0.55$ (50% ethyl acetate in hexanes) Silica gel, visible UV.



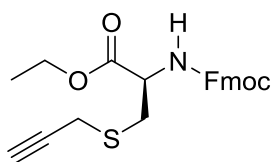
N-acetyl-*S*-(prop-2-yn-1-yl)cysteine ethyl ester (**7.11c**). Followed general procedure D: dicobalt hexacarbonyl complexed alkyne **7.10c** (23 mg, 0.045 mmol), acetone (4.0 mL), and ceric ammonium nitrate (99 mg, 0.18 mmol). The reaction was complete after 10 min of stirring. The work-up afforded 9 mg of alkyne **7.11c** in 83% yield as a colorless oil. Further purification was not performed. ¹H NMR (500 MHz, CDCl₃) 6.42 (bs, 1H), 4.86 (dt, *J* = 7.5, 5.0 Hz, 1H), 4.25 (q, *J* = 7.0 Hz, 2H), 3.31 (dd, *J* = 17.0, 2.5 Hz, 1H), 3.25-3.21 (m, 2H), 3.14 (dd, *J* = 14.3, 5.3 Hz, 1H), 2.30 (t, *J* = 2.5 Hz, 1H), 2.08 (s, 3H), 1.31 (t, *J* = 7.0 Hz, 3H) ppm. ¹³C NMR (125 MHz, CDCl₃) 170.9, 170.3, 79.4, 72.1, 62.2, 51.9, 33.9, 23.3, 20.0, 14.3 ppm. Impurity present at 29.8 ppm. IR (thin film) 3287, 2919, 2850, 2361, 1739, 1660, 1539, 1374, 1213, 1028 cm⁻¹. HRMS (FTMS + p ESI Full ms)

[*M*+*H*]⁺ calc'd for C₁₀H₁₆O₃NS, 230.0845; found, 230.0846. *R*_f = 0.23 (50% ethyl acetate in hexanes) Silica gel, potassium permanganate.



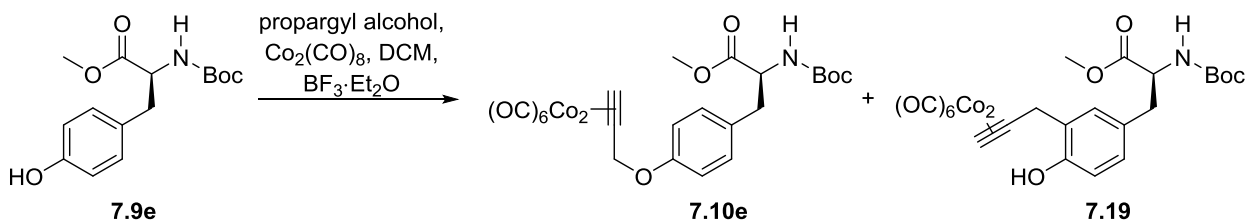
Dicobalt hexacarbonyl complexed *N*-(((9H-fluoren-9-yl)methoxy)carbonyl)-*S*-(prop-2-yn-1-yl)-*L*-cysteine ethyl ester (**7.10d**). **Method A:** Followed general procedure C2: Dicobalt octacarbonyl (55 mg, 0.16 mmol), propargyl alcohol (9 mg, 0.16 mmol), dichloromethane (1.1 mL), *N*-Fmoc-*L*-cysteine ethyl ester (**7.9d**) (30 mg, 0.081 mmol) dissolved in dichloromethane (0.6 mL), and boron trifluoride diethyl etherate (25 μL, 0.20 mmol). The reaction was stirred for 45 min. The crude residue was purified by silica gel flash column chromatography (gradient of 5-20% ethyl acetate in hexanes) to afford 40 mg of **7.10d** in 71% yield, as a red oil.

Method B: Followed general procedure C1: $\text{Co}_2(\text{CO})_6$ -methyl propargyl ether **7.6b** (45 mg, 0.13 mmol), dichloromethane (0.6 mL), *N*-Fmoc-L-cysteine ethyl ester (**7.9d**) (24 mg, 0.063 mmol) dissolved in dichloromethane (0.6 mL), and boron trifluoride diethyl etherate (20 μL , 0.156 mmol). The reaction was stirred for 2 h. The crude residue was purified by silica gel flash column chromatography (gradient of 10-20% diethyl ether in hexanes) to afford 29 mg of **7.10d** in 67% yield. ^1H NMR (400 MHz, CDCl_3) 7.77 (d, $J = 7.6$ Hz, 2H), 7.60 (d, $J = 7.6$ Hz, 2H), 7.41 (app t, $J = 7.6$ Hz, 2H), 7.32 (app t, $J = 7.6$ Hz, 2H), 6.13 (s, 1H), 5.66 (d, $J = 7.6$ Hz, 1H), 4.66 (dt, $J = 7.6, 5.0$ Hz, 1H), 4.44-4.35 (m, 2H), 4.28-4.22 (m, 3H), 3.99 (s, 2H), 3.19 (dd, $J = 14.0, 4.8$ Hz, 1H), 3.09 (dd, $J = 14.0, 5.2$ Hz, 1H), 1.32 (t, $J = 7.2$ Hz, 3H) ppm. ^{13}C NMR (125 MHz, CDCl_3) 199.5 (6 C), 170.7, 155.9, 143.93, 143.86, 141.5 (2 C), 127.9 (2 C), 127.2 (2 C), 125.2 (2 C), 120.2 (2 C), 92.1, 73.4, 67.5, 62.3, 53.9, 47.3, 36.9, 35.1, 14.3 ppm. IR (thin film) 3345, 3070, 2923, 2094, 2053, 2023, 1726, 1507, 1450, 1339, 1204, 1052, 759, 741 cm^{-1} . HRMS (FTMS + p ESI Full ms) $[\text{M}+\text{H}]^+$ calc'd for $\text{C}_{29}\text{H}_{24}\text{O}_{10}\text{NCO}_2\text{S}$, 695.9779; found, 695.9745. $R_f = 0.36$ (20% ethyl acetate in hexanes) Silica gel, visible UV.



Ethyl *N*-(((9H-fluoren-9-yl)methoxy)carbonyl)-*S*-(prop-2-yn-1-yl)-*L*-cysteinate (**7.11d**). Followed general procedure D: Dicobalt hexacarbonyl complexed alkyne **7.10d** (22 mg, 0.032 mmol), acetone (3.5 mL), and ceric ammonium nitrate (69 mg, 0.13 mmol). The reaction was complete after 10 min of stirring. The work-up afforded 12 mg of alkyne **7.11d** in 92% yield as an off white oil. Further purification was not performed. ^1H NMR (400 MHz, CDCl_3) 7.77 (d, $J = 7.4$ Hz, 2H), 7.61 (d, $J = 7.4$ Hz, 2H), 7.41 (app t, $J = 7.4$ Hz, 2H), 7.32 (app tt, $J = 7.4, 1.2$ Hz, 2H), 5.64 (d, $J = 7.6$ Hz, 1H), 4.65 (dt, $J = 8.0, 5.2$ Hz, 1H), 4.46-4.38 (m, 2H), 4.28-4.23 (m, 3H), 3.32-3.22 (m, 2H), 3.22 (dd, $J = 14.4, 4.8$ Hz, 1H), 3.14 (dd, $J = 14.0, 5.6$ Hz, 1H), 2.26 (t, $J = 2.6$ Hz, 1H), 1.31 (t, $J = 7.2$ Hz, 3H) ppm. ^{13}C NMR (125 MHz, CDCl_3) 170.8, 155.9, 144.0, 143.9, 141.5 (2 C), 127.9 (2 C), 127.2 (2 C), 125.2 (2 C), 120.2 (2 C), 79.4, 72.1, 67.3, 62.2, 53.7, 47.3, 34.0, 20.1, 14.3

ppm. Trace impurity observed at 29.8 ppm. IR (thin film) 3291, 2924, 1723, 1517, 1450, 1339, 1210, 1051, 760, 741 cm^{-1} . HRMS (FTMS + p ESI Full ms) $[\text{M}+\text{H}]^+$ calc'd for $\text{C}_{23}\text{H}_{24}\text{O}_4\text{NS}$, 410.1421; found, 410.1424. $R_f = 0.26$ (20% ethyl acetate in hexanes) Silica gel, UV.



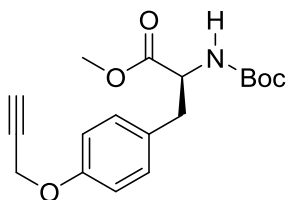
$\text{Co}_2(\text{CO})_6$ -*N*-[(1,1-dimethylethoxy)carbonyl]-*O*-(prop-2-yn-1-yl)-*L*-tyrosine methyl ester (**7.10e**). **Method A:** Follows general procedure C2: propargyl alcohol (75.9 mg, 1.35 mmol), dichloromethane (5 mL), dicobalt octacarbonyl (510 mg, 1.49 mmol), *N*-Boc-*L*-tyrosine methyl ester **7.9e** (200 mg, 0.68 mmol)³⁶² and boron trifluoride diethyl etherate (210 μL , 1.70 mmol). The reaction stirred for 1 h. Both **7.10e** and **7.19** were observed by TLC. The crude residue was purified by silica gel flash column chromatography (gradient of 10-40% ethyl acetate in hexanes) to afford 187 mg of **7.10e** in 45% yield as a dark red/brown oil and no **7.19** was isolated.

In a separate experiment, **7.10e** was afforded in 32% yield and byproduct **7.19** was isolated in trace amounts. The ^1H NMR of this sample of **7.19** is included in the **Section 7.7**. Further characterization was not obtained due to small amounts.

Method B: Follows general procedure C2: methyl propargyl ether (19 mg, 0.27 mmol), dichloromethane (2.0 mL), dicobalt octacarbonyl (93 mg, 0.27 mmol), *N*-Boc-*L*-tyrosine methyl ester **7.9e** (40.0 mg, 0.135 mmol) and boron trifluoride diethyl etherate (42 μL , 0.338 mmol). The reaction stirred for 3 h. Both **7.10e** and **7.19** were observed by TLC. The crude residue was purified by silica gel flash column chromatography (gradient of 15-30% ethyl acetate in hexanes) to afford 19 mg of **7.10e** in 23% yield as a dark red/brown oil. Large amounts of baseline material was observed.

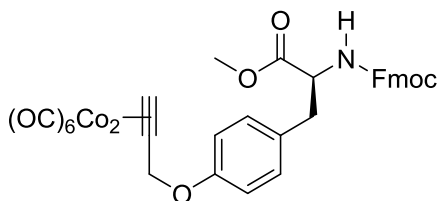
Data for **7.10e**: ^1H NMR (500 MHz, CDCl_3): 7.05 (d, $J = 7.0$ Hz, 2H), 6.88 (d, $J = 8.0$ Hz, 2H), 6.05 (s, 1H), 5.15 (s, 2H), 4.95 (bs, 1H), 4.55 (bs, 1H), 3.72 (s, 3H), 3.03 (m, 2H), 1.42 (s, 9H) ppm. ^{13}C NMR (125 MHz, CDCl_3) 199.3 (6 C), 172.4, 157.3, 155.1, 130.4 (2C), 128.6, 114.7 (2C), 89.5, 79.9, 71.7, 68.2, 54.5, 52.2, 37.5, 28.3 (3 C) ppm. Impurities seen at 129.7, 124.2, 28.8, 26.7. IR (thin film) 3445, 3368, 2979, 2956, 2929, 2097, 2056, 1746, 1716, 1612, 1585, 1510, 1445, 1392, 1367, 1244, 1216, 1172, 1111, 1059, 1018, 839, 779, 519, 497 cm^{-1} . HRMS (FTMS + p ESI Full ms) $[\text{M}+\text{Na}]^+$ calc'd for $\text{C}_{24}\text{H}_{23}\text{Co}_2\text{NO}_{10}\text{Na}$ 625.9878 m/z; found 625.9877 m/z. $R_f = 0.44$ (20% ethyl acetate in hexanes) Silica gel, visible, UV.

Data for **7.19**: ^1H NMR (400 MHz, CDCl_3) 6.95 (s, 1H), 6.88 (d, $J = 8.0$ Hz, 1H), 6.70-6.62 (m, 1H), 6.07 (s, 1H), 4.91-4.87 (m, 1 H), 4.79-4.71 (m, 1H), 4.58-4.49 (m, 1H), 4.10 (s, 1H), 3.72 (s, 3H), 3.08-2.92 (m, 2H), 1.43 (s, 9H) ppm. $R_f = 0.26$ (20% ethyl acetate in hexanes) Silica gel, visible UV.



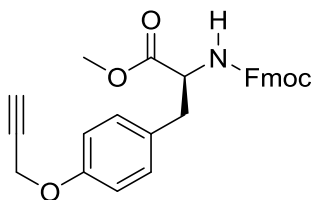
N-[(1,1-dimethylethoxy)carbonyl]-*O*-(prop-2-yn-1-yl)-*L*-tyrosine methyl ester (**7.11e**). Follows general procedure D: cobalt complex **7.10e** (186 mg, 0.31 mmol, 1 equiv), acetone (10 mL), and ceric ammonium nitrate (1.7 g, 3.1 mmol, 10 equiv). The reaction stirred for 30 min. The crude residue was purified by silica gel flash column chromatography (gradient of 0-50% ethyl acetate in hexanes) to afford 73.4 mg of alkyne **7.11e** in 75% yield as a clear oil. ^1H NMR (500 MHz, CDCl_3) 7.05 (d, $J = 8.5$ Hz, 2H), 6.90 (d, $J = 8.5$ Hz, 2H), 4.96 (br d, $J = 8.0$ Hz, 1H), 4.66 (d, $J = 2.5$ Hz, 2H), 4.59-4.49 (m, 1H), 3.71 (s, 3H), 3.08-2.97 (m, 2H), 2.51 (t, $J = 2.0$ Hz, 1H), 1.41 (s, 9H) ppm. ^{13}C NMR (125 MHz, CDCl_3). 172.4, 156.7, 155.1, 130.3 (2C), 129.0, 115.0 (2C), 79.9, 78.6, 75.5, 55.8, 54.5, 52.2, 37.5, 28.3 (3C) ppm. Impurities seen at 61.3, 37.7, 36.2, 19.6, 19.4, 14.1. IR (thin film) 3368, 3288, 2977, 2956, 2929, 2868, 2121, 1743, 1712, 1611, 1586, 1506, 1438, 1392, 1366, 1218, 1165, 1113, 1058, 1027, 924, 825, 644 cm^{-1} . HRMS

(FTMS + p ESI Full ms) $[M+H]^+$ calc'd for $C_{18}H_{24}NO_5$ 334.1649 m/z; found 334.1640 m/z. $R_f = 0.27$ (20% ethyl acetate in hexanes) Silica gel, visible UV.

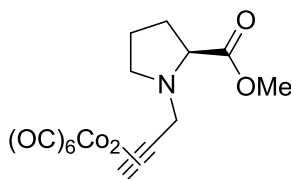


$Co_2(CO)_6$ -*N*-[[(9H-fluoren-9-yl)methoxy]carbonyl]-*O*-(prop-2-yn-1-yl)-L-tyrosine methyl ester (**7.10f**). **Method A.** Follows general procedure C2: propargyl alcohol (27.0 mg, 0.48 mmol), dichloromethane (5 mL), dicobalt octacarbonyl (164 mg, 0.48 mmol, 2 equiv), *N*-Fmoc-L-tyrosine methyl ester **7.9f** (100 mg, 0.24 mmol) and boron trifluoride diethyl etherate (74 μ L, 0.60 mmol). The reaction stirred for 1 h. The crude residue was purified by silica gel flash column chromatography (gradient of 10-40% ethyl acetate in hexanes) to afford 22.3 mg of **7.10f** in 6% yield as a dark red/brown sticky solid.

Method B: Follows general procedure C2: Methyl propargyl ether (16.8 mg, 0.240 mmol), dichloromethane (5 mL), dicobalt octacarbonyl (82.1 mg, 0.240 mmol), *N*-Fmoc-L-tyrosine methyl ester **7.9f** (50.0 mg, 0.120 mmol), dissolved in dichloromethane (5 mL), and boron trifluoride diethyl etherate (40 μ L, 0.300 mmol). The crude residue was purified by silica gel flash column chromatography (gradient of 10-50% ethyl acetate in hexanes) to afford 64.9 mg of **7.10f** in 73% yield. 1H NMR (500 MHz, $CDCl_3$) 7.78 (d, $J = 7.5$ Hz, 2H), 7.58 (s, 2H), 7.40-7.39 (m, 2H), 7.33-7.32 (m, 2H), 7.01 (d, $J = 7.0$ Hz, 2H), 6.87 (d, $J = 7.5$ Hz, 2H), 6.05 (s, 1H), 5.23 (d, $J = 7.5$ Hz, 1H), 5.15 (s, 2H), 4.65 (bs, 1H), 4.48-4.34 (m, 2H), 4.22 (bs, 1H), 3.75 (s, 3H), 3.08 (m, 2H) ppm. ^{13}C NMR (125 MHz, $CDCl_3$) 199.3 (6C), 171.9, 157.3, 155.5, 143.9, 143.8, 141.4 (2C), 130.4 (2C), 128.3, 127.7 (2C), 127.1 (2C), 125.1, 125.0, 120.0 (2C), 114.8 (2C), 89.4, 71.7, 68.2, 66.9, 54.9, 52.4, 47.2, 37.3 ppm. IR (thin film) 3429, 3066, 3033, 2951, 2923, 2896, 2852, 2096, 2054, 2022, 1724, 1610, 1583, 1510, 1449, 1347, 1242, 1213, 1177, 1033, 757, 741, 518, 494 cm^{-1} . HRMS (FTMS + p ESI Full ms) $[M+H]^+$ calc'd for $C_{34}H_{25}Co_2NO_{11}$ 742.0164 m/z; found 742.0170 m/z. $R_f = 0.50$ (30% ethyl acetate in hexanes) Silica gel, visible UV.

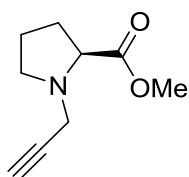


N-[[(9H-fluoren-9-yl)methoxy]carbonyl]-*O*-(prop-2-yn-1-yl)-*L*-tyrosine methyl ester (**7.11f**). Follows general procedure D: cobalt complex **7.10f** (46.4 mg, 0.063 mmol), acetone (2 mL), and ceric ammonium nitrate (34.3 mg, 0.630 mmol). The reaction stirred for 30 min. The crude residue was purified by silica gel flash column chromatography (gradient of 0-50% ethyl acetate in hexanes) to afford 23.0 mg of alkyne **7.11f** in 81% yield as a white solid. Melting Point: 94-95 °C. ¹H NMR (500 MHz, CDCl₃) 7.77 (d, *J* = 7.5 Hz, 2H), 7.57 (app t, *J* = 7.0 Hz, 2H), 7.41 (app t, *J* = 7.0 Hz, 2H), 7.32 (app t, *J* = 7.0 Hz, 2H), 7.01 (d, *J* = 8.9 Hz, 2H), 6.89 (d, *J* = 8.0, 2H), 5.24 (d, *J* = 8.5 Hz, 1H), 4.66 (s, 2H), 4.46 (dd, *J* = 11.0, 7.0 Hz, 1H), 4.37-4.34 (m, 1H), 4.21 (t, *J* = 6.5, 1H), 3.74 (s, 3H), 3.12-3.03 (m, 2H), 2.50 (s, 1H) ppm. ¹³C NMR (125 MHz, CDCl₃) 171.9, 156.8, 155.5, 143.9 (2C), 141.3 (2C), 130.4 (2C), 128.6, 127.7 (2C), 127.1 (2C), 125.1 (2C), 120.0 (2C), 115.0 (2C), 78.2, 75.5, 66.9, 55.8, 54.8, 52.4, 47.2, 37.4 ppm. IR (thin film) 3286, 2956, 2923, 2852, 2049, 2022, 1723, 1608, 1511, 1462, 1449, 1377, 1344, 1259, 1240, 1218, 1177, 1108, 1051, 1026, 757, 741 cm⁻¹. HRMS (FTMS + p ESI Full ms) [M+H]⁺ calc'd for C₂₈H₂₅NO₅ 456.1806 m/z; found 456.1793 m/z. R_f = 0.23 (30% ethyl acetate in hexanes) Silica gel, visible UV.

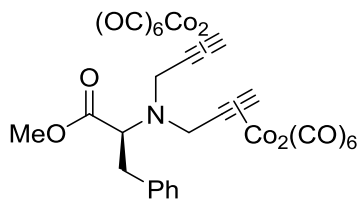


Co₂(CO)₆-*N*-propargyl-*L*-proline methyl ester (**7.10g**). Follows general procedure C3: Tetrafluoroborate salt **6c** (140 mg, 0.340 mmol), dichloromethane (5 mL), *L*-proline methyl ester **7.9g** (57 mg, 0.442 mmol) dissolved in dichloromethane (1.8 mL). The

reaction stirred for 1.5 h. The crude residue was purified by silica gel flash column chromatography (gradient of 5-10% diethyl ether in hexanes) to afford 75 mg of cobalt complexed alkyne **7.10g** in 46% yield as a red oil. ^1H NMR (300 MHz, CDCl_3) 6.05 (s, 1H), 4.23 (d, $J = 15.6$ Hz, 1H), 3.97 (d, $J = 15.3$ Hz, 1H), 3.71 (s, 3H), 3.53 (dd, $J = 8.1$, 5.1 Hz, 1H), 3.23-3.14 (m, 1H), 2.71 (q, $J = 8.1$ Hz, 1H), 2.13, 1.78 (m, 4H) ppm. ^{13}C NMR (100 MHz, CDCl_3) 199.9 (6C), 174.3, 91.8, 73.4, 64.2, 56.1, 52.8, 51.9, 29.4, 23.5 ppm. IR (thin film) 2955, 2798, 2093, 2020, 1736, 1551, 1437, 1356, 1278, 1199, 1173 cm^{-1} . HRMS (FTMS + p ESI Full ms) $[\text{M}+\text{H}]^+$ calc'd for $\text{C}_{15}\text{H}_{14}\text{O}_8\text{NCo}_2$, 453.9378; found, 453.9361. $R_f = 0.37$ (20% diethyl ether in hexanes) Silica gel, UV, potassium permanganate.

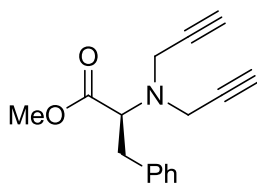


N-propargyl-L-proline methyl ester (**7.11g**). Followed general procedure D: Dicobalt hexacarbonyl complexed alkyne **7.10g** (20 mg, 0.044 mmol), acetone (5.0 mL), and ceric ammonium nitrate (97 mg, 0.18 mmol). After 1 h of stirring, **7.10g** remained, as evidenced by proton NMR. An additional amount of ceric ammonium nitrate (10 mg, 0.018 mmol) was added and stirred for 20 min. The work-up afforded 5 mg of alkyne **7.11g** in 68% yield as a colorless oil. Further purification was not performed. Characterization via ^1H NMR, ^{13}C NMR, and HRMS was obtained; however, **7.11g** appears to be unstable leading to decomposition and poor reproducibility of these data. ^1H NMR (400 MHz, CDCl_3) 3.74 (s, 3H), 3.61 (t, $J = 2.4$ Hz, 2H), 3.45 (dd, $J = 8.8$, 6.8 Hz, 1H), 3.09-3.04 (m, 1H), 2.73 (td, $J = 8.8$, 7.6 Hz, 1H), 2.21 (t, $J = 2.4$ Hz, 1H), 2.19-2.11 (m, 1H), 2.03-1.76 (m, 3H) ppm. ^{13}C NMR (100 MHz, CDCl_3) 174.3, 78.5, 73.3, 62.7, 52.3, 52.2, 41.3, 29.8, 23.4 ppm. Impurity present at 30.5 ppm. HRMS (FTMS + p ESI Full ms) $[\text{M}+\text{H}]^+$ calc'd for $\text{C}_9\text{H}_{14}\text{O}_2\text{N}$, 168.1019; found, 168.1013.



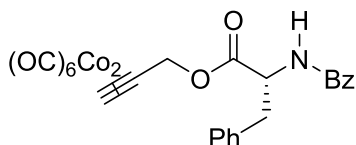
Bis(dicobalt hexacarbonyl) complexed *N,N*-di(prop-2-ynyl)-*L*-phenylalanine methyl ester (**7.10h**). Follows general procedure C3: Tetrafluoroborate salt **7.6c** (46 mg, 0.11 mmol, 1 equiv), dichloromethane (2 mL), *L*-phenyl alanine methyl ester **7.9h** (20 mg, 0.11 mmol, 1 equiv) dissolved in dichloromethane (0.3 mL). The reaction stirred for 1.5 h. The crude residue was purified by silica gel flash column chromatography (gradient of 2-20% diethyl ether in hexanes) to afford 46 mg of cobalt complexed dialkyne **7.10h** in 59% yield as a red oil. The yield was calculated using tetrafluoroborate salt **7.6c** as the limiting reagent. ^1H NMR (300 MHz, CDCl_3) 7.31-7.22 (m, 3H), 7.17 (d, $J = 7.2$ Hz, 2H), 6.10 (s, 2H), 4.41 (d, $J = 15.9$ Hz, 2H), 4.04-3.99 (m, 3H), 3.56 (s, 3H), 3.21 (t, $J = 12.0$ Hz, 1H), 2.96-2.92 (m, 1H) ppm. ^{13}C NMR (100 MHz, CDCl_3) 199.7 (12C), 172.0, 137.3, 129.3 (2C), 128.7 (2C), 126.9, 91.1 (2C), 73.8 (2C), 64.4, 55.1 (2C), 51.3, 36.5 ppm. IR (thin film) 2093, 3052, 2017, 1735, 1425, 1200, 1165 cm^{-1} . HRMS (FTMS + p ESI Full ms)

$[\text{M}+\text{H}]^+$ calc'd for $\text{C}_{28}\text{H}_{18}\text{O}_{14}\text{NC}_4$, 827.8050; found, 827.8084. $R_f = 0.48$ (10% diethyl ether in hexanes) Silica gel, UV visible.

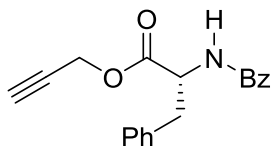


N,N-di(prop-2-ynyl)-*L*-phenylalanine methyl ester (**7.11h**). Followed general procedure D: Dicobalt hexacarbonyl complexed dialkyne **7.10h** (21 mg, 0.025 mmol, 1 equiv), acetone (4.0 mL), and ceric ammonium nitrate (111 mg, 0.20 mmol, 8 equiv). The reaction was complete after 20 min of stirring. The crude residue was purified using silica gel flash column chromatography (gradient of 15-30% diethyl ether in hexanes), which afforded 4 mg of alkyne **7.11h** in 56% yield as an oil. ^1H NMR (400 MHz, CDCl_3) 7.30-7.26 (m, 2H), 7.23-7.7.18 (m, 3H), 3.75 (t, $J = 7.6$ Hz, 1H), 3.68 (d, $J = 2.4$ Hz, 4H), 3.57

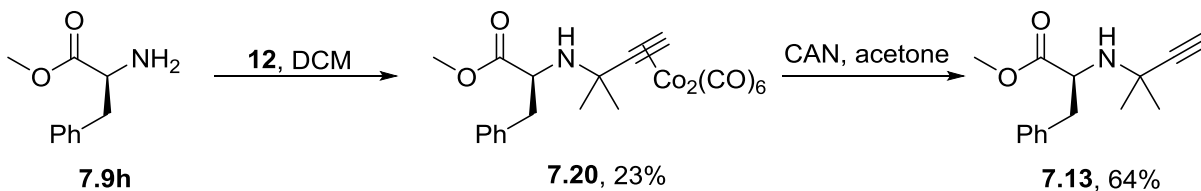
(s, 3H), 3.05 (d, $J = 7.6$ Hz, 2H), 2.25 (t, $J = 2.4$ Hz, 2H) ppm. ^{13}C NMR (100 MHz, CDCl_3) 172.1, 137.5, 129.3 (2 C), 128.6 (2 C), 126.8, 79.3 (2 C), 73.1 (2 C), 65.9, 51.5, 40.1 (2 C), 36.5 ppm. IR (thin film) 3250, 2991, 2914, 2813, 2344, 1714, 1478, 1421, 1347, 1199, 1153, 1112, 740, 692, 623 cm^{-1} . HRMS (FTMS + p ESI Full ms) $[\text{M}+\text{H}]^+$ calc'd for $\text{C}_{16}\text{H}_{18}\text{O}_2\text{N}$, 256.1332; found, 256.1335. $R_f = 0.37$ (20% diethyl ether in hexanes) Silica gel, UV, potassium permanganate.



Dicobalt hexacarbonyl prop-2-yn-1-yl benzoylphenylalaninate complex (**7.10i**). Follows general procedure C2: propargyl alcohol (11 mg, 0.20 mmol), dichloromethane (1.1 mL), dicobalt octacarbonyl (69 mg, 0.20 mmol), *N*-benzoyl-D-phenylalanine (**7.9i**) (27 mg, 0.10 mmol, 1 equiv), dissolved in dichloromethane (1.0 mL), and boron trifluoride diethyl etherate (32 μL , 0.26 mmol). The reaction stirred for 2 h. The crude residue was purified by silica gel flash column chromatography (10% ethyl acetate in hexanes) to afford 35 mg of **7.10i** in 60% yield as a dark red oil. ^1H NMR (400 MHz, CDCl_3) 7.72-7.70 (m, 1H), 7.51 (t, $J = 7.6$ Hz, 1H), 7.42 (t, $J = 7.6$ Hz, 2H), 7.31-7.28 (m, 3H), 7.17-7.15 (m, 2H), 6.55 (d, $J = 7.2$ Hz, 1H), 6.08 (s, 2H), 5.44 (d, $J = 14.4$ Hz, 1H), 5.24 (d, $J = 14.0$ Hz, 1H), 5.18 (dt, $J = 7.6, 5.6$ Hz, 1H), 3.36 (dd, $J = 14.0, 5.6$ Hz, 1H), 3.27 (dd, $J = 14.0, 6.0$ Hz, 1H) ppm. ^{13}C NMR (125 MHz, CDCl_3) 199.1 (6C), 171.5, 166.9, 135.9, 134.0, 131.9, 129.5 (2C), 128.9 (2C), 128.8 (2C), 127.5, 127.2 (2C), 87.2, 72.4, 66.8, 53.8, 38.0 ppm. IR (thin film) 3031, 2925, 2097, 2056, 2025, 1746, 1647, 1531, 1487, 1178, 700 cm^{-1} . HRMS (FTMS + p ESI Full ms) $[\text{M}+\text{Na}]^+$ calc'd for $\text{C}_{25}\text{H}_{17}\text{O}_9\text{NCo}_2$, 615.9460; found, 615.9453. $R_f = 0.34$ (20% ethyl acetate in hexanes) Silica gel, visible UV.

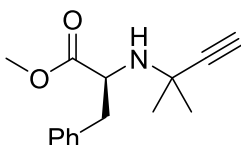


Prop-2-yn-1-yl benzoylphenylalaninate (**7.11i**). Followed general procedure D: Dicobalt hexacarbonyl complexed alkyne **7.10i** (20 mg, 0.034 mmol), acetone (2.5 mL), and ceric ammonium nitrate (75 mg, 0.138 mmol). The reaction was complete after 10 min of stirring. Reaction work up afforded 10 mg of pure alkyne **7.11i** as a white sticky solid in 90% yield. Purification by silica gel column was not performed. ^1H NMR (400 MHz, CDCl_3) 7.72-7.70 (m, 2H), 7.53-7.47 (m, 1H), 7.45-7.41 (m, 2H), 7.32-7.26 (m, 3H), 7.19-7.17 (m, 2H), 6.53 (d, $J = 7.6$ Hz, 1H), 5.14 (dt, $J = 7.6, 5.6$ Hz, 1H), 4.82 (dd, $J = 15.6, 2.6$ Hz, 1H), 4.73 (dd, $J = 15.6, 2.6$ Hz, 1H), 3.33 (dd, $J = 13.8, 5.8$ Hz, 1H), 3.27 (dd, $J = 13.8, 5.4$ Hz, 1H), 2.54 (t, $J = 2.4$ Hz, 1H) ppm. Impurities seen at 1.43, 1.25, 0.88 ppm. ^{13}C NMR (125 MHz, CDCl_3) 171.0, 167.0, 135.7, 134.0, 132.0, 129.6 (2C), 128.83 (2C), 128.80 (2C), 127.5, 127.2 (2C), 75.8, 53.5, 53.0, 37.9, 29.8 ppm. IR (thin film) 3396, 3277, 3070, 2920, 2851, 2131, 1762, 1647, 1521, 1488, 1205, 1171 cm^{-1} . HRMS (FTMS + p ESI Full ms) $[\text{M}+\text{H}]^+$ calc'd for $\text{C}_{19}\text{H}_{17}\text{O}_3\text{N}$, 308.1281; found, 308.1282. $R_f = 0.21$ (20% ethyl acetate in hexanes) Silica gel, UV.

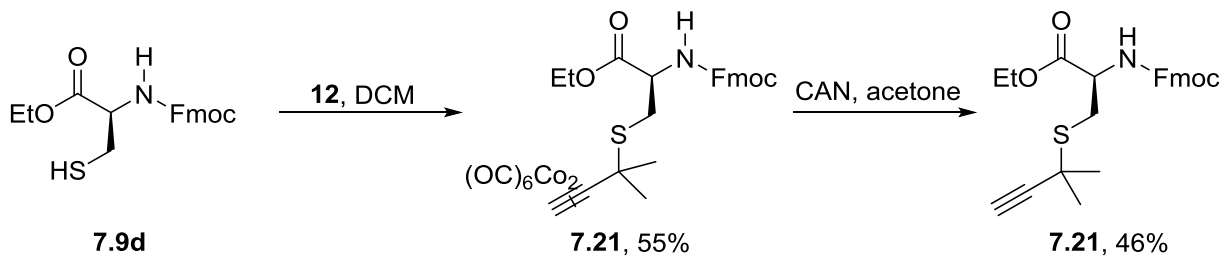


$\text{Co}_2(\text{CO})_6$ -*N*-(1,1-dimethyl-3-propynyl)-*L*-phenylalanine methyl ester (**7.20**). Follows general procedure C3: Tetrafluoroborate salt **7.12** (77 mg, 0.18 mmol, 1.3 equiv), dichloromethane (2.5 mL), *L*-phenylalanine methyl ester **7.9h** (24 mg, 0.14 mmol, 1 equiv) dissolved in dichloromethane (0.5 mL). The reaction stirred for 40 min. The crude residue was purified by silica gel flash column chromatography (gradient of 5-20% diethyl ether in hexanes) to afford 16 mg of cobalt complexed alkyne **S7** in 23% yield as a red oil. ^1H NMR (400 MHz, CDCl_3) 7.29-7.17 (m, 5 H), 5.99 (s, 1H), 3.72 (dt, $J = 7.6,$

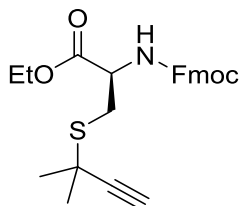
3.2 Hz, 1H), 3.62 (s, 3H), 2.92-2.81 (m, 2H), 1.90 (d, $J = 8.4$ Hz, 1H), 1.29 (s, 3H), 1.20 (3H) ppm. ^{13}C NMR (100 MHz, CDCl_3) 200.1 (6C), 176.6, 137.6, 129.6 (2C), 128.4 (2C), 126.8, 107.3, 72.2, 58.0, 56.7, 52.0, 41.9, 32.1, 30.9 ppm. IR (thin film) 2973, 2927, 2092, 2050, 2019, 1739, 1455, 1194, 1172, 700 cm^{-1} . HRMS (FTMS + p ESI Full ms) $[\text{M}+\text{H}]^+$ calc'd for $\text{C}_{21}\text{H}_{20}\text{O}_8\text{NCO}_2$, 531.9847; found, 531.9848. $R_f = 0.35$ (10% diethyl ether in hexanes) Silica gel, Visible, UV.



N-(1,1-dimethyl-3-propynyl)-*L*-phenylalanine methyl ester (**7.13**). Followed general procedure D: $\text{Co}_2(\text{CO})_6$ -alkyne **7.20** (12 mg, 0.023 mmol), acetone (4.0 mL), and ceric ammonium nitrate (50 mg, 0.090 mmol). The reaction was complete after 20 min of stirring as indicated by consumption of **S7**, as evidenced by TLC. However, **7.13** was not visible by TLC until after the reaction work up. The crude residue was purified by silica gel flash column chromatography (10% diethyl ether in hexanes) which afforded 4 mg of alkyne **7.13** in 64% yield as a colorless oil. ^1H NMR (400 MHz, CDCl_3) 7.30-7.26 (m, 2H), 7.23-7.19 (m, 3H), 3.73 (dd, $J = 7.8, 6.4$ Hz, 1H), 3.63 (s, 3H), 2.93 (dd, $J = 13.4, 6.4$ Hz, 1H), 2.84 (dd, $J = 13.4, 7.8$ Hz, 1H), 2.18 (s, 1H), 1.92 (bs, 1H), 1.31 (s, 3H), 1.19 (s, 3H) ppm. ^{13}C NMR (100 MHz, CDCl_3) 176.3, 137.5, 129.6 (2C), 128.4 (2C), 126.8, 88.5, 70.1, 58.9, 51.7, 49.6, 41.4, 30.3, 29.6 ppm. IR (thin film) 3286, 3027, 2977, 2929, 2368, 1736, 1458, 1438, 1196, 1171, 700 cm^{-1} . HRMS (FTMS + p ESI Full ms) $[\text{M}+\text{H}]^+$ calc'd for $\text{C}_{15}\text{H}_{20}\text{O}_2\text{N}$, 246.1489; found, 246.1478. $R_f = 0.33$ (20% diethyl ether in hexanes) Silica gel, UV, potassium permanganate.

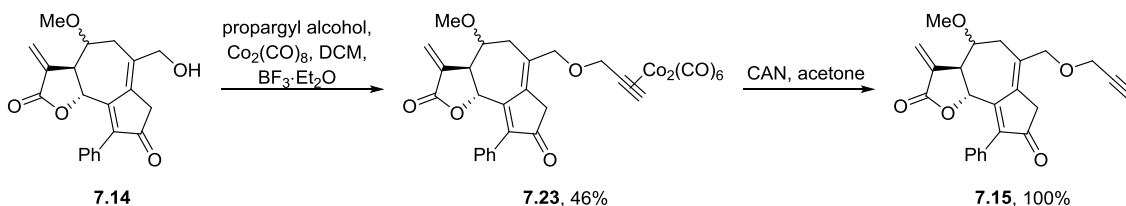


Co₂(CO)₆-Ethyl *N*-(((9H-fluoren-9-yl)methoxy)carbonyl)-*S*-(1,1-dimethyl-3-propynyl)-*L*-cysteinate (**7.21**). Follows general procedure C3: Tetrafluoroborate salt **7.12** (62 mg, 0.14 mmol, 1.3 equiv), dichloromethane (1.5 mL), *N*-(((9H-fluoren-9-yl)methoxy)carbonyl)-*L*-cysteine ethyl ester **7.9d** (42 mg, 0.11 mmol, 1 equiv) dissolved in dichloromethane (0.8 mL). The reaction stirred for 2 h. The crude residue was purified by silica gel flash column chromatography (gradient of 15-30% diethyl ether in hexanes) to afford 42 mg of cobalt complexed alkyne **7.21** in 55% yield as a red oil. ¹H NMR (400 MHz, CDCl₃) 7.77 (d, *J* = 7.6 Hz, 2H), 7.60 (d, *J* = 7.2 Hz, 2H), 7.41 (t, *J* = 7.4 Hz, 2H), 7.32 (t, *J* = 7.4 Hz, 2H), 6.23 (s, 1H), 5.59 (d, *J* = 7.6 Hz, 1H), 4.71-4.66 (m, 1H), 4.39 (d, *J* = 7.2 Hz, 2H), 4.27-4.21 (m, 3H), 3.19-3.10 (m, 2H), 1.621 (s, 3H), 1.616 (s, 3H), 1.30 (t, *J* = 7.2 Hz, 3H) ppm. ¹³C NMR (125 MHz, CDCl₃) 199.8 (6C), 170.5, 155.8, 144.0, 143.9, 141.5 (2C), 127.9 (2C), 127.2 (2C), 125.3 (2C), 120.2 (2C), 105.0, 73.1, 67.4, 62.2, 53.6, 48.9, 47.3, 32.7 (2C), 32.4, 14.3 ppm. IR (thin film) 3338, 3070, 2979, 2092, 2053, 2022, 1725, 1510, 1451, 1200, 1052, 759, 740 cm⁻¹. HRMS (FTMS + p ESI Full ms) [M+NH₄]⁺ calc'd for C₃₁H₃₁O₁₀N₂SCo₂, 741.0358; found, 741.0379. R_f = 0.18 (20% diethyl ether in hexanes) Silica gel, visible, UV.



N-(((9H-fluoren-9-yl)methoxy)carbonyl)-*S*-(1,1-dimethyl-3-propynyl)-*L*-cysteine ethyl ester (**7.22**). Followed general procedure D: Co₂(CO)₆-alkyne **7.22** (47 mg, 0.069 mmol), acetone (6.9 mL), and ceric ammonium nitrate (152 mg, 0.28 mmol). The reaction was

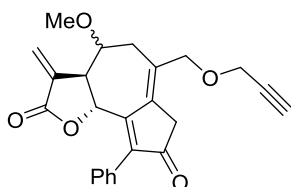
complete after 15 min of stirring. The crude residue was purified by silica gel flash column chromatography (20% diethyl ether in hexanes) which afforded 14 mg of alkyne **7.22** in 46% yield as a colorless oil. ¹H NMR (400 MHz, CDCl₃) 7.77 (d, *J* = 7.6 Hz, 2H), 7.63-7.58 (m, 2H), 7.40 (app t, *J* = 7.4 Hz, 2H), 7.30 (app t, *J* = 7.4 Hz, 2H), 5.65 (d, *J* = 8.0 Hz, 1H), 4.69 (dt, *J* = 8.0, 5.2 Hz, 1H), 4.44-4.37 (m, 2H), 4.27-4.21 (m, 3H), 3.28-3.19 (m, 2H), 2.37 (s, 1H), 1.57 (s, 6H), 1.30 (t, *J* = 7.0 Hz, 3H) ppm. ¹³C NMR (100 MHz, CDCl₃) 170.7, 155.9, 144.0, 143.9, 141.5, 141.4, 127.9 (2C), 127.2 (2C), 125.3 (2C), 120.1 (2C), 87.8, 70.9, 67.3, 62.1, 53.6, 47.3, 38.7, 33.2, 30.79, 30.75, 14.3 ppm. IR (thin film) 3292, 2976, 2925, 2365, 1719, 1509, 1449, 1339, 1208, 1051, 759, 740 cm⁻¹. HRMS (FTMS + p ESI Full ms) [M+H]⁺ calc'd for C₂₅H₂₈O₄NS, 438.1734; found, 438.1725. R_f = 0.23 (30% diethyl ether in hexanes) Silica gel, UV, potassium permanganate.



Dicobalt hexacarbonyl complexed 4-methoxy-3-methylene-9-phenyl-6-((prop-2-yn-1-yl)oxy)methyl)-3a,5,7,9b-tetrahydroazuleno[4,5-b]furan-2,8(3H,4H)-dione (**7.23**).

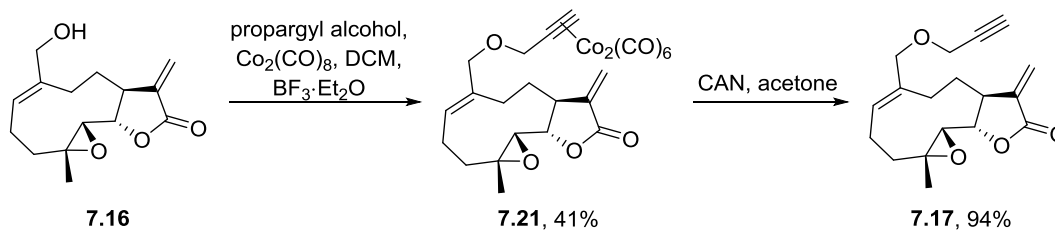
Follows general procedure C2: propargyl alcohol (5 mg, 0.091 mmol), dichloromethane (0.60 mL), dicobalt octacarbonyl (31 mg, 0.091 mmol), alcohol **7.14**³⁶³ (16 mg, 0.045 mmol), dissolved in dichloromethane (0.40 mL), and boron trifluoride diethyl etherate (15 μ L, 0.11 mmol). The reaction was monitored by TLC and stirred for 2 h. The crude residue was purified by silica gel flash column chromatography (gradient of 10-30% ethyl acetate in hexanes) to afford 14 mg of **7.23** as a mixture of two diastereomers (2.1:1) in 46% yield as a dark red/brown oil. ¹H NMR (400 MHz, CDCl₃) 7.40-7.35 (m, 3 H), 7.31-7.26 (m, 2 H), 6.34 (d, *J* = 3.6 Hz, 1 H)**, 6.24 (d, *J* = 3.2 Hz, 1 H)*, 6.09 (s, 1 H), 5.86 (d, *J* = 3.2 Hz, 1 H)*, 5.78 (d, *J* = 9.6 Hz, 1 H)**, 5.47 (d, *J* = 3.2 Hz, 1 H)**, 5.38 (d, *J* = 10.4 Hz, 1 H)*, 4.69 (d, *J* = 13.6 Hz, 2 H)*, 4.63 (d, *J* = 13.2 Hz, 2 H)**, 4.33 (d, *J* = 12.4 Hz, 2 H)**, 4.25 (d, *J* = 12.8 Hz, 2 H)*, 4.10-4.05 (m, 1 H)**, 3.88-3.86

(m, 1 H)*, 3.51 (s, 3 H)*, 3.39 (s, 3H)**, 3.32-3.14 (m, 4 H), 2.52-2.41 (m, 1 H) ppm. ¹³C NMR (100 MHz, CDCl₃) 201.4*(6C), 201.1** (6C), 199.6, 168.3**, 167.9*, 162.2**, 161.5*, 144.0**, 143.0*, 137.2*, 135.0**, 134.4*, 133.6**, 131.6*, 130.72**, 130.65*, 130.3**, 130.0*, 129.9**, 128.84**, 128.77*, 127.8**, 127.7*, 122.8**, 122.2*, 90.7**, 90.6*, 81.8*, 75.7*, 74.7**, 73.6**, 73.4*, 73.3**, 71.9*, 71.6**, 71.4**, 71.1*, 57.2**, 56.5*, 49.8*, 40.0**, 39.7*, 33.8**, 29.8**, 29.5* ppm. IR (thin film) 2927, 2829, 2372, 2093, 2051, 2022, 1773, 1702, 12.68, 1096, 1018, 697 cm⁻¹. *Major diastereomer, **minor diastereomer. HRMS (FTMS + p ESI Full ms) [M+H]⁺ calc'd for C₃₀H₂₃O₁₁CO₂, 676.9899; found, 676.9903. R_f = 0.26*, 0.22** (30% ethyl acetate/hexanes) Silica gel, Visible, UV.



4-Methoxy-3-methylene-9-phenyl-6-((prop-2-yn-1-yloxy)methyl)-3a,5,7,9b-tetrahydroazuleno[4,5-b]furan-2,8(3H,4H)-dione (**7.15**). Follows general procedure D: cobalt complex **7.23** (14 mg, 0.021 mmol, 1 equiv), acetone (1.5 mL), and ceric ammonium nitrate (68 mg, 0.12 mmol, 6 equiv). The reaction stirred for 15 min. The reaction afforded 9 mg of alkyne **7.15** as a mixture of two diastereomers (2.1:1) in quantitative yield as a colorless oil. The crude material was not purified further. ¹H NMR (400 MHz, CDCl₃) 7.38-7.35 (m, 3 H), 7.30-7.24 (m, 2 H), 6.36 (d, *J* = 3.2 Hz, 1 H)**, 6.24 (d, *J* = 3.2 Hz, 1 H)*, 5.88 (d, *J* = 2.8 Hz, 1 H)*, 5.78 (d, *J* = 9.6 Hz, 1 H)**, 5.52 (d, *J* = 3.2 Hz, 1 H)**, 5.38 (d, *J* = 10.4 Hz, 1 H)*, 4.23-4.16 (m, 4 H), 4.09-4.06 (m, 1 H)**, 3.87-3.84 (m, 1 H)*, 3.51 (s, 3 H)*, 3.43 (s, 3 H)**, 3.38-3.12 (m, 4 H), 2.52-2.46 (m, 2 H) ppm. ¹³C NMR (150 MHz, CDCl₃) 201.5*, 201.3**, 168.3**, 167.9*, 161.9**, 161.4*, 144.2**, 143.2*, 137.2*, 135.8**, 135.4*, 133.6**, 130.9*, 130.73**, 130.65*, 129.93 (2C)*, 129.89 (2C)**, 129.7**, 128.9**, 128.8*, 127.80 (2C)**, 127.75 (2C)*, 122.9**, 122.2*, 81.8*, 79.5*, 79.3*, 75.7*, 75.6**, 75.4*, 74.8**, 73.8**, 71.9**, 71.5*, 57.8**, 57.4**, 57.2*, 56.5*, 49.8*, 49.7**, 40.0**, 39.7*, 30.0*, 29.7** ppm.

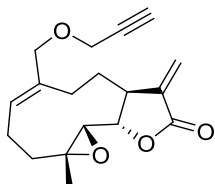
Minor impurities observed: 67.6, 34.2, 29.9, 24.0, 22.9, 14.3 ppm. *Major diastereomer, **minor diastereomer. IR (thin film) 3279, 2933, 2852, 2115, 1769, 1703, 1492, 1445, 1269, 1134, 1095, 699 cm^{-1} . HRMS (FTMS + p ESI Full ms) $[\text{M}+\text{H}]^+$ calc'd for $\text{C}_{24}\text{H}_{23}\text{O}_5$, 391.1540; found, 391.1525. $R_f = 0.18$ (40% ethyl acetate/hexanes) Silica gel, UV, potassium permanganate.



$\text{Co}_2(\text{CO})_6$ -*O*-(prop-2-ynyl)-MelB (**7.21**). **Method A:** Follows general procedure C2: Propargyl alcohol (4 mg, 0.076 mmol), dichloromethane (0.5 mL), dicobalt octacarbonyl (26 mg, 0.076 mmol), Melampomagnolide B (**MelB**, **7.16**)^{250d} (10 mg, 0.038 mmol), dissolved in dichloromethane (0.3 mL), and boron trifluoride diethyl etherate (12 μL , 0.095 mmol). The reaction was quenched after 10 min of stirring despite a small amount of Mel B remaining in the reaction. The crude residue was purified by silica gel flash column chromatography (gradient of 10-20% ethyl acetate in hexanes) to afford 9 mg of **7.21** in 41% yield as a dark red oil.

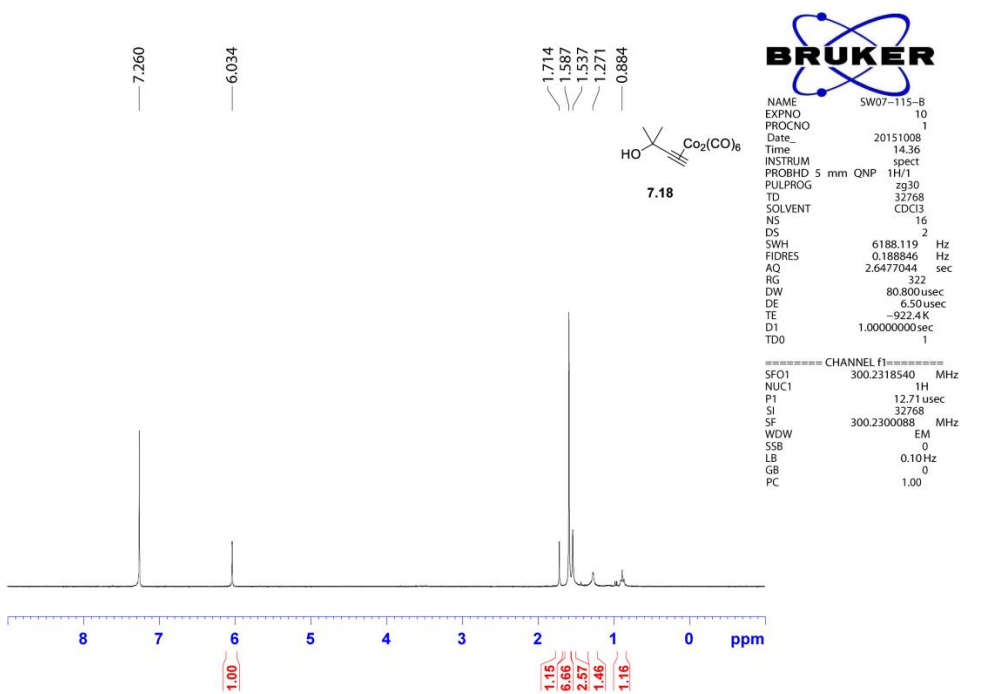
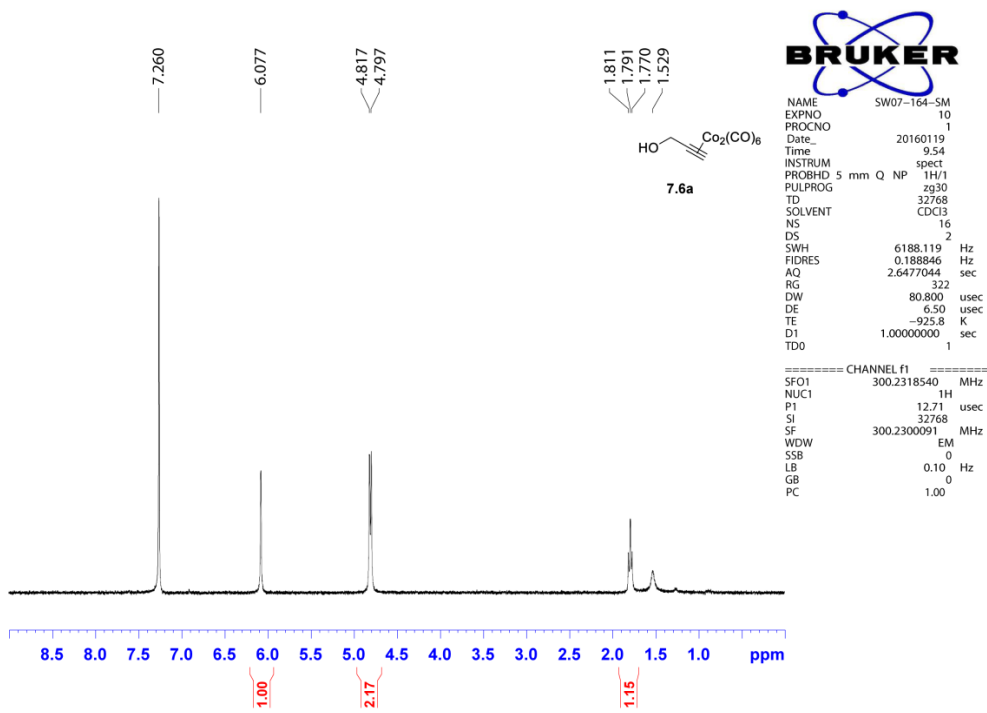
Method B: Follows general procedure C2: Methyl propargyl ether (8 mg, 0.11 mmol), dichloromethane (0.8 mL), dicobalt octacarbonyl (39 mg, 0.11 mmol), Mel B (**7.16**) (15 mg, 0.057 mmol), dissolved in dichloromethane (0.4 mL), and boron trifluoride diethyl etherate (18 μL , 0.14 mmol). The reaction was quenched after 40 min of stirring despite a small amount of Mel B remaining in the reaction. The crude residue was purified by silica gel flash column chromatography (gradient of 10-20% ethyl acetate in hexanes) to afford 13 mg of **7.24** in 39% yield. ^1H NMR (400 MHz, CDCl_3) 6.25 (s, 1H), 6.04 (s, 1H), 5.67 (br s, 1H), 5.51 (s, 1H), 4.62 (d, $J = 13.2$ Hz, 1H), 4.53 (d, $J = 12.8$ Hz, 1H), 4.25 (d, $J = 11.2$ Hz, 1H), 3.98 (d, $J = 12.0$ Hz, 1H), 3.86 (t, $J = 9.6$ Hz, 1H), 2.87-2.85 (m, 2H), 2.43-2.31 (m, 4H), 2.22-2.15 (m, 2H), 1.67-1.64 (m, 1H), 1.55 (s, 3H), 1.12-1.06 (m, 1H) ppm. ^{13}C NMR (100 MHz, CDCl_3) 199.6 (6C), 169.6, 139.1, 136.8, 129.4,

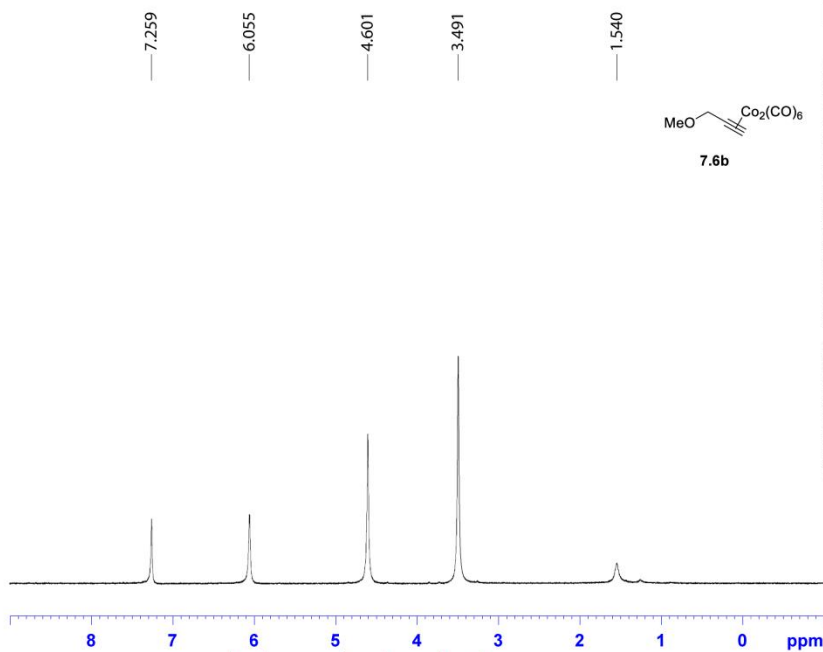
120.2, 91.1, 81.2, 73.8, 71.8, 70.3, 63.6, 60.2, 43.2, 36.9, 25.7, 24.3, 23.8, 18.1 ppm. IR (thin film) 2931, 2360, 2095, 2053, 2023, 1770, 1262, 1138, 1075, 995 cm^{-1} . HRMS (FTMS + p ESI Full ms) $[\text{M}+\text{H}]^+$ calc'd for $\text{C}_{24}\text{H}_{23}\text{O}_{10}\text{Co}_2$, 588.9950; found, 588.9946. R_f = 0.19 (20% ethyl acetate in hexanes) Silica gel, visible, UV.



O-(prop-2-ynyl)-Mel B (**7.17**). Followed general procedure B: $\text{Co}_2(\text{CO})_6$ -alkyne **7.24** (9 mg, 0.015 mmol), acetone (1.5 mL), and ceric ammonium nitrate (34 mg, 0.061 mmol). The reaction was complete after 10 min of stirring. Reaction work up afforded 4 mg of pure alkyne **7.17** as a colorless oil in 94% yield. Further purification was not performed. ^1H NMR (400 MHz, CDCl_3) 6.24 (d, J = 3.6 Hz, 1H), 5.70-5.66 (m, 1H), 5.55 (d, J = 3.2 Hz, 1H), 4.18 (dd, J = 16.0, 2.4 Hz, 1H), 4.16 (d, J = 10.8 Hz, 1H), 4.08 (dd, J = 16.0, 2.4 Hz, 1H), 3.90 (d, J = 11.6 Hz, 1H), 3.86 (t, J = 9.2 Hz, 1H), 2.96-2.82 (m, 1H), 2.86 (d, J = 9.6 Hz, 1H), 2.53-2.45 (m, 1H), 2.44 (t, J = 2.4 Hz, 1H), 2.40-2.27 (m, 3H), 2.22-2.14 (m, 2H), 1.68-1.62 (m, 1H), 1.55 (s, 3H), 1.14-1.07 (m, 1H) ppm. ^{13}C NMR (125 MHz, CDCl_3) 169.6, 139.2, 136.6, 130.4, 120.1, 81.3, 79.7, 74.8, 72.9, 63.6, 60.1, 57.4, 43.1, 36.9, 25.9, 24.6, 23.9, 18.2 ppm. IR (thin film) 3274, 2921, 2850, 2112, 1764, 1261, 1138, 1073, 993, 815 cm^{-1} . HRMS (FTMS + p ESI Full ms) $[\text{M}+\text{H}]^+$ calc'd for $\text{C}_{18}\text{H}_{23}\text{O}_4$, 303.1591; found, 303.1595. R_f = 0.20 (30% ethyl acetate in hexanes) Silica gel, UV, potassium permanganate.

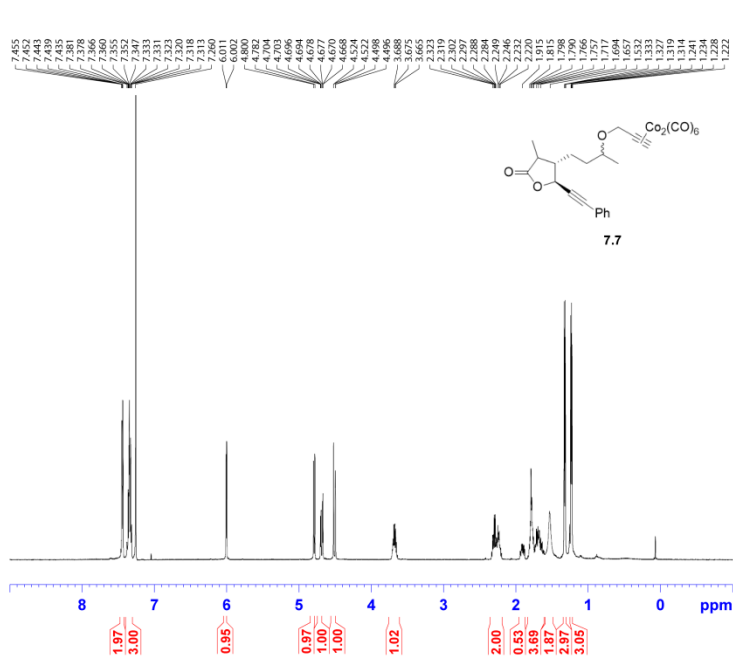
7.7 Spectral Data





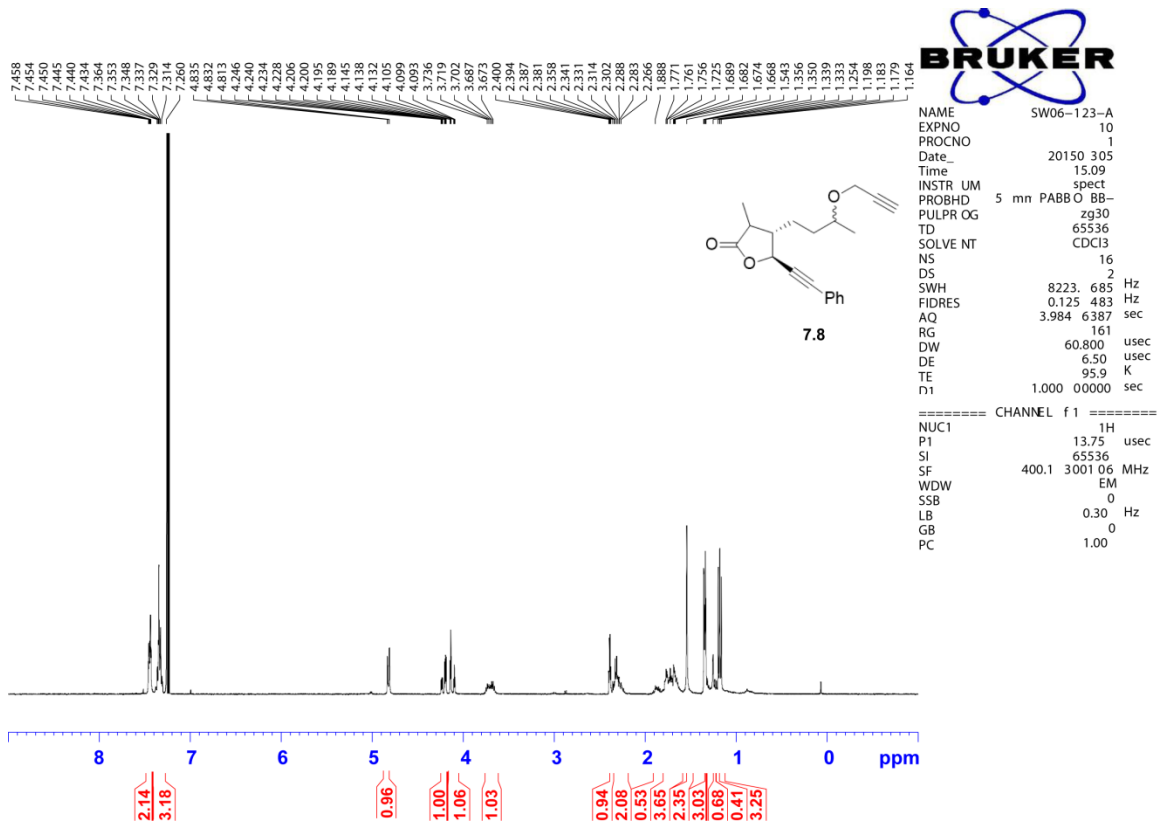
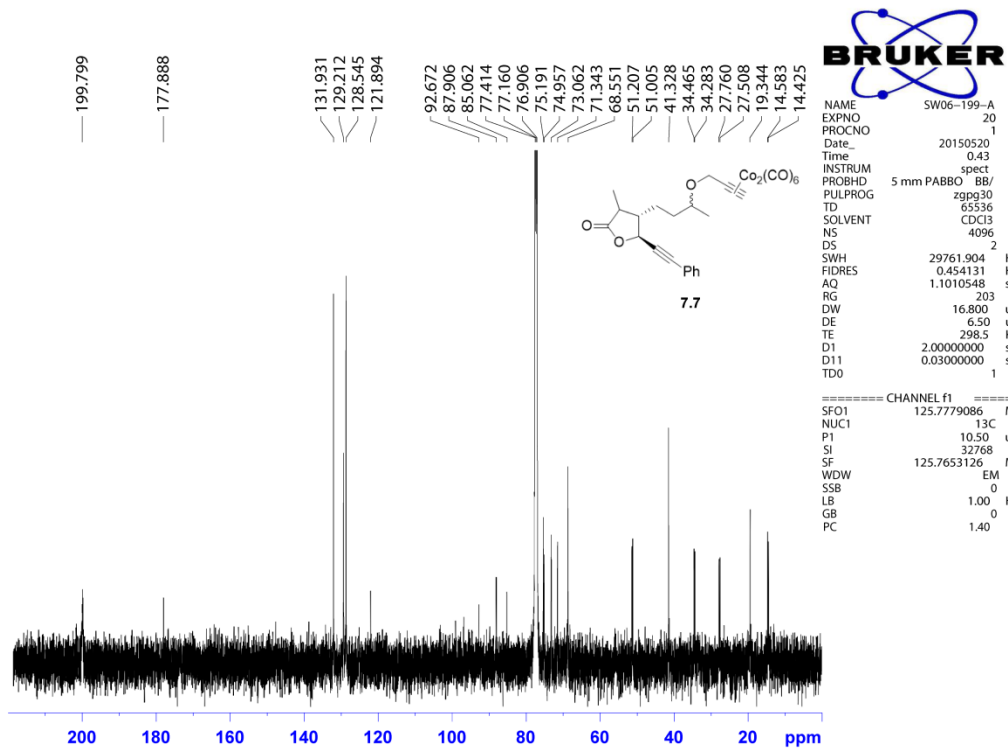
NAME SW07-052-cr
 EXPNO 10
 PROCNO 1
 Date_ 20150728
 Time 15.47
 INSTRUM spect
 PROBHD 5 mm QNP
 PULPROG zg30
 TD 32768
 SOLVENT CDCl₃
 NS 16
 DS 2
 SWH 6188.119 Hz
 FIDRES 0.188846 Hz
 AQ 2.6477044 sec
 RG 322
 DW 80.800 usec
 DE 6.50 usec
 TE -930.4 K
 D1 1.00000000 sec
 TDO 1

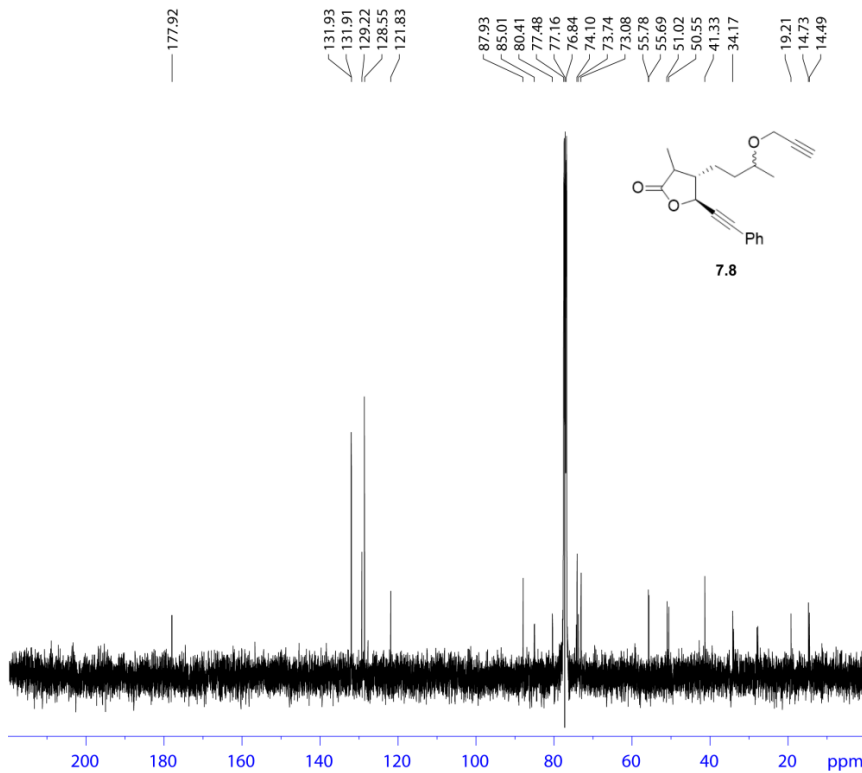
===== CHANNEL f1 =====
 SFO1 300.2318540 MHz
 NUC1 1H
 P1 12.71 usec
 SI 32768
 SF 300.2300091 MHz
 WDW EM
 SSB 0
 LB 0.10 Hz
 GB 0
 PC 1.00



NAME SW06-199-A
 EXPNO 10
 PROCNO 1
 Date_ 20150518
 Time 12.47
 INSTRUM spect
 PROBHD 5 mm PABBO
 PULPROG zg30
 TD 65536
 SOLVENT CDCl₃
 NS 16
 DS 2
 SWH 10000.000 Hz
 FIDRES 0.152586 Hz
 AQ 3.2788500 sec
 RG 203
 DW 50.000 usec
 DE 6.50 usec
 TE 298.2 K
 D1 1.00000000 sec
 TDO 1

===== CHANNEL f1 =====
 SFO1 500.1630887 MHz
 NUC1 1H
 P1 11.45 usec
 SI 65536
 SF 500.1600119 MHz
 WDW EM
 SSB 0
 LB 0.30 Hz
 GB 0
 PC 1.00





```

NAME SW06-123-A
EXPNO 2
PROCNO 1
Date_ 20150307
Time 14.50
INSTRUM spect
PROBHD 5 mm PADUL 13C
PULPROG zgpg30
TD 65536
SOLVENT CDCl3
NS 4394
DS 4
SWH 24038.461 Hz
FIDRES 0.366798 Hz
AQ 1.3631988 sec
RG 45.2
DW 20.800 usec
DE 6.50 usec
TE 295.4 K
D1 3.0000000 sec
D11 0.0300000 sec
TD0 1

```

```

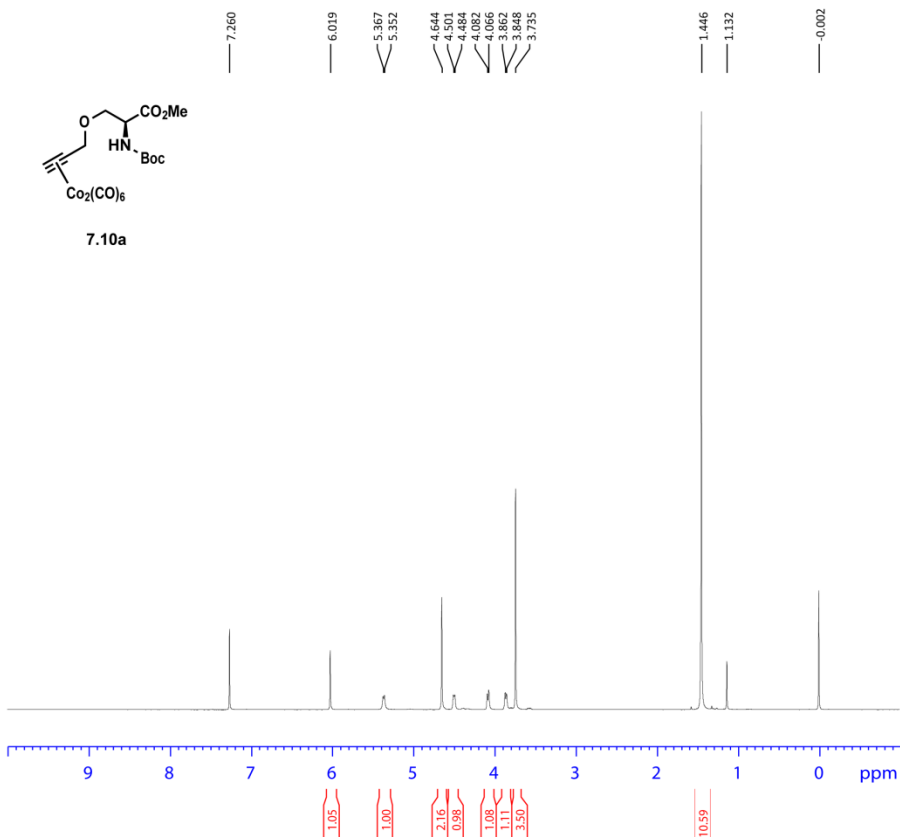
===== CHANNEL f1 =====
NUC1 13C
P1 10.00 usec
PL1 -0.44 dB
PL1W 39.19395828 W
SFO1 100.6479773 MHz

```

```

===== CHANNEL f2 =====
CPDPRG2 waltz16
NUC2 1H
PCPD2 90.00 usec
PL2 -3.90 dB
PL12 15.81 dB
PL13 120.00 dB
PL2W 21.64248466 W
PL12W 0.23137002 W
PL13W 0.00000000 W
SFO2 400.2316009 MHz
SI 32768
SF 100.6379009 MHz
WDW EM
SSB 0
LB 1.00 Hz
GB 0
PC 1.40

```



```

Current Data Parameters
NAME 05-123
EXPNO 1
PROCNO 1

```

```

F2 - Acquisition Parameters
Date_ 20150728
Time 10.10
INSTRUM spect
PROBHD 5 mm PABBO BB/
PULPROG zg30
TD 65536
SOLVENT CDCl3
NS 16
DS 2
SWH 10000.000 Hz
FIDRES 0.152588 Hz
AQ 3.2767999 sec
RG 148.37
DW 50.000 usec
DE 13.29 usec
TE 298.1 K
D1 1.0000000 sec
TD0 1

```

```

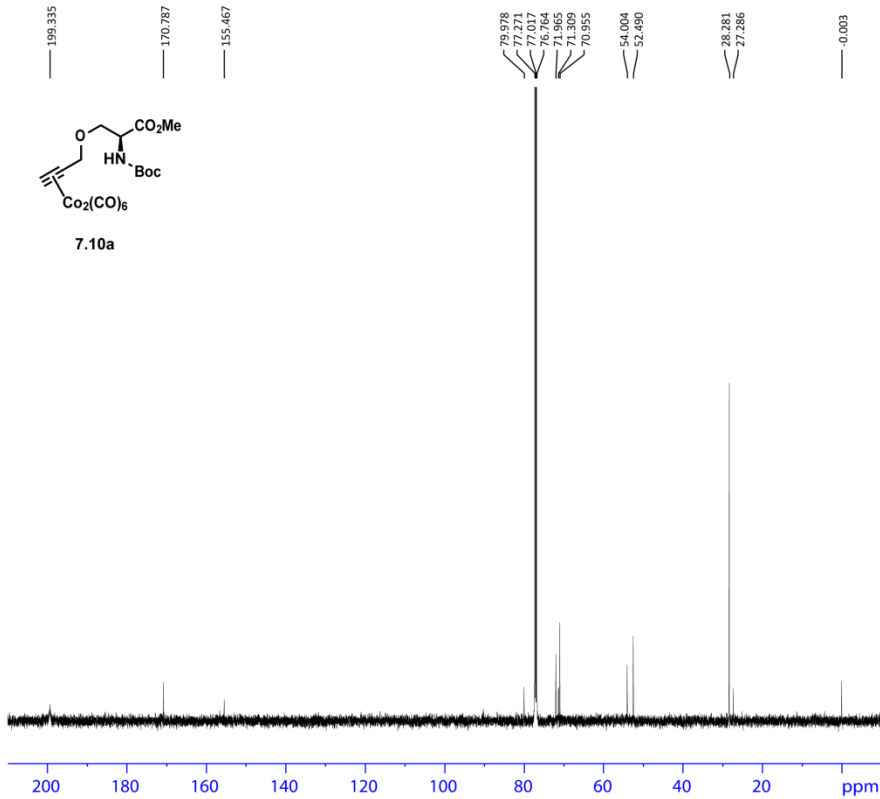
===== CHANNEL f1 =====
SFO1 500.1330885 MHz
NUC1 1H
P1 10.99 usec
PLW1 15.00000000 W

```

```

F2 - Processing parameters
SI 65536
SF 500.1300142 MHz
WDW EM
SSB 0
LB 0.30 Hz
GB 0
PC 1.00

```

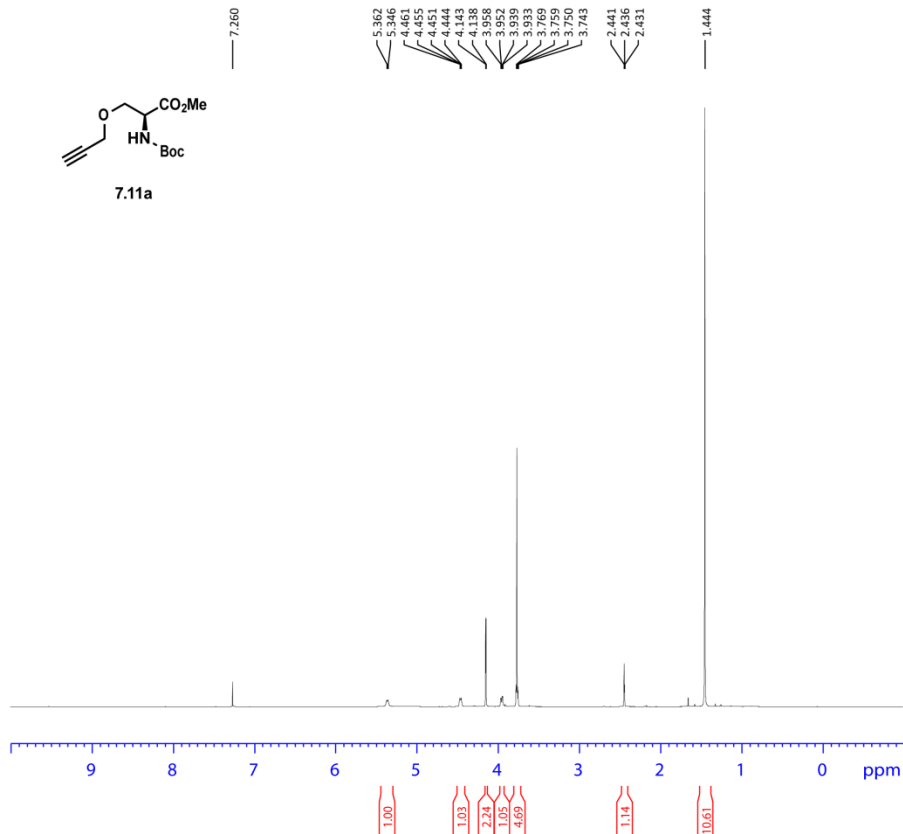
Current Data Parameters
 NAME 05-123
 EXPNO 2
 PROCNO 1

F2 - Acquisition Parameters
 Date_ 20150728
 Time 10.48
 INSTRUM spect
 PROBHD 5 mm PABBO BB/
 PULPROG zgpg30
 TD 65536
 SOLVENT CDCl3
 NS 500
 DS 2
 SWH 29761.904 Hz
 FIDRES 0.454131 Hz
 AQ 1.1010048 sec
 RG 186.69
 DW 16.800 usec
 DE 6.50 usec
 TE 298.1 K
 D1 2.0000000 sec
 D11 0.0300000 sec
 TDO 1

===== CHANNEL f1 =====
 SFO1 125.7703643 MHz
 NUC1 13C
 P1 10.00 usec
 PLW1 84.00000000 W

===== CHANNEL f2 =====
 SFO2 500.1320005 MHz
 NUC2 1H
 CPDPRG2 waltz16
 PCPD2 80.00 usec
 PLW2 15.00000000 W
 PLW12 0.28308001 W
 PLW13 0.18117000 W

F2 - Processing parameters
 SI 32768
 SF 125.7577890 MHz
 WDW EM
 SSB 0
 LB 1.00 Hz
 GB 0
 PC 1.40

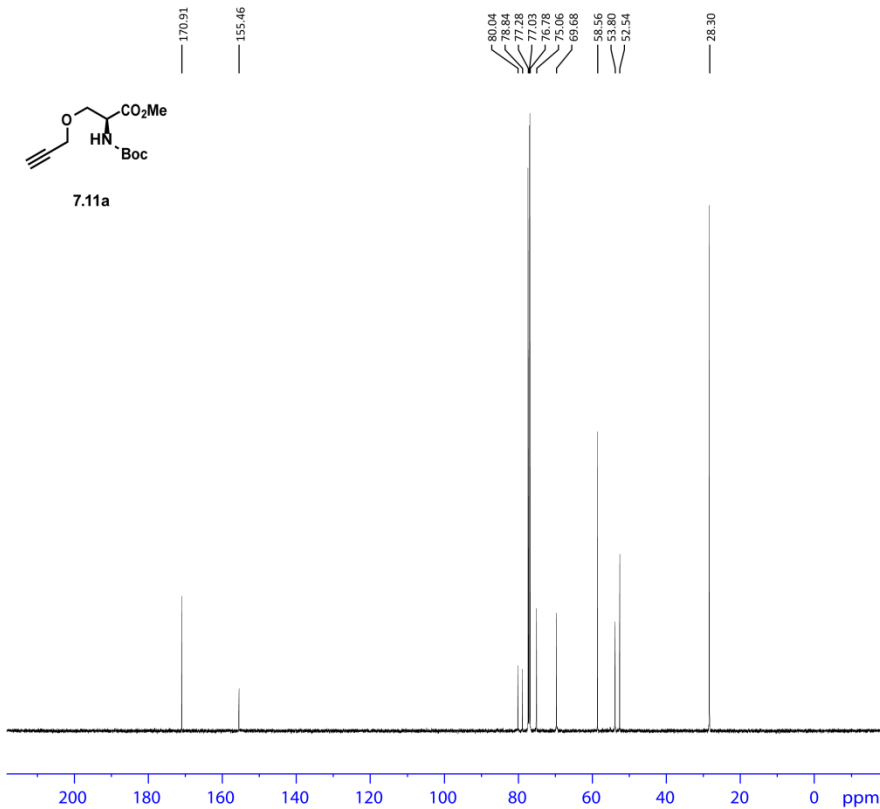


Current Data Parameters
 NAME 05-36 F1
 EXPNO 1
 PROCNO 1

F2 - Acquisition Parameters
 Date_ 20150423
 Time 13.17
 INSTRUM spect
 PROBHD 5 mm PABBO BB/
 PULPROG zg30
 TD 219998
 SOLVENT CDCl3
 NS 16
 DS 2
 SWH 10000.000 Hz
 FIDRES 0.045455 Hz
 AQ 10.9998999 sec
 RG 86.1
 DW 50.000 usec
 DE 13.29 usec
 TE 298.1 K
 D1 1.0000000 sec
 TDO 1

===== CHANNEL f1 =====
 SFO1 500.1330885 MHz
 NUC1 1H
 P1 10.99 usec
 PLW1 15.00000000 W

F2 - Processing parameters
 SI 65536
 SF 500.1300134 MHz
 WDW EM
 SSB 0
 LB 0.30 Hz
 GB 0
 PC 1.00



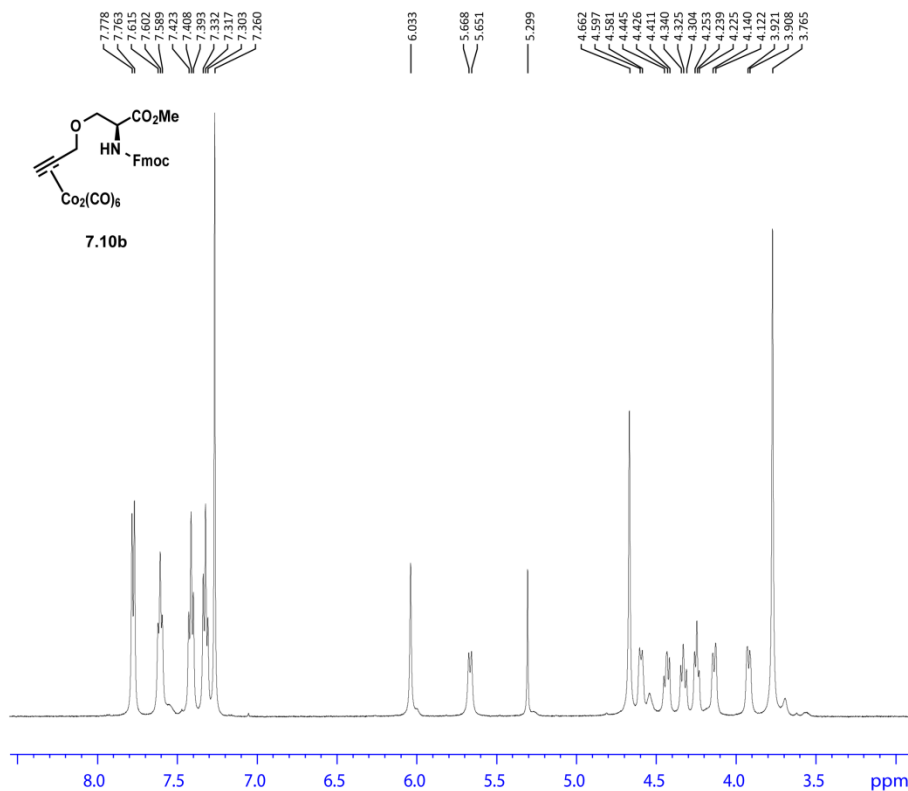
Current Data Parameters
 NAME 05-36 F1
 EXPNO 2
 PROCNO 1

F2 - Acquisition Parameters
 Date_ 20150425
 Time 23.07
 INSTRUM spect
 PROBHD 5 mm PABBO BB/
 PULPROG zgpg30
 TD 65536
 SOLVENT CDCl₃
 NS 1024
 DS 4
 SWH 29761.904 Hz
 FIDRES 0.454131 Hz
 AQ 1.1010048 sec
 RG 186.69
 DW 16.800 usec
 DE 6.50 usec
 TE 298.1 K
 D1 2.0000000 sec
 D11 0.03000000 sec
 TDO 1

===== CHANNEL f1 =====
 SFO1 125.7703637 MHz
 NUC1 13C
 P1 10.00 usec
 PLW1 84.00000000 W

===== CHANNEL f2 =====
 SFO2 500.1320005 MHz
 NUC2 1H
 CPDPRGJ2 waltz16
 PCPD2 80.00 usec
 PLW2 15.00000000 W
 PLW12 0.28308001 W
 PLW13 0.18117000 W

F2 - Processing parameters
 SI 32768
 SF 125.7577890 MHz
 WDW EM
 SSB 0
 LB 1.00 Hz
 GB 0
 PC 1.40

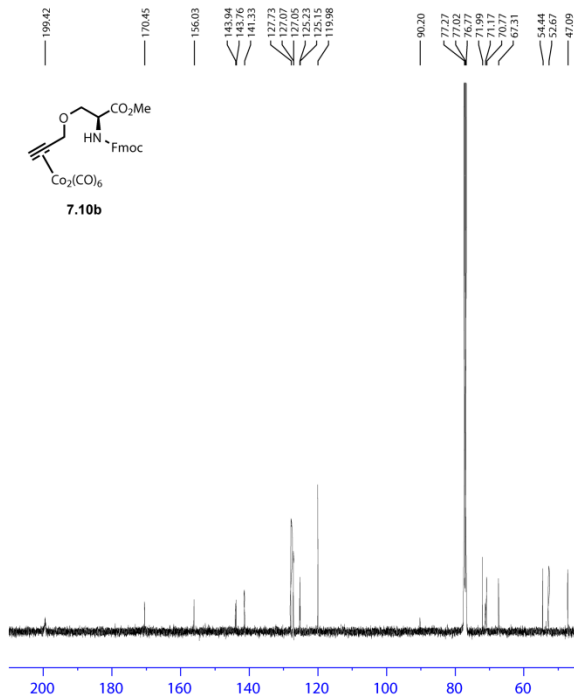


Current Data Parameters
 NAME 05-53 F2
 EXPNO 1
 PROCNO 1

F2 - Acquisition Parameters
 Date_ 20150511
 Time 21.51
 INSTRUM spect
 PROBHD 5 mm PABBO BB/
 PULPROG zg30
 TD 65536
 SOLVENT CDCl₃
 NS 16
 DS 2
 SWH 10000.000 Hz
 FIDRES 0.152588 Hz
 AQ 3.2767999 sec
 RG 186.69
 DW 50.000 usec
 DE 13.29 usec
 TE 298.1 K
 D1 1.0000000 sec
 TDO 1

===== CHANNEL f1 =====
 SFO1 500.1330885 MHz
 NUC1 1H
 P1 10.99 usec
 PLW1 15.00000000 W

F2 - Processing parameters
 SI 65536
 SF 500.1300137 MHz
 WDW EM
 SSB 0
 LB 0.30 Hz
 GB 0
 PC 1.00



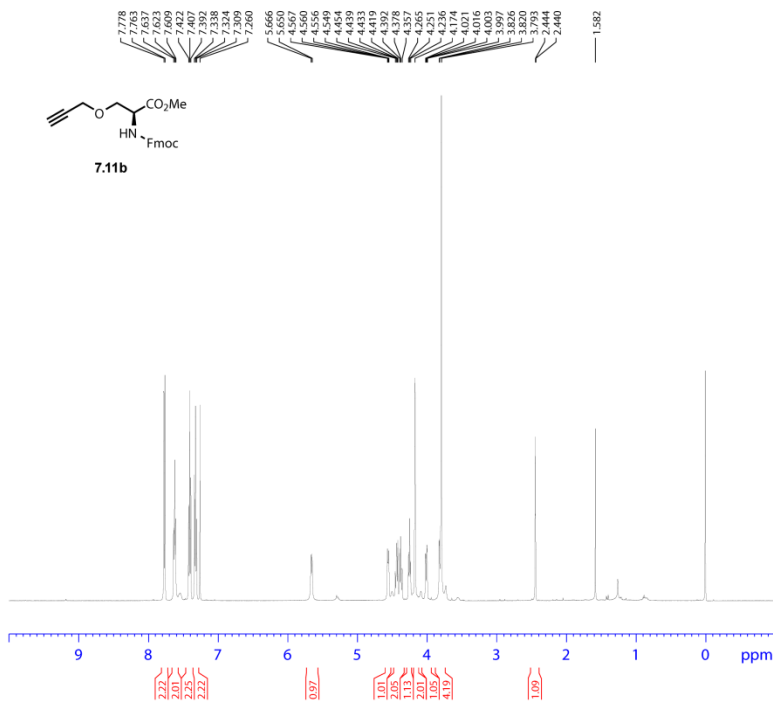
Current Data Parameters
 NAME 05-53 F2
 EXPNO 2
 PROCNO 1

F2 - Acquisition Parameters
 Date_ 20150512
 Time 0.43
 INSTRUM spect
 PROBHD 5 mm PABBO BB/
 PULPROG zgpg30
 TD 65536
 SOLVENT CDCl3
 NS 3000
 DS 4
 SWH 29761.904 Hz
 FIDRES 0.454131 Hz
 AQ 1.1010048 sec
 RG 186.69
 DW 16.800 usec
 DE 6.50 usec
 TE 298.1 K
 D1 2.00000000 sec
 D11 0.03000000 sec
 TDO 1

===== CHANNEL f1 =====
 SFO1 125.7703637 MHz
 NUC1 13C
 P1 10.00 usec
 PLW1 84.00000000 W

===== CHANNEL f2 =====
 SFO2 500.1320005 MHz
 NUC2 1H
 CPDPRG2 waltz16
 PCPD2 80.00 usec
 PLW2 15.00000000 W
 PLW12 0.28308001 W
 PLW13 0.18117000 W

F2 - Processing parameters
 SI 32768
 SF 125.7577890 MHz
 WDW EM
 SSB 0
 LB 1.00 Hz
 GB 0
 PC 1.40

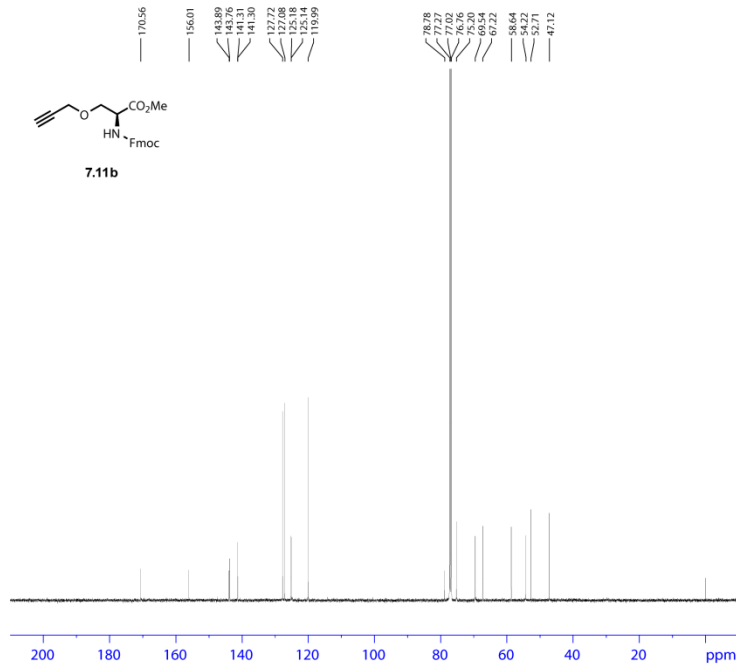


Current Data Parameters
 NAME 05-131
 EXPNO 1
 PROCNO 1

F2 - Acquisition Parameters
 Date_ 20150727
 Time 19.59
 INSTRUM spect
 PROBHD 5 mm PABBO BB/
 PULPROG zg30
 TD 199998
 SOLVENT CDCl3
 NS 16
 DS 2
 SWH 10000.000 Hz
 FIDRES 0.050000 Hz
 AQ 9.9998999 sec
 RG 86.1
 DW 50.000 usec
 DE 13.29 usec
 TE 298.1 K
 D1 1.00000000 sec
 TDO 1

===== CHANNEL f1 =====
 SFO1 500.1330885 MHz
 NUC1 1H
 P1 10.99 usec
 PLW1 15.00000000 W

F2 - Processing parameters
 SI 65536
 SF 500.1330139 MHz
 WDW EM
 SSB 0
 LB 0.30 Hz
 GB 0
 PC 1.00



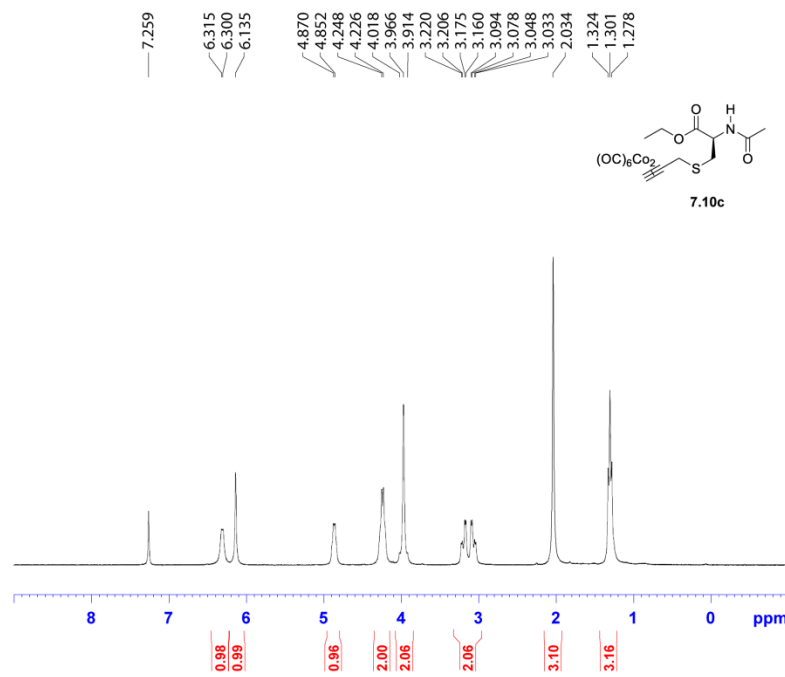
Current Data Parameters
 NAME 05-131
 EXPNO 2
 PROCNO 1

F2 - Acquisition Parameters
 Date_ 20150727
 Time 23.52
 INSTRUM spect
 PROBHD 5 mm PABBO BB/
 PULPROG zgpg30
 TD 65536
 SOLVENT CDCl3
 NS 2000
 DS 4
 SWH 29761.904 Hz
 FIDRES 0.454131 Hz
 AQ 1.1010048 sec
 RG 186.69
 DW 16.800 usec
 DE 6.50 usec
 TE 298.1 K
 D1 2.0000000 sec
 D11 0.03000000 sec
 TDO 1

===== CHANNEL f1 =====
 SFO1 125.7703637 MHz
 NUC1 13C
 P1 10.00 usec
 PLW1 84.0000000 W

===== CHANNEL f2 =====
 SFO2 500.1320005 MHz
 NUC2 1H
 CPDPRG2 waltz16
 PCPD2 80.00 usec
 PLW2 15.0000000 W
 PLW12 0.28308001 W
 PLW13 0.18117000 W

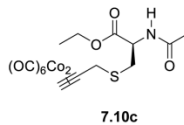
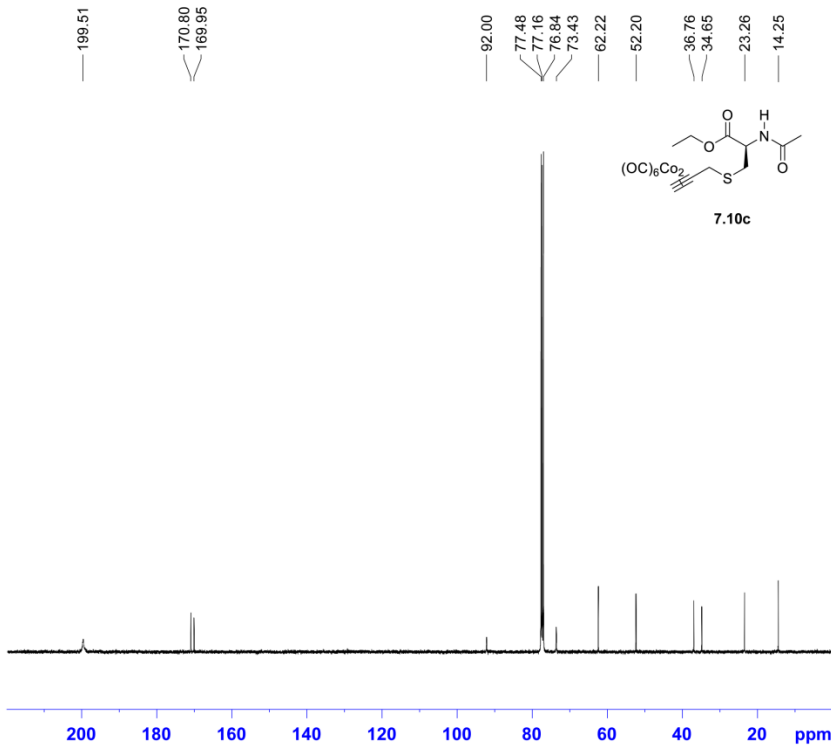
F2 - Processing parameters
 SI 32768
 SF 125.7577906 MHz
 WDW EM
 SSB 0
 LB 1.00 Hz
 GB 0
 PC 1.40



NAME SW06-102-C
 EXPNO 10
 PROCNO 1

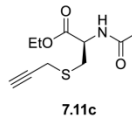
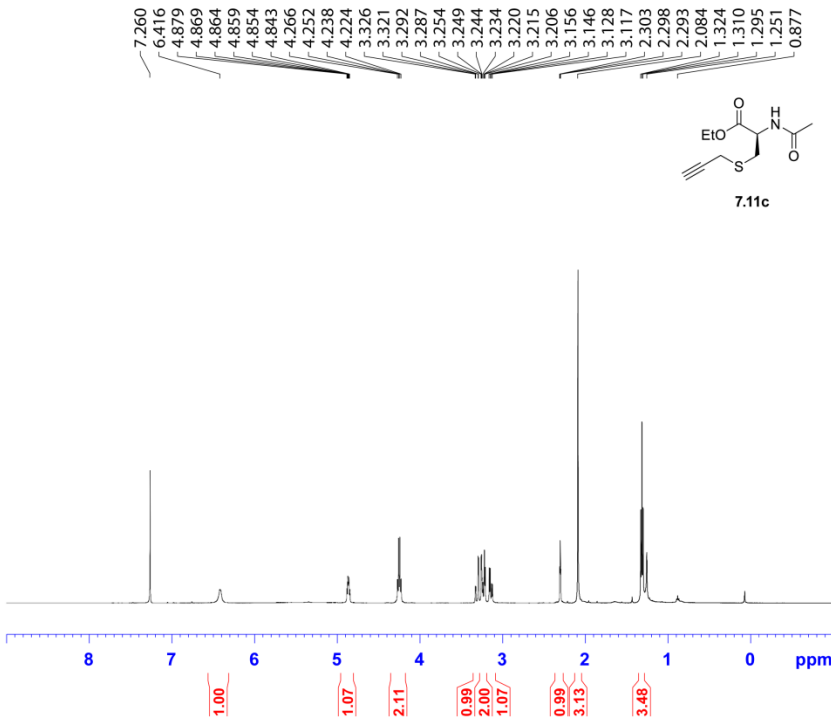
Date_ 20150213
 Time 16.20
 INSTRUM spect
 PROBHD 5 mm QNP
 PULPROG zg30
 TD 32768
 SOLVENT CDCl3
 NS 16
 DS 2
 SWH 6188.119 Hz
 FIDRES 0.188846 Hz
 AQ 2.6477044 sec
 RG 128
 DW 80.800 usec
 DE 6.50 usec
 TE -929.4 K
 D1 1.0000000 sec
 TDO 1

===== CHANNEL f1 =====
 SFO1 300.2318540 MHz
 NUC1 1H
 P1 12.71 usec
 SI 32768
 SF 300.2300093 MHz
 WDW EM
 SSB 0
 LB 0.10 Hz
 GB 0
 PC 1.00



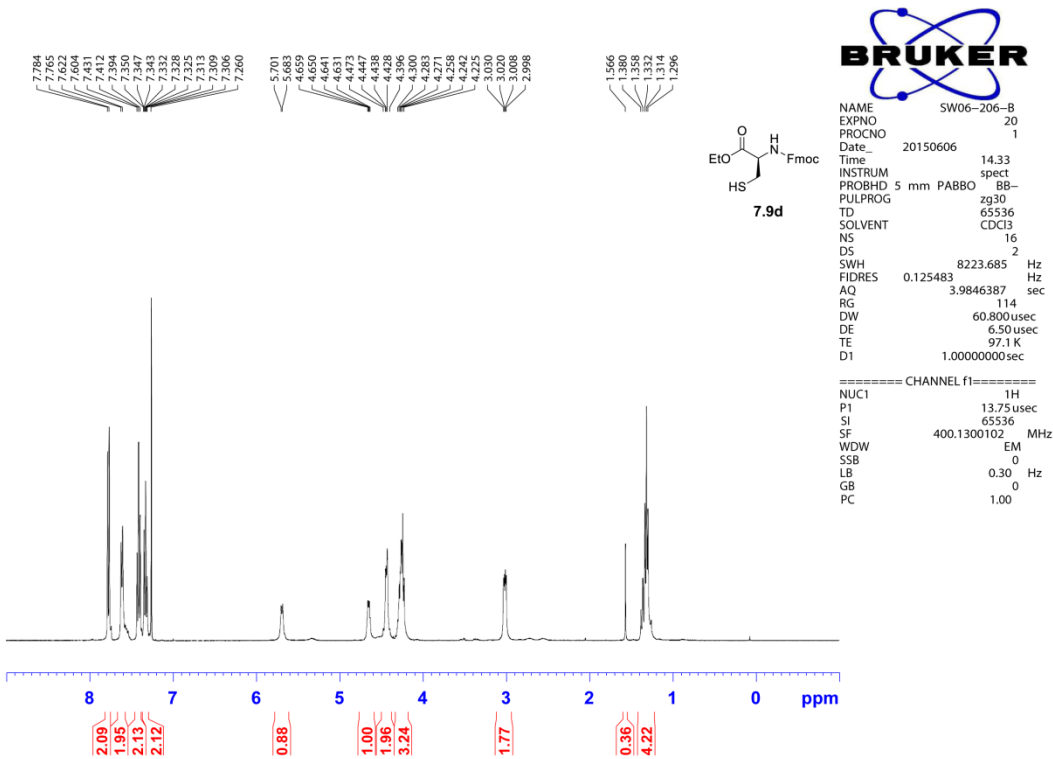
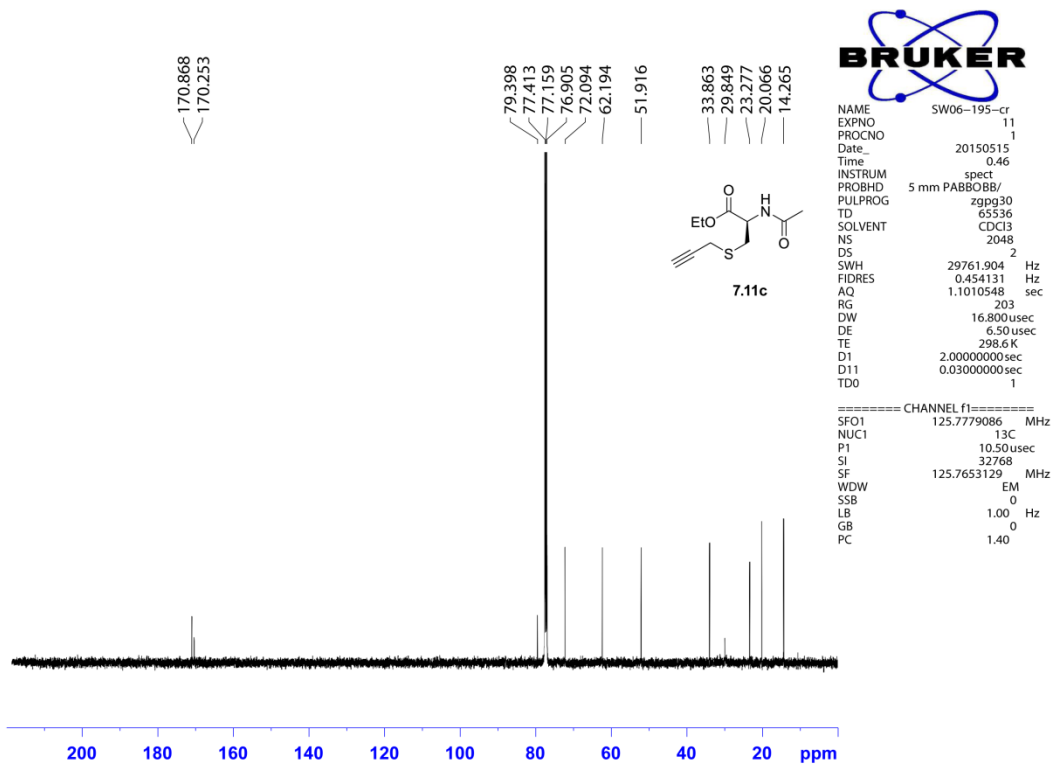
NAME SW06-102-C
 EXPNO 10
 PROCNO 1
 Date_ 20150214
 Time 5.45
 INSTRUM spect
 PROBHD 5 mm PABBO BB-
 PULPROG zgpg30
 TD 65536
 SOLVENT CDCl3
 NS 3072
 DS 4
 SWH 24038.461 Hz
 FIDRES 0.366798 Hz
 AQ 1.3631988 sec
 RG 203
 DW 20.800usec
 DE 6.50usec
 TE 97.6 K
 D1 2.00000000sec
 D11 0.03000000sec

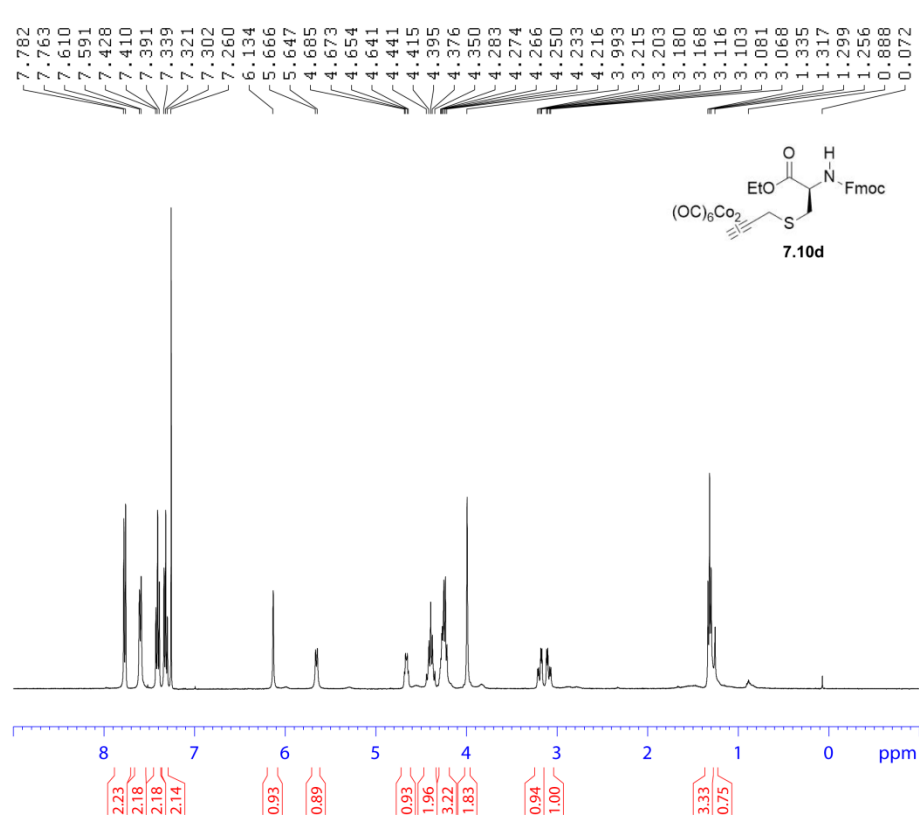
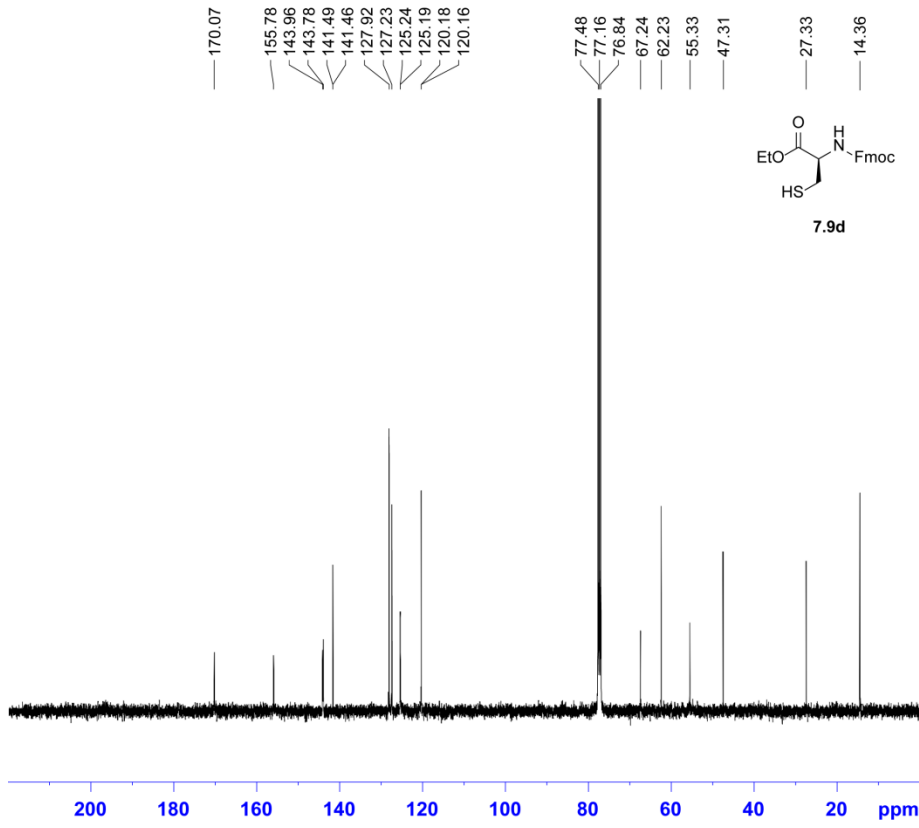
===== CHANNEL f1 =====
 NUC1 13C
 P1 10.00usec
 SI 32768
 SF 100.6127552 MHz
 WDW EM
 SSB 0
 LB 1.00 Hz
 GB 0
 PC 1.40

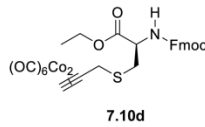
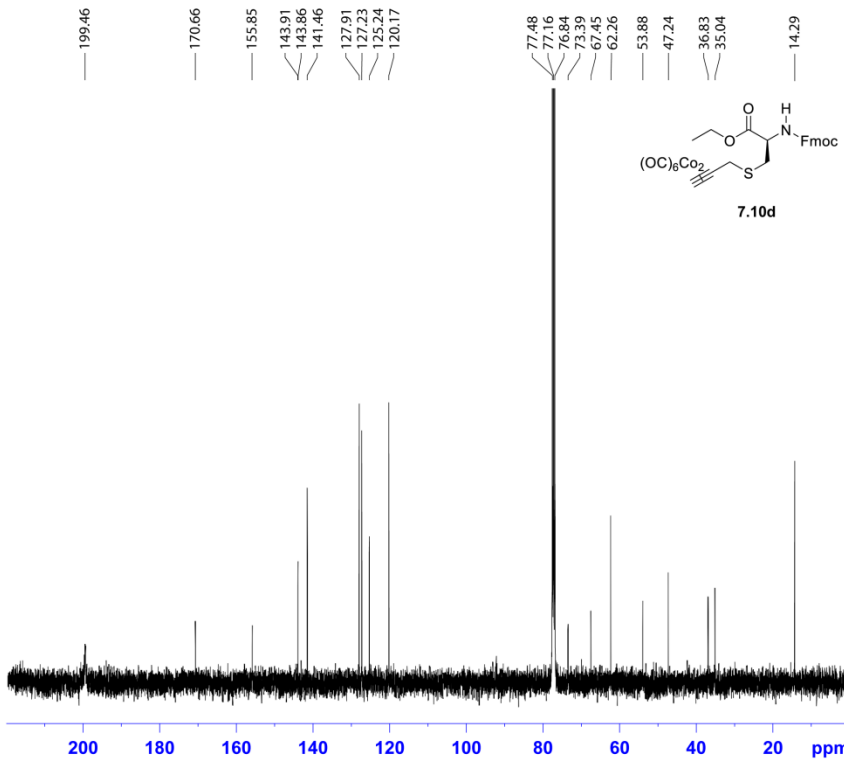


NAME SW06-195-cr
 EXPNO 10
 PROCNO 1
 Date_ 20150513
 Time 17.30
 INSTRUM spect
 PROBHD 5 mm PABBO BB/
 PULPROG zg30
 TD 65536
 SOLVENT CDCl3
 NS 16
 DS 2
 SWH 10000.000 Hz
 FIDRES 0.152588 Hz
 AQ 3.2768500 sec
 RG 203
 DW 50.000usec
 DE 6.50usec
 TE 298.2 K
 D1 1.00000000sec
 TDO 1

===== CHANNEL f1 =====
 SFO1 500.1630887 MHz
 NUC1 1H
 P1 11.45usec
 SI 65536
 SF 500.1600124 MHz
 WDW EM
 SSB 0
 LB 0.30 Hz
 GB 0
 PC 1.00







```

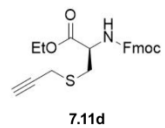
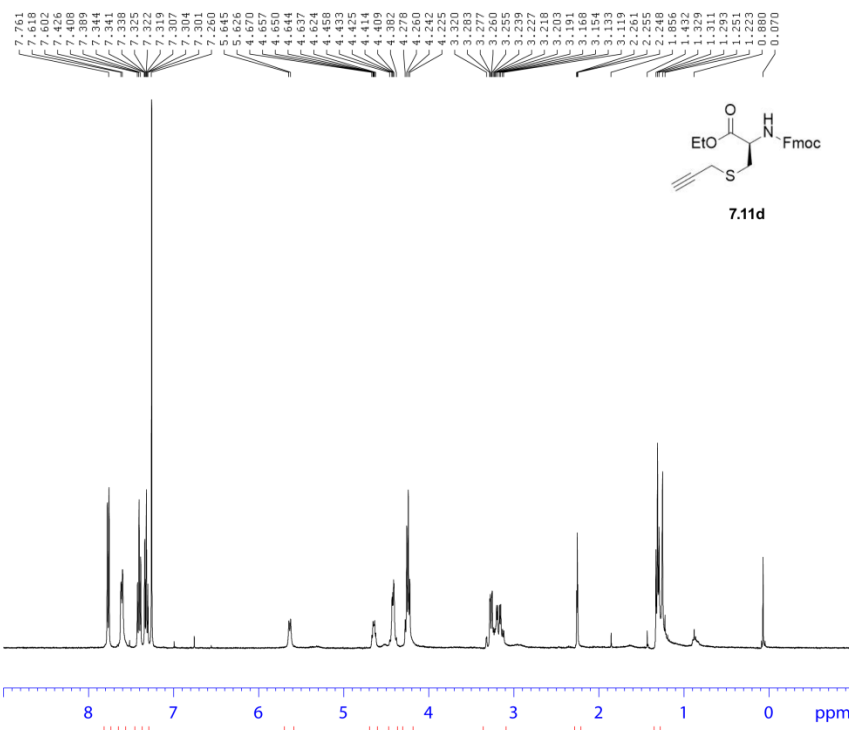
NAME SW06-138-C
EXPNO 11
PROCNO 1
Date_ 20150401
Time 1.15
INSTRUM spect
PROBHD 5 mm PABBO BB-
PULPROG zgpg30
TD 65536
SOLVENT CDCl3
NS 2048
DS 4
SWH 24038.461 Hz
FIDRES 0.366798 Hz
AQ 1.3631988 sec
RG 203
DW 20.800 usec
DE 6.50 usec
TE 96.9 K
D1 2.00000000 sec
D11 0.03000000 sec

```

```

===== CHANNEL f1 =====
NUC1 13C
P1 10.00 usec
SI 32768
SF 100.6127549 MHz
WDW EM
SSB 0
LB 1.00 Hz
GB 0
PC 1.40

```



```

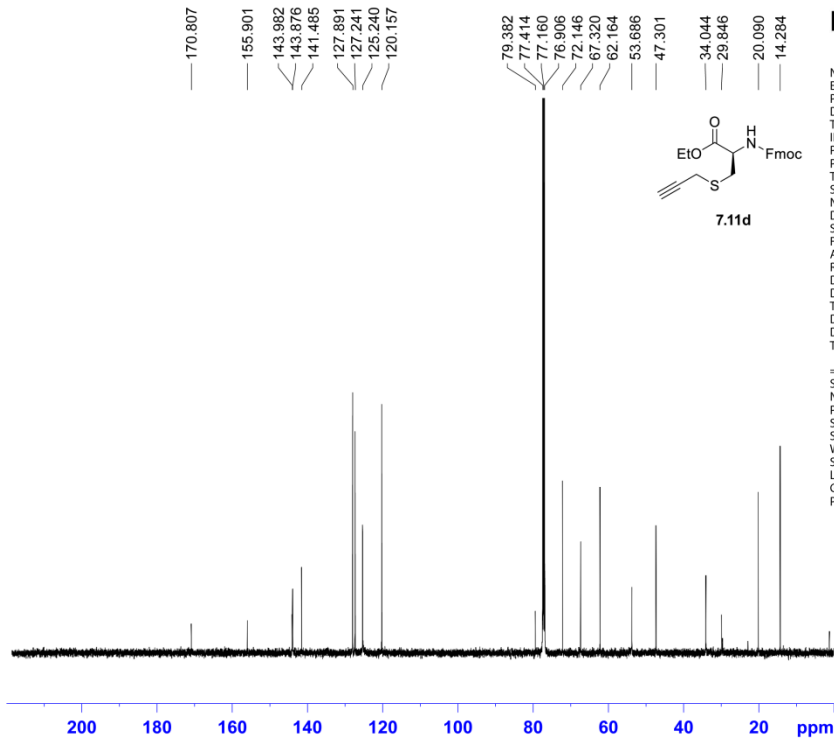
NAME SW06-164-cr
EXPNO 10
PROCNO 1
Date_ 20150415
Time 16.06
INSTRUM spect
PROBHD 5 mm PABBO BB-
PULPROG zg30
TD 65536
SOLVENT CDCl3
NS 16
DS 2
SWH 8223.685 Hz
FIDRES 0.125483 Hz
AQ 3.9846387 sec
RG 161
DW 60.800 usec
DE 6.50 usec
TE 90.5 K
D1 1.00000000 sec

```

```

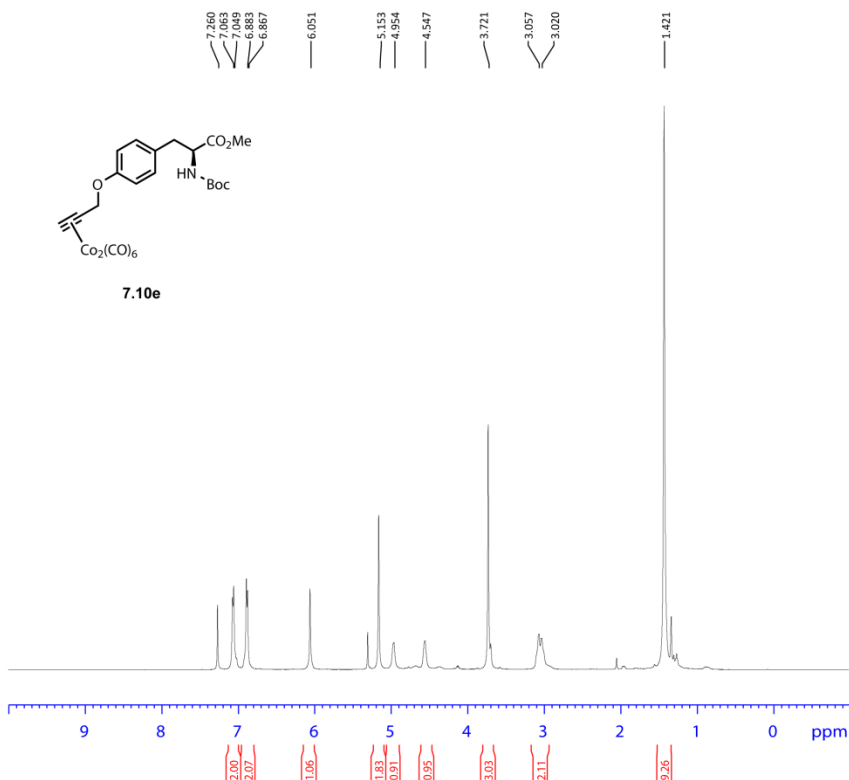
===== CHANNEL f1 =====
NUC1 1H
P1 13.75 usec
SI 65536
SF 400.1300100 MHz
WDW EM
SSB 0
LB 0.30 Hz
GB 0
PC 1.00

```

NAME SW06-164 cr
EXPNO 11
PROCNO 1
Date_ 20150512
Time 6.40
INSTRUM spect
PROBHD 5 mm PABBO BB/
PULPROG zgpg30
TD 65536
SOLVENT CDCl3
NS 2048
DS 2
SWH 29761.904 Hz
FIDRES 0.454131 Hz
AQ 1.1010548 sec
RG 203
DW 16.800 usec
DE 6.50 usec
TE 298.6 K
D1 2.00000000 sec
D11 0.03000000 sec
TDO 1

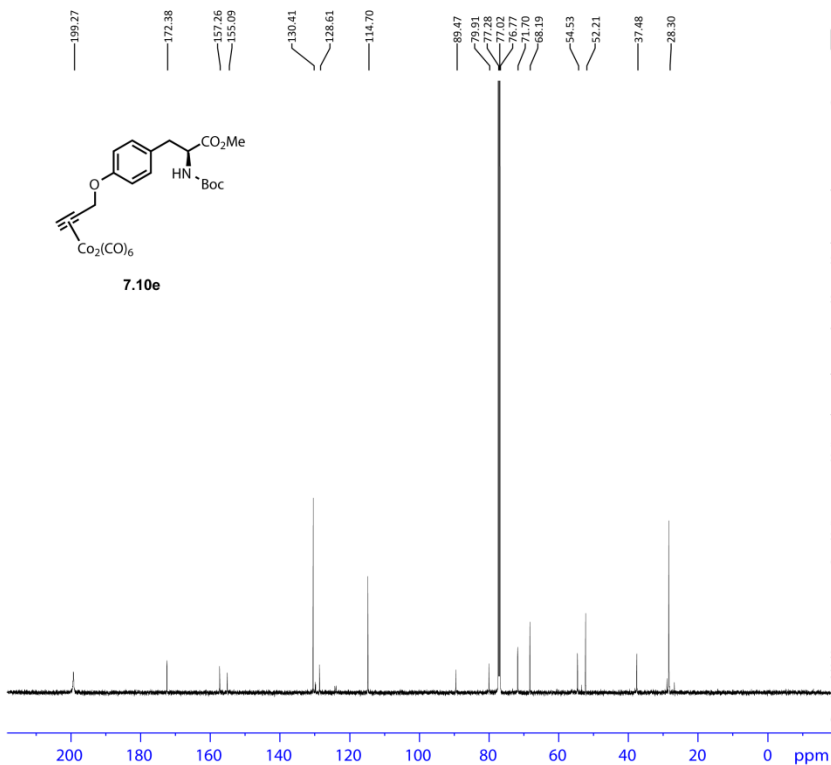
===== CHANNEL f1 =====
SFO1 125.7779086 MHz
NUC1 13C
P1 10.50 usec
SI 32768
SF 125.7653142 MHz
WDW EM
SSB 0
LB 1.00 Hz
GB 0
PC 1.40



Current Data Parameters
NAME 05-67A
EXPNO 1
PROCNO 1

F2 - Acquisition Parameters
Date_ 20150512
Time 19.33
INSTRUM spect
PROBHD 5 mm PABBO BB/
PULPROG zg30
TD 219998
SOLVENT CDCl3
NS 16
DS 2
SWH 10000.000 Hz
FIDRES 0.045455 Hz
AQ 10.9989999 sec
RG 86.1
DW 50.000 usec
DE 13.29 usec
TE 298.1 K
D1 1.00000000 sec
TDO 1

===== CHANNEL f1 =====
SFO1 500.1330885 MHz
NUC1 1H
P1 10.99 usec
PLW1 15.00000000 W
F2 - Processing parameters
SI 65536
SF 500.1300141 MHz
WDW EM
SSB 0
LB 0.30 Hz
GB 0
PC 1.00



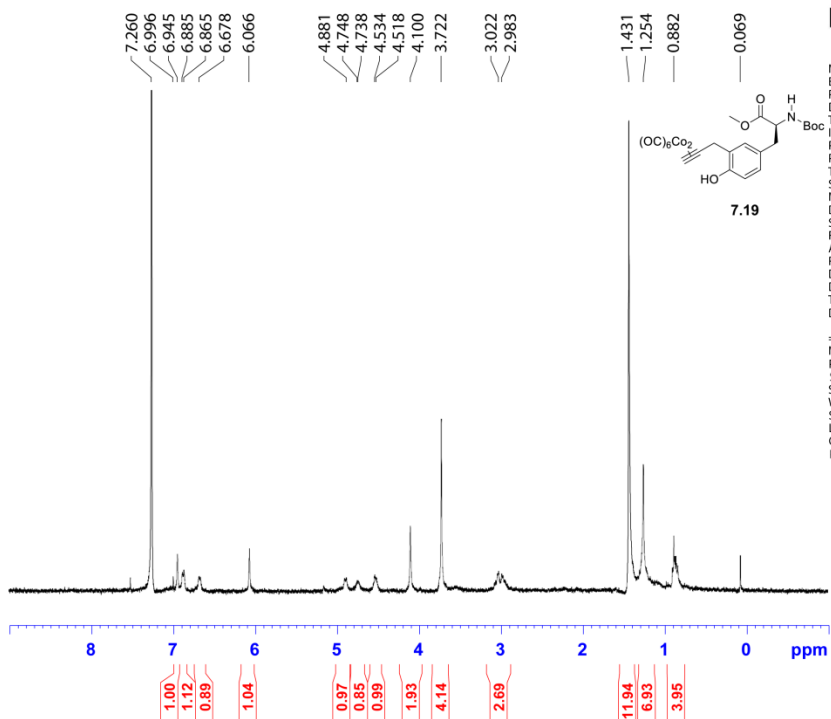
Current Data Parameters
 NAME 05-67A
 EXPNO 2
 PROCNO 1

F2 - Acquisition Parameters
 Date_ 20150512
 Time 23.50
 INSTRUM spect
 PROBHD 5 mm PABBO BB/
 PULPROG zgpg30
 TD 65536
 SOLVENT CDCl3
 NS 2000
 DS 4
 SWH 29761.904 Hz
 FIDRES 0.454131 Hz
 AQ 1.1010048 sec
 RG 186.69
 DW 16.800 usec
 DE 6.50 usec
 TE 298.1 K
 D1 2.0000000 sec
 D11 0.0300000 sec
 TD0 1

===== CHANNEL f1 =====
 SFO1 125.703637 MHz
 NUC1 13C
 P1 10.00 usec
 PLW1 84.0000000 W

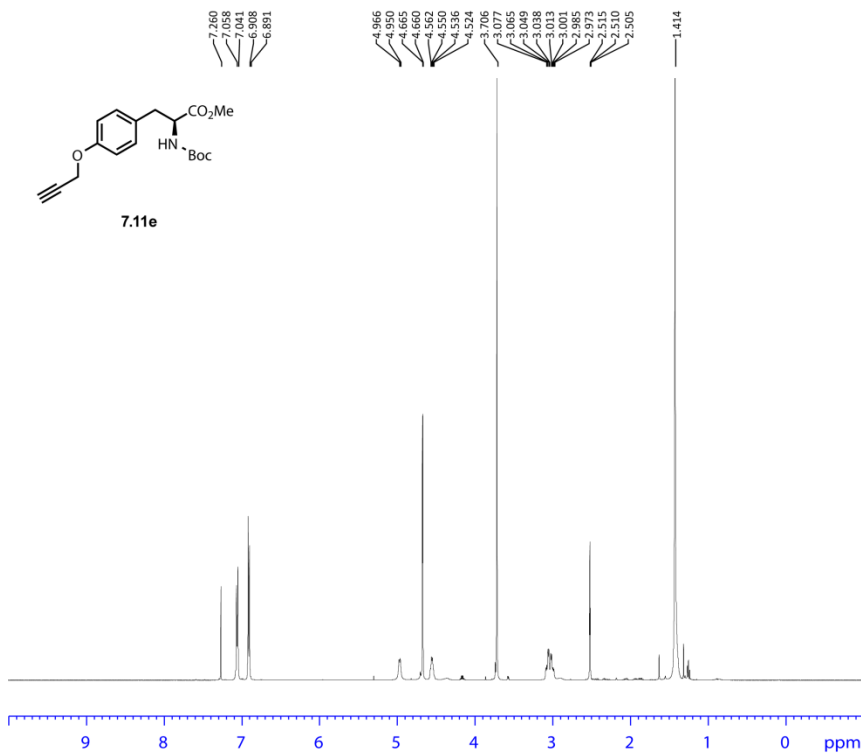
===== CHANNEL f2 =====
 SFO2 500.1320005 MHz
 NUC2 1H
 CPDPRG2 waltz16
 PCPD2 80.00 usec
 PLW2 15.0000000 W
 PLW12 0.28308001 W
 PLW13 0.18117000 W

F2 - Processing parameters
 SI 32768
 SF 125.7577890 MHz
 WDW EM
 SSB 0
 LB 1.00 Hz
 GB 0
 PC 1.40



NAME SW06-166-D
 EXPNO 10
 PROCNO 1
 Date_ 20150421
 Time 17.09
 INSTRUM spect
 PROBHD 5 mm PABBO BB-
 PULPROG zg30
 TD 65536
 SOLVENT CDCl3
 NS 16
 DS 2
 SWH 8223.685 Hz
 FIDRES 0.125483 Hz
 AQ 3.9846387 sec
 RG 181
 DW 60.800 usec
 DE 6.50 usec
 TE 94.1 K
 D1 1.0000000 sec

===== CHANNEL f1 =====
 NUC1 1H
 P1 13.75 usec
 SI 65536
 SF 400.1300096 MHz
 WDW EM
 SSB 0
 LB 0.30 Hz
 GB 0
 PC 1.00

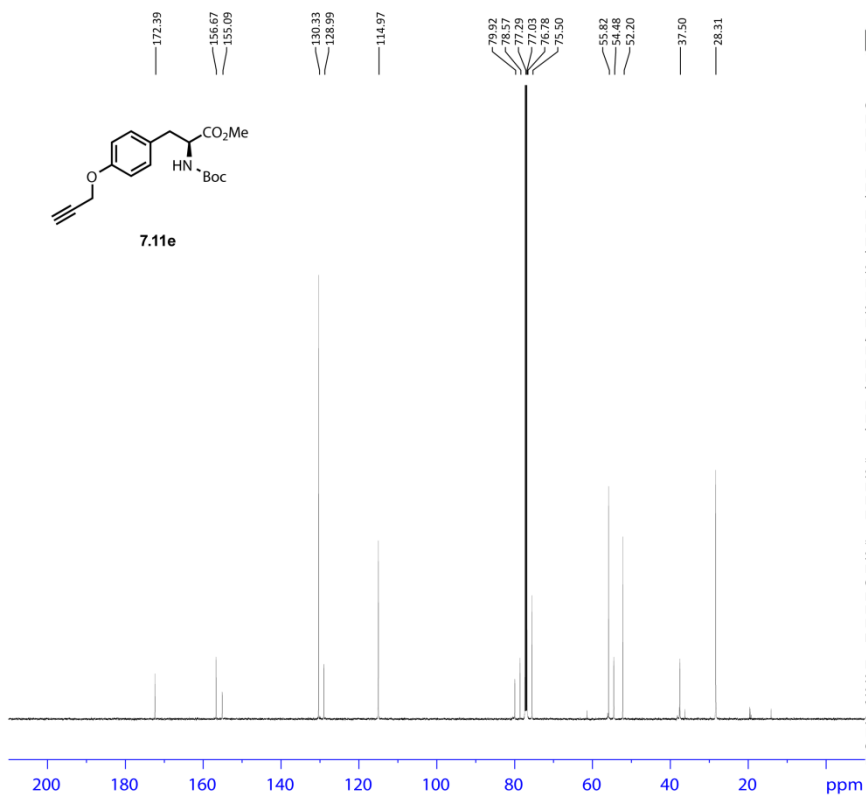


Current Data Parameters
 NAME 05-21B-2
 EXPNO 1
 PROCNO 1

F2 - Acquisition Parameters
 Date_ 20150414
 Time 14.05
 INSTRUM spect
 PROBHD 5 mm PABBO BB/
 PULPROG zg30
 TD 219998
 SOLVENT CDCl3
 NS 16
 DS 2
 SWH 10000.000 Hz
 FIDRES 0.045455 Hz
 AQ 10.9998999 sec
 RG 86.1
 DW 50.000 usec
 DE 13.29 usec
 TE 298.1 K
 D1 1.0000000 sec
 TDO 1

===== CHANNEL f1 =====
 SFO1 500.1330885 MHz
 NUC1 1H
 P1 10.99 usec
 PLW1 15.00000000 W

F2 - Processing parameters
 SI 65536
 SF 500.1300136 MHz
 WDW EM
 SSB 0
 LB 0.30 Hz
 GB 0
 PC 1.00



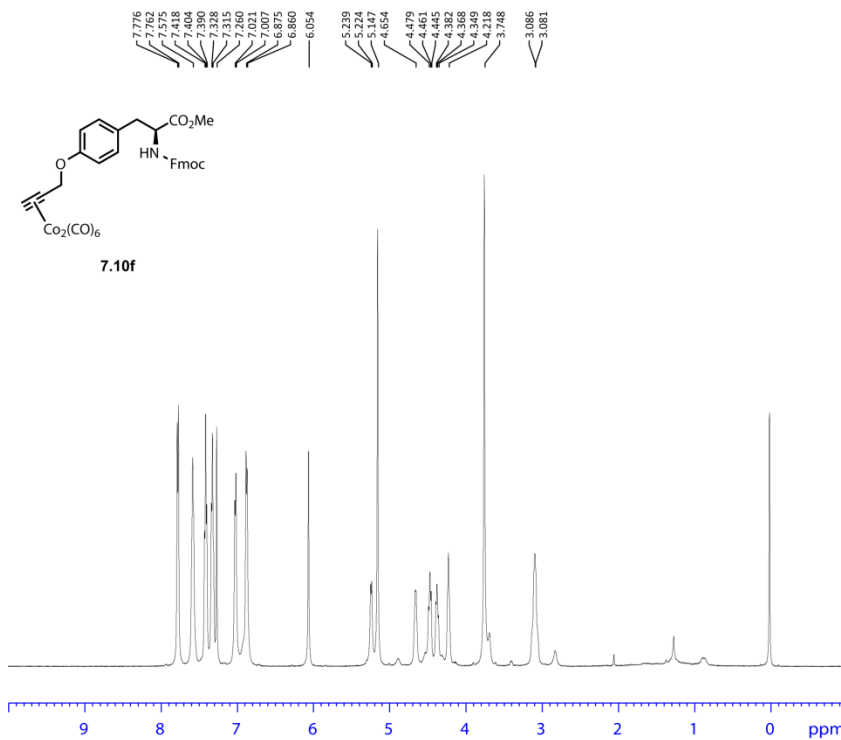
Current Data Parameters
 NAME 05-21B-2
 EXPNO 2
 PROCNO 1

F2 - Acquisition Parameters
 Date_ 20150415
 Time 0.42
 INSTRUM spect
 PROBHD 5 mm PABBO BB/
 PULPROG zgpg30
 TD 65536
 SOLVENT CDCl3
 NS 3000
 DS 4
 SWH 29761.904 Hz
 FIDRES 0.454131 Hz
 AQ 1.1010048 sec
 RG 186.69
 DW 16.800 usec
 DE 6.50 usec
 TE 298.1 K
 D1 2.0000000 sec
 D11 0.03000000 sec
 TDO 1

===== CHANNEL f1 =====
 SFO1 125.7703637 MHz
 NUC1 13C
 P1 10.00 usec
 PLW1 84.00000000 W

===== CHANNEL f2 =====
 SFO2 500.1320005 MHz
 NUC2 1H
 CPDPRG2 waltz16
 PCPD2 80.00 usec
 PLW2 15.00000000 W
 PLW12 0.28308001 W
 PLW13 0.18117000 W

F2 - Processing parameters
 SI 32768
 SF 125.7577890 MHz
 WDW EM
 SSB 0
 LB 1.00 Hz
 GB 0
 PC 1.40

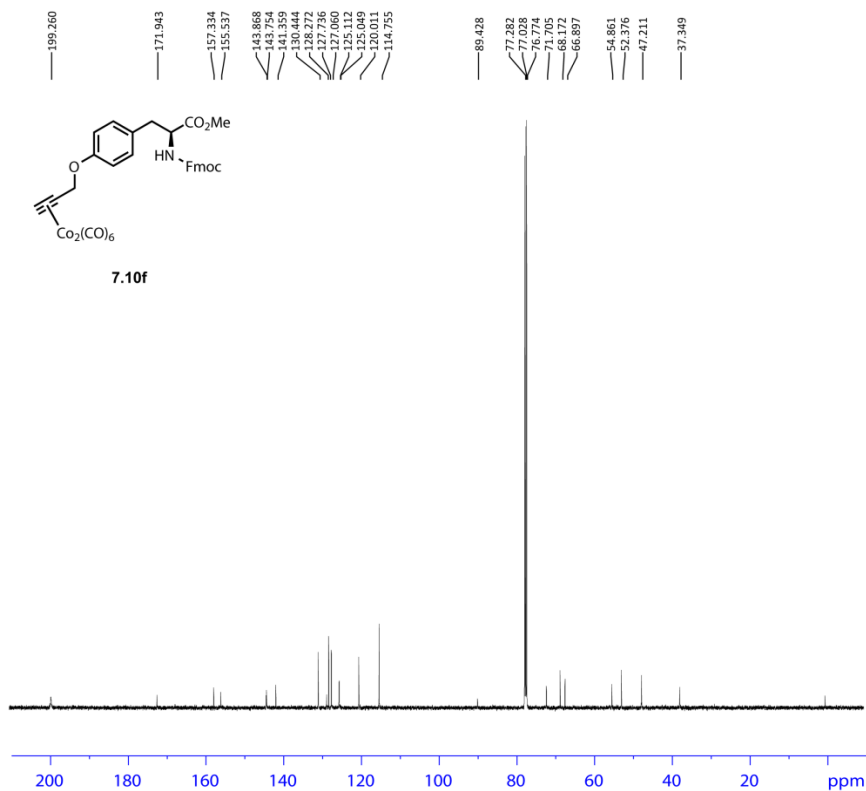


Current Data Parameters
 NAME 05-129
 EXPNO 1
 PROCNO 1

F2 - Acquisition Parameters
 Date_ 20150718
 Time 14.58
 INSTRUM spect
 PROBHD 5 mm PABBO BB/
 PULPROG zg30
 TD 65536
 SOLVENT CDCl3
 NS 16
 DS 2
 SWH 10000.000 Hz
 FIDRES 0.152588 Hz
 AQ 3.2767999 sec
 RG 148.37
 DW 50.000 usec
 DE 13.29 usec
 TE 298.1 K
 D1 1.00000000 sec
 TDO 1

==== CHANNEL f1 =====
 SFO1 500.1330885 MHz
 NUC1 1H
 P1 10.99 usec
 PLW1 15.00000000 W

F2 - Processing parameters
 SI 65536
 SF 500.1300152 MHz
 WDW EM
 SSB 0
 LB 0.30 Hz
 GB 0
 PC 1.00



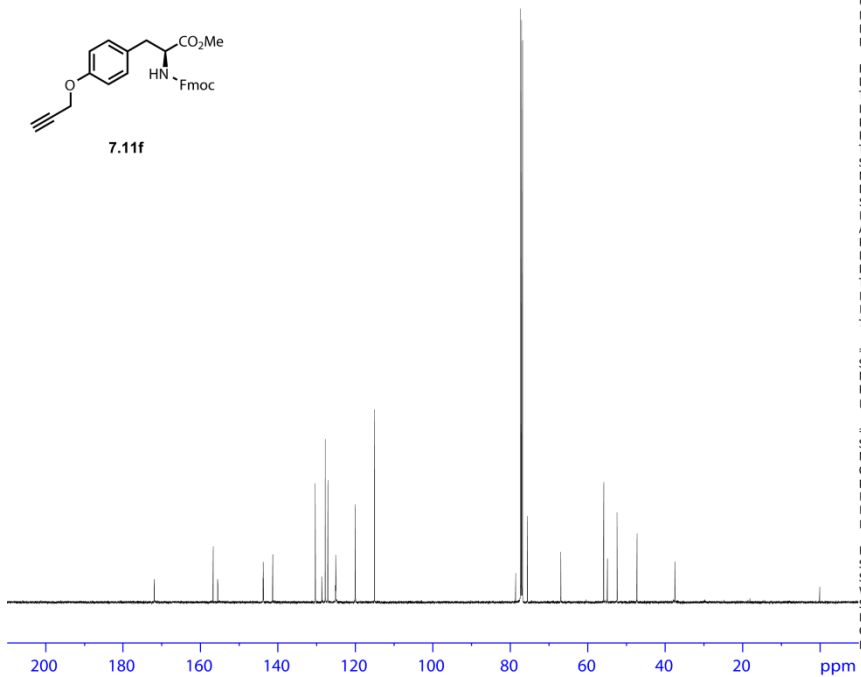
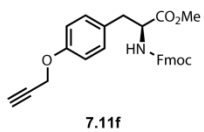
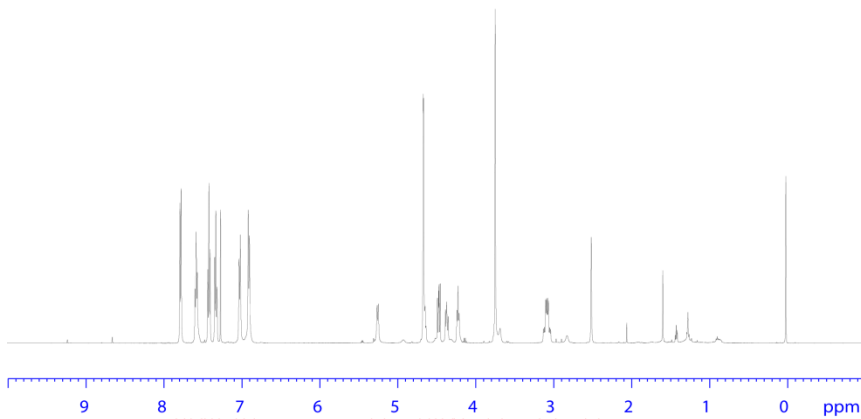
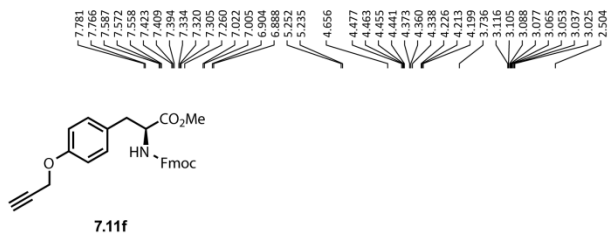
Current Data Parameters
 NAME 05-129
 EXPNO 2
 PROCNO 1

F2 - Acquisition Parameters
 Date_ 20150718
 Time 15.52
 INSTRUM spect
 PROBHD 5 mm PABBO BB/
 PULPROG zgpg30
 TD 65536
 SOLVENT CDCl3
 NS 800
 DS 2
 SWH 29761.904 Hz
 FIDRES 0.454131 Hz
 AQ 1.1010048 sec
 RG 186.69
 DW 16.800 usec
 DE 6.50 usec
 TE 298.1 K
 D1 2.00000000 sec
 D11 0.03000000 sec
 TDO 1

==== CHANNEL f1 =====
 SFO1 125.7703643 MHz
 NUC1 13C
 P1 10.00 usec
 PLW1 84.00000000 W

==== CHANNEL f2 =====
 SFO2 500.1320005 MHz
 NUC2 1H
 CPDPRG2 waltz16
 PCPD2 80.00 usec
 PLW2 15.00000000 W
 PLW12 0.28308001 W
 PLW13 0.18117000 W

F2 - Processing parameters
 SI 32768
 SF 125.7577890 MHz
 WDW EM
 SSB 0
 LB 1.00 Hz
 GB 0
 PC 1.40



Current Data Parameters
NAME 05-133
EXPNO 1
PROCNO 1

F2 - Acquisition Parameters
Date_ 20150728
Time 14.03
INSTRUM spect
PROBHD 5 mm PABBO BB/
PULPROG zg30
TD 199998
SOLVENT CDCl3
NS 16
DS 2
SWH 10000.000 Hz
FIDRES 0.050000 Hz
AQ 9.9989999 sec
RG 86.1
DW 50.000 usec
DE 13.29 usec
TE 298.1 K
D1 1.0000000 sec
TD0 1

===== CHANNEL f1 =====
SFO1 500.130885 MHz
NUC1 1H
P1 10.99 usec
PLW1 15.0000000 W

F2 - Processing parameters
SI 65536
SF 500.1300141 MHz
WDW EM
SSB 0
LB 0.30 Hz
GB 0
PC 1.00



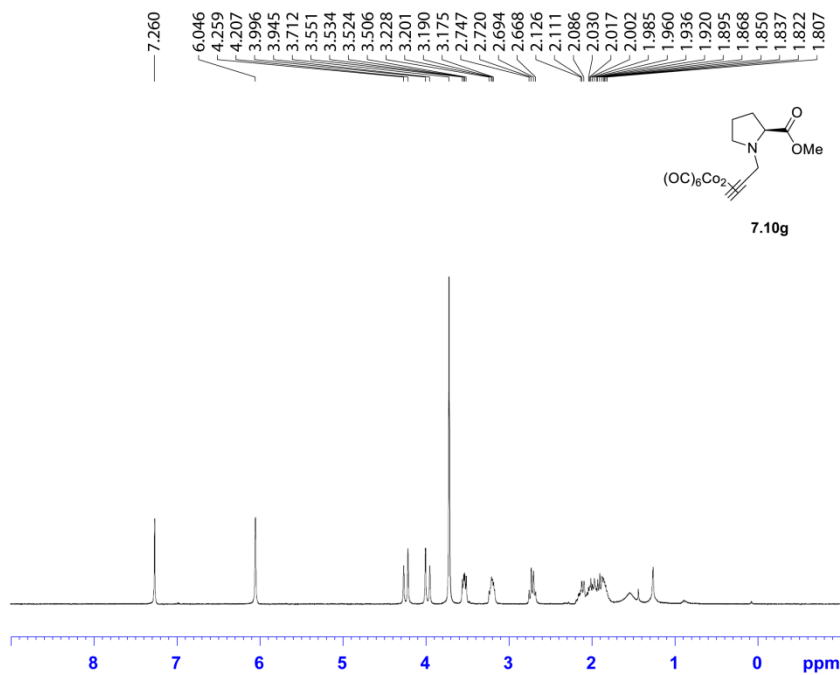
Current Data Parameters
NAME 05-133
EXPNO 2
PROCNO 1

F2 - Acquisition Parameters
Date_ 20150728
Time 23.52
INSTRUM spect
PROBHD 5 mm PABBO BB/
PULPROG zgpg30
TD 65536
SOLVENT CDCl3
NS 2000
DS 4
SWH 29761.904 Hz
FIDRES 0.454131 Hz
AQ 1.1010048 sec
RG 186.69
DW 16.800 usec
DE 6.50 usec
TE 298.1 K
D1 2.0000000 sec
D11 0.0300000 sec
TD0 1

===== CHANNEL f1 =====
SFO1 125.7703637 MHz
NUC1 13C
P1 10.00 usec
PLW1 84.0000000 W

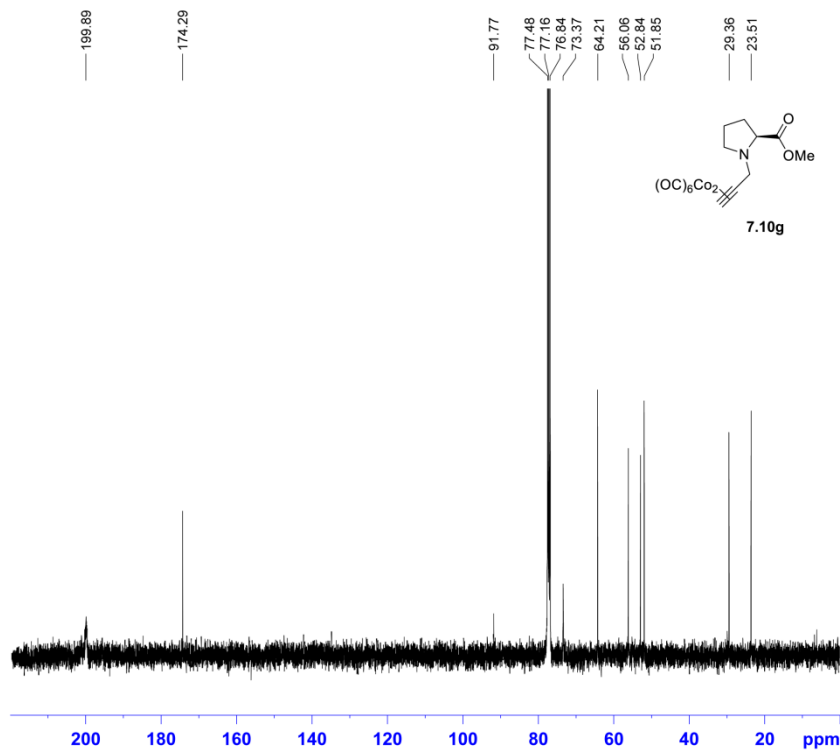
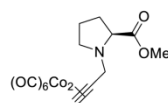
===== CHANNEL f2 =====
SFO2 500.1320005 MHz
NUC2 1H
CPDPRG2 waltz16
PCPD2 80.00 usec
PLW2 15.0000000 W
PLW12 0.28308001 W
PLW13 0.18117000 W

F2 - Processing parameters
SI 32768
SF 125.7577914 MHz
WDW EM
SSB 0
LB 1.00 Hz
GB 0
PC 1.40



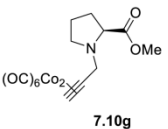
NAME SW07-060-C
EXPNO 10
PROCNO 1
Date_ 20150804
Time 18.03
INSTRUM spect
PROBHD 5 mm QNP
PULPROG zg30
TD 32768
SOLVENT CDCl3
NS 16
DS 2
SWH 6188.1 19 Hz
FIDRES 0.188846 Hz
AQ 2.6477044 sec
RG 322
DW 80.800 usec
DE 6.50 usec
TE -922.2 K
D1 1.00000000 sec
TDO 1

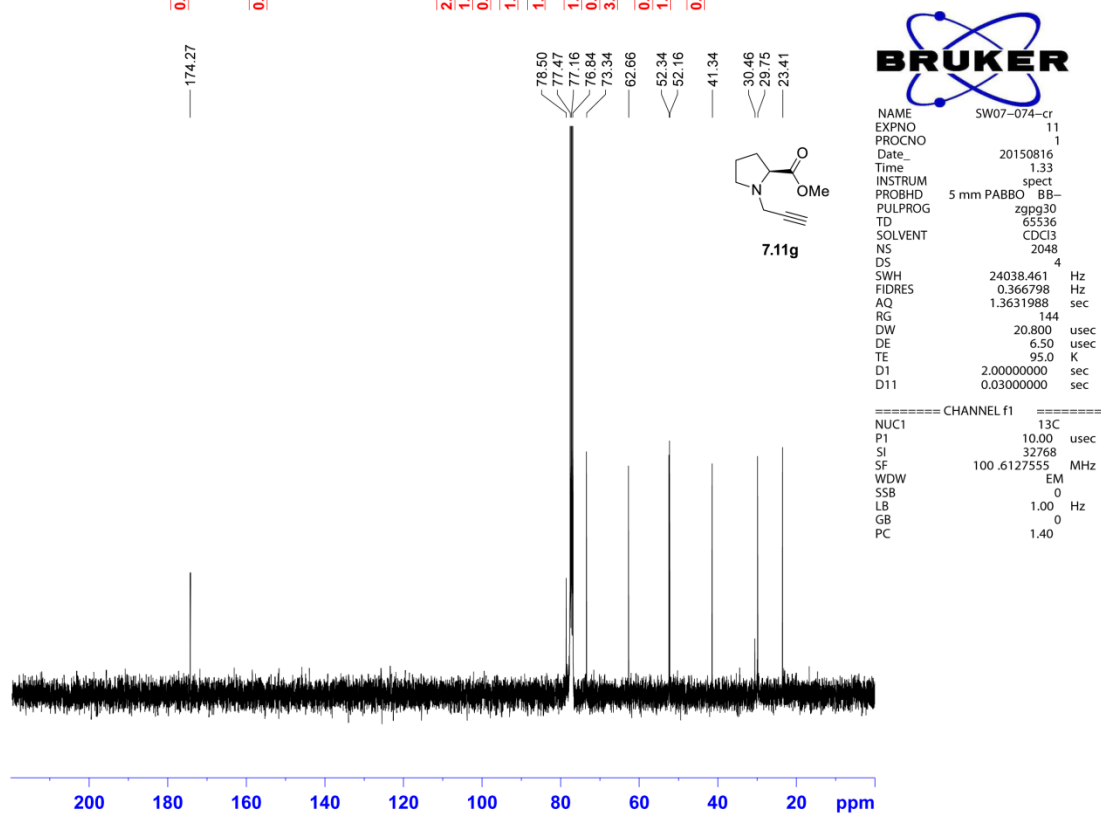
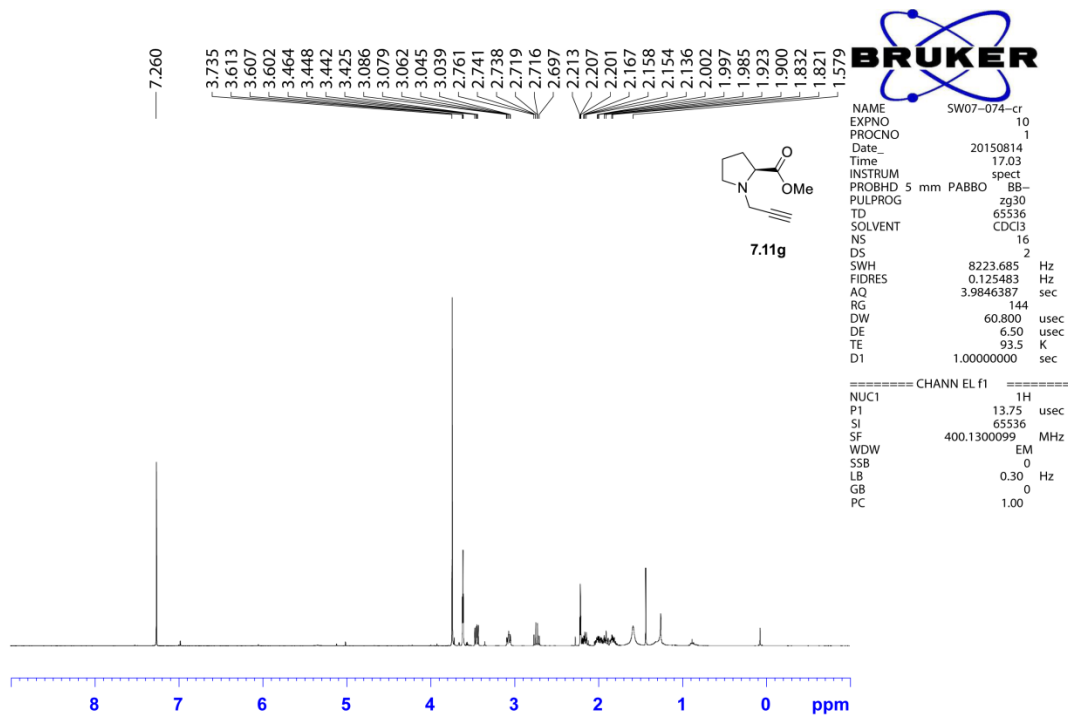
===== CHANNEL f1 =====
SFO1 300.2318540 MHz
NUC1 1H
P1 12.71 usec
SI 32768
SF 300.2300085 MHz
WDW EM
SSB 0
LB 0.10 Hz
GB 0
PC 1.00

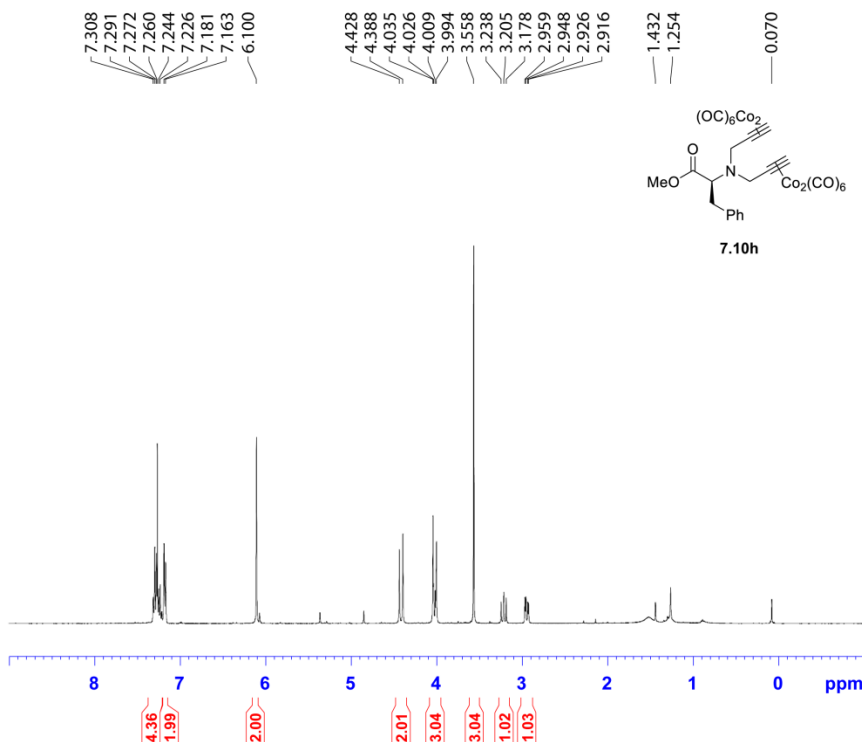


NAME SW07-060-C
EXPNO 10
PROCNO 1
Date_ 20150805
Time 4.43
INSTRUM spect
PROBHD 5 mm PABBO BB-
PULPROG zgpg30
TD 65536
SOLVENT CDCl3
NS 2048
DS 4
SWH 24038.461 Hz
FIDRES 0.366798 Hz
AQ 1.3631988 sec
RG 181
DW 20.800 usec
DE 6.50 usec
TE 95.5 K
D1 2.00000000 sec
D11 0.03000000 sec

===== CHANNEL f1 =====
NUC1 13C
P1 10.00 usec
SI 32768
SF 100.6127546 MHz
WDW EM
SSB 0
LB 1.00 Hz
GB 0
PC 1.40

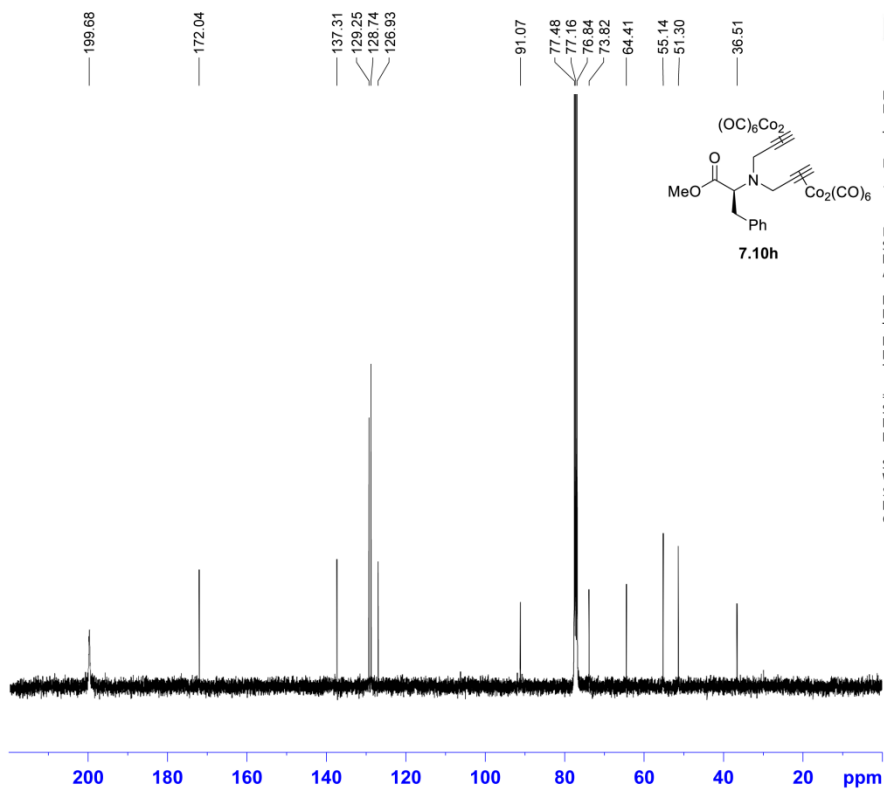






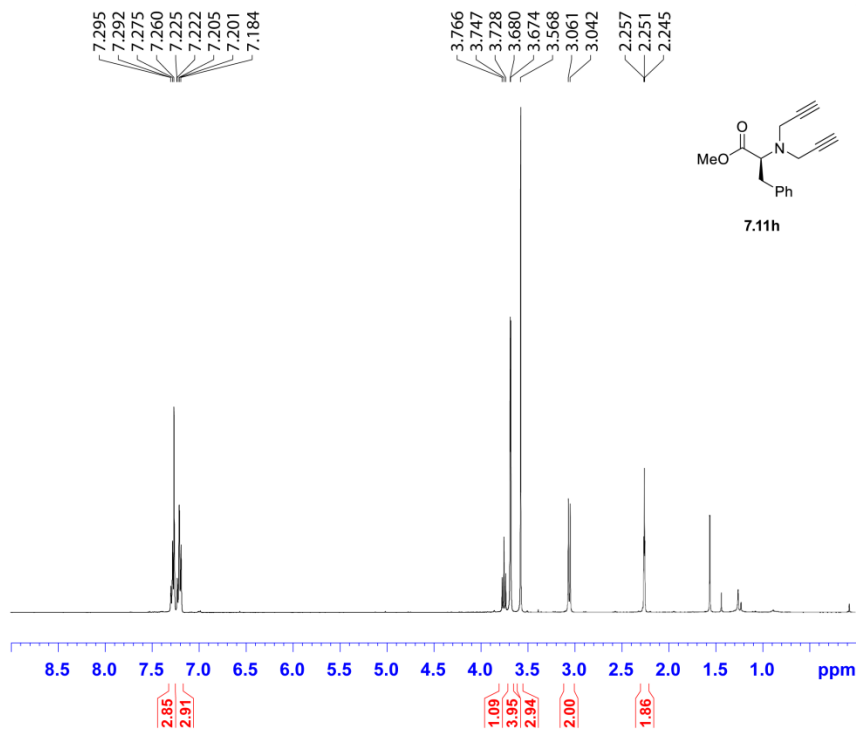
NAME SW07-111-B
 EXPNO 10
 PROCNO 1
 Date_ 20151013
 Time 14.03
 INSTRUM spect
 PROBHD 5 mm PABBO BB-
 PULPROG zg30
 TD 65536
 SOLVENT CDCl3
 NS 16
 DS 2
 SWH 8012.820 Hz
 FIDRES 0.122266 Hz
 AQ 4.0894966 sec
 RG 144
 DW 62.400 usec
 DE 6.50 usec
 TE 96.7 K
 D1 1.00000000 sec
 TDO 1

===== CHANNEL f1 =====
 SFO1 400.1324710 MHz
 NUC1 1H
 P1 13.75 usec
 SI 65536
 SF 400.1300107 MHz
 WDW EM
 SSB 0
 LB 0.30 Hz
 GB 0
 PC 1.00



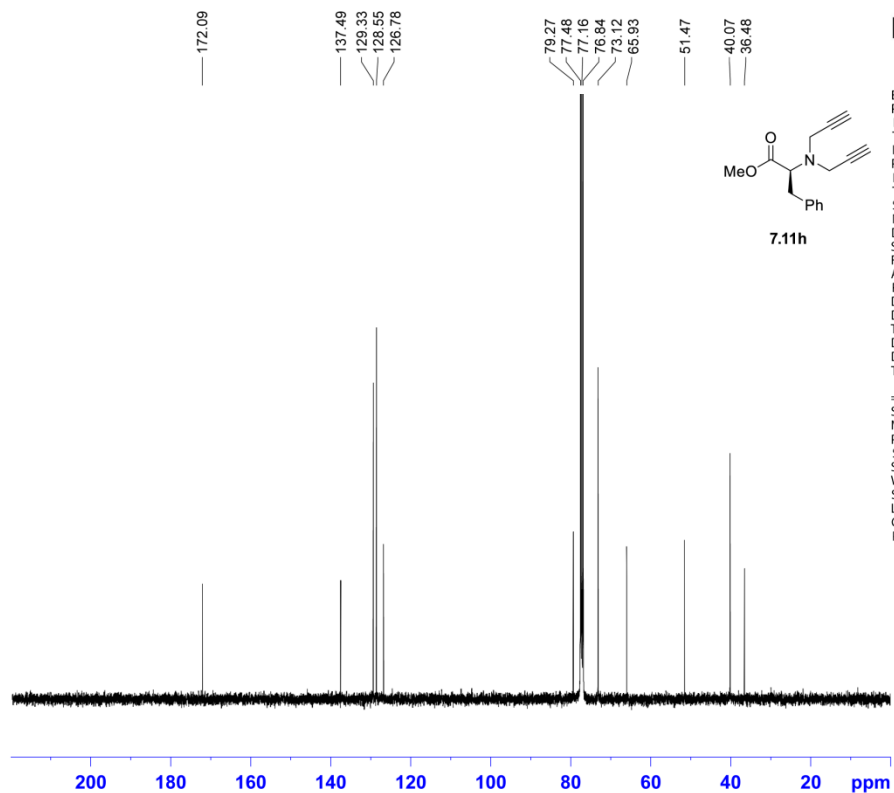
NAME SW07-111-B
 EXPNO 11
 PROCNO 1
 Date_ 20151014
 Time 3.34
 INSTRUM spect
 PROBHD 5 mm PABBO BB-
 PULPROG zgpg30
 TD 65536
 SOLVENT CDCl3
 NS 3072
 DS 4
 SWH 24038.461 Hz
 FIDRES 0.366798 Hz
 AQ 1.3631988 sec
 RG 203
 DW 20.800 usec
 DE 6.50 usec
 TE 97.8 K
 D1 2.00000000 sec
 D11 0.03000000 sec
 TDO 1

===== CHANNEL f1 =====
 SFO1 100.6228293 MHz
 NUC1 13C
 P1 10.00 usec
 SI 32768
 SF 100.6127541 MHz
 WDW EM
 SSB 0
 LB 1.00 Hz
 GB 0
 PC 1.40



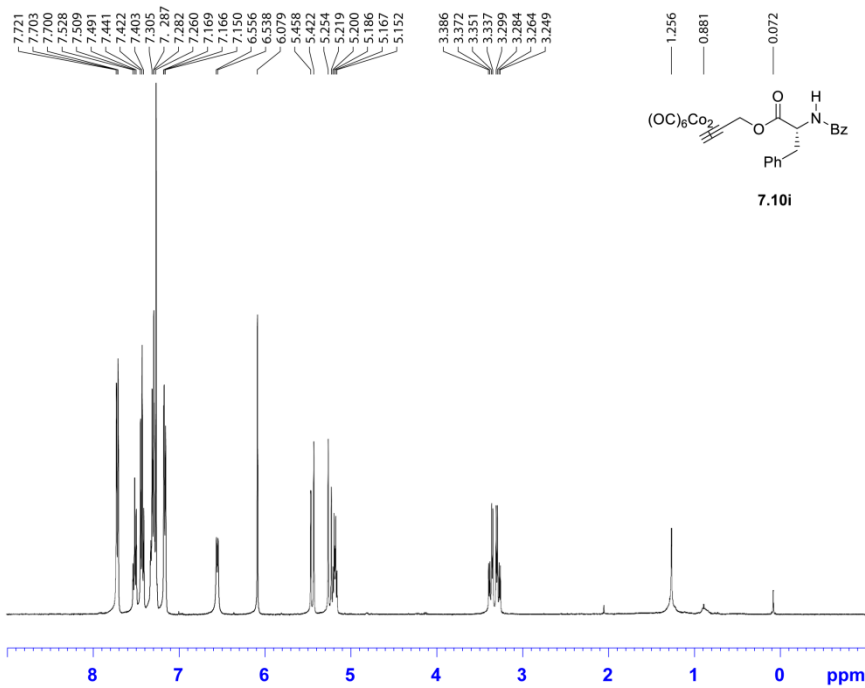
NAME SW07-118-A
EXPNO 10
PROCNO 1
Date_ 20151014
Time 18.07
INSTRUM spect
PROBHD 5 mm PABBO BB-
PULPROG zg30
TD 65536
SOLVENT CDCl3
NS 16
DS 2
SWH 8012.820 Hz
FIDRES 0.122266 Hz
AQ 4.0894966 sec
RG 128
DW 62.400 usec
DE 6.50 usec
TE 96.8 K
D1 1.00000000 sec
TD0 1

===== CHANNEL f1 =====
SFO1 400.1324710 MHz
NUC1 1H
P1 13.75 usec
SI 65536
SF 400.1300106 MHz
WDW EM
SSB 0
LB 0.30 Hz
GB 0
PC 1.00



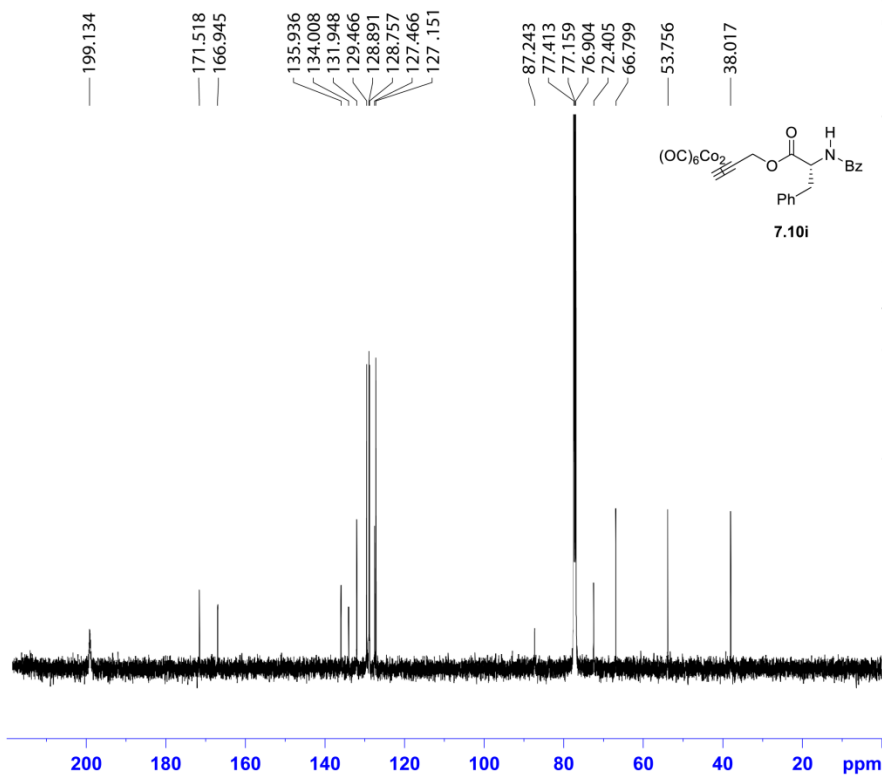
NAME SW07-118-A
EXPNO 11
PROCNO 1
Date_ 20151014
Time 23.00
INSTRUM spect
PROBHD 5 mm PABBO BB-
PULPROG zgpg30
TD 65536
SOLVENT CDCl3
NS 3072
DS 4
SWH 24038.461 Hz
FIDRES 0.366798 Hz
AQ 1.3631988 sec
RG 181
DW 20.800 usec
DE 6.50 usec
TE 97.9 K
D1 2.00000000 sec
D11 0.03000000 sec
TD0 1

===== CHANNEL f1 =====
SFO1 100.6228293 MHz
NUC1 13C
P1 10.00 usec
SI 32768
SF 100.6127546 MHz
WDW EM
SSB 0
LB 1.00 Hz
GB 0
PC 1.40



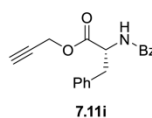
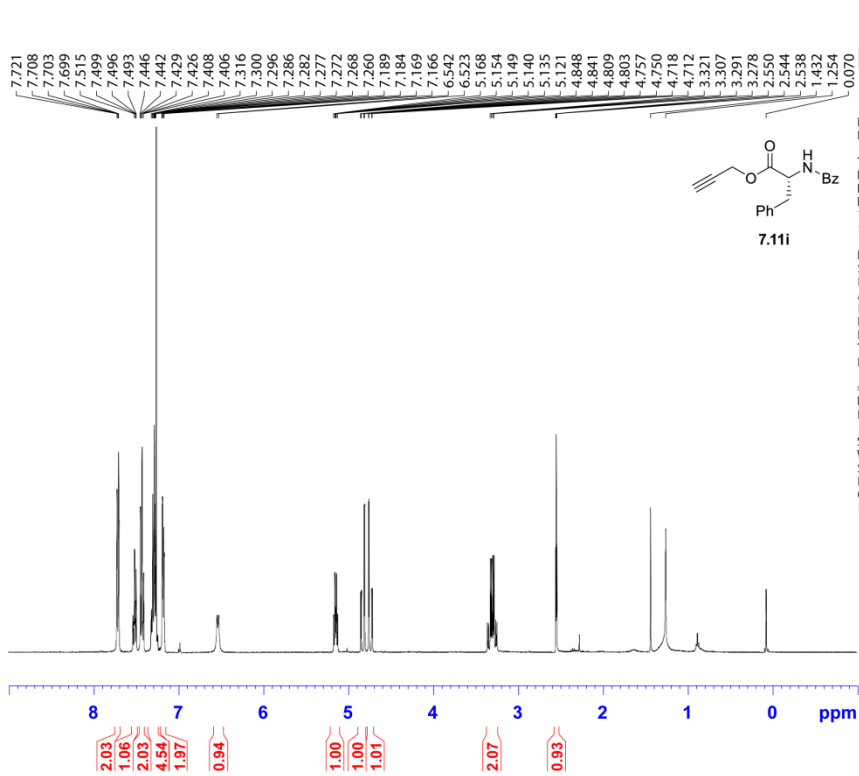
NAME SW06-065-C
 EXPNO 10
 PROCNO 1
 Date_ 20150108
 Time_ 18.42
 INSTRUM spect
 PROBHD 5 mm PABBO BB-
 PULPROG zg30
 TD 65536
 SOLVENT CDCl3
 NS 16
 DS 2
 SWH 8223.685 Hz
 FIDRES 0.125483 Hz
 AQ 3.9846387 sec
 RG 128
 DW 60.800 usec
 DE 6.50 usec
 TE 96.1 K
 D1 1.00000000 sec

===== CHANNEL f1 =====
 NUC1 1H
 P1 13.75 usec
 SI 65536
 SF 400.1300108 MHz
 WDW EM
 SSB 0
 LB 0.30 Hz
 GB 0
 PC 1.00



NAME SW06-169-C
 EXPNO 10
 PROCNO 1
 Date_ 20150425
 Time_ 2.37
 INSTRUM spect
 PROBHD 5 mm PABBO BB/
 PULPROG zgpg30
 TD 65536
 SOLVENT CDCl3
 NS 2048
 DS 2
 SWH 29761.904 Hz
 FIDRES 0.454131 Hz
 AQ 1.1010548 sec
 RG 203
 DW 16.800 usec
 DE 6.50 usec
 TE 299.2 K
 D1 2.00000000 sec
 D11 0.03000000 sec
 TD0 1

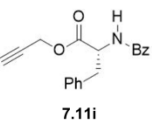
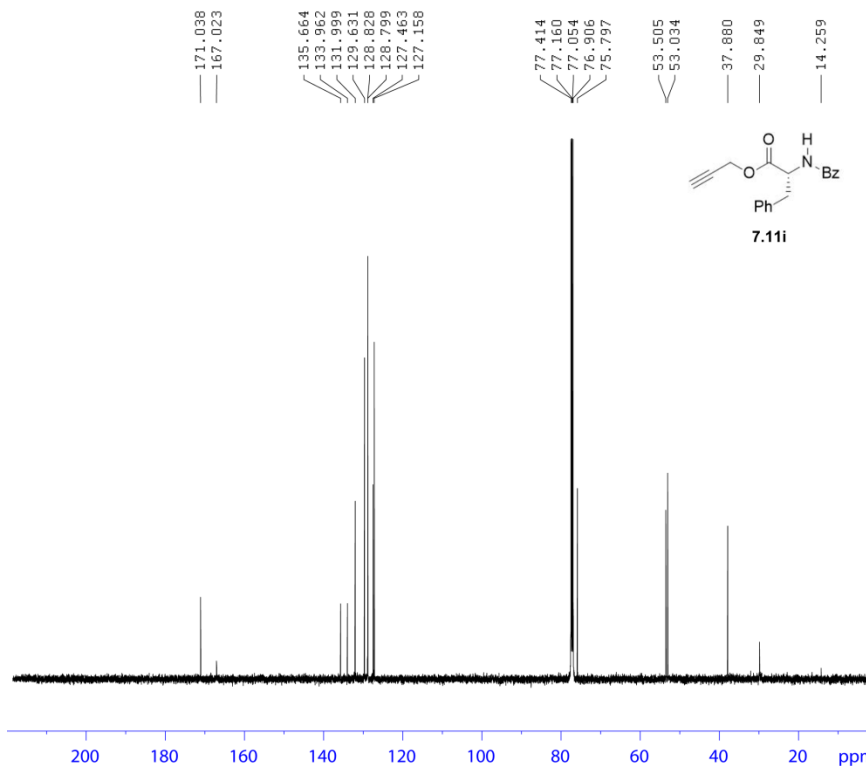
===== CHANNEL f1 =====
 SFO1 125.7779086 MHz
 NUC1 13C
 P1 10.50 usec
 SI 32768
 SF 125.7653129 MHz
 WDW EM
 SSB 0
 LB 1.00 Hz
 GB 0
 PC 1.40



NAME	SW06-165-cr
EXPNO	10
PROCNO	1
Date_	2015 0415
Time	16.11
INSTRUM	spect
PROBHD	5 mm PABBO BB-
PULPROG	zg30
TD	65536
SOLVENT	CDCl3
NS	16
DS	2
SWH	8223.685 Hz
FIDRES	0.125483 Hz
AQ	3.9846387 sec
RG	144
DW	60.800 usec
DE	6.50 usec
TE	90.6 K
D1	1.0000000 sec

==== CHANNEL f1 =====

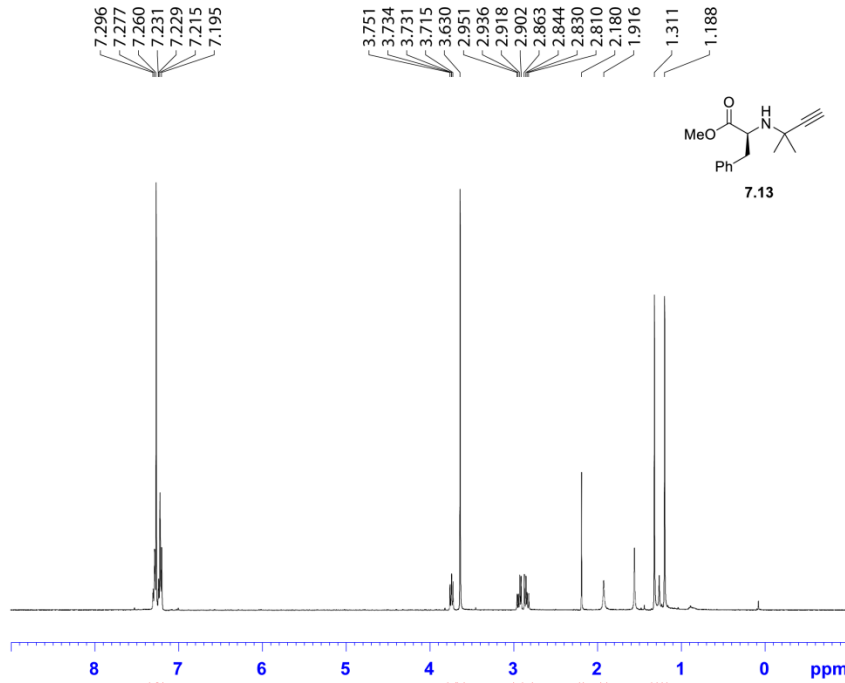
NUC1	1H
P1	13.75 usec
SI	65536
SF	400.130098 MHz
WDW	EM
SSB	0
LB	0.30 Hz
GB	0
PC	1.00



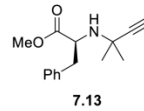
NAME	SW06-165-cr
EXPNO	11
PROCNO	1
Date_	20150502
Time	0.44
INSTRUM	spect
PROBHD	5 mm PABBO BB/
PULPROG	zpgp30
TD	65536
SOLVENT	CDCl3
NS	2048
DS	2
SWH	29761.904 Hz
FIDRES	0.454131 Hz
AQ	1.1010548 sec
RG	203
DW	16.800 usec
DE	6.50 usec
TE	298.2 K
D1	2.0000000 sec
D11	0.03000000 sec
TD0	1

==== CHANNEL f1 =====

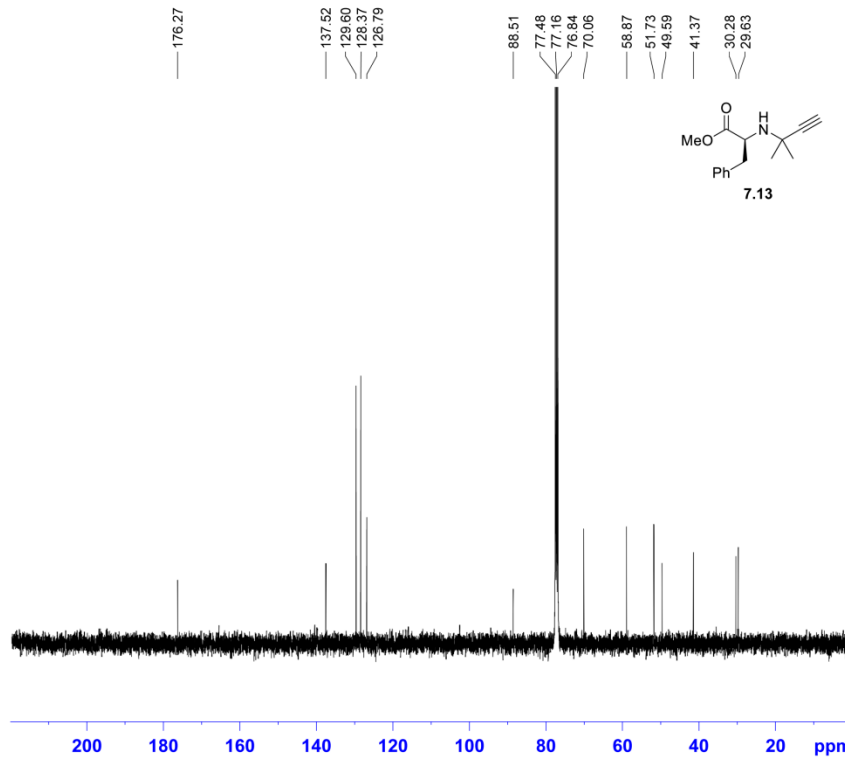
SF01	125.7779086 MHz
NUC1	13C
P1	10.50 usec
SI	32768
SF	125.7653137 MHz
WDW	EM
SSB	0
LB	1.00 Hz
GB	0
PC	1.40



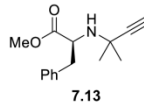
NAME SW07-131-A
 EXPNO 10
 PROCNO 1
 Date_ 20151103
 Time 17.21
 INSTRUM spect
 PROBHD 5 mm PABBO BB-
 PULPROG zg30
 TD 65536
 SOLVENT CDCl3
 NS 16
 DS 2
 SWH 8012.820 Hz
 FIDRES 0.122266 Hz
 AQ 4.0894966 sec
 RG 144
 DW 62.400 usec
 DE 6.50 usec
 TE 91.8 K
 D1 1.00000000 sec
 TD0 1



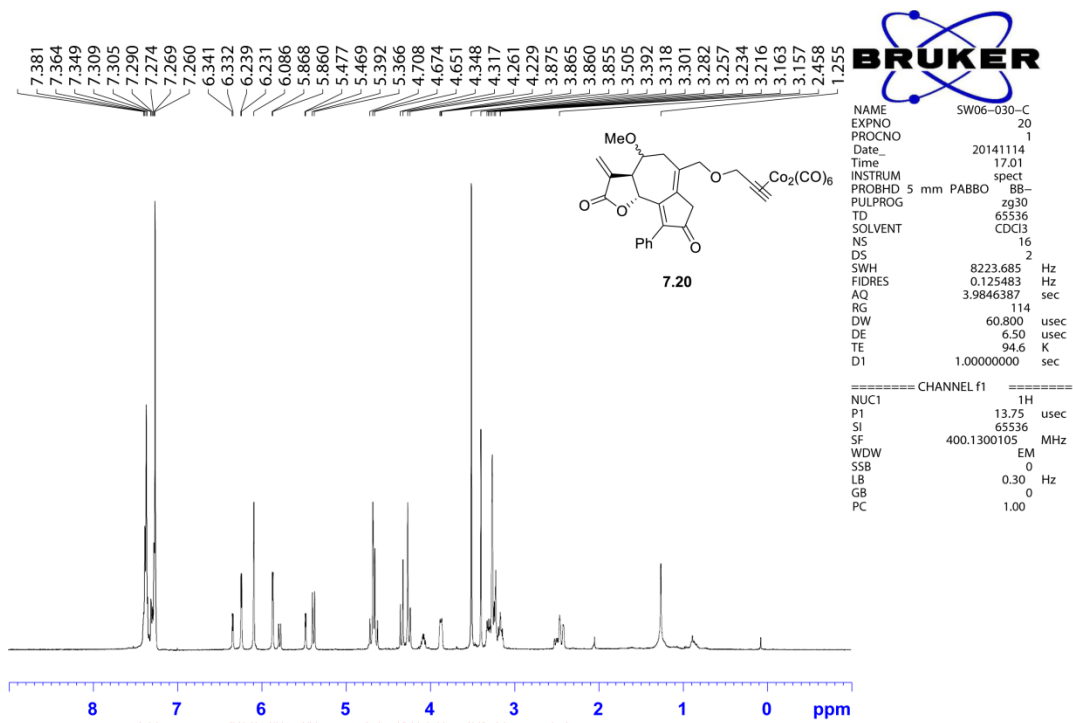
===== CHANNEL f1 =====
 SFO1 400.1324710 MHz
 NUC1 1H
 P1 13.75 usec
 SI 65536
 SF 400.1300105 MHz
 WDW EM
 SSB 0
 LB 0.30 Hz
 GB 0
 PC 1.00



NAME SW07-131-A
 EXPNO 11
 PROCNO 1
 Date_ 20151103
 Time 23.00
 INSTRUM spect
 PROBHD 5 mm PABBO BB-
 PULPROG zgpg30
 TD 65536
 SOLVENT CDCl3
 NS 3072
 DS 4
 SWH 24038.461 Hz
 FIDRES 0.366798 Hz
 AQ 1.3631988 sec
 RG 203
 DW 20.800 usec
 DE 6.50 usec
 TE 97.2 K
 D1 2.00000000 sec
 D11 0.03000000 sec
 TD0 1

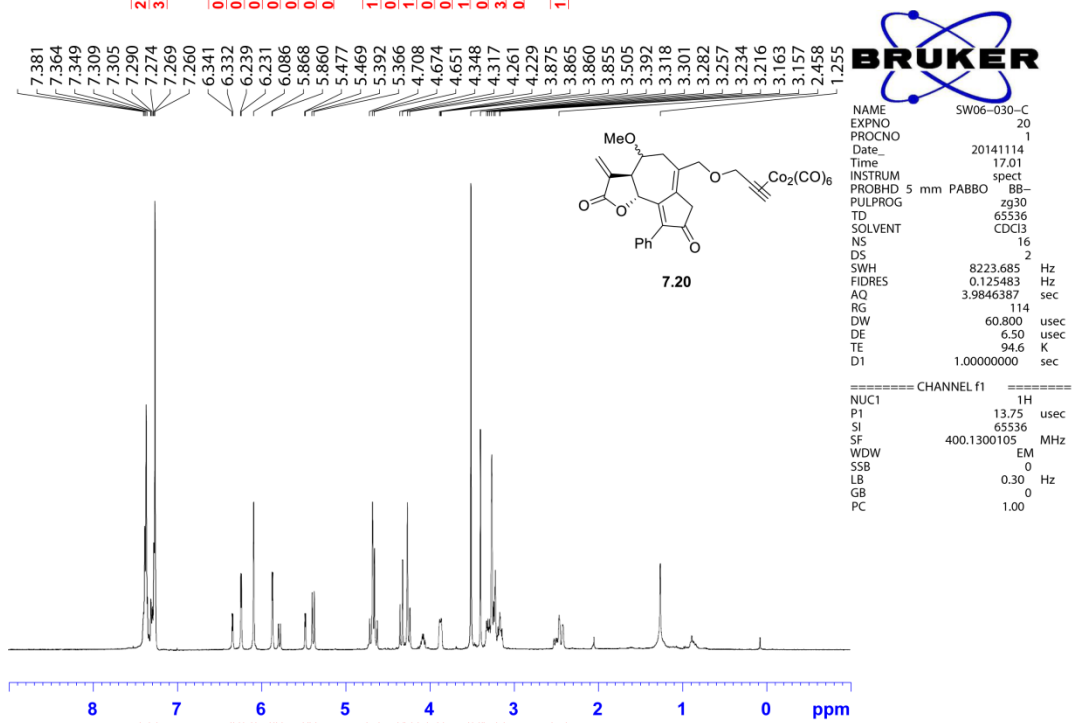


===== CHANNEL f1 =====
 SFO1 100.6228293 MHz
 NUC1 13C
 P1 10.00 usec
 SI 32768
 SF 100.6127542 MHz
 WDW EM
 SSB 0
 LB 1.00 Hz
 GB 0
 PC 1.40



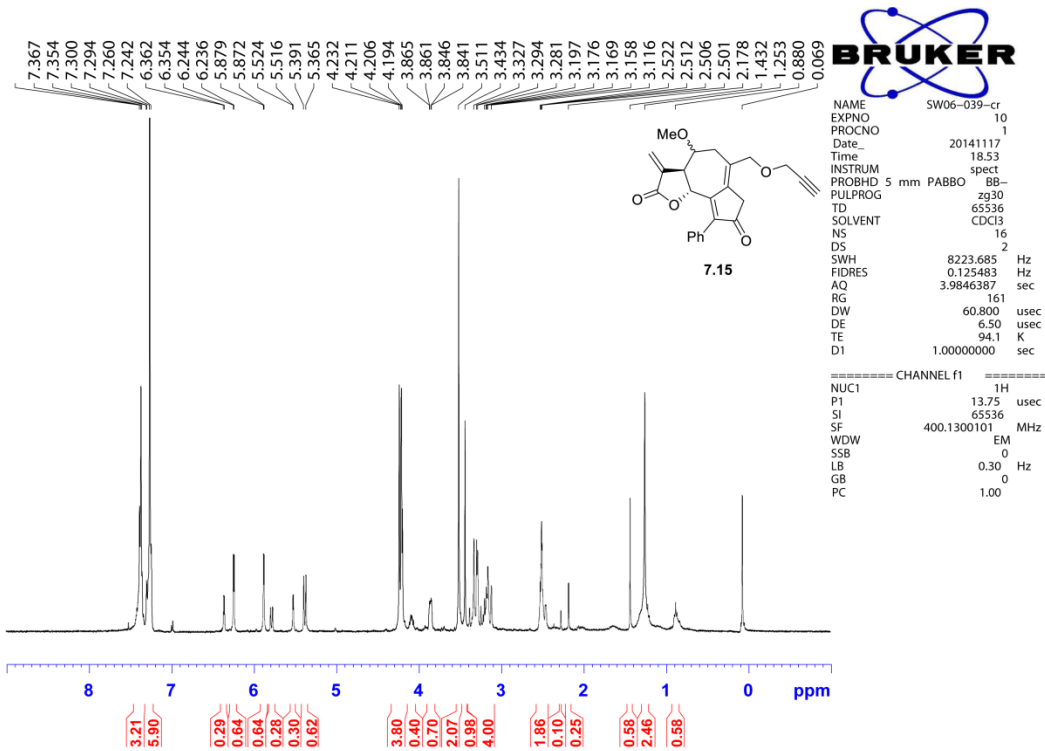
NAME SW06-030-C
 EXPNO 20
 PROCNO 1
 Date_ 20141114
 Time 17.01
 INSTRUM spect
 PROBHD 5 mm PABBO BB-
 PULPROG zg30
 TD 65536
 SOLVENT CDCl3
 NS 16
 DS 2
 SWH 8223.685 Hz
 FIDRES 0.125483 Hz
 AQ 3.9846387 sec
 RG 114
 DW 60.800 usec
 DE 6.50 usec
 TE 94.6 K
 D1 1.00000000 sec

===== CHANNEL f1 =====
 NUC1 1H
 P1 13.75 usec
 SI 65536
 SF 400.1300105 MHz
 WDW EM
 SSB 0
 LB 0.30 Hz
 GB 0
 PC 1.00



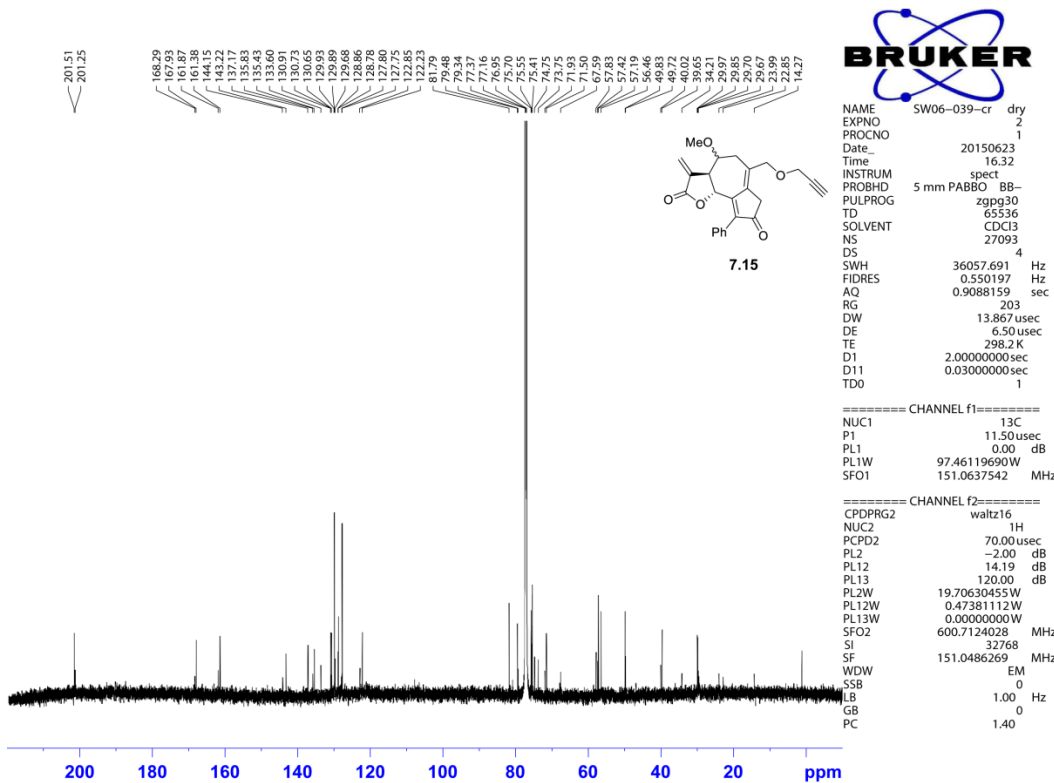
NAME SW06-030-C
 EXPNO 20
 PROCNO 1
 Date_ 20141114
 Time 17.01
 INSTRUM spect
 PROBHD 5 mm PABBO BB-
 PULPROG zg30
 TD 65536
 SOLVENT CDCl3
 NS 16
 DS 2
 SWH 8223.685 Hz
 FIDRES 0.125483 Hz
 AQ 3.9846387 sec
 RG 114
 DW 60.800 usec
 DE 6.50 usec
 TE 94.6 K
 D1 1.00000000 sec

===== CHANNEL f1 =====
 NUC1 1H
 P1 13.75 usec
 SI 65536
 SF 400.1300105 MHz
 WDW EM
 SSB 0
 LB 0.30 Hz
 GB 0
 PC 1.00



NAME SW06-039-cr
 EXPNO 10
 PROCNO 1
 Date_ 20141117
 Time 18.53
 INSTRUM spect
 PROBHD 5 mm PABBO BB-
 PULPROG zg30
 TD 65536
 SOLVENT CDCl3
 NS 16
 DS 2
 SWH 8223.685 Hz
 FIDRES 0.125483 Hz
 AQ 3.9846387 sec
 RG 161
 DW 60.800 usec
 DE 6.50 usec
 TE 94.1 K
 D1 1.00000000 sec

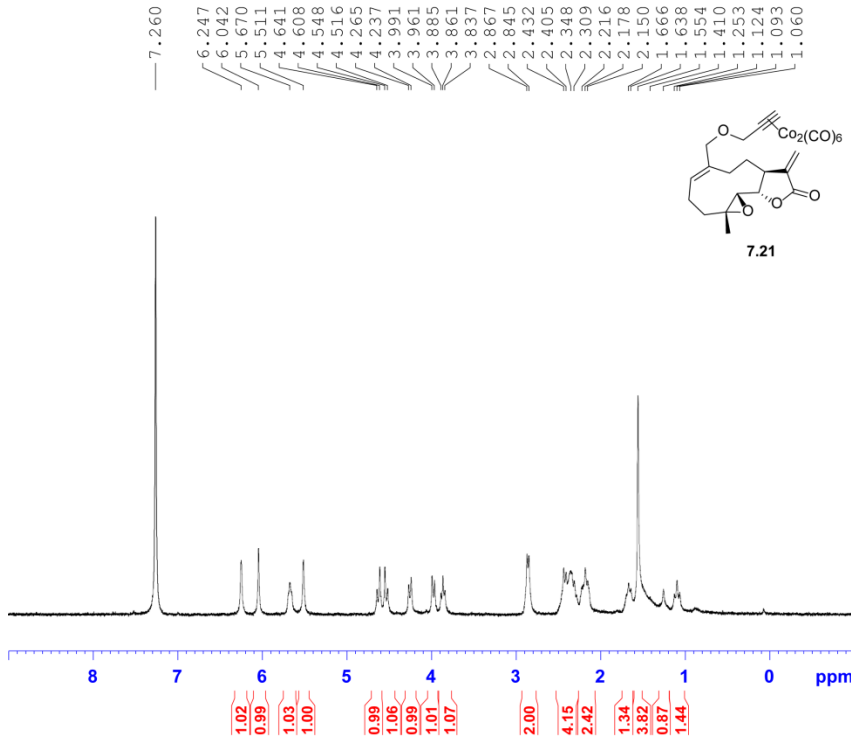
===== CHANNEL f1 =====
 NUC1 1H
 P1 13.75 usec
 SI 65536
 SF 400.1300101 MHz
 WDW EM
 SSB 0
 LB 0.30 Hz
 GB 0
 PC 1.00



NAME SW06-039-cr dry
 EXPNO 2
 PROCNO 1
 Date_ 20150623
 Time 16.32
 INSTRUM spect
 PROBHD 5 mm PABBO BB-
 PULPROG zgpg30
 TD 65536
 SOLVENT CDCl3
 NS 27093
 DS 4
 SWH 36057.691 Hz
 FIDRES 0.550197 Hz
 AQ 0.9088159 sec
 RG 203
 DW 13.867 usec
 DE 6.50 usec
 TE 298.2 K
 D1 2.00000000 sec
 D10 0.03000000 sec
 TD0 1

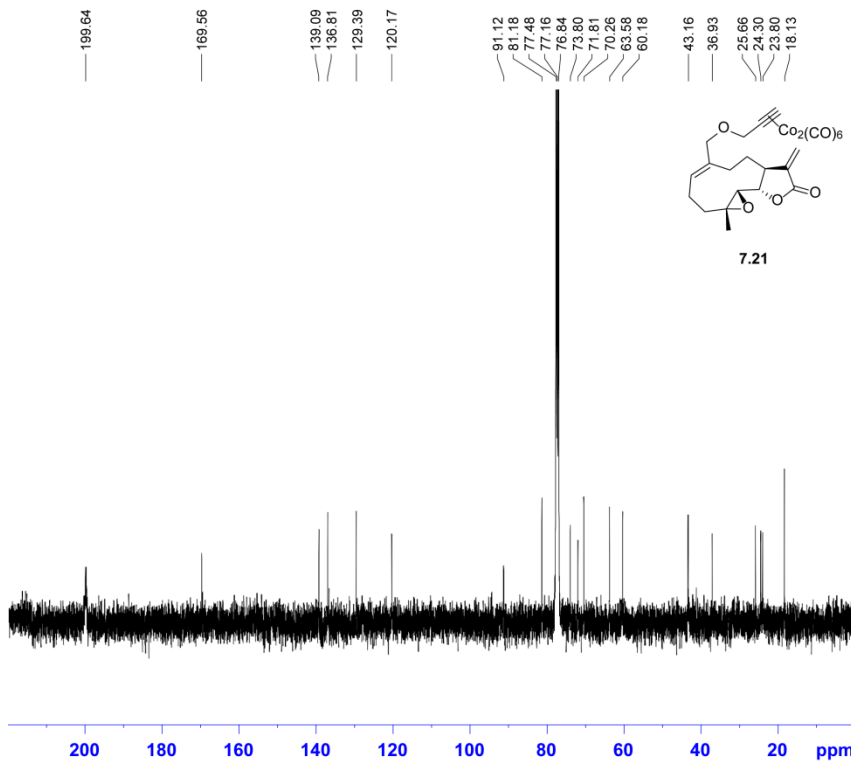
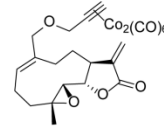
===== CHANNEL f1 =====
 NUC1 13C
 P1 11.50 usec
 PL1 0.00 dB
 PL1W 97.46119690W
 SFO1 151.0637542 MHz

===== CHANNEL f2 =====
 CPDPRG2 waltz16
 NUC2 1H
 PCPD2 70.00 usec
 PL2 -2.00 dB
 PL12 14.19 dB
 PL13 120.00 dB
 PL2W 19.70630455W
 PL12W 0.47381112W
 PL13W 0.00000000W
 SFO2 600.7124028 MHz
 SI 32768
 SF 151.0486269 MHz
 WDW EM
 SSB 0
 LB 1.00 Hz
 GB 0
 PC 1.40



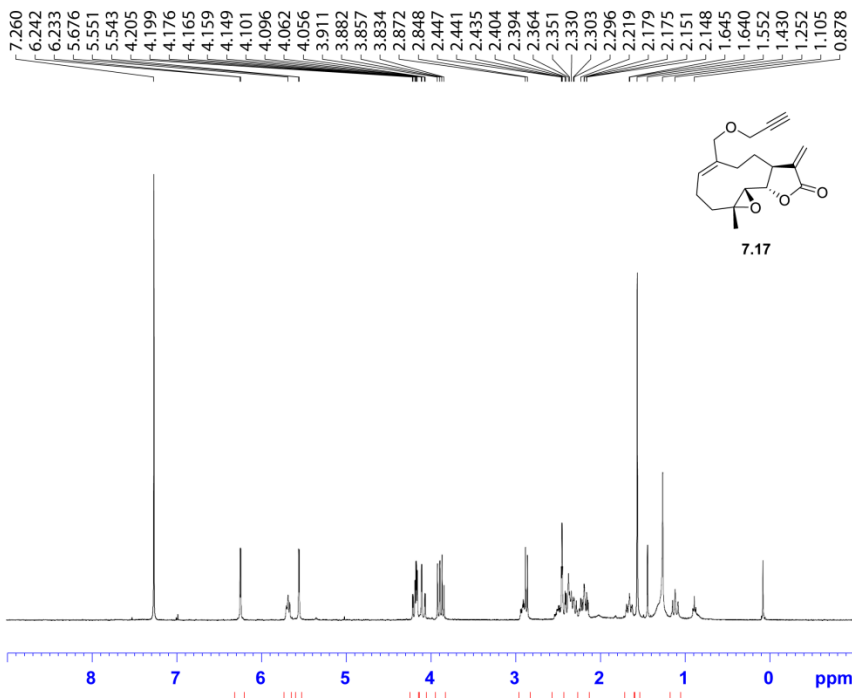
NAME SW06-183-C
EXPNO 20
PROCNO 1
Date_ 20150507
Time_ 12.52
INSTRUM spect
PROBHD 5 mm FAPBO BB-
PULPROG zg30
TD 65536
SOLVENT CDCl3
NS 16
DS 2
SWH 8223.685 Hz
FIDRES 0.125483 Hz
AQ 3.9846387 sec
RG 181
DW 60.800 usec
DE 6.50 usec
TE 90.6 K
D1 1.00000000 sec

===== CHANNEL f1 =====
NUC1 1H
P1 13.75 usec
SI 65536
SF 400.1300102 MHz
WDW EM
SSB 0
LB 0.30 Hz
GB 0
PC 1.00



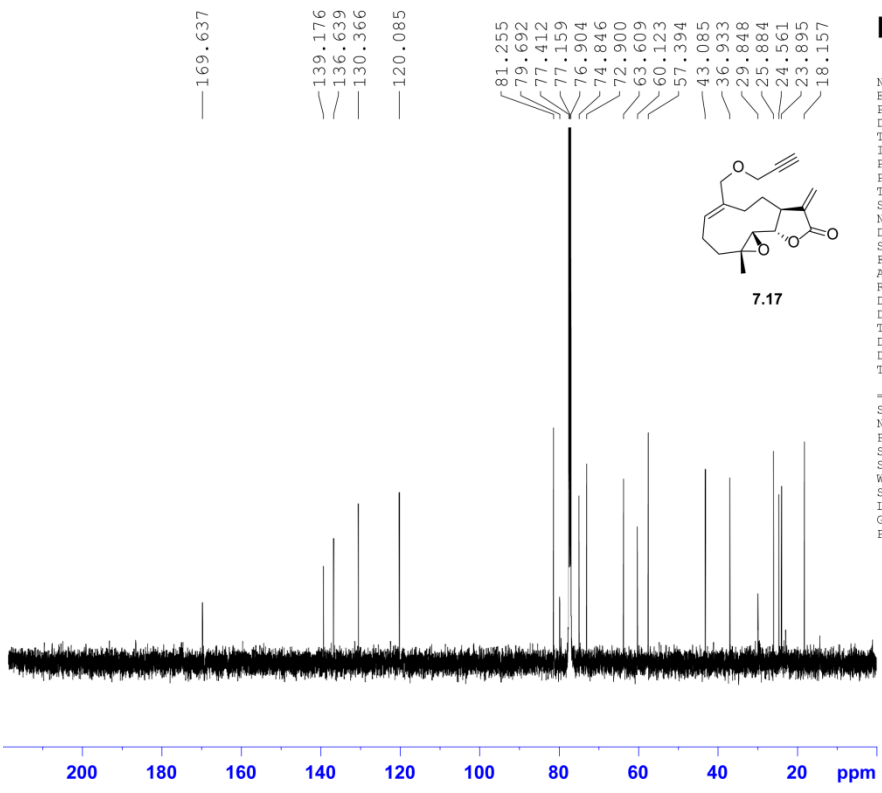
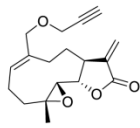
NAME SW06-183-C
EXPNO 11
PROCNO 1
Date_ 20150505
Time_ 7.27
INSTRUM spect
PROBHD 5 mm PABBO BB-
PULPROG zgpg30
TD 65536
SOLVENT CDCl3
NS 2048
DS 4
SWH 24038.461 Hz
FIDRES 0.366798 Hz
AQ 1.3631988 sec
RG 203
DW 20.800 usec
DE 6.50 usec
TE 95.3 K
D1 2.00000000 sec
D11 0.03000000 sec

===== CHANNEL f1 =====
NUC1 13C
P1 10.00 usec
SI 32768
SF 100.6127547 MHz
WDW EM
SSB 0
LB 1.00 Hz
GB 0
PC 1.40



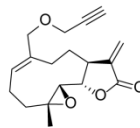
NAME SW06-191-cr
EXPNO 10
PROCNO 1
Date_ 20150512
Time 17.34
INSTRUM spect
PROBHD 5 mm PABBO BB-
PULPROG zg30
TD 65536
SOLVENT CDCl3
NS 16
DS 2
SWH 8223.685 Hz
FIDRES 0.125483 Hz
AQ 3.9846387 sec
RG 161
DW 60.800 usec
DE 6.50 usec
TE 3049.3 K
D1 1.00000000 sec

===== CHANNEL f1 =====
NUC1 1H
P1 13.75 usec
SI 65536
SF 400.1300100 MHz
WDW EM
SSB 0
LB 0.30 Hz
GB 0
PC 1.00



NAME SW06-191-cr
EXPNO 10
PROCNO 1
Date_ 20150513
Time 6.46
INSTRUM spect
PROBHD 5 mm PABBO BB/
PULPROG zgpg30
TD 65536
SOLVENT CDCl3
NS 2048
DS 2
SWH 29761.904 Hz
FIDRES 0.454131 Hz
AQ 1.1010548 sec
RG 203
DW 16.800 usec
DE 6.50 usec
TE 298.5 K
D1 2.00000000 sec
D11 0.03000000 sec
TD0 1

===== CHANNEL f1 =====
SF01 125.7779086 MHz
NUC1 13C
P1 10.50 usec
SI 32768
SF 125.7653131 MHz
WDW EM
SSB 0
LB 1.00 Hz
GB 0
PC 1.40



7.8 Acknowledgements

We gratefully acknowledge the NIH (R21-CA194661 to DAH and R01-GM054161 to KMB) and the Department of Defense (PC141033 to DAH) for funding. Mass spectrometry performed at the University of Minnesota was conducted at the Masonic Cancer Center Analytical Biochemistry Core Facility, which is supported by the National Institute of Health (P30-CA77598).

Bibliography

1. (a) Roeder, R. G., The role of general initiation factors in transcription by RNA polymerase II. *Trends Biochem. Sci.* **1996**, *21*, 327-35; (b) Roeder, R. G., Nuclear RNA polymerases: role of general initiation factors and cofactors in eukaryotic transcription. *Methods in Enzymol.* **1996**, *273*, 165-71; (c) Kuhlman, T. C.; Cho, H.; Reinberg, D.; Hernandez, N., The general transcription factors IIA, IIB, IIF, and IIE are required for RNA polymerase II transcription from the human U1 small nuclear RNA promoter. *Mol. Cell. Biol.* **1999**, *19*, 2130-41; (d) Orphanides, G.; Lagrange, T.; Reinberg, D., The general transcription factors of RNA polymerase II. *Genes Dev.* **1996**, *10*, 2657-83.
2. Chapman, R. D.; Heidemann, M.; Albert, T. K.; Mailhammer, R.; Flatley, A.; Meisterernst, M.; Kremmer, E.; Eick, D., Transcribing RNA polymerase II is phosphorylated at CTD residue serine-7. *Science* **2007**, *318*, 1780-2.
3. Kornberg, R. D., Mediator and the mechanism of transcriptional activation. *Trends in Biochem. Sci.* **2005**, *30*, 235-9.
4. (a) Malik, S.; Roeder, R. G., Dynamic regulation of pol II transcription by the mammalian Mediator complex. *Trends in Biochem. Sci.* **2005**, *30*, 256-63; (b) de Laat, W.; Klous, P.; Kooren, J.; Noordermeer, D.; Palstra, R. J.; Simonis, M.; Splinter, E.; Grosveld, F., Three-dimensional organization of gene expression in erythroid cells. *Curr. Top. Dev. Biol.* **2008**, *82*, 117-39; (c) Ptashne, M., Gene regulation by proteins acting nearby and at a distance. *Nature* **1986**, *322*, 697-701; (d) Cullen, K. E.; Kladde, M. P.; Seyfred, M. A., Interaction between transcription regulatory regions of prolactin chromatin. *Science* **1993**, *261*, 203-6; (e) Dekker, J.; Rippe, K.; Dekker, M.; Kleckner, N., Capturing chromosome conformation. *Science* **2002**, *295*, 1306-11.
5. (a) Banerji, J.; Olson, L.; Schaffner, W., A lymphocyte-specific cellular enhancer is located downstream of the joining region in immunoglobulin heavy chain genes. *Cell* **1983**, *33*, 729-40; (b) Gillies, S. D.; Morrison, S. L.; Oi, V. T.; Tonegawa, S., A tissue-specific transcription enhancer element is located in the major intron of a rearranged immunoglobulin heavy chain gene. *Cell* **1983**, *33*, 717-28.
6. (a) Lettice, L. A.; Heaney, S. J.; Purdie, L. A.; Li, L.; de Beer, P.; Oostra, B. A.; Goode, D.; Elgar, G.; Hill, R. E.; de Graaff, E., A long-range Shh enhancer regulates expression in the developing limb and fin and is associated with preaxial polydactyly. *Hum. Mol. Gen.* **2003**, *12*, 1725-35; (b) Sagai, T.; Hosoya, M.; Mizushima, Y.; Tamura, M.; Shiroishi, T., Elimination of a long-range cis-regulatory module causes complete loss of limb-specific Shh expression and truncation of the mouse limb. *Development* **2005**, *132*, 797-803.
7. (a) Sato, S.; Tomomori-Sato, C.; Parmely, T. J.; Florens, L.; Zybailov, B.; Swanson, S. K.; Banks, C. A.; Jin, J.; Cai, Y.; Washburn, M. P.; Conaway, J. W.; Conaway, R.

- C., A set of consensus mammalian mediator subunits identified by multidimensional protein identification technology. *Mol. Cell* **2004**, *14*, 685-91; (b) Wang, G.; Cantin, G. T.; Stevens, J. L.; Berk, A. J., Characterization of mediator complexes from HeLa cell nuclear extract. *Mol. Cell. Biol.* **2001**, *21*, 4604-13; (c) Ryu, S.; Tjian, R., Purification of transcription cofactor complex CRSP. *Proc. Natl. Acad. Sci. U.S.A.* **1999**, *96*, 7137-42; (d) Taatjes, D. J.; Naar, A. M.; Andel, F., 3rd; Nogales, E.; Tjian, R., Structure, function, and activator-induced conformations of the CRSP coactivator. *Science* **2002**, *295*, 1058-62.
8. (a) Mittler, G.; Kremmer, E.; Timmers, H. T.; Meisterernst, M., Novel critical role of a human Mediator complex for basal RNA polymerase II transcription. *EMBO reports* **2001**, *2*, 808-13; (b) Wu, S. Y.; Zhou, T.; Chiang, C. M., Human mediator enhances activator-facilitated recruitment of RNA polymerase II and promoter recognition by TATA-binding protein (TBP) independently of TBP-associated factors. *Mol. Cell. Biol.* **2003**, *23*, 6229-42.
 9. (a) The NF- κ B heterodimer binds to over 600 gene targets. For a comprehensive list visit: <http://www.bu.edu/nf-kb/gene-resources/target-genes/>. Gilmore, T. D. et al; (b) Oeckinghaus, A.; Ghosh, S., The NF- κ B family of transcription factors and its regulation. *Cold Spring Harb. Perspect. Biol.* **2009**, *1*, a000034.
 10. Bolton, E. C.; So, A. Y.; Chaivorapol, C.; Haqq, C. M.; Li, H.; Yamamoto, K. R., Cell- and gene-specific regulation of primary target genes by the androgen receptor. *Genes Dev.* **2007**, *21*, 2005-17.
 11. Lelli, K. M.; Slattery, M.; Mann, R. S., Disentangling the many layers of eukaryotic transcriptional regulation. *Annu. Rev. Genet.* **2012**, *46*, 43-68.
 12. Thanos, D.; Maniatis, T., Virus induction of human IFN β gene expression requires the assembly of an enhanceosome. *Cell* **1995**, *83*, 1091-100.
 13. (a) Liu, H.; Sidiropoulos, P.; Song, G.; Pagliari, L. J.; Birrer, M. J.; Stein, B.; Anrather, J.; Pope, R. M., TNF- α gene expression in macrophages: regulation by NF- κ B is independent of c-Jun or C/EBP β . *J. Immunol.* **2000**, *164*, 4277-85; (b) Falvo, J. V.; Ugliarolo, A. M.; Brinkman, B. M.; Merika, M.; Parekh, B. S.; Tsai, E. Y.; King, H. C.; Morielli, A. D.; Peralta, E. G.; Maniatis, T.; Thanos, D.; Goldfeld, A. E., Stimulus-specific assembly of enhancer complexes on the tumor necrosis factor α gene promoter. *Mol. Cell. Biol.* **2000**, *20*, 2239-47.
 14. Meijssing, S. H.; Pufall, M. A.; So, A. Y.; Bates, D. L.; Chen, L.; Yamamoto, K. R., DNA binding site sequence directs glucocorticoid receptor structure and activity. *Science* **2009**, *324*, 407-10.
 15. Reich, N. C.; Liu, L., Tracking STAT nuclear traffic. *Nature reviews. Immunology* **2006**, *6*, 602-12.

16. (a) Beg, A. A.; Ruben, S. M.; Scheinman, R. I.; Haskill, S.; Rosen, C. A.; Baldwin, A. S., Jr., I κ B interacts with the nuclear localization sequences of the subunits of NF- κ B: a mechanism for cytoplasmic retention. *Genes Dev.* **1992**, *6*, 1899-913; (b) Ganchi, P. A.; Sun, S. C.; Greene, W. C.; Ballard, D. W., I κ B/MAD-3 masks the nuclear localization signal of NF- κ B p65 and requires the transactivation domain to inhibit NF- κ B p65 DNA binding. *Mol. Biol. Cell* **1992**, *3*, 1339-52; (c) Henkel, T.; Zabel, U.; van Zee, K.; Muller, J. M.; Fanning, E.; Baeuerle, P. A., Intramolecular masking of the nuclear location signal and dimerization domain in the precursor for the p50 NF- κ B subunit. *Cell* **1992**, *68*, 1121-33.
17. Huang, B.; Yang, X. D.; Lamb, A.; Chen, L. F., Posttranslational modifications of NF- κ B: another layer of regulation for NF- κ B signaling pathway. *Cell. Signal* **2010**, *22*, 1282-90.
18. Masoud, G. N.; Li, W., HIF-1 α pathway: role, regulation and intervention for cancer therapy. *Acta. Pharm. Sin. B* **2015**, *5*, 378-89.
19. (a) Hamamoto, R.; Saloura, V.; Nakamura, Y., Critical roles of non-histone protein lysine methylation in human tumorigenesis. *Nature Rev. Cancer* **2015**, *15*, 110-124; (b) Yang, Y.; Bedford, M. T., Protein arginine methyltransferases and cancer. *Nature Rev. Cancer* **2013**, *13*, 37-50.
20. Lu, T.; Jackson, M. W.; Wang, B.; Yang, M.; Chance, M. R.; Miyagi, M.; Gudkov, A. V.; Stark, G. R., Regulation of NF- κ B by NSD1/FBXL11-dependent reversible lysine methylation of p65. *Proc. Natl. Acad. Sci. U.S.A.* **2010**, *107*, 46-51.
21. (a) Cho, E. C.; Zheng, S.; Munro, S.; Liu, G.; Carr, S. M.; Moehlenbrink, J.; Lu, Y. C.; Stimson, L.; Khan, O.; Konietzny, R.; McGouran, J.; Coutts, A. S.; Kessler, B.; Kerr, D. J.; Thangue, N. B., Arginine methylation controls growth regulation by E2F-1. *EMBO J.* **2012**, *31*, 1785-97; (b) Jansson, M.; Durant, S. T.; Cho, E. C.; Sheahan, S.; Edelmann, M.; Kessler, B.; La Thangue, N. B., Arginine methylation regulates the p53 response. *Nature cell biology* **2008**, *10*, 1431-9; (c) Bandyopadhyay, S.; Harris, D. P.; Adams, G. N.; Lause, G. E.; McHugh, A.; Tillmaand, E. G.; Money, A.; Willard, B.; Fox, P. L.; Dicorleto, P. E., HOXA9 methylation by PRMT5 is essential for endothelial cell expression of leukocyte adhesion molecules. *Mol. Cell. Biol.* **2012**, *32*, 1202-13.
22. (a) Spange, S.; Wagner, T.; Heinzl, T.; Kramer, O. H., Acetylation of non-histone proteins modulates Cell. Signal at multiple levels. *The international journal of biochemistry & cell biology* **2009**, *41*, 185-98; (b) Ogryzko, V. V.; Schiltz, R. L.; Russanova, V.; Howard, B. H.; Nakatani, Y., The transcriptional coactivators p300 and CBP are histone acetyltransferases. *Cell* **1996**, *87*, 953-9.
23. (a) Na, S. Y.; Lee, S. K.; Han, S. J.; Choi, H. S.; Im, S. Y.; Lee, J. W., Steroid receptor coactivator-1 interacts with the p50 subunit and coactivates nuclear factor κ B-mediated transactivations. *J. Biol. Chem.* **1998**, *273*, 10831-4; (b) Lee, S. K.; Kim,

- H. J.; Na, S. Y.; Kim, T. S.; Choi, H. S.; Im, S. Y.; Lee, J. W., Steroid receptor coactivator-1 coactivates activating protein-1-mediated transactivations through interaction with the c-Jun and c-Fos subunits. *J. Biol. Chem.* **1998**, *273*, 16651-4; (c) Li, G.; Heaton, J. H.; Gelehrter, T. D., Role of steroid receptor coactivators in glucocorticoid and transforming growth factor β regulation of plasminogen activator inhibitor gene expression. *Mol. Endocrinol.* **2006**, *20*, 1025-34; (d) Gao, Z.; Chiao, P.; Zhang, X.; Zhang, X.; Lazar, M. A.; Seto, E.; Young, H. A.; Ye, J., Coactivators and corepressors of NF- κ B in I κ B α gene promoter. *J. Biol. Chem.* **2005**, *280*, 21091-8; (e) Batsche, E.; Desroches, J.; Bilodeau, S.; Gauthier, Y.; Drouin, J., Rb enhances p160/SRC coactivator-dependent activity of nuclear receptors and hormone responsiveness. *J. Biol. Chem.* **2005**, *280*, 19746-56; (f) Lee, S. K.; Kim, H. J.; Kim, J. W.; Lee, J. W., Steroid receptor coactivator-1 and its family members differentially regulate transactivation by the tumor suppressor protein p53. *Mol. Endocrinol.* **1999**, *13*, 1924-33.
24. Stanya, K. J.; Kao, H. Y., New insights into the functions and regulation of the transcriptional corepressors SMRT and N-CoR. *Cell Div.* **2009**, *4*, 7.
25. (a) Hoberg, J. E.; Yeung, F.; Mayo, M. W., SMRT derepression by the I κ B kinase α : a prerequisite to NF- κ B transcription and survival. *Mol. Cell* **2004**, *16*, 245-55; (b) Hoberg, J. E.; Popko, A. E.; Ramsey, C. S.; Mayo, M. W., I κ B kinase α -mediated derepression of SMRT potentiates acetylation of RelA/p65 by p300. *Mol. Cell. Biol.* **2006**, *26*, 457-71; (c) Hong, S. H.; Privalsky, M. L., The SMRT corepressor is regulated by a MEK-1 kinase pathway: inhibition of corepressor function is associated with SMRT phosphorylation and nuclear export. *Mol. Cell. Biol.* **2000**, *20*, 6612-25.
26. Wingender, E.; Schoeps, T.; Haubrock, M.; Donitz, J., TFClass: a classification of human transcription factors and their rodent orthologs. *Nucleic Acid Res.* **2015**, *43* (Database issue), D97-102.
27. <http://tfclass.bioinf.med.uni-goettingen.de/tfclass>
28. Glover, J. N.; Harrison, S. C., Crystal structure of the heterodimeric bZIP transcription factor c-Fos-c-Jun bound to DNA. *Nature* **1995**, *373*, 257-61.
29. Schwabe, J. W.; Chapman, L.; Finch, J. T.; Rhodes, D., The crystal structure of the estrogen receptor DNA-binding domain bound to DNA: how receptors discriminate between their response elements. *Cell* **1993**, *75*, 567-78.
30. Chen, F. E.; Huang, D. B.; Chen, Y. Q.; Ghosh, G., Crystal structure of p50/p65 heterodimer of transcription factor NF- κ B bound to DNA. *Nature* **1998**, *391*, 410-3.
31. (a) Chen, F. E.; Huang, D. B.; Chen, Y. Q.; Ghosh, G., Crystal structure of p50/p65 heterodimer of transcription factor NF- κ B bound to DNA. *Nature* **1998**, *391*, 410-413; (b) Urban, M. B.; Baeuerle, P. A., The 65-kD subunit of NF- κ B is a receptor for

- I κ B and a modulator of DNA-binding specificity. *Genes Dev.* **1990**, *4*, 1975-84; (c) Thanos, D.; Maniatis, T., The high mobility group protein HMG I(Y) is required for NF- κ B-dependent virus induction of the human IFN- β gene. *Cell* **1992**, *71*, 777-89; (d) Wrangé, O.; Eriksson, P.; Perlmann, T., The purified activated glucocorticoid receptor is a homodimer. *J. Biol. Chem.* **1989**, *264*, 5253-9; (e) Perlmann, T.; Eriksson, P.; Wrangé, O., Quantitative analysis of the glucocorticoid receptor-DNA interaction at the mouse mammary tumor virus glucocorticoid response element. *J. Biol. Chem.* **1990**, *265*, 17222-9; (f) Bonham, A. J.; Wentz, N.; Osslund, L. M.; Prussin, A. J., 2nd; Vinkemeier, U.; Reich, N. O., STAT1:DNA sequence-dependent binding modulation by phosphorylation, protein:protein interactions and small-molecule inhibition. *Nucleic Acid Res.* **2013**, *41*, 754-63.
32. (a) Naar, A. M.; Lemon, B. D.; Tjian, R., Transcriptional coactivator complexes. *Annu. Rev. Biochem.* **2001**, *70*, 475-501; (b) Weake, V. M.; Workman, J. L., Inducible gene expression: diverse regulatory mechanisms. *Nature Rev. Genet.* **2010**, *11*, 426-37.
33. Frieze, S.; Farnham, P. J., Transcription factor effector domains. *Subcell. Biochem.* **2011**, *52*, 261-77.
34. Hayden, M. S.; Ghosh, S., Signaling to NF- κ B. *Genes Dev.* **2004**, *18*, 2195-224.
35. (a) Cha-Molstad, H.; Agrawal, A.; Zhang, D.; Samols, D.; Kushner, I., The Rel family member p50 mediates cytokine-induced C-reactive protein expression by a novel mechanism. *J. Immunol.* **2000**, *165*, 4592-7; (b) Fujita, T.; Nolan, G. P.; Liou, H. C.; Scott, M. L.; Baltimore, D., The candidate proto-oncogene bcl-3 encodes a transcriptional coactivator that activates through NF- κ B p50 homodimers. *Genes Dev.* **1993**, *7*, 1354-63; (c) Heissmeyer, V.; Krappmann, D.; Wulczyn, F. G.; Scheidereit, C., NF- κ B p105 is a target of I κ B kinases and controls signal induction of Bcl-3-p50 complexes. *EMBO J.* **1999**, *18*, 4766-78; (d) Dechend, R.; Hirano, F.; Lehmann, K.; Heissmeyer, V.; Ansieau, S.; Wulczyn, F. G.; Scheidereit, C.; Leutz, A., The Bcl-3 oncoprotein acts as a bridging factor between NF- κ B/Rel and nuclear co-regulators. *Oncogene* **1999**, *18*, 3316-23.
36. Zhong, H.; May, M. J.; Jimi, E.; Ghosh, S., The phosphorylation status of nuclear NF- κ B determines its association with CBP/p300 or HDAC-1. *Mol. Cell* **2002**, *9*, 625-36.
37. Baeuerle, P. A.; Baltimore, D., Activation of DNA-binding activity in an apparently cytoplasmic precursor of the NF- κ B transcription factor. *Cell* **1988**, *53*, 211-7.
38. Pomerantz, J. L.; Baltimore, D., Two pathways to NF- κ B. *Mol. Cell* **2002**, *10*, 693-5.
39. (a) Liou, H. C.; Sha, W. C.; Scott, M. L.; Baltimore, D., Sequential induction of NF- κ B/Rel family proteins during B-cell terminal differentiation. *Mol. Cell. Biol.* **1994**, *14*, 5349-59; (b) Liou, H. C.; Hsia, C. Y., Distinctions between c-Rel and other NF-

- κ B proteins in immunity and disease. *BioEssays: News and Reviews in Molecular, Cellular and Developmental Biology* **2003**, *25*, 767-80.
40. (a) Busam, K.; Gieringer, C.; Freudenberg, M.; Hohmann, H. P., Staphylococcus aureus and derived exotoxins induce nuclear factor κ B-like activity in murine bone marrow macrophages. *Infect. Immun.* **1992**, *60*, 2008-15; (b) Dyer, R. B.; Collaco, C. R.; Niesel, D. W.; Herzog, N. K., Shigella flexneri invasion of HeLa cells induces NF- κ B DNA-binding activity. *Infect. Immun.* **1993**, *61*, 4427-33; (c) Trede, N. S.; Castigli, E.; Geha, R. S.; Chatila, T., Microbial superantigens induce NF- κ B in the human monocytic cell line THP-1. *J. Immunol.* **1993**, *150*, 5604-13; (d) Zhang, Y.; Broser, M.; Rom, W. N., Activation of the interleukin 6 gene by Mycobacterium tuberculosis or lipopolysaccharide is mediated by nuclear factors NF-IL6 and NF- κ B. *Proc. Natl. Acad. Sci. U.S.A.* **1994**, *91*, 2225-9; (e) Munzenmaier, A.; Lange, C.; Glocker, E.; Covacci, A.; Moran, A.; Bereswill, S.; Baeuerle, P. A.; Kist, M.; Pahl, H. L., A secreted/shed product of Helicobacter pylori activates transcription factor nuclear factor- κ B. *J. Immunol.* **1997**, *159*, 6140-7; (f) Klebanoff, S. J.; Watts, D. H.; Mehlin, C.; Headley, C. M., Lactobacilli and vaginal host defense: activation of the human immunodeficiency virus type 1 long terminal repeat, cytokine production, and NF- κ B. *J. Infect. Dis.* **1999**, *179*, 653-60; (g) Hashemi, F. B.; Ghassemi, M.; Roebuck, K. A.; Spear, G. T., Activation of human immunodeficiency virus type 1 expression by Gardnerella vaginalis. *J. Infect. Dis.* **1999**, *179*, 924-30; (h) Eaves-Pyles, T.; Szabo, C.; Salzman, A. L., Bacterial invasion is not required for activation of NF- κ B in enterocytes. *Infect. Immun.* **1999**, *67*, 800-4; (i) Hauf, N.; Goebel, W.; Serfling, E.; Kuhn, M., Listeria monocytogenes infection enhances transcription factor NF- κ B in P388D1 macrophage-like cells. *Infect. Immun.* **1994**, *62*, 2740-7; (j) Hauf, N.; Goebel, W.; Fiedler, F.; Sokolovic, Z.; Kuhn, M., Listeria monocytogenes infection of P388D1 macrophages results in a biphasic NF- κ B (RelA/p50) activation induced by lipoteichoic acid and bacterial phospholipases and mediated by I κ B α and I κ B β degradation. *Proc. Natl. Acad. Sci. U.S.A.* **1997**, *94*, 9394-9; (k) Dokter, W. H.; Dijkstra, A. J.; Koopmans, S. B.; Stulp, B. K.; Keck, W.; Halie, M. R.; Vellenga, E., G(Anh)MTetra, a natural bacterial cell wall breakdown product, induces interleukin-1 β and interleukin-6 expression in human monocytes. A study of the molecular mechanisms involved in inflammatory cytokine expression. *J. Biol. Chem.* **1994**, *269*, 4201-6; (l) Naumann, M.; Wessler, S.; Bartsch, C.; Wieland, B.; Meyer, T. F., Neisseria gonorrhoeae epithelial cell interaction leads to the activation of the transcription factors nuclear factor κ B and activator protein 1 and the induction of inflammatory cytokines. *J. Exp. Med.* **1997**, *186*, 247-58; (m) Rawadi, G.; Garcia, J.; Lemercier, B.; Roman-Roman, S., Signal transduction pathways involved in the activation of NF- κ B, AP-1, and c-fos by Mycoplasma fermentans membrane lipoproteins in macrophages. *J. Immunol.* **1999**, *162*, 2193-203.
41. (a) Siddiqui, A.; Gaynor, R.; Srinivasan, A.; Mapoles, J.; Farr, R. W., trans-activation of viral enhancers including long terminal repeat of the human immunodeficiency virus by the hepatitis B virus X protein. *Virology* **1989**, *169*, 479-84; (b) Bachelerie, F.; Alcamì, J.; Arenzana-Seisdedos, F.; Virelizier, J. L., HIV enhancer activity

- perpetuated by NF- κ B induction on infection of monocytes. *Nature* **1991**, 350, 709-12.
42. Sen, R.; Baltimore, D., Inducibility of κ immunoglobulin enhancer-binding protein Nf- κ B by a posttranslational mechanism. *Cell* **1986**, 47, 921-8.
 43. (a) Jobin, C.; Haskill, S.; Mayer, L.; Panja, A.; Sartor, R. B., Evidence for altered regulation of I κ B α degradation in human colonic epithelial cells. *J. Immunol.* **1997**, 158, 226-34; (b) Auron, P. E., The interleukin 1 receptor: ligand interactions and signal transduction. *Cytokine & Growth Factor Rev.* **1998**, 9, 221-37; (c) Osborn, L.; Kunkel, S.; Nabel, G. J., Tumor necrosis factor α and interleukin 1 stimulate the human immunodeficiency virus enhancer by activation of the nuclear factor κ B. *Proc. Natl. Acad. Sci. U.S.A.* **1989**, 86, 2336-40.
 44. (a) Hazan, U.; Thomas, D.; Alcamì, J.; Bachelierie, F.; Israel, N.; Yssel, H.; Virelizier, J. L.; Arenzana-Seisdedos, F., Stimulation of a human T-cell clone with anti-CD3 or tumor necrosis factor induces NF- κ B translocation but not human immunodeficiency virus 1 enhancer-dependent transcription. *Proc. Natl. Acad. Sci. U.S.A.* **1990**, 87, 7861-5; (b) Arima, N.; Matsushita, K.; Suruga, Y.; Ohtsubo, H.; Fujiwara, H.; Hidaka, S.; Arimura, K.; Kukita, T.; Yamaguchi, K.; Fukumori, J.; Tanaka, H., IL-2-induced growth of CD8⁺ T cell polyclonal leukemia cells mediated by NF- κ B induction and IL-2 receptor α expression. *Leuk. Res.* **1998**, 22, 265-73.
 45. Grohmann, U.; Belladonna, M. L.; Bianchi, R.; Orabona, C.; Ayroldi, E.; Fioretti, M. C.; Puccetti, P., IL-12 acts directly on DC to promote nuclear localization of NF- κ B and primes DC for IL-12 production. *Immunity* **1998**, 9, 315-23.
 46. McDonald, P. P.; Russo, M. P.; Ferrini, S.; Cassatella, M. A., Interleukin-15 (IL-15) induces NF- κ B activation and IL-8 production in human neutrophils. *Blood* **1998**, 92, 4828-35.
 47. Shalom-Barak, T.; Quach, J.; Lotz, M., Interleukin-17-induced gene expression in articular chondrocytes is associated with activation of mitogen-activated protein kinases and NF- κ B. *J. Biol. Chem.* **1998**, 273, 27467-73.
 48. Kojima, H.; Aizawa, Y.; Yanai, Y.; Nagaoka, K.; Takeuchi, M.; Ohta, T.; Ikegami, H.; Ikeda, M.; Kurimoto, M., An essential role for NF- κ B in IL-18-induced IFN- γ expression in KG-1 cells. *J. Immunol.* **1999**, 162, 5063-9.
 49. Stein, B.; Kramer, M.; Rahmsdorf, H. J.; Ponta, H.; Herrlich, P., UV-induced transcription from the human immunodeficiency virus type 1 (HIV-1) long terminal repeat and UV-induced secretion of an extracellular factor that induces HIV-1 transcription in nonirradiated cells. *J. Virol.* **1989**, 63, 4540-4.
 50. Pahl, H. L., Activators and target genes of Rel/NF- κ B transcription factors. *Oncogene* **1999**, 18, 6853-66.

51. Scheidereit, C., I κ B kinase complexes: gateways to NF- κ B activation and transcription. *Oncogene* **2006**, *25*, 6685-705.
52. (a) Chen, Z. J.; Parent, L.; Maniatis, T., Site-specific phosphorylation of I κ B α by a novel ubiquitination-dependent protein kinase activity. *Cell* **1996**, *84*, 853-62; (b) DiDonato, J. A.; Hayakawa, M.; Rothwarf, D. M.; Zandi, E.; Karin, M., A cytokine-responsive I κ B kinase that activates the transcription factor NF- κ B. *Nature* **1997**, *388*, 548-54; (c) Yamaoka, S.; Courtois, G.; Bessia, C.; Whiteside, S. T.; Weil, R.; Agou, F.; Kirk, H. E.; Kay, R. J.; Israel, A., Complementation cloning of NEMO, a component of the I κ B kinase complex essential for NF- κ B activation. *Cell* **1998**, *93*, 1231-40; (d) Mercurio, F.; Zhu, H.; Murray, B. W.; Shevchenko, A.; Bennett, B. L.; Li, J.; Young, D. B.; Barbosa, M.; Mann, M.; Manning, A.; Rao, A., IKK-1 and IKK-2: cytokine-activated I κ B kinases essential for NF- κ B activation. *Science* **1997**, *278*, 860-6.
53. (a) Woronicz, J. D.; Gao, X.; Cao, Z.; Rothe, M.; Goeddel, D. V., I κ B kinase- β : NF- κ B activation and complex formation with I κ B kinase- α and NIK. *Science* **1997**, *278*, 866-9; (b) Rothwarf, D. M.; Zandi, E.; Natoli, G.; Karin, M., IKK- γ is an essential regulatory subunit of the I κ B kinase complex. *Nature* **1998**, *395*, 297-300; (c) Delhase, M.; Hayakawa, M.; Chen, Y.; Karin, M., Positive and negative regulation of I κ B kinase activity through IKK β subunit phosphorylation. *Science* **1999**, *284*, 309-13.
54. Wang, C.; Deng, L.; Hong, M.; Akkaraju, G. R.; Inoue, J.; Chen, Z. J., TAK1 is a ubiquitin-dependent kinase of MKK and IKK. *Nature* **2001**, *412*, 346-51.
55. (a) Huang, Q.; Yang, J.; Lin, Y.; Walker, C.; Cheng, J.; Liu, Z. G.; Su, B., Differential regulation of interleukin 1 receptor and Toll-like receptor signaling by MEKK3. *Nature Immunol.* **2004**, *5*, 98-103; (b) Yang, J.; Lin, Y.; Guo, Z.; Cheng, J.; Huang, J.; Deng, L.; Liao, W.; Chen, Z.; Liu, Z.; Su, B., The essential role of MEKK3 in TNF-induced NF- κ B activation. *Nature Immunol.* **2001**, *2*, 620-4.
56. Huang, W. C.; Chen, J. J.; Chen, C. C., c-Src-dependent tyrosine phosphorylation of IKK β is involved in tumor necrosis factor- α -induced intercellular adhesion molecule-1 expression. *J. Biol. Chem.* **2003**, *278* (11), 9944-52.
57. Tang, E. D.; Inohara, N.; Wang, C. Y.; Nunez, G.; Guan, K. L., Roles for homotypic interactions and transautophosphorylation in I κ B kinase β (IKK β) activation. *J. Biol. Chem.* **2003**, *278*, 38566-70.
58. Inohara, N.; Koseki, T.; Lin, J.; del Peso, L.; Lucas, P. C.; Chen, F. F.; Ogura, Y.; Nunez, G., An induced proximity model for NF- κ B activation in the Nod1/RICK and RIP signaling pathways. *J. Biol. Chem.* **2000**, *275*, 27823-31.
59. Poyet, J. L.; Srinivasula, S. M.; Lin, J. H.; Fernandes-Alnemri, T.; Yamaoka, S.; Tsichlis, P. N.; Alnemri, E. S., Activation of the I κ B kinases by RIP via IKK/NEMO-mediated oligomerization. *J. Biol. Chem.* **2000**, *275*, 37966-77.

60. Deng, L.; Wang, C.; Spencer, E.; Yang, L.; Braun, A.; You, J.; Slaughter, C.; Pickart, C.; Chen, Z. J., Activation of the I κ B kinase complex by TRAF6 requires a dimeric ubiquitin-conjugating enzyme complex and a unique polyubiquitin chain. *Cell* **2000**, *103*, 351-61.
61. (a) Abbott, D. W.; Wilkins, A.; Asara, J. M.; Cantley, L. C., The Crohn's disease protein, NOD2, requires RIP2 in order to induce ubiquitinylation of a novel site on NEMO. *Curr. Biol.* **2004**, *14*, 2217-27; (b) Sun, L.; Deng, L.; Ea, C. K.; Xia, Z. P.; Chen, Z. J., The TRAF6 ubiquitin ligase and TAK1 kinase mediate IKK activation by BCL10 and MALT1 in T lymphocytes. *Mol. Cell* **2004**, *14*, 289-301; (c) Zhou, H.; Wertz, I.; O'Rourke, K.; Ultsch, M.; Seshagiri, S.; Eby, M.; Xiao, W.; Dixit, V. M., Bcl10 activates the NF- κ B pathway through ubiquitination of NEMO. *Nature* **2004**, *427*, 167-71; (d) Ea, C. K.; Deng, L.; Xia, Z. P.; Pineda, G.; Chen, Z. J., Activation of IKK by TNF α requires site-specific ubiquitination of RIP1 and polyubiquitin binding by NEMO. *Mol. Cell* **2006**, *22*, 245-57; (e) Tang, E. D.; Wang, C. Y.; Xiong, Y.; Guan, K. L., A role for NF- κ B essential modifier/I κ B kinase- γ (NEMO/IKK γ) ubiquitination in the activation of the I κ B kinase complex by tumor necrosis factor- α . *J. Biol. Chem.* **2003**, *278*, 37297-305.
62. (a) Huang, T. T.; Wuerzberger-Davis, S. M.; Wu, Z. H.; Miyamoto, S., Sequential modification of NEMO/IKK γ by SUMO-1 and ubiquitin mediates NF- κ B activation by genotoxic stress. *Cell* **2003**, *115*, 565-76; (b) Carter, R. S.; Pennington, K. N.; Ungurait, B. J.; Ballard, D. W., In vivo identification of inducible phosphoacceptors in the IKK γ /NEMO subunit of human I κ B kinase. *J. Biol. Chem.* **2003**, *278*, 19642-8; (c) Prajapati, S.; Gaynor, R. B., Regulation of I κ B kinase (IKK) γ /NEMO function by IKK β -mediated phosphorylation. *J. Biol. Chem.* **2002**, *277*, 24331-9.
63. Zabel, U.; Henkel, T.; Silva, M. S.; Baeuerle, P. A., Nuclear uptake control of NF- κ B by MAD-3, an I κ B protein present in the nucleus. *EMBO J.* **1993**, *12*, 201-11.
64. (a) Chen, Z.; Hagler, J.; Palombella, V. J.; Melandri, F.; Scherer, D.; Ballard, D.; Maniatis, T., Signal-induced site-specific phosphorylation targets I κ B α to the ubiquitin-proteasome pathway. *Genes Dev.* **1995**, *9*, 1586-97; (b) Scherer, D. C.; Brockman, J. A.; Chen, Z.; Maniatis, T.; Ballard, D. W., Signal-induced degradation of I κ B α requires site-specific ubiquitination. *Proc. Natl. Acad. Sci. U.S.A.* **1995**, *92*, 11259-63; (c) DiDonato, J.; Mercurio, F.; Rosette, C.; Wu-Li, J.; Suyang, H.; Ghosh, S.; Karin, M., Mapping of the inducible I κ B phosphorylation sites that signal its ubiquitination and degradation. *Mol. Cell. Biol.* **1996**, *16*, 1295-304; (d) Roff, M.; Thompson, J.; Rodriguez, M. S.; Jacque, J. M.; Baleux, F.; Arenzana-Seisdedos, F.; Hay, R. T., Role of I κ B α ubiquitination in signal-induced activation of NF κ B in vivo. *J. Biol. Chem.* **1996**, *271*, 7844-50.
65. (a) Zhong, H.; SuYang, H.; Erdjument-Bromage, H.; Tempst, P.; Ghosh, S., The transcriptional activity of NF- κ B is regulated by the I κ B-associated PKAc subunit through a cyclic AMP-independent mechanism. *Cell* **1997**, *89*, 413-24; (b) Zhong, H.; Voll, R. E.; Ghosh, S., Phosphorylation of NF- κ B p65 by PKA stimulates

- transcriptional activity by promoting a novel bivalent interaction with the coactivator CBP/p300. *Mol. Cell* **1998**, *1*, 661-71; (c) Vermeulen, L.; De Wilde, G.; Van Damme, P.; Vanden Berghe, W.; Haegeman, G., Transcriptional activation of the NF- κ B p65 subunit by mitogen- and stress-activated protein kinase-1 (MSK1). *EMBO J.* **2003**, *22*, 1313-24; (d) Jacks, K. A.; Koch, C. A., Differential regulation of mitogen- and stress-activated protein kinase-1 and -2 (MSK1 and MSK2) by CK2 following UV radiation. *J. Biol. Chem.* **2010**, *285*, 1661-70.
66. (a) Bird, T. A.; Schooley, K.; Dower, S. K.; Hagen, H.; Virca, G. D., Activation of nuclear transcription factor NF- κ B by interleukin-1 is accompanied by casein kinase II-mediated phosphorylation of the p65 subunit. *J. Biol. Chem.* **1997**, *272*, 32606-12; (b) Wang, D.; Baldwin, A. S., Jr., Activation of nuclear factor- κ B-dependent transcription by tumor necrosis factor- α is mediated through phosphorylation of RelA/p65 on serine 529. *J. Biol. Chem.* **1998**, *273*, 29411-6; (c) Wang, D.; Westerheide, S. D.; Hanson, J. L.; Baldwin, A. S., Jr., Tumor necrosis factor α -induced phosphorylation of RelA/p65 on Ser529 is controlled by casein kinase II. *J. Biol. Chem.* **2000**, *275*, 32592-7.
67. (a) Sakurai, H.; Chiba, H.; Miyoshi, H.; Sugita, T.; Toriumi, W., I κ B kinases phosphorylate NF- κ B p65 subunit on serine 536 in the transactivation domain. *J. Biol. Chem.* **1999**, *274*, 30353-6; (b) Sakurai, H.; Suzuki, S.; Kawasaki, N.; Nakano, H.; Okazaki, T.; Chino, A.; Doi, T.; Saiki, I., Tumor necrosis factor- α -induced IKK phosphorylation of NF- κ B p65 on serine 536 is mediated through the TRAF2, TRAF5, and TAK1 signaling pathway. *J. Biol. Chem.* **2003**, *278*, 36916-23.
68. (a) Tojima, Y.; Fujimoto, A.; Delhase, M.; Chen, Y.; Hatakeyama, S.; Nakayama, K.; Kaneko, Y.; Nimura, Y.; Motoyama, N.; Ikeda, K.; Karin, M.; Nakanishi, M., NAK is an I κ B kinase-activating kinase. *Nature* **2000**, *404*, 778-82; (b) Fujita, F.; Taniguchi, Y.; Kato, T.; Narita, Y.; Furuya, A.; Ogawa, T.; Sakurai, H.; Joh, T.; Itoh, M.; Delhase, M.; Karin, M.; Nakanishi, M., Identification of NAP1, a regulatory subunit of I κ B kinase-related kinases that potentiates NF- κ B signaling. *Mol. Cell. Biol.* **2003**, *23*, 7780-93.
69. Schwabe, R. F.; Brenner, D. A., Role of glycogen synthase kinase-3 in TNF- α -induced NF- κ B activation and apoptosis in hepatocytes. *Am. J. Physiol. Gastrointest. Liver. Physiol.* **2002**, *283*, G204-11.
70. Buss, H.; Dorrie, A.; Schmitz, M. L.; Frank, R.; Livingstone, M.; Resch, K.; Kracht, M., Phosphorylation of serine 468 by GSK-3 β negatively regulates basal p65 NF- κ B activity. *J. Biol. Chem.* **2004**, *279*, 49571-4.
71. (a) Leitges, M.; Sanz, L.; Martin, P.; Duran, A.; Braun, U.; Garcia, J. F.; Camacho, F.; Diaz-Meco, M. T.; Rennert, P. D.; Moscat, J., Targeted disruption of the ζ PKC gene results in the impairment of the NF- κ B pathway. *Mol. Cell* **2001**, *8*, 771-80; (b) Duran, A.; Diaz-Meco, M. T.; Moscat, J., Essential role of RelA Ser311

- phosphorylation by ζ PKC in NF- κ B transcriptional activation. *EMBO J.* **2003**, *22*, 3910-8.
72. Bohuslav, J.; Chen, L. F.; Kwon, H.; Mu, Y.; Greene, W. C., p53 induces NF- κ B activation by an I κ B kinase-independent mechanism involving phosphorylation of p65 by ribosomal S6 kinase 1. *J. Biol. Chem.* **2004**, *279*, 26115-25.
73. Chen, L.; Fischle, W.; Verdin, E.; Greene, W. C., Duration of nuclear NF- κ B action regulated by reversible acetylation. *Science* **2001**, *293*, 1653-7.
74. Chen, L. F.; Mu, Y.; Greene, W. C., Acetylation of RelA at discrete sites regulates distinct nuclear functions of NF- κ B. *EMBO J.* **2002**, *21*, 6539-48.
75. (a) Arenzana-Seisdedos, F.; Thompson, J.; Rodriguez, M. S.; Bachelier, F.; Thomas, D.; Hay, R. T., Inducible nuclear expression of newly synthesized I κ B α negatively regulates DNA-binding and transcriptional activities of NF- κ B. *Mol. Cell. Biol.* **1995**, *15*, 2689-96; (b) Arenzana-Seisdedos, F.; Turpin, P.; Rodriguez, M.; Thomas, D.; Hay, R. T.; Virelizier, J. L.; Dargemont, C., Nuclear localization of I κ B α promotes active transport of NF- κ B from the nucleus to the cytoplasm. *J. Cell. Sci.* **1997**, *110*, 369-78.
76. Zou, Z.; Huang, B.; Wu, X.; Zhang, H.; Qi, J.; Bradner, J.; Nair, S.; Chen, L. F., Brd4 maintains constitutively active NF- κ B in cancer cells by binding to acetylated RelA. *Oncogene* **2014**, *33*, 2395-404.
77. Kiernan, R.; Bres, V.; Ng, R. W.; Coudart, M. P.; El Messaoudi, S.; Sardet, C.; Jin, D. Y.; Emiliani, S.; Benkirane, M., Post-activation turn-off of NF- κ B-dependent transcription is regulated by acetylation of p65. *J. Biol. Chem.* **2003**, *278*, 2758-66.
78. (a) Buerki, C.; Rothgiesser, K. M.; Valovka, T.; Owen, H. R.; Rehrauer, H.; Fey, M.; Lane, W. S.; Hottiger, M. O., Functional relevance of novel p300-mediated lysine 314 and 315 acetylation of RelA/p65. *Nucleic Acid Res.* **2008**, *36*, 1665-80; (b) Rothgiesser, K. M.; Fey, M.; Hottiger, M. O., Acetylation of p65 at lysine 314 is important for late NF- κ B-dependent gene expression. *BMC Genomics* **2010**, *11*, 22.
79. Ashburner, B. P.; Westerheide, S. D.; Baldwin, A. S., Jr., The p65 (RelA) subunit of NF- κ B interacts with the histone deacetylase (HDAC) corepressors HDAC1 and HDAC2 to negatively regulate gene expression. *Mol. Cell. Biol.* **2001**, *21*, 7065-77.
80. Yeung, F.; Hoberg, J. E.; Ramsey, C. S.; Keller, M. D.; Jones, D. R.; Frye, R. A.; Mayo, M. W., Modulation of NF- κ B-dependent transcription and cell survival by the SIRT1 deacetylase. *EMBO J.* **2004**, *23* (12), 2369-80.
81. (a) Xiao, G.; Harhaj, E. W.; Sun, S. C., NF- κ B-inducing kinase regulates the processing of NF- κ B2 p100. *Mol. Cell* **2001**, *7*, 401-9; (b) Senftleben, U.; Cao, Y.; Xiao, G.; Greten, F. R.; Krahn, G.; Bonizzi, G.; Chen, Y.; Hu, Y.; Fong, A.; Sun, S.

- C.; Karin, M., Activation by IKK α of a second, evolutionary conserved, NF- κ B signaling pathway. *Science* **2001**, *293*, 1495-9.
82. Ling, L.; Cao, Z.; Goeddel, D. V., NF- κ B-inducing kinase activates IKK- α by phosphorylation of Ser-176. *Proc. Natl. Acad. Sci. U.S.A.* **1998**, *95*, 3792-7.
83. Xiao, G.; Cvijic, M. E.; Fong, A.; Harhaj, E. W.; Uhlik, M. T.; Waterfield, M.; Sun, S. C., Retroviral oncoprotein Tax induces processing of NF- κ B2/p100 in T cells: evidence for the involvement of IKK α . *EMBO J.* **2001**, *20*, 6805-15.
84. Xiao, G.; Fong, A.; Sun, S. C., Induction of p100 processing by NF- κ B-inducing kinase involves docking I κ B kinase α (IKK α) to p100 and IKK α -mediated phosphorylation. *J. Biol. Chem.* **2004**, *279*, 30099-105.
85. (a) Amir, R. E.; Haecker, H.; Karin, M.; Ciechanover, A., Mechanism of processing of the NF- κ B2 p100 precursor: identification of the specific polyubiquitin chain-anchoring lysine residue and analysis of the role of NEDD8-modification on the SCF(β -TrCP) ubiquitin ligase. *Oncogene* **2004**, *23*, 2540-7; (b) Liang, C.; Zhang, M.; Sun, S. C., β -TrCP binding and processing of NF- κ B2/p100 involve its phosphorylation at serines 866 and 870. *Cell. Signal* **2006**, *18*, 1309-17.
86. Solan, N. J.; Miyoshi, H.; Carmona, E. M.; Bren, G. D.; Paya, C. V., RelB cellular regulation and transcriptional activity are regulated by p100. *J. Biol. Chem.* **2002**, *277*, 1405-18.
87. Liao, G.; Sun, S. C., Regulation of NF- κ B2/p100 processing by its nuclear shuttling. *Oncogene* **2003**, *22*, 4868-74.
88. Mordmuller, B.; Krappmann, D.; Esen, M.; Wegener, E.; Scheidereit, C., Lymphotoxin and lipopolysaccharide induce NF- κ B-p52 generation by a co-translational mechanism. *EMBO reports* **2003**, *4*, 82-87.
89. Liao, G.; Zhang, M.; Harhaj, E. W.; Sun, S. C., Regulation of the NF- κ B-inducing kinase by tumor necrosis factor receptor-associated factor 3-induced degradation. *J. Biol. Chem.* **2004**, *279*, 26243-50.
90. Zarnegar, B. J.; Wang, Y.; Mahoney, D. J.; Dempsey, P. W.; Cheung, H. H.; He, J.; Shiba, T.; Yang, X.; Yeh, W. C.; Mak, T. W.; Korneluk, R. G.; Cheng, G., Noncanonical NF- κ B activation requires coordinated assembly of a regulatory complex of the adaptors cIAP1, cIAP2, TRAF2 and TRAF3 and the kinase NIK. *Nature Immunol.* **2008**, *9*, 1371-8.
91. (a) Morrison, M. D.; Reiley, W.; Zhang, M.; Sun, S. C., An atypical tumor necrosis factor (TNF) receptor-associated factor-binding motif of B cell-activating factor belonging to the TNF family (BAFF) receptor mediates induction of the noncanonical NF- κ B signaling pathway. *J. Biol. Chem.* **2005**, *280*, 10018-24; (b) Vallabhapurapu,

- S.; Matsuzawa, A.; Zhang, W.; Tseng, P. H.; Keats, J. J.; Wang, H.; Vignali, D. A.; Bergsagel, P. L.; Karin, M., Nonredundant and complementary functions of TRAF2 and TRAF3 in a ubiquitination cascade that activates NIK-dependent alternative NF- κ B signaling. *Nature Immunol.* **2008**, *9*, 1364-70.
92. Claudio, E.; Brown, K.; Park, S.; Wang, H.; Siebenlist, U., BAFF-induced NEMO-independent processing of NF- κ B2 in maturing B cells. *Nature Immunol.* **2002**, *3*, 958-65.
93. Sun, S. C., The noncanonical NF- κ B pathway. *Immunol. Rev.* **2012**, *246*, 125-40.
94. (a) Sun, S. C.; Faye, I., Cecropia immunoresponsive factor, an insect immunoresponsive factor with DNA-binding properties similar to nuclear-factor κ B. *FEBS J.* **1992**, *204*, 885-92; (b) Derudder, E.; Dejardin, E.; Pritchard, L. L.; Green, D. R.; Korner, M.; Baud, V., RelB/p50 dimers are differentially regulated by tumor necrosis factor- α and lymphotoxin- β receptor activation: critical roles for p100. *J. Biol. Chem.* **2003**, *278*, 23278-84; (c) Yilmaz, Z. B.; Weih, D. S.; Sivakumar, V.; Weih, F., RelB is required for Peyer's patch development: differential regulation of p52-RelB by lymphotoxin and TNF. *EMBO J.* **2003**, *22*, 121-30.
95. Jacque, E.; Tchenio, T.; Piton, G.; Romeo, P. H.; Baud, V., RelA repression of RelB activity induces selective gene activation downstream of TNF receptors. *Proc. Natl. Acad. Sci. U.S.A.* **2005**, *102*, 14635-40.
96. Gerondakis, S.; Grumont, R.; Gugasyan, R.; Wong, L.; Isomura, I.; Ho, W.; Banerjee, A., Unravelling the complexities of the NF- κ B signalling pathway using mouse knockout and transgenic models. *Oncogene* **2006**, *25*, 6781-99.
97. (a) Li, Q.; Van Antwerp, D.; Mercurio, F.; Lee, K. F.; Verma, I. M., Severe liver degeneration in mice lacking the I κ B kinase 2 gene. *Science* **1999**, *284*, 321-5; (b) Senftleben, U.; Li, Z. W.; Baud, V.; Karin, M., IKK β is essential for protecting T cells from TNF α -induced apoptosis. *Immunity* **2001**, *14*, 217-30; (c) Beg, A. A.; Sha, W. C.; Bronson, R. T.; Ghosh, S.; Baltimore, D., Embryonic lethality and liver degeneration in mice lacking the RelA component of NF- κ B. *Nature* **1995**, *376*, 167-70; (d) Beg, A. A.; Baltimore, D., An essential role for NF- κ B in preventing TNF- α -induced cell death. *Science* **1996**, *274*, 782-4; (e) Prendes, M.; Zheng, Y.; Beg, A. A., Regulation of developing B cell survival by RelA-containing NF- κ B complexes. *J. Immunol.* **2003**, *171*, 3963-9.
98. Alcamo, E.; Mizgerd, J. P.; Horwitz, B. H.; Bronson, R.; Beg, A. A.; Scott, M.; Doerschuk, C. M.; Hynes, R. O.; Baltimore, D., Targeted mutation of TNF receptor I rescues the RelA-deficient mouse and reveals a critical role for NF- κ B in leukocyte recruitment. *J. Immunol.* **2001**, *167*, 1592-600.
99. Courtois, G.; Gilmore, T. D., Mutations in the NF- κ B signaling pathway: implications for human disease. *Oncogene* **2006**, *25*, 6831-43.

100. (a) Marok, R.; Winyard, P. G.; Coumbe, A.; Kus, M. L.; Gaffney, K.; Blades, S.; Mapp, P. I.; Morris, C. J.; Blake, D. R.; Kaltschmidt, C.; Baeuerle, P. A., Activation of the transcription factor nuclear factor- κ B in human inflamed synovial tissue. *Arthritis. Rheumatism*. **1996**, *39*, 583-91; (b) Han, Z.; Boyle, D. L.; Manning, A. M.; Firestein, G. S., AP-1 and NF- κ B regulation in rheumatoid arthritis and murine collagen-induced arthritis. *Autoimmunity* **1998**, *28*, 197-208.
101. (a) Hofmann, M. A.; Schiekofer, S.; Isermann, B.; Kanitz, M.; Henkels, M.; Joswig, M.; Treusch, A.; Morcos, M.; Weiss, T.; Borcea, V.; Abdel Khalek, A. K.; Amiral, J.; Tritschler, H.; Ritz, E.; Wahl, P.; Ziegler, R.; Bierhaus, A.; Nawroth, P. P., Peripheral blood mononuclear cells isolated from patients with diabetic nephropathy show increased activation of the oxidative-stress sensitive transcription factor NF- κ B. *Diabetologia* **1999**, *42*, 222-32; (b) Mollah, Z. U.; Pai, S.; Moore, C.; O'Sullivan, B. J.; Harrison, M. J.; Peng, J.; Phillips, K.; Prins, J. B.; Cardinal, J.; Thomas, R., Abnormal NF- κ B function characterizes human type 1 diabetes dendritic cells and monocytes. *J. Immunol.* **2008**, *180*, 3166-75.
102. (a) Rogler, G.; Brand, K.; Vogl, D.; Page, S.; Hofmeister, R.; Andus, T.; Knuechel, R.; Baeuerle, P. A.; Scholmerich, J.; Gross, V., Nuclear factor κ B is activated in macrophages and epithelial cells of inflamed intestinal mucosa. *Gastroenterology* **1998**, *115*, 357-69; (b) Schreiber, S.; Nikolaus, S.; Hampe, J., Activation of nuclear factor κ B inflammatory bowel disease. *Gut* **1998**, *42*, 477-84; (c) Ellis, R. D.; Goodlad, J. R.; Limb, G. A.; Powell, J. J.; Thompson, R. P.; Punchard, N. A., Activation of nuclear factor κ B in Crohn's disease. *Inflamm. Res.* **1998**, *47*, 440-5.
103. (a) Gveric, D.; Kaltschmidt, C.; Cuzner, M. L.; Newcombe, J., Transcription factor NF- κ B and inhibitor I κ B α are localized in macrophages in active multiple sclerosis lesions. *J. Neuropathol. Exp. Neurol.* **1998**, *57*, 168-78; (b) Mc Guire, C.; Prinz, M.; Beyaert, R.; van Loo, G., Nuclear factor κ B (NF- κ B) in multiple sclerosis pathology. *Trends Mol. Med.* **2013**, *19*, 604-13.
104. Herrington, F. D.; Carmody, R. J.; Goodyear, C. S., Modulation of NF- κ B Signaling as a Therapeutic Target in Autoimmunity. *J. Biomol. Screen* **2016**, *21*, 223-42.
105. Lakota, K., Artenjak, A., Cucnik, S., Brguljan-Hitij, J., Cegovnik, B., Salobir, B., accetto, R.; Bozic, B., Rozman, B., and Sodin-Semrl, S., Atherogenesis, Inflammation and Autoimmunity. *Atherogenesis*. Parthasarathy, S., Ed. Interchopin: Online: 2012; Vol. 1, pp 187-202.
106. Monaco, C.; Paleolog, E., Nuclear factor κ B: a potential therapeutic target in atherosclerosis and thrombosis. *Cardiovasc. Res.* **2004**, *61*, 671-82.
107. (a) Bu, D. X.; Erl, W.; de Martin, R.; Hansson, G. K.; Yan, Z. Q., IKK β -dependent NF- κ B pathway controls vascular inflammation and intimal hyperplasia.

- FASEB J.* **2005**, *19*, 1293-5; (b) Hansson, G. K., Inflammation, atherosclerosis, and coronary artery disease. *New Engl. J. Med.* **2005**, *352*, 1685-95.
108. Marienfeld, R.; Neumann, M.; Chuvpilo, S.; Escher, C.; Kneitz, B.; Avots, A.; Schimpl, A.; Serfling, E., Cyclosporin A interferes with the inducible degradation of NF- κ B inhibitors, but not with the processing of p105/NF- κ B1 in T cells. *European J. Immunol.* **1997**, *27*, 1601-9.
109. (a) Karin, M., *NF- κ B in Health and Disease*. Springer: 2011; Vol. 349; (b) Hoesel, B.; Schmid, J. A., The complexity of NF- κ B signaling in inflammation and cancer. *Mol. Cancer* **2013**, *12*, 86.
110. Pikarsky, E.; Porat, R. M.; Stein, I.; Abramovitch, R.; Amit, S.; Kasem, S.; Gutkovich-Pyest, E.; Urieli-Shoval, S.; Galun, E.; Ben-Neriah, Y., NF- κ B functions as a tumour promoter in inflammation-associated cancer. *Nature* **2004**, *431*, 461-6.
111. Gilmore, T. D., Multiple mutations contribute to the oncogenicity of the retroviral oncoprotein v-Rel. *Oncogene* **1999**, *18*, 6925-37.
112. Karin, M., NF- κ B as a critical link between inflammation and cancer. *Cold Spring Harb. Perspect. Biol.* **2009**, *1*, a000141.
113. Landskron, G.; De la Fuente, M.; Thuwajit, P.; Thuwajit, C.; Hermoso, M. A., Chronic inflammation and cytokines in the tumor microenvironment. *J. Immunol. Res.* **2014**, *2014*, 149185.
114. Hewamana, S.; Alghazal, S.; Lin, T. T.; Clement, M.; Jenkins, C.; Guzman, M. L.; Jordan, C. T.; Neelakantan, S.; Crooks, P. A.; Burnett, A. K.; Pratt, G.; Fegan, C.; Rowntree, C.; Brennan, P.; Pepper, C., The NF- κ B subunit RelA is associated with in vitro survival and clinical disease progression in chronic lymphocytic leukemia and represents a promising therapeutic target. *Blood* **2008**, *111*, 4681-9.
115. (a) Khan, I. N.; Al-Karim, S.; Bora, R. S.; Chaudhary, A. G.; Saini, K. S., Cancer stem cells: a challenging paradigm for designing targeted drug therapies. *Drug. Discov. Today* **2015**, *20*, 1205-16; (b) Pattabiraman, D. R.; Weinberg, R. A., Tackling the cancer stem cells - what challenges do they pose? *Nature. Rev. Drug. Discov.* **2014**, *13*, 497-512.
116. Pardee, K.; Necakov, A. S.; Krause, H., Nuclear Receptors: Small Molecule Sensors that Coordinate Growth, Metabolism and Reproduction. *Subcell. Biochem.* **2011**, *52*, 123-53.
117. Tan, M. H.; Li, J.; Xu, H. E.; Melcher, K.; Yong, E. L., Androgen receptor: structure, role in prostate cancer and drug discovery. *Acta Pharmacol. Sin.* **2015**, *36*, 3-23.

118. Jenster, G.; van der Korput, H. A.; Trapman, J.; Brinkmann, A. O., Identification of two transcription activation units in the N-terminal domain of the human androgen receptor. *J. Biol. Chem.* **1995**, *270*, 7341-6.
119. Callewaert, L.; Van Tilborgh, N.; Claessens, F., Interplay between two hormone-independent activation domains in the androgen receptor. *Cancer Res.* **2006**, *66*, 543-53.
120. (a) McEwan, I. J., Molecular mechanisms of androgen receptor-mediated gene regulation: structure-function analysis of the AF-1 domain. *Endocr. Relat. Cancer* **2004**, *11*, 281-93; (b) He, B.; Kemppainen, J. A.; Voegel, J. J.; Gronemeyer, H.; Wilson, E. M., Activation function 2 in the human androgen receptor ligand binding domain mediates interdomain communication with the NH(2)-terminal domain. *J. Biol. Chem.* **1999**, *274*, 37219-25.
121. Haelens, A.; Tanner, T.; Denayer, S.; Callewaert, L.; Claessens, F., The hinge region regulates DNA binding, nuclear translocation, and transactivation of the androgen receptor. *Cancer Res.* **2007**, *67*, 4514-23.
122. (a) Jenster, G.; Trapman, J.; Brinkmann, A. O., Nuclear import of the human androgen receptor. *Biochem. J.* **1993**, *293*, 761-8; (b) Cutress, M. L.; Whitaker, H. C.; Mills, I. G.; Stewart, M.; Neal, D. E., Structural basis for the nuclear import of the human androgen receptor. *J. Cell. Sci.* **2008**, *121*, 957-68.
123. (a) Bohen, S. P. a. Y., K.R., Modulation of Steroid Receptor Signal Transduction by Heat Shock Proteins. In *The Biology of Heat Shock Proteins and Molecular Chaperones*, Morimoto, R. I., Tissieres, A., Georgopoulos, C., Ed. Cold Spring Harbor Laboratory Press: Cold Spring Harbor, 1994; (b) Veldscholte, J.; Berrevoets, C. A.; Zegers, N. D.; van der Kwast, T. H.; Grootegoed, J. A.; Mulder, E., Hormone-induced dissociation of the androgen receptor-heat-shock protein complex: use of a new monoclonal antibody to distinguish transformed from nontransformed receptors. *Biochemistry* **1992**, *31*, 7422-30.
124. Marivoet, S.; Van Dijck, P.; Verhoeven, G.; Heyns, W., Interaction of the 90-kDa heat shock protein with native and in vitro translated androgen receptor and receptor fragments. *Mol. Cell. Endocrinol.* **1992**, *88*, 165-74.
125. Fang, Y.; Fliss, A. E.; Robins, D. M.; Caplan, A. J., Hsp90 regulates androgen receptor hormone binding affinity in vivo. *J. Biol. Chem.* **1996**, *271*, 28697-702.
126. (a) Davies, T. H.; Ning, Y. M.; Sanchez, E. R., A new first step in activation of steroid receptors: hormone-induced switching of FKBP51 and FKBP52 immunophilins. *J. Biol. Chem.* **2002**, *277*, 4597-600; (b) Cano, L. Q.; Lavery, D. N.; Bevan, C. L., Mini-review: Foldosome regulation of androgen receptor action in prostate cancer. *Mol. Cell. Endocrinol.* **2013**, *369*, 52-62.

127. (a) Hohfeld, J.; Minami, Y.; Hartl, F. U., Hip, a novel cochaperone involved in the eukaryotic Hsc70/Hsp40 reaction cycle. *Cell* **1995**, *83*, 589-98; (b) Freeman, B. C.; Felts, S. J.; Toft, D. O.; Yamamoto, K. R., The p23 molecular chaperones act at a late step in intracellular receptor action to differentially affect ligand efficacies. *Genes Dev.* **2000**, *14*, 422-34.
128. Georget, V.; Terouanne, B.; Nicolas, J. C.; Sultan, C., Mechanism of antiandrogen action: key role of hsp90 in conformational change and transcriptional activity of the androgen receptor. *Biochemistry* **2002**, *41*, 11824-31.
129. He, B.; Lee, L. W.; Minges, J. T.; Wilson, E. M., Dependence of selective gene activation on the androgen receptor NH₂- and COOH-terminal interaction. *J. Biol. Chem.* **2002**, *277*, 25631-9.
130. He, B.; Kemppainen, J. A.; Wilson, E. M., FXXLF and WXXLF sequences mediate the NH₂-terminal interaction with the ligand binding domain of the androgen receptor. *J. Biol. Chem.* **2000**, *275*, 22986-94.
131. Ikonen, T.; Palvimo, J. J.; Janne, O. A., Interaction between the amino- and carboxyl-terminal regions of the rat androgen receptor modulates transcriptional activity and is influenced by nuclear receptor coactivators. *J. Biol. Chem.* **1997**, *272*, 29821-8.
132. Black, B. E.; Vitto, M. J.; Gioeli, D.; Spencer, A.; Afshar, N.; Conaway, M. R.; Weber, M. J.; Paschal, B. M., Transient, ligand-dependent arrest of the androgen receptor in subnuclear foci alters phosphorylation and coactivator interactions. *Mol. Endocrinol.* **2004**, *18*, 834-50.
133. (a) Georget, V.; Lobaccaro, J. M.; Terouanne, B.; Mangeat, P.; Nicolas, J. C.; Sultan, C., Trafficking of the androgen receptor in living cells with fused green fluorescent protein-androgen receptor. *Mol. Cell. Endocrinol.* **1997**, *129*, 17-26; (b) Pratt, W. B.; Silverstein, A. M.; Galigniana, M. D., A model for the cytoplasmic trafficking of signalling proteins involving the hsp90-binding immunophilins and p50cdc37. *Cell. Signal* **1999**, *11*, 839-51; (c) Shaffer, P. L.; Jivan, A.; Dollins, D. E.; Claessens, F.; Gewirth, D. T., Structural basis of androgen receptor binding to selective androgen response elements. *Proc. Natl. Acad. Sci. U.S.A.* **2004**, *101*, 4758-63.
134. Heinlein, C. A.; Chang, C., Androgen receptor (AR) coregulators: an overview. *Endocrine Revs.* **2002**, *23*, 175-200.
135. Dasgupta, S.; Lonard, D. M.; O'Malley, B. W., Nuclear receptor coactivators: master regulators of human health and disease. *Annu. Rev. Med.* **2014**, *65*, 279-92.
136. (a) Heemers, H. V.; Tindall, D. J., Androgen receptor (AR) coregulators: a diversity of functions converging on and regulating the AR transcriptional complex.

- Endocrine Revs.* **2007**, *28*, 778-808; (b) Berrevoets, C. A.; Doesburg, P.; Steketeer, K.; Trapman, J.; Brinkmann, A. O., Functional interactions of the AF-2 activation domain core region of the human androgen receptor with the amino-terminal domain and with the transcriptional coactivator TIF2 (transcriptional intermediary factor2). *Mol. Endocrinol.* **1998**, *12*, 1172-83; (c) Bevan, C. L.; Hoare, S.; Claessens, F.; Heery, D. M.; Parker, M. G., The AF1 and AF2 domains of the androgen receptor interact with distinct regions of SRC1. *Mol. Cell. Biol.* **1999**, *19*, 8383-92; (d) Zhou, X. E.; Suino-Powell, K. M.; Li, J.; He, Y.; Mackeigan, J. P.; Melcher, K.; Yong, E. L.; Xu, H. E., Identification of SRC3/AIB1 as a preferred coactivator for hormone-activated androgen receptor. *J. Biol. Chem.* **2010**, *285*, 9161-71.
137. Fu, M.; Wang, C.; Reutens, A. T.; Wang, J.; Angeletti, R. H.; Siconolfi-Baez, L.; Ogryzko, V.; Avantiaggiati, M. L.; Pestell, R. G., p300 and p300/cAMP-response element-binding protein-associated factor acetylate the androgen receptor at sites governing hormone-dependent transactivation. *J. Biol. Chem.* **2000**, *275*, 20853-60.
138. Gaughan, L.; Brady, M. E.; Cook, S.; Neal, D. E.; Robson, C. N., Tip60 is a co-activator specific for class I nuclear hormone receptors. *J. Biol. Chem.* **2001**, *276*, 46841-8.
139. Wang, Z.; Wang, Z.; Guo, J.; Li, Y.; Bavarva, J. H.; Qian, C.; Brahimi-Horn, M. C.; Tan, D.; Liu, W., Inactivation of androgen-induced regulator ARD1 inhibits androgen receptor acetylation and prostate tumorigenesis. *Proc. Natl. Acad. Sci. U.S.A.* **2012**, *109*, 3053-8.
140. Koryakina, Y.; Ta, H. Q.; Gioeli, D., Androgen receptor phosphorylation: biological context and functional consequences. *Endocr. Relat. Cancer* **2014**, *21*, T131-45.
141. (a) Jenster, G.; de Ruiter, P. E.; van der Korput, H. A.; Kuiper, G. G.; Trapman, J.; Brinkmann, A. O., Changes in the abundance of androgen receptor isotypes: effects of ligand treatment, glutamine-stretch variation, and mutation of putative phosphorylation sites. *Biochemistry* **1994**, *33*, 14064-72; (b) Wong, H. Y.; Burghoorn, J. A.; Van Leeuwen, M.; De Ruiter, P. E.; Schippers, E.; Blok, L. J.; Li, K. W.; Dekker, H. L.; De Jong, L.; Trapman, J.; Grootegoed, J. A.; Brinkmann, A. O., Phosphorylation of androgen receptor isoforms. *Biochem. J.* **2004**, *383*, 267-76.
142. Coffey, K.; Robson, C. N., Regulation of the androgen receptor by post-translational modifications. *J. Endocrinol.* **2012**, *215*, 221-37.
143. Gordon, V.; Bhadel, S.; Wunderlich, W.; Zhang, J.; Ficarro, S. B.; Mollah, S. A.; Shabanowitz, J.; Hunt, D. F.; Xenarios, I.; Hahn, W. C.; Conaway, M.; Carey, M. F.; Gioeli, D., CDK9 regulates AR promoter selectivity and cell growth through serine 81 phosphorylation. *Mol. Endocrinol.* **2010**, *24*, 2267-80.

144. (a) Karantanos, T.; Corn, P. G.; Thompson, T. C., Prostate cancer progression after androgen deprivation therapy: mechanisms of castrate resistance and novel therapeutic approaches. *Oncogene* **2013**, *32*, 5501-11; (b) Harris, W. P.; Mostaghel, E. A.; Nelson, P. S.; Montgomery, B., Androgen deprivation therapy: progress in understanding mechanisms of resistance and optimizing androgen depletion. *Nature Rev. Urol.* **2009**, *6*, 76-85.
145. Assi, R.; Temraz, S.; Shamseddine, A.; Mukherji, D., New Compounds Targeting the Androgen Receptor for Treatment of Advanced Prostate Cancer. *Curr. Drug Targets* **2016**, *17*, 290-302.
146. (a) Rowlands, M. G.; Barrie, S. E.; Chan, F.; Houghton, J.; Jarman, M.; McCague, R.; Potter, G. A., Esters of 3-pyridylacetic acid that combine potent inhibition of 17 α -hydroxylase/C17,20-lyase (cytochrome P45017 α) with resistance to esterase hydrolysis. *J. Med. Chem.* **1995**, *38*, 4191-7; (b) Basch, E.; Autio, K.; Ryan, C. J.; Mulders, P.; Shore, N.; Kheoh, T.; Fizazi, K.; Logothetis, C. J.; Rathkopf, D.; Smith, M. R.; Mainwaring, P. N.; Hao, Y.; Griffin, T.; Li, S.; Meyers, M. L.; Molina, A.; Cleeland, C., Abiraterone acetate plus prednisone versus prednisone alone in chemotherapy-naïve men with metastatic castration-resistant prostate cancer: patient-reported outcome results of a randomised phase 3 trial. *The Lancet. Oncology* **2013**, *14*, 1193-9; (c) Mostaghel, E. A.; Marck, B. T.; Plymate, S. R.; Vessella, R. L.; Balk, S.; Matsumoto, A. M.; Nelson, P. S.; Montgomery, R. B., Resistance to CYP17A1 inhibition with abiraterone in castration-resistant prostate cancer: induction of steroidogenesis and androgen receptor splice variants. *Clinical Cancer Res.* **2011**, *17*, 5913-25.
147. (a) Scher, H. I.; Beer, T. M.; Higano, C. S.; Anand, A.; Taplin, M. E.; Efsthathiou, E.; Rathkopf, D.; Shelkey, J.; Yu, E. Y.; Alumkal, J.; Hung, D.; Hirmand, M.; Seely, L.; Morris, M. J.; Danila, D. C.; Humm, J.; Larson, S.; Fleisher, M.; Sawyers, C. L.; Prostate Cancer Foundation/Department of Defense Prostate Cancer Clinical Trials, C., Antitumour activity of MDV3100 in castration-resistant prostate cancer: a phase 1-2 study. *Lancet* **2010**, *375*, 1437-46; (b) Jung, M. E.; Ouk, S.; Yoo, D.; Sawyers, C. L.; Chen, C.; Tran, C.; Wongvipat, J., Structure-activity relationship for thiohydantoin androgen receptor antagonists for castration-resistant prostate cancer (CRPC). *J. Med. Chem.* **2010**, *53*, 2779-96.
148. (a) Claessens, F.; Helsen, C.; Prekovic, S.; Van den Broeck, T.; Spans, L.; Van Poppel, H.; Joniau, S., Emerging mechanisms of enzalutamide resistance in prostate cancer. *Nature Rev. Urol.* **2014**, *11*, 712-6; (b) Zong, Y.; Goldstein, A. S., Adaptation or selection--mechanisms of castration-resistant prostate cancer. *Nature Rev. Urol.* **2013**, *10*, 90-8.
149. Korpál, M.; Korn, J. M.; Gao, X.; Rakiec, D. P.; Ruddy, D. A.; Doshi, S.; Yuan, J.; Kovats, S. G.; Kim, S.; Cooke, V. G.; Monahan, J. E.; Stegmeier, F.; Roberts, T. M.; Sellers, W. R.; Zhou, W.; Zhu, P., An F876L mutation in androgen receptor

- confers genetic and phenotypic resistance to MDV3100 (enzalutamide). *Cancer Discov.* **2013**, *3*, 1030-43.
150. Monaghan, A. E.; McEwan, I. J., A sting in the tail: the N-terminal domain of the androgen receptor as a drug target. *Asian J. Andrology* **2016**, *18*, 687-94.
151. Andersen, R. J.; Mawji, N. R.; Wang, J.; Wang, G.; Haile, S.; Myung, J. K.; Watt, K.; Tam, T.; Yang, Y. C.; Banuelos, C. A.; Williams, D. E.; McEwan, I. J.; Wang, Y.; Sadar, M. D., Regression of castrate-recurrent prostate cancer by a small-molecule inhibitor of the amino-terminus domain of the androgen receptor. *Cancer Cell* **2010**, *17*, 535-46.
152. Myung, J. K.; Banuelos, C. A.; Fernandez, J. G.; Mawji, N. R.; Wang, J.; Tien, A. H.; Yang, Y. C.; Tavakoli, I.; Haile, S.; Watt, K.; McEwan, I. J.; Plymate, S.; Andersen, R. J.; Sadar, M. D., An androgen receptor N-terminal domain antagonist for treating prostate cancer. *J. Clin. Invest.* **2013**, *123*, 2948-60.
153. Brand, L. J.; Olson, M. E.; Ravindranathan, P.; Guo, H.; Kempema, A. M.; Andrews, T. E.; Chen, X.; Raj, G. V.; Harki, D. A.; Dehm, S. M., EPI-001 is a selective peroxisome proliferator-activated receptor- γ modulator with inhibitory effects on androgen receptor expression and activity in prostate cancer. *Oncotarget* **2015**, *6*, 3811-24.
154. Vaquerizas, J. M.; Kummerfeld, S. K.; Teichmann, S. A.; Luscombe, N. M., A census of human transcription factors: function, expression and evolution. *Nature Rev. Genet.* **2009**, *10*, 252-63.
155. (a) Darnell, J. E., Jr., Transcription factors as targets for cancer therapy. *Nature Rev. Cancer* **2002**, *2*, 740-9; (b) Koehler, A. N., A complex task? Direct modulation of transcription factors with small molecules. *Curr. Opin. Chem. Biol.* **2010**, *14*, 331-40.
156. (a) Moreira, I. S.; Fernandes, P. A.; Ramos, M. J., Hot spots--a review of the protein-protein interface determinant amino-acid residues. *Proteins* **2007**, *68*, 803-12; (b) Lo Conte, L.; Chothia, C.; Janin, J., The atomic structure of protein-protein recognition sites. *J. Mol. Biol.* **1999**, *285*, 2177-98; (c) Perot, S.; Sperandio, O.; Miteva, M. A.; Camproux, A. C.; Villoutreix, B. O., Druggable pockets and binding site centric chemical space: a paradigm shift in drug discovery. *Drug. Discov. Today* **2010**, *15*, 656-67.
157. Ivanov, A. A.; Khuri, F. R.; Fu, H., Targeting protein-protein interactions as an anticancer strategy. *Trends Pharmacol. Sci.* **2013**, *34*, 393-400.
158. (a) Berg, T., Inhibition of transcription factors with small organic molecules. *Curr. Opin. Chem. Biol.* **2008**, *12*, 464-71; (b) Nair, S. K.; Burley, S. K., X-ray

- structures of Myc-Max and Mad-Max recognizing DNA. Molecular bases of regulation by proto-oncogenic transcription factors. *Cell* **2003**, *112*, 193-205.
159. (a) Fontaine, F.; Overman, J.; Francois, M., Pharmacological manipulation of transcription factor protein-protein interactions: opportunities and obstacles. *Cell. Regen.* **2015**, *4*, 2; (b) Hagenbuchner, J.; Ausserlechner, M. J., Targeting transcription factors by small compounds--Current strategies and future implications. *Biochem. Pharmacol.* **2016**, *107*, 1-13.
160. (a) Dutzmann, J.; Daniel, J. M.; Bauersachs, J.; Hilfiker-Kleiner, D.; Sedding, D. G., Emerging translational approaches to target STAT3 signalling and its impact on vascular disease. *Cardiovasc. Res.* **2015**, *106*, 365-74; (b) Vohwinkel, C. U.; Hoegl, S.; Eltzschig, H. K., Hypoxia signaling during acute lung injury. *J. Appl. Physiol.* **2015**, *119*, 1157-63; (c) Yang, C. J.; Fan, Z. X.; Yang, J.; Yang, J., Activating transcription factor 3: A promising therapeutic target for remission myocardial ischemia reperfusion injury. *Int. J. Cardiol.* **2015**, *201*, 102-3.
161. Rask-Andersen, M.; Almen, M. S.; Schioth, H. B., Trends in the exploitation of novel drug targets. *Nature. Rev. Drug. Discov.* **2011**, *10*, 579-90.
162. Gilmore, T. D.; Herscovitch, M., Inhibitors of NF- κ B signaling: 785 and counting. *Oncogene* **2006**, *25*, 6887-99.
163. (a) Housman, G.; Byler, S.; Heerboth, S.; Lapinska, K.; Longacre, M.; Snyder, N.; Sarkar, S., Drug resistance in cancer: an overview. *Cancers* **2014**, *6*, 1769-92; (b) Huang, L.; Fu, L., Mechanisms of resistance to EGFR tyrosine kinase inhibitors. *Acta. Pharm. Sin. B* **2015**, *5*, 390-401.
164. Druker, B. J.; Tamura, S.; Buchdunger, E.; Ohno, S.; Segal, G. M.; Fanning, S.; Zimmermann, J.; Lydon, N. B., Effects of a selective inhibitor of the Abl tyrosine kinase on the growth of Bcr-Abl positive cells. *Nature Med.* **1996**, *2*, 561-6.
165. (a) Gorre, M. E.; Mohammed, M.; Ellwood, K.; Hsu, N.; Paquette, R.; Rao, P. N.; Sawyers, C. L., Clinical resistance to STI-571 cancer therapy caused by BCR-ABL gene mutation or amplification. *Science* **2001**, *293*, 876-80; (b) Bixby, D.; Talpaz, M., Mechanisms of resistance to tyrosine kinase inhibitors in chronic myeloid leukemia and recent therapeutic strategies to overcome resistance. *Hematology* **2009**, 461-76; (c) Valent, P., Standard treatment of Ph⁺ CML in 2010: how, when and where not to use what BCR/ABL1 kinase inhibitor? *Eur. J. Clin. Investigation* **2010**, *40*, 918-31.
166. Kubo, T.; Yamamoto, H.; Lockwood, W. W.; Valencia, I.; Soh, J.; Peyton, M.; Jida, M.; Otani, H.; Fujii, T.; Ouchida, M.; Takigawa, N.; Kiura, K.; Shimizu, K.; Date, H.; Minna, J. D.; Varella-Garcia, M.; Lam, W. L.; Gazdar, A. F.; Toyooka, S., MET gene amplification or EGFR mutation activate MET in lung cancers untreated with EGFR tyrosine kinase inhibitors. *Int. J. Cancer* **2009**, *124*, 1778-84.

167. (a) Shanmugam, M. K., Lee, J.H., Chai, E.Z.P., Kanchi, M.M., Kar, S., Arfuso, F., Dharmarajan, A., Kumar, A.P., Ramar, P.S., Looi, C.Y., Mustafa, M.R., Tergaonkar, V., Bishayee, A., Ahn, K.S., Sethi, G., Cancer Prevention and Therapy Through the Modulation of Transcription Factors by Bioactive Natural Compounds. *Seminars in Cancer Biology* **2016**, ASAP; (b) Ye, N.; Ding, Y.; Wild, C.; Shen, Q.; Zhou, J., Small molecule inhibitors targeting activator protein 1 (AP-1). *J. Med. Chem.* **2014**, *57*, 6930-48.
168. Zhao, Y.; Aguilar, A.; Bernard, D.; Wang, S., Small-molecule inhibitors of the MDM2-p53 protein-protein interaction (MDM2 Inhibitors) in clinical trials for cancer treatment. *J. Med. Chem.* **2015**, *58*, 1038-52.
169. (a) Freedman, D. A.; Wu, L.; Levine, A. J., Functions of the MDM2 oncoprotein. *Cell. Mol. Life Sci.* **1999**, *55*, 96-107; (b) Ganguli, G.; Abecassis, J.; Wasylyk, B., MDM2 induces hyperplasia and premalignant lesions when expressed in the basal layer of the epidermis. *EMBO J.* **2000**, *19*, 5135-47.
170. (a) Finley, A.; Copeland, R. A., Small molecule control of chromatin remodeling. *Chemistry & Biology* **2014**, *21* (9), 1196-210; (b) Kumar, R.; Li, D. Q.; Muller, S.; Knapp, S., Epigenomic regulation of oncogenesis by chromatin remodeling. *Oncogene* **2016**, *35*, 4423-36.
171. (a) Prince, H. M.; Bishton, M. J.; Harrison, S. J., Clinical studies of histone deacetylase inhibitors. *Clin. Cancer Res.* **2009**, *15*, 3958-69; (b) Furumai, R.; Matsuyama, A.; Kobashi, N.; Lee, K. H.; Nishiyama, M.; Nakajima, H.; Tanaka, A.; Komatsu, Y.; Nishino, N.; Yoshida, M.; Horinouchi, S., FK228 (depsipeptide) as a natural prodrug that inhibits class I histone deacetylases. *Cancer Res.* **2002**, *62*, 4916-21.
172. Mann, B. S.; Johnson, J. R.; Cohen, M. H.; Justice, R.; Pazdur, R., FDA approval summary: vorinostat for treatment of advanced primary cutaneous T-cell lymphoma. *The Oncologist* **2007**, *12*, 1247-52.
173. Lee, J. H.; Choy, M. L.; Marks, P. A., Mechanisms of resistance to histone deacetylase inhibitors. *Adv. Cancer Res.* **2012**, *116*, 39-86.
174. (a) Rosato, R. R.; Kolla, S. S.; Hock, S. K.; Almenara, J. A.; Patel, A.; Amin, S.; Atadja, P.; Fisher, P. B.; Dent, P.; Grant, S., Histone deacetylase inhibitors activate NF- κ B in human leukemia cells through an ATM/NEMO-related pathway. *J. Biol. Chem.* **2010**, *285*, 10064-77; (b) Fantin, V. R.; Loboda, A.; Paweletz, C. P.; Hendrickson, R. C.; Pierce, J. W.; Roth, J. A.; Li, L.; Gooden, F.; Korenchuk, S.; Hou, X. S.; Harrington, E. A.; Randolph, S.; Reilly, J. F.; Ware, C. M.; Kadin, M. E.; Frankel, S. R.; Richon, V. M., Constitutive activation of signal transducers and activators of transcription predicts vorinostat resistance in cutaneous T-cell lymphoma. *Cancer Res.* **2008**, *68*, 3785-94; (c) Zhou, J.; Bi, C.; Chng, W. J.; Cheong, L. L.; Liu, S. C.; Mahara, S.; Tay, K. G.; Zeng, Q.; Li, J.; Guo, K.; Tan, C. P.; Yu, H.;

- Albert, D. H.; Chen, C. S., PRL-3, a metastasis associated tyrosine phosphatase, is involved in FLT3-ITD signaling and implicated in anti-AML therapy. *PLoS one* **2011**, *6*, e19798.
175. (a) Wade, W. S.; Mrksich, M.; Dervan, P. B., Design of Peptides That Bind in the Minor Groove of DNA at 5'-(a,T)G(a,T)C(a,T)-3' Sequences by a Dimeric Side-by-Side Motif. *J. Am. Chem. Soc.* **1992**, *114*, 8783-8794; (b) Griffin, L. C.; Kiessling, L. L.; Beal, P. A.; Gillespie, P.; Dervan, P. B., Recognition of All 4 Base-Pairs of Double-Helical DNA by Triple-Helix Formation - Design of Nonnatural Deoxyribonucleosides for Pyrimidine.Purine Base Pair Binding. *J. Am. Chem. Soc.* **1992**, *114*, 7976-7982; (c) Leung, C. H.; Chan, D. S.; Ma, V. P.; Ma, D. L., DNA-binding small molecules as inhibitors of transcription factors. *Med.Res. Rev.* **2013**, *33*, 823-46.
176. Chenoweth, D. M.; Dervan, P. B., Allosteric modulation of DNA by small molecules. *Proc. Natl. Acad. Sci. U.S.A.* **2009**, *106*, 13175-9.
177. Dervan, P. B., Molecular recognition of DNA by small molecules. *Bioorg. Med. Chem.* **2001**, *9*, 2215-35.
178. (a) Mysore, V. S.; Szablowski, J.; Dervan, P. B.; Frost, P. J., A DNA-binding Molecule Targeting the Adaptive Hypoxic Response in Multiple Myeloma Has Potent Antitumor Activity. *Mol. Cancer Res.* **2016**, *14*, 253-66; (b) Raskatov, J. A.; Meier, J. L.; Puckett, J. W.; Yang, F.; Ramakrishnan, P.; Dervan, P. B., Modulation of NF- κ B-dependent gene transcription using programmable DNA minor groove binders. *Proc. Natl. Acad. Sci. U.S.A.* **2012**, *109*, 1023-8.
179. (a) Yeh, J. E.; Toniolo, P. A.; Frank, D. A., Targeting transcription factors: promising new strategies for cancer therapy. *Curr. Opin. Oncol.* **2013**, *25*, 652-8; (b) Singh, P.; Singh, M. K.; Chaudhary, D.; Chauhan, V.; Bharadwaj, P.; Pandey, A.; Upadhyay, N.; Dhaked, R. K., Small-molecule quinolinol inhibitor identified provides protection against BoNT/A in mice. *PLoS one* **2012**, *7*, e47110.
180. (a) Cheatle Jarvela, A. M.; Hinman, V. F., Evolution of transcription factor function as a mechanism for changing metazoan developmental gene regulatory networks. *EvoDevo* **2015**, *6*, 3; (b) Siggers, T.; Gordan, R., Protein-DNA binding: complexities and multi-protein codes. *Nucleic Acid Res.* **2014**, *42*, 2099-111; (c) Wray, G. A., The evolutionary significance of cis-regulatory mutations. *Nature Rev. Genet.* **2007**, *8*, 206-16.
181. (a) Adams, R. H., W., Helenalin. I. Isolation and Properties. *J. Am. Chem. Soc.* **1949**, *71*, 2546-2551; (b) Kos, O.; Lindenmeyer, M. T.; Tubaro, A.; Sosa, S.; Merfort, I., New sesquiterpene lactones from Arnica tincture prepared from fresh flowerheads of Arnica montana. *Planta Med.* **2005**, *71*, 1044-52.

182. (a) Hall, I. H.; Lee, K. H.; Mar, E. C.; Starnes, C. O.; Waddell, T. G., Antitumor agents. 21. A proposed mechanism for inhibition of cancer growth by tenulin and helenalin and related cyclopentenones. *J. Med. Chem.* **1977**, *20*, 333-7; (b) Grippo, A. A.; Hall, I. H.; Kiyokawa, H.; Muraoka, O.; Shen, Y. C.; Lee, K. H., The cytotoxicity of helenalin, its mono and difunctional esters, and related sesquiterpene lactones in murine and human tumor cells. *Drug Des. Discov.* **1992**, *8*, 191-206; (c) Merfort, I., Perspectives on sesquiterpene lactones in inflammation and cancer. *Curr. Drug Targets* **2011**, *12*, 1560-73.
183. (a) Schmidt, T. J., Helenanolide-type sesquiterpene lactones--III. Rates and stereochemistry in the reaction of helenalin and related helenanolides with sulfhydryl containing biomolecules. *Bioorg. Med. Chem.* **1997**, *5*, 645-53; (b) Schmidt, T. J.; Lyss, G.; Pahl, H. L.; Merfort, I., Helenanolide type sesquiterpene lactones. Part 5: the role of glutathione addition under physiological conditions. *Bioorg. Med. Chem.* **1999**, *7*, 2849-55; (c) Buchele, B.; Zugmaier, W.; Lunov, O.; Syrovets, T.; Merfort, I.; Simmet, T., Surface plasmon resonance analysis of nuclear factor- κ B protein interactions with the sesquiterpene lactone helenalin. *Anal. Biochem.* **2010**, *401*, 30-7.
184. Lyss, G.; Knorre, A.; Schmidt, T. J.; Pahl, H. L.; Merfort, I., The anti-inflammatory sesquiterpene lactone helenalin inhibits the transcription factor NF- κ B by directly targeting p65. *J. Biol. Chem.* **1998**, *273*, 33508-16.
185. Rungeler, P.; Castro, V.; Mora, G.; Goren, N.; Vichnewski, W.; Pahl, H. L.; Merfort, I.; Schmidt, T. J., Inhibition of transcription factor NF- κ B by sesquiterpene lactones: a proposed molecular mechanism of action. *Bioorg. Med. Chem.* **1999**, *7* (11), 2343-52.
186. Garcia-Pineros, A. J.; Castro, V.; Mora, G.; Schmidt, T. J.; Strunck, E.; Pahl, H. L.; Merfort, I., Cysteine 38 in p65/NF- κ B plays a crucial role in DNA binding inhibition by sesquiterpene lactones. *J. Biol. Chem.* **2001**, *276* (43), 39713-20.
187. (a) Kim, K.; Kim, S. J.; Han, Y. T.; Hong, S. J.; An, H.; Chang, D. J.; Kim, T.; Lim, B.; Lee, J.; Surh, Y. J.; Suh, Y. G., Identification of small molecule inhibitors of the STAT3 signaling pathway: Insights into their structural features and mode of action. *Bioorg. Med. Chem. Lett.* **2015**, *25*, 5444-8; (b) Furqan, M.; Akinleye, A.; Mukhi, N.; Mittal, V.; Chen, Y.; Liu, D., STAT inhibitors for cancer therapy. *J. Hemat. Oncol.* **2013**, *6*, 90.
188. Huang, W.; Dong, Z.; Wang, F.; Peng, H.; Liu, J. Y.; Zhang, J. T., A small molecule compound targeting STAT3 DNA-binding domain inhibits cancer cell proliferation, migration, and invasion. *ACS Chem. Biol.* **2014**, *9*, 1188-96.
189. Huang, W.; Dong, Z.; Chen, Y.; Wang, F.; Wang, C. J.; Peng, H.; He, Y.; Hangoc, G.; Pollok, K.; Sandusky, G.; Fu, X. Y.; Broxmeyer, H. E.; Zhang, Z. Y.; Liu, J. Y.; Zhang, J. T., Small-molecule inhibitors targeting the DNA-binding domain

- of STAT3 suppress tumor growth, metastasis and STAT3 target gene expression in vivo. *Oncogene* **2016**, *35*, 802.
190. Fletcher, S.; Prochownik, E. V., Small-molecule inhibitors of the Myc oncoprotein. *Biochim. Biophys. Acta* **2015**, *1849*, 525-43.
191. Brooks, T. A.; Hurley, L. H., Targeting MYC Expression through G-Quadruplexes. *Genes & Cancer* **2010**, *1*, 641-649.
192. (a) Kraeft, S. K.; Traincart, F.; Mesnildrey, S.; Bourdais, J.; Veron, M.; Chen, L. B., Nuclear localization of nucleoside diphosphate kinase type B (nm23-H2) in cultured cells. *Exper. Cell Res.* **1996**, *227*, 63-9; (b) Dexheimer, T. S.; Carey, S. S.; Zuohe, S.; Gokhale, V. M.; Hu, X.; Murata, L. B.; Maes, E. M.; Weichsel, A.; Sun, D.; Meuillet, E. J.; Montfort, W. R.; Hurley, L. H., NM23-H2 may play an indirect role in transcriptional activation of c-myc gene expression but does not cleave the nuclease hypersensitive element III(1). *Mol. Cancer. Ther.* **2009**, *8*, 1363-77.
193. Li, Y.; Tong, Y.; Wong, Y. H., Regulatory functions of Nm23-H2 in tumorigenesis: insights from biochemical to clinical perspectives. *Naunyn-Schmiedeberg's Archives of Pharmacology* **2015**, *388*, 243-56.
194. Shan, C.; Lin, J.; Hou, J. Q.; Liu, H. Y.; Chen, S. B.; Chen, A. C.; Ou, T. M.; Tan, J. H.; Li, D.; Gu, L. Q.; Huang, Z. S., Chemical intervention of the NM23-H2 transcriptional programme on c-MYC via a novel small molecule. *Nucleic Acid Res.* **2015**, *43*, 6677-91.
195. Khedkar, S. A.; Sun, X.; Rigby, A. C.; Feinberg, M. W., Discovery of small molecule inhibitors to Kruppel-like factor 10 (KLF10): implications for modulation of T regulatory cell differentiation. *J. Med. Chem.* **2015**, *58*, 1466-78.
196. (a) Cao, Z.; Wara, A. K.; Icli, B.; Sun, X.; Packard, R. R.; Esen, F.; Stapleton, C. J.; Subramaniam, M.; Kretschmer, K.; Apostolou, I.; von Boehmer, H.; Hansson, G. K.; Spelsberg, T. C.; Libby, P.; Feinberg, M. W., Kruppel-like factor KLF10 targets transforming growth factor- β 1 to regulate CD4(+)CD25(-) T cells and T regulatory cells. *J. Biol. Chem.* **2009**, *284*, 24914-24; (b) Venuprasad, K.; Huang, H.; Harada, Y.; Elly, C.; Subramaniam, M.; Spelsberg, T.; Su, J.; Liu, Y. C., The E3 ubiquitin ligase Itch regulates expression of transcription factor Foxp3 and airway inflammation by enhancing the function of transcription factor TIEG1. *Nature Immunol.* **2008**, *9*, 245-53.
197. (a) Dalal, K.; Roshan-Moniri, M.; Sharma, A.; Li, H.; Ban, F.; Hassona, M. D.; Hsing, M.; Singh, K.; LeBlanc, E.; Dehm, S.; Tomlinson Guns, E. S.; Cherkasov, A.; Rennie, P. S., Selectively targeting the DNA-binding domain of the androgen receptor as a prospective therapy for prostate cancer. *J. Biol. Chem.* **2014**, *289*, 26417-29; (b) Li, H.; Ban, F.; Dalal, K.; Leblanc, E.; Frewin, K.; Ma, D.; Adomat, H.; Rennie, P. S.; Cherkasov, A., Discovery of small-molecule inhibitors selectively

- targeting the DNA-binding domain of the human androgen receptor. *J. Med. Chem.* **2014**, *57*, 6458-67.
198. (a) Xiao, G.; Fu, J., NF- κ B and Cancer: a Paradigm of Yin-Yang. *American journal of Cancer Res.* **2011**, *1*, 192-221; (b) Aggarwal, B. B., Nuclear factor- κ B the enemy within. *Cancer Cell* **2004**, *6*, 203-208; (c) Huxford, T.; Ghosh, G., A structural guide to proteins of the NF- κ B signaling module. *Cold Spring Harb. Perspect. Biol.* **2009**, *1*, a000075; (d) Hayden, M. S., Ghosh, S., Shared principles in NF- κ B signaling. *Cell* **2008**, *132*, 344-362.
199. (a) Greten, F. R.; Karin, M., The IKK/NF- κ B activation pathway-a target for prevention and treatment of cancer. *Cancer Lett.* **2004**, *206*, 193-9; (b) Pande, V.; Sousa, S. F.; Ramos, M. J., Direct covalent modification as a strategy to inhibit nuclear factor- κ B. *Curr Med Chem* **2009**, *16*, 4261-73; (c) Wang, W.; Nag, S. A.; Zhang, R., Targeting the NF κ B signaling pathways for breast cancer prevention and therapy. *Curr Med Chem* **2015**, *22*, 264-89; (d) Karin, M.; Yamamoto, Y.; Wang, Q. M., The IKK NF- κ B system: A treasure trove for drug development. *Nat. Rev. Drug Discov.* **2004**, *3*, 17-26.
200. Gupta, S. C.; Sundaram, C.; Reuter, S.; Aggarwal, B. B., Inhibiting NF- κ B activation by small molecules as a therapeutic strategy. *Biochim. Biophys. Acta* **2010**, *1799*, 775-87.
201. (a) Kojima, T.; Wang, X.; Fujiwara, K.; Osaka, S.; Yoshida, Y.; Osaka, E.; Taniguchi, M.; Ueno, T.; Fukuda, N.; Soma, M.; Tokuhashi, Y.; Nagase, H., Inhibition of human osteosarcoma cell migration and invasion by a gene silencer, pyrrole-imidazole polyamide, targeted at the human MMP9 NF- κ B binding site. *Biol. Pharm. Bull.* **2014**, *37*, 1460-5; (b) Wurtz, N. R.; Pomerantz, J. L.; Baltimore, D.; Dervan, P. B., Inhibition of DNA binding by NF- κ B with pyrrole-imidazole polyamides. *Biochemistry* **2002**, *41*, 7604-9; (c) Chenoweth, D. M.; Poposki, J. A.; Marques, M. A.; Dervan, P. B., Programmable oligomers targeting 5'-GGGG-3' in the minor groove of DNA and NF- κ B binding inhibition. *Bioorg. Med. Chem.* **2007**, *15*, 759-70; (d) Yang, F.; Nickols, N. G.; Li, B. C.; Szablowski, J. O.; Hamilton, S. R.; Meier, J. L.; Wang, C. M.; Dervan, P. B., Animal toxicity of hairpin pyrrole-imidazole polyamides varies with the turn unit. *J. Med. Chem.* **2013**, *56*, 7449-57.
202. Siedle, B.; Garcia-Pineros, A. J.; Murillo, R.; Schulte-Monting, J.; Castro, V.; Rungeler, P.; Klaas, C. A.; Da Costa, F. B.; Kisiel, W.; Merfort, I., Quantitative structure - Activity relationship of sesquiterpene lactones as inhibitors of the transcription factor NF- κ B. *J. Med. Chem.* **2004**, *47*, 6042-6054.
203. Pettit, G. R.; Budzinskic; Cragg, G. M.; Brown, P.; Johnston, L. D., Antineoplastic Agents 34. Helonium-Autumnale-L. *J. Med. Chem.* **1974**, *17*, 1013-1016.

204. Lamson, P. D., On the pharmacological action of helenalin, the active principle of helenium autumnale. *J. Pharmacol. Exp. Ther.* **1913**, *4*, 471-489.
205. Kitson, R. R.; Millemaggi, A.; Taylor, R. J., The renaissance of α -methylene- γ -butyrolactones: new synthetic approaches. *Angew. Chem. Int. Ed.* **2009**, *48*, 9426-51.
206. (a) Lee, K. H.; Ibuka, T.; Mar, E. C.; Hall, I. H., Anti-tumor agents. 31. Helenalin sym-dimethylethylenediamine reaction products and related derivatives. *J. Med. Chem.* **1978**, *21*, 698-701; (b) Lee, K. H.; Huang, E. S.; Furukawa, H., Antitumor Agents. 3. Synthesis and cytotoxic activity of helenalin amine adducts and related derivatives. *J. Med. Chem.* **1972**, *15*, 609-611; (c) Lee, K. H.; Kim, S. H.; Furukawa, H.; Piantadosi, C.; Huang, E. S., Antitumor Agents. 11. Synthesis and cytotoxic activity of epoxides of helenalin related derivatives. *J. Med. Chem.* **1975**, *18*, 59-63.
207. Cys38 and Cys120 of p65 are spatially separated by 7.7 Å in the PDB 1VKX. This distance is similar to spatial separation of the two electrophilic carbons in helenalin (~ 7 Å) from two published crystal structures and a computationally minimized structure.
208. (a) Kastrati, I.; Siklos, M. I.; Calderon-Gierszal, E. L.; El-Shennawy, L.; Georgieva, G.; Thayer, E. N.; Thatcher, G. R.; Frasar, J., Dimethyl Fumarate Inhibits the Nuclear Factor κ B Pathway in Breast Cancer Cells by Covalent Modification of p65 Protein. *J. Biol. Chem.* **2016**, *291*, 3639-47; (b) Han, Y.; Englert, J. A.; Yang, R.; Delude, R. L.; Fink, M. P., Ethyl pyruvate inhibits nuclear factor- κ B-dependent signaling by directly targeting p65. *J. Pharmacol. Exp. Ther.* **2005**, *312*, 1097-105; (c) Sethi, G.; Ahn, K. S.; Aggarwal, B. B., Targeting nuclear factor- κ B activation pathway by thymoquinone: role in suppression of antiapoptotic gene products and enhancement of apoptosis. *Mol. Cancer Res.* **2008**, *6*, 1059-70; (d) Liang, M. C.; Bardhan, S.; Pace, E. A.; Rosman, D.; Beutler, J. A.; Porco, J. A., Jr.; Gilmore, T. D., Inhibition of transcription factor NF- κ B signaling proteins IKK β and p65 through specific cysteine residues by epoxyquinone A monomer: correlation with its anti-cancer cell growth activity. *Biochem. Pharmacol.* **2006**, *71*, 634-45; (e) Rana, S.; Blowers, E. C.; Tebbe, C.; Contreras, J. I.; Radhakrishnan, P.; Kizhake, S.; Zhou, T.; Rajule, R. N.; Arnst, J. L.; Munkarah, A. R.; Rattan, R.; Natarajan, A., Isatin Derived Spirocyclic Analogues with α -Methylene- γ -butyrolactone as Anticancer Agents: A Structure-Activity Relationship Study. *J. Med. Chem.* **2016**, *59*, 5121-7.
209. Yamamoto, M.; Horie, R.; Takeiri, M.; Kozawa, I.; Umezawa, K., Inactivation of NF- κ B components by covalent binding of (-)-dehydroxymethylepoxyquinomicin to specific cysteine residues. *J. Med. Chem.* **2008**, *51*, 5780-8.
210. (a) Fronczek, F. R.; Ober, A. G.; Fischer, N. H., Helenalin, a Pseudoguaianolide from Helenium-Amarum. *Acta Crystallogr. C* **1987**, *43*, 358-360; (b) Watson, W. H.; Kashyap, R. P., The Structures of 2 Sesquiterpene Lactones. *Acta Crystallogr. C* **1990**, *46*, 1524-1528.

211. Deny, L. J.; Traboulsi, H.; Cantin, A. M.; Marsault, E.; Richter, M. V.; Belanger, G., Bis-Michael Acceptors as Novel Probes to Study the Keap1/Nrf2/ARE Pathway. *J. Med. Chem.* **2016**, ASAP.
212. (a) Grieco, P. A.; Majetich, G. F.; Ohfuné, Y., Pseudoguaianolides .1. Stereospecific Total Synthesis of the Ambrosanolides DI-Ambrosin and DI-Damsin. *J. Am. Chem. Soc.* **1982**, *104*, 4226-4233; (b) Grieco, P. A.; Ohfuné, Y.; Majetich, G. F.; Wang, C. L. J., Pseudoguaianolides .2. Stereocontrolled Total Synthesis of the Helenanolide DI-Helenalin. *J. Am. Chem. Soc.* **1982**, *104*, 4233-4240; (c) Ohfuné, Y.; Grieco, P. A.; Wang, C. L. J.; Majetich, G., Stereospecific Total Synthesis of DI-Helenalin - General Route to Helenanolides and Ambrosanolides. *J. Am. Chem. Soc.* **1978**, *100*, 5946-5948; (d) Roberts, M. R.; Schlessinger, R. H., Total Synthesis of DI-Helenalin. *J. Am. Chem. Soc.* **1979**, *101*, 7626-7627.
213. Hodgson, D. M.; Talbot, E. P. A.; Clark, B. P., Stereoselective Synthesis of β -(Hydroxymethylaryl/alkyl)- α -methylene- γ -butyrolactones. *Org. Lett.* **2011**, *13*, 2594-2597.
214. (a) Ramachandran, P. V.; Chen, G. M.; Brown, H. C., Chiral synthesis via organoboranes .42. Selective reductions .57. Efficient kinetic resolution of representative α -tertiary ketones with B-chlorodiisopinocampheylborane. *J. Org. Chem.* **1996**, *61*, 88-94; (b) Sato, K. S., S.; Kojima, Y., A New Synthesis of 3-Methylcyclopent-2-en-2-ol-1-one. *J. Org. Chem.* **1967**, *32*, 339-341; (c) Lee, K. H.; Mar, E. C.; Okamoto, M.; Hall, I. H., Antitumor agents 32. Synthesis and antitumor activity of cyclopentenone derivatives related to helenalin. *J. Med. Chem.* **1978**, *21*, 819-22.
215. Nicolaou, K. C.; Montagnon, T.; Baran, P. S.; Zhong, Y. L., Iodine(V) reagents in organic synthesis. Part 4. o-iodoxybenzoic acid as a chemospecific tool for single electron transfer-based oxidation processes. *J. Am. Chem. Soc.* **2002**, *124*, 2245-2258.
216. Fuchs, M.; Schober, M.; Orthaber, A.; Faber, K., Asymmetric Synthesis of β -Substituted α -Methylenebutyrolactones via TRIP-Catalyzed Allylation: Mechanistic Studies and Application to the Synthesis of (S)-(-)-Hydroxymatairesinol. *Adv. Synth. Catal.* **2013**, *355*, 2499-2505.
217. (a) Ando, K.; Takemasa, Y.; Tomioka, K.; Koga, K., Stereoselective Reactions .21. Asymmetric Alkylation of α Alkyl β -Keto-Esters to α,α -Dialkyl β -Keto-Esters Having Either (R)-Chiral or (S)-Chiral Quaternary Center Depending on the Solvent System. *Tetrahedron* **1993**, *49*, 1579-1588; (b) Fukuyama, Y.; Matsumoto, K.; Tono, Y.; Yokoyama, R.; Takahashi, H.; Minami, H.; Okazaki, H.; Mitsumoto, Y., Total syntheses of neuroprotective mastigophorenes A and B. *Tetrahedron* **2001**, *57*, 7127-7135; (c) Fukuyama, Y.; Kiriya, Y.; Kodama, M., Total synthesis of herbertenediol, an isocuparane sesquiterpene isolated from liverworts. *Tetrahedron Lett* **1996**, *37*, 1261-1264; (d) Lee, J. N.; Oya, S.; Snyder, J. K., Asymmetric

- Oxidation of B-Ketoesters with Benzoyl Peroxide - Enantioselective Formation of Protected Tertiary Alcohols. *Tetrahedron Lett.* **1991**, *32*, 5899-5902.
218. (a) Ito, Y.; Hirao, T.; Saegusa, T., Synthesis of α,β -Unsaturated Carbonyl-Compounds by Palladium(II)-Catalyzed Dehydrosilylation of Silyl Enol Ethers. *J. Org. Chem.* **1978**, *43*, 1011-1013; (b) Larock, R. C.; Hightower, T. R.; Kraus, G. A.; Hahn, P.; Zheng, D., A Simple, Effective, New, Palladium-Catalyzed Conversion of Enol Silanes to Enones and Enals. *Tetrahedron Lett* **1995**, *36*, 2423-2426.
219. Hexum, J. K.; Tello-Aburto, R.; Struntz, N. B.; Harned, A. M.; Harki, D. A., Bicyclic Cyclohexenones as Inhibitors of NF- κ B Signaling. *ACS Med. Chem. Lett.* **2012**, *3*, 459-464.
220. Rostovtsev, V. V.; Green, L. G.; Fokin, V. V.; Sharpless, K. B., A stepwise Huisgen cycloaddition process: copper(I)-catalyzed regioselective "ligation" of azides and terminal alkynes. *Angew. Chem. Int. Ed.* **2002**, *41*, 2596-9.
221. Frigerio, M.; Santagostino, M.; Sputore, S., A user-friendly entry to 2-iodoxybenzoic acid (IBX). *J. Org. Chem.* **1999**, *64*, 4537-4538.
222. (a) Kozawa, I.; Akashi, Y.; Takiguchi, K.; Sasaki, D.; Sawamoto, D.; Takao, K.; Tadano, K., Stereoselective double alkylation of the acetoacetate ester α -carbon on a D-glucose-derived template: Application to the synthesis of enantiopure cycloalkenones bearing an asymmetric quaternary carbon. *Synlett* **2007**, 399-402; (b) Kato, K.; Suzuki, H.; Tanaka, H.; Miyasaka, T.; Baba, M.; Yamaguchi, K.; Akita, H., Stereoselective synthesis of 4'- α -alkylcarbovir derivatives based on an asymmetric synthesis or chemoenzymatic procedure. *Chem. Pharm. Bull.* **1999**, *47*, 1256-1264; (c) Kumar, R.; Rej, R. K.; Halder, J.; Mandal, H.; Nanda, S., Enantiopure hydroxymethylated cycloalkenols as privileged small molecular multifunctional scaffolds for the asymmetric synthesis of carbocycles. *Tetrahedron-Asymmetr.* **2016**, *27*, 498-512.
223. Friscourt, F.; Fahrni, C. J.; Boons, G. J., A fluorogenic probe for the catalyst-free detection of azide-tagged molecules. *J. Am. Chem. Soc.* **2012**, *134*, 18809-15.
224. (a) Shevchenko, A.; Wilm, M.; Vorm, O.; Mann, M., Mass spectrometric sequencing of proteins from silver stained polyacrylamide gels. *Anal. Chem.* **1996**, *68* (5), 850-858; (b) Shevchenko, A.; Tomas, H.; Havlis, J.; Olsen, J. V.; Mann, M., In-gel digestion for mass spectrometric characterization of proteins and proteomes. *Nature Protocols* **2006**, *1*, 2856-60.
225. Yates, J. R., 3rd; Eng, J. K.; McCormack, A. L., Mining genomes: correlating tandem mass spectra of modified and unmodified peptides to sequences in nucleotide databases. *Anal. Chem.* **1995**, *67*, 3202-10.
226. APEX II, Bruker Analytical X-ray Systems, Madison, WI (2011).

227. SHELXTL V2008/4, Bruker Analytical X-ray Systems, Madison, WI (2008).
228. SAINT+ V7.34, Bruker Analytical X-ray Systems, Madison, WI (2003).
229. Widen, J. C., Kempema, A.M., Villalta, P.W., Harki, D.A., Targeting NF- κ B p65 with a Helenalin Inspired Bis-electrophile. *ACS Chem. Biol.* **2016**, ASAP.
230. (a) Beinke, S.; Ley, S. C., Functions of NF- κ B1 and NF- κ B2 in immune cell biology. *Biochem. J.* **2004**, *382*, 393-409; (b) Hayden, M. S.; West, A. P.; Ghosh, S., NF- κ B and the immune response. *Oncogene* **2006**, *25*, 6758-80; (c) Hayden, M. S.; Ghosh, S., NF- κ B, the first quarter-century: remarkable progress and outstanding questions. *Genes Dev.* **2012**, *26*, 203-34; (d) Mitchell, S.; Vargas, J.; Hoffmann, A., Signaling via the NF κ B system. *Systems Biol. Med.* **2016**, *8*, 227-41.
231. Basseres, D. S.; Baldwin, A. S., Nuclear factor- κ B and inhibitor of κ B kinase pathways in oncogenic initiation and progression. *Oncogene* **2006**, *25*, 6817-30.
232. For a comprehensive list of inhibitors of the NF- κ B pathway visit: <http://www.bu.edu/nf-kb/physiological-mediators/inhibitors/>.
233. (a) Avonto, C.; Tagliatela-Scafati, O.; Pollastro, F.; Minassi, A.; Di Marzo, V.; De Petrocellis, L.; Appendino, G., An NMR spectroscopic method to identify and classify thiol-trapping agents: revival of Michael acceptors for drug discovery? *Angew. Chem. Int. Ed.* **2011**, *50*, 467-71; (b) Appendino, G.; Minassi, A.; Collado, J. A.; Pollastro, F.; Chianese, G.; Tagliatela-Scafati, O.; Ayyari, M.; Garcia, V.; Munoz, E., The Thia-Michael Reactivity of Zerumbone and Related Cross-Conjugated Dienones: Disentangling Stoichiometry, Regiochemistry, and Addition Mode with an NMR-Spectroscopy-Based Cysteamine Assay. *Eur. J. Org. Chem.* **2015**, 3721-3726.
234. (a) Schmidt, T. J., Helenanolide type sesquiterpene lactones .1. Conformations and molecular dynamics of helenalin, its esters and 11,13-dihydro derivatives. *J. Mol. Struct.* **1996**, *385*, 99-112; (b) Carson, M. S.; Tully, L. E., A New Synthesis of A-Methylene Lactones. *P. Roy Irish Acad. B* **1983**, *83*, 33-38.
235. Paryzek, Z.; Koenig, H.; Tabaczka, B., Ammonium formate/palladium on carbon: A versatile system for catalytic hydrogen transfer reduction of carbon-carbon double bonds. *Synthesis-Stuttgart* **2003**, 2594-2594.
236. Siegel, S., Smith, G.V., Stereochemistry and the Mechanism of Hydrogenation of Cycloolefins on a Platinum Catalyst. *J. Am. Chem. Soc.* **1960**, *82*, 6082-6087.
237. Wen, B.; Hexum, J. K.; Widen, J. C.; Harki, D. A.; Brummond, K. M., A redox economical synthesis of bioactive 6,12-guaianolides. *Org. Lett.* **2013**, *15*, 2644-7.

238. Ghantous, A.; Gali-Muhtasib, H.; Vuorela, H.; Saliba, N. A.; Darwiche, N., What made sesquiterpene lactones reach cancer clinical trials? *Drug. Discov. Today* **2010**, *15*, 668-78.
239. Knight, D. W., Feverfew: chemistry and biological activity. *Nat. Prod. Rep.* **1995**, *12*, 271-6.
240. (a) Ghantous, A.; Sinjab, A.; Herceg, Z.; Darwiche, N., Parthenolide: from plant shoots to cancer roots. *Drug. Discov. Today* **2013**, *18*, 894-905; (b) Kreuger, M. R.; Grootjans, S.; Biavatti, M. W.; Vandenabeele, P.; D'Herde, K., Sesquiterpene lactones as drugs with multiple targets in cancer treatment: focus on parthenolide. *Anti-Cancer Drugs* **2012**, *23*, 883-96.
241. Guzman, M. L.; Rossi, R. M.; Karnischky, L.; Li, X.; Peterson, D. R.; Howard, D. S.; Jordan, C. T., The sesquiterpene lactone parthenolide induces apoptosis of human acute myelogenous leukemia stem and progenitor cells. *Blood* **2005**, *105*, 4163-9.
242. (a) Lapidot, T.; Sirard, C.; Vormoor, J.; Murdoch, B.; Hoang, T.; Caceres-Cortes, J.; Minden, M.; Paterson, B.; Caligiuri, M. A.; Dick, J. E., A cell initiating human acute myeloid leukaemia after transplantation into SCID mice. *Nature* **1994**, *367*, 645-8; (b) Hope, K. J.; Jin, L.; Dick, J. E., Acute myeloid leukemia originates from a hierarchy of leukemic stem cell classes that differ in self-renewal capacity. *Nature Immunol.* **2004**, *5*, 738-43.
243. (a) Crews, L. A.; Jamieson, C. H., Selective elimination of leukemia stem cells: hitting a moving target. *Cancer Lett.* **2013**, *338*, 15-22; (b) Jordan, C. T., Targeting myeloid leukemia stem cells. *Science Transl. Med.* **2010**, *2*, 31ps21; (c) Dick, J. E., Stem cell concepts renew cancer research. *Blood* **2008**, *112*, 4793-807; (d) Horton, S. J.; Huntly, B. J., Recent advances in acute myeloid leukemia stem cell biology. *Haematologica* **2012**, *97*, 966-74; (e) Guzman, M. L.; Allan, J. N., Concise review: Leukemia stem cells in personalized medicine. *Stem Cells* **2014**, *32*, 844-51.
244. Amorim, M. H.; Gil da Costa, R. M.; Lopes, C.; Bastos, M. M., Sesquiterpene lactones: adverse health effects and toxicity mechanisms. *Crit. Rev. Toxicol.* **2013**, *43*, 559-79.
245. (a) Curry, E. A., 3rd; Murry, D. J.; Yoder, C.; Fife, K.; Armstrong, V.; Nakshatri, H.; O'Connell, M.; Sweeney, C. J., Phase I dose escalation trial of feverfew with standardized doses of parthenolide in patients with cancer. *Invest. New Drugs* **2004**, *22*, 299-305; (b) Sweeney, C. J.; Mehrotra, S.; Sadaria, M. R.; Kumar, S.; Shortle, N. H.; Roman, Y.; Sheridan, C.; Campbell, R. A.; Murry, D. J.; Badve, S.; Nakshatri, H., The sesquiterpene lactone parthenolide in combination with docetaxel reduces metastasis and improves survival in a xenograft model of breast cancer. *Mol. Cancer Ther.* **2005**, *4*, 1004-12.

246. (a) Guzman, M. L.; Rossi, R. M.; Neelakantan, S.; Li, X.; Corbett, C. A.; Hassane, D. C.; Becker, M. W.; Bennett, J. M.; Sullivan, E.; Lachowicz, J. L.; Vaughan, A.; Sweeney, C. J.; Matthews, W.; Carroll, M.; Liesveld, J. L.; Crooks, P. A.; Jordan, C. T., An orally bioavailable parthenolide analog selectively eradicates acute myelogenous leukemia stem and progenitor cells. *Blood* **2007**, *110*, 4427-35; (b) Neelakantan, S.; Nasim, S.; Guzman, M. L.; Jordan, C. T.; Crooks, P. A., Aminoparthenolides as novel anti-leukemic agents: Discovery of the NF- κ B inhibitor, DMAPT (LC-1). *Bioorg. Med. Chem. Lett.* **2009**, *19*, 4346-9.
247. (a) Hejchman, E.; Haugwitz, R. D.; Cushman, M., Synthesis and cytotoxicity of water-soluble ambrosin prodrug candidates. *J. Med. Chem.* **1995**, *38*, 3407-10; (b) Woods, J. R.; Mo, H. P.; Bieberich, A. A.; Alavanja, T.; Colby, D. A., Amino-derivatives of the sesquiterpene lactone class of natural products as prodrugs. *MedChemComm* **2013**, *4*, 27-33; (c) Zhang, Q.; Lu, Y.; Ding, Y.; Zhai, J.; Ji, Q.; Ma, W.; Yang, M.; Fan, H.; Long, J.; Tong, Z.; Shi, Y.; Jia, Y.; Han, B.; Zhang, W.; Qiu, C.; Ma, X.; Li, Q.; Shi, Q.; Zhang, H.; Li, D.; Zhang, J.; Lin, J.; Li, L. Y.; Gao, Y.; Chen, Y., Guaianolide sesquiterpene lactones, a source to discover agents that selectively inhibit acute myelogenous leukemia stem and progenitor cells. *J. Med. Chem.* **2012**, *55*, 8757-69; (d) Nasim, S.; Crooks, P. A., Antileukemic activity of aminoparthenolide analogs. *Bioorg. Med. Chem. Lett.* **2008**, *18*, 3870-3; (e) Hwang, D. R.; Wu, Y. S.; Chang, C. W.; Lien, T. W.; Chen, W. C.; Tan, U. K.; Hsu, J. T.; Hsieh, H. P., Synthesis and anti-viral activity of a series of sesquiterpene lactones and analogues in the subgenomic HCV replicon system. *Bioorg. Med. Chem.* **2006**, *14*, 83-91; (f) Matsuda, H.; Toguchida, I.; Ninomiya, K.; Kageura, T.; Morikawa, T.; Yoshikawa, M., Effects of sesquiterpenes and amino acid-sesquiterpene conjugates from the roots of *Saussurea lappa* on inducible nitric oxide synthase and heat shock protein in lipopolysaccharide-activated macrophages. *Bioorg. Med. Chem.* **2003**, *11*, 709-15; (g) Srivastava, S. K.; Abraham, A.; Bhat, B.; Jaggi, M.; Singh, A. T.; Sanna, V. K.; Singh, G.; Agarwal, S. K.; Mukherjee, R.; Burman, A. C., Synthesis of 13-amino costunolide derivatives as anticancer agents. *Bioorg. Med. Chem. Lett.* **2006**, *16*, 4195-9.
248. (a) Castaneda-Acosta, J.; Fischer, N. H.; Vargas, D., Biomimetic transformations of parthenolide. *J. Nat. Prod.* **1993**, *56*, 90-8; (b) An, Y.; Guo, W.; Li, L.; Xu, C.; Yang, D.; Wang, S.; Lu, Y.; Zhang, Q.; Zhai, J.; Fan, H.; Qiu, C.; Qi, J.; Chen, Y.; Yuan, S., Micheliolide derivative DMAMCL inhibits glioma cell growth in vitro and in vivo. *PLoS One* **2015**, *10*, e0116202.
249. (a) Neukirch, H.; Kaneider, N. C.; Wiedermann, C. J.; Guerriero, A.; D'Ambrosio, M., Parthenolide and its photochemically synthesized 1(10)Z isomer: chemical reactivity and structure-activity relationship studies in human leucocyte chemotaxis. *Bioorg. Med. Chem.* **2003**, *11*, 1503-10; (b) Long, J.; Zhang, S. F.; Wang, P. P.; Zhang, X. M.; Yang, Z. J.; Zhang, Q.; Chen, Y., Total syntheses of parthenolide and its analogues with macrocyclic stereocontrol. *J. Med. Chem.* **2014**, *57*, 7098-112; (c) Dell'Agli, M.; Galli, G. V.; Bosisio, E.; D'Ambrosio, M., Inhibition of NF- κ B and

- metalloproteinase-9 expression and secretion by parthenolide derivatives. *Bioorg. Med. Chem. Lett.* **2009**, *19*, 1858-60.
250. (a) Kwok, B. H.; Koh, B.; Ndubuisi, M. I.; Elofsson, M.; Crews, C. M., The anti-inflammatory natural product parthenolide from the medicinal herb Feverfew directly binds to and inhibits I κ B kinase. *Chemistry & Biology* **2001**, *8*, 759-66; (b) Macias, F. A.; Velasco, R. F.; Alvarez, J. A.; Castellano, D.; Galindo, J. C. G., Synthesis of melampolides and cis,cis-germacranolides as natural herbicide models. *Tetrahedron* **2004**, *60*, 8477-8488; (c) Nasim, S.; Pei, S.; Hagen, F. K.; Jordan, C. T.; Crooks, P. A., Melampomagnolide B: a new antileukemic sesquiterpene. *Bioorg. Med. Chem.* **2011**, *19* (4), 1515-9; (d) El-Faraly, F. S., Melampolides from *Magnoli grandiflora*. *Phytochemistry* **1984**, *23*, 2372; (e) Janganati, V.; Penthala, N. R.; Madadi, N. R.; Chen, Z.; Crooks, P. A., Anti-cancer activity of carbamate derivatives of melampomagnolide B. *Bioorg. Med. Chem. Lett.* **2014**, *24*, 3499-502.
251. Kolev, J. N.; O'Dwyer, K. M.; Jordan, C. T.; Fasan, R., Discovery of potent parthenolide-based antileukemic agents enabled by late-stage P450-mediated C-H functionalization. *ACS Chem. Biol.* **2014**, *9*, 164-73.
252. (a) Raj, L.; Ide, T.; Gurkar, A. U.; Foley, M.; Schenone, M.; Li, X.; Tolliday, N. J.; Golub, T. R.; Carr, S. A.; Shamji, A. F.; Stern, A. M.; Mandinova, A.; Schreiber, S. L.; Lee, S. W., Selective killing of cancer cells by a small molecule targeting the stress response to ROS. *Nature* **2011**, *475*, 231-4; (b) Schumacker, P. T., Reactive oxygen species in cancer cells: live by the sword, die by the sword. *Cancer Cell* **2006**, *10*, 175-6; (c) Skalska, J.; Brookes, P. S.; Nadtochiy, S. M.; Hilchey, S. P.; Jordan, C. T.; Guzman, M. L.; Maggirwar, S. B.; Briehl, M. M.; Bernstein, S. H., Modulation of cell surface protein free thiols: a potential novel mechanism of action of the sesquiterpene lactone parthenolide. *PLoS One* **2009**, *4*, e8115; (d) Lagadinou, E. D.; Sach, A.; Callahan, K.; Rossi, R. M.; Neering, S. J.; Minhajuddin, M.; Ashton, J. M.; Pei, S.; Grose, V.; O'Dwyer, K. M.; Liesveld, J. L.; Brookes, P. S.; Becker, M. W.; Jordan, C. T., BCL-2 inhibition targets oxidative phosphorylation and selectively eradicates quiescent human leukemia stem cells. *Cell Stem Cell* **2013**, *12*, 329-41; (e) Diehn, M.; Cho, R. W.; Lobo, N. A.; Kalisky, T.; Dorie, M. J.; Kulp, A. N.; Qian, D.; Lam, J. S.; Ailles, L. E.; Wong, M.; Joshua, B.; Kaplan, M. J.; Wapnir, I.; Dirbas, F. M.; Somlo, G.; Garberoglio, C.; Paz, B.; Shen, J.; Lau, S. K.; Quake, S. R.; Brown, J. M.; Weissman, I. L.; Clarke, M. F., Association of reactive oxygen species levels and radioresistance in cancer stem cells. *Nature* **2009**, *458*, 780-3; (f) Shanmugam, R.; Kusumanchi, P.; Cheng, L.; Crooks, P.; Neelakantan, S.; Matthews, W.; Nakshatri, H.; Sweeney, C. J., A water-soluble parthenolide analogue suppresses in vivo prostate cancer growth by targeting NF κ B and generating reactive oxygen species. *The Prostate* **2010**, *70*, 1074-86; (g) Trachootham, D.; Alexandre, J.; Huang, P., Targeting cancer cells by ROS-mediated mechanisms: a radical therapeutic approach? *Nature Rev. Drug. Discov.* **2009**, *8*, 579-91; (h) Adams, D. J.; Boskovic, Z. V.; Theriault, J. R.; Wang, A. J.; Stern, A. M.; Wagner, B. K.; Shamji, A. F.; Schreiber, S. L., Discovery of small-molecule enhancers of reactive oxygen species that are nontoxic or cause genotype-selective cell death. *ACS Chem. Biol.* **2013**, *8*, 923-9; (i) Pei, S.;

- Minhajuddin, M.; Callahan, K. P.; Balys, M.; Ashton, J. M.; Neering, S. J.; Lagadinou, E. D.; Corbett, C.; Ye, H.; Liesveld, J. L.; O'Dwyer, K. M.; Li, Z.; Shi, L.; Greninger, P.; Settleman, J.; Benes, C.; Hagen, F. K.; Munger, J.; Crooks, P. A.; Becker, M. W.; Jordan, C. T., Targeting aberrant glutathione metabolism to eradicate human acute myelogenous leukemia cells. *J. Biol. Chem.* **2013**, *288*, 33542-58; (j) Wen, J.; You, K. R.; Lee, S. Y.; Song, C. H.; Kim, D. G., Oxidative stress-mediated apoptosis. The anticancer effect of the sesquiterpene lactone parthenolide. *J. Biol. Chem.* **2002**, *277*, 38954-64.
253. (a) Jain, T. C.; Banks, C. M.; McCloskey, J. E., Reversible Dimethylamine Addition as a Protecting Reaction for α,β -Unsaturated Methylene Groups of γ -Lactones and Its Regeneration by Basic Elimination of Quaternary Ammonium-Salts - Convenient Synthesis of Dehydrosaussurea Lactone. *Tetrahedron* **1976**, *32*, 765-768; (b) Lee, K. H.; Furukawa, H., Antitumor agents. 3. Synthesis and cytotoxic activity of helenalin amine adducts and related derivatives. *J. Med. Chem.* **1972**, *15*, 609-11.
254. Demeijere, A., Bonding Properties of Cyclopropane and Their Chemical Consequences. *Angew. Chem. Int. Ed.* **1979**, *18*, 809-826.
255. Long, J.; Ding, Y. H.; Wang, P. P.; Zhang, Q.; Chen, Y., Protection-group-free semisyntheses of parthenolide and its cyclopropyl analogue. *J. Org. Chem.* **2013**, *78*, 10512-8.
256. (a) Furukawa, J., Kawabata, N., Nishimura, J., A stereospecific synthesis of cyclopropane derivatives from olefins. *Tetrahedron* **1968**, *31*, 3495; (b) Simmons, H. E., Smith, R.D., A New Synthesis of Cyclopropanes from olefins. *J. Am. Chem. Soc.* **1958**, *80*, 5323-5324; (c) Simmons, H. E., Smith, R.D., A New Synthesis of Cyclopropanes. *J. Am. Chem. Soc.* **1959**, *81*, 4256-4264.
257. Acosta, J. C.; Fronczek, F. R.; Fischer, N. H., Micheliolide. *Acta Crystallogr. C* **1991**, *47*, 2702-2704.
258. (a) Batist, G.; Tulpule, A.; Sinha, B. K.; Katki, A. G.; Myers, C. E.; Cowan, K. H., Overexpression of a novel anionic glutathione transferase in multidrug-resistant human breast cancer cells. *J. Biol. Chem.* **1986**, *261*, 15544-9; (b) Ke, W.; Yu, P.; Wang, J.; Wang, R.; Guo, C.; Zhou, L.; Li, C.; Li, K., MCF-7/ADR cells (re-designated NCI/ADR-RES) are not derived from MCF-7 breast cancer cells: a loss for breast cancer multidrug-resistant research. *Medical Oncol.* **2011**, *28*, S135-41.
259. (a) Hirschmann-Jax, C.; Foster, A. E.; Wulf, G. G.; Nuchtern, J. G.; Jax, T. W.; Gobel, U.; Goodell, M. A.; Brenner, M. K., A distinct "side population" of cells with high drug efflux capacity in human tumor cells. *Proc. Natl. Acad. Sci. U.S.A.* **2004**, *101*, 14228-33; (b) Holohan, C.; Van Schaeybroeck, S.; Longley, D. B.; Johnston, P. G., Cancer drug resistance: an evolving paradigm. *Nature Rev. Cancer* **2013**, *13*, 714-26; (c) Sotiropoulou, P. A.; Christodoulou, M. S.; Silvani, A.; Herold-Mende, C.;

- Passarella, D., Chemical approaches to targeting drug resistance in cancer stem cells. *Drug. Discov. Today* **2014**, *19*, 1547-62.
260. Swaminathan, S. K.; Olin, M. R.; Forster, C. L.; Cruz, K. S.; Panyam, J.; Ohlfest, J. R., Identification of a novel monoclonal antibody recognizing CD133. *Journal of immunological methods* **2010**, *361*, 110-5.
261. Andrews, T. E.; Wang, D.; Harki, D. A., Cell surface markers of cancer stem cells: diagnostic macromolecules and targets for drug delivery. *Drug Deliv. Transl. Res.* **2013**, *3*, 121-42.
262. (a) Kwok, B. H. B.; Koh, B.; Ndubuisi, M. I.; Elofsson, M.; Crews, C. M., The anti-inflammatory natural product parthenolide from the medicinal herb Feverfew directly binds to and inhibits I κ B kinase. *Chemistry & Biology* **2001**, *8*, 759-766; (b) Hexum, J. K.; Becker, C. M.; Kempema, A. M.; Ohlfest, J. R.; Largaespada, D. A.; Harki, D. A., Parthenolide prodrug LC-1 slows growth of intracranial glioma. *Bioorg. Med. Chem. Lett.* **2015**, *25*, 2493-5.
263. (a) Bhatia, M.; Wang, J. C.; Kapp, U.; Bonnet, D.; Dick, J. E., Purification of primitive human hematopoietic cells capable of repopulating immune-deficient mice. *Proc. Natl. Acad. Sci. U.S.A.* **1997**, *94*, 5320-5; (b) Laroche, A.; Vormoor, J.; Hanenberg, H.; Wang, J. C.; Bhatia, M.; Lapidot, T.; Moritz, T.; Murdoch, B.; Xiao, X. L.; Kato, I.; Williams, D. A.; Dick, J. E., Identification of primitive human hematopoietic cells capable of repopulating NOD/SCID mouse bone marrow: implications for gene therapy. *Nature Medicine* **1996**, *2*, 1329-37.
264. Sundman-Engberg, B.; Tidefelt, U.; Paul, C., Toxicity of cytostatic drugs to normal bone marrow cells in vitro. *Cancer Chemother. Pharmacol.* **1998**, *42*, 17-23.
265. Bedigian, H. G.; Taylor, B. A.; Meier, H., Expression of murine leukemia viruses in the highly lymphomatous BXH-2 recombinant inbred mouse strain. *J. Virol.* **1981**, *39*, 632-40.
266. (a) Largaespada, D. A.; Shaughnessy, J. D., Jr.; Jenkins, N. A.; Copeland, N. G., Retroviral integration at the Evi-2 locus in BXH-2 myeloid leukemia cell lines disrupts Nf1 expression without changes in steady-state Ras-GTP levels. *J. Virol.* **1995**, *69*, 5095-102; (b) Yin, B.; Kogan, S. C.; Dickins, R. A.; Lowe, S. W.; Largaespada, D. A., Trp53 loss during in vitro selection contributes to acquired Ara-C resistance in acute myeloid leukemia. *Exper. Hematol.* **2006**, *34*, 631-41.
267. Rathe, S. K.; Moriarity, B. S.; Stoltenberg, C. B.; Kurata, M.; Aumann, N. K.; Rahrman, E. P.; Bailey, N. J.; Melrose, E. G.; Beckmann, D. A.; Liska, C. R.; Largaespada, D. A., Using RNA-seq and targeted nucleases to identify mechanisms of drug resistance in acute myeloid leukemia. *Scientific Reports* **2014**, *4*, 6048.

268. (a) McDermott, S. P.; Eppert, K.; Notta, F.; Isaac, M.; Datti, A.; Al-Awar, R.; Wrana, J.; Minden, M. D.; Dick, J. E., A small molecule screening strategy with validation on human leukemia stem cells uncovers the therapeutic efficacy of kinetin riboside. *Blood* **2012**, *119*, 1200-7; (b) Mathema, V. B.; Koh, Y. S.; Thakuri, B. C.; Sillanpaa, M., Parthenolide, a sesquiterpene lactone, expresses multiple anti-cancer and anti-inflammatory activities. *Inflammation* **2012**, *35*, 560-5.
269. Pajak, B.; Gajkowska, B.; Orzechowski, A., Molecular basis of parthenolide-dependent proapoptotic activity in cancer cells. *Folia Histochemica et Cytobiologica* **2008**, *46*, 129-35.
270. Tartier, L.; McCarey, Y. L.; Biaglow, J. E.; Kochevar, I. E.; Held, K. D., Apoptosis induced by dithiothreitol in HL-60 cells shows early activation of caspase 3 and is independent of mitochondria. *Cell Death Diff.* **2000**, *7*, 1002-10.
271. (a) Singh, J.; Petter, R. C.; Baillie, T. A.; Whitty, A., The resurgence of covalent drugs. *Nature. Rev. Drug. Discov.* **2011**, *10*, 307-17; (b) Potashman, M. H.; Duggan, M. E., Covalent modifiers: an orthogonal approach to drug design. *J. Med. Chem.* **2009**, *52*, 1231-46.
272. Warner, J. K.; Wang, J. C.; Takenaka, K.; Doulatov, S.; McKenzie, J. L.; Harrington, L.; Dick, J. E., Direct evidence for cooperating genetic events in the leukemic transformation of normal human hematopoietic cells. *Leukemia* **2005**, *19*, 1794-805.
273. An Empirical correction for absorption anisotropy, R. Blessing. *Acta Cryst.* **1995**, *A51*, 33-38.
274. SAINT+ V7.68A, Bruker Analytical X-ray Systems, Madison, WI (2011).
275. Kempema, A. M.; Widen, J. C.; Hexum, J. K.; Andrews, T. E.; Wang, D.; Rathe, S. K.; Meece, F. A.; Noble, K. E.; Sachs, Z.; Largaespada, D. A.; Harki, D. A., Synthesis and antileukemic activities of C1-C10-modified parthenolide analogues. *Bioorg. Med. Chem.* **2015**, *23*, 4737-45.
276. SMART V5.054, Bruker Analytical X-ray Systems, Madison, WI (2001).
277. SHELXTL V6.14, Bruker Analytical X-ray Systems, Madison, WI (2000).
278. SAINT+ V6.45A, Bruker Analytical X-ray Systems, Madison, WI (2003).
279. (a) Meng, E. C.; Pettersen, E. F.; Couch, G. S.; Huang, C. C.; Ferrin, T. E., Tools for integrated sequence-structure analysis with UCSF Chimera. *BMC Bioinformatics* **2006**, *7*, 339; (b) Pettersen, E. F.; Goddard, T. D.; Huang, C. C.; Couch, G. S.; Greenblatt, D. M.; Meng, E. C.; Ferrin, T. E., UCSF chimera - A visualization system for exploratory research and analysis. *J. Comput. Chem.* **2004**, *25*, 1605-1612.

280. Wang, D. Synthesis and evaluation of parthenolide analogues: chemical probes and therapeutic agents. M.S. Thesis, University of Minnesota, March 2013.
281. (a) Kreso, A.; Dick, J. E., Evolution of the cancer stem cell model. *Cell Stem Cell* **2014**, *14*, 275-91; (b) Clarke, M. F.; Dick, J. E.; Dirks, P. B.; Eaves, C. J.; Jamieson, C. H.; Jones, D. L.; Visvader, J.; Weissman, I. L.; Wahl, G. M., Cancer stem cells--perspectives on current status and future directions: AACR Workshop on cancer stem cells. *Cancer Res.* **2006**, *66*, 9339-44.
282. Majeti, R.; Park, C. Y.; Weissman, I. L., Identification of a hierarchy of multipotent hematopoietic progenitors in human cord blood. *Cell Stem Cell* **2007**, *1*, 635-45.
283. (a) Bonnet, D.; Dick, J. E., Human acute myeloid leukemia is organized as a hierarchy that originates from a primitive hematopoietic cell. *Nature Medicine* **1997**, *3*, 730-737; (b) Lumkul, R.; Gorin, N. C.; Malehorn, M. T.; Hoehn, G. T.; Zheng, R.; Baldwin, B.; Small, D.; Gore, S.; Smith, D.; Meltzer, P. S.; Civin, C. I., Human AML cells in NOD/SCID mice: engraftment potential and gene expression. *Leukemia* **2002**, *16*, 1818-26.
284. Taussig, D. C.; Miraki-Moud, F.; Anjos-Afonso, F.; Pearce, D. J.; Allen, K.; Ridler, C.; Lillington, D.; Oakervee, H.; Cavenagh, J.; Agrawal, S. G.; Lister, T. A.; Gribben, J. G.; Bonnet, D., Anti-CD38 antibody-mediated clearance of human repopulating cells masks the heterogeneity of leukemia-initiating cells. *Blood* **2008**, *112*, 568-75.
285. Kadia, T. M.; Ravandi, F.; Cortes, J.; Kantarjian, H., New drugs in acute myeloid leukemia. *Annals of Oncology* **2016**, *27*, 770-8.
286. Gupta, V.; Tallman, M. S.; Weisdorf, D. J., Allogeneic hematopoietic cell transplantation for adults with acute myeloid leukemia: myths, controversies, and unknowns. *Blood* **2011**, *117*, 2307-18.
287. Dohner, H.; Estey, E. H.; Amadori, S.; Appelbaum, F. R.; Buchner, T.; Burnett, A. K.; Dombret, H.; Fenaux, P.; Grimwade, D.; Larson, R. A.; Lo-Coco, F.; Naoe, T.; Niederwieser, D.; Ossenkoppele, G. J.; Sanz, M. A.; Sierra, J.; Tallman, M. S.; Lowenberg, B.; Bloomfield, C. D.; European, L., Diagnosis and management of acute myeloid leukemia in adults: recommendations from an international expert panel, on behalf of the European LeukemiaNet. *Blood* **2010**, *115*, 453-74.
288. Dohner, H.; Weisdorf, D. J.; Bloomfield, C. D., Acute Myeloid Leukemia. *New Engl. J. Med.* **2015**, *373*, 1136-52.
289. (a) Neelakantan, S.; Surjawan, I.; Karacelik, H.; Hicks, C. L.; Crooks, P. A., Synthesis of novel isoluminol probes and their use in rapid bacterial assays. *Bioorg. Med. Chem. Lett.* **2009**, *19*, 5722-6; (b) Han, P.; Saunders, D. R.; Woods, R. L.; Luo,

- G., Trajectory prediction of saccadic eye movements using a compressed exponential model. *Journal of Vision* **2013**, *13*
290. Garcia-Pineros, A. J.; Lindenmeyer, M. T.; Merfort, I., Role of cysteine residues of p65/NF- κ B on the inhibition by the sesquiterpene lactone parthenolide and N-ethyl maleimide, and on its transactivating potential. *Life Sciences* **2004**, *75*, 841-56.
291. Lee, J.; Bogoy, M., Target deconvolution techniques in modern phenotypic profiling. *Curr. Opin. Chem. Biol.* **2013**, *17*, 118-26.
292. (a) Tanaka, Y.; Bond, M. R.; Kohler, J. J., Photocrosslinkers illuminate interactions in living cells. *Molecular BioSys.* **2008**, *4*, 473-80; (b) Smith, E.; Collins, I., Photoaffinity labeling in target- and binding-site identification. *Future Med. Chem.* **2015**, *7*, 159-83.
293. Elferaly, F. S., Melampolides from Magnolia-Grandiflora. *Phytochemistry* **1984**, *23*, 2372-2374.
294. Swanton, C., Intratumor heterogeneity: evolution through space and time. *Cancer Res.* **2012**, *72*, 4875-82.
295. (a) Goodspeed, A.; Heiser, L. M.; Gray, J. W.; Costello, J. C., Tumor-Derived Cell Lines as Molecular Models of Cancer Pharmacogenomics. *Mol. Cancer Res.* **2016**, *14*, 3-13; (b) Bruserud, O.; Gjertsen, B. T.; Foss, B.; Huang, T. S., New strategies in the treatment of acute myelogenous leukemia (AML): in vitro culture of aml cells--the present use in experimental studies and the possible importance for future therapeutic approaches. *Stem Cells* **2001**, *19*, 1-11.
296. (a) Meldal, M.; Tornøe, C. W., Cu-catalyzed azide-alkyne cycloaddition. *Chemical Revs.* **2008**, *108*, 2952-3015; (b) Sletten, E. M.; Bertozzi, C. R., Bioorthogonal chemistry: fishing for selectivity in a sea of functionality. *Angew. Chem. Int. Ed.* **2009**, *48*, 6974-98; (c) Tang, W.; Becker, M. L., "Click" reactions: a versatile toolbox for the synthesis of peptide-conjugates. *Chemical Society reviews* **2014**, *43*, 7013-39; (d) Martell, J.; Weerapana, E., Applications of copper-catalyzed click chemistry in activity-based protein profiling. *Molecules* **2014**, *19*, 1378-93; (e) Tiwari, V. K.; Mishra, B. B.; Mishra, K. B.; Mishra, N.; Singh, A. S.; Chen, X., Cu-Catalyzed Click Reaction in Carbohydrate Chemistry. *Chemical Revs.* **2016**, *116*, 3086-240.
297. Jayakumar, A.; Tai, M. H.; Huang, W. Y.; al-Feel, W.; Hsu, M.; Abu-Elheiga, L.; Chirala, S. S.; Wakil, S. J., Human fatty acid synthase: properties and molecular cloning. *Proc. Natl. Acad. Sci. U.S.A.* **1995**, *92*, 8695-9.
298. Kzhyshkowska, J.; Rusch, A.; Wolf, H.; Dobner, T., Regulation of transcription by the heterogeneous nuclear ribonucleoprotein E1B-AP5 is mediated by complex

- formation with the novel bromodomain-containing protein BRD7. *Biochem. J.* **2003**, *371*, 385-93.
299. Gabler, S.; Schutt, H.; Groitl, P.; Wolf, H.; Shenk, T.; Dobner, T., E1B 55-kilodalton-associated protein: a cellular protein with RNA-binding activity implicated in nucleocytoplasmic transport of adenovirus and cellular mRNAs. *J. Virol.* **1998**, *72*, 7960-71.
300. Ishimi, Y., A DNA helicase activity is associated with an MCM4, -6, and -7 protein complex. (vol 272, pg 24508, 1997). *J. Biol. Chem.* **1998**, *273*, 23616-23616.
301. Robinson, A. J.; Kunji, E. R. S.; Gross, A., Mitochondrial carrier homolog 2 (MTCH2): The recruitment and evolution of a mitochondrial carrier protein to a critical player in apoptosis. *Exper. Cell Res.* **2012**, *318*, 1316-1323.
302. Zaltsman, Y.; Shachnai, L.; Yivgi-Ohana, N.; Schwarz, M.; Maryanovich, M.; Houtkooper, R. H.; Vaz, F. M.; De Leonardis, F.; Fiermonte, G.; Palmieri, F.; Gillissen, B.; Daniel, P. T.; Jimenez, E.; Walsh, S.; Koehler, C. M.; Roy, S. S.; Walter, L.; Hajnoczky, G.; Gross, A., MTCH2/MIMP is a major facilitator of tBID recruitment to mitochondria. *Nature Cell Biol.* **2010**, *12*, 553-562.
303. Maryanovich, M.; Zaltsman, Y.; Ruggiero, A.; Goldman, A.; Shachnai, L.; Zaidman, S. L.; Porat, Z.; Golan, K.; Lapidot, T.; Gross, A., An MTCH2 pathway repressing mitochondria metabolism regulates haematopoietic stem cell fate. *Nature Commun.* **2015**, *6*.
304. (a) Blewitt, M. E.; Gendrel, A. V.; Pang, Z. Y.; Sparrow, D. B.; Whitelaw, N.; Craig, J. M.; Apedaile, A.; Hilton, D. J.; Dunwoodie, S. L.; Brockdorff, N.; Kay, G. F.; Whitelaw, E., SmcHD1, containing a structural-maintenance-of-chromosomes hinge domain, has a critical role in X inactivation. *Nature Genet.* **2008**, *40*, 663-669; (b) Gendrel, A. V.; Apedaile, A.; Coker, H.; Termanis, A.; Zvetkova, I.; Godwin, J.; Tang, Y. A.; Huntley, D.; Montana, G.; Taylor, S.; Giannoulatou, E.; Heard, E.; Stancheva, I.; Brockdorff, N., Smchd1-Dependent and -Independent Pathways Determine Developmental Dynamics of CpG Island Methylation on the Inactive X Chromosome. *Dev. Cell* **2012**, *23*, 265-279.
305. Will, C. L.; Urlaub, H.; Achsel, T.; Gentzel, M.; Wilm, M.; Luhrmann, R., Characterization of novel SF3b and 17S U2 snRNP proteins, including a human Prp5p homologue and an SF3b DEAD-box protein. *EMBO J.* **2002**, *21*, 4978-4988.
306. Kisselev, A. F.; van der Linden, W. A.; Overkleeft, H. S., Proteasome inhibitors: an expanding army attacking a unique target. *Chemistry & Biology* **2012**, *19*, 99-115.
307. (a) Obeng, E. A.; Carlson, L. M.; Gutman, D. M.; Harrington, W. J., Jr.; Lee, K. P.; Boise, L. H., Proteasome inhibitors induce a terminal unfolded protein response in multiple myeloma cells. *Blood* **2006**, *107*, 4907-16; (b) Meister, S.; Schubert, U.;

- Neubert, K.; Herrmann, K.; Burger, R.; Gramatzki, M.; Hahn, S.; Schreiber, S.; Wilhelm, S.; Herrmann, M.; Jack, H. M.; Voll, R. E., Extensive immunoglobulin production sensitizes myeloma cells for proteasome inhibition. *Cancer Res.* **2007**, *67*, 1783-92.
308. El-Amm, J.; Tabbara, I. A., Emerging therapies in multiple myeloma. *Am. J. Clin. Oncol.* **2015**, *38*, 315-21.
309. Cerini, C.; Kerjan, P.; Astier, M.; Gratecos, D.; Mirande, M.; Semeriva, M., A component of the multisynthetase complex is a multifunctional aminoacyl-tRNA synthetase. *EMBO J.* **1991**, *10*, 4267-77.
310. Sampath, P.; Mazumder, B.; Seshadri, V.; Gerber, C. A.; Chavatte, L.; Kinter, M.; Ting, S. M.; Dignam, J. D.; Kim, S.; Driscoll, D. M.; Fox, P. L., Noncanonical function of glutamyl-prolyl-tRNA synthetase: gene-specific silencing of translation. *Cell* **2004**, *119*, 195-208.
311. Arif, A.; Chatterjee, P.; Moodt, R. A.; Fox, P. L., Heterotrimeric GAIT complex drives transcript-selective translation inhibition in murine macrophages. *Mol. Cell. Biol.* **2012**, *32*, 5046-55.
312. Mukhopadhyay, R.; Jia, J.; Arif, A.; Ray, P. S.; Fox, P. L., The GAIT system: a gatekeeper of inflammatory gene expression. *Trends Biochem. Sci.* **2009**, *34*, 324-31.
313. Wang, Q.; Li, N.; Wang, X.; Shen, J.; Hong, X.; Yu, H.; Zhang, Y.; Wan, T.; Zhang, L.; Wang, J.; Cao, X., Membrane protein hMYADM preferentially expressed in myeloid cells is up-regulated during differentiation of stem cells and myeloid leukemia cells. *Life Sciences* **2007**, *80*, 420-9.
314. Chai, Z.; Brereton, P.; Suzuki, T.; Sasano, H.; Obeyesekere, V.; Escher, G.; Saffery, R.; Fuller, P.; Enriquez, C.; Krozowski, Z., 17 β -hydroxysteroid dehydrogenase type XI localizes to human steroidogenic cells. *Endocrinology* **2003**, *144*, 2084-91.
315. (a) Kobayashi, Y.; Suzuki, K.; Kobayashi, H.; Ohashi, S.; Koike, K.; Macchi, P.; Kiebler, M.; Anzai, K., C9orf10 protein, a novel protein component of Pura-containing mRNA-protein particles (Pura-mRNPs): characterization of developmental and regional expressions in the mouse brain. *J. Histochem. Cytochem.* **2008**, *56*, 723-31; (b) Angenstein, F.; Evans, A. M.; Ling, S. C.; Settlage, R. E.; Ficarro, S.; Carrero-Martinez, F. A.; Shabanowitz, J.; Hunt, D. F.; Greenough, W. T., Proteomic characterization of messenger ribonucleoprotein complexes bound to nontranslated or translated poly(A) mRNAs in the rat cerebral cortex. *J. Biol. Chem.* **2005**, *280*, 6496-503.

316. Tanaka, M.; Sasaki, K.; Kamata, R.; Hoshino, Y.; Yanagihara, K.; Sakai, R., A novel RNA-binding protein, Ossa/C9orf10, regulates activity of Src kinases to protect cells from oxidative stress-induced apoptosis. *Mol. Cell. Biol.* **2009**, *29*, 402-13.
317. (a) Guan, Y.; Gerhard, B.; Hogge, D. E., Detection, isolation, and stimulation of quiescent primitive leukemic progenitor cells from patients with acute myeloid leukemia (AML). *Blood* **2003**, *101*, 3142-9; (b) D'Anneo, A.; Carlisi, D.; Lauricella, M.; Emanuele, S.; Di Fiore, R.; Vento, R.; Tesoriere, G., Parthenolide induces caspase-independent and AIF-mediated cell death in human osteosarcoma and melanoma cells. *J. Cell. Physiol.* **2013**, *228*, 952-67; (c) Kwak, S. W.; Park, E. S.; Lee, C. S., Parthenolide induces apoptosis by activating the mitochondrial and death receptor pathways and inhibits FAK-mediated cell invasion. *Molecular and cellular biochemistry* **2014**, *385* (1-2), 133-44; (d) D'Anneo, A.; Carlisi, D.; Emanuele, S.; Buttitta, G.; Di Fiore, R.; Vento, R.; Tesoriere, G.; Lauricella, M., Parthenolide induces superoxide anion production by stimulating EGF receptor in MDA-MB-231 breast cancer cells. *Int. J. Oncol.* **2013**, *43*, 1895-900.
318. Sander, J. D.; Joung, J. K., CRISPR-Cas systems for editing, regulating and targeting genomes. *Nature Biotech.* **2014**, *32*, 347-55.
319. Pereira, D. S.; Dorrell, C.; Ito, C. Y.; Gan, O. I.; Murdoch, B.; Rao, V. N.; Zou, J. P.; Reddy, E. S.; Dick, J. E., Retroviral transduction of TLS-ERG initiates a leukemogenic program in normal human hematopoietic cells. *Proc. Natl. Acad. Sci. U.S.A.* **1998**, *95*, 8239-44.
320. Guschin, D. Y.; Waite, A. J.; Katibah, G. E.; Miller, J. C.; Holmes, M. C.; Rebar, E. J., A rapid and general assay for monitoring endogenous gene modification. *Methods in Mol. Biol.* **2010**, *649*, 247-56.
321. Yang, B.; Wen, X.; Kodali, N. S.; Oleykowski, C. A.; Miller, C. G.; Kulinski, J.; Besack, D.; Yeung, J. A.; Kowalski, D.; Yeung, A. T., Purification, cloning, and characterization of the CEL I nuclease. *Biochemistry* **2000**, *39*, 3533-41.
322. Rathe, S. K.; Moriarity, B. S.; Stoltenberg, C. B.; Kurata, M.; Aumann, N. K.; Rahrman, E. P.; Bailey, N. J.; Melrose, E. G.; Beckmann, D. A.; Liska, C. R.; Largaespada, D. A., Using RNA-seq and targeted nucleases to identify mechanisms of drug resistance in acute myeloid leukemia. *Scientific Reports* **2014**, *4*.
323. Siegel, R. L.; Miller, K. D.; Jemal, A., Cancer Statistics, 2016. *CA Cancer J. Clin.* **2016**, *66*, 7-30.
324. Bechis, S. K.; Carroll, P. R.; Cooperberg, M. R., Impact of Age at Diagnosis on Prostate Cancer Treatment and Survival. *J. Clin. Oncol.* **2011**, *29*, 235-241.
325. Heidenreich, A.; Bastian, P. J.; Bellmunt, J.; Bolla, M.; Joniau, S.; van der Kwast, T.; Mason, M.; Matveev, V.; Wiegel, T.; Zattoni, F.; Mottet, N., EAU Guidelines on

- Prostate Cancer. Part II: Treatment of Advanced, Relapsing, and Castration-Resistant Prostate Cancer. *Eur. Urol.* **2014**, *65*, 467-479.
326. Huggins, C. S., R.E.; Hodges, C.V., The effects of castration on advanced carcinoma of the prostate gland. *Arch. Surg.* **1941**, *43*, 209-223.
327. Gomella, L. G., Effective testosterone suppression for prostate cancer: is there a best castration therapy? *Revs. Urol.* **2009**, *11*, 52-60.
328. Ross, R. W.; Xie, W.; Regan, M. M.; Pomerantz, M.; Nakabayashi, M.; Daskivich, T. J.; Sartor, O.; Taplin, M. E.; Kantoff, P. W.; Oh, W. K., Efficacy of androgen deprivation therapy (ADT) in patients with advanced prostate cancer: association between Gleason score, prostate-specific antigen level, and prior ADT exposure with duration of ADT effect. *Cancer* **2008**, *112*, 1247-53.
329. Ferraldeschi, R.; Pezaro, C.; Karavasili, V.; de Bono, J., Abiraterone and novel antiandrogens: overcoming castration resistance in prostate cancer. *Annu. Rev. Med.* **2013**, *64*, 1-13.
330. Bambury, R. M.; Rathkopf, D. E., Novel and next-generation androgen receptor-directed therapies for prostate cancer: Beyond abiraterone and enzalutamide. *Urologic Oncol.* **2016**, *34*, 348-55.
331. Dehm, S. M.; Schmidt, L. J.; Heemers, H. V.; Vessella, R. L.; Tindall, D. J., Splicing of a novel androgen receptor exon generates a constitutively active androgen receptor that mediates prostate cancer therapy resistance. *Cancer Res.* **2008**, *68*, 5469-77.
332. (a) Sun, S.; Sprenger, C. C.; Vessella, R. L.; Haugk, K.; Soriano, K.; Mostaghel, E. A.; Page, S. T.; Coleman, I. M.; Nguyen, H. M.; Sun, H.; Nelson, P. S.; Plymate, S. R., Castration resistance in human prostate cancer is conferred by a frequently occurring androgen receptor splice variant. *J. Clin. Invest.* **2010**, *120*, 2715-30; (b) Hornberg, E.; Ylitalo, E. B.; Crnalic, S.; Antti, H.; Stattin, P.; Widmark, A.; Bergh, A.; Wikstrom, P., Expression of androgen receptor splice variants in prostate cancer bone metastases is associated with castration-resistance and short survival. *PLoS One* **2011**, *6*, e19059.
333. Jenster, G.; van der Korput, H. A.; van Vroonhoven, C.; van der Kwast, T. H.; Trapman, J.; Brinkmann, A. O., Domains of the human androgen receptor involved in steroid binding, transcriptional activation, and subcellular localization. *Mol. Endocrinol.* **1991**, *5*, 1396-404.
334. Clinical trial information: <https://clinicaltrials.gov/ct2/show/NCT02606123>.
335. (a) Andersen, R. J. F., J.G.; Sadar, M.D.; Mawji, N.; Banuelos, A.C. Bisphenol compounds and methods for their use. **2012**; (b) Mawji, N. W., J.; Banuelos, A.C.;

- Andersen, R.J.; Fernandez, J.G.; Sadar, M.D. Ester derivatives of androgen receptor modulators and method for their use. **2014**.
336. Krongrad, A.; Wilson, C. M.; Wilson, J. D.; Allman, D. R.; McPhaul, M. J., Androgen increases androgen receptor protein while decreasing receptor mRNA in LNCaP cells. *Mol. Cell. Endocrinol.* **1991**, *76*, 79-88.
337. Barnes, J. C.; Ehrlich, D. J.; Gao, A. X.; Leibfarth, F. A.; Jiang, Y.; Zhou, E.; Jamison, T. F.; Johnson, J. A., Iterative exponential growth of stereo- and sequence-controlled polymers. *Nature Chem.* **2015**, *7*, 810-5.
338. Chomczynski, P.; Sacchi, N., The single-step method of RNA isolation by acid guanidinium thiocyanate-phenol-chloroform extraction: twenty-something years on. *Nature Protocols* **2006**, *1*, 581-5.
339. (a) Johansson, H., Pedersen, D.S., Azide- and Alkyne-derivatised α -amino acids. *Eur. J. Org. Chem.* **2012**, *2012*, 4267-4281; (b) Lehmann, J.; Wright, M. H.; Sieber, S. A., Making a Long Journey Short: Alkyne Functionalization of Natural Product Scaffolds. *Chemistry* **2016**, *22*, 4666-78.
340. Gushwa, N. N.; Kang, S.; Chen, J.; Taunton, J., Selective targeting of distinct active site nucleophiles by irreversible SRC-family kinase inhibitors. *J. Am. Chem. Soc.* **2012**, *134*, 20214-7.
341. Cohen, M. S.; Hadjivassiliou, H.; Taunton, J., A clickable inhibitor reveals context-dependent autoactivation of p90 RSK. *Nature Chem. Biol.* **2007**, *3*, 156-60.
342. Bottcher, T.; Sieber, S. A., Showdomycin as a versatile chemical tool for the detection of pathogenesis-associated enzymes in bacteria. *J. Am. Chem. Soc.* **2010**, *132*, 6964-72.
343. Wirth, T.; Pestel, G. F.; Ganal, V.; Kirmeier, T.; Schuberth, I.; Rein, T.; Tietze, L. F.; Sieber, S. A., The two faces of potent antitumor duocarmycin-based drugs: a structural dissection reveals disparate motifs for DNA versus aldehyde dehydrogenase 1 affinity. *Angew. Chem. Int. Ed.* **2013**, *52*, 6921-5.
344. Li, J.; Cisar, J. S.; Zhou, C. Y.; Vera, B.; Williams, H.; Rodriguez, A. D.; Cravatt, B. F.; Romo, D., Simultaneous structure-activity studies and arming of natural products by C-H amination reveal cellular targets of eupalmerin acetate. *Nature Chem.* **2013**, *5*, 510-7.
345. (a) Cravatt, B. F.; Wright, A. T.; Kozarich, J. W., Activity-based protein profiling: from enzyme chemistry to proteomic chemistry. *Annu. Rev. Biochem.* **2008**, *77*, 383-414; (b) Nodwell, M. B.; Sieber, S. A., ABPP methodology: introduction and overview. *Topics Curr. Chem.* **2012**, *324*, 1-41; (c) Willems, L. I.; Overkleeft, H. S.; van Kasteren, S. I., Current developments in activity-based protein profiling.

- Bioconjugate Chem.* **2014**, *25*, 1181-91; (d) Yang, P.; Liu, K., Activity-based protein profiling: recent advances in probe development and applications. *ChemBioChem* **2015**, *16*, 712-24.
346. Bottcher, T.; Pitscheider, M.; Sieber, S. A., Natural products and their biological targets: proteomic and metabolomic labeling strategies. *Angew. Chem. Int. Ed.* **2010**, *49*, 2680-98.
347. (a) Etmayer, P.; Amidon, G. L.; Clement, B.; Testa, B., Lessons learned from marketed and investigational prodrugs. *J. Med. Chem.* **2004**, *47*, 2393-404; (b) Li, B.; Sedlacek, M.; Manoharan, I.; Boopathy, R.; Duysen, E. G.; Masson, P.; Lockridge, O., Butyrylcholinesterase, paraoxonase, and albumin esterase, but not carboxylesterase, are present in human plasma. *Biochem. Pharmacol.* **2005**, *70*, 1673-84.
348. (a) Lockwood, R. F.; Nicholas, K. M., Transition Metal-Stabilized Carbenium Ions as Synthetic Intermediates .1. A-[(Alkynyl)Dicobalt Hexacarbonyl] Carbenium Ions as Propargylating Agents. *Tetrahedron Lett.* **1977**, 4163-4166; (b) Nicholas, K. M., Chemistry and Synthetic Utility of Cobalt-Complexed Propargyl Cations. *Accounts Chem. Res.* **1987**, *20*, 207-214; (c) Teobald, B. J., The Nicholas reaction: the use of dicobalt hexacarbonyl-stabilised propargylic cations in synthesis. *Tetrahedron* **2002**, *58*, 4133-4170; (d) Diaz, D. D.; Bncort, J. M.; Martin, V. S., The Nicholas reaction: A powerful tool for the stereoselective synthesis of bioactive compounds. *Synlett.* **2007**, 343-359.
349. (a) Diaz, D. D.; Martin, V. S., CO₂(CO)₍₈₎-Assisted synthesis of propargylic unsymmetrical ethers by reaction of alcohols with propargylic alcohols. *Tetrahedron Lett* **2000**, *41*, 9993-9996; (b) Hope-Weeks, L. J.; Mays, M. J.; Solan, G. A., Coordinated 1,3-diyne diols as organometallic building blocks for large macrocycles containing oxygen and unsaturated donor units. *Eur. J. Inorg. Chem.* **2007**, 3101-3114; (c) Ortega, N.; Martin, V. S.; Martin, T., An approach to lauroxanes by iterative use of Co(2)(CO)(6)-acetylenic complexes. a formal synthesis of (+)-laurencin. *J. Org. Chem.* **2010**, *75*, 6660-72.
350. Hayashi, Y.; Yamaguchi, H.; Toyoshima, M.; Okado, K.; Toyo, T.; Shoji, M., Formal total synthesis of fostriecin by 1,4-asymmetric induction with an alkyne-cobalt complex. *Org. Lett.* **2008**, *10*, 1405-8.
351. Ahmad Fuaad, A. A.; Azmi, F.; Skwarczynski, M.; Toth, I., Peptide conjugation via CuAAC 'click' chemistry. *Molecules* **2013**, *18*, 13148-74.
352. Struthers, H.; Spingler, B.; Mindt, T. L.; Schibli, R., "Click-to-chelate": design and incorporation of triazole-containing metal-chelating systems into biomolecules of diagnostic and therapeutic interest. *Chemistry Eur. J.* **2008**, *14*, 6173-83.

353. Hope-Weeks, L. J.; Mays, M. J.; Woods, A. D., Synthesis of thio and mixed donor atom macrocycles containing coordinated diyne units. *J. Chem. Soc. Dalton*. **2002**, 1812-1819.
354. Evans, E. F.; Lewis, N. J.; Kapfer, I.; Macdonald, G.; Taylor, R. J. K., N-tert-butoxycarbonyl (BOC) deprotection using boron trifluoride etherate. *Synthetic Commun.* **1997**, *27*, 1819-1825.
355. Amouri, H.; Begue, J. P.; Chennoufi, A.; Bonnet-Delpon, D.; Gruselle, M.; Malezieux, B., Cobalt-Induced C-N and C-C Bond Formation via Metal-Stabilized α -CF(3) Carbenium Ion. *Org. Lett.* **2000**, *2*, 807-809.
356. Shea, K. M.; Closser, K. D.; Quintal, M. M., Nicholas reactions with carboxylic acids for the synthesis of macrocyclic diolides. *J. Org. Chem.* **2005**, *70*, 9088-91.
357. (a) Macias, F. A.; Galindo, J. C. G.; Massanet, G. M., Natural Product Models as Allelochemicals .1. Potential Allelopathic Activity of Several Sesquiterpene Lactone Models. *Phytochemistry* **1992**, *31*, 1969-1977; (b) Nasim, S.; Pei, S. S.; Hagen, F. K.; Jordan, C. T.; Crooks, P. A., Melampomagnolide B: A new antileukemic sesquiterpene. *Bioorg. Med. Chem.* **2011**, *19*, 1515-1519; (c) Janganati, V.; Penthala, N. R.; Madadi, N. R.; Chen, Z.; Crooks, P. A., Anti-cancer activity of carbamate derivatives of melampomagnolide B. *Bioorg. Med. Chem. Lett.* **2014**, *24*, 3499-3502.
358. Conner, R. E., Nicholas, K.M., Isolation, characterization, and stability of α -[(ethynyl)dicobalt hexacarbonyl] carbonium ions. *J. Organomet. Chem.* **1977**, *125*, C45-C48.
359. Oh, J. E.; Lee, K. H., Synthesis of novel unnatural amino acid as a building block and its incorporation into an antimicrobial peptide. *Bioorg. Med. Chem.* **1999**, *7*, 2985-90.
360. Zhang, F.; Zhang, W.; Zhang, Y.; Curran, D. P.; Liu, G., Synthesis and applications of a light-fluorous glycosyl donor. *J. Org. Chem.* **2009**, *74*, 2594-7.
361. Aroyan, C. E.; Dermenci, A.; Miller, S. J., Development of a cysteine-catalyzed enantioselective Rauhut-Currier reaction. *J. Org. Chem.* **2010**, *75*, 5784-96.
362. Page, P. C. B.; Buckley, B. R.; Farah, M. M.; Blacker, A. J., Binaphthalene-Derived Iminium Salt Catalysts for Highly Enantioselective Asymmetric Epoxidation. *Eur J. Org. Chem.* **2009**, 3413-3426.
363. Alcohol 14 was synthesized according to procedures previously reported and was used as a mixture of two diastereomers (2.4:1): *Org. Lett.* **2013**, *15*, 2644-2647.